INVESTIGATION AND COMPARISON OF BEARING DEVICES USED IN HIGH-SPEED RAILWAY BRIDGES UNDER EARTHQUAKE IMPACT

A THESIS SUBMITTED TO
THE GRADUATE SCHOOL OF NATURAL AND APPLIED SCIENCES
OF
MIDDLE EAST TECHNICAL UNIVERSITY

BY

UĞUR AŞCI

IN PARTIAL FULFILLMENT OF THE REQUIREMENTS
FOR
THE DEGREE OF MASTER OF SCIENCE
IN
EARTHQUAKE STUDIES

DECEMBER 2019

Approval of the thesis:

INVESTIGATION AND COMPARISON OF BEARING DEVICES USED IN HIGH-SPEED RAILWAY BRIDGES UNDER EARTHQUAKE IMPACT

submitted by **UĞUR AŞCI** in partial fulfillment of the requirements for the degree of **Master of Science in Earthquake Studies Department, Middle East Technical University** by,

Prof. Dr. Halil Kalıpçılar
Dean, Graduate School of **Natural and Applied Sciences** _____

Prof. Dr. Ayşegül Askan Gündoğan
Head of Department, **Earthquake Studies** _____

Prof. Dr. Alp Caner
Supervisor, **Earthquake Studies, METU** _____

Prof. Dr. Ayşen Dener Akkaya
Co-Supervisor, **Statistics, METU** _____

Examining Committee Members:

Prof. Dr. Murat Altuğ Erberik
Earthquake Studies, METU _____

Prof. Dr. Alp Caner
Earthquake Studies, METU _____

Prof. Dr. Ayşen Dener Akkaya
Statistics, METU _____

Assist. Prof. Dr. Onur Pekcan
Civil Engineering, METU _____

Assoc. Prof. Dr. Alper Aldemir
Civil Engineering, Hacettepe University _____

Date: 05.12.2019

I hereby declare that all information in this document has been obtained and presented in accordance with academic rules and ethical conduct. I also declare that, as required by these rules and conduct, I have fully cited and referenced all material and results that are not original to this work.

Name, Surname: Uğur AŞCI

Signature:

ABSTRACT

INVESTIGATION AND COMPARISON OF BEARING DEVICES USED IN HIGH-SPEED RAILWAY BRIDGES UNDER EARTHQUAKE IMPACT

AŞCI, Uğur
Master of Science, Earthquake Studies
Supervisor: Prof. Dr. Alp Caner
Co-Supervisor: Prof. Dr. Ayşen Dener Akkaya

December 2019, 205 pages

This study covers the investigation of behavior and comparison of two bearing types (elastomeric and pot bearings) under earthquake effects.

Real earthquake records are used in this study. Earthquake selection is an important process. The plan behind the selection process is to cover the earthquakes with high occurrence rates in real life and to gain more realistic results. Magnitudes of selected earthquakes are 6.0, 6.5 or 7.0. The location assumed at which the effects of earthquakes investigated is 15 to 30 km away from the fault. Soil class of the assumed location is either C or D. Depending on earthquake magnitude and soil properties, 6 data groups are formed. In each group, 7 different earthquake data are taken into consideration.

To make a comparison between the behavior of different bearing types, elastomeric and pot bearings are chosen since they are the most widely used bearing types. For elastomeric bearing used cases; case 1 is using elastomeric bearing under each beam and case 2 is using less elastomeric bearing under the cross beam. In pot bearing case, say case 3, the same amount of bearings is taken into the account as in case 2 of elastomeric bearing is used.

This study has been done for the bridge which is 95-meter-long with 3 spans and 2 piers. Each pier has a height of 15 meters. For the analytic model and structural analysis finite element program, SAP2000 v.14.2.2 has been used.

Within this study behavior of bearings under real earthquake effect depending upon magnitude and soil properties are investigated.

Keywords: High-Speed Railway Bridges, Bearing Devices, Elastomeric Bearing, Pot Bearing, Earthquake Effects on Bearings

ÖZ

YÜKSEK HIZLI TREN KÖPRÜLERİNDE KULLANILAN MESNETLERİN DEPREM ETKİSİ ALTINDAKİ DAVRANIŞLARININ ARAŞTIRILMASI VE BİRBİRLERİYLE KIYASLANMASI

AŞCI, Uğur
Yüksek Lisans, Deprem Çalışmaları
Tez Danışmanı: Prof. Dr. Alp Caner
Ortak Tez Danışmanı: Prof. Dr. Ayşen Dener Akkaya

Aralık 2019, 205 sayfa

Bu çalışma, yüksek hızlı tren köprülerinde kullanılan mesnet elemanlarının çeşitli deprem etkileri altındaki davranışlarının incelenmesini ve farklı mesnet tiplerinin (elastomer mesnet ve pot mesnet) deprem etkileri altındaki davranışlarının birbirleriyle kıyaslanmasını içermektedir.

Bu çalışmada gerçek deprem verileri kullanılmıştır. Depremler seçilirken günlük yaşamda en çok karşılaşılan durumlarla örtüştürülerek gerçekçi yaklaşımlar ve sonuçlar elde edilmesi planlanmıştır. 6.0, 6.5, 7.0 büyüklüğündeki depremlerin, deprem merkezinden en az 15 km en fazla 30 km mesafede yer alan C ve D sınıfı zemin üzerindeki etkilerinin değerlendirilmesi amaçlanmıştır. Deprem büyüklüğü ve zemin sınıfı parametreleri ile 6 farklı veri grubu oluşturulmuş, her veri grubu için 7 farklı deprem verisi kullanılmıştır.

Mesnet tipine göre davranış kıyaslaması için kullanım yaygınlığı göz önüne alınarak elastomer mesnet ve pot mesnet tipleri seçilmiştir. Elastomer mesnet tipi kullanılarak modellenen köprülerde her bir kirişin altına bir elastomer mesnet konması bir durum; enleme kirişi yardımıyla daha az sayıda elastomer mesnet kullanılması ikinci bir

durum; pot mesnet kullanılarak modellenen köprü durumu da üçüncü durum olarak değerlendirilmiştir.

95 metre uzunluğunda, 3 açıklıklı, orta ayak yükseklikleri 15 er metre olan simetrik bir köprü hesaplar için seçilmiştir. Köprünün analizler için kullanılacak sayısal modeli SAP2000 v14.2.2 kullanılarak oluşturulmuş ve deprem verileri ile mesnet özellikleri modele uygulanarak analizleri yapılmıştır.

Bu çalışma ile mesnet tiplerinin gerçek deprem verileri altındaki davranışları, zemin sınıfına ve deprem büyüklüklerine bağlı olarak değerlendirilmiştir.

Anahtar Kelimeler: Yüksek Hızlı Tren Köprüleri, Mesnet Elemanları, Elastomer Mesnet, Pot Mesnet, Depremin Mesnetlere Etkileri

To My Family

ACKNOWLEDGEMENTS

I would like to thank Prof. Dr. Alp Caner, Prof Dr. Ayşegül Askan Gündoğan and Assoc. Prof. Dr. Alper Aldemir for their support, encouragement, and help from the very beginning until the end of this study.

I would like to thank Prof. Dr. Ayşen Dener Akkaya and Assoc. Prof. Dr. Berna Burçak Başbuğ Erkan for their precious help and support throughout this study.

I would like to thank Prof. Dr. Murat Altuğ Erberik and Assist. Prof. Dr. Onur Pekcan for their precious feedbacks and positive criticism.

My Wife Nurper Erdin Aşcı deserves very special thanks for her unlimited support, patience, belief in me, encouragement and love.

I am proud of being their son and brother; I want to express my gratefulness to my Dad Osman Aşcı, my Mom Nuran Aşcı and my Brother Umut Aşcı for their endless patience, support, belief in me and love.

I also want to thank my Father-in-law Sermet Erdin and my Mother-in-law Yeşim Erdin for their encouragement and help to create the extra time needed to conduct this study.

My dear Son Mert Aşcı also deserves special thanks however he has not been aware of that today; this study stole so much from our playing time.

I also want to put the names of my colleagues Ayhan Akray and Özer Gündüz here for their support and motivation, and I am happy to walk through the same destination with them.

And I want to thank Hakan Veysi Alkan and Hakan Acunsal for their permission, patience, support and making way for creating the extra time needed to conduct this study.

TABLE OF CONTENTS

LIST OF TABLES

TABLES

LIST OF FIGURES

FIGURES

LIST OF ABBREVIATIONS

A : Acceleration (cm/s^2)

a : Half of the distance between the beams

a_{cr} : Creep deflection divided by initial dead load deflection

A_{eb} : Area of the elastomeric bearing (mm^2)

AASHTO : American Association of State Highways and Transportation Officials

C.J. : Construction joint

C_p : The clearance distance of the pot wall (mm)

D : Displacement (mm)

D_{ed} : Diameter of the elastomeric disc of a pot bearing (mm)

D_p : Internal diameter of pot bearing (mm)

E : Modulus of elasticity ($kg/m/s^2$)

E.B. : Expansion bearing

EBC-3 : Elastomeric bearing analysis case

EBC10-REF : Reference analysis case

E.J. : Expansion joint

F.B. : Fixed bearing

F_y : Yield strength of steel (MPa)

g : Gravitational acceleration (cm/s^2)

GM : Ground motion

G_{eb} : Shear modulus of the elastomeric bearing

$\mathbf{h_{layer}}$ **:** Height of each layer between steel plates in an elastomeric bearing (mm)

$\mathbf{h_{p1}}$ **:** Pot cavity (mm)

$\mathbf{h_{p2}}$ **:** Clear distance between pot wall and top plate (mm)

$\mathbf{h_{r}}$ **:** Height of the elastomeric disc of a pot bearing (mm)

$\mathbf{h_{ri}}$ **:** Thickness of i^{th} elastomeric layer (mm)

$\mathbf{h_{rt}}$ **:** Height between the uppermost and the lowest steel plates (mm)

$\mathbf{h_{total,p}}$ **:** Total height of pot bearing (mm)

$\mathbf{H_{u}}$ **:** Lateral load (N) from applicable strength and extreme load combinations in Table 3.4.1-1 of AASHTO LRFD Bridge Design Specifications

$\mathbf{h_{wf}}$ **:** Pot wall free height (mm)

$\mathbf{h_{wr}}$ **:** Height from top of the rim to underside of the piston (mm)

$\mathbf{k_{rot,l}}$ **:** Rotational spring stiffness coefficient about longitudinal direction (kNm/rad)

$\mathbf{k_{rot,t}}$ **:** Rotational spring stiffness coefficient about transverse direction (kNm/rad)

$\mathbf{k_{rot,v}}$ **:** Rotational spring stiffness coefficient about vertical direction (kNm/rad)

$\mathbf{k_{tr}}$ **:** Translational spring stiffness coefficient of elastomeric bearing in both transverse and longitudinal directions (kN/m)

$\mathbf{k_{vr}}$ **:** Spring stiffness coefficient of elastomeric bearing in the vertical direction (kN/m)

LFD **:** Load factor design

LRFD **:** Load resistance factor design

L_{eb} **:** Length of the elastomeric bearing (mm)

L_1 **:** Distance between two expansion joints (m)

M **:** Earthquake Magnitude

M_i **:** Moment (kN.m)

PBC-3 **:** Pot bearing analysis case

PEER **:** The Pacific Earthquake Engineering and Research Center

PGA **:** Peak ground acceleration (g)

PGD **:** Peak ground displacement (cm)

PGV **:** Peak ground velocity (cm/s)

PTFE **:** Polytetrafluoroethylene

P_{eb} **:** Total vertical load on an elastomeric bearing (N/m^2)

R.B. ELV. **:** Rail bound elevation (m)

R.L. ELV. **:** Redline elevation (m)

R_{jb} **:** Distance between the epicenter and the seismograph. It is proposed by Joyner and Boore. (km)

R_o **:** Radial distance from the center of the pot to object in question (e.g., pot wall, anchor bolt, etc.) (mm)

R_{rup} **:** The closest distance between the fault plane and the station (km)

SF **:** Shape Factor of the thickest layer of the bearing

T **:** Period in seconds

TCDD **:** General Directorate of State Railways

TSBC **:** Turkish Seismic Building Code

$\mathbf{t_{ap}}$ **:** Thickness of anchorage plate (mm)

$\mathbf{t_b}$ **:** Thickness of base of a pot bearing (mm)

$\mathbf{t_{ptfe}}$ **:** Thickness of the polytetrafluoroethylene layer (mm)

$\mathbf{t_w}$ **:** Pot wall thickness (mm)

V **:** Velocity (m/s)

$\mathbf{V_i}$ **:** Shear force (kN)

$\mathbf{V_{S30}}$ **:** Harmonic mean of shear wave velocities in first 30 meters of a soil profile (m/s)

$\mathbf{W_{eb}}$ **:** Width of the elastomeric bearing (mm)

$\mathbf{W_{sup,eb}}$ **:** Weight of superstructure exerted on each elastomeric bearing (kN)

LIST OF SYMBOLS

σ_{eb} : Compression pressure on an elastomeric bearing (MPa)

δc^{i} : Instant pressure deformation (m)

ε_{ci} : Instant pressure strain (/m)

ε_{creep} : Creep strain (/m)

δ_{c} : Creep deflection (mm)

$\delta_{s,max}$: The maximum shear deformation of the bearing (mm)

α_{c} : Thermal coefficient of concrete (/C^{o})

α_{sh} : Shrinkage coefficient of concrete

Δ_{T} : Temperature change (C^{o})

θ_{TL} : Rotation due to total load (rad)

$\sigma_{c,d}$: Compression pressure of elastomeric bearing due to dead load (MPa)

σ_{all} : Allowable compression pressure on an elastomeric bearing (MPa)

θ_{u} : Maximum strength limit state design rotation angle (rad)

δ_{LL} : Deflection due to live load of a pot bearing (mm)

ε_{Li} : Instantaneous live load compressive strain in ith elastomer layer

δ_{DL} : Deflection due to dead load (mm)

ε_{di} : Initial dead load compressive strain in ith elastomer layer

δ_{ul} : Long-term deflections including the creep deflection

σ_{s} : Average compressive stress due to total service load combinations

δ_{vfl} : Vertical deflection due to factored load (mm)

CHAPTER 1

INTRODUCTION

1.1. General

With the enhancement in technology, it is getting easier day by day to reach instantly to any information wherever it has come into service. The enhancement makes improvements in railway technology like any other subject. The first railway line was opened on 27 September 1825 and from that day; there is a remarkable development in railway technology. In 1903 the experimental train designed by Siemens & Halske and the rail car by AEG passed 200 km/h speed. In 1964, the first high-speed railway line was put into operation in Japan from Tokyo to Osaka. After such achievements, speed records also have been upgraded. In the aspect of passenger trains, from 2015 world record is held by Japanese LO Maglev with a speed of 603 km/h. In the beginning, the high-speed term was being used for the speed above 200 km/h. Recently, it is used for speed above 250 km/h. More than 25 countries have high-speed railway lines that are in operation or under construction today. To provide route alignments that are suitable for operation of high-speed trains; bridges, viaducts, and tunnels are needed today more than needed in the past. That increases the need for the design and construction of high-speed railway bridges. Both from higher operational velocities and lower serviceability tolerance limits, high-speed railway bridges differ from conventional railway bridges and highway bridges.

Earthquakes have existed from very old times, and they have been generally very harmful events. With the help of technological enhancements in the construction sector, construction materials have been improved and make people more capable to construct earthquake-resistant structures. In spite of the technological advancements, earthquakes are still sudden and mortal events that cannot be predicted before its

occurrence. After the start of using some construction materials like concrete, steel, reinforced concrete, autoclaved aerated concrete, etc. humanity tries to prevent the vital effects of earthquakes. The design stage should be performed by considering the effects of earthquakes carefully.

To prevent undesirable effects of impacts like earthquakes, dynamic loads, etc. the use of seismic isolators, bearing devices and/or other types of dampers is a good solution. Generally, bearing devices are used in the design and construction of any kind of bridge for limiting the displacements. Types of bearings commonly used in ordinary bridges (except special bridges like long-span, cable-stayed, balanced-cantilever, etc.) are almost the same depending on the design habits and the opportunities offered by the manufacturers. The behavior of the bridge under an earthquake impact may be different depending on the soil conditions of bridge location. Within this study, the behavior of bearings under real earthquake effects depending upon the magnitude and soil properties are investigated.

1.2. Definitions

Definitions of some subjects, which may be needed to make it easier to understand this study, are explained in this section.

1.2.1. Seismic Waves, Records and Ground Motion Data

An earthquake can be described simply as the motions of ground due to fault activities. When an earthquake occurred, ground motion propagates waves through the earth. In some cases, like earthquakes with high magnitudes, seismic waves can travel all around the world. By the enhancement in technology, the instruments called seismographs are being used to record these waves and their existence at any point. The sample sketch showing the working principle of a seismograph (seismometer) can be seen in Figure 1.1. The data recorded by a seismograph is called seismogram which

forms the seismic record of an earthquake. The data gathered from a specific seismograph for a specific earthquake is also the ground motion data of the location on which the seismograph exists.

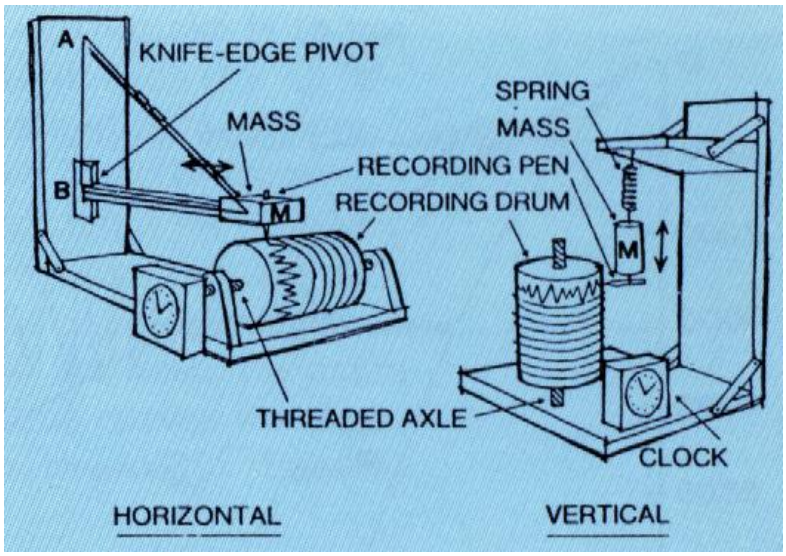

Figure 1.1. Sample Sketch for Working Principle of a Seismograph (Seismometer)

1.2.2. Fault Mechanisms

1.2.2.1. Normal Fault

If the mass above the fault (Footwall) moves downward relative to the mass below (Hanging Wall) in a fault, then that fault is called as “Normal Fault”. (Figure 1.2)

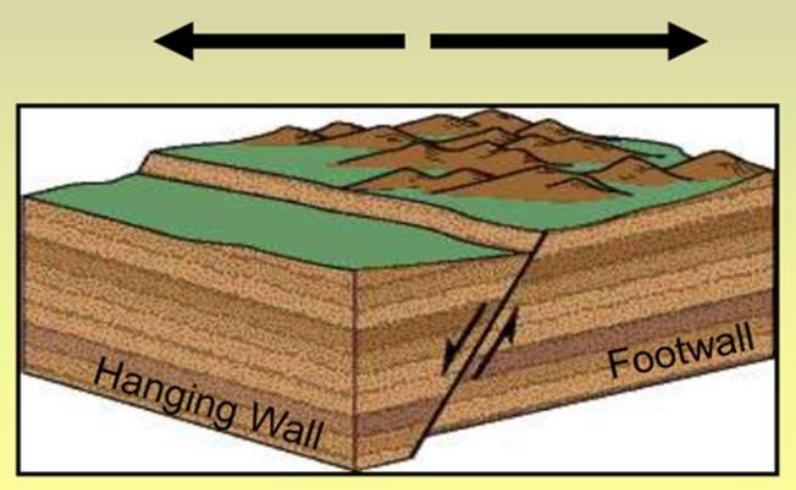

Figure 1.2. Normal Fault

1.2.2.2. Thrust (Reverse) Fault

If the mass above the fault moves upward relative to the mass below in a fault, then that fault is called as “Thrust (Reverse) Fault”. (Figure 1.3)

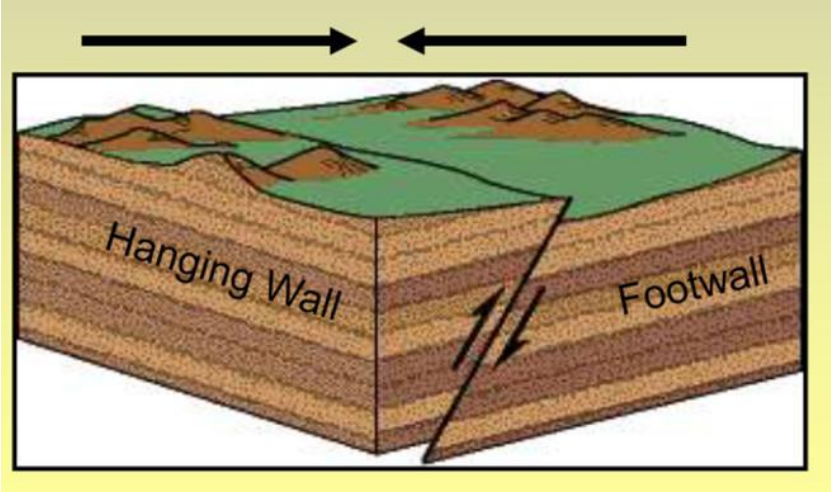

Figure 1.3. Thrust (Reverse) Fault

1.2.2.3. Strike-Slip Fault

If the masses sliding horizontally by rubbing each other at the boundary between them in a fault, then that fault is called as “Strike-Slip Fault”. (Figure 1.4) North-Anatolian and East-Anatolian faults are strike-slip faults.

The fault type chosen for this study is the strike-slip fault. The aim behind that decision is to increase the similarity of this study’s results to the most common real situations in Turkey.

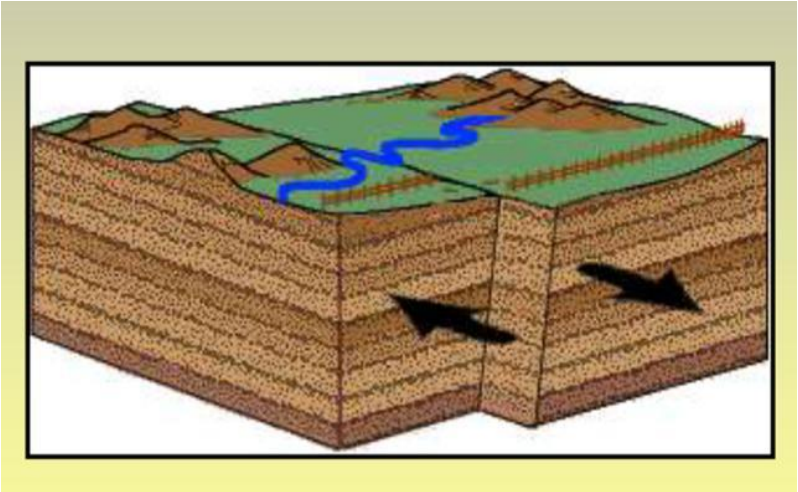

Figure 1.4. Strike-Slip Fault

The pictures used in Figures 1.2, 1.3 and 1.4 are adapted from the USGS web site (https://earthquake.usgs.gov/learn/topics/keeping_track.php).

1.2.3. Hypocenter and Epicenter

The point that rupture begins called **hypocenter** or focus and the projected point directly to the surface is called **epicenter**.

1.2.4. Distance from Fault

The arrival of seismic waves to a point located far away from the fault takes a while and seismic waves lose their energies while propagation. If the site, where a bridge will be constructed, is close enough to the fault then the effect of the earthquake on that location will be similar to the effect on the fault. On the other hand, if the distance of the site from the fault is high enough the effect of the earthquake will be so less.

In AASHTO LRFD Bridge Design Specifications; Near-field effects are taken into consideration if the distance from the fault is less than 6 miles (9,656 km ~= 10 km). In this study, the R_{jb} distance from the fault is taken as between 15-30 km. The reason behind this decision is the same as the reason for fault mechanism type and soil class selection; to increase the similarity of this study's results within the real situations in Turkey. Therefore, there is no need to compute the near-field effect of earthquakes taken into consideration

1.2.5. Arias Intensity of an Earthquake

Arias Intensity is one of the measures of intensity of an earthquake calculated by taking time integral of the acceleration of that earthquake. Its unit is "m/s". Arturo Arias is the engineer proposed the formula given below for the calculation of Arias Intensity:

$$I_a = \frac{\pi}{2g}\int_0^{\infty}[a(t)]^2 dt$$

1.3. Literature Review

1.3.1. Previous Studies

(Marioni, 2006) studied the bearings of high-speed railway bridges in September 2006. He gave some information about the European high-speed rail system. The

study mentioned the types of bearings used in Europe. Specifically, the author states that pot bearing was the common one for high-speed railway bridges. He also described the characteristics, strengths, and weaknesses of bearings.

(Yu et al., 2018) compared the spherical steel bearings and the friction pendulum bearing (FPB) by conducting numerical analysis on longitudinal seismic responses in their study. They used OpenSEES (Open System for Earthquake Engineering and Simulation) software for creating the finite element model of bridge and track structures. Three earthquake ground motion data were applied to the longitudinal direction of the bridge. According to their study, FPB is more effective to use with the purpose of longitudinal earthquake resistance with large deformation of bearing.

(Tang et al., 2011) investigated the behavior of fabricated lead rubber bearing (LRB) which is comparable to the others a new type of bearing. They formed a finite element model for a simply supported high-speed railway bridge with five 32m long spans. They stated that ANSYS software was used for finite element analysis of the structure. Data of El-Centro, Taft and Parkfield earthquakes were considered in their studies as earthquake ground motion data and ICE series of high-speed trains are used in calculations. Their study shows that LRB can reduce deformations at the top of piers when its dynamic properties were chosen carefully and correctly.

(Zou et al., 2019) tried and verified a new bearing system for high-speed railway bridges by either doing a shaking table test and numerical simulations in June 2019. They called the function separation system (FSI) for the system that separates the bearing function from the isolation function. The results obtained from the shaking table test and from numerical simulations were verified by each other. This study shows that scientists are still doing researches for new bearing systems to use in high-speed railway bridges since it is a significant subject.

(Ülker-kaustell, 2017) studied the dynamic behavior of pot bearings by creating a small pot-bearing prototype, testing it in the laboratory, developing a simple macro-element of pot bearings and validating the element with the existing bridge's

measurements. According to the study, the friction coefficient of a uni-directional bearing is higher than the one of a multi-directional bearing and the effect arisen from the difference between kinetic and static frictions are negligible.

1.4. The Objective and The Scope of This Study

In the known literature, comparison of the response of bridges with elastomeric bearing and pot bearing has not been studied in detail. The objective of this study is to understand the bridge behavior with elastomeric and pot bearings for high-speed railways under real earthquake effects for two different soil types and to provide a comparison between the earthquake responses of the elastomeric and pot bearings used in bridges over high-speed railways. By utilizing analytic models and doing a finite element analysis with ground motion data of real earthquakes, this study will constitute realistic results which can be a good reference for designers. After gathering the results of forty-two cases for each bearing, they will be compared with each other and will be presented.

1.4.1. The Methodology of the Study

This study kicks off with specifying the characteristics of ground motion data needed and gathering them from the database of PEER. Chapter 2 presents the main characteristic properties of them and provides some sample graphs about them. There are 42 separate ground motion data depending on the magnitude and soil class type.

In chapter 3, general information about the selected fictive bridge is stated in a detailed way. Drawings of the bridge are also given in that section. Meanwhile bearing types and their some specifications are explained in this section.

Chapter 4 includes information about the method of analysis (Linear Direct Integration Time History Analysis), 3D models formed via using Sap2000 software for the three cases and the results of 126 cases. Sap2000 v14.2.2 is used for finite element analysis

of all cases. Analysis cases differ from each other according to their bearing type and formations. The first one of the cases includes two elastomeric bearings under each beam, the second one includes 6 elastomeric bearings for 10 girders and the last one includes pot bearings.

Chapter 5 is the section for comparisons. All results gathered by the analysis done compared among each other based on three main parameters; the magnitude of earthquakes, soil classes and bearing type and formation.

At the end of the study, works done are summarized and presented in Chapter 6. Chapter 6 also includes suggestions for future studies that shall be done regarding this study.

CHAPTER 2

SELECTION AND HANDLING OF GROUND MOTION DATA

2.1. Selection of Ground Motion Data

Earthquakes are able to occur anywhere completely around the world. To get realistic results and catch up on the cases with high occurrence rates within this study, the selection of earthquakes and records of them holds a big role. At the very beginning of the study, ground motion data was specified and selected from PEER Database. The distance from fault is set to between 15 and 30 kilometers. The near-fault effect is not considered in this study since the number of bridges in region 2 is more than the number of bridges in region 1. Where, region 1 refers to the area of a circle with radii less than 15 km. and region 2 refers to the area of the part of the circle with the same center and its radius is changing from 15km. to 30km. Soil classes are considered as ZC and ZD since the effect of an earthquake will be worse in these soil classes than ZA and ZB. ZE and ZF soil classes are also not considered because liquefaction takes place generally during an earthquake in ZE and ZF type soil classes. Liquefaction is a different subject with specific content, so it will not be studied in this study. Soil classification can be seen in Table 2.13. Ground motions exist in the PEER database and selected data by the criteria mentioned above are given in the Tables from “Table 2.1” to “Table 2.12”. By selecting ground motion data according to these specifications, the location of the bridge to be taken into account in this study approaches the real case.

Table 2.1. *Ground Motion Data List from PEER Database with the Magnitude between 5.75 - 6.25 located on Soil Class ZC*

Ground Motion Data List from PEER Database with the Magnitude between 5.75 - 6.25 located on Soil Class ZC										
No	Case Code	Arias Intensity (m/sec)	Earthquake Name	Year	Station Name	Magnitude	Mechanism	Rjb (km)	Rrup (km)	Vs30 (m/sec)
1		0,1	"Westmorland"	1981	"Superstition Mtn Camera"	5,9	strike slip	19,26	19,37	362,38
2		0,3	"Joshua Tree_ CA "	1992	"North Palm Springs Fire Sta #36"	6,1	strike slip	21,4	21,97	367,84
3		0	"Chalfant Valley-01"	1986	"Benton"	5,77	strike slip	24,25	24,33	370,94
4		0,4	"Chalfant Valley-02"	1986	"Benton"	6,19	strike slip	21,55	21,92	370,94
5		0,2	"Livermore-01"	1980	"San Ramon - Eastman Kodak"	5,8	strike slip	15,19	17,24	377,51
6		0,2	"Chi-Chi_ Taiwan-04"	1999	"CHY034"	6,2	strike slip	28,45	28,49	378,75
7		0,1	"Chalfant Valley-02"	1986	"Convict Creek"	6,19	strike slip	29,35	31,19	382,12
8		0,1	"Livermore-01"	1980	"San Ramon Fire Station"	5,8	strike slip	15,84	17,93	384,47
9		0,2	"Joshua Tree_ CA "	1992	"Morongo Valley Fire Station"	6,1	strike slip	21,73	22,3	396,41
10		0,2	"Livermore-01"	1980	"Del Valle Dam (Toe)"	5,8	strike slip	23,92	24,95	403,37
11		0,1	"Parkfield"	1966	"Cholame - Shandon Array #12"	6,19	strike slip	17,64	17,64	408,93
12		0	"Parkfield-02_ CA"	2004	"COALINGA - PRIEST VALLEY"	6	strike slip	21,88	22,02	412,79
13	60CI1	0,4	"Joshua Tree_ CA "	1992	"Whitewater Trout Farm"	6,1	strike slip	28,97	29,4	425,02
14		0,1	"Chi-Chi_ Taiwan-04"	1999	"CHY024"	6,2	strike slip	19,67	19,73	427,73
15		0,2	"Chi-Chi_ Taiwan-04"	1999	"CHY006"	6,2	strike slip	24,58	24,62	438,19
16		0	"Chalfant Valley-01"	1986	"Lake Crowley - Shehorn Res."	5,77	strike slip	24,37	24,45	456,83
17	60CI2	0,1	"Chalfant Valley-02"	1986	"Lake Crowley - Shehorn Res."	6,19	strike slip	22,08	24,47	456,83
18	60CI3	0,1	"Morgan Hill"	1984	"Corralitos"	6,19	strike slip	23,23	23,24	462,24
19	60CI4	0,1	"Chi-Chi_ Taiwan-04"	1999	"TCU122"	6,2	strike slip	23,14	23,19	475,46
20		0,1	"Chi-Chi_ Taiwan-04"	1999	"TCU116"	6,2	strike slip	28,72	28,76	493,09
21		0	"Livermore-01"	1980	"APEEL 3E Hayward CSUH"	5,8	strike slip	29,19	30,59	517,06
22	60CI5	0,5	"Parkfield"	1966	"Temblor pre-1969"	6,19	strike slip	15,96	15,96	527,92
23		0,1	"Chalfant Valley-02"	1986	"Long Valley Dam (Downst)"	6,19	strike slip	18,3	21,12	537,16
24		0,1	"Chalfant Valley-02"	1986	"Long Valley Dam (L Abut)"	6,19	strike slip	18,3	21,12	537,16
25		0,3	"Chi-Chi_ Taiwan-04"	1999	"CHY028"	6,2	strike slip	17,63	17,7	542,61
26		0,1	"Chi-Chi_ Taiwan-04"	1999	"CHY029"	6,2	strike slip	25,75	25,79	544,74
27		0	"Potenza_ Italy"	1990	"Brienza"	5,8	strike slip	25,89	26,2	561,04
28		0,3	"Chi-Chi_ Taiwan-04"	1999	"CHY035"	6,2	strike slip	25,01	25,06	573,04
29	60CI6	0,1	"Mammoth Lakes-06"	1980	"Bishop - Paradise Lodge"	5,94	strike slip	18,85	23,86	585,12
30	60CI7	0,2	"Basso Tirreno_ Italy"	1978	"Naso"	6	strike slip	17,15	19,59	620,56
31		0,1	"Chi-Chi_ Taiwan-04"	1999	"TCU084"	6,2	strike slip	26,83	27,13	665,2
32		0	"Chi-Chi_ Taiwan-04"	1999	"TCU089"	6,2	strike slip	27,25	27,52	671,52

Table 2.2. *Selected Ground Motion Data List from PEER Database with the Magnitude between 5.75 - 6.25 located on Soil Class ZC*

Selected Ground Motion Data List from PEER Database with the Magnitude between 5.75 - 6.25 located on Soil Class ZC													
No	Case Code	Arias Intensity (m/sec)	Earthquake Name	Year	Station Name	Magnitude	Mechanism	Rjb (km)	Rrup (km)	Vs30 (m/sec)	PGA (g)	PGV (cm/s)	PGD (cm)
1	60CI1	0,4	"Joshua Tree_ CA "	1992	Whitewater Trout Farm	6,1	strike slip	28,97	29,40	425,02	0,21	11,59	1,55
2	60CI2	0,1	"Chalfant Valley-02"	1986	Lake Crowley - Shehorn Res.	6,19	strike slip	22,08	24,47	456,83	0,16	5,58	0,97
3	60CI3	0,1	"Morgan Hill"	1984	Corralitos	6,19	strike slip	23,23	23,24	462,24	0,07	7,99	2,36
4	60CI4	0,1	"Chi-Chi_ Taiwan-04"	1999	TCU122	6,2	strike slip	23,14	23,19	475,46	0,06	14,51	8,38
5	60CI5	0,5	"Parkfield"	1966	Temblor pre-1969	6,19	strike slip	15,96	15,96	527,92	0,36	11,78	5,55
6	60CI6	0,1	"Mammoth Lakes-06"	1980	Bishop - Paradise Lodge	5,94	strike slip	18,85	23,86	585,12	0,11	5,47	1,65
7	60CI7	0,2	"Basso Tirreno_ Italy"	1978	Naso	6	strike slip	17,15	19,59	620,56	0,15	16,80	3,09

Table 2.3. *Ground Motion Data List from PEER Database with the Magnitude between 6.25 - 6.75 located on Soil Class ZC*

Ground Motion Data List from PEER Database with the Magnitude between 6.25 - 6.75 located on Soil Class ZC										
No	Case Code	Arias Intensity (m/sec)	Earthquake Name	Year	Station Name	Magnitude	Mechanism	Rjb (km)	Rrup (km)	Vs30 (m/sec)
1	65CI1	0,2	"Imperial Valley-06"	1979	"Superstition Mtn Camera"	6,53	strike slip	24,61	24,61	362,38
2	65CI2	0,3	"Big Bear-01"	1992	"Highland Fire Station"	6,46	strike slip	26,18	26,47	362,39
3	65CI3	0,5	"Big Bear-01"	1992	"Morongo Valley Fire Station"	6,46	strike slip	27,96	29,06	396,41
4	65CI4	1,3	"Imperial Valley-06"	1979	"Cerro Prieto"	6,53	strike slip	15,19	15,19	471,53
5	65CI5	7,2	"Tottori_ Japan"	2000	"OKY004"	6,61	strike slip	19,72	19,72	475,8
6	65CI6	2,6	"Tottori_ Japan"	2000	"SMNH02"	6,61	strike slip	23,64	23,64	502,66
7	65CI7	1,3	"Tottori_ Japan"	2000	"OKYH09"	6,61	strike slip	21,22	21,22	518,92
8		0,6	"Tottori_ Japan"	2000	"OKYH08"	6,61	strike slip	24,84	24,84	694,21
9		1,2	"Tottori_ Japan"	2000	"OKYH14"	6,61	strike slip	26,51	26,51	709,86

Table 2.4. *Selected Ground Motion Data List from PEER Database with the Magnitude between 6.25 - 6.75 located on Soil Class ZC*

Selected Ground Motion Data List from PEER Database with the Magnitude between 6.25 - 6.75 located on Soil Class ZC													
No		Arias Intensity (m/sec)	Earthquake Name	Year	Station Name	Magnitude	Mechanism	Rjb (km)	Rrup (km)	Vs30 (m/sec)	PGA (g)	PGV (cm/s)	PGD (cm)
1	65CI1	0,2	"Imperial Valley-06"	1979	Superstition Mtn Camera	6,53	strike slip	24,61	24,61	362,38	0,15	8,92	2,32
2	65CI2	0,3	"Big Bear-01"	1992	Highland Fire Station	6,46	strike slip	26,18	26,47	362,39	0,16	6,11	2,80
3	65CI3	0,5	"Big Bear-01"	1992	Morongo Valley Fire Station	6,46	strike slip	27,96	29,06	396,41	0,15	15,97	3,74
4	65CI4	1,3	"Imperial Valley-06"	1979	Cerro Prieto	6,53	strike slip	15,19	15,19	471,53	0,16	8,05	1,96
5	65CI5	7,2	"Tottori_ Japan"	2000	OKY004	6,61	strike slip	19,72	19,72	475,80	0,82	11,79	0,75
6	65CI6	2,6	"Tottori_ Japan"	2000	SMNH02	6,61	strike slip	23,64	23,64	502,66	0,58	21,17	8,98
7	65CI7	1,3	"Tottori_ Japan"	2000	OKYH09	6,61	strike slip	21,22	21,22	518,92	0,29	8,45	4,51

Table 2.5. *Ground Motion Data List from PEER Database with the Magnitude between 6.75 - 7.25 located on Soil Class ZC*

(GM Data referred in the cell filled with red color is an incorrect data)

Ground Motion Data List from PEER Database with the Magnitude between 6.75 - 7.25 located on Soil Class ZC										
No	Case Code	Arias Intensity (m/sec)	Earthquake Name	Year	Station Name	Magnitude	Mechanism	Rjb (km)	Rrup (km)	Vs30 (m/sec)
1	70CI1	0,7	"Landers"	1992	"North Palm Springs Fire Sta #36"	7,28	strike slip	26,95	26,95	367,84
2	70CI2	1,2	"Landers"	1992	"Fun Valley"	7,28	strike slip	25,02	25,02	388,63
3	70CI3	1	"Darfield_ New Zealand"	2010	"SPFS"	7	strike slip	29,86	29,86	389,54
4	70CI4	1,2	"Landers"	1992	"Morongo Valley Fire Station"	7,28	strike slip	17,36	17,36	396,41
5	70CI5	4,1	"Darfield_ New Zealand"	2010	"Heathcote Valley Primary School "	7	strike slip	24,36	24,47	422
6	70CI6	0,6	"Landers"	1992	"Whitewater Trout Farm"	7,28	strike slip	27,05	27,05	425,02
7	70CI7	0,7	"Darfield_ New Zealand"	2010	"LPCC"	7	strike slip	25,21	25,67	649,67
8		0	"Duzce_ Turkey"	1999	"Lamont 362"	7,14	strike slip	23,41	23,41	517

Table 2.6. *Selected Ground Motion Data List from PEER Database with the Magnitude between 6.75 - 7.25 located on Soil Class ZC*

Selected Ground Motion Data List from PEER Database with the Magnitude between 6.75 - 7.25 located on Soil Class ZC													
No		Arias Intensity (m/sec)	Earthquake Name	Year	Station Name	Magnitude	Mechanism	Rjb (km)	Rrup (km)	Vs30 (m/sec)	PGA (g)	PGV (cm/s)	PGD (cm)
1	70CI1	0,7	"Landers"	1992	North Palm Springs Fire Sta #36	7,28	strike slip	26,95	26,95	367,84	0,21	15,58	6,80
2	70CI2	1,2	"Landers"	1992	Fun Valley	7,28	strike slip	25,02	25,02	388,63	0,16	21,57	7,51
3	70CI3	1	"Darfield_ New Zealand"	2010	SPFS	7	strike slip	29,86	29,86	389,54	0,22	24,81	9,38
4	70CI4	1,2	"Landers"	1992	Morongo Valley Fire Station	7,28	strike slip	17,36	17,36	396,41	0,58	37,85	15,06
5	70CI5	4,1	"Darfield_ New Zealand"	2010	Heathcote Valley Primary Schoo	7	strike slip	24,36	24,47	422,00	0,12	8,72	4,65
6	70CI6	0,6	"Landers"	1992	Whitewater Trout Farm	7,28	strike slip	27,05	27,05	425,02	0,14	14,61	6,43
7	70CI7	0,7	"Darfield_ New Zealand"	2010	LPCC	7	strike slip	25,21	25,67	649,67	0,26	30,29	21,27

Table 2.7. *Ground Motion Data List from PEER Database with the Magnitude between 5.75 - 6.25 located on Soil Class ZD*

Ground Motion Data List from PEER Database with the Magnitude between 5.75 - 6.25 located on Soil Class ZD										
No	Case Code	Arias Intensity (m/sec)	Earthquake Name	Year	Station Name	Magnitude	Mechanism	Rjb (km)	Rrup (km)	Vs30 (m/sec)
1		0,3	"Westmorland"	1981	"Brawley Airport"	5,9	strike slip	15,28	15,41	208,71
2	60DI1	0,2	"Westmorland"	1981	"Niland Fire Station"	5,9	strike slip	15,16	15,29	212
3	60DI2	0,1	"Morgan Hill"	1984	"Hollister Differential Array #3"	6,19	strike slip	26,42	26,43	215,54
4	60DI3	0,1	"Parkfield-02_CA"	2004	"Parkfield - Gold Hill 6W"	6	strike slip	15,45	15,79	232,44
5	60DI4	0,1	"Morgan Hill"	1984	"Agnews State Hospital"	6,19	strike slip	24,48	24,49	239,69
6	60DI5	0,4	"Chi-Chi_Taiwan-04"	1999	"CHY101"	6,2	strike slip	21,62	21,67	258,89
7		0,1	"Chi-Chi_Taiwan-04"	1999	"CHY025"	6,2	strike slip	29,2	29,23	277,5
8	60DI6	1,3	"Joshua Tree_CA "	1992	"Indio - Jackson Road"	6,1	strike slip	25,04	25,53	292,12
9	60DI7	0,1	"Chalfant Valley-01"	1986	"Bishop - LADWP South St"	5,77	strike slip	23,38	23,47	303,47
10		0	"Parkfield-02_CA"	2004	"Monarch Peak"	6	strike slip	29,31	29,43	308
11		0,1	"Parkfield-02_CA"	2004	"Coalinga - Fire Station 39"	6	strike slip	22,45	22,59	333,61
12		0,6	"Joshua Tree_CA "	1992	"Thousand Palms Post Office"	6,1	strike slip	17,15	17,86	333,89
13		0	"Morgan Hill"	1984	"San Juan Bautista_24 Polk St"	6,19	strike slip	27,15	27,15	335,5
14		0,7	"Westmorland"	1981	"Parachute Test Site"	5,9	strike slip	16,54	16,66	348,69
15		0	"Parkfield-02_CA"	2004	"Parkfield - Cholame 12W"	6	strike slip	15,49	15,83	359,03
16		0,1	"Bishop (Rnd Val)"	1984	"McGee Creek - Surface"	5,82	strike slip	21,79	22,75	359,23
17		0,1	"Chalfant Valley-02"	1986	"McGee Creek - Surface"	6,19	strike slip	28,2	30,11	359,23

Table 2.8. *Enter the Table Caption here*

Selected Ground Motion Data List from PEER Database with the Magnitude between 5.75 - 6.25 located on Soil Class ZD													
No		Arias Intensity (m/sec)	Earthquake Name	Year	Station Name	Magnitude	Mechanism	Rjb (km)	Rrup (km)	Vs30 (m/sec)	PGA (g)	PGV (cm/s)	PGD (cm)
1	60DI1	0,2	"Westmorland"	1981	Niland Fire Station	5,9	strike slip	15,16	15,29	212,00	0,15	7,57	1,15
2	60DI2	0,1	"Morgan Hill"	1984	Hollister Differential Array #3	6,19	strike slip	26,42	26,43	215,54	0,08	9,49	3,57
3	60DI3	0,1	"Parkfield-02_CA"	2004	Parkfield - Gold Hill 6W	6	strike slip	15,45	15,79	232,44	0,09	4,94	2,29
4	60DI4	0,1	"Morgan Hill"	1984	Agnews State Hospital	6,19	strike slip	24,48	24,49	239,69	0,03	5,62	2,02
5	60DI5	0,4	"Chi-Chi_Taiwan-04"	1999	CHY101	6,2	strike slip	21,62	21,67	258,89	0,15	18,85	12,64
6	60DI6	1,3	"Joshua Tree_CA "	1992	Indio - Jackson Road	6,1	strike slip	25,04	25,53	292,12	0,41	31,91	8,90
7	60DI7	0,1	"Chalfant Valley-01"	1986	Bishop - LADWP South St	5,77	strike slip	23,38	23,47	303,47	0,13	7,86	2,31

Table 2.9. *Ground Motion Data List from PEER Database with the Magnitude between 6.25 - 6.75 located on Soil Class ZD*

(GM Data referred in the cell filled with red color is an incorrect data)

Ground Motion Data List from PEER Database with the Magnitude between 6.25 - 6.75 located on Soil Class ZD										
No	Case Code	Arias Intensity (m/sec)	Earthquake Name	Year	Station Name	Magnitude	Mechanism	Rjb (km)	Rrup (km)	Vs30 (m/sec)
1		0,4	"Superstition Hills-02"	1987	"Salton Sea Wildlife Refuge"	6,54	strike slip	25,88	25,88	191,14
2	65DI1	1,1	"Superstition Hills-02"	1987	"El Centro Imp. Co. Cent"	6,54	strike slip	18,2	18,2	192,05
3	65DI2	0,4	"Imperial Valley-06"	1979	"El Centro Array #12"	6,53	strike slip	17,94	17,94	196,88
4	65DI3	0,1	"Imperial Valley-06"	1979	"Calipatria Fire Station"	6,53	strike slip	23,17	24,6	205,78
5		0,5	"Superstition Hills-02"	1987	"Calipatria Fire Station"	6,54	strike slip	27	27	205,78
6		0,3	"Superstition Hills-02"	1987	"Brawley Airport"	6,54	strike slip	17,03	17,03	208,71
7	65DI4	0,5	"Northern Calif-03"	1954	"Ferndale City Hall"	6,5	strike slip	26,72	27,02	219,31
8	65DI5	0,3	"Imperial Valley-06"	1979	"El Centro Array #1"	6,53	strike slip	19,76	21,68	237,33
9		3,3	"Imperial Valley-06"	1979	"Delta"	6,53	strike slip	22,03	22,03	242,05
10	65DI6	0,4	"Victoria_ Mexico"	1980	"Chihuahua"	6,33	strike slip	18,53	18,96	242,05
11		0,3	"Imperial Valley-06"	1979	"El Centro Array #13"	6,53	strike slip	21,98	21,98	249,92
12		0,3	"Superstition Hills-02"	1987	"Kornbloom Road (temp)"	6,54	strike slip	18,48	18,48	266,01
13	65DI7	0,8	"Tottori_ Japan"	2000	"OKY005"	6,61	strike slip	28,81	28,82	293,37
14		0,6	"Superstition Hills-02"	1987	"Plaster City"	6,54	strike slip	22,25	22,25	316,64
15		2	"Tottori_ Japan"	2000	"SMN003"	6,61	strike slip	25,52	25,53	343,97

Table 2.10. *Selected Ground Motion Data List from PEER Database with the Magnitude between 6.25 - 6.75 located on Soil Class ZD*

Selected Ground Motion Data List from PEER Database with the Magnitude between 6.25 - 6.75 located on Soil Class ZD													
No		Arias Intensity (m/sec)	Earthquake Name	Year	Station Name	Magnitude	Mechanism	Rjb (km)	Rrup (km)	Vs30 (m/sec)	PGA (g)	PGV (cm/s)	PGD (cm)
1	65DI1	1,1	"Superstition Hills-02"	1987	El Centro Imp. Co. Cent	6,54	strike slip	18,20	18,20	192,05	0,36	48,07	21,86
2	65DI2	0,4	"Imperial Valley-06"	1979	El Centro Array #12	6,53	strike slip	17,94	17,94	196,88	0,14	18,11	17,33
3	65DI3	0,1	"Imperial Valley-06"	1979	Calipatria Fire Station	6,53	strike slip	23,17	24,60	205,78	0,13	15,60	11,12
4	65DI4	0,5	"Northern Calif-03"	1954	Ferndale City Hall	6,5	strike slip	26,72	27,02	219,31	0,16	34,80	14,63
5	65DI5	0,3	"Imperial Valley-06"	1979	El Centro Array #1	6,53	strike slip	19,76	21,68	237,33	0,13	16,06	7,70
6	65DI6	0,4	"Victoria_ Mexico"	1980	Chihuahua	6,33	strike slip	18,53	18,96	242,05	0,15	8,84	4,61
7	65DI7	0,8	"Tottori_ Japan"	2000	OKY005	6,61	strike slip	28,81	28,82	293,37	0,29	6,21	0,97

Table 2.11. *Ground Motion Data List from PEER Database with the Magnitude between 6.75 - 7.25 located on Soil Class ZD*

Ground Motion Data List from PEER Database with the Magnitude between 6.75 - 7.25 located on Soil Class ZD										
No	Case Code	Arias Intensity (m/sec)	Earthquake Name	Year	Station Name	Magnitude	Mechanism	Rjb (km)	Rrup (km)	Vs30 (m/sec)
1		1,1	"El Mayor-Cucapah_ Mexico"	2010	"El Centro - Meloland Geotechnic"	7,2	strike slip	28,53	29	186,21
2		0,9	"Darfield_ New Zealand"	2010	"Christchurch Botanical Gardens"	7	strike slip	18,05	18,05	187
3		1,2	"Darfield_ New Zealand"	2010	"Christchurch Hospital"	7	strike slip	18,4	18,4	194
4		5,5	"El Mayor-Cucapah_ Mexico"	2010	"El Centro Array #11"	7,2	strike slip	15,36	16,21	196,25
5		1,3	"Darfield_ New Zealand"	2010	"Christchurch Cathedral College"	7	strike slip	19,89	19,89	198
6		4,3	"El Mayor-Cucapah_ Mexico"	2010	"El Centro Differential Array"	7,2	strike slip	22,83	23,42	202,26
7		3,6	"El Mayor-Cucapah_ Mexico"	2010	"El Centro Array #10"	7,2	strike slip	19,36	20,05	202,85
8		1,1	"Darfield_ New Zealand"	2010	"Christchurch Cashmere High School"	7	strike slip	17,64	17,64	204
9		0,6	"Darfield_ New Zealand"	2010	"Hulverstone Drive Pumping Station"	7	strike slip	25,4	25,4	206
10		1,3	"Darfield_ New Zealand"	2010	"Pages Road Pumping Station"	7	strike slip	24,55	24,55	206
11		1	"Darfield_ New Zealand"	2010	"Shirley Library"	7	strike slip	22,33	22,33	207
12		1,6	"El Mayor-Cucapah_ Mexico"	2010	"El Centro Array #7"	7,2	strike slip	27,42	27,91	210,51
13		0,8	"Darfield_ New Zealand"	2010	"NNBS North New Brighton School "	7	strike slip	26,76	26,76	211
14		3,7	"El Mayor-Cucapah_ Mexico"	2010	"El Centro - Imperial & Ross"	7,2	strike slip	19,39	20,08	229,25
15		2,4	"El Mayor-Cucapah_ Mexico"	2010	"Calexico Fire Station"	7,2	strike slip	19,12	20,46	231,23
16	70DI1	2,3	"El Mayor-Cucapah_ Mexico"	2010	"Chihuahua"	7,2	strike slip	18,21	19,47	242,05
17	70DI2	2,1	"El Mayor-Cucapah_ Mexico"	2010	"TAMAULIPAS"	7,2	strike slip	25,32	26,55	242,05
18	70DI3	0,9	"Darfield_ New Zealand"	2010	"Styx Mill Transfer Station "	7	strike slip	20,86	20,86	247,5
19	70DI4	0,3	"Darfield_ New Zealand"	2010	"ADCS"	7	strike slip	28,46	31,41	249,28
20	70DI5	0,6	"Kobe_ Japan"	1995	"Abeno"	6,9	strike slip	24,85	24,85	256
21	70DI6	1,4	"Kobe_ Japan"	1995	"Fukushima"	6,9	strike slip	17,85	17,85	256
22	70DI7	1,2	"Kobe_ Japan"	1995	"Morigawachi"	6,9	strike slip	24,78	24,78	256
23		0,2	"Kobe_ Japan"	1995	"OSAJ"	6,9	strike slip	21,35	21,35	256
24		0,6	"Kobe_ Japan"	1995	"Sakai"	6,9	strike slip	28,08	28,08	256
25		0,8	"Kobe_ Japan"	1995	"Shin-Osaka"	6,9	strike slip	19,14	19,15	256
26		1,1	"Kobe_ Japan"	1995	"Yae"	6,9	strike slip	27,77	27,77	256
27		1,3	"Darfield_ New Zealand"	2010	"Papanui High School "	7	strike slip	18,73	18,73	263,2
28		0,7	"Darfield_ New Zealand"	2010	"SBRC"	7	strike slip	21,31	24,34	263,2
29		3,5	"El Mayor-Cucapah_ Mexico"	2010	"El Centro - Meloland Geot. Array"	7,2	strike slip	28,53	29	264,57
30		1,2	"El Mayor-Cucapah_ Mexico"	2010	"El Centro - Meadows Union School"	7,2	strike slip	27,81	28,3	276,25
31		0,2	"Darfield_ New Zealand"	2010	"DORC"	7	strike slip	29,96	32,91	280,26
32		1,7	"Kobe_ Japan"	1995	"Kakogawa"	6,9	strike slip	22,5	22,5	312
33		0,1	"Darfield_ New Zealand"	2010	"WSFC"	7	strike slip	24,36	26,93	344,02
34		0,7	"Landers"	1992	"North Palm Springs"	7,28	strike slip	26,84	26,84	344,67
35		2,2	"Landers"	1992	"Coolwater"	7,28	strike slip	19,74	19,74	352,98
36		0,9	"Landers"	1992	"Yermo Fire Station"	7,28	strike slip	23,62	23,62	353,63
37		0,4	"Landers"	1992	"Mission Creek Fault"	7,28	strike slip	26,96	26,96	355,42
38		0,7	"Landers"	1992	"Desert Hot Springs"	7,28	strike slip	21,78	21,78	359

Table 2.12. *Selected Ground Motion Data List from PEER Database with the Magnitude between 6.75 - 7.25 located on Soil Class ZD*

Selected Ground Motion Data List from PEER Database with the Magnitude between 6.75 - 7.25 located on Soil Class ZD													
No		Arias Intensity (m/sec)	Earthquake Name	Year	Station Name	Magnitude	Mechanism	Rjb (km)	Rrup (km)	Vs30 (m/sec)	PGA (g)	PGV (cm/s)	PGD (cm)
1	70DI1	2,3	"El Mayor-Cucapah_ Mexico"	2010	Chihuahua	7,2	strike slip	18,21	19,47	242,05	0,21	38,25	48,23
2	70DI2	2,1	"El Mayor-Cucapah_ Mexico"	2010	TAMAULIPAS	7,2	strike slip	25,32	26,55	242,05	0,23	52,82	39,29
3	70DI3	0,9	"Darfield_ New Zealand"	2010	Styx Mill Transfer Station	7	strike slip	20,86	20,86	247,50	0,17	60,16	44,09
4	70DI4	0,3	"Darfield_ New Zealand"	2010	ADCS	7	strike slip	28,46	31,41	249,28	0,11	11,08	7,00
5	70DI5	0,6	"Kobe_ Japan"	1995	Abeno	6,9	strike slip	24,85	24,85	256,00	0,23	12,39	2,16
6	70DI6	1,4	"Kobe_ Japan"	1995	Fukushima	6,9	strike slip	17,85	17,85	256,00	0,22	15,13	3,71
7	70DI7	1,2	"Kobe_ Japan"	1995	Morigawachi	6,9	strike slip	24,78	24,78	256,00	0,18	13,18	2,51

Table 2.13. *Local Soil Types Given in TSBC-2018*

Yerel Zemin Sınıfı	Zemin Cinsi	Üst 30 metrede ortalama		
		$(V_S)_{30}$ [m/s]	$(N_{60})_{30}$ [darbe /30 cm]	$(c_u)_{30}$ [kPa]
ZA	Sağlam, sert kayalar	> 1500	–	–
ZB	Az ayrışmış, orta sağlam kayalar	760 – 1500	–	–
ZC	Çok sıkı kum, çakıl ve sert kil tabakaları veya ayrışmış, çok çatlaklı zayıf kayalar	360 – 760	> 50	> 250
ZD	Orta sıkı – sıkı kum, çakıl veya çok katı kil tabakaları	180 – 360	15 – 50	70 – 250
ZE	Gevşek kum, çakıl veya yumuşak – katı kil tabakaları veya $PI > 20$ ve $w > \%\ 40$ koşullarını sağlayan toplamda 3 metreden daha kalın yumuşak kil tabakası $(c_u < 25\ \text{kPa})$ içeren profiller	< 180	< 15	< 70
ZF	Sahaya özel araştırma ve değerlendirme gerektiren zeminler: 1) Deprem etkisi altında çökme ve potansiyel göçme riskine sahip zeminler (sıvılaşabilir zeminler, yüksek derecede hassas killer, göçebilir zayıf çimentolu zeminler vb.), 2) Toplam kalınlığı 3 metreden fazla turba ve/veya organik içeriği yüksek killer, 3) Toplam kalınlığı 8 metreden fazla olan yüksek plastisiteli (PI >50) killer, 4) Çok kalın (> 35 m) yumuşak veya orta katı killer.			

Selected ground motion records are coded for ease of understanding and handling throughout this study. Each ground motion record has a unique code. Therefore 210 codes are used to describe them individually. Subcodes used for that purpose are; 60, 65, 70, C, D, I, 1, 2, 3, 4, 5, 6, 7, h1, h2 and up. Since they are not used as separate

letters, used only in groups of codes like 60CI1_h1 they have not to cause any misunderstanding or ambiguity. Assumed meanings of codes are listed below:

60 : Stands for the magnitude of an earthquake (6.0 -+0.25)

65 : Stands for the magnitude of an earthquake (6.5 -+0.25)

70 : Stands for the magnitude of an earthquake (7.0 -+0.25)

C : Stands for soil class ZC shown in Table 2.13.

D : Stands for soil class ZD shown in Table 2.13.

I : Stands for the intermediate distance (between 15 and 30 km) from fault

h1 : Horizontal direction 1 of a ground motion

h2 : Horizontal direction 2 of a ground motion

up : Vertical direction of a ground motion

1, 2, 3, 4, 5, 6 and 7 : Stands for just the number assigned to the ground motion; it is not showing any order of any property

60CI1_h1 : Ground motion data in horizontal 1 direction of an earthquake with 6.0 -+0,25 Magnitude, ZC class soil, intermediate distance, ground motion number 1

70DI3_up : Ground motion data in the vertical direction of an earthquake with 7.0 -+0,25 Magnitude, ZD class soil, intermediate distance, ground motion number 3

2.2. Acceleration, Velocity and Displacement Graphs

Acceleration, velocity and displacement graphs of the 65DI1 earthquake are given in this part as a sample. Acceleration, velocity and displacement graphs of all ground motion records are provided in Appendix A which is provided in the attached compact disc (CD).

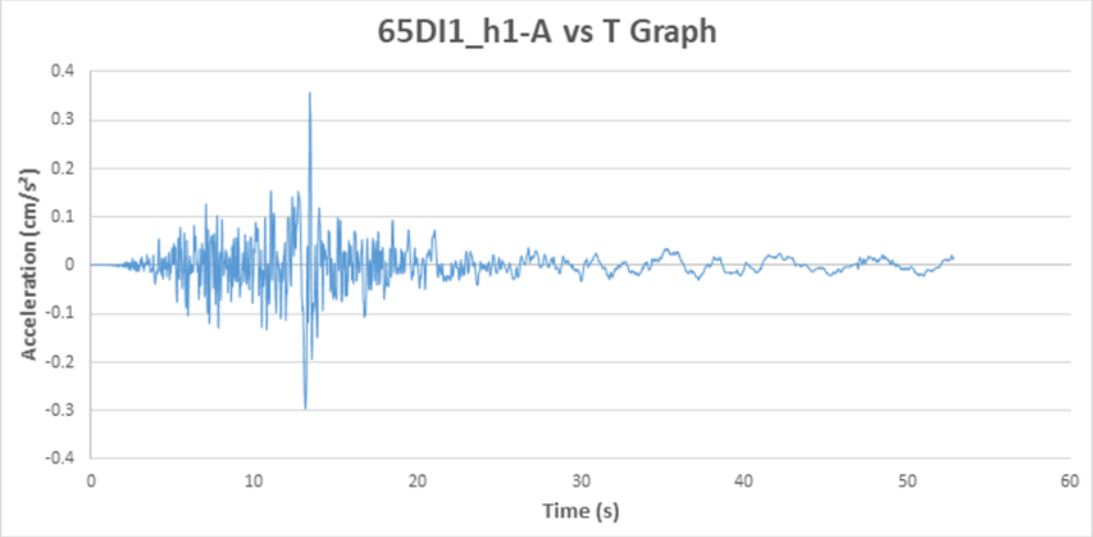

Figure 2.1. Acceleration vs Time Graph of Ground Motion for 65DI1_h1

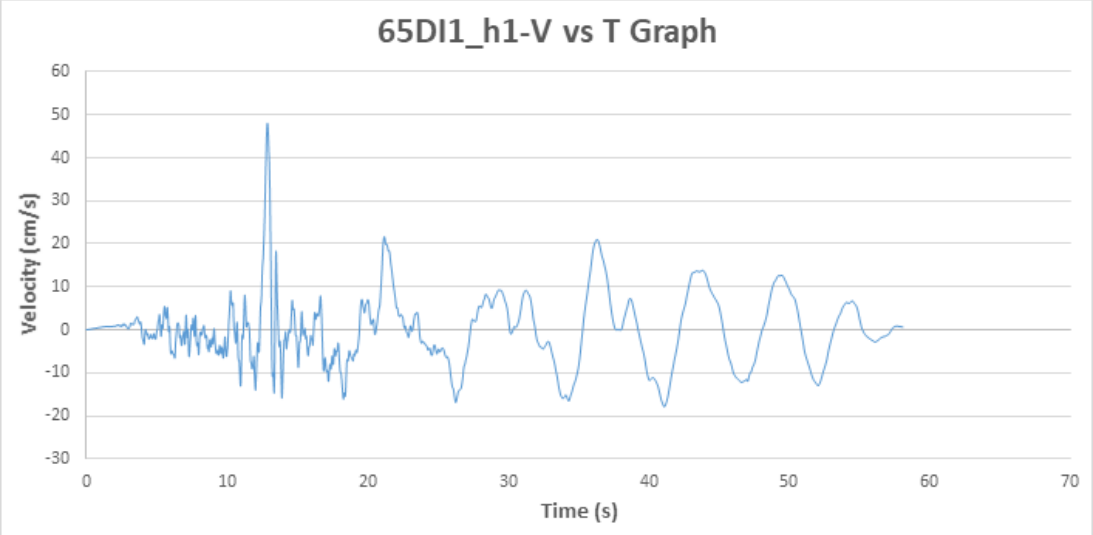

Figure 2.2. Velocity vs Time Graph of Ground Motion for 65DI1_h1

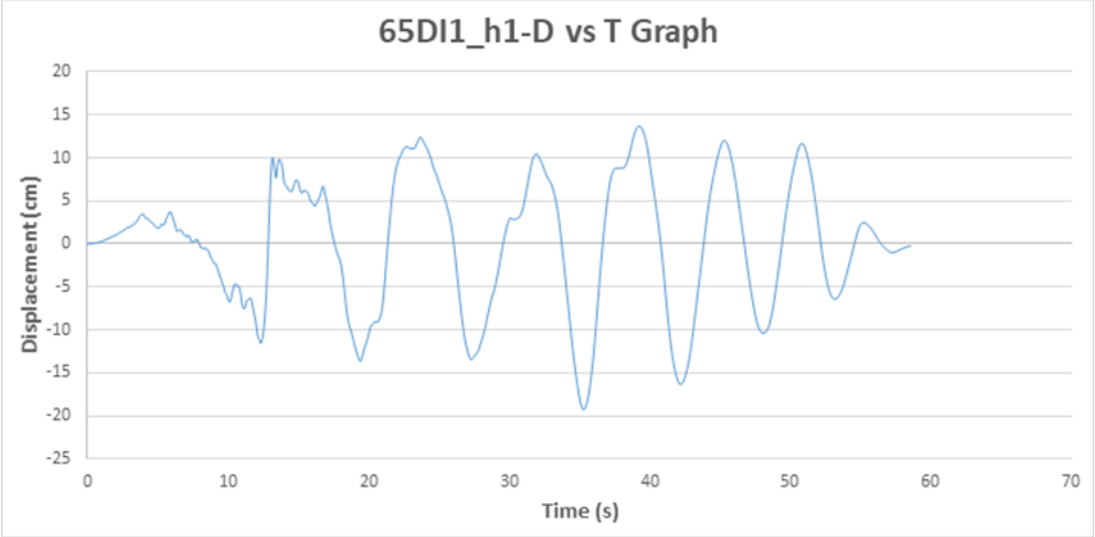

Figure 2.3. Displacement vs Time Graph of Ground Motion for 65DI1_h1

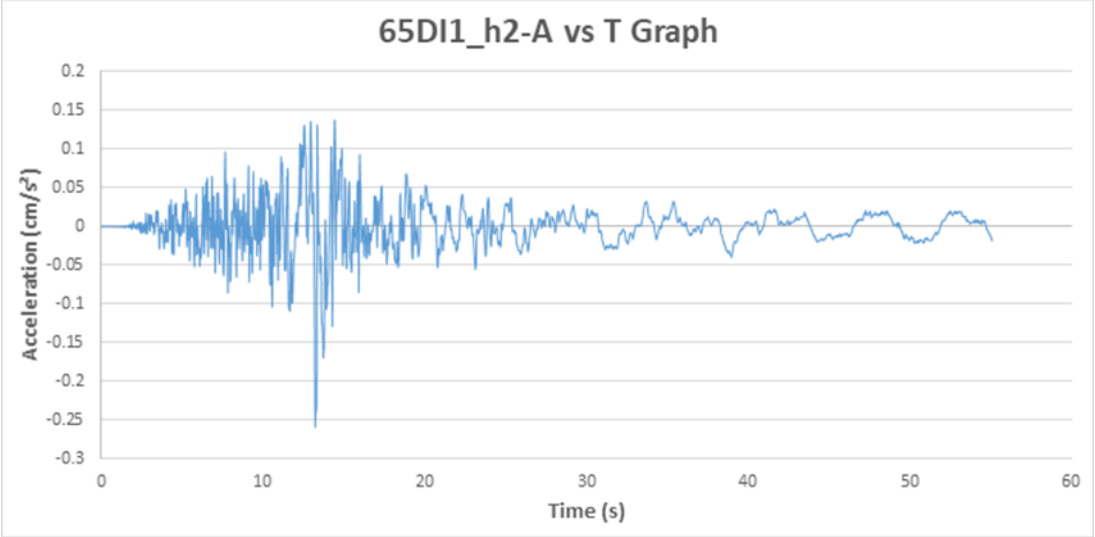

Figure 2.4. Acceleration vs Time Graph of Ground Motion for 65DI1_h2

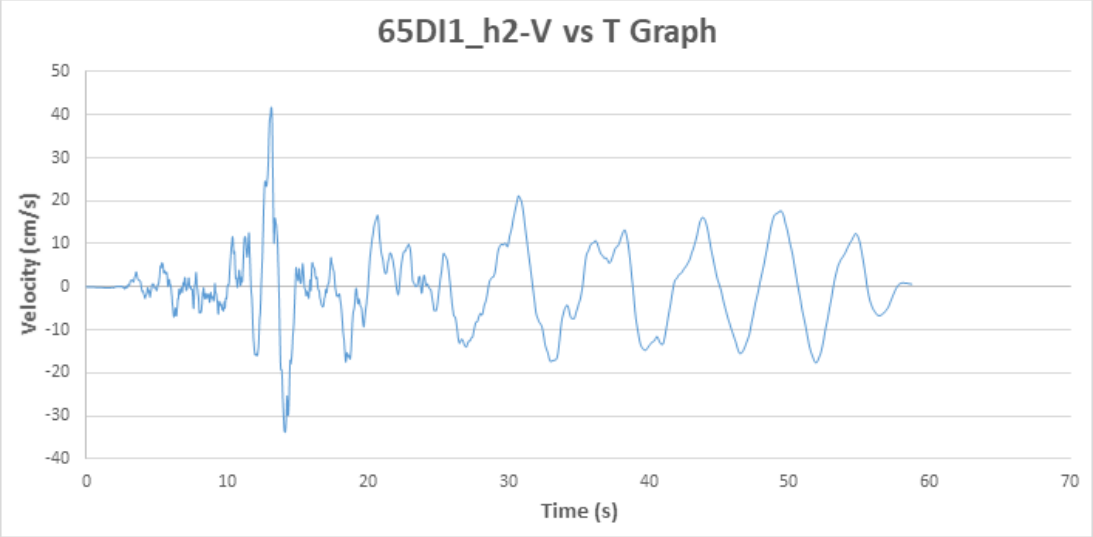

Figure 2.5. Velocity vs Time Graph of Ground Motion for 65DI1_h2

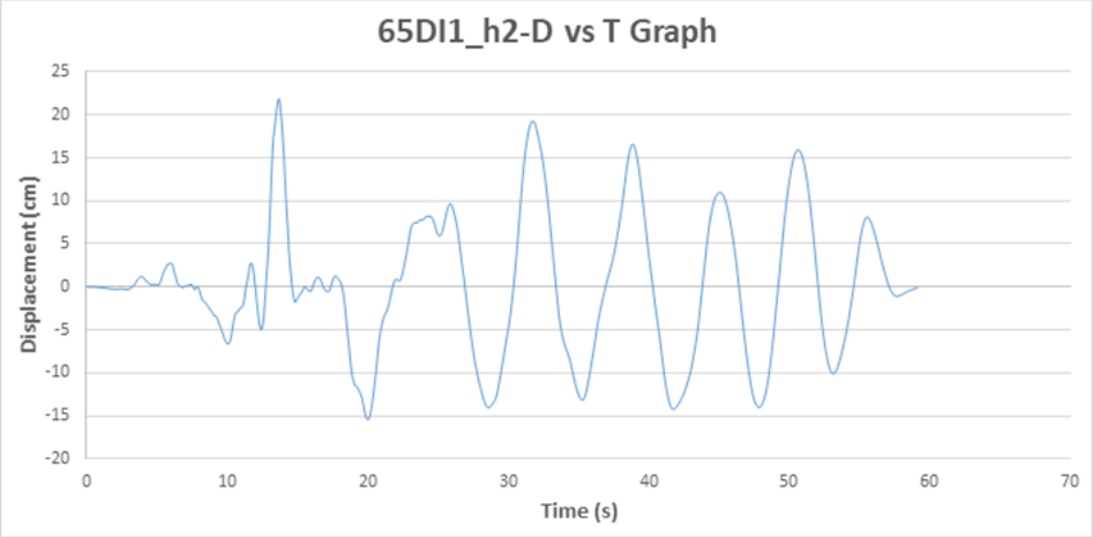

Figure 2.6. Displacement vs Time Graph of Ground Motion for 65DI1_h2

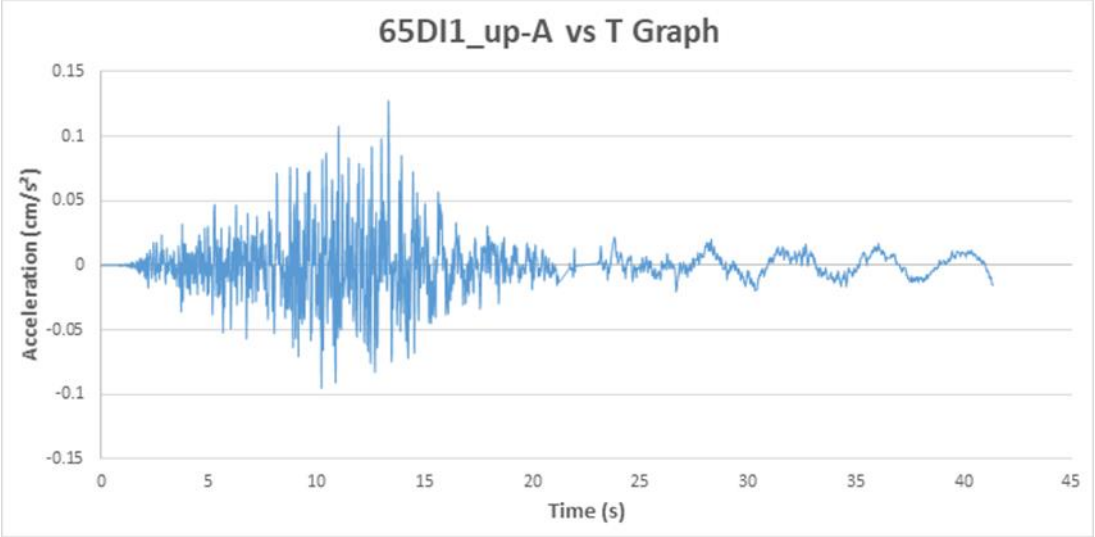

Figure 2.7. Acceleration vs Time Graph of Ground Motion for 65DI1_up

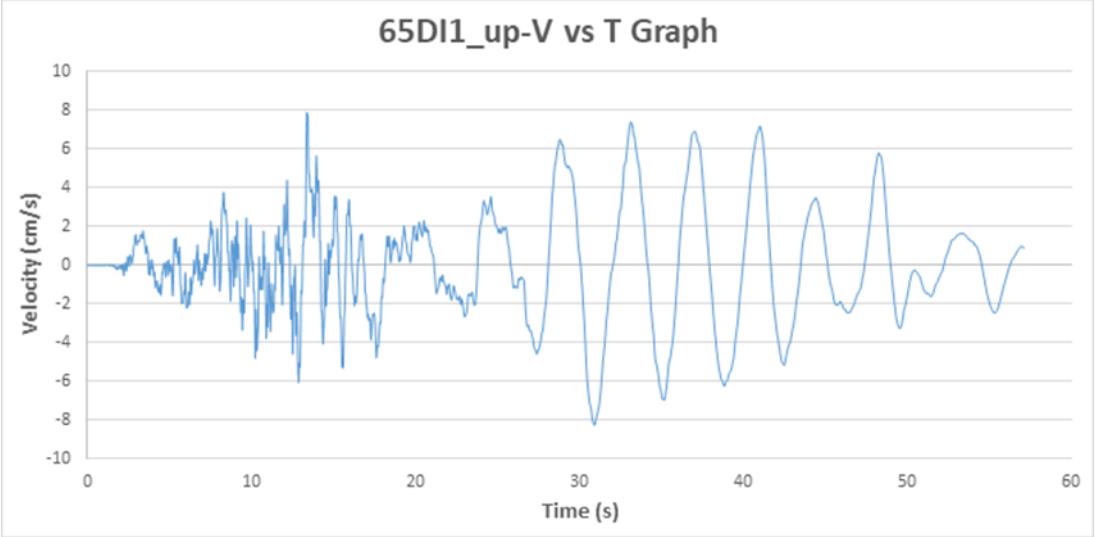

Figure 2.8. Velocity vs Time Graph of Ground Motion for 65DI1_up

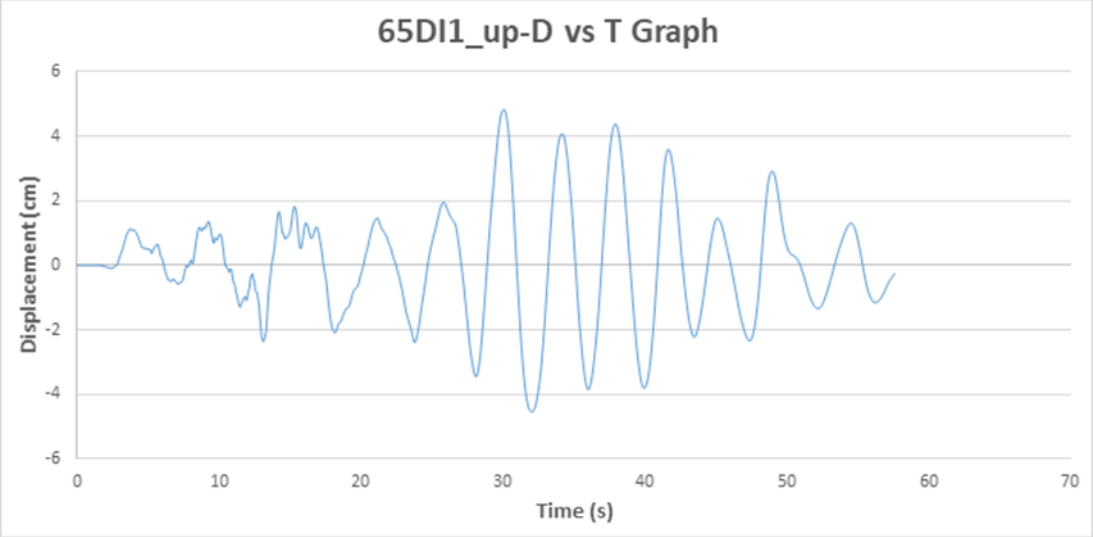

Figure 2.9. Displacement vs Time Graph of Ground Motion for 65DI1_up

2.3. Fourier Amplitude Spectra Graphs

To gather the information of whether the structure is amplified by an earthquake data or not, Fourier Amplitude Spectra Graphs are obtained via using the "Seismosignal 2016 Release 1" software. Some sample Fourier Amplitude Graphs are provided below and graphs of all records are provided in Appendix B which is provided in the attached CD. The sample graphs belong to the earthquake 65DI1 which has a magnitude of 6.5; soil class ZD, the distance from fault is between 15 km and 30 km. The three graphs show the Fourier Amplitude Spectra for horizontal direction 1, horizontal direction 2 and vertical directions of the ground motion, respectively.

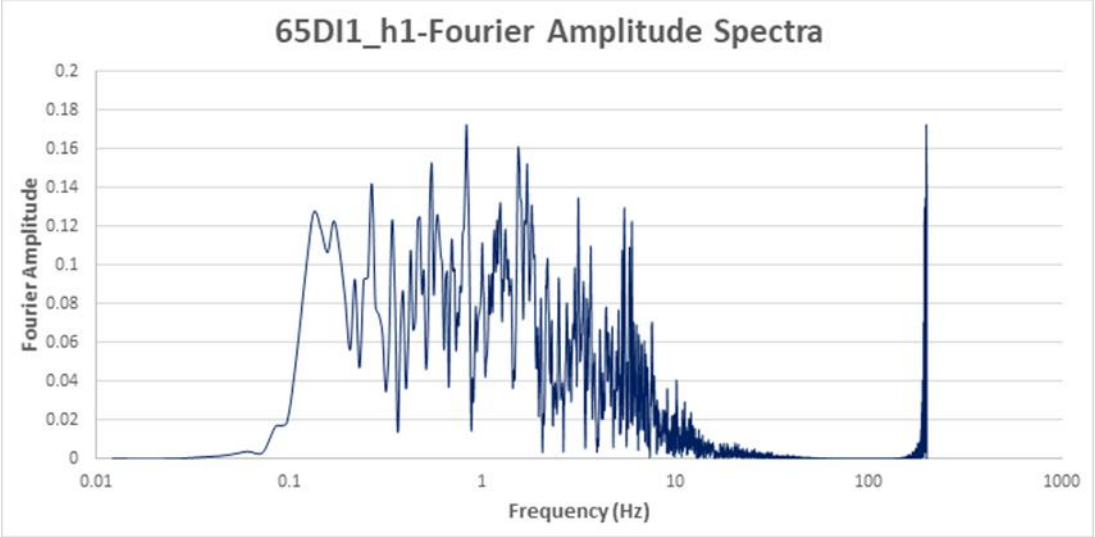

Figure 2.10. Fourier Amplitude Spectra Graph of Ground Motion for 65DI1_h1

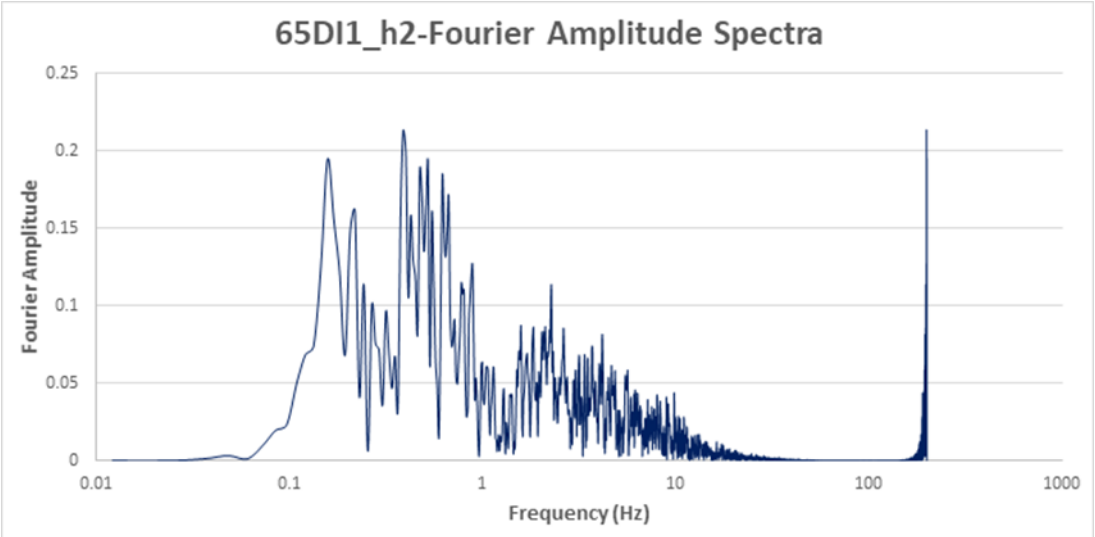

Figure 2.11. Fourier Amplitude Spectra Graph of Ground Motion for 65DI1_h2

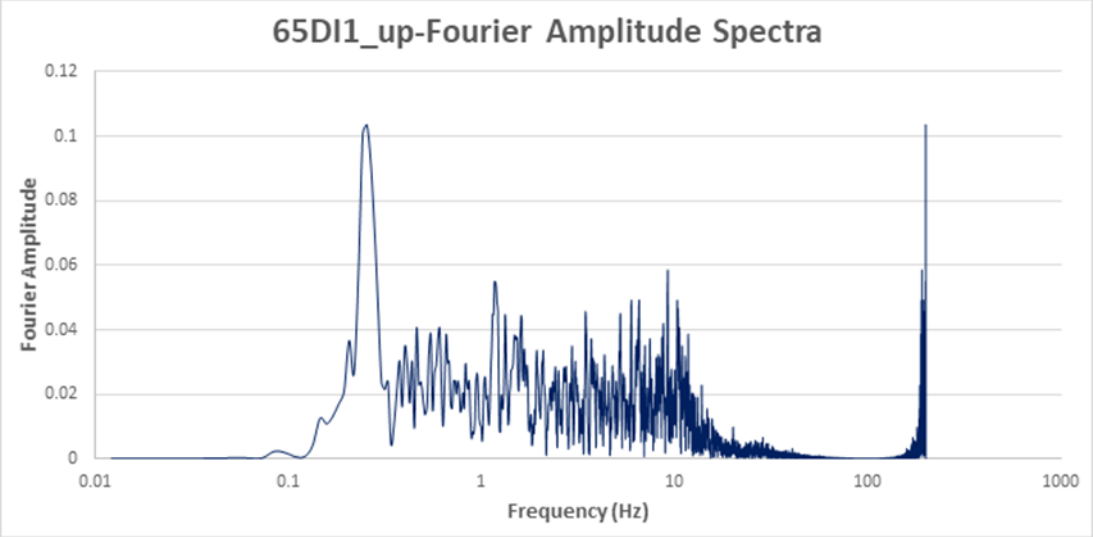

Figure 2.12. Fourier Amplitude Spectra Graph of Ground Motion for 65DI1_up

2.4. Response Spectrum Graphs

In this part, some sample Response Spectrum Graphs are provided below and graphs of all records are provided in Appendix C which is provided in the attached CD. As same in the previous part; the sample graphs belong to the earthquake 65DI1 which has a magnitude of 6.5, soil class ZD, the distance from fault is between 15 km and 30 km. The three graphs show the response spectra for horizontal direction 1, horizontal direction 2 and vertical directions of ground motion, respectively.

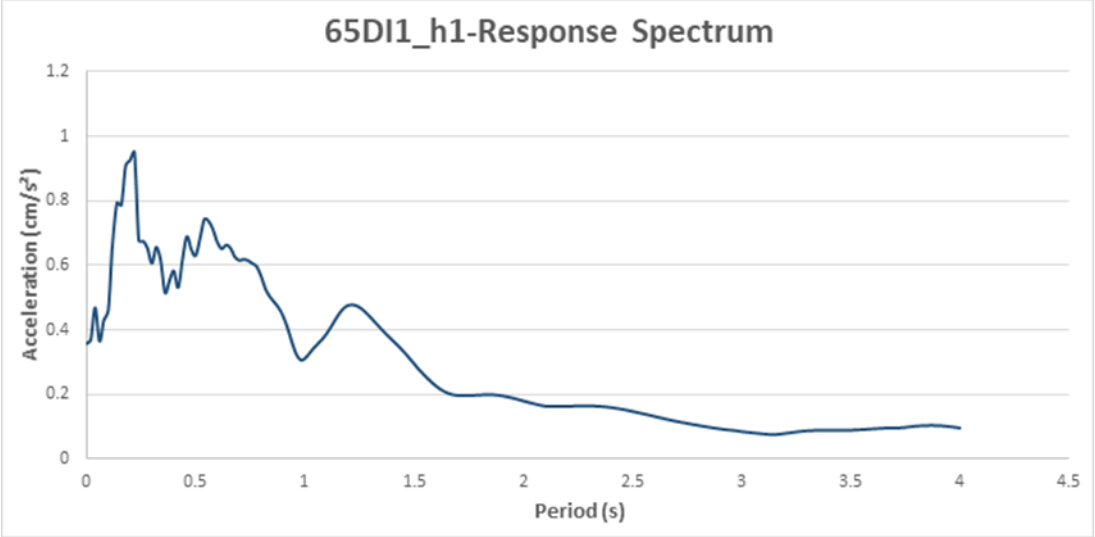

Figure 2.13. Response Spectrum Graph of Ground Motion for 65DI1_h1

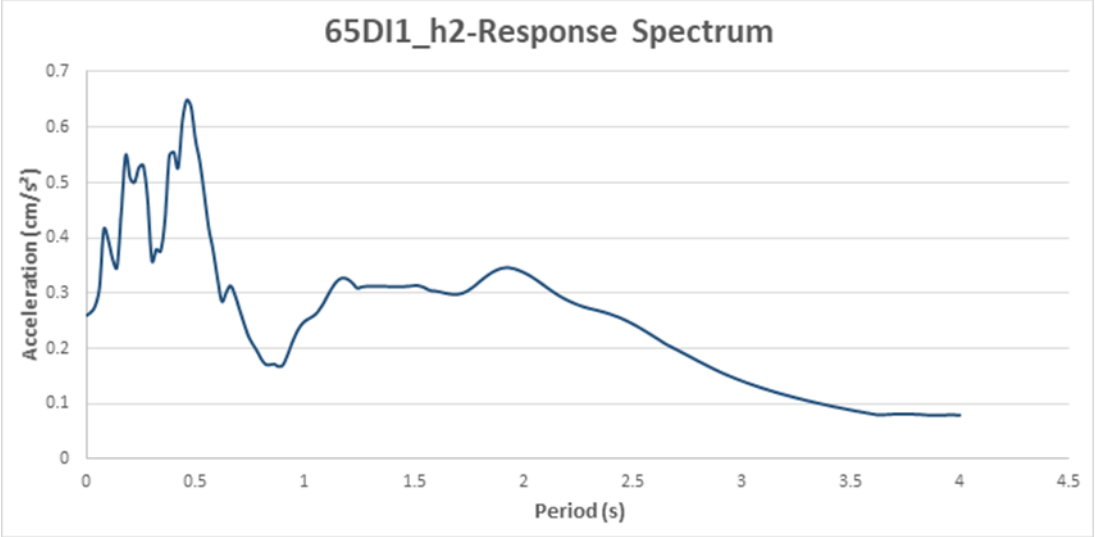

Figure 2.14. Response Spectrum Graph of Ground Motion for 65DI1_h2

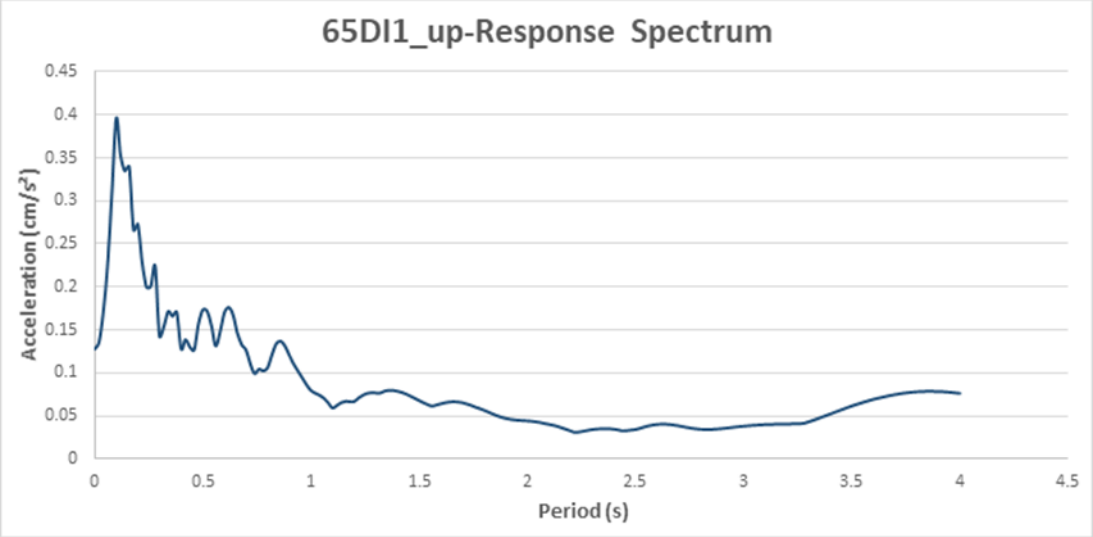

Figure 2.15. Response Spectrum Graph of Ground Motion for 65DI1_up

CHAPTER 3

SELECTION OF BRIDGE AND BEARING TYPES

3.1. Main Properties of the Selected Bridge

An ordinary, symmetric 95m long bridge is selected for this study. It has two spans, 2 piers with 15 meters height, 10 meters high abutments. Its superstructure consists of 10 precast reinforced concrete I girders with 1.90 meters height, concrete slab, precast panels, steel pedestrian guard rails. The cross-sectional view of the superstructure, longitudinal view of the bridge, cross-sectional view and dimensions of precast I girders are provided in Figures 3.1., 3.2. and 3.3., respectively. The abbreviations used are given in the "List of Abbreviations".

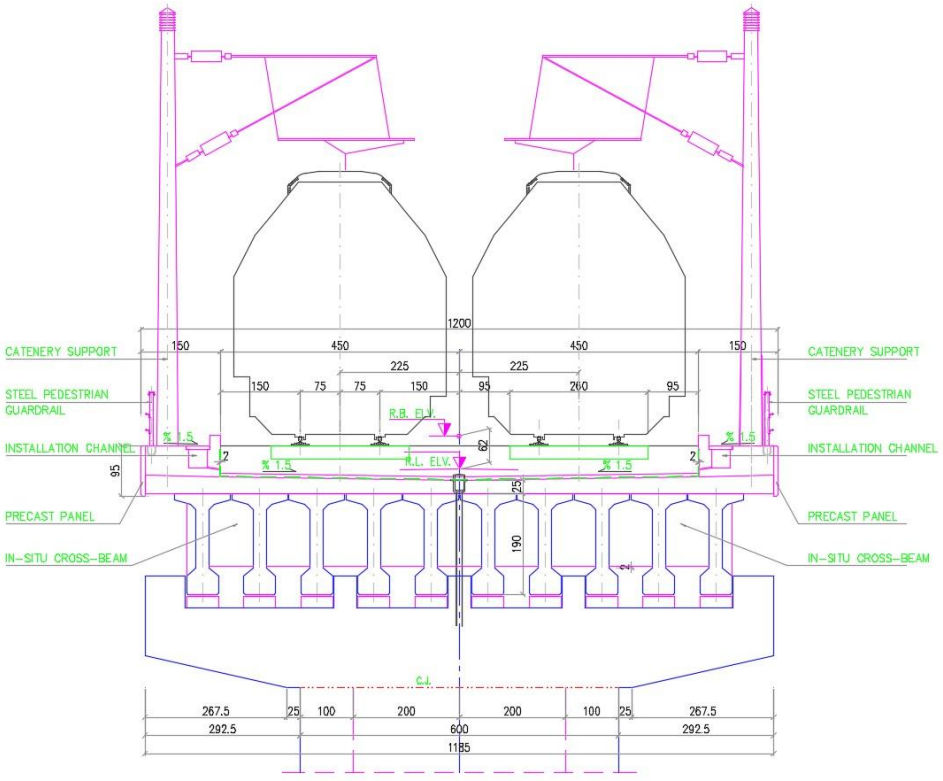

Figure 3.1. Cross-Sectional View of Superstructure

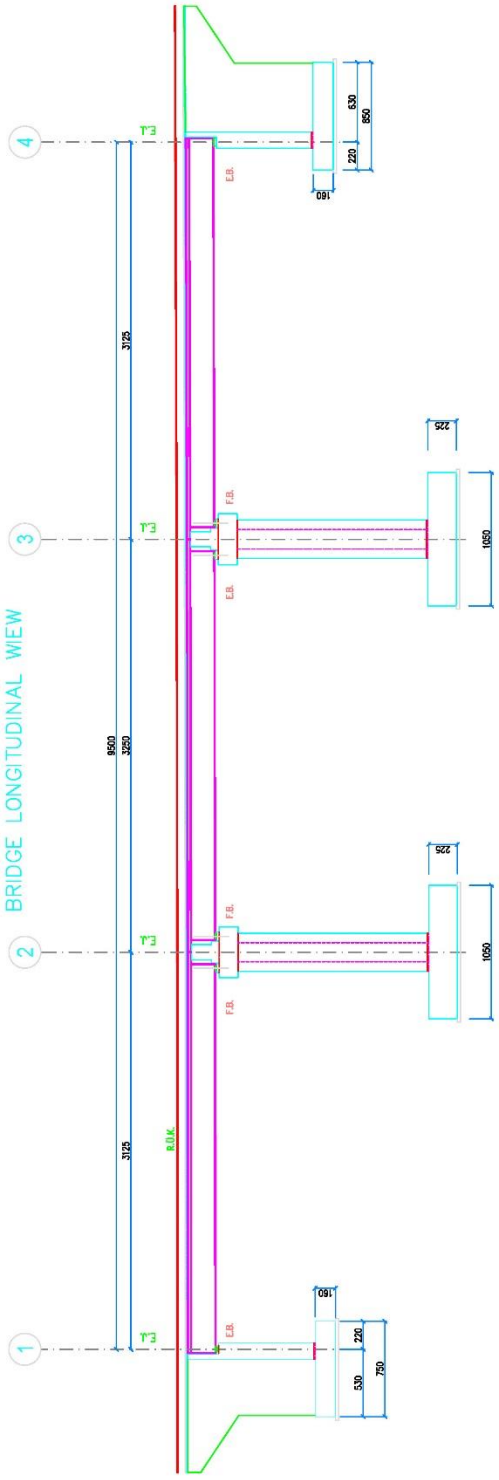

Figure 3.2. Longitudinal View of the Bridge

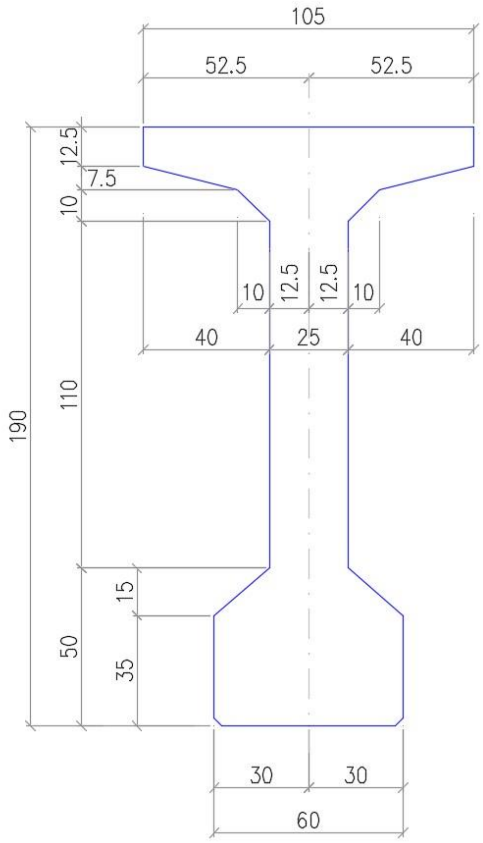

Figure 3.3. Cross-Sectional View and Dimensions of Precast I Girders

3.2. Selected Bearing Types

Elastomeric bearings, pot bearings, lead rubber bearings, friction pendulum bearings, spherical bearings are some of the bearing types used in high-speed railway bridges all around the world. Elastomeric and pot bearings are the most commonly used ones among all bearings are being concerned, so in this study elastomeric and pot bearings are investigated.

3.2.1. Elastomeric Bearings

3.2.1.1. Definition

Elastomeric bearings are generally made from the material called “neoprene”. It can be either plain bearing pads, which is made of only by neoprene material or laminated bearing, which is made of neoprene and layers of steel plates within the neoprene. In this study, a laminated bearing type is used. As a sample drawing for the structure of elastomeric bearings; the ones used are given in Figures 3.4, 3.5, 3.6 and 3.7.

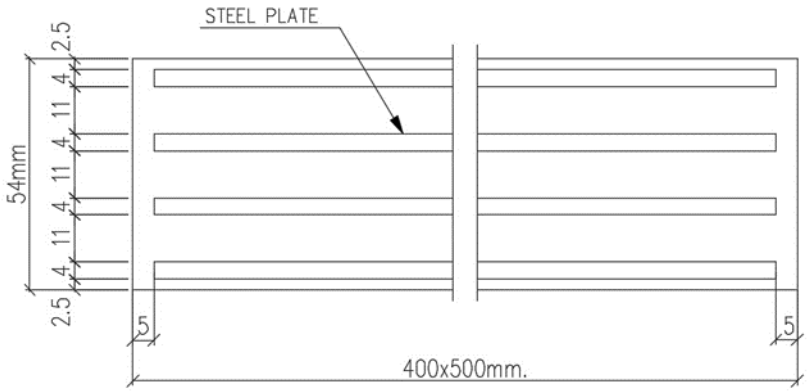

Figure 3.4. Elastomeric Expansion Bearing used in EBC10-REF Case (Cross-Sectional View)

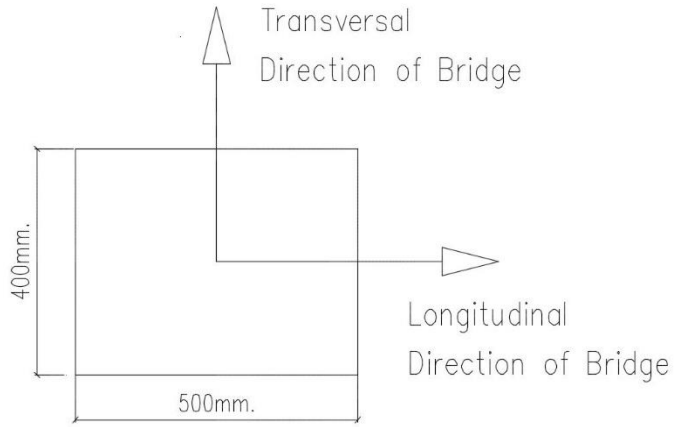

Figure 3.5. Elastomeric Expansion Bearing used in EBC10-REF Case (Top View)

Width of the elastomeric bearing, W_{eb} = 400 mm

Length of the elastomeric bearing, L_{eb} = 500 mm

Height of the elastomeric bearing, H_{eb} = 54 mm

Height between the uppermost and the lowest steel plates, h_{rt} = 33 mm

Shear modulus of the material used for elastomeric bearing, G_{eb} = 1 N/mm^2

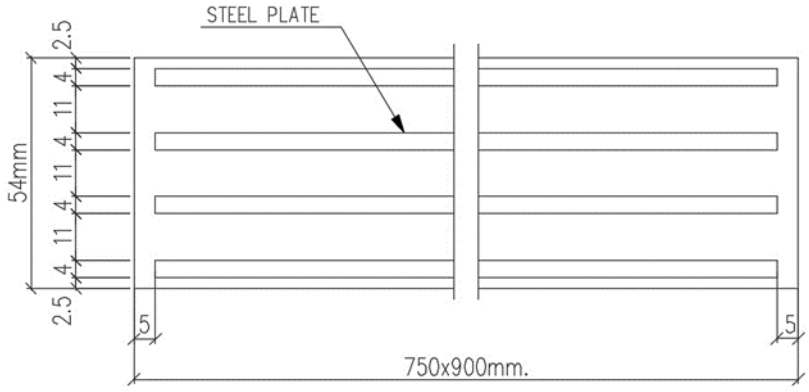

Figure 3.6. Elastomeric Expansion Bearing used in EBC3 (Cross-Sectional View)

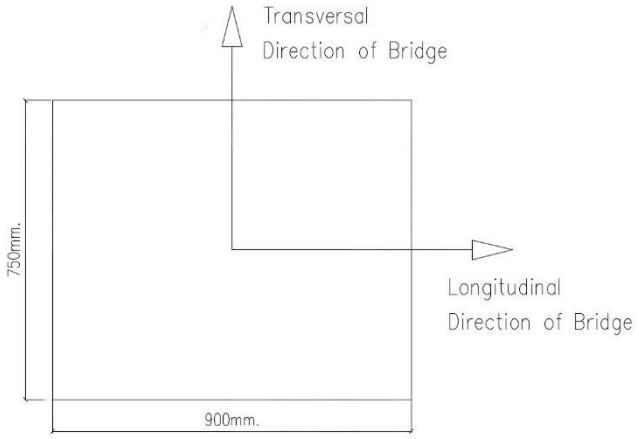

Figure 3.7. Elastomeric Expansion Bearing used in EBC3 (Top View)

Width of the elastomeric bearing, W = 750 mm

Length of the elastomeric bearing, L = 900 mm

Height of the elastomeric bearing, H = 54 mm

Height between the uppermost and the lowest steel plates, h_{rt} = 33 mm

Shear modulus of the material used for elastomeric bearing, G = 1 N/mm^2

3.2.1.2. Design Check of Elastomeric Bearings According to AASHTO

For the design check of the elastomeric bearings used in this study, the steps mentioned in section 14.6 of the code; "AASHTO (American Association of State Highways and Transportation Officials) Standard Specifications for Highway Bridges, Seventeenth Edition, 2002" are followed. The calculations made for the design check of the initially assumed dimensions and material properties, given in section 3.2.1.1, are given below. For the sake of understanding, abbreviations used in this part are provided in the "List of Abbreviations" at the beginning of this thesis report.

3.2.1.2.1. Design of Elastomeric Bearings Used in Reference Analysis Case (EBC10-REF)

- **Compression Check:**

It is specified in AASHTO 14.6.6.3.2 that the limit for compressive stress is 1000 psi which is approximately 6,89 MPa.

Total vertical load on an elastomeric bearing, P_{eb} = 1.271,85 kN

Area of the elastomeric bearing, A_{eb} = 0,4 x 0,5 = 0,2 m^2

Compression pressure on an elastomeric bearing, $\sigma_{eb} = P_{eb} / A_{eb}$

σ_{eb} = 6.359,25 kN / m^2 => 922,295 psi < 1000 psi (14.6.6.3.2)

- **Vertical Displacement Check**

Instant pressure deformation is the sum of the deformations gathered by using the instant strains and the height of the elastomer between the uppermost and the lowest steel plates; $\delta_c^i = \sum \varepsilon_{ci} h_{rt}$ (14.6.5.3.3-1)

Where;

ε_{ebi} **:** Instant pressure strain (/m)

h_{rt} **:** Height between the uppermost and the lowest steel plates (mm)

For obtaining the instant strain shape factor (SF) and the compressive stress due to total vertical load on an elastomeric bearing (σ_{eb}) is needed according to Figure 14.6.5.3.3-1 in AASHTO.

$SF = (L_{eb} \times W_{eb}) / (2 \times h_{layer} \times (L_{eb} + W_{eb})) = 10$

Where;

L_{eb} : Length of the elastomeric bearing (mm)

W_{eb} : Width of the elastomeric bearing (mm)

h_{layer} : Height of each layer between steel plates in an elastomeric bearing (mm)

For SF > 6,0; 60 Durometer Compressive Strain Equation:

$\varepsilon = C\sigma_{eb}^{x}$ where the constant C = 0,65 x (σ_{eb}/1000)^0,5 and x = 0,25^((SF/12)^0,15)

C = 0,624 x = 0,26 => ε = 3,68 => ε_{ebi} = 0,00368

Therefore; instantaneous deflection δ_c^i = 0,00368 x 33 = 1,21 mm.

For creep deflection after 25 years; from table 14.6.5.2-1, strain for creep will be;

$\varepsilon_{creep} = 0,35$

Thus; the creep deflection, $\delta_c = 1,35 \times 1,21 = 1,634$ mm. $< 0,07 \times h_{rt} = 2,31$ mm

- **Stability Check**

In order to satisfy the stability requirements given in part 14.6.6.3.6 of AASHTO; the total thickness of the elastomeric bearing should be less than one-third of the length or width of itself. Namely,

$L_{eb} => 3h_{rt}$ 400 => 99 (14.6.6.3.6)

$W_{eb} => 3h_{rt}$ 500 => 99

Where;

L_{eb} : Length of the elastomeric bearing (mm)

W_{eb} : Width of the elastomeric bearing (mm)

h_{rt} **:** Height between the uppermost and the lowest steel plates (mm)

- **Shear Deformation Check**

The maximum deformation caused by shrinkage, thermal effects, creep, post-tensioning, etc. should be less than half of the height between the uppermost and the lowest steel plates. Therefore, the maximum shear deformation of the bearing will be;
$\delta_{s,max} < h_{rt} / 2 = 1,65$ cm (14.6.5.3.4)

Where;

Δ_T : The temperature change considered in thermal effects to the elastomeric bearing. It is taken into account to be 35 ^oC.

Thermal coefficient of concrete, α_c = 0,0000108 /^{o}C (8.5.3)

Shrinkage coefficient of concrete, α_{sh} = 0,0002000 (8.5.4)

Distance between two expansion joints, L_1 = 32,50 m.

Elongation of one bearing = (L_1 x α_c x Δ_T) / 2 = 0,61 cm.

Shortening of one bearing = ((L_1 x α_c x Δ_T) + (L_1 x α_{sh})) / 2 = 1,26 cm.

- **Rotation Limit**

Limiting the rotation aims to prevent uplift of any corner of the elastomeric bearing. The limit for the rotation, θ_{TL}, can be calculated by the formula;

$\theta_{TL} < (2\delta_c / W_{eb})$ = 0,00817 rad

Where;

δ_c : Creep deflection (mm)

W_{eb} : Width of the elastomeric bearing (mm)

Bearings are modeled as linear link elements in the structural analysis software having three dimensional (horizontal, vertical and rotational) stiffness properties. The calculation process of stiffness coefficients is provided below.

- **Horizontal (Longitudinal and Transverse) Direction Spring Stiffness Coefficients**

Translational spring stiffness coefficient of elastomeric bearing in both transverse and longitudinal directions, k_{tr}, is directly proportional to the shear modulus of the elastomeric bearing (G_{eb}) and area of the elastomeric bearing (A_{eb}). Height of the

elastomeric bearing diversely affects the stiffness coefficient in the horizontal direction;

$k_{tr} = (G_{eb} \times A_{eb}) / h_{rt} = 6.061$ kN/m

Where,

G_{eb} : Shear modulus of the elastomeric bearing

A_{eb} : Area of the elastomeric bearing (mm^2)

h_{rt} : Height between the uppermost and the lowest steel plates (mm)

- **Vertical Direction Spring Stiffness Coefficients**

Spring stiffness coefficient of elastomeric bearing in the vertical direction, k_{vr}, is a function of the modulus of elasticity, area of the elastomeric bearing and the height between the uppermost and the lowest steel plates (h_{rt}). The formula for k_{vr} is:

$k_{vr} = (E \times A_{eb}) / h_{rt}$

Modulus of elasticity, E is the pressure per each unit of strain. The strain is gathered by using Figure 14.6.5.3.3-1 from AASHTO. For using specified Figure, shape factor (SF) and compressive stress are needed.

Shape factor is a function of length and width of elastomeric bearing (L_{eb} and W_{eb}) and height of each steel layer (h_{layer});

$SF = (L_{eb} \times W_{eb}) / (2 \times h_{layer} \times (L_{eb} + W_{eb})) = 10$

The compressive stress, that will be used for finding shape factor is, the amount of the load on an elastomeric bearing due to the weight of the superstructure per unit area:

$\sigma_{c,d} = W_{sup,eb} / A_{eb} = 3.150$ kN / m^2

Since $\sigma_{c,d} = 3.150$ kN / m^2 , SF = 10 and By using the Figure 14.6.5.3.3-1 in AASHTO; $\varepsilon_{c,d} \sim= 0{,}02$ and $E = \sigma_{c,d} / \varepsilon_{c,d} = 157{,}5$ N / mm^2

Therefore the spring stiffness coefficient which can be used for modeling elastomeric bearing as alink element, k_{vr} = 954.545 N / mm.

- **Rotation About Transverse Direction Spring Stiffness Coefficients**

The value for spring stiffness coefficient for rotation about transverse direction, $k_{rot,t}$, is so small and it can be neglected. Therefore, the spring coefficient for rotation about the transverse direction of the link element is assumed to be zero.

$k_{rot,t}$ = 0 kN.m/rad

- **Rotation About Longitudinal Direction Spring Stiffness Coefficients**

The system itself is very stiff and very hard to rotate about the longitudinal direction. Therefore, the value of the spring stiffness coefficient of rotation about longitudinal direction, $k_{rot,l}$, is assumed to be 10^8 kN.m/rad in order to take the behavior of the system into consideration while introducing the link element to the structural analysis program.

$k_{rot,l}$ = 10^8 kN.m/rad

- **Rotation About Vertical Direction Spring Stiffness Coefficients**

If there will be a rotation about vertical direction, the angle of rotation will be the same for each elastomeric bearing even though they are placed under different beams. It is shown in Figure 3.8. Initially, by assuming a unit rotation about the vertical direction and with the information stated in the previous sentence, shear forces and moments exerted on each elastomeric bearing can be calculated. After computing the moment reactions, the rotational spring stiffness coefficient can be obtained by the formula; $k_{rot,v} = (2 \times \sum M_i) / \theta$

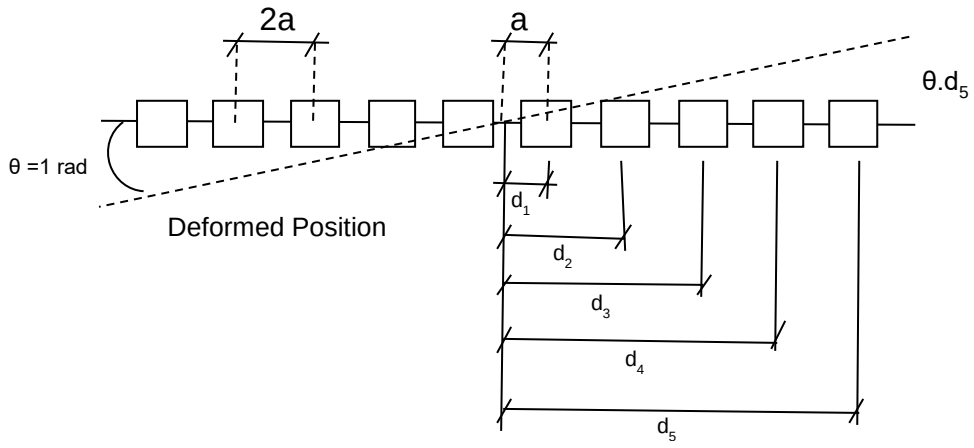

Figure 3.8. Rotation About the Vertical Direction

Shear forces exerted on each elastomeric bearing can be regarded as the force for moving the system in the vertical direction for unit rotation. Since the rotations are so small, the tangent of the rotation angle can be taken as the angle itself ($\tan(\theta) = \theta$). So, the vertical displacement is the result of the mathematical operation: "$\theta.d_i$". By using vertical displacement values and translational spring stiffness coefficient of elastomeric bearing, shear force, V_i, can be calculated:

$V_1 = k_{tr}.\theta.d_1$, $V_2 = k_{tr}.\theta.d_2$, $V_3 = k_{tr}.\theta.d_3$, $V_4 = k_{tr}.\theta.d_4$ and $V_5 = k_{tr}.\theta.d_5$

Afterward, moments, M_i, can be obtained by multiplying shear force values by the moment arms, d_i :

$M_1 = V_1.d_1$, $M_2 = V_2.d_2$, $M_3 = V_3.d_3$, $M_4 = V_4.d_4$, $M_5 = V_5.d_5$

Finally, by using the formula, "$k_{rot,v} = (2 \times \sum M_i) / \theta$" spring stiffness coefficient of elastomeric bearings for rotation about vertical direction can be gathered:

$k_{rot,v}$ = 577.813 kN.m/rad

Where;

$k_{rot,v}$: Spring stiffness coefficient of elastomeric bearings for rotation about vertical direction (kN.m/rad)

k_{tr} : Translational spring stiffness coefficient of elastomeric bearing in both transverse and longitudinal directions (kN/m)

a : Half of the distance between the beams

θ : Angle of rotation about the vertical direction

d_i : Distance from the centerline of the system in the horizontal direction

V_i : The shear force exerted on each elastomeric bearing due to the rotation with the angle θ

M_i : The moment exerted on each elastomeric bearing due to the rotation with the angle θ

3.2.1.2.2. Design of Elastomeric Bearings Used in Elastomeric Bearing Analysis Case (EBC)

- **Compression Check:**

It is specified in AASHTO 14.6.6.3.2 that the limit for compressive stress is 1000 psi which is approximately 6,89 MPa.

Total Vertical Load on an Elastomeric Bearing, P_{eb} = 4.239,50 kN

Area of the elastomeric bearing , A_{eb} = 0,75 x 0,9 = 0,675 m^2

Compression pressure on an elastomeric bearing , $\sigma_{eb} = P_{eb} / A_{eb}$

σ_{eb} = 6.280,74 kN / m^2 => 910,944 psi < 1000 psi (14.6.6.3.2)

- **Vertical Displacement Check**

Instant pressure deformation is the sum of the deformations gathered by using the instant strains and the height of the elastomer between the uppermost and the lowest steel plates, $\delta c^i = \sum \varepsilon_{ci} h_{rt}$ (14.6.5.3.3-1)

Where;

ε_{ebi} **:** Instant pressure strain (/m)

h_{rt} **:** Height between the uppermost and the lowest steel plates (mm)

For obtaining the instant strain shape factor (SF) and the compressive stress due to total vertical load on an elastomeric bearing (σ_{eb}) is needed according to Figure 14.6.5.3.3-1 in AASHTO.

$SF = (L_{eb} \times W_{eb}) / (2 \times h_{layer} \times (L_{eb} + W_{eb})) = 19$

Where;

L_{eb} : Length of the elastomeric bearing (mm)

W_{eb} : Width of the elastomeric bearing (mm)

h_{layer} : Height of each layer between steel plates in an elastomeric bearing (mm)

For SF > 6,0; 60 Durometer Compressive Strain Equation:

$\varepsilon = C\sigma_{eb}^{x}$ where C = 0,65 x (σ/1000)^0,5 and x = 0,25^((SF/12)^0,15)

C = 0,624 x = 0,226 => ε = 2,92

ε_{ci} = 0,00292

Therefore; instantaneous deflection δc^i = 0,00292 x 54 = 0,158 cm.

For creep deflection after 25 years; from table 14.6.5.2-1, strain for creep will be;

ε_{creep} = 0,35

Thus; the creep deflection, δ_c = 1,35 x 1,58 = 2,133 mm. < 0,07 x h_{rt} = 2,31 mm

- **Stability Check**

In order to satisfy the stability requirements given in part 14.6.6.3.6 of AASHTO; the total thickness of the elastomeric bearing should be less than one-third of the length or width of itself. Namely,

L_{eb} => $3h_{rt}$ 750 => 99 (14.4.1.5)

W_{eb} => $5h_{rt}$ 900 => 165

Where;

L_{eb} : Length of the elastomeric bearing (mm)

W_{eb} : Width of the elastomeric bearing (mm)

h_{rt} **:** Height between the uppermost and the lowest steel plates (mm)

- **Shear Deformation Check**

The maximum deformation caused by shrinkage, thermal effects, creep, post-tensioning, etc. should be less than half of the height between the uppermost and the lowest steel plates. Therefore, the maximum shear deformation of the bearing will be; $\delta_{s,max} < h_{rt} / 2 = 4{,}10$ cm (14.6.5.3.4)

Where;

Δ_T : The temperature change considered in thermal effects to the elastomeric bearing. It is taken into account to be 35 ºC.

Thermal coefficient of concrete, $\alpha_c = 0{,}0000108$ /C^o (8.5.3)

Shrinkage coefficient of concrete, $\alpha_{sh} = 0{,}0002000$ (8.5.4)

Distance between two expansion joints, $L_1 = 32{,}50$ m.

Elongation of one bearing = $(L_1 \times \alpha_c \times \Delta_T) / 2 = 0{,}61$ cm.

Shortening of one bearing = $((L_1 \times \alpha_c \times \Delta_{T)} + (L_1 \times \alpha_{sh})) / 2 = 1{,}26$ cm.

- **Rotation Limit**

Limiting the rotation aims to prevent uplift of any corner of the elastomeric bearing. The limit for the rotation, θ_{TL}, can be calculated by the formula;

$\theta_{TL} < (2\delta_c / W_{eb}) = 0{,}010665$ rad

Where;

δ_c : Creep deflection (mm)

W_{eb} : Width of the elastomeric bearing (mm)

As mentioned before bearings are modeled as linear link elements in the structural analysis software having three dimensional (horizontal, vertical and rotational) stiffness properties. The calculation process of stiffness coefficients is provided below.

- **Horizontal (Longitudinal and Transverse) Direction Spring Stiffness Coefficients**

Translational spring stiffness coefficient of elastomeric bearing in both transverse and longitudinal directions, k_{tr}, is directly proportional to the shear modulus of the elastomeric bearing (G_{eb}) and area of the elastomeric bearing (A_{eb}). Height of the elastomeric bearing diversely affects the stiffness coefficient in the horizontal direction;

$k_{tr} = (G_{eb} \times A_{eb}) / h_{rt} = 20.455$ N/mm

k_{tr} is same for both longitudinal and transverse direction of the bridge.

Where,

G_{eb} : Shear modulus of the elastomeric bearing

A_{eb} : Area of the elastomeric bearing (mm^2)

h_{rt} : Height between the uppermost and the lowest steel plates (mm)

- **Vertical Direction Spring Stiffness Coefficients**

Spring stiffness coefficient of elastomeric bearing in the vertical direction, k_{vr}, is a function of the modulus of elasticity, area of the elastomeric bearing and the height between the uppermost and the lowest steel plates (h_{rt}). The formula for k_{vr} is:

$k_{vr} = (E \times A_{eb}) / h_{rt}$

Modulus of elasticity, E is the pressure per each unit of strain. The strain is gathered by using Figure 14.6.5.3.3-1 from AASHTO. For using specified Figure, shape factor (SF) and compressive stress are needed.

Shape factor is a function of length and width of elastomeric bearing (L_{eb} and W_{eb}) and height of each steel layer (h_{layer});

$SF = (L_{eb} \times W_{eb}) / (2 \times h_{layer} \times (L_{eb} + W_{eb})) = 19$

The compressive stress, that will be used for finding shape factor is, the amount of the load on an elastomeric bearing due to the weight of the superstructure per unit area:

$\sigma_c = W_{sup,eb} / A_{eb} = 3.111{,}1 \text{ kN} / \text{m}^2$

for using Figure 14.6.5.3.3-1;

Since $\sigma_{c,d} = 3.111{,}1 \text{ kN} / \text{m}^2$, SF = 19 and By using the Figure 14.6.5.3.3-1 in AASHTO; $\varepsilon_{c,d} \sim= 0{,}02$ and $E = \sigma_{c,d} / \varepsilon_{c,d} = 155{,}56 \text{ N} / \text{mm}^2$

Therefore the spring stiffness coefficient which can be used for modeling elastomeric bearing as alink element, $k_{vr} = 3.181.818 \text{ N} / \text{mm}$

- **Rotation About Transverse Direction Spring Stiffness Coefficients**

The value for spring stiffness coefficient for rotation about transverse direction, $k_{rot,t}$, is so small and it can be neglected. Therefore, the spring coefficient for rotation about the transverse direction of the link element is assumed to be zero, $k_{rot,t} = 0 \text{ kN.m/rad}$

- **Rotation About Longitudinal Direction Spring Stiffness Coefficients**

The system itself is very stiff and very hard to rotate about the longitudinal direction. Therefore, the value of the spring stiffness coefficient of rotation about longitudinal direction, $k_{rot,l}$, is assumed to be 10^8 kN.m/rad in order to take the behavior of the system into consideration while introducing the link element to the structural analysis program.

$k_{rot,l}$ = 10^8 kN.m/rad

- **Rotation About Vertical Direction Spring Stiffness Coefficients**

If there will be a rotation about vertical direction, the angle of rotation will be the same for each elastomeric bearing even though they are placed under different beams. It is shown in Figure 3.9. Initially, by assuming a unit rotation about the vertical direction and with the information stated in the previous sentence, shear forces and moments exerted on each elastomeric bearing can be calculated. After computing the moment reactions, the rotational spring stiffness coefficient can be obtained by the formula;
$k_{rot,v} = (2 \times \sum M_i) / \theta$

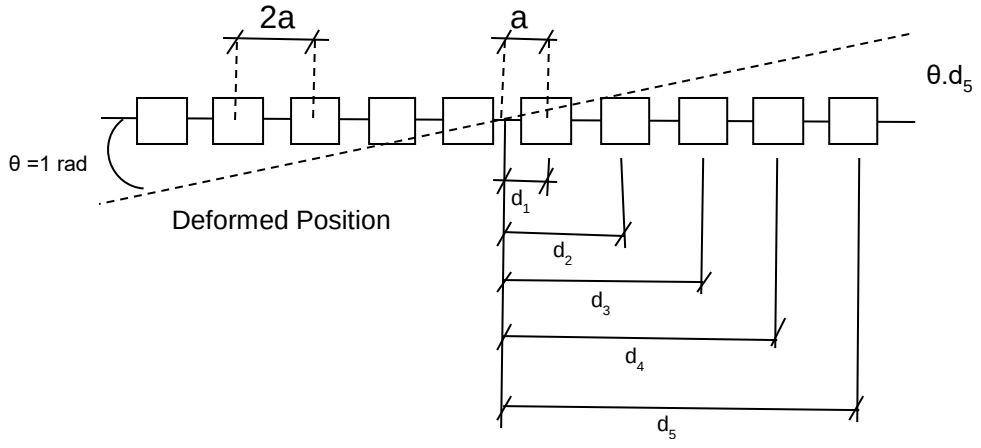

Figure 3.9. Rotation About the Vertical Direction

Shear forces exerted on each elastomeric bearing can be regarded as the force for moving the system in vertical direction for unit rotation. Since the rotations are so small, the tangent of the rotation angle can be taken as the angle itself ($\tan(\theta) = \theta$). So, the vertical displacement is the result of the mathematical operation: "$\theta.d_i$". By using vertical displacement values and translational spring stiffness coefficient of elastomeric bearing, shear force, V_i, can be calculated:

$V_1 = k_{tr}.\theta.d_1$, $V_2 = k_{tr}.\theta.d_2$, $V_3 = k_{tr}.\theta.d_3$, $V_4 = k_{tr}.\theta.d_4$ and $V_5 = k_{tr}.\theta.d_5$

Afterward, moments, M_i, can be obtained by multiplying shear force values by the moment arms, d_i :

$M_1 = V_1.d_1$, $M_2 = V_2.d_2$, $M_3 = V_3.d_3$, $M_4 = V_4.d_4$, $M_5 = V_5.d_5$

Finally, by using the formula, "$k_{rot,v} = (2 \times \sum M_i) / \theta$" spring stiffness coefficient of elastomeric bearings for rotation about vertical direction can be gathered:

$k_{rot,v}$ = 70.204.219 kN.m/rad

Where;

$k_{rot,v}$: Spring stiffness coefficient of elastomeric bearings for rotation about vertical direction (kN.m/rad)

k_{tr} : Translational spring stiffness coefficient of elastomeric bearing in both transverse and longitudinal directions (kN/m)

a : Half of the distance between the beams

θ : Angle of rotation about the vertical direction

d_i : Distance from the centerline of the system in the horizontal direction

V_i : The shear force exerted on each elastomeric bearing due to the rotation with the angle θ

M_i : The moment exerted on each elastomeric bearing due to the rotation with the angle θ

3.2.2. Pot Bearings

3.2.2.1. Definition

Characteristics of a pot bearing can differ from one producer to another but generally they are made up of neoprene (elastomeric pad), steel plates up and down outside and there is an internal steel ring inside of it. (Figure 3.10.)

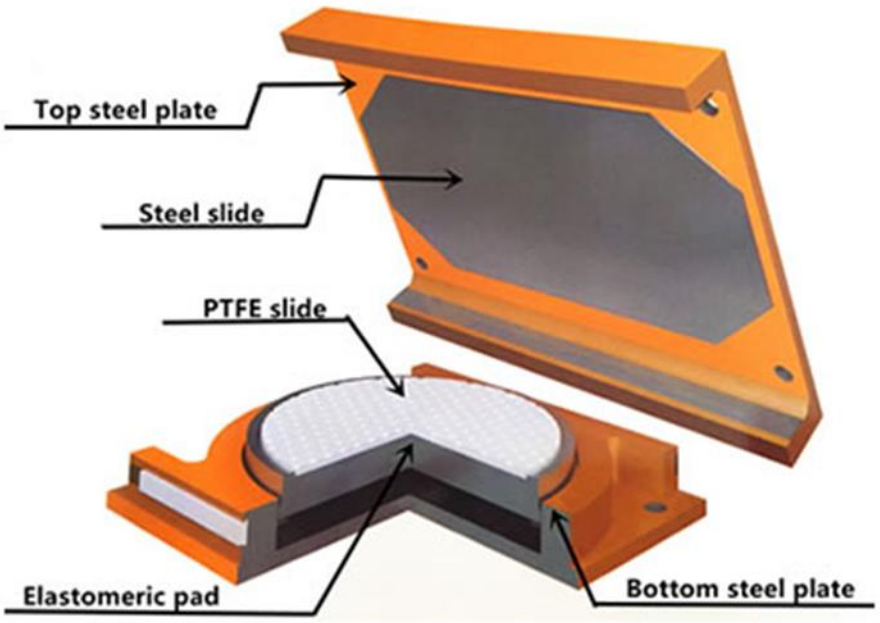

Figure 3.10. General View of a Sample Pot Bearing

The fixed and guided pot bearings are used in this study. (Figure 3.11., Figure 3.12., Figure 3.13. and Figure 3.14.) Figures 3.10, 3.11, 3.12, 3.13 and 3.14 are retrieved from https://www.bridgebearing.org/bridgebearing/pot-bearing.html.

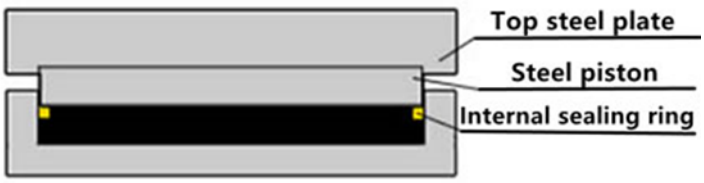

Figure 3.11. General View of a Fixed Pot Bearing

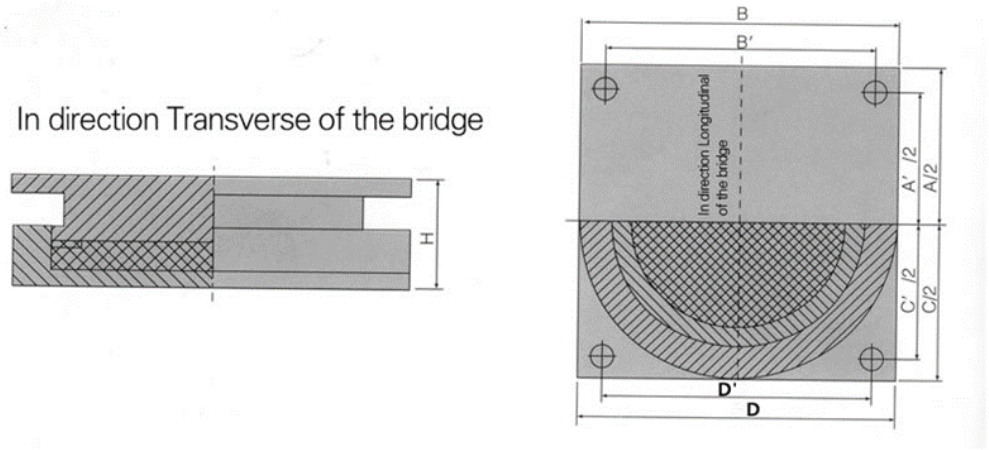

Figure 3.12. Cross-Sectional View of a Fixed Pot Bearing

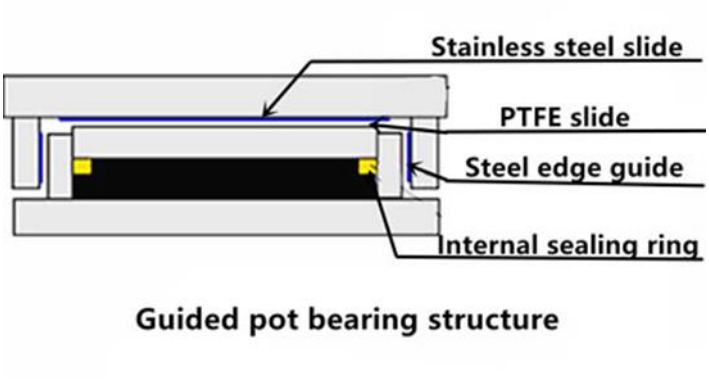

Figure 3.13. General View of a Guided Pot Bearing

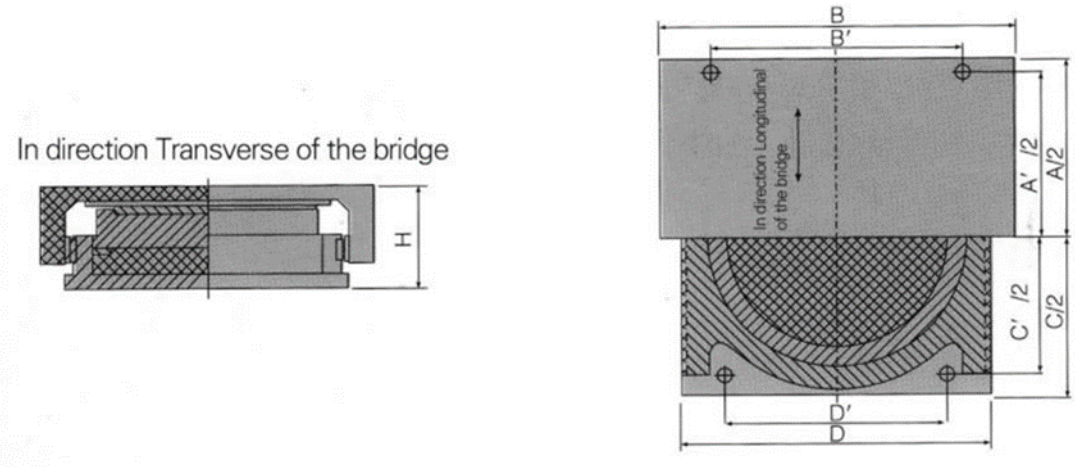

Figure 3.14. Cross-Sectional View of a Guided Pot Bearing

3.2.2.2. Design of Pot Bearings Used in Analysis Case PBC According to AASHTO LRFD Bridge Design Specifications

- **Compressive strength of the elastomeric disc**

It is specified in AASHTO LRFD Bridge Design Specifications, part 14.7.4.4, the average compressive strength of the elastomeric disc is limited up to 25 Mpa, $\sigma_{all} \leq 25$ Mpa

Where, σ_{all} : Allowable compression pressure on an elastomeric pad

- **The diameter of the elastomeric disc**

It is stated in the AASHTO LRFD Bridge Design Specifications that diameter of the elastomeric disc which is equal to the internal diameter of the pot bearing is related with the allowable compression stress and unfactored vertical load:

$D_p = 2 \times \sqrt{((\text{Unfactored Vertical Load}) \times 1000 / \pi / \sigma_{all})}$

Where;

D_p : Diameter of elastomeric disc = Internal diameter of pot bearing

Since the allowable compression pressure on the elastomeric disc should be less than or equal to 25 Mpa, and total vertical load on an elastomeric bearing, P_{eb} = 4.239,50 kN

Therefore, the diameter of the elastomeric pad should be at least; 464,67 mm.

- **The thickness of the elastomeric disc**

It is stated in the part 14.7.4.3-1 of AASHTO LRFD Bridge Design Specifications that the height of the elastomeric pad should be less than or equal to the result of the multiplication; 3,33 times the diameter of the elastomeric pad, D_p, and the design rotation angle, θ_u :

$h_r \geq 3{,}33.Dp.\theta u$ (AASHTO LRFD Bridge Design Specifications 14.7.4.3-1) (mm)

Where;

D_p : Diameter of elastomeric disc = Internal diameter of pot bearing

θ_u : Design rotation angle specified in Article 14.4.2 in AASHTO LRFD Bridge Design Specifications (rad.)

- **Compressive deflection**

Deflections that occurred due to compression are handled separately for the dead load and the live load according to the AASHTO LRFD Bridge Design Specifications in part 14.7.5.3.3. For the deflection due to the live load, the instantaneous live load compressive strain in i^{th} elastomer layer and thickness of i^{th} elastomeric layer are needed:

$\delta_{LL} = \sum \varepsilon_{Li} h_{ri}$ (14.7.5.3.3-1)

Where;

ε_{Li} = the instantaneous live load compressive strain in i^{th} elastomer layer

h_{ri} = the thickness of i^{th} elastomeric layer (mm)

In the same manner, deflection due to dead load is calculated by using the initial dead load compressive strain in i^{th} elastomer layer, ε_{di} and the thickness of i^{th} elastomeric layer, h_{ri} :

$\delta_{DL} = \sum \varepsilon_{di} h_{ri}$ (14.7.5.3.3-2)

Where;

ε_{di} = the initial dead load compressive strain in i^{th} elastomer layer

h_{ri} = the thickness of i^{th} elastomeric layer (mm)

The long-term dead load deflections including the creep effects are simply the summation of the instantaneous dead load deflection, δ_{DL} and the deflection due to creep effect.:

$\delta_{ul} = \delta_{DL} + a_{cr} \delta_{DL}$ (14.7.5.3.3-3)

Where;

a_{cr} = creep deflection divided by initial dead load deflection

- **Pot wall thickness**

According to the part 14.7.4.6 of AASHTO LRFD Bridge Design Specifications, the pot wall thickness, t_w, has a limitation regarding the formulas 14.7.4.6.5 and 14.7.4.6.6. They are namely;

$t_w \geq ((D_p \sigma_s) / (1{,}25 \times F_y)$ (14.7.4.6-5) and $t_w \geq 20$ mm. (14.7.4.6-6)

Where;

D_p = Internal diameter of pot bearing (mm)

σ_s = Average compressive stress due to total service load combinations (MPa)

F_y = Steel yield strength (MPa)

- **Pot base thickness**

As stated in the code AASHTO LRFD Bridge Design Specifications part 14.7.4.6, the minimum value for the pot base thickness, t_b, should be greater than 20 millimeters or the value of six percent of the internal diameter of the pot bearing, D_p :

$t_b \geq 0{,}06 \times D_p$ (14.7.4.6-1) and

$t_b \geq 20$ mm. (14.7.4.6-2)

Where;

D_p : Internal diameter of pot bearing (mm)

- **Pot wall free height (Height from top of the rim to underside of the piston)**

In part 14.7.4.7 of the code AASHTO LRFD Bridge Design Specifications, the limitations for the pot wall free height, h_{wf}, are specified. There are three different cases to check for the suitability of the free height of the pot wall:

- $h_{wf} \geq (1,5 \times H_u) / (D_p \times F_y)$ (14.7.4.7-2)
- $h_{wf} \geq 3$ mm. (14.7.4.7-3) and
- $h_{wf} \geq 0,03D_p$ (14.7.4.7-4)

Where;

h_{wf} : Pot wall free height (mm)

H_u : Lateral load (N) from applicable strength and extreme load combinations in Table 3.4.1-1 of AASHTO LRFD Bridge Design Specifications

D_p : Internal diameter of pot bearing (mm)

F_y : Yield strength of steel (MPa)

- **Pot cavity**

The cavity depth for the pot bearing is stated in part 14.7.4.3 of AASHTO LRFD Bridge Design Specifications as:

$h_{p1} \geq (0,5D_p\theta_u) + h_r + h_{wf}$ (C14.7.4.3-1)

Where;

D_p : Internal diameter of pot bearing (mm)

θ_u : Design rotation angle (rad)

h_r : Height of the elastomeric disc of a pot bearing (mm)

h_{wf} : Pot wall free height = Height from top of the rim to underside of the piston (mm)

- **Clear space between the top of pot wall and top of the piston**

The clear space in the vertical direction between the top of the wall and the top of the piston can be calculated according to the formula (C14.7.4.3-2) in the part 14.7.4.3 of AASHTO LRFD Bridge Design Specifications: $h_{p2} \geq (R_o\theta_u) - 2\delta_{ufl} - 3$ (14.7.4.3-2)

Where;

R_o : Radial distance from the center of the pot to object in question (e.g., pot wall, anchor bolt, etc.) (mm)

θ_u : Design rotation angle (rad)

δ_{vfl} : Vertical deflection due to factored load (mm)

R_o = radial distance from the center of the pot to object in question (e.g., pot wall, anchor bolt, etc.) (mm)

- **Clear space between the outer face of the piston rim and the outer wall of the pot**

The piston should have a diameter less than the inside diameter of the pot. The clear space between them, C_p, should satisfy the two specifications:

- $C_p \geq 0{,}5$ mm. and
- $C_p = \theta_u \text{ x } (h_{wf} – (D_p \text{ x } \theta_u) / 2)$ (14.7.4.7-5)

Where;

C_p : The clearance distance of the pot wall (mm)

θ_u : Design rotation angle (rad)

h_{wf} : Pot wall free height = Height from top of the rim to underside of the piston (mm)

D_p : Internal diameter of pot bearing (mm)

- **The Total height of the bearing**

The total height of the pot bearing is calculated by simply adding the base thickness (two times), pot cavity, clear distance between the pot wall and the top plate, thickness of anchorage plate (two times) and the thickness of the polytetrafluoroethylene layer:

$h_{total,p} = 2 \times t_b + h_{p1} + h_{p2} + 2 \times t_{ap} \times t_b + t_{ptfe}$

Where;

t_b : Thickness of base of a pot bearing (mm)

h_{p1} : Pot cavity (mm)

h_{p2} : Clear distance between pot wall and top plate (mm)

t_{ap} : Thickness of anchorage plate (mm)

t_{ptfe} : Thickness of the polytetrafluoroethylene layer (mm)

In order to introduce the pot bearings as link elements to the structural analysis software, Sap2000 v.14.2.2; spring stiffness coefficients of the elastomeric disc are used. They are gathered via the same procedure used for elastomeric bearings as shown in section 3.2.1.2.2 of this study.

CHAPTER 4

STRUCTURAL MODEL AND FINITE ELEMENT ANALYSIS

4.1. Analysis Method Followed

For this study, analytical models are formed by the help of the software Sap2000 v14.2.2. Frame elements, link elements, joints, and restraints are used for composing the structural analysis model of the bridge. As mentioned in section 2, all earthquake ground motions used in this study belong to real earthquake records. They are all applied to the structure as time history functions. That functions formed the acceleration load functions as inputs of linear direct integration time history method. All data were manually checked and it is understood that the first 30 seconds of all the data includes the peaks and the effective durations. Therefore, 1500 time steps are taken into account with a step size of 0,02 seconds. It means the portions of ground motion records including the time from 0 to 30 seconds are considered in this study. Sample load case information is given in Figure 4.1 and Figure 4.2.

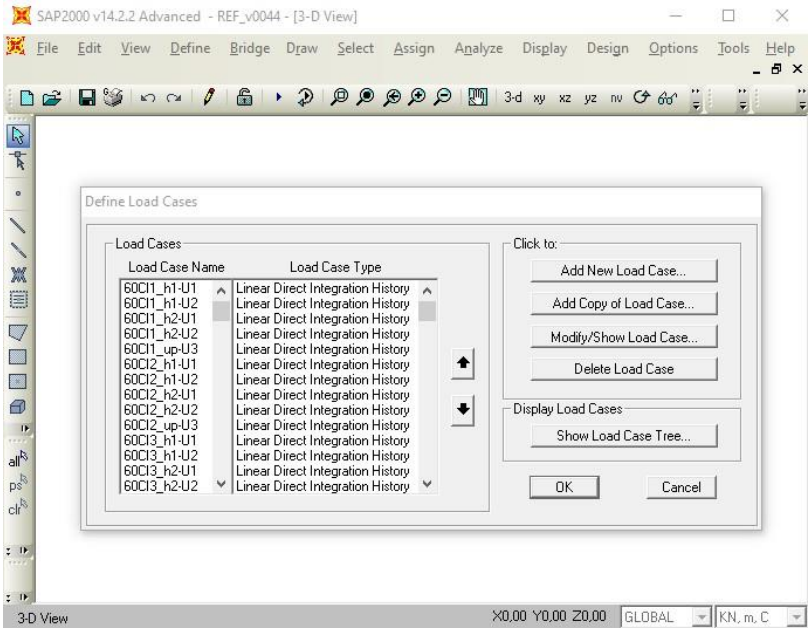

Figure 4.1. Load Cases Defined

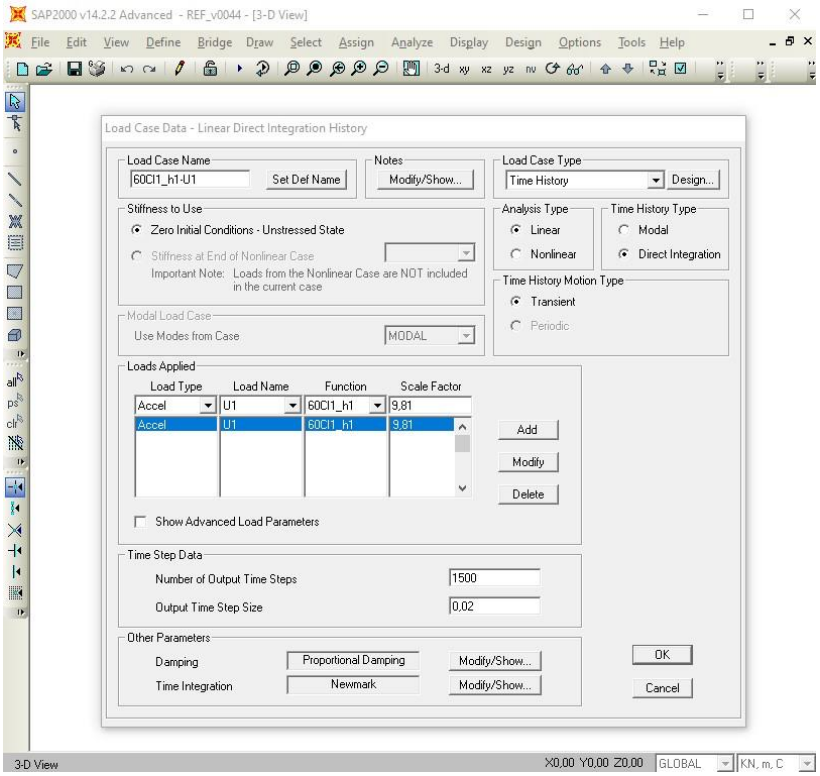

Figure 4.2. Sample Load Case Defined

4.2. Analysis Cases

With this study, elastomeric and pot bearings used in bridges over high-speed railways will be compared under various earthquake effects. For this purpose, initially, 3 different models of the selected bridge for each analysis cases were formed.

Case 1 is the reference case. The bridge in case 1 has two elastomeric bearings under each precast I girder (One elastomeric bearing for each end). Totally, twenty elastomeric bearings are utilized in each span. It is chosen as the "Reference Analysis Case (EBC10-REF) since it is the most widely used design case for bridges in Turkey and in many other countries. The number "10" in the abbreviated name stands for the number of elastomeric bearings used for one end of each span.

The bridge formed for case 2 has three elastomeric bearings under the cross beam for 10 precast I girders in one end. Totally six elastomeric bearings are utilized for ten girders in one span. The name "Elastomeric Bearing Case (EBC-3)" was given to the second analysis case. The number "3" in the abbreviated name stands for the number of elastomeric beams used for one end of each span.

Case 3 has the name of "Pot Bearing Case (PBC-3). It has the same number of bearings as used in case 2. The idea of locating the bearings is also the same. Totally six pot bearings are used for ten girders in each span under the crossbeam. The number "3" in the abbreviated name stands for the number of pot bearings used for one end of each span as done for the other two analysis cases.

Specific properties of structural models including bearing formation, assignment of bearing and frame element numbers, etc. are given below for each case.

4.2.1. Case 1: Reference Analysis Case, EBC10-REF, Elastomeric Bearings under Each Beam

In this part of the study, an analytic model of the bridge for case 1; namely Reference Analysis Case (EBC10-REF), was formed and analyzed in Sap2000 v14.2.2 software.

4.2.1.1. Analytical Model for Structural Analysis

In Figure 4.3, a closer look to the bearings and in Figure 4.4, the analytical model for structural analysis of the bridge composed for this case are given. Frame elements are used for piers, girders, crossbeams, cap beams and abutments; link elements are introduced for bearings. Elastomeric bearings are used in this analysis case. Properties of the link elements (stiffness coefficients, fixity, etc.) used for introducing the bearings to the software are given in Figures 4.5 and 4.6.

While introducing bearings as link elements to the software, arbitrary numbers are assigned to the link elements. These assigned numbers of bearings are given in Figure 4.7. The case for frame elements is also the same; the assigned numbers of frames are also given in Figure 4.8.

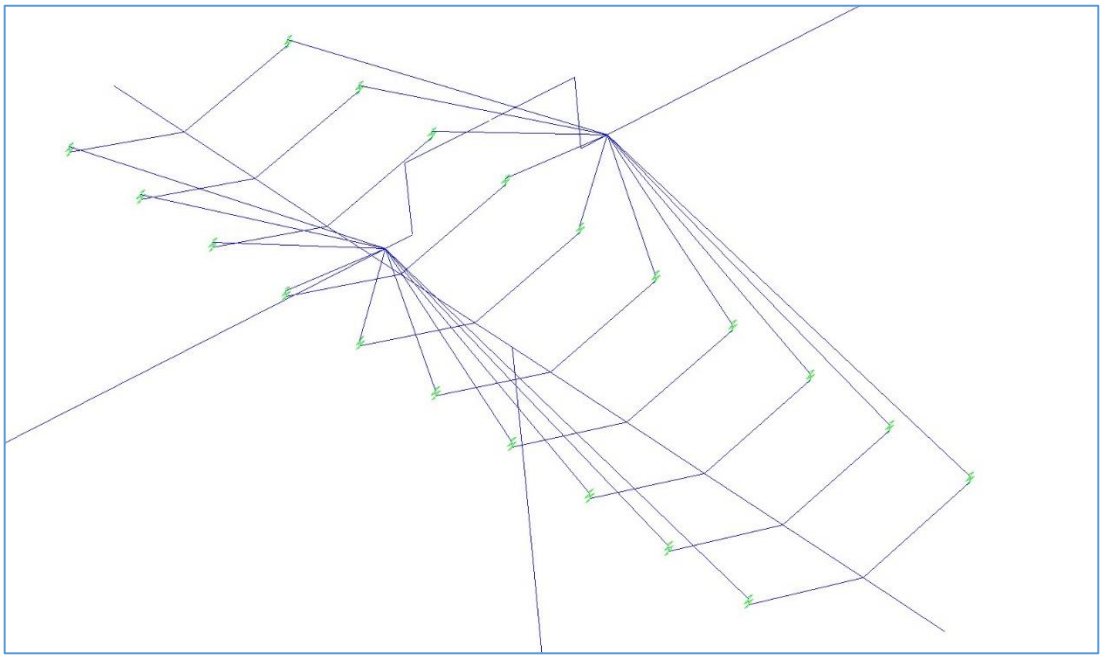

Figure 4.3. Close View of the Bearings for the Analysis Case 1 (EBC10-REF)

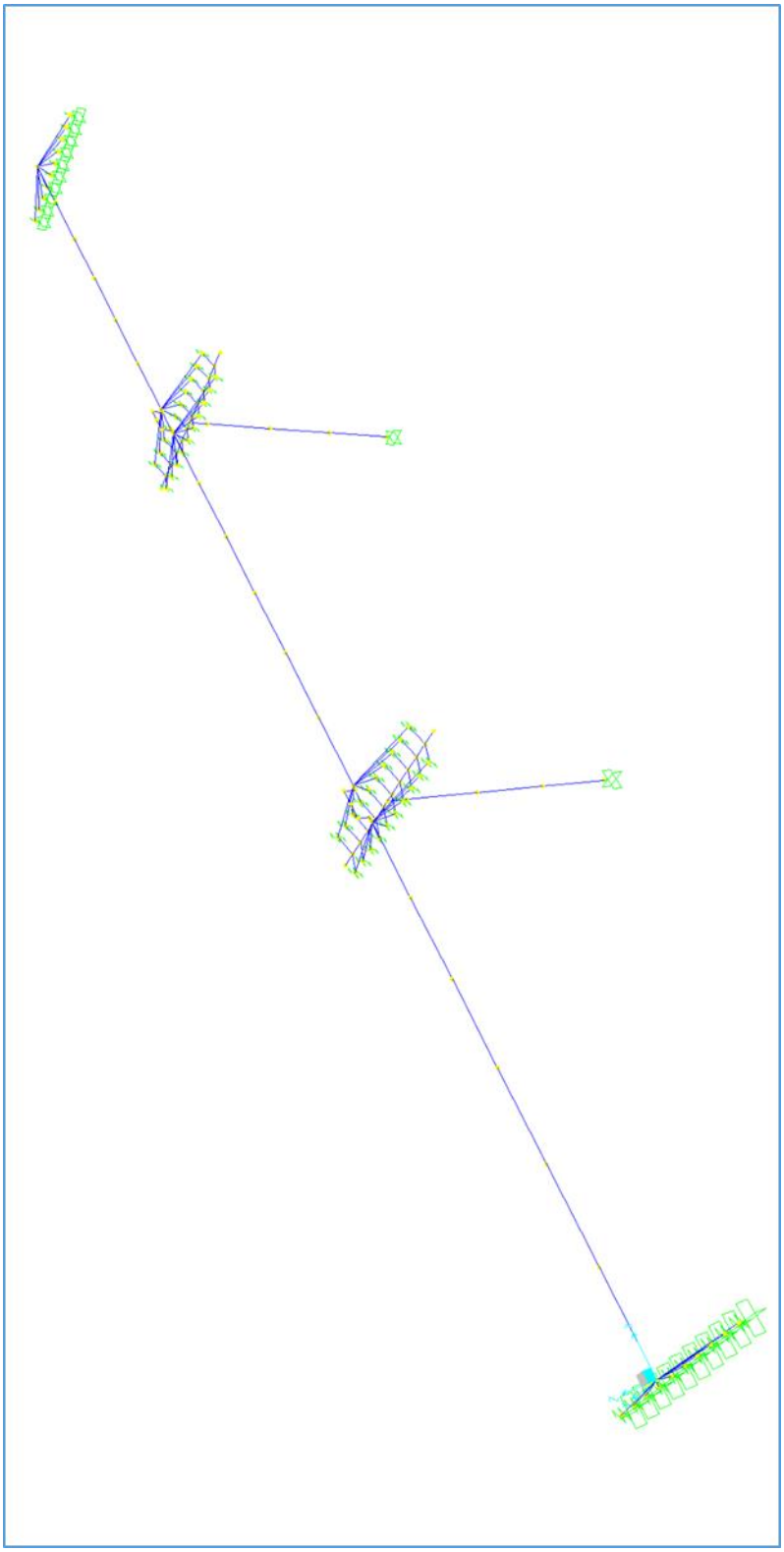

Figure 4.4. General View of Analytical Model of Analysis Case 1 (EBC10-REF)

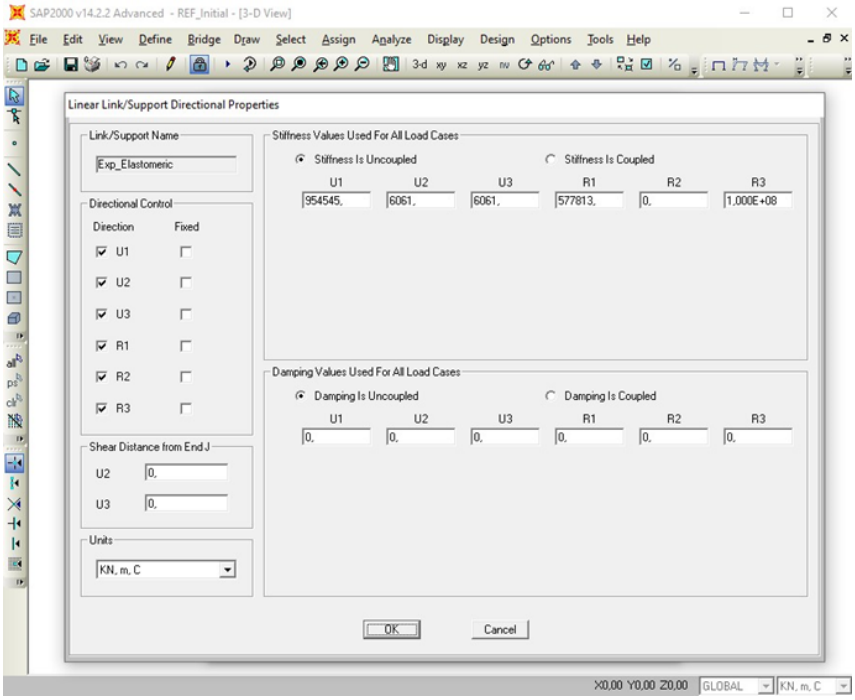

Figure 4.5. Stiffness Properties of Expansion Elastomeric Bearings

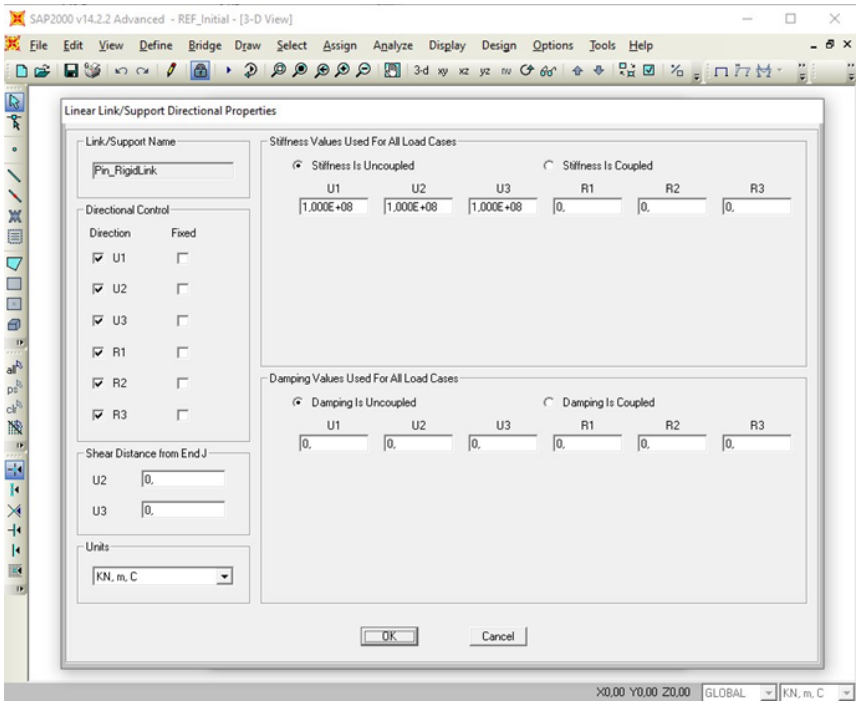

Figure 4.6. Stiffness Properties of Fixed Elastomeric Bearing

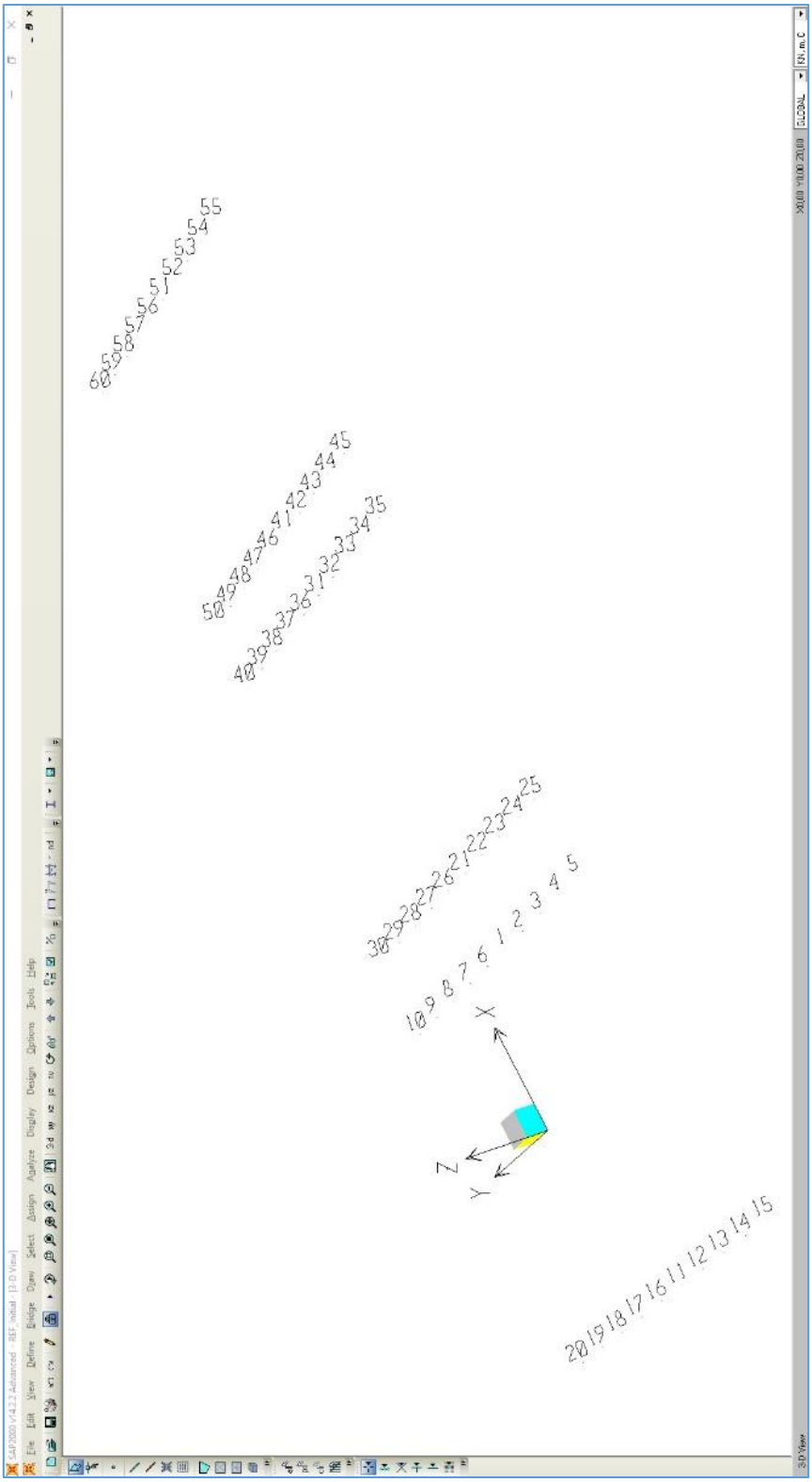

Figure 4.7. Number Assignments of Bearings for the Model of Analysis Case 1 (EBC10-REF)

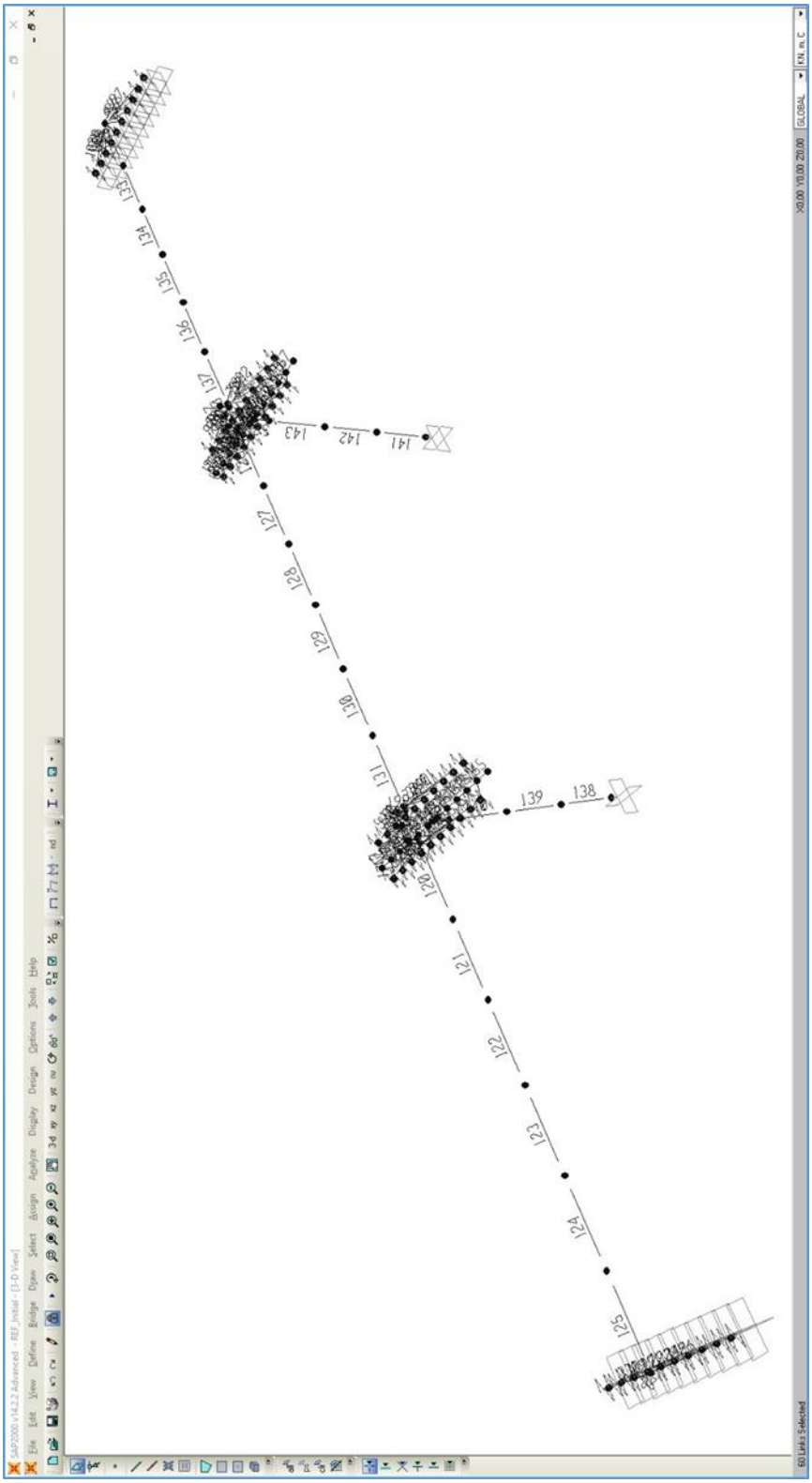

Figure 4.8. Number Assignments of Frames for the Model of Analysis Case 1 (EBC10-REF)

4.2.1.2. Analysis Results

Shape and period of the first mode, relative displacements of bearings, vertical reactions exerted on bearings, column base-end maximum shear and maximum moment reactions of both piers are obtained from the software and shown below as histograms. Histogram type graph is used since there is not any relation or correlation between earthquakes among themselves applied to the structure.

Initially, stiffness properties arising from geometric properties of bearings are assigned to the link elements. When the structural analysis was completed, it was seen that under the effect of three earthquakes, which are 60DI6, 70DI1 and 65DI1, the horizontal displacement exceeded 10 cm. Since the gap between the beam and the cap-beam is 10 centimeters and when the horizontal displacement exceeds 10 centimeters it means that the beam hits the cap beam. In order to limit the horizontal displacement to 10 centimeter, the spring-stiffness coefficient values of bearings just in the longitudinal direction of the bridge were iterated. During the iteration process, it was aimed to limit the horizontal displacement and for staying on the safe side, the iteration process was finalized when the horizontal displacement value reached to a little bit less than 10 centimeters. The characteristics of the iterated structural model and analysis results of the iterated model are provided in sections 4.2.1.3 and 4.2.1.4, respectively.

When presenting the analysis results in this section, it is intentionally done that, horizontal displacements of bearings with the assigned number of 16 is provided. In the iterated case, the horizontal displacement of the bearing with the assigned number of 15 has higher displacement values. Since the difference of the results for bearing-15 and bearing-16 is less enough, results for both of them are provided. When doing the comparison between the results of analysis cases, the maximum results for the bearings are taken into consideration.

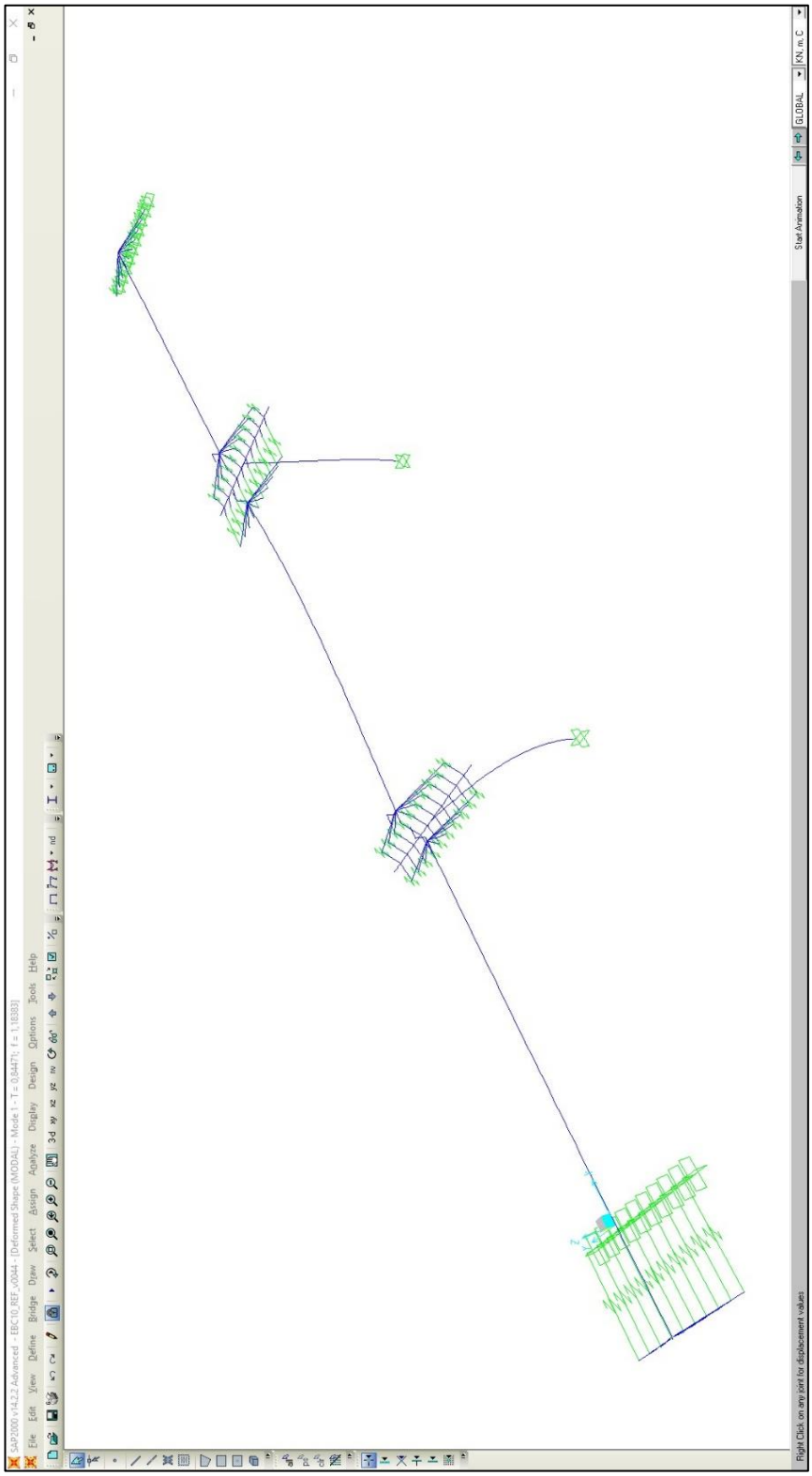

Figure 4.9. Shape and Period (T~=0,84s) of First Mode

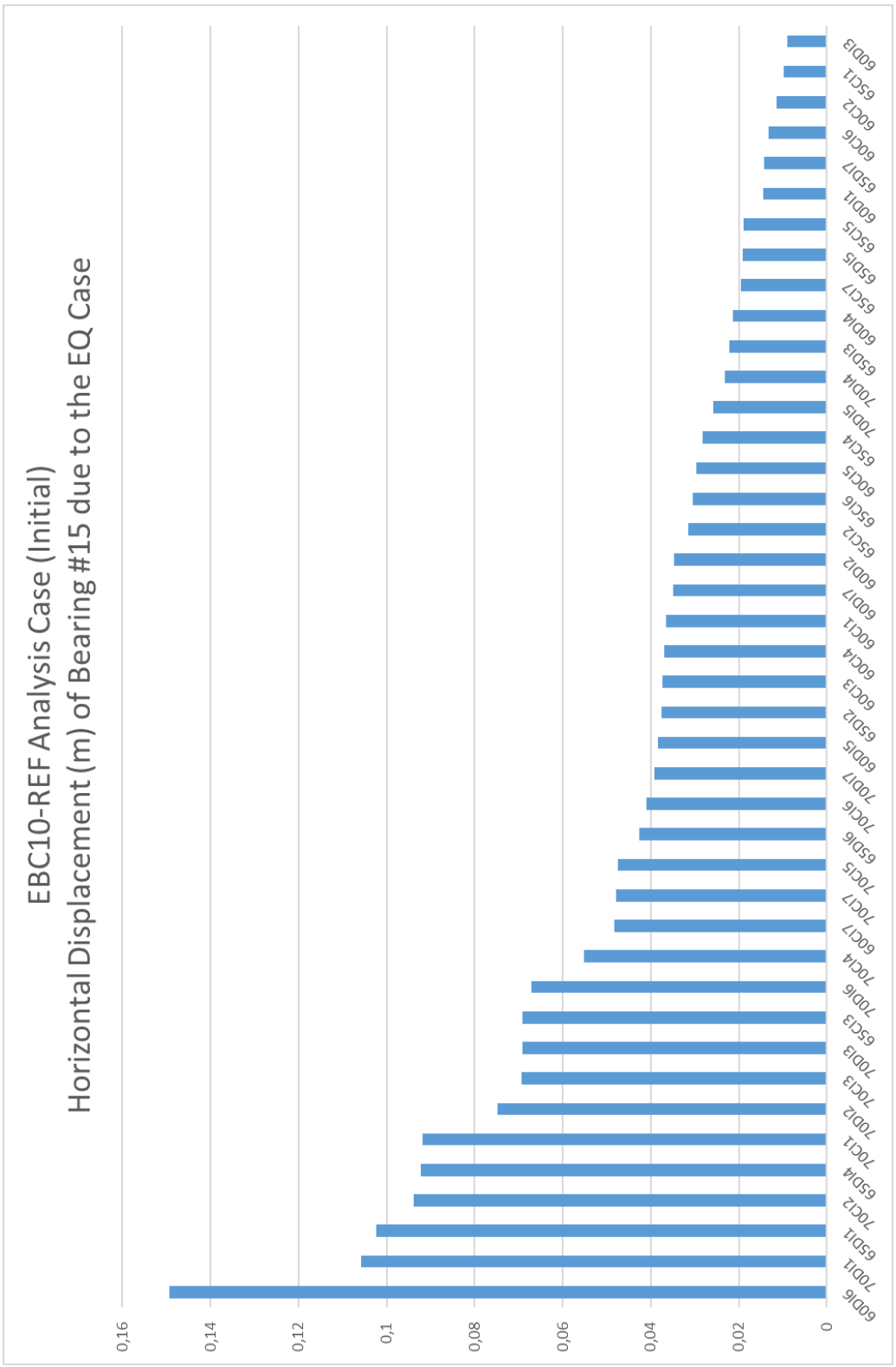

Figure 4.10. Horizontal Displacement (m) of Bearing #15 due to EQ Case

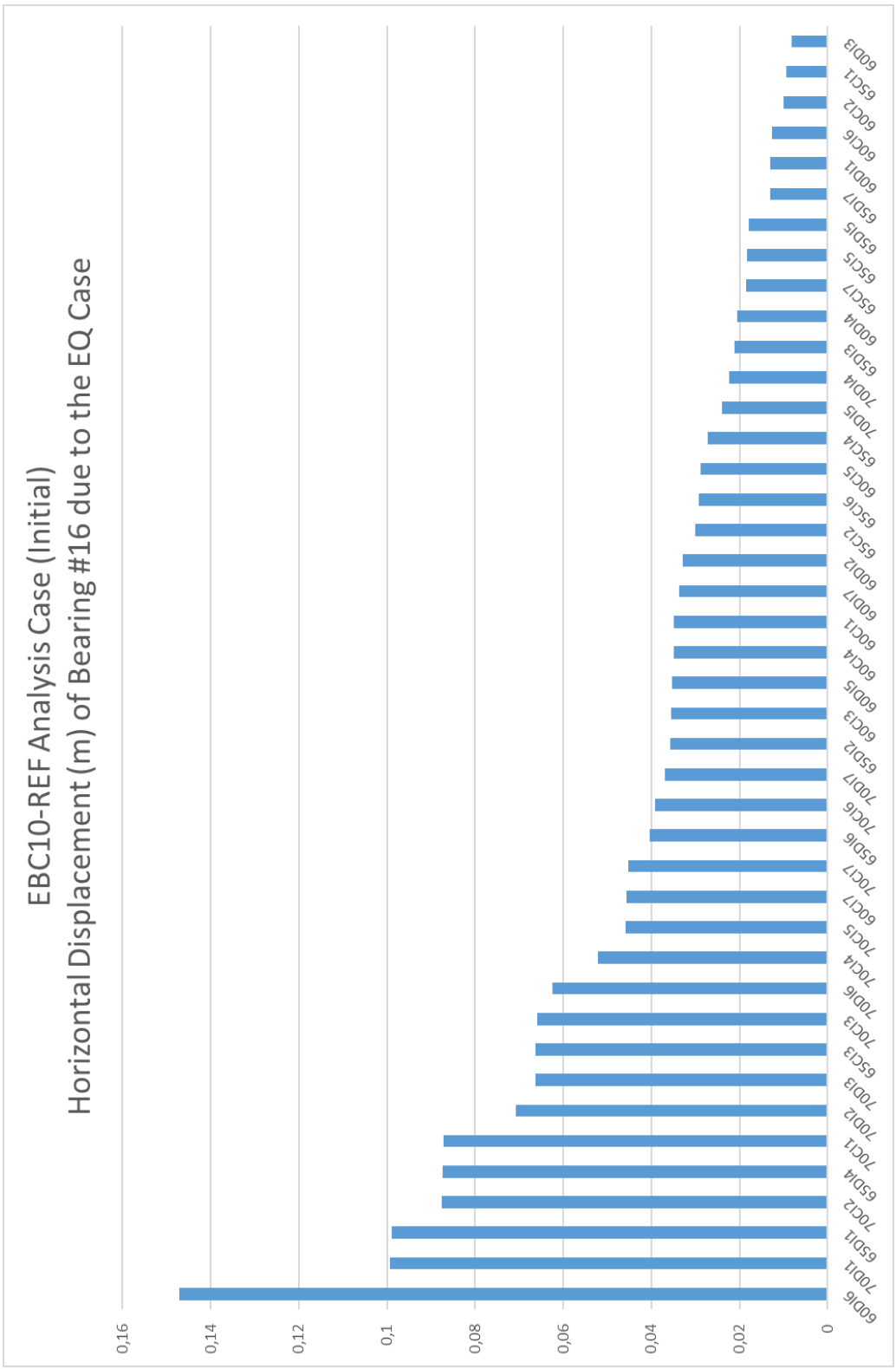

Figure 4.11. Horizontal Displacement (m) of Bearing #16 due to EQ Case

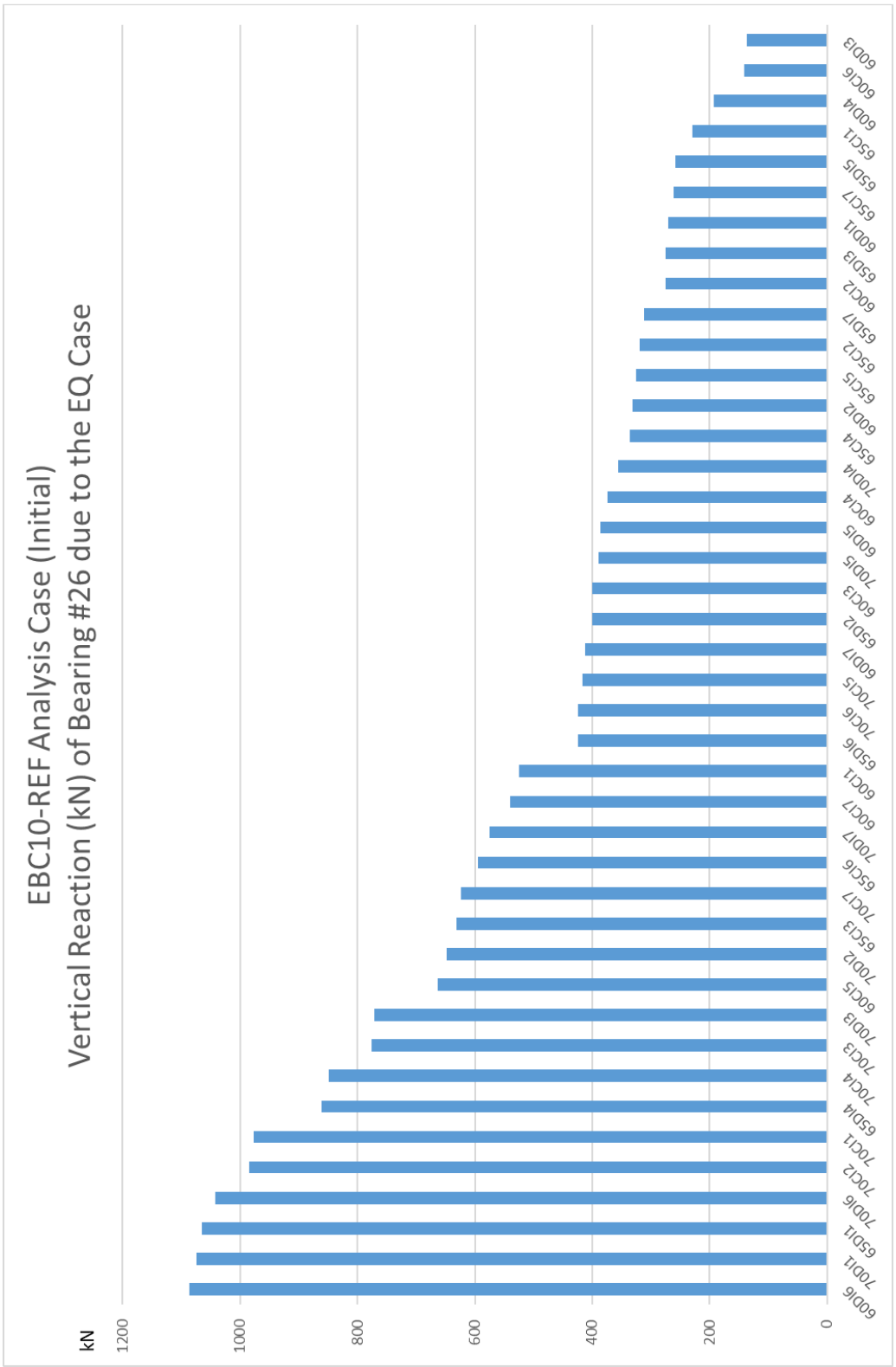

Figure 4.12. Vertical Reaction (kN) of Bearing #26 due to EQ Case

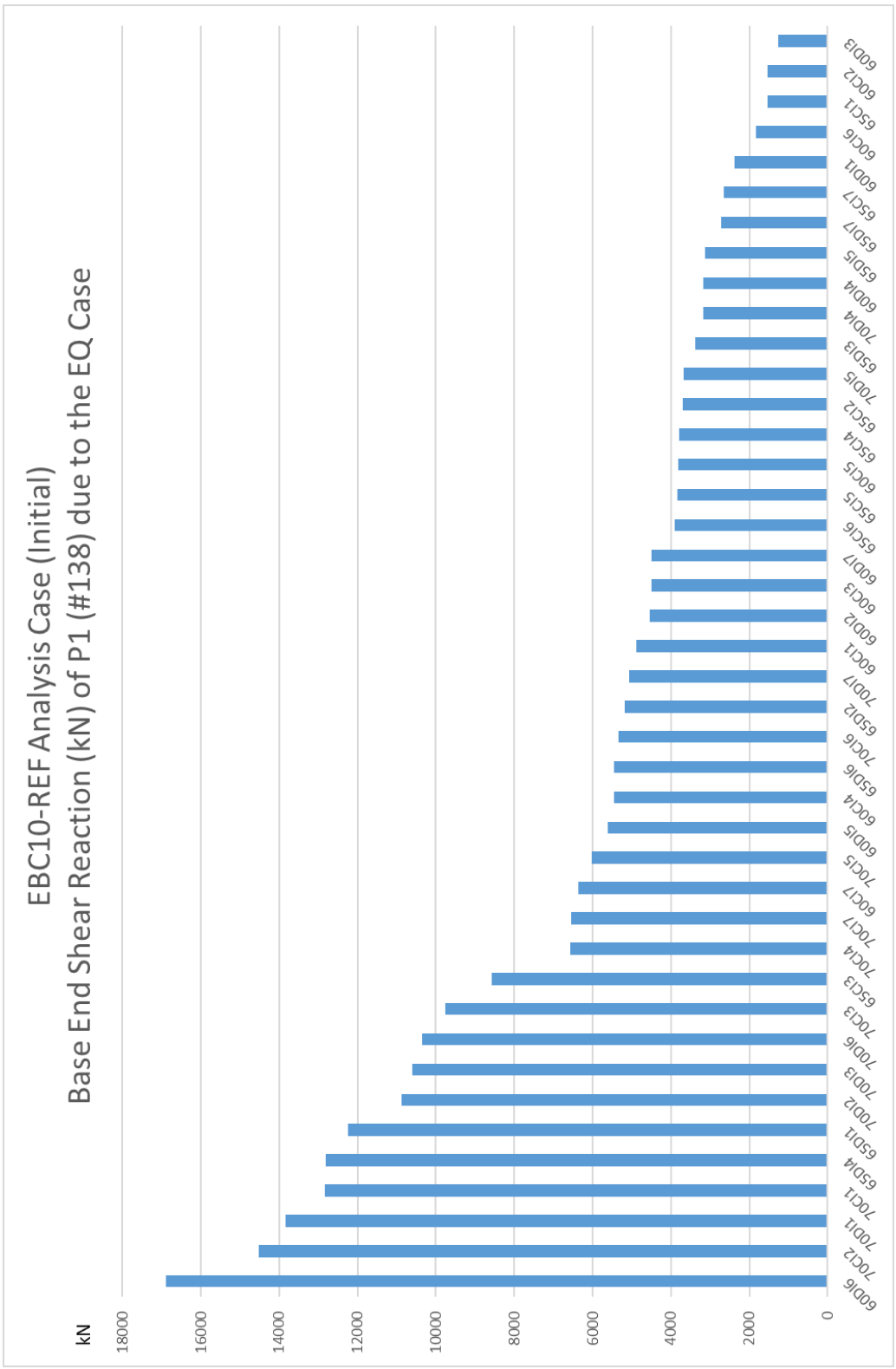

Figure 4.13. Base End Shear Reaction (kN) of P1 (#138) due to EQ Case

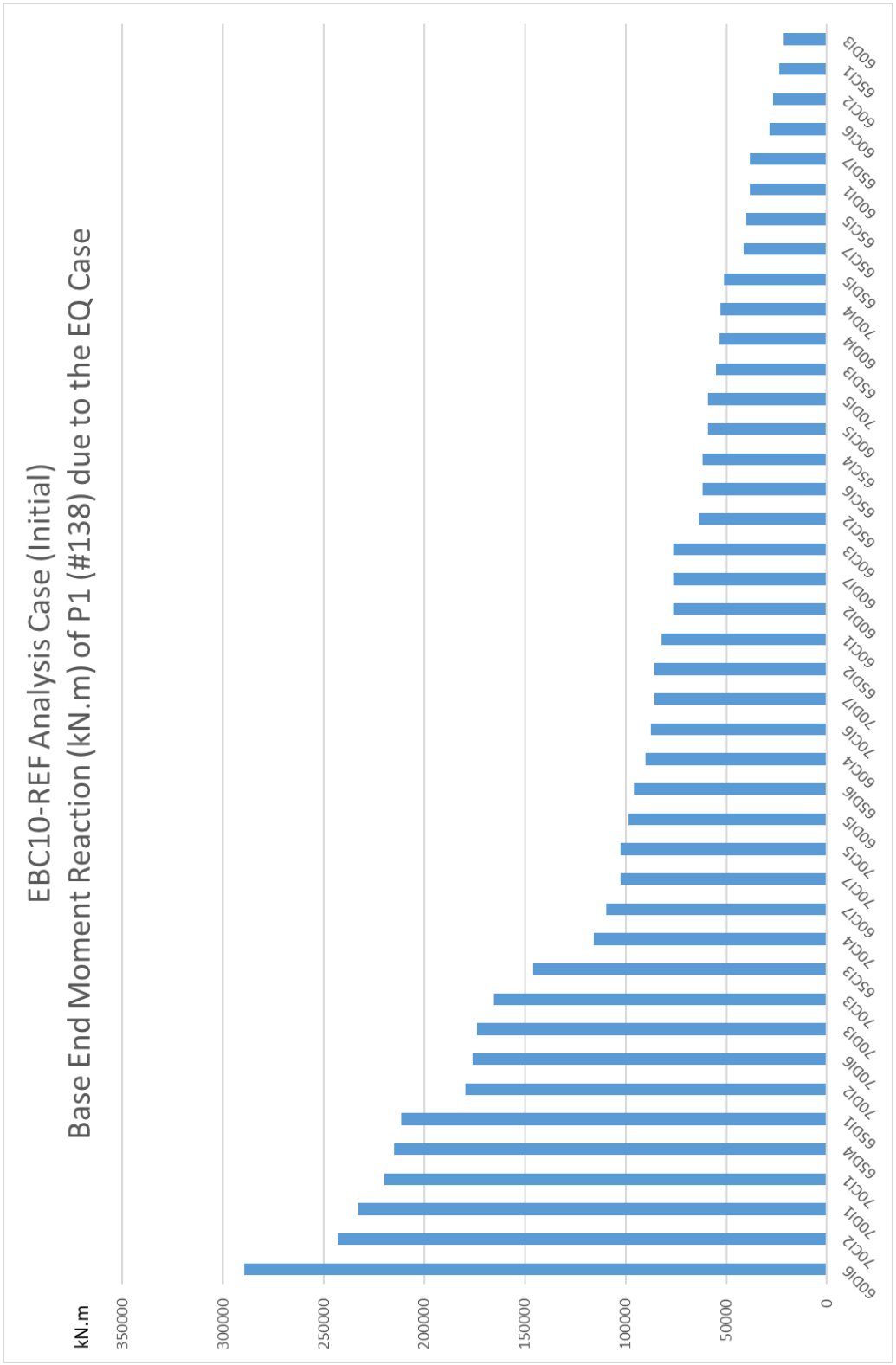

Figure 4.14. Base End Moment Reaction (kN.m) of P1 (#138) due to EQ Case

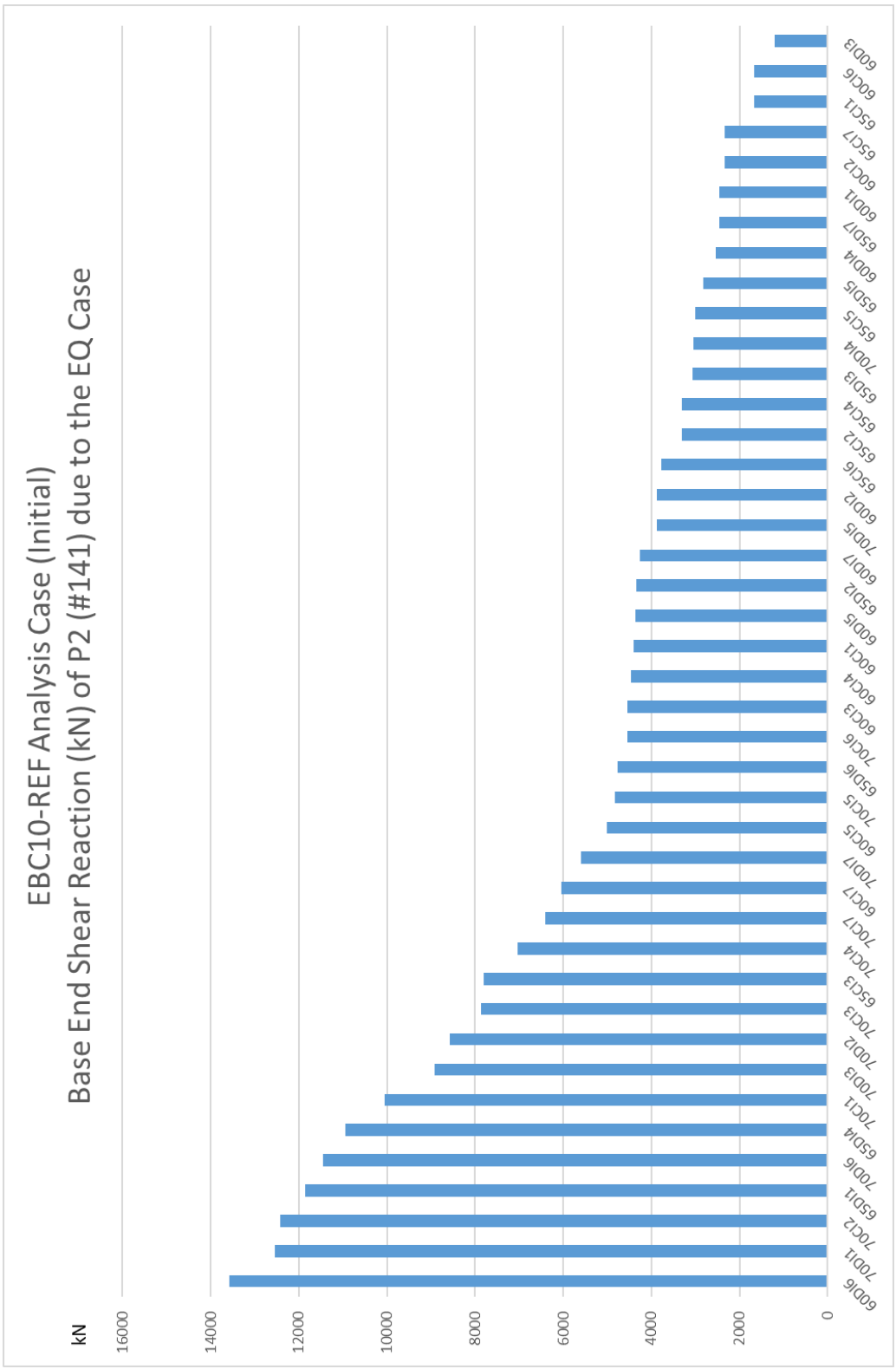

Figure 4.15. Base End Shear Reaction (kN) of P2 (#141) due to EQ Case

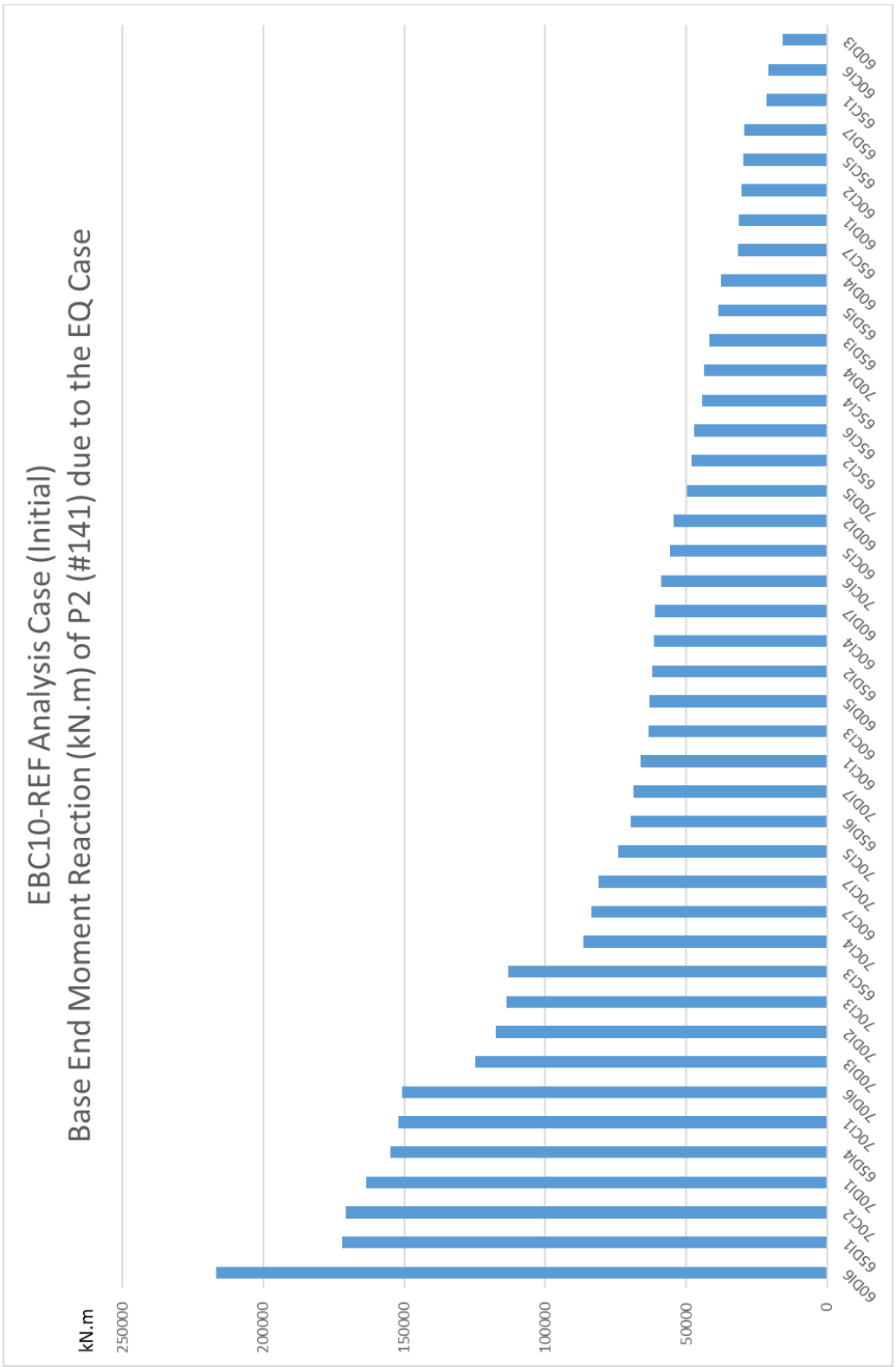

Figure 4.16. Base End Moment Reaction (kN.m) of P2 (#141) due to EQ Case

4.2.1.3. Specific Properties of the Structure (Iterated Stiffness)

As mentioned in section 4.2.1.2, when relative displacements of bearings exceed 10 centimeters; actually it means that beams hit the structure. Thus, it is decided that stiffness values of bearings are iterated by generating some other analytical models to achieve the maximum relative displacement of bearings under any earthquake applied to the bridge within this study.

Final stiffness values of elastomeric bearings standing upon the desired relative displacement limit, which is 10 centimeters, are shown below in Figure 4.17, and Figure 4.18.

Results obtained from the structural analysis of the bridge via using the bearings with specified properties are provided in part 4.2.1.4.

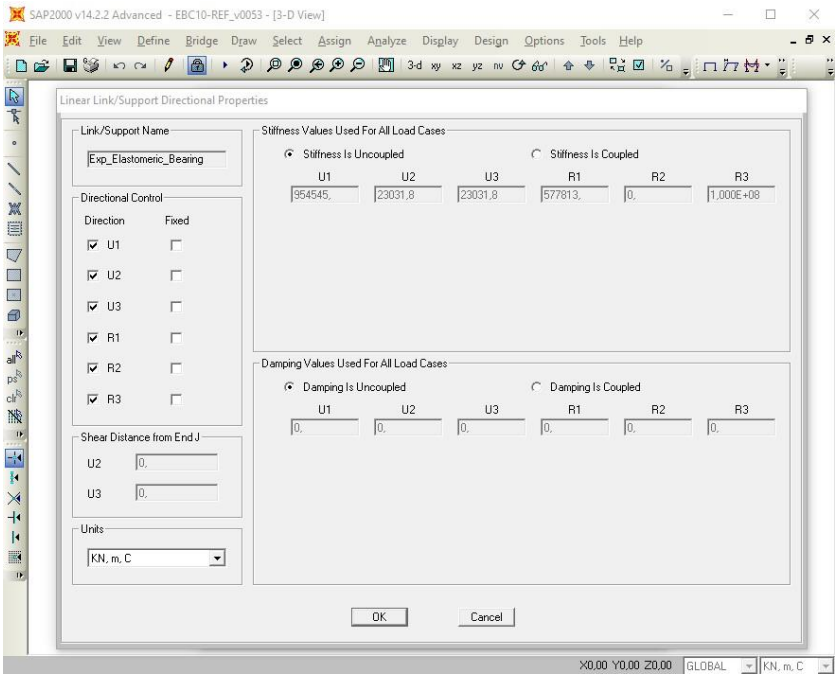

Figure 4.17. Stiffness Properties of Expansion Elastomeric Bearings

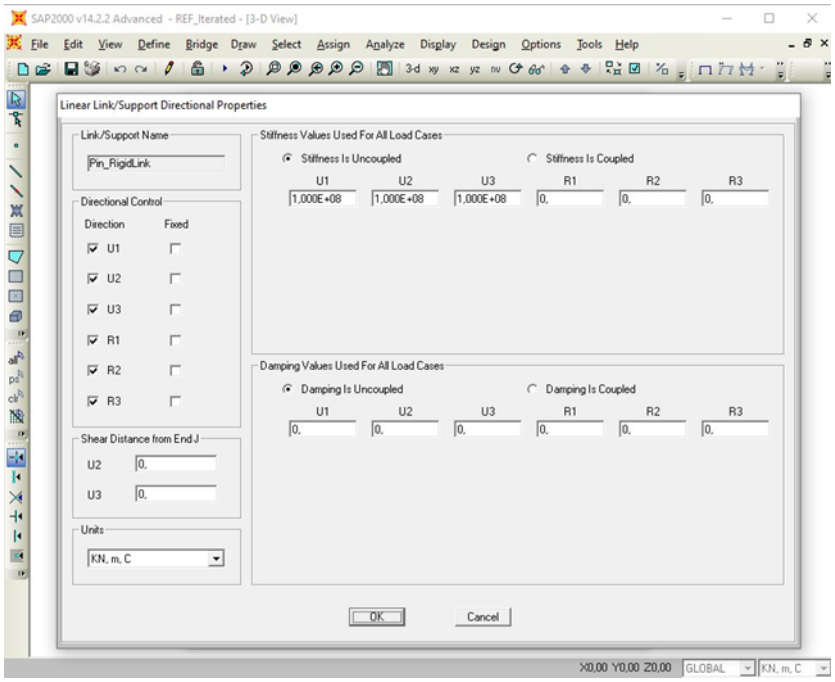

Figure 4.18. Stiffness Properties of Fixed Elastomeric Bearings

4.2.1.4. Analysis Results of the Structure (Iterated Stiffness)

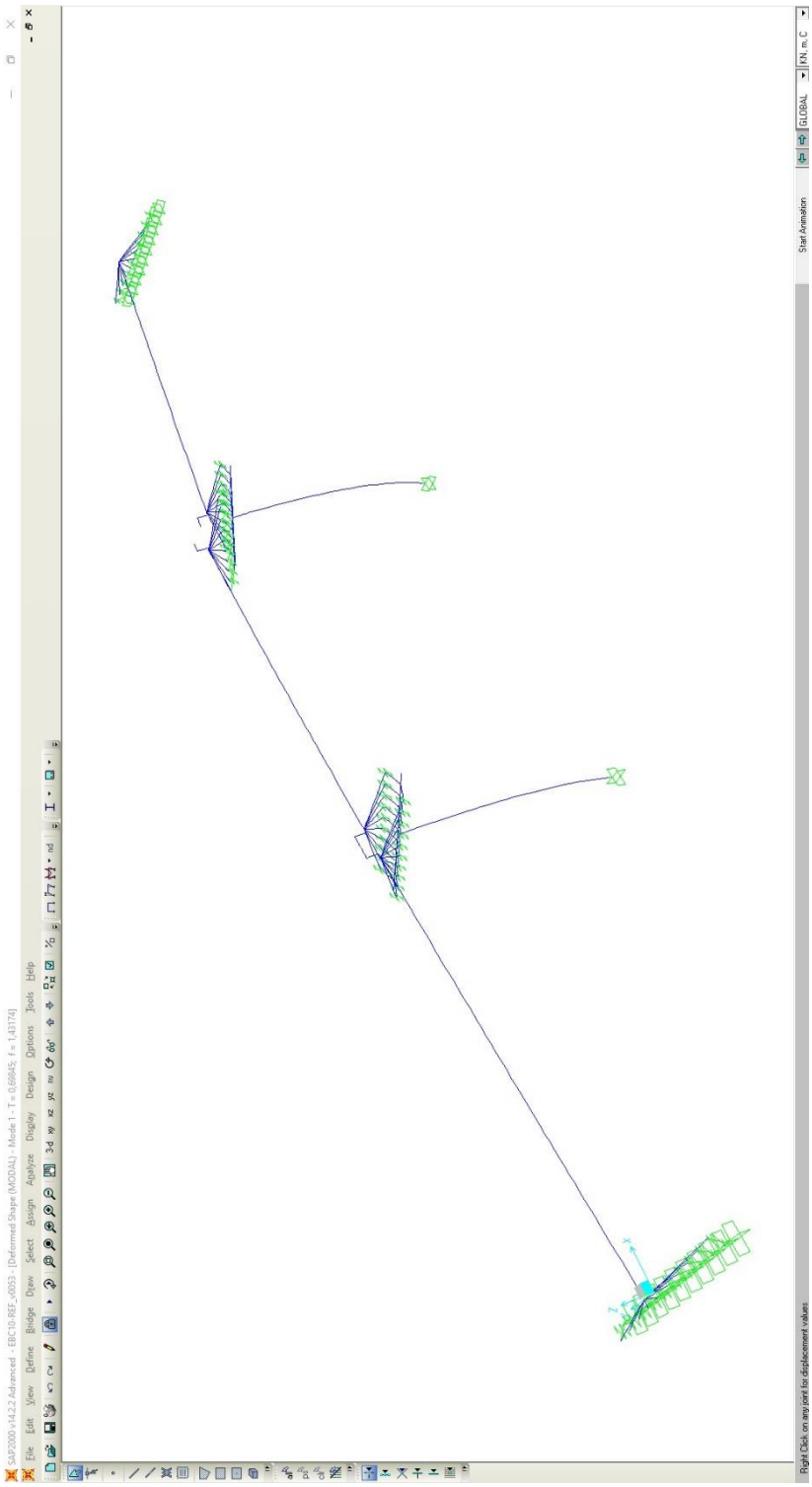

Figure 4.19. Shape and Period (T~=0,70s) of First Mode

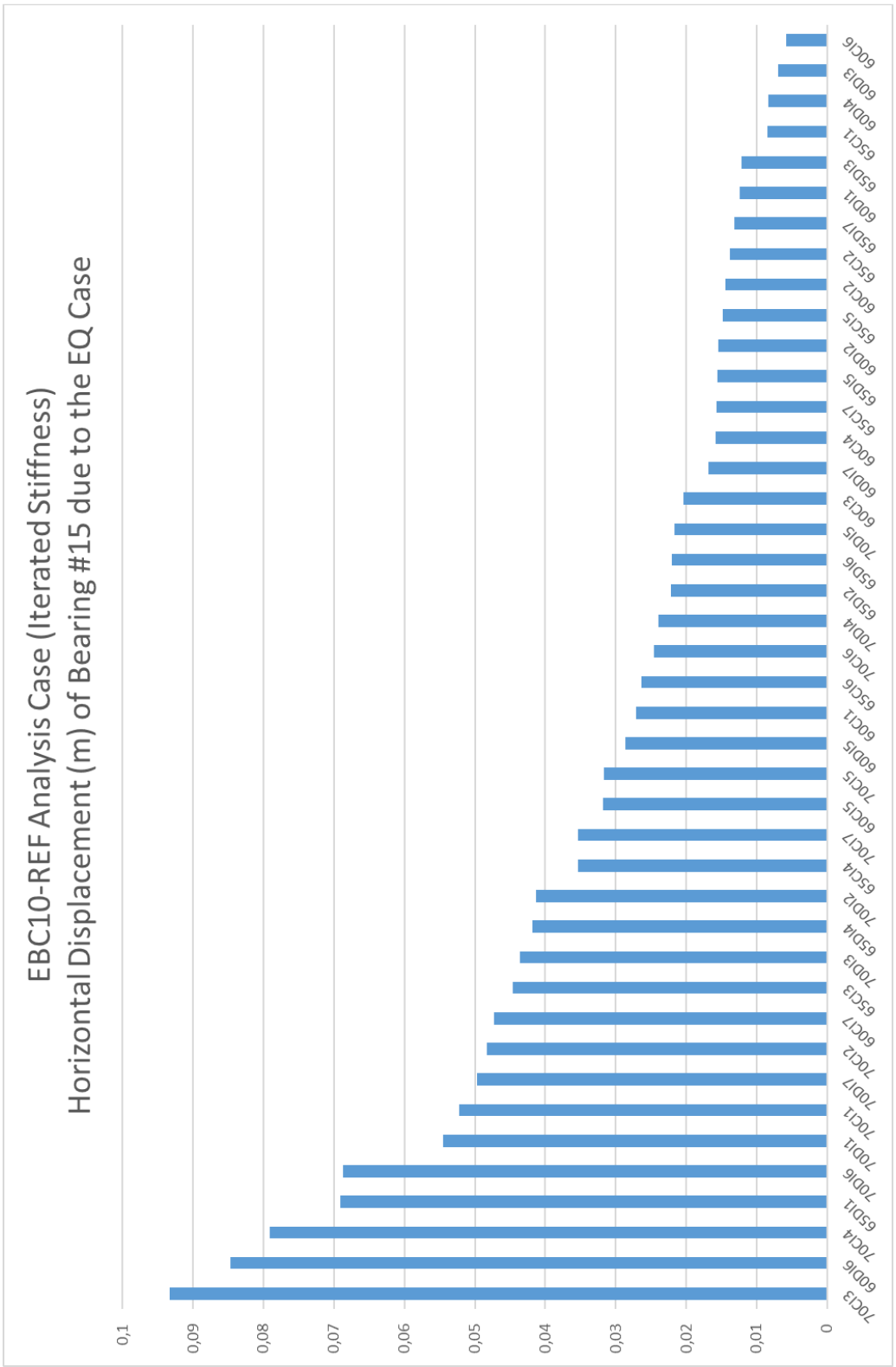

Figure 4.20. Horizontal Displacement (m) of Bearing #15 due to EQ Case (with iterated stiffness)

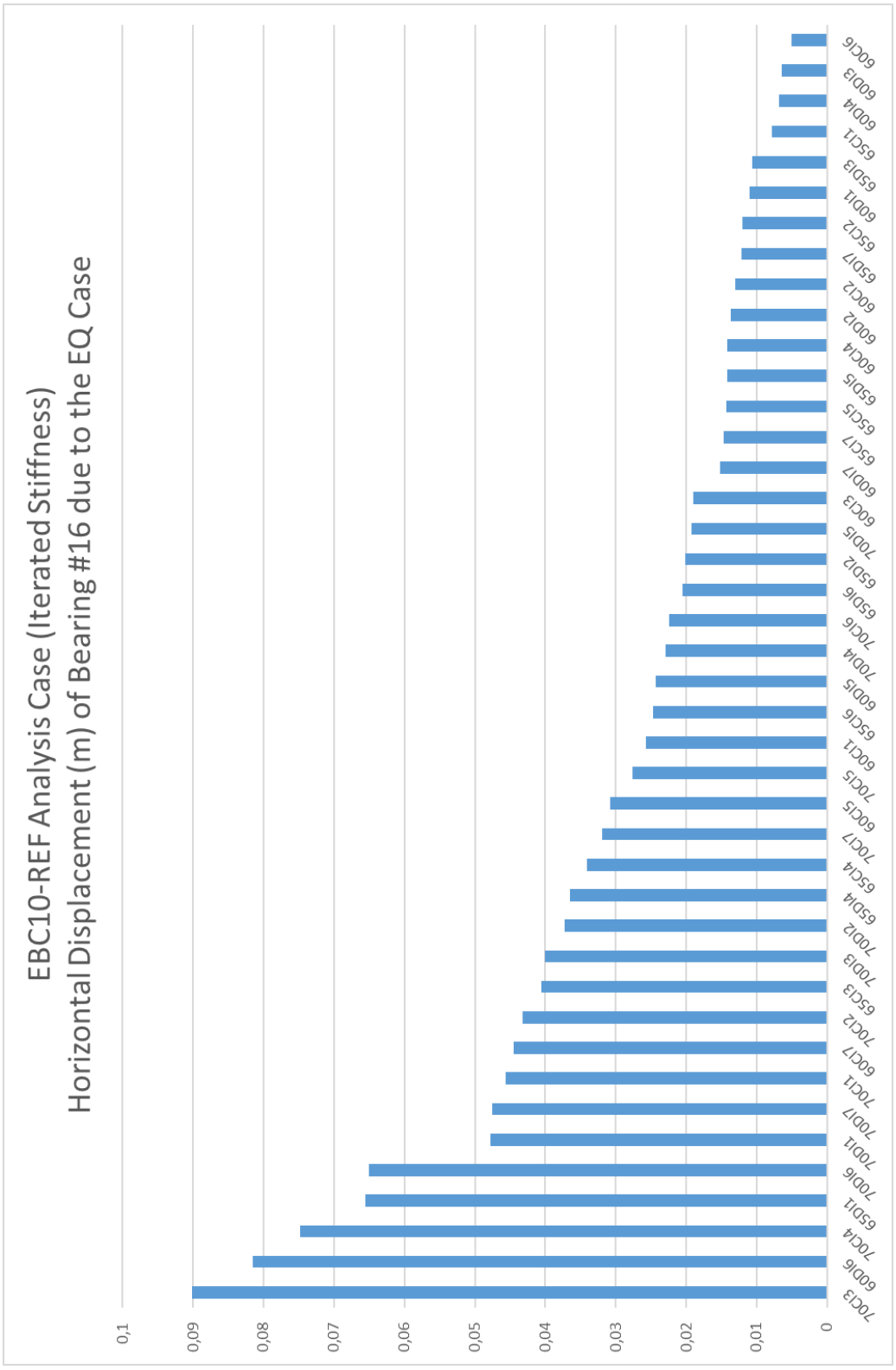

Figure 4.21. Horizontal Displacement (m) of Bearing #16 due to EQ Case (with iterated stiffness)

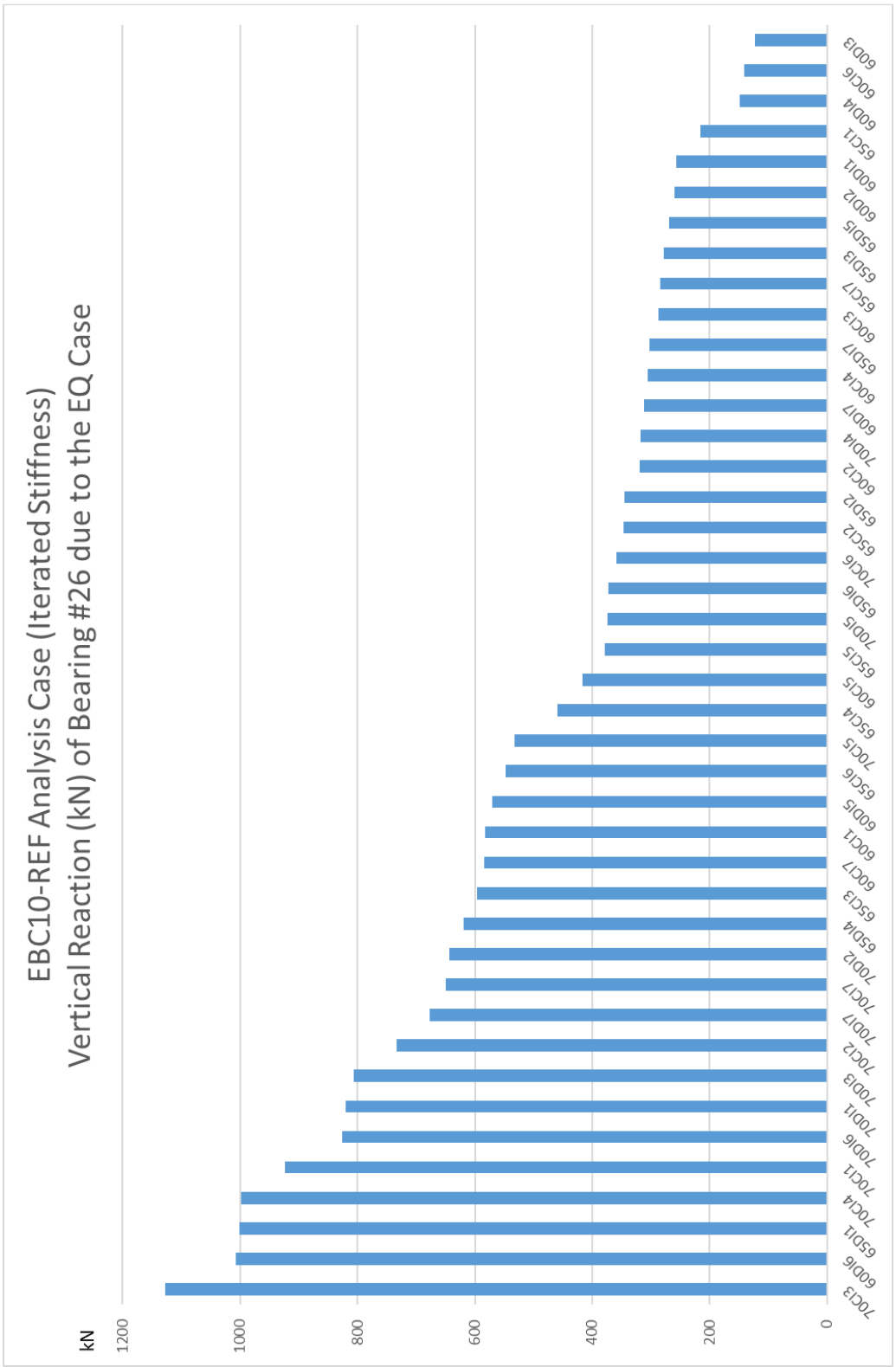

Figure 4.22. Vertical Reaction (kN) of Bearing #26 due to EQ Case (with iterated stiffness)

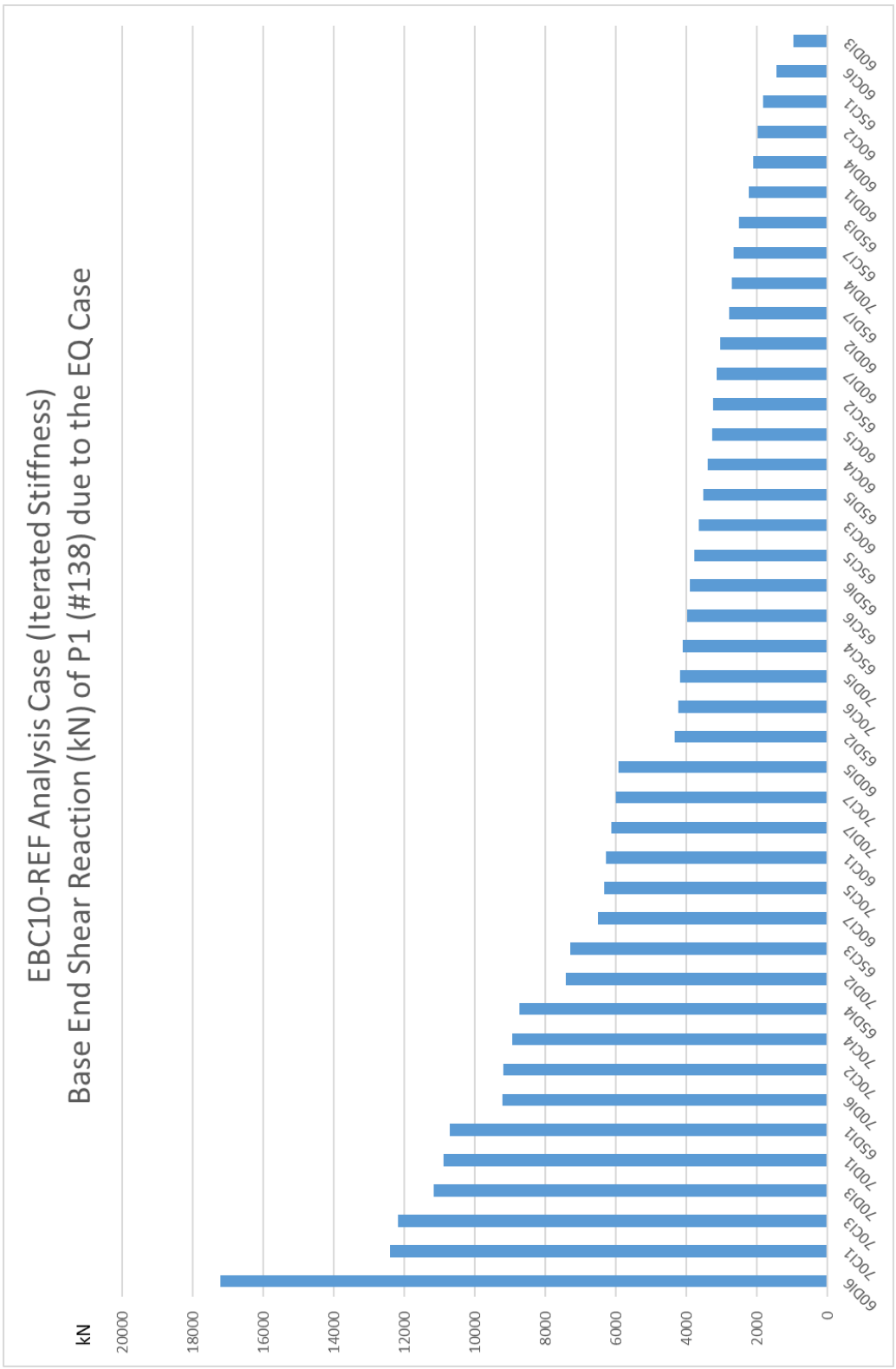

Figure 4.23. Base End Shear Reaction (kN) of P1 (#138) due to EQ Case (with iterated stiffness)

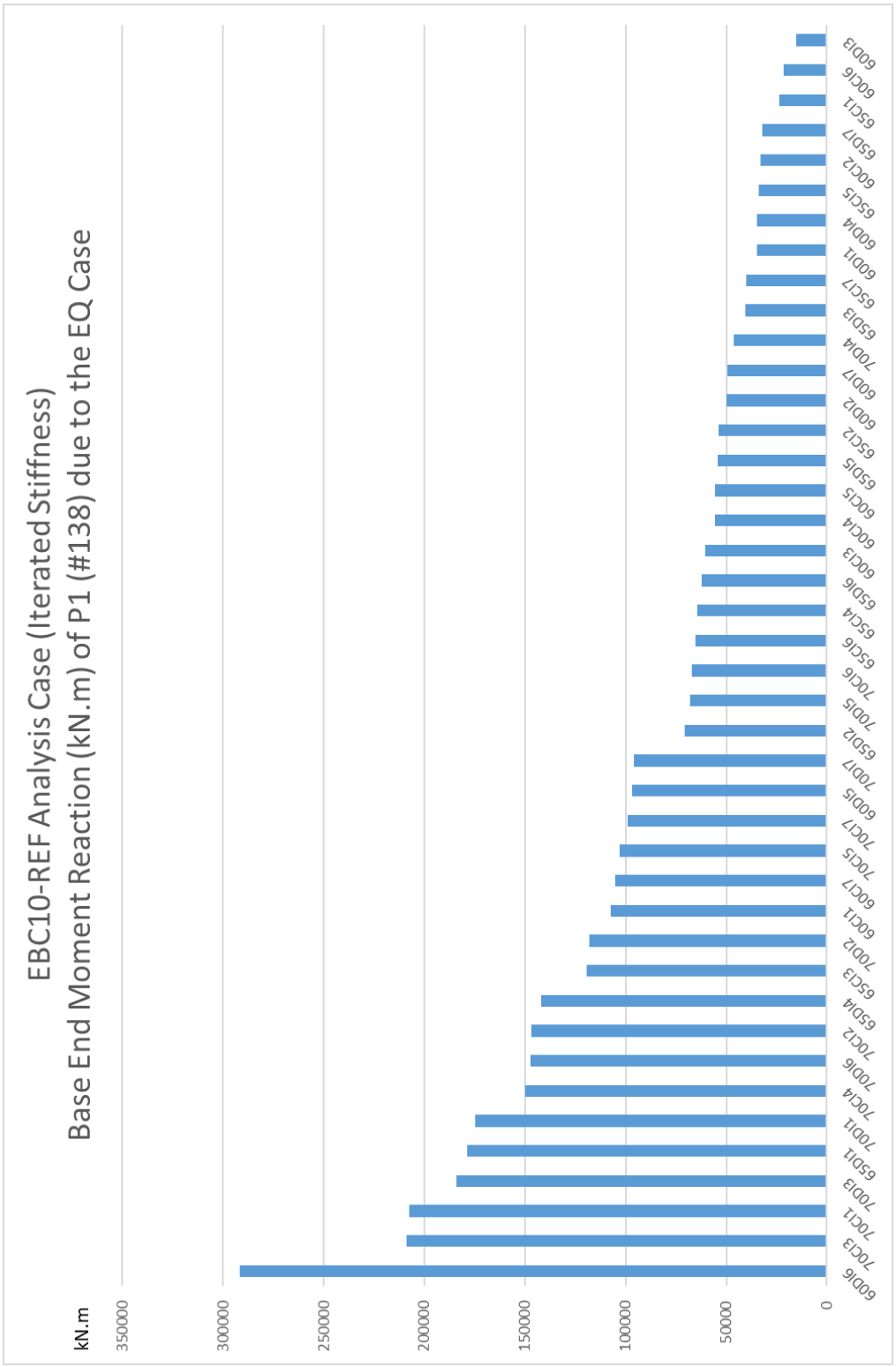

Figure 4.24. Base End Moment Reaction (kN.m) of P1 (#138) due to EQ Case (with iterated stiffness)

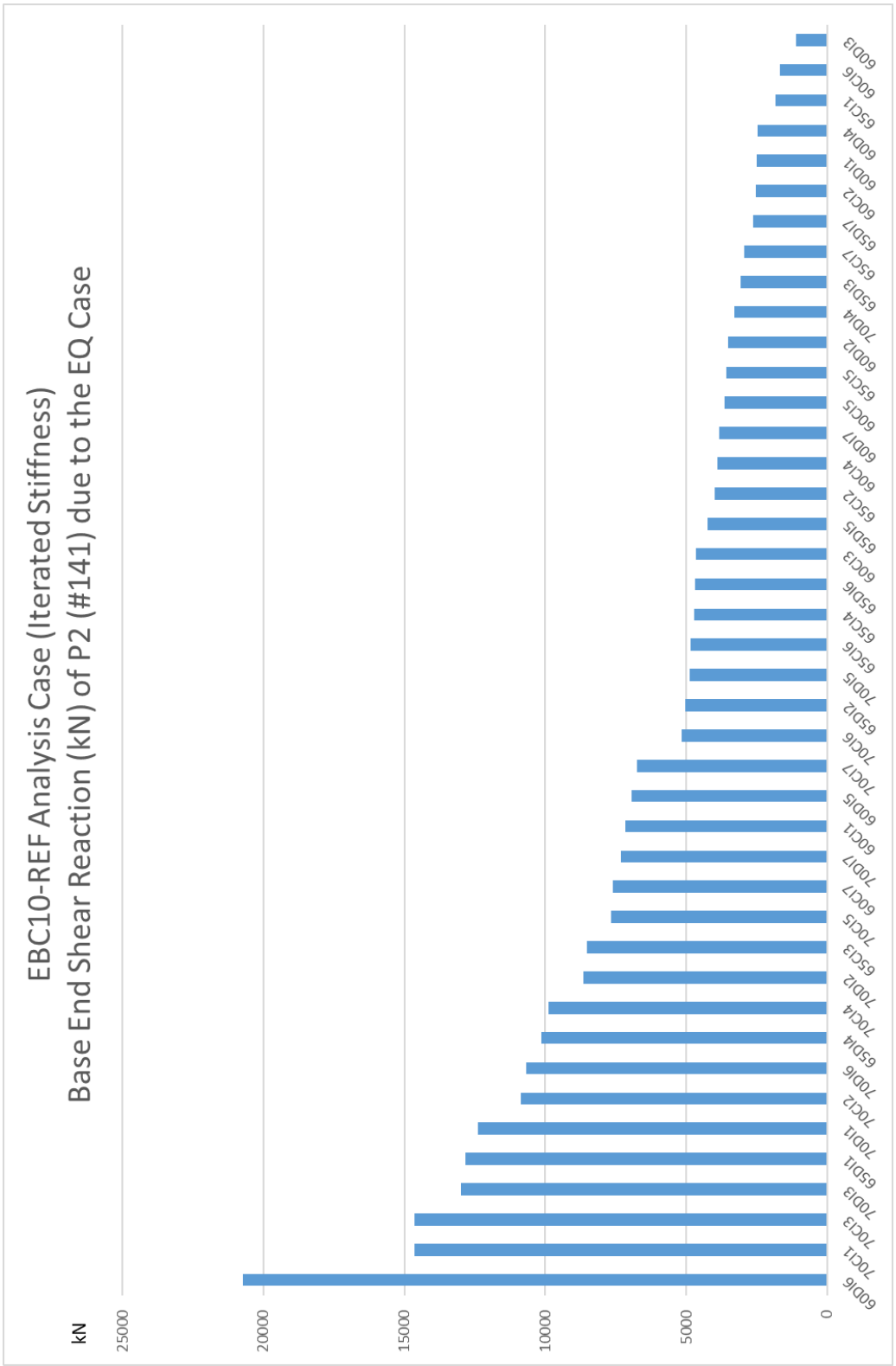

Figure 4.25. Base End Shear Reaction (kN) of P2 (#141) due to EQ Case (with iterated stiffness)

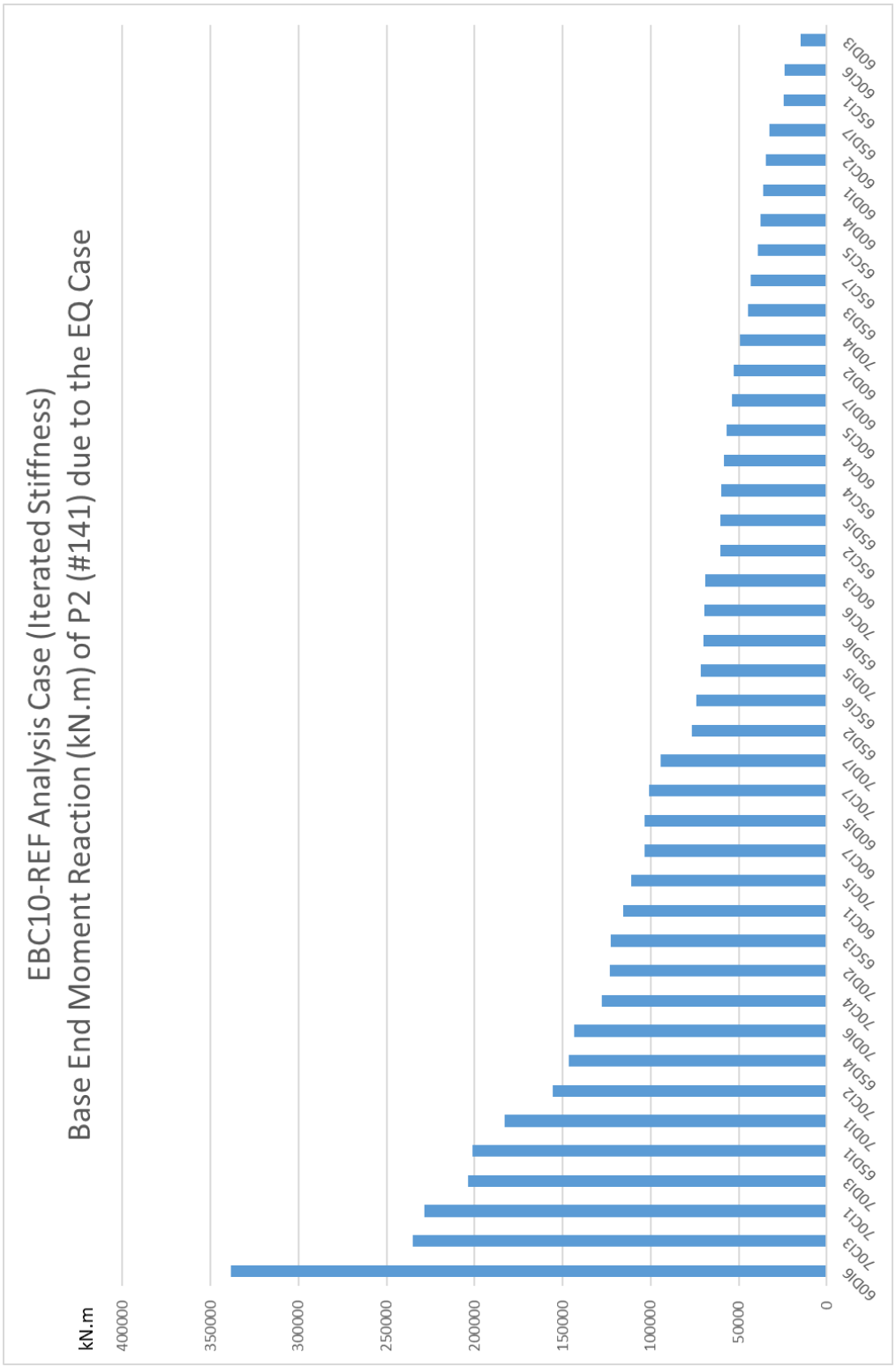

Figure 4.26. Base End Moment Reaction (kN.m) of P2 (#141) due to EQ Case (with iterated stiffness)

4.2.2. Case 2: Elastomeric Bearing Case, EBC-3, Limited Amount of (3) Elastomeric Bearings under Cross Beam

In this part of the study, an analytic model of the bridge for analysis case 2 was formed and analyzed in Sap2000 software.

4.2.2.1. Analytical Model for Structural Analysis

In Figure 4.27, a closer look to the bearings, and in Figure 4.28, an analytical model for the structural analysis of the bridge are given. Frame elements are used for piers, girders, crossbeams, cap beams and abutments; link elements are introduced for bearings. Properties of the link elements (stiffness coefficients, fixity, etc.) used for introducing the bearings to the software are given in Figure 4.29 and Figure 4.30.

While introducing link and frame elements to the software, arbitrary numbers are assigned to the elements. The assigned numbers of link elements regarding bearings are given in Figure 4.31. The case for frame elements is also the same; the assigned numbers of frames are also given in Figure 4.32.

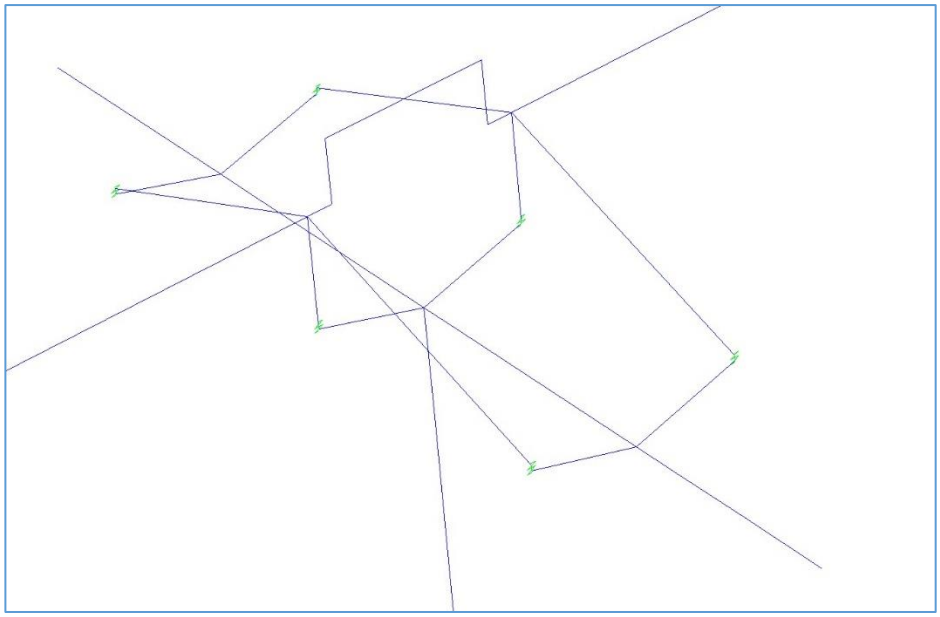

Figure 4.27. Close View of the Bearings for the Analysis Case 2 (EBC-3)

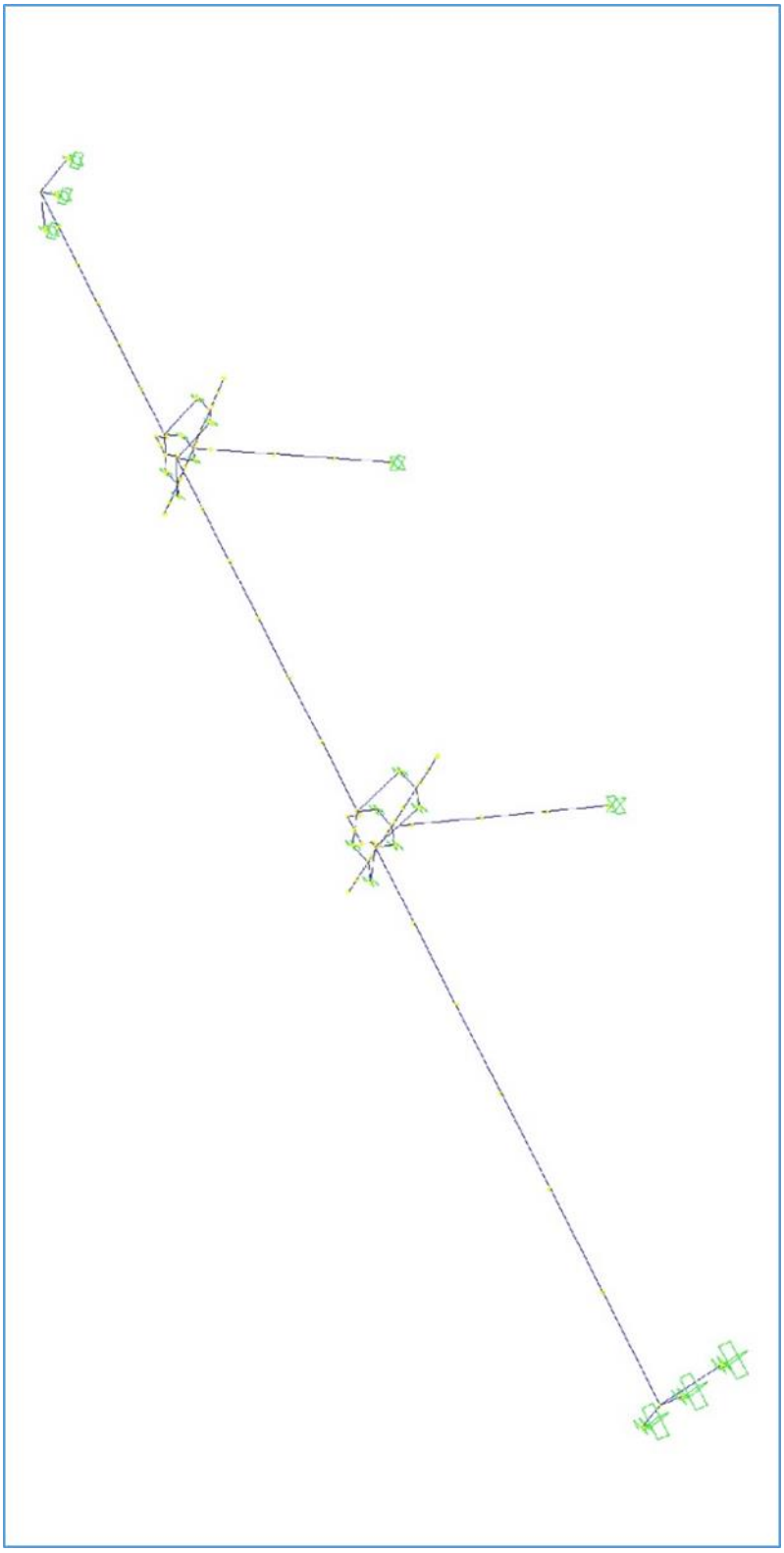

Figure 4.28. General View of 3-D Structural Model of Analysis Case 2 (EBC-3)

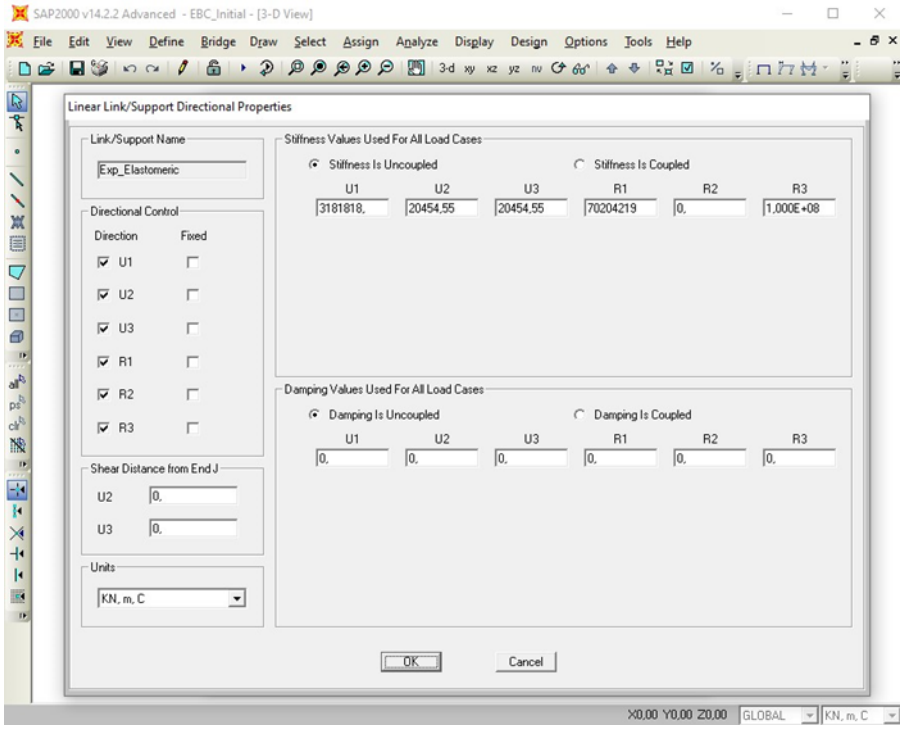

Figure 4.29. Stiffness Properties of Expansion Elastomeric Bearings

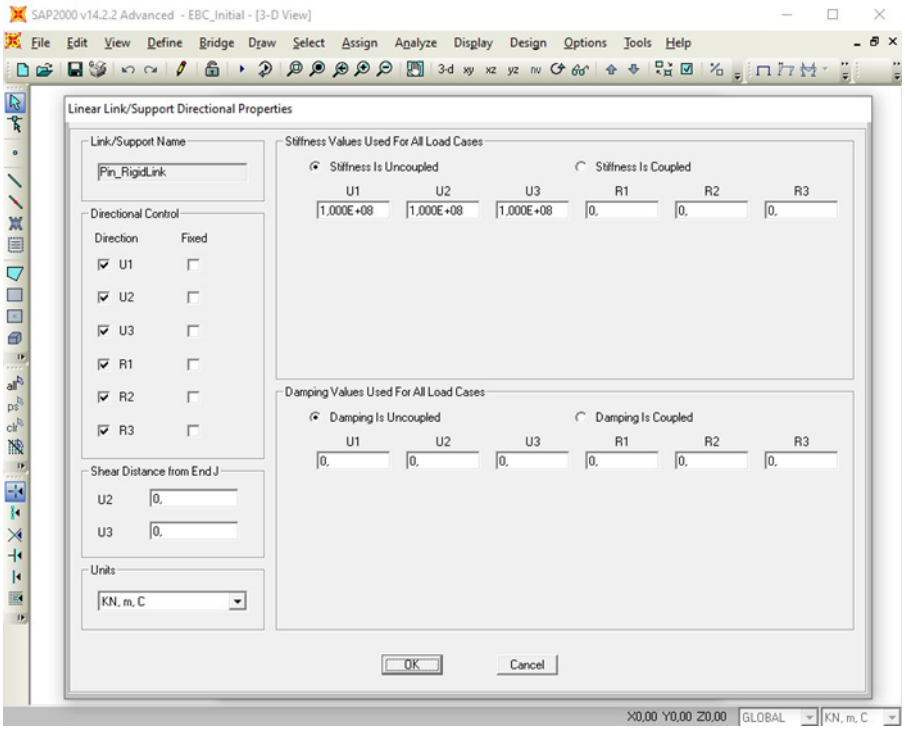

Figure 4.30. Stiffness Properties of Fixed Elastomeric Bearings

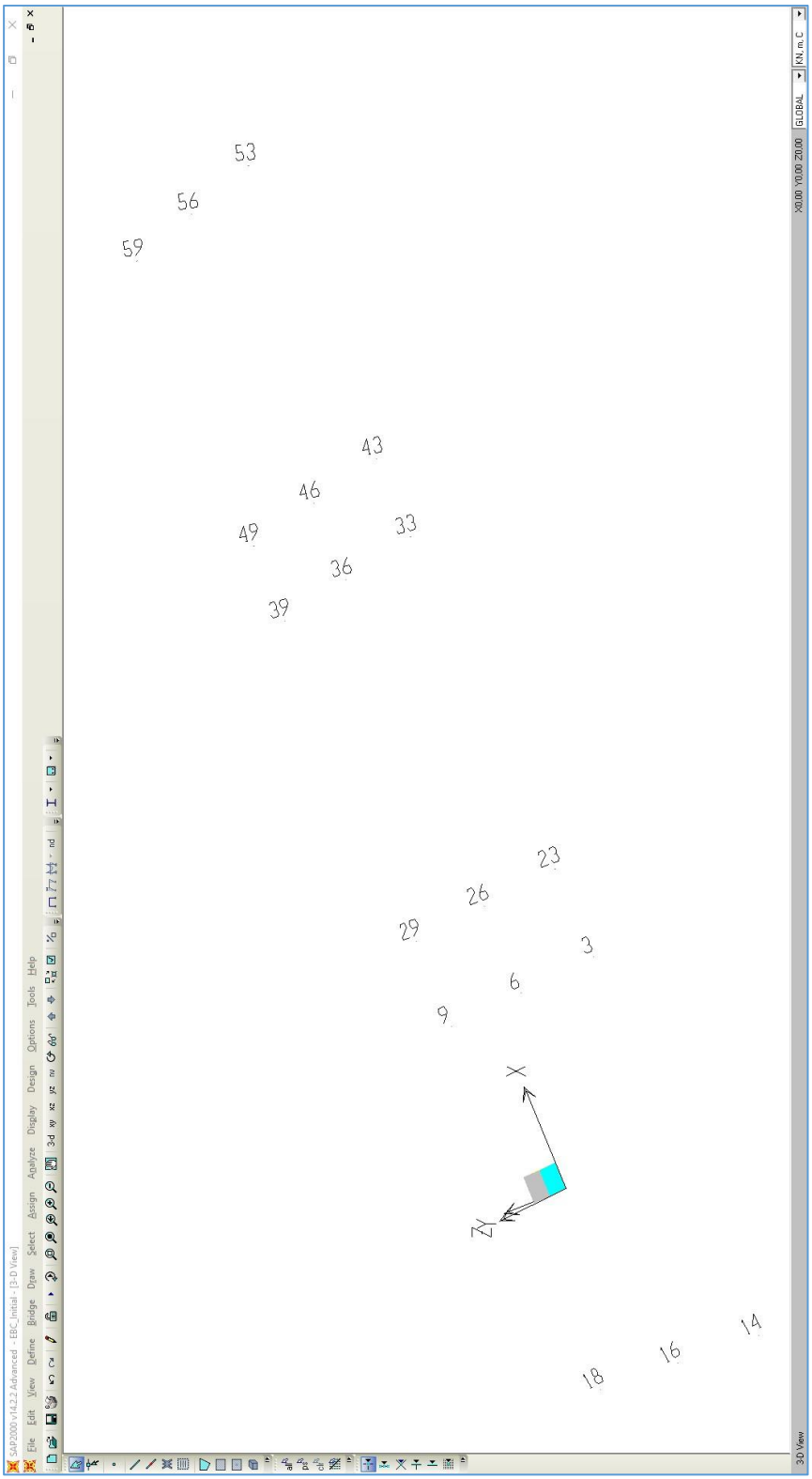

Figure 4.31. Number Assignments of Bearings for the Model of Analysis Case 2 (EBC-3)

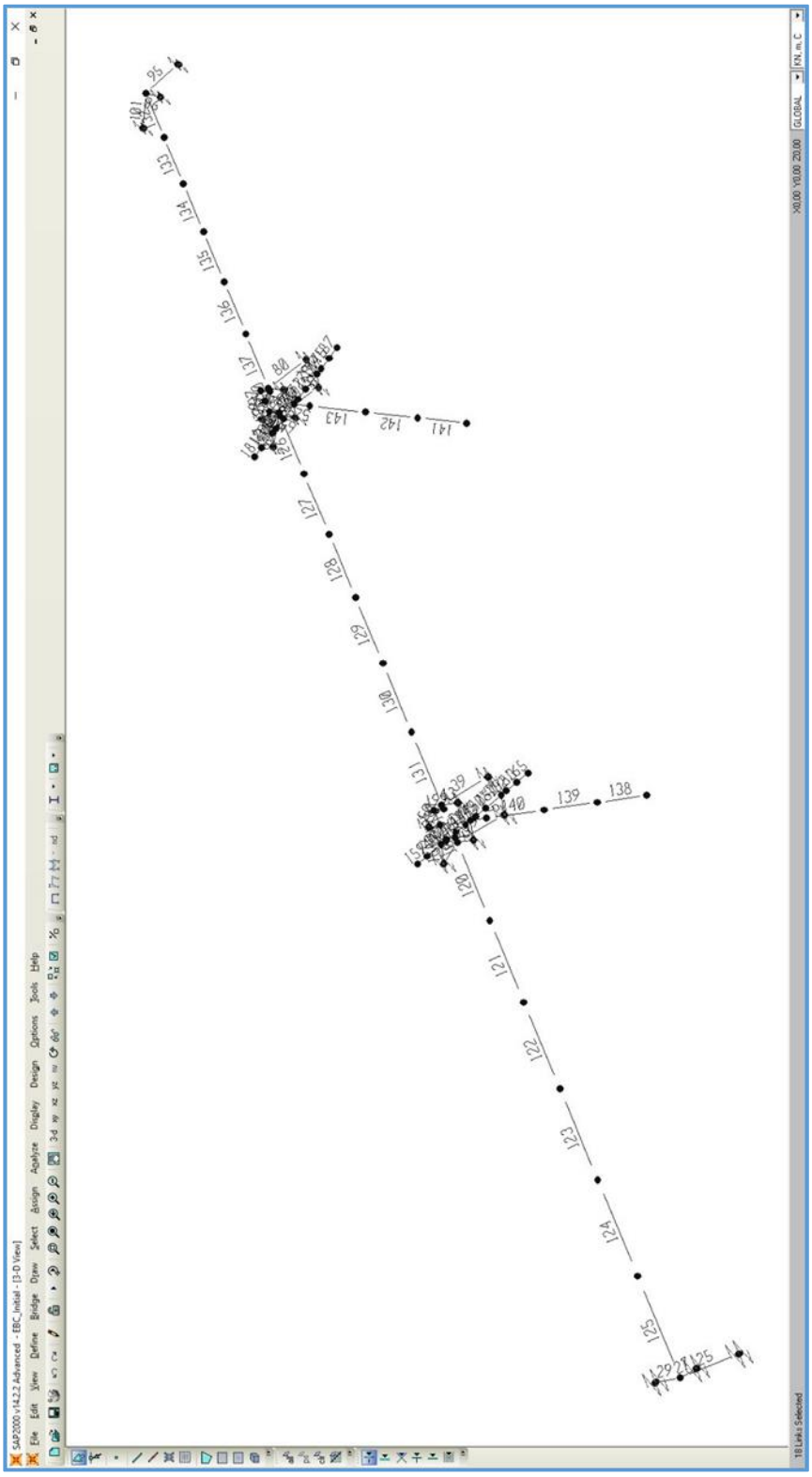

Figure 4.32. Number Assignment of Frames for the Model of Analysis Case 2 (EBC-3)

4.2.2.2. Analysis Results

Shape and period of the first mode, relative displacements of bearings, vertical reactions exerted on bearings, column base-end maximum shear and maximum moment reactions are obtained from the software and shown below as histograms. Histogram type graph is used since there is not any relationship between earthquakes applied to the structure.

Like the process done in Reference Analysis Case (EBC10-REF), initially, stiffness properties arising from geometric properties of bearings are assigned to the link elements. When the structural analysis was completed, like the situation in the reference analysis case, it was seen that under the effect of one earthquake which is 60DI6 the horizontal displacement exceeded 10 cm. In order to limit the horizontal displacement to 10 centimeters for the earthquakes, which creates higher horizontal displacements, the spring-stiffness coefficient values of bearings just in the longitudinal direction of the bridge were iterated. During the iteration process, it was aimed to limit the horizontal displacement and for staying in the safe side, the iteration process was finalized when the horizontal displacement value reached to a little bit less than 10 centimeters. The characteristics of the iterated structural model and analysis results of the iterated model are provided in sections 4.2.2.3 and 4.2.2.4, respectively.

When presenting the analysis results for this analysis case, it is intentionally done that, horizontal displacements of bearings with the assigned number of 16 is provided since the highest horizontal displacements are exerted to that bearing. In the initial case, the vertical reaction of the bearing with the assigned number of 26 has higher values, so the results of that bearing are provided. In the iterated case, the horizontal displacement of the bearing with the assigned number of 16 has higher displacement values. But for the vertical reaction results, the highest values are obtained from bearing-18. Since the difference of the results for bearing-18 and bearing-26 is less enough, results for both of them are provided. When doing the comparison between

the results of analysis cases, the maximum results for the bearings are taken into consideration.

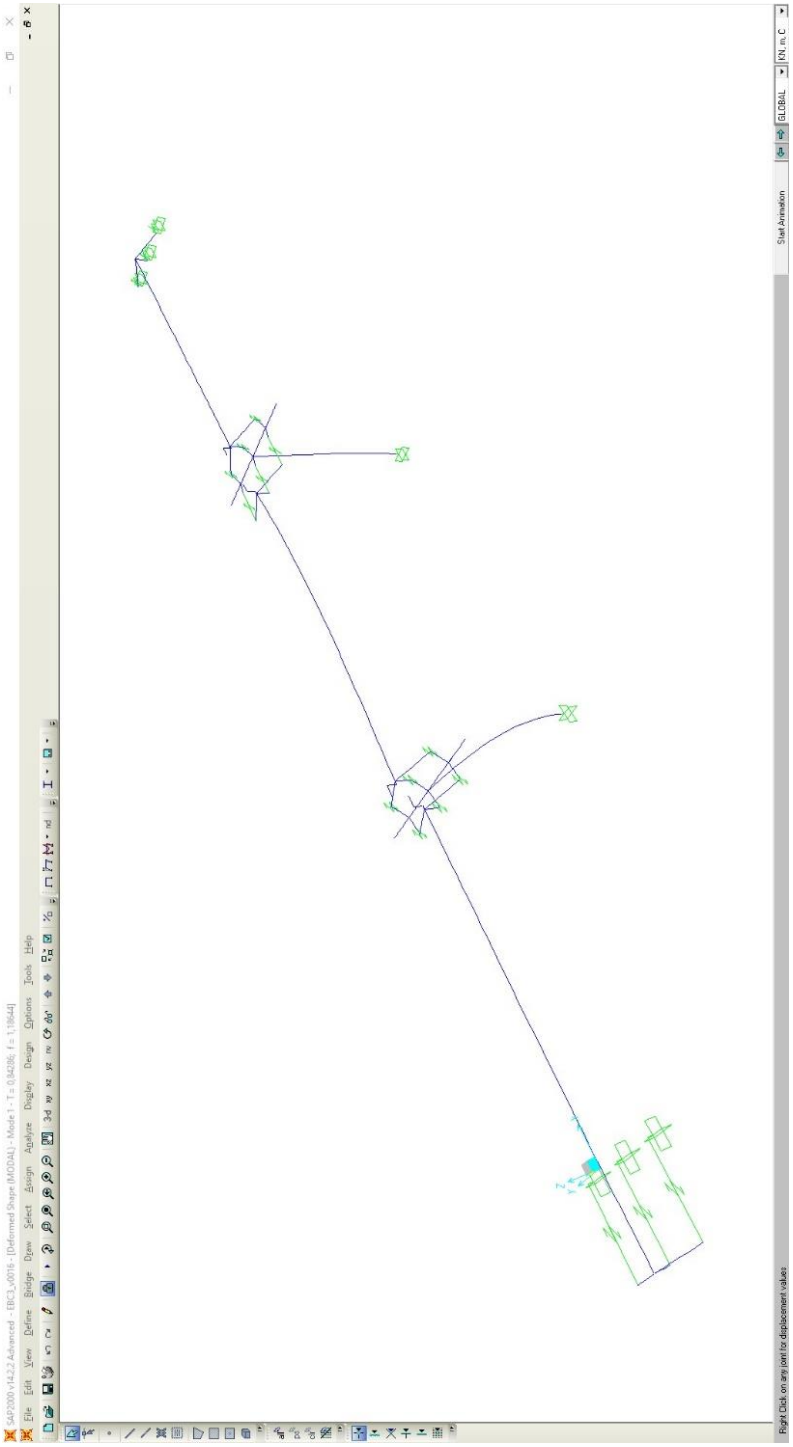

Figure 4.33. Shape and Period (T~=0,84s) of First Mode

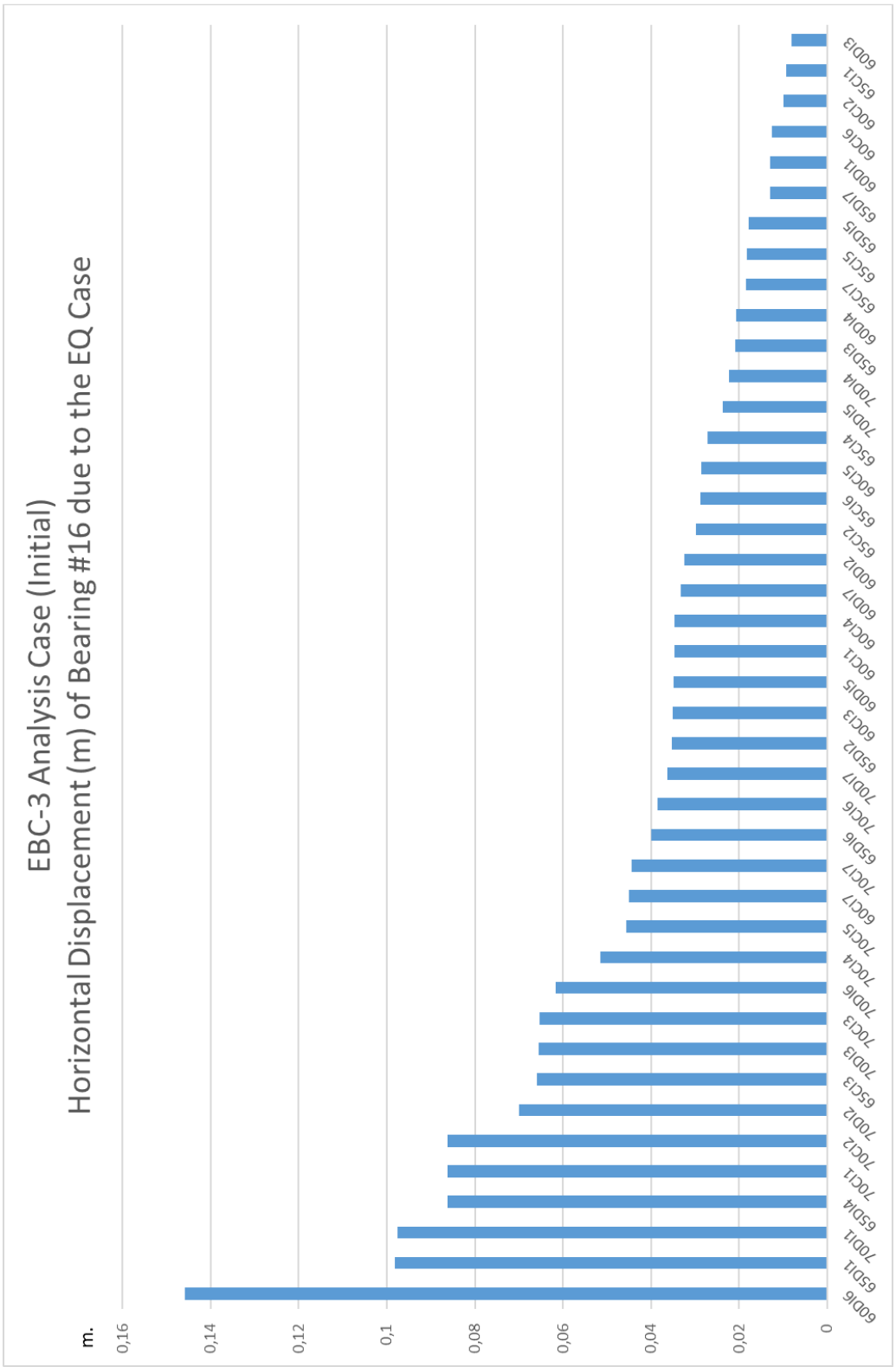

Figure 4.34. Horizontal Displacement (m) of Bearing #16 due to EQ Case

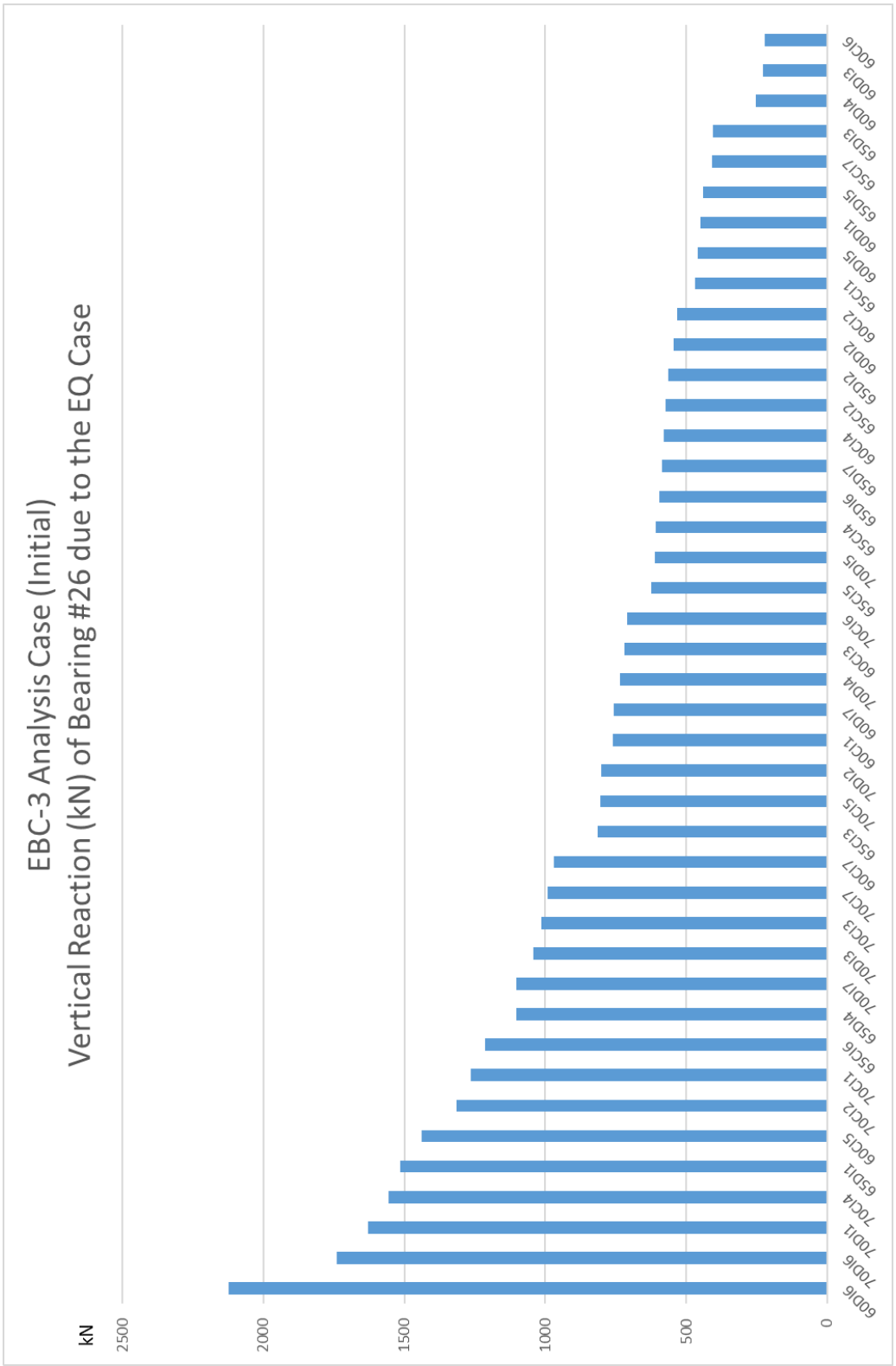

Figure 4.35. Vertical Reaction (kN) of Bearing #26 due to EQ Case

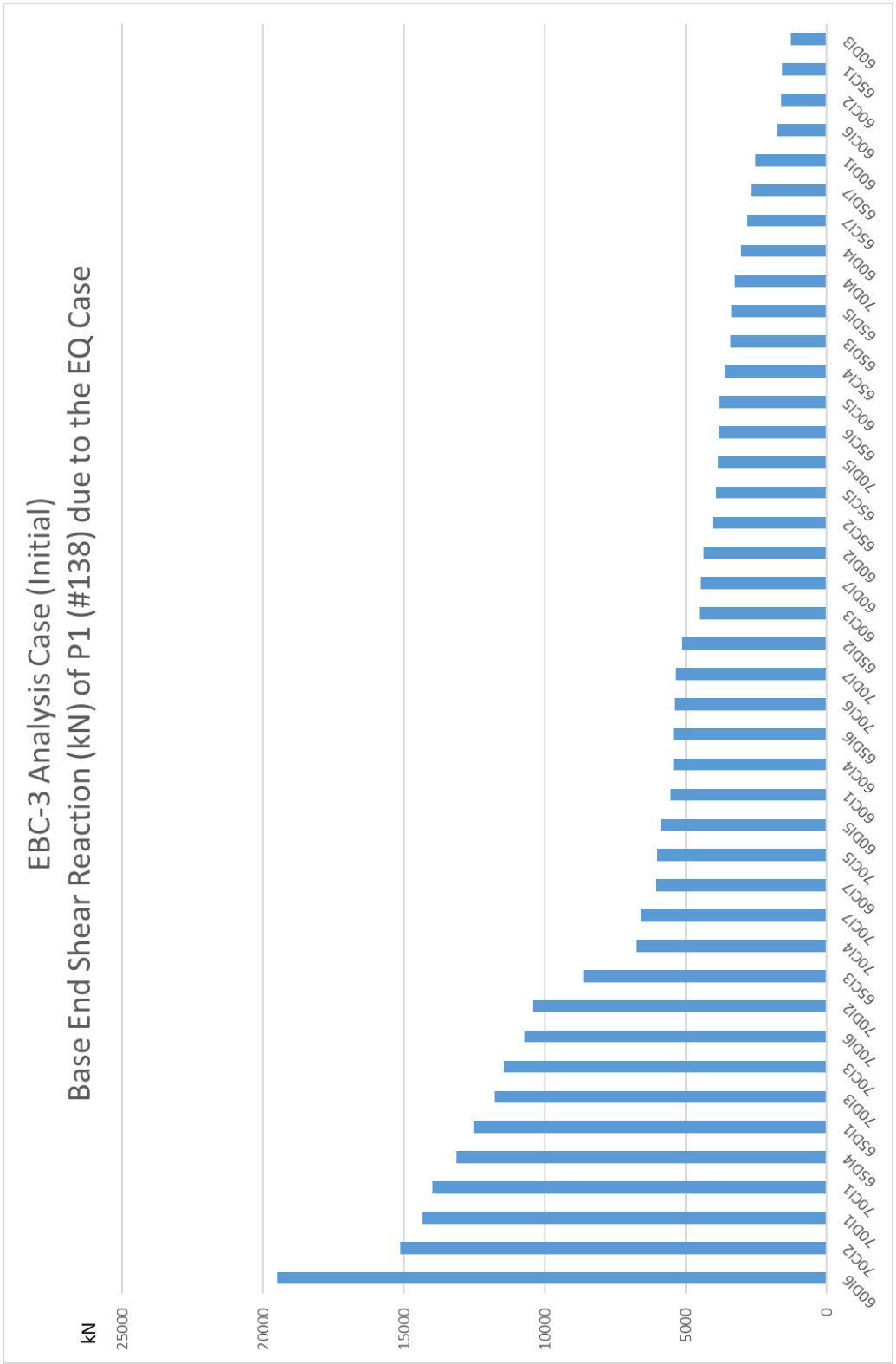

Figure 4.36. Base End Shear Reaction (kN) of P1 (#138) due to EQ Case

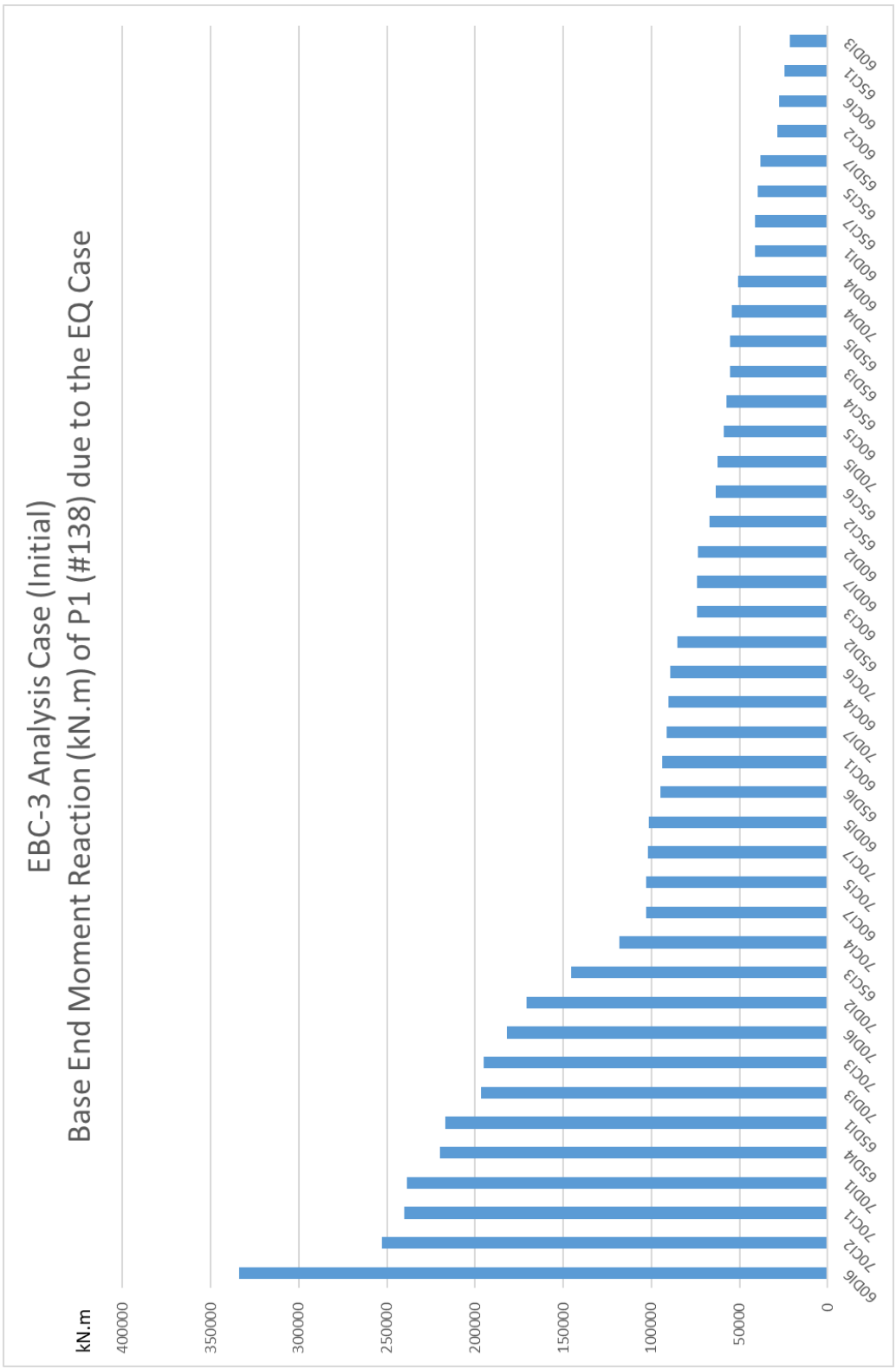

Figure 4.37. Base End Moment Reaction (kN.m) of P1 (#138) due to EQ Case

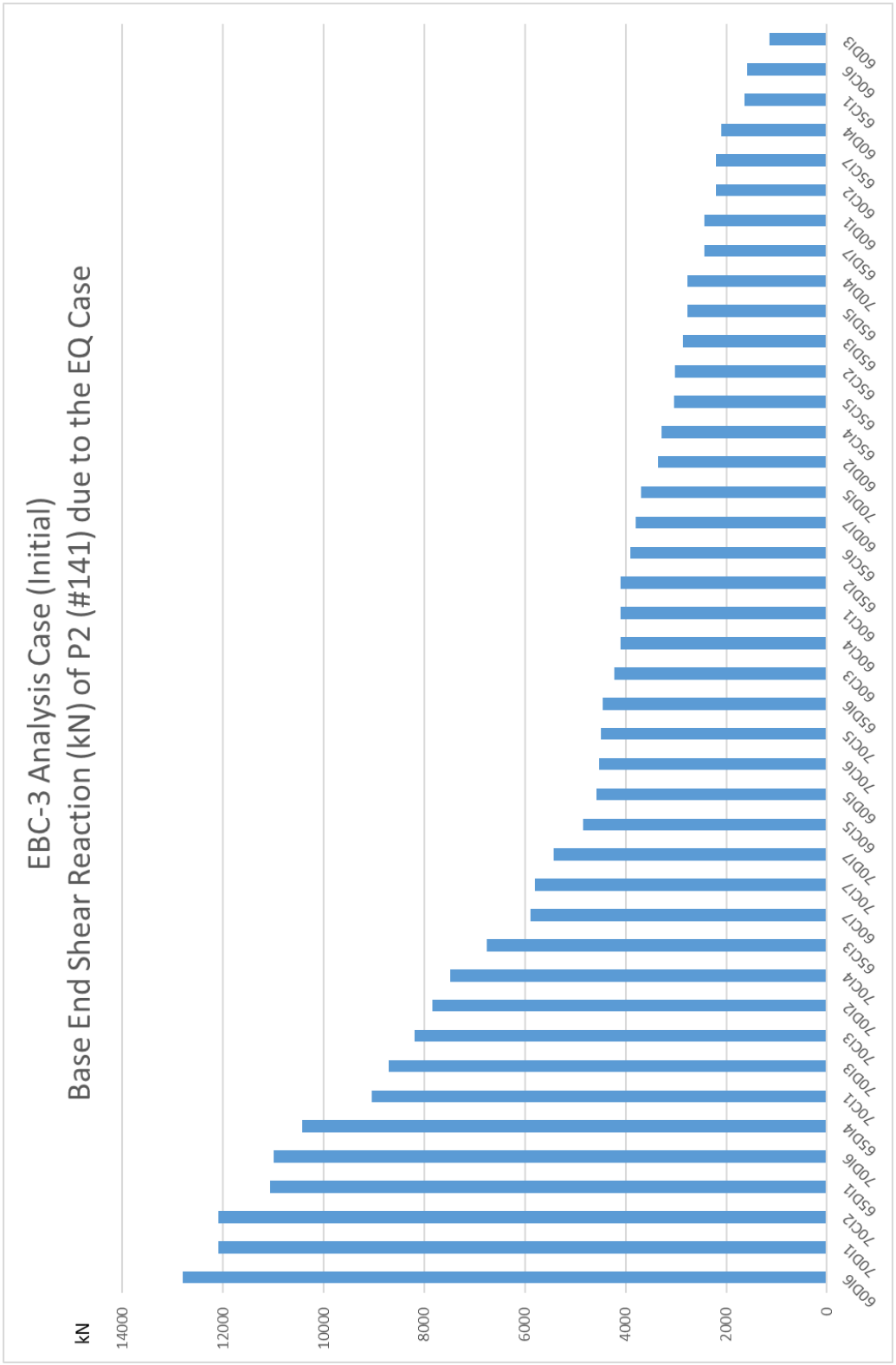

Figure 4.38. Base End Shear Reaction (kN) of P2 (#141) due to EQ Case

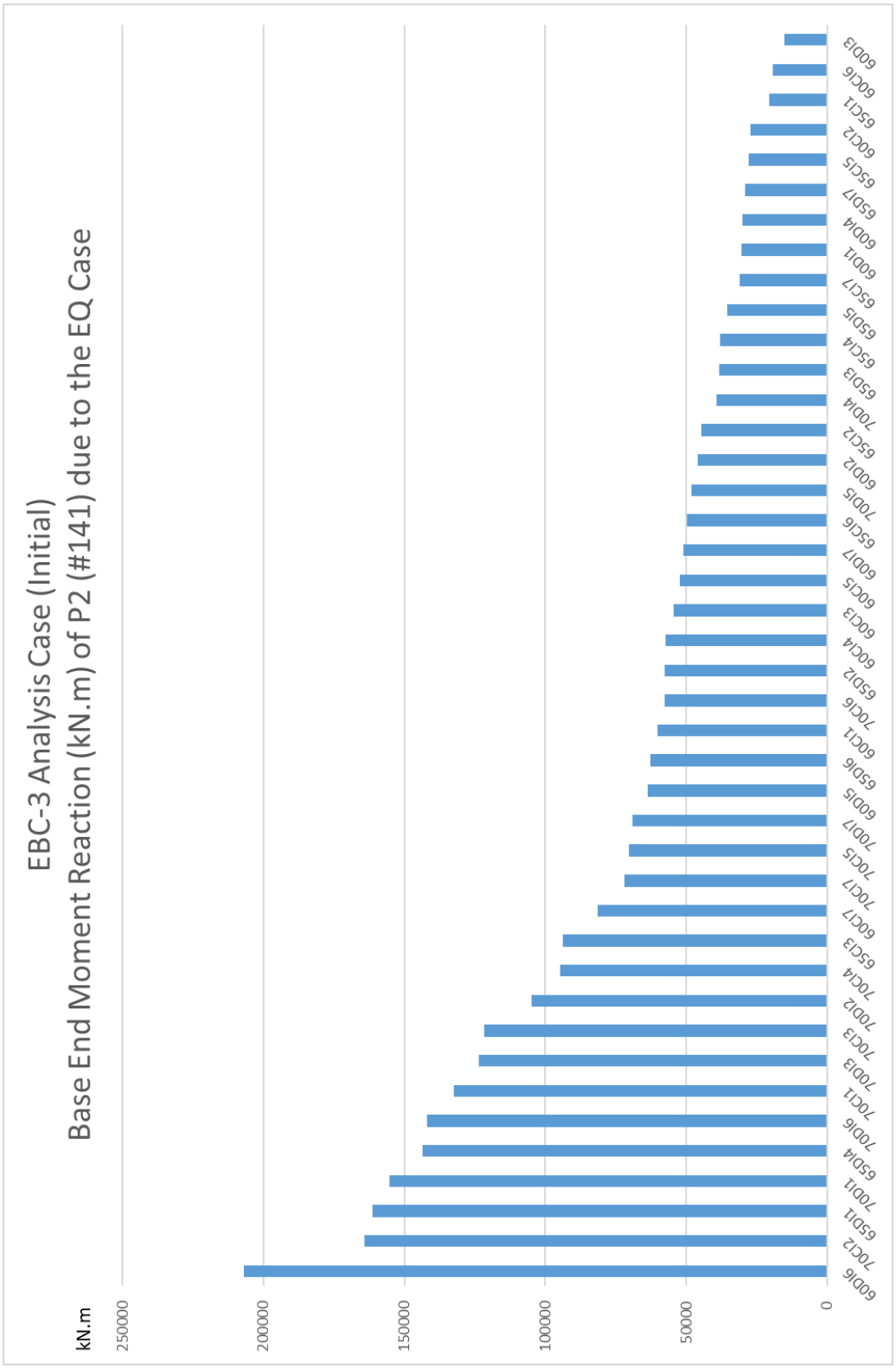

Figure 4.39. Base End Moment Reaction (kN.m) of P2 (#141) due to EQ Case

4.2.2.3. Specific Properties of the Structure (Iterated Stiffness)

As described before; when relative displacements of bearings exceed 10 centimeters; bearing stiffness values are needed to be iterated to ensure that the relative displacements are staying within the desired limit, 10 centimeters. Stiffness values of bearings are iterated by generating some other analytical models to achieve the maximum relative displacement of bearings under any earthquake applied to the bridge within this study.

Final stiffness values of elastomeric bearings standing upon the desired relative displacement limit are shown below in Figure 4.40 and Figure 4.41.

Results obtained from the structural analysis of the bridge via using bearings with specified properties are provided in part 4.2.2.4.

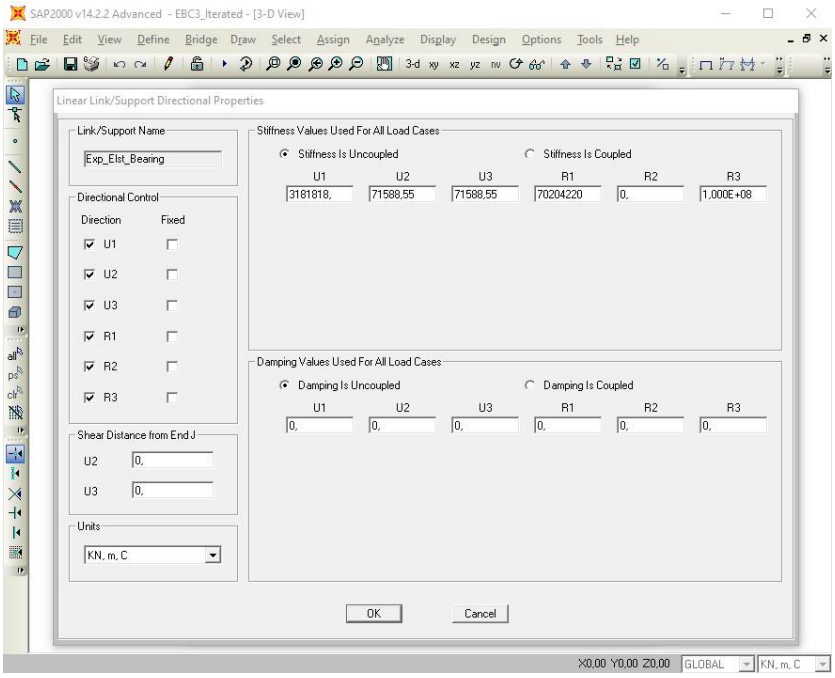

Figure 4.40. Stiffness Properties of Expansion Elastomeric Bearings

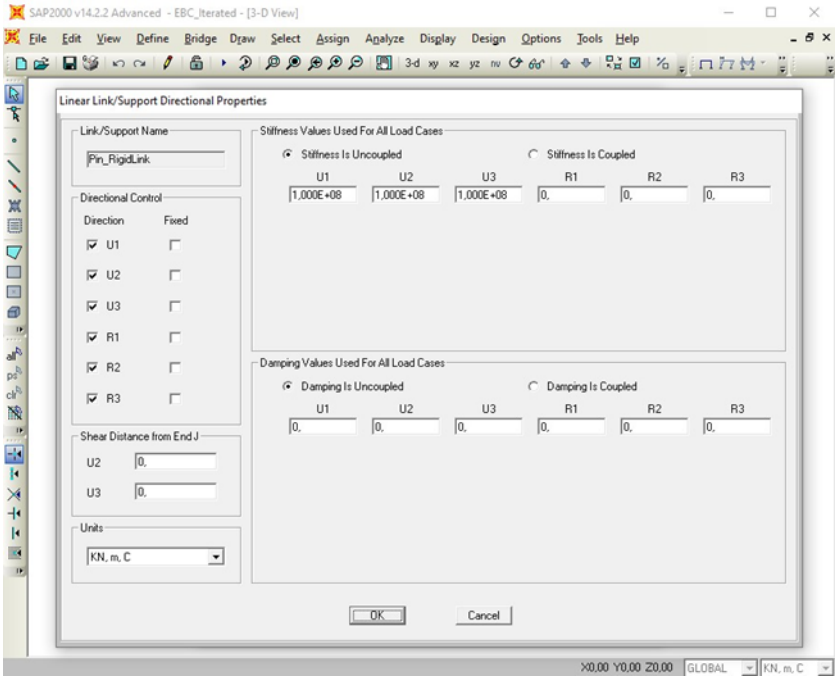

Figure 4.41. Stiffness Properties of Fixed Elastomeric Bearings

4.2.2.4. Analysis Results of the Structure (Iterated Stiffness)

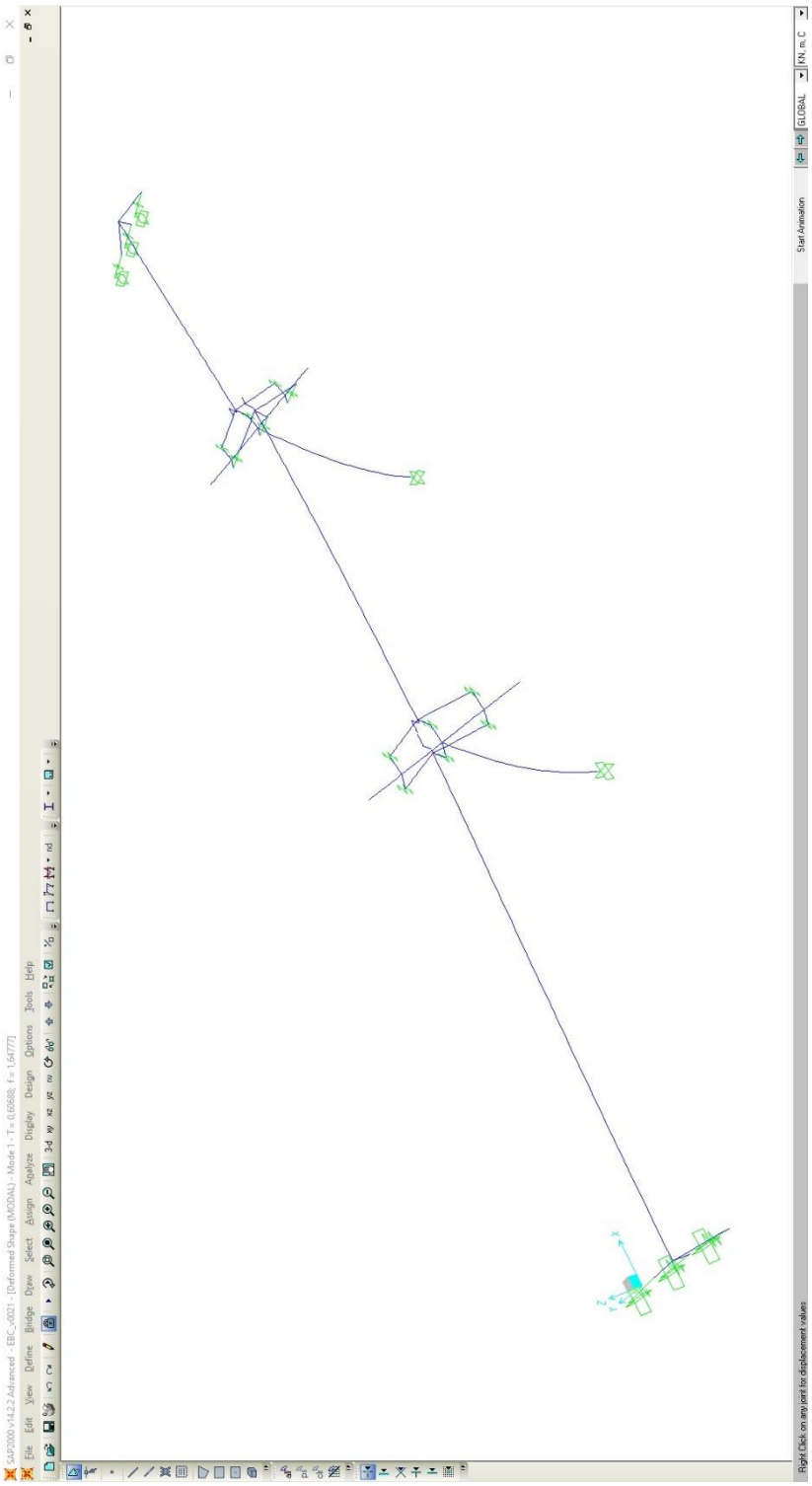

Figure 4.42. Shape and Period (T~=0,61s) of First Mode

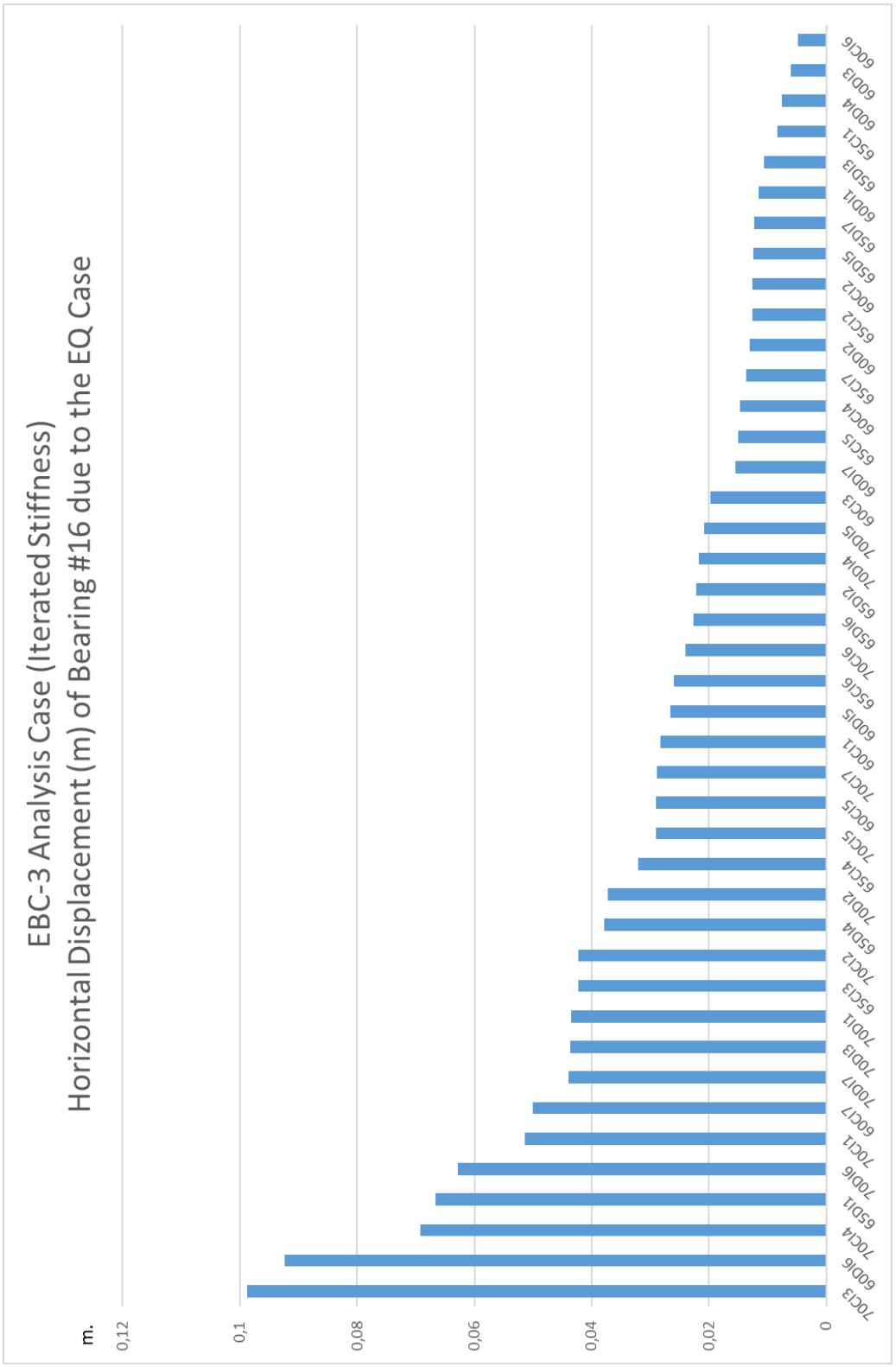

Figure 4.43. Horizontal Displacement (m) of Bearing #16 due to EQ Case (with iterated stiffness)

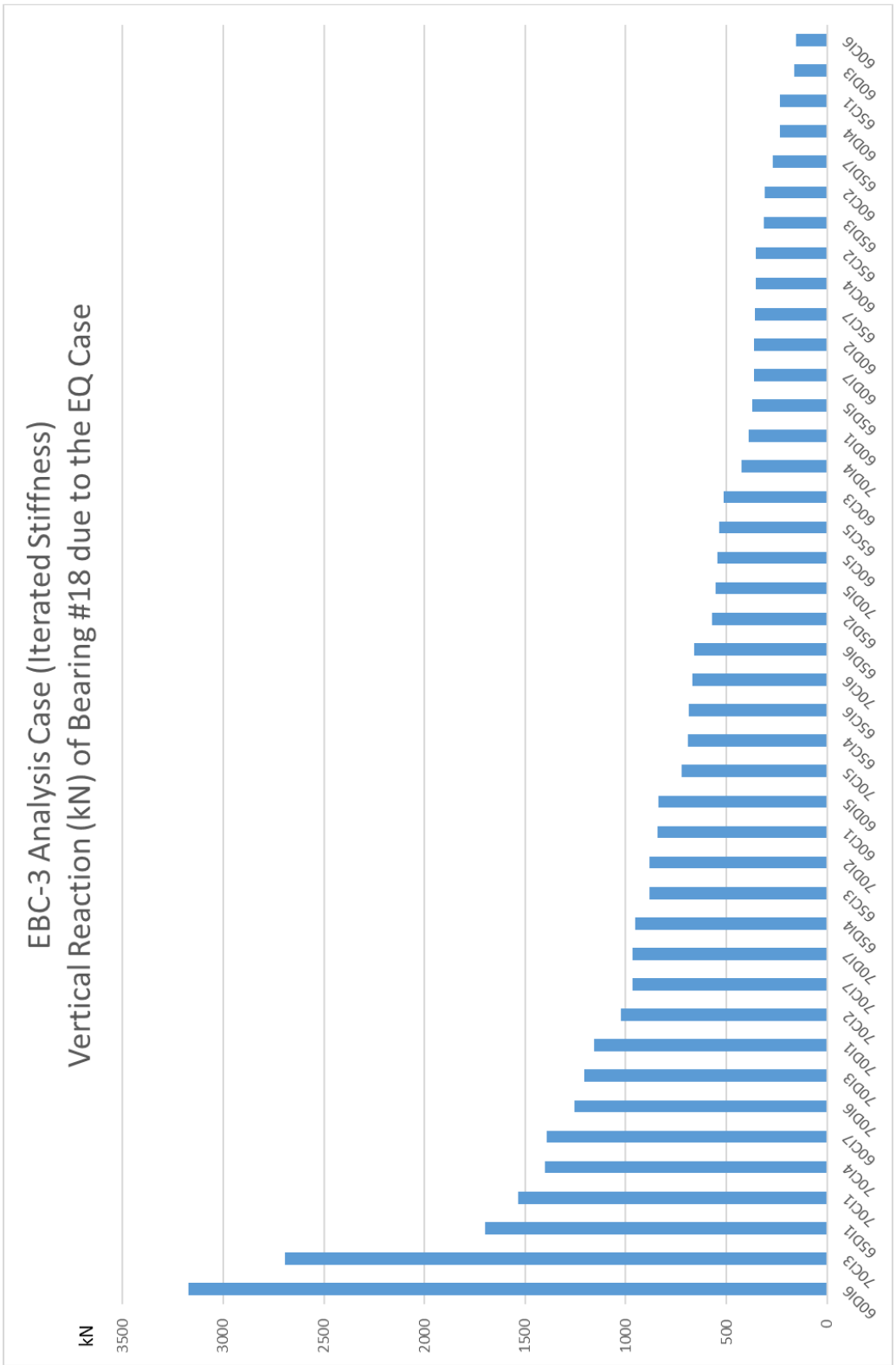

Figure 4.44. Vertical Reaction (kN) of Bearing #18 due to EQ Case (with iterated stiffness)

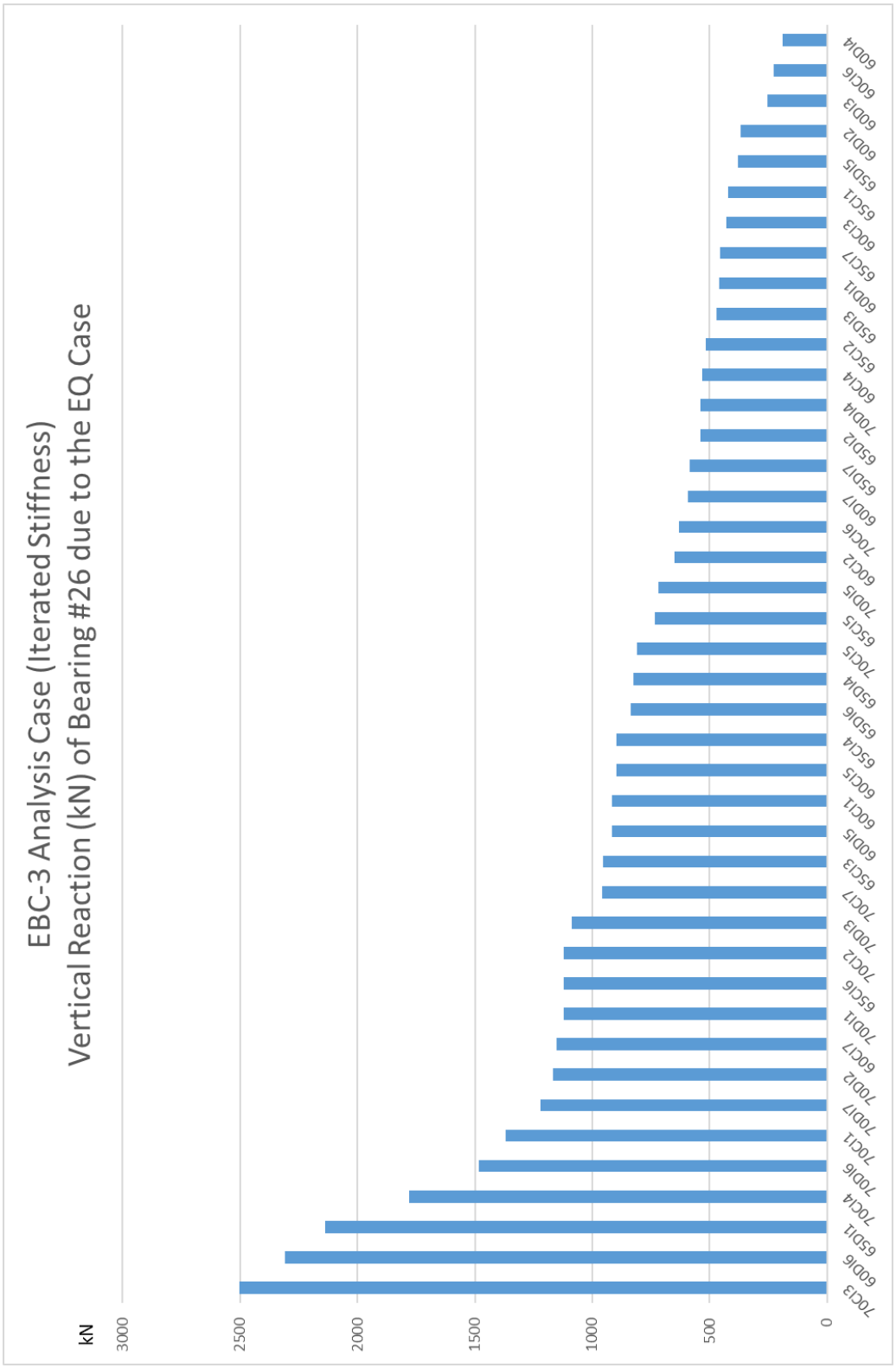

Figure 4.45. Vertical Reaction (kN) of Bearing #26 due to EQ Case (with iterated stiffness)

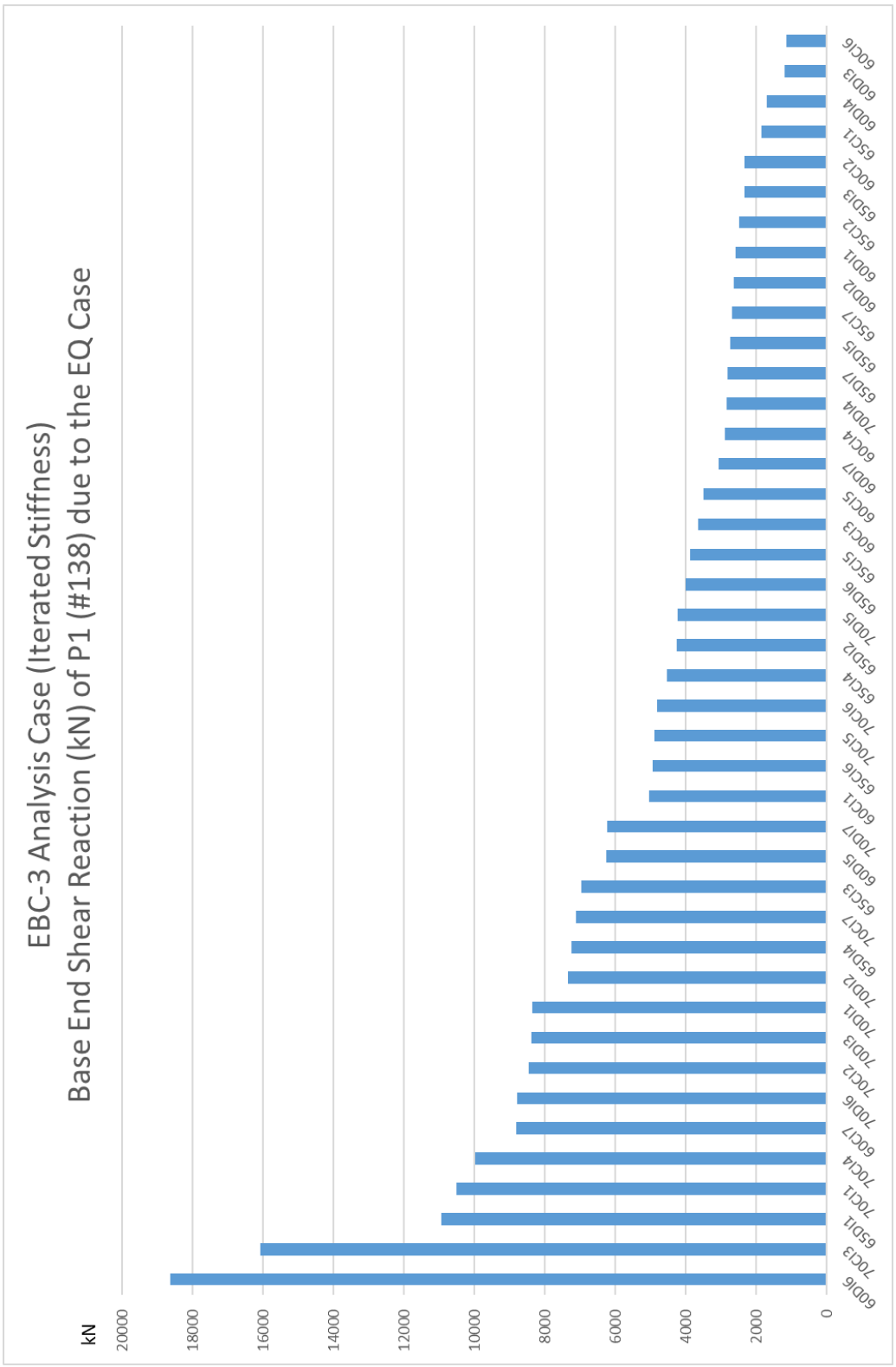

Figure 4.46. Base End Shear Reaction (kN) of P1 (#138) due to EQ Case (with iterated stiffness)

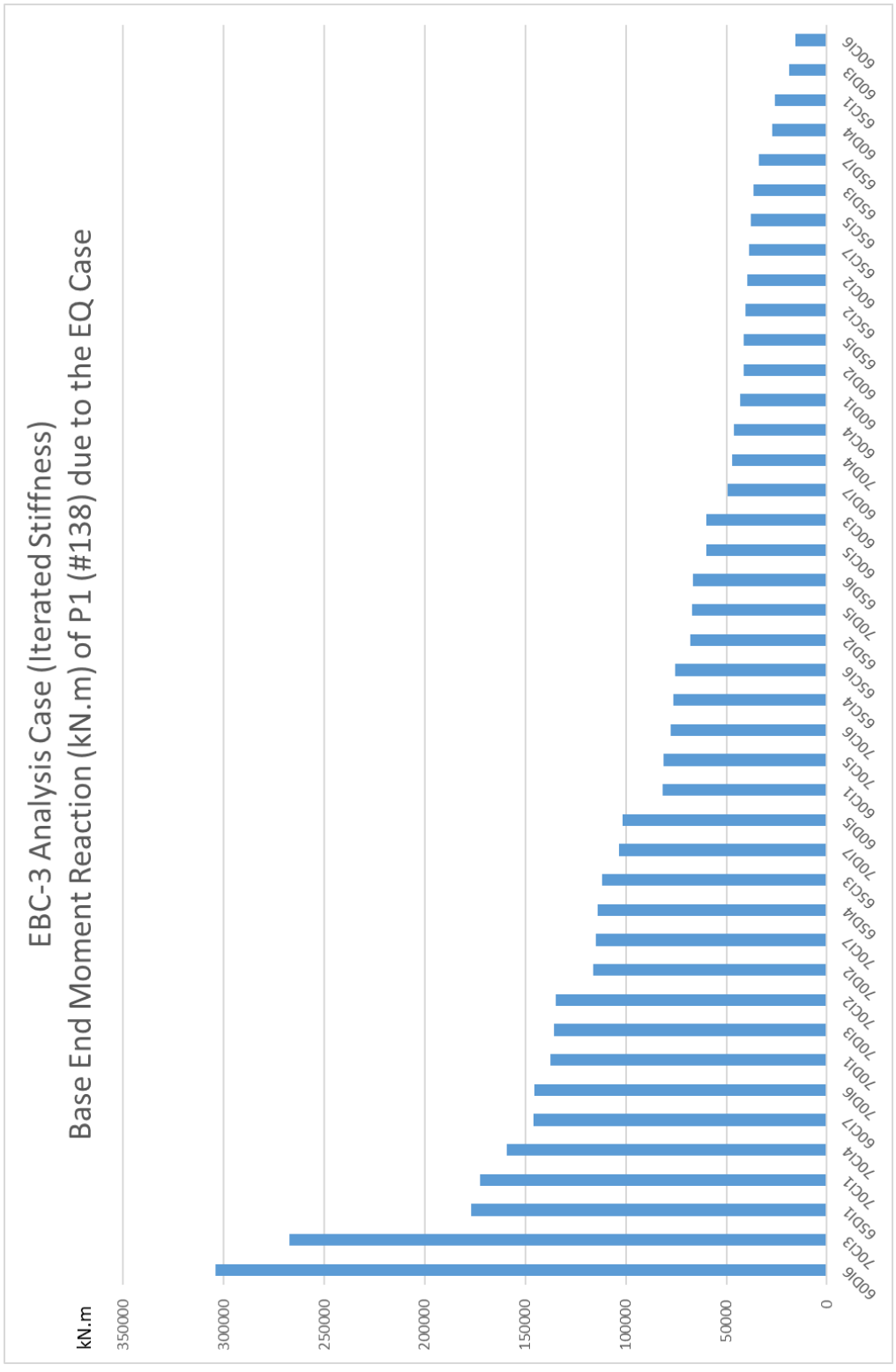

Figure 4.47. Base End Moment Reaction (kN.m) of P1 (#138) due to EQ Case (with iterated stiffness)

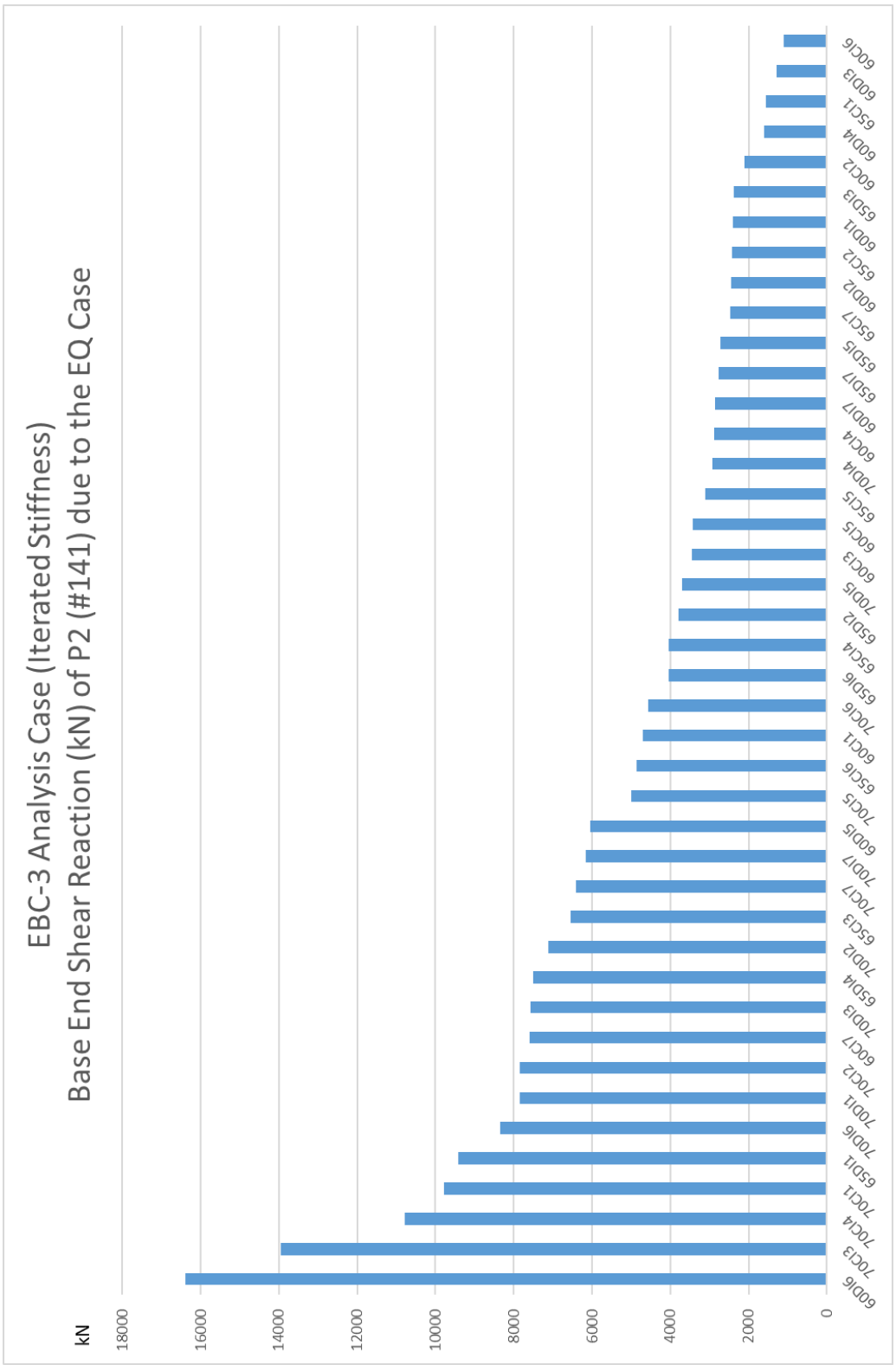

Figure 4.48. Base End Shear Reaction (kN) of P2 (#141) due to EQ Case (with iterated stiffness)

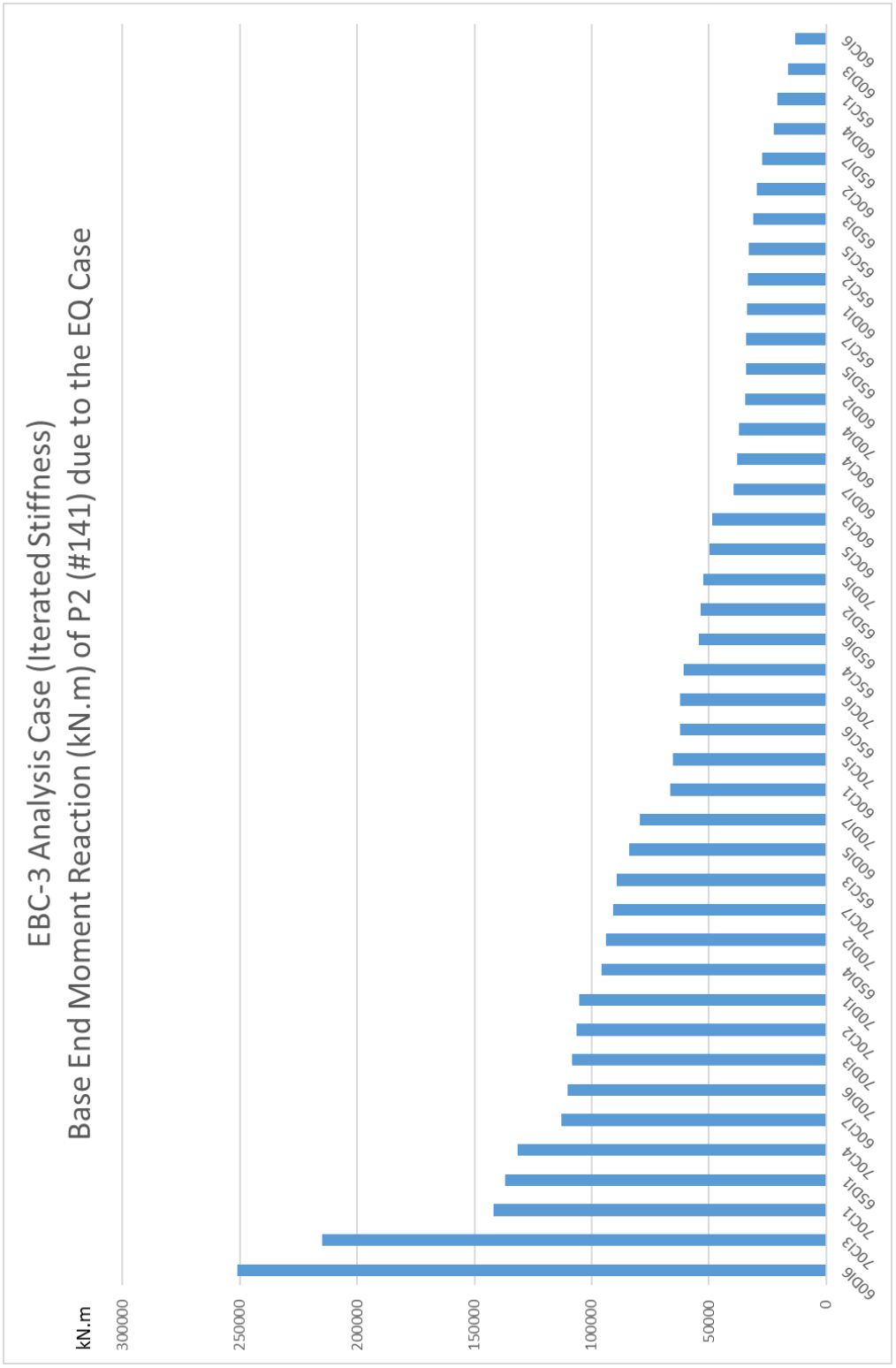

Figure 4.49. Base End Moment Reaction (kN.m) of P2 (#141) due to EQ Case (with iterated stiffness)

4.2.3. Case 3: Pot Bearing Case, PBC-3, 3 Pot Bearings under Cross Beam

An analytic model of the bridge for case 3 was formed and analyzed in Sap2000 software. The number of bearings used in this case is the same as the one in case 2. In this case, a totally six pot bearings are used for ten girders in each span.

4.2.3.1. Analytical Model for Structural Analysis

In Figure 4.50, a closer look to the bearings and in Figure 4.51, an analytical model for the structural analysis of the bridge are given. Frame elements are used for piers, girders, crossbeams, cap beams and abutments; link elements are introduced for bearings. Properties of the link elements (stiffness coefficients, fixity, etc.) used for introducing the bearings to the software are given in Figure 4.52 and Figure 4.53.

As being same with the procedure of the previous two cases, software used for structural analysis assigns arbitrary numbers to the link and frame elements. The assigned numbers of bearings and the assigned numbers of frames are provided in Figure 4.54 and Figure 4.55, respectively.

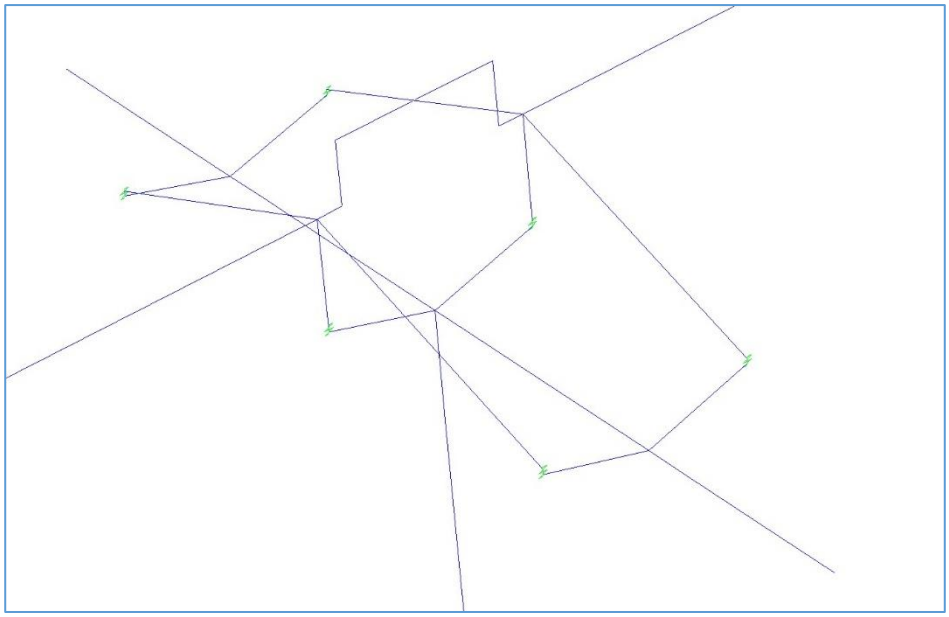

Figure 4.50. Close View of the Bearings for the Analysis Case 3 (PBC-3)

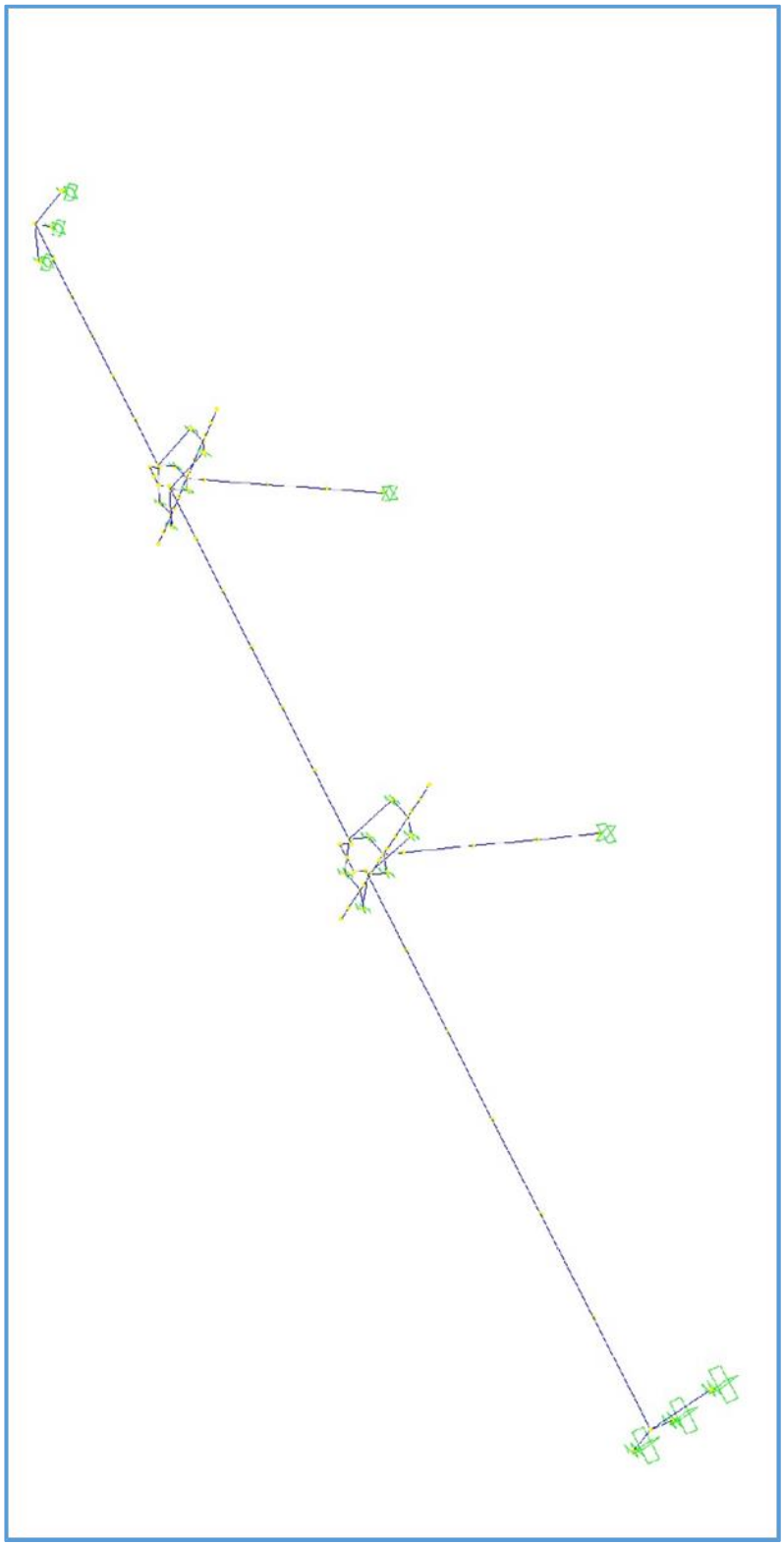

Figure 4.51. General View of 3-D Structural Model of Analysis Case 3 (PBC-3)

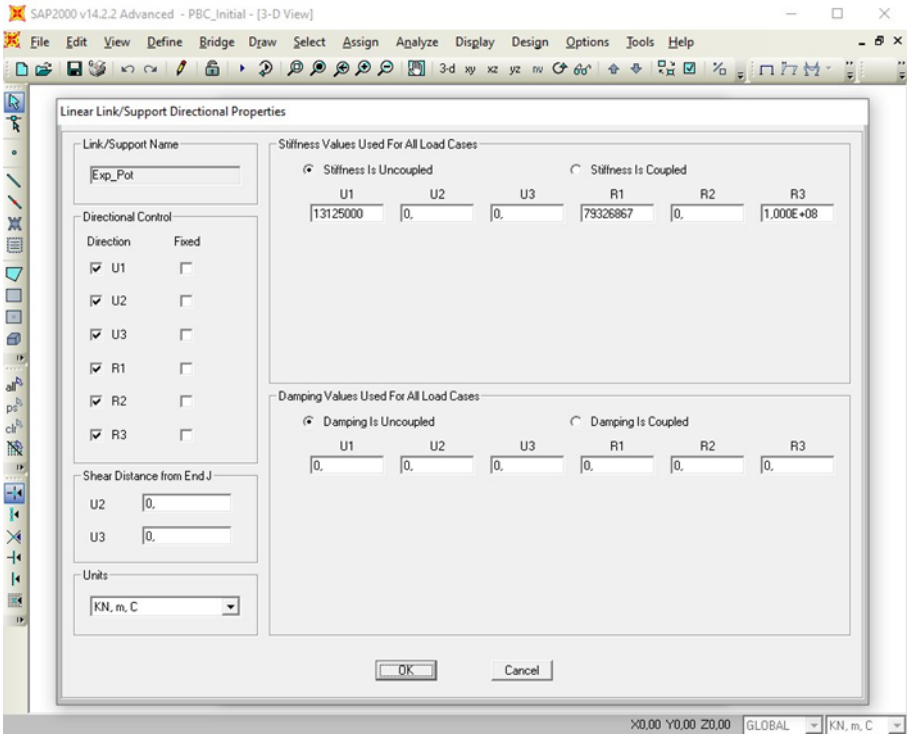

Figure 4.52. Stiffness Properties of Expansion Pot Bearings

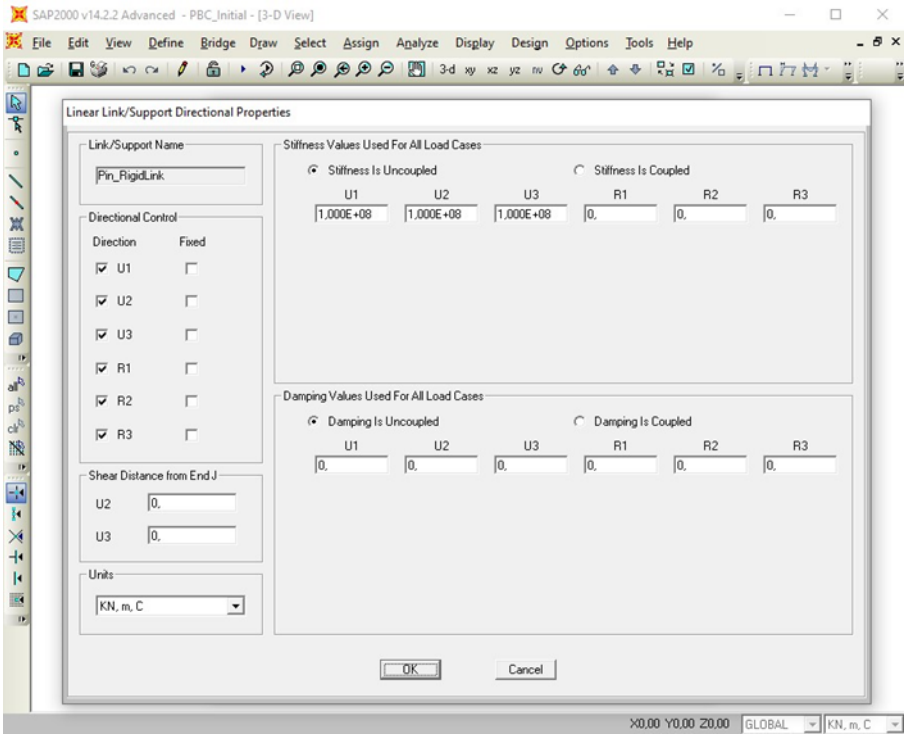

Figure 4.53. Stiffness Properties of Fixed Pot Bearings

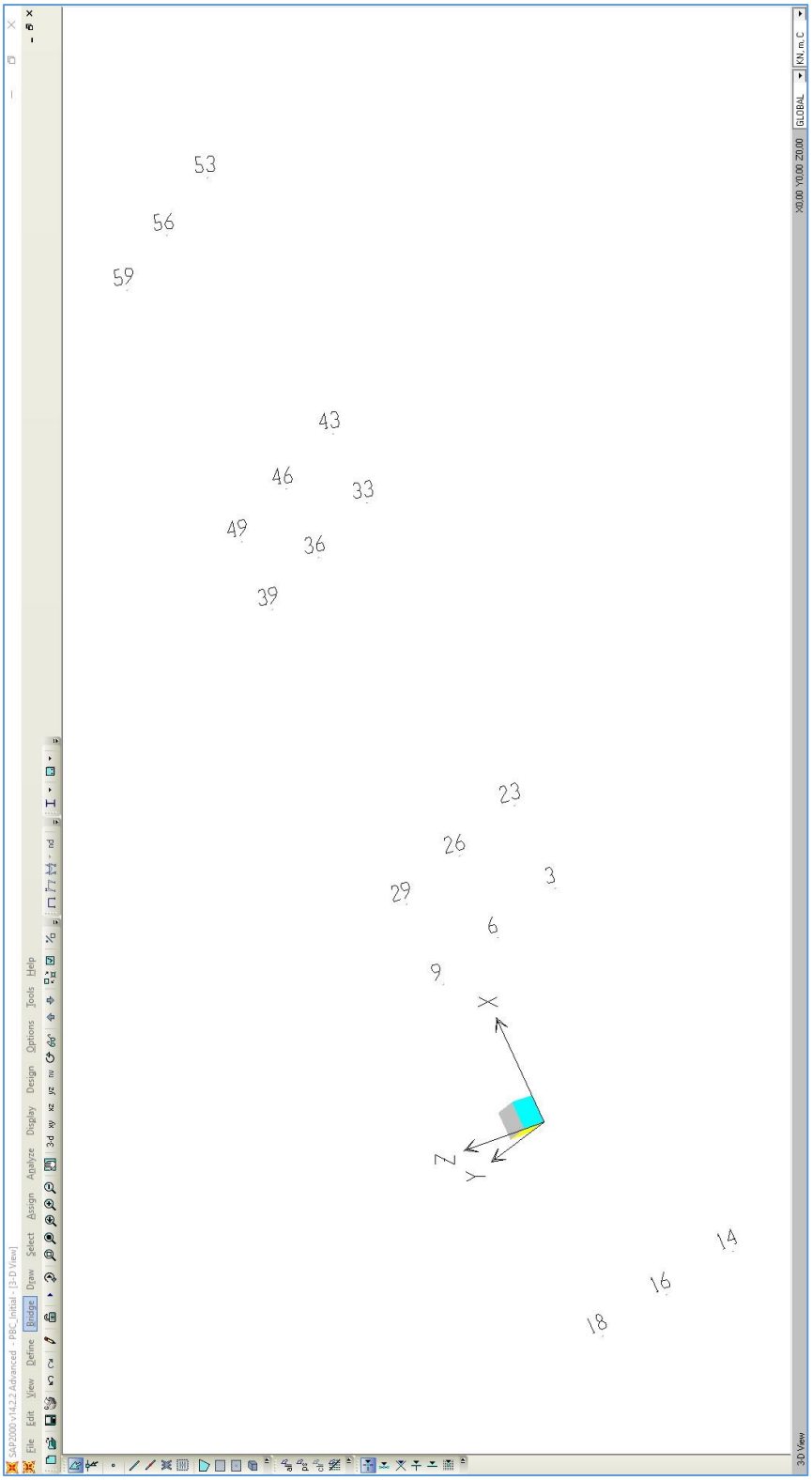

Figure 4.54. Number Assignment of Bearingsfor the Model of Analysis Case 3 (PBC-3)

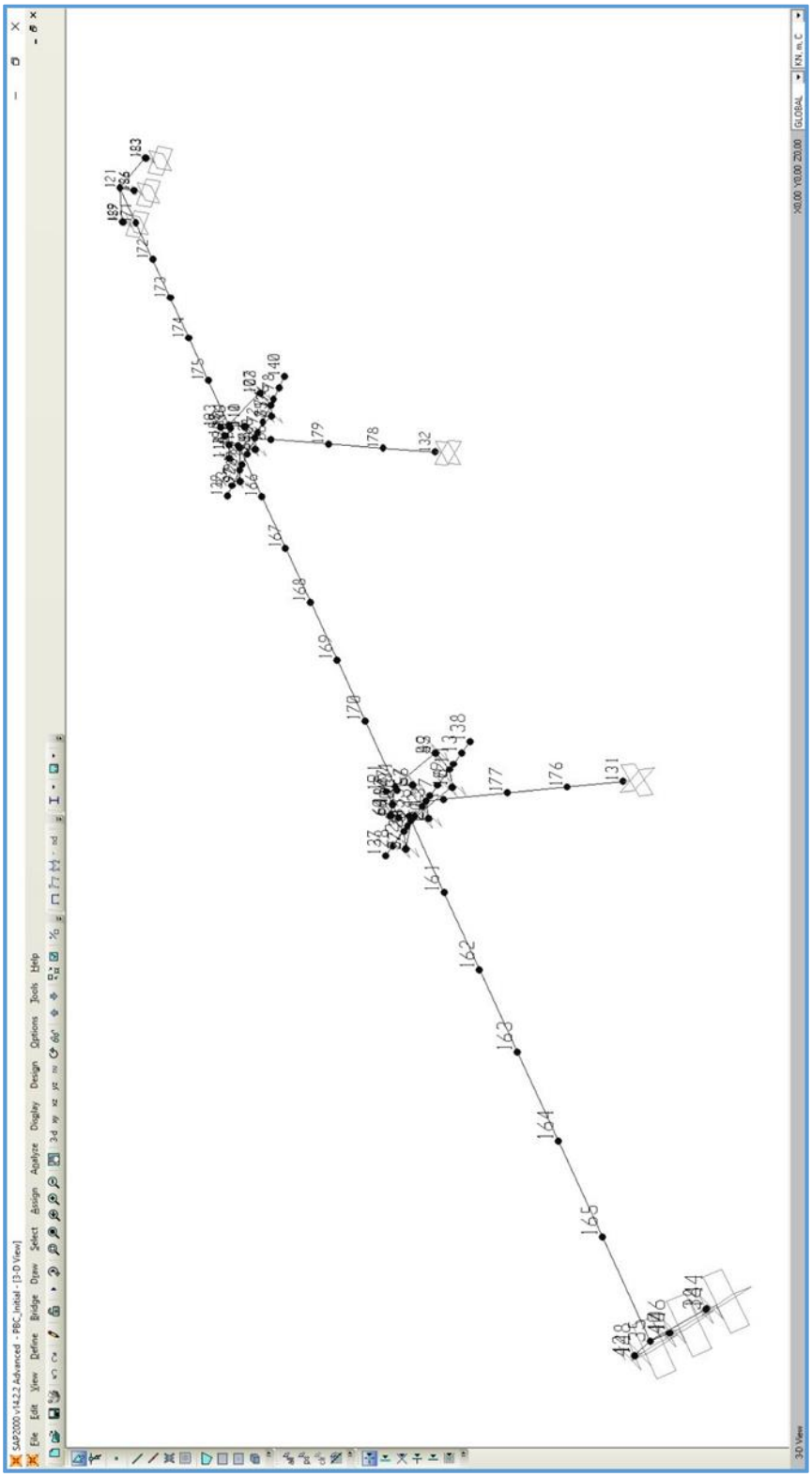

Figure 4.55. Number Assignment of Frames for the Model of Analysis Case 3 (PBC-3)

4.2.3.2. Analysis Results

Shape and period of the first mode, relative displacements of bearings, vertical reactions exerted on bearings, column base-end maximum shear and maximum moment reactions are obtained from the software and shown below as histograms. Histogram type graph is used since there is not any relationship between earthquakes applied to the structure.

As the process was done in the previous two analysis cases (REF and EBC), initially stiffness properties arising from geometric properties of bearings are assigned to the link elements. When the structural analysis was completed, it was seen that under the effect of earthquakes coded as 60DI6, 65DI4, and 70CI3, the horizontal displacement exceeded 10 cm. In order to limit the horizontal displacement to 10 centimeters, the spring stiffness coefficient values of bearings just in the longitudinal direction of the bridge were iterated. During the iteration process, it was aimed to limit the horizontal displacement and for staying on the safe side, the iteration process was finalized when the horizontal displacement value reached a little bit less than 10 centimeters. The characteristics of the iterated structural model and analysis results of the iterated model are provided in sections 4.2.3.3 and 4.2.3.4, respectively.

When presenting the analysis results for this analysis case, horizontal displacements of bearings with the assigned number of 33 for the initial model and 16 for the iterated model are provided since the highest horizontal displacements are exerted to those bearings. For presenting vertical reaction exerted on bearings, the selected bearing is bearing-26 because the highest vertical reaction values are exerted on bearing-26. In the iterated case, the horizontal displacement of the bearing with the assigned number of 16 has higher displacement values. But for the vertical reaction results, the highest values are obtained from bearing-18. Since the difference of the results for bearing-18 and bearing-26 is less enough, results for both of them are provided. When doing the comparison between the results of analysis cases, the maximum results for the bearings are taken into consideration.

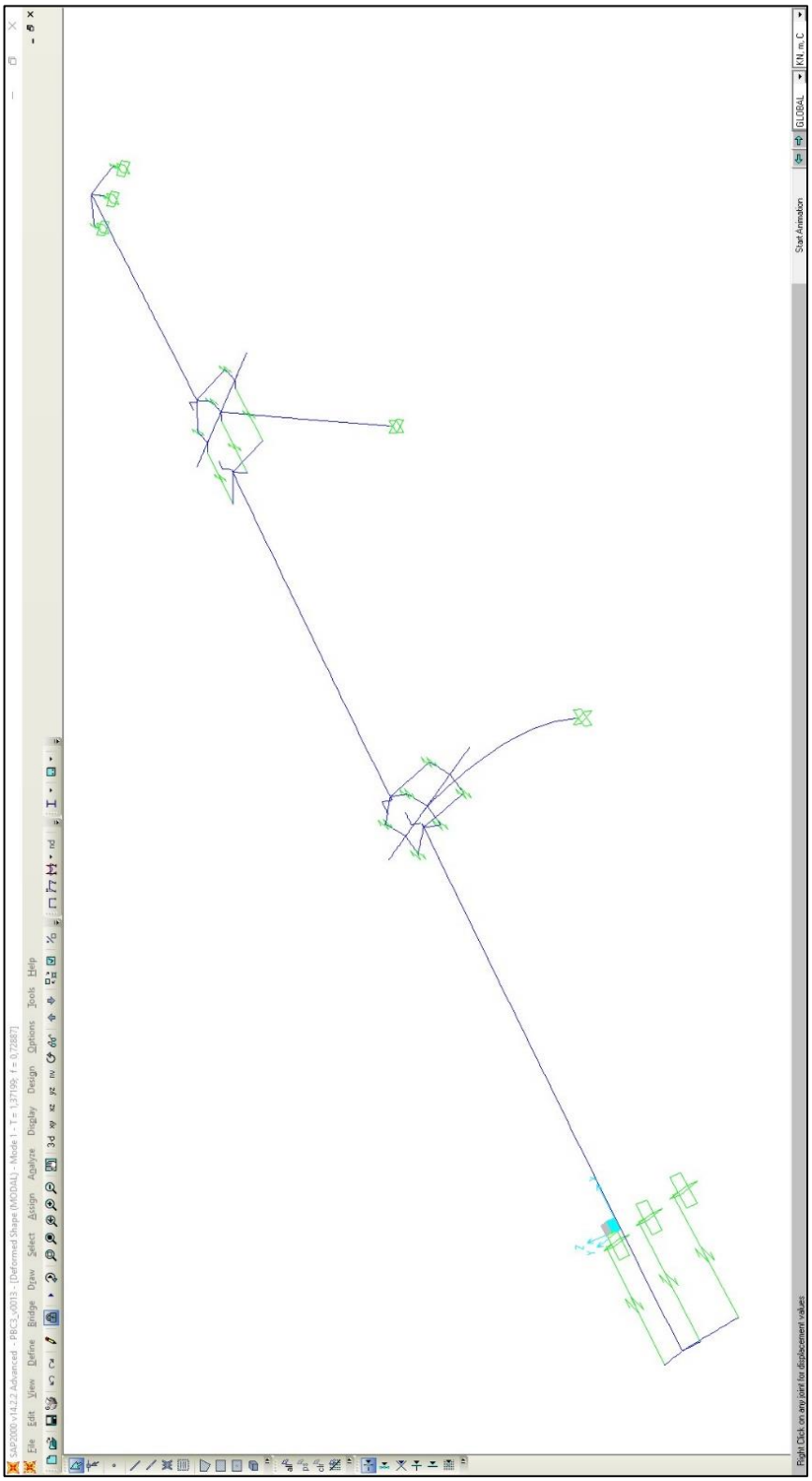

Figure 4.56. Shape and Period (T~=1,37s) of First Mode

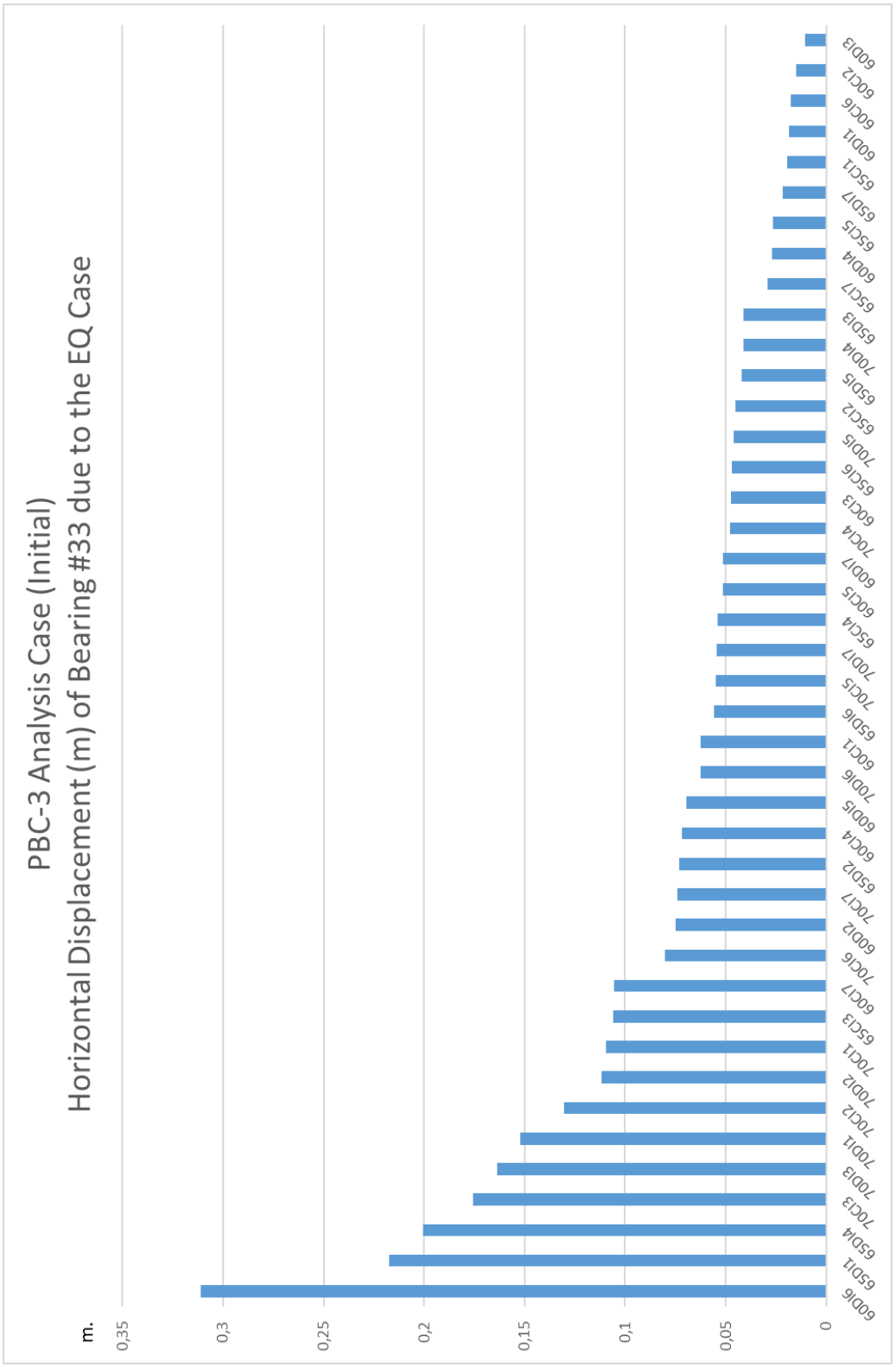

Figure 4.57. Horizontal Displacement (m) of Bearing #33 due to EQ Case

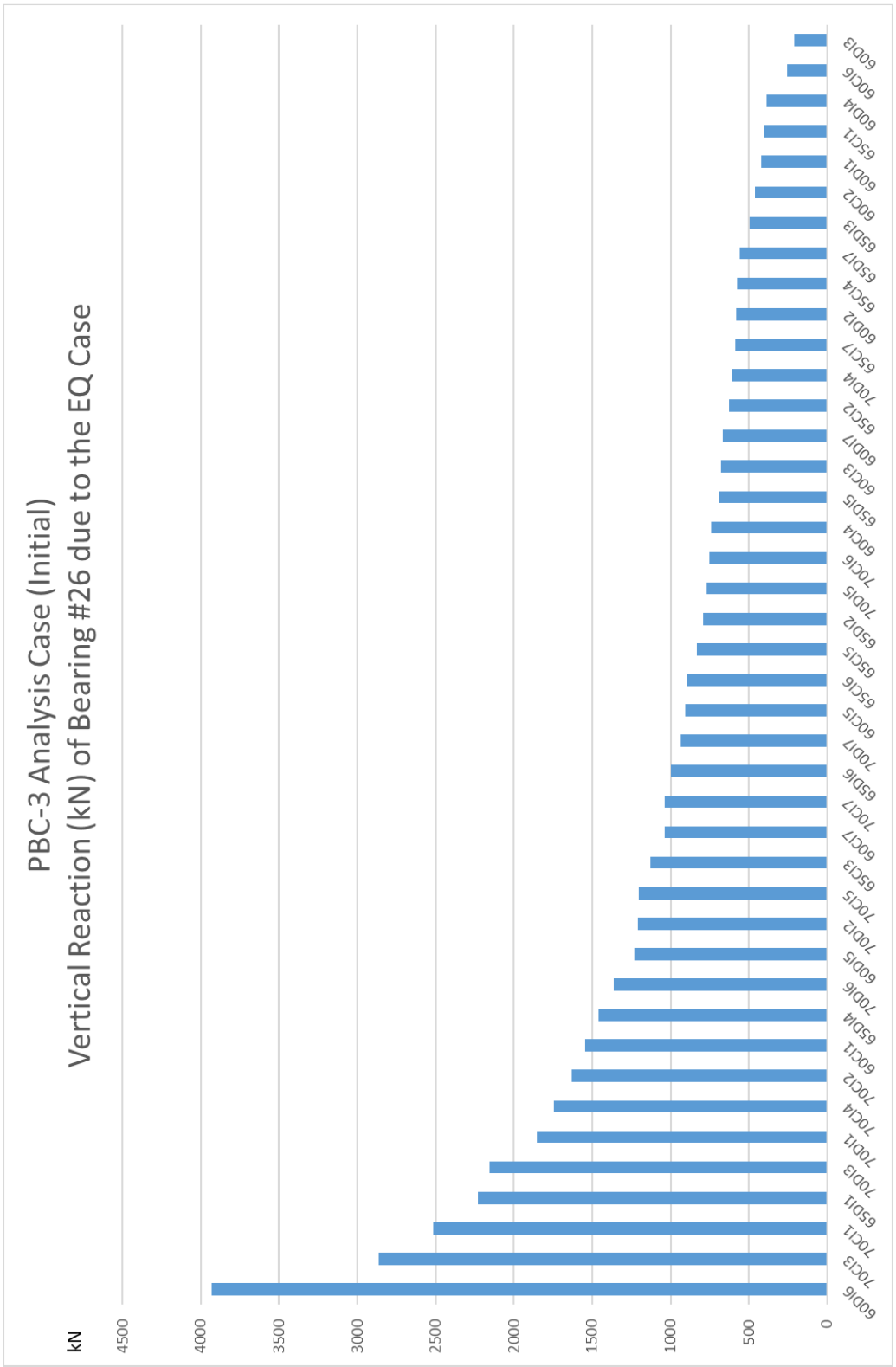

Figure 4.58. Vertical Reaction (kN) of Bearing #26 due to EQ Case

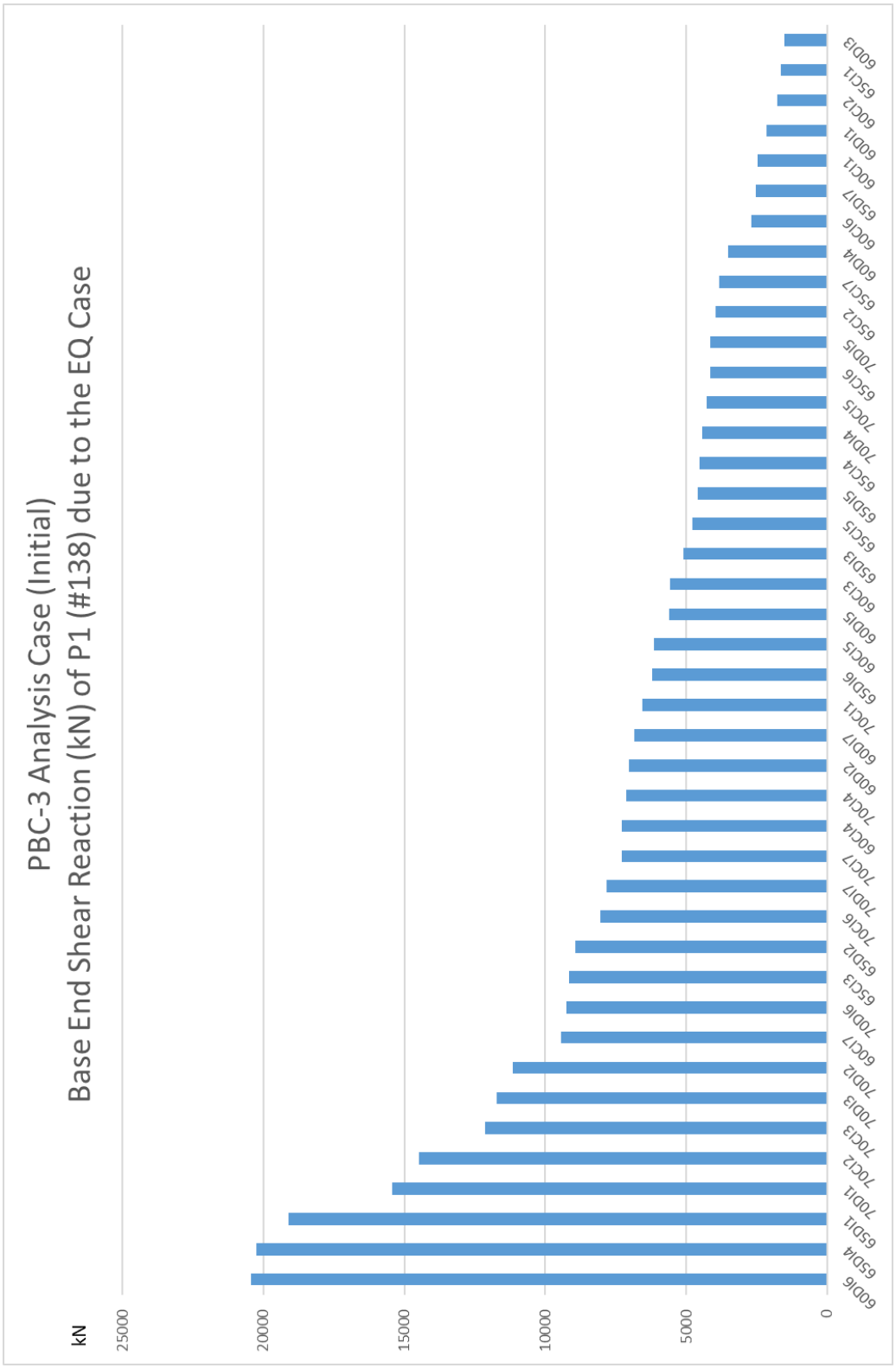

Figure 4.59. Base End Shear Reaction (kN) of P1 (#138) due to EQ Case

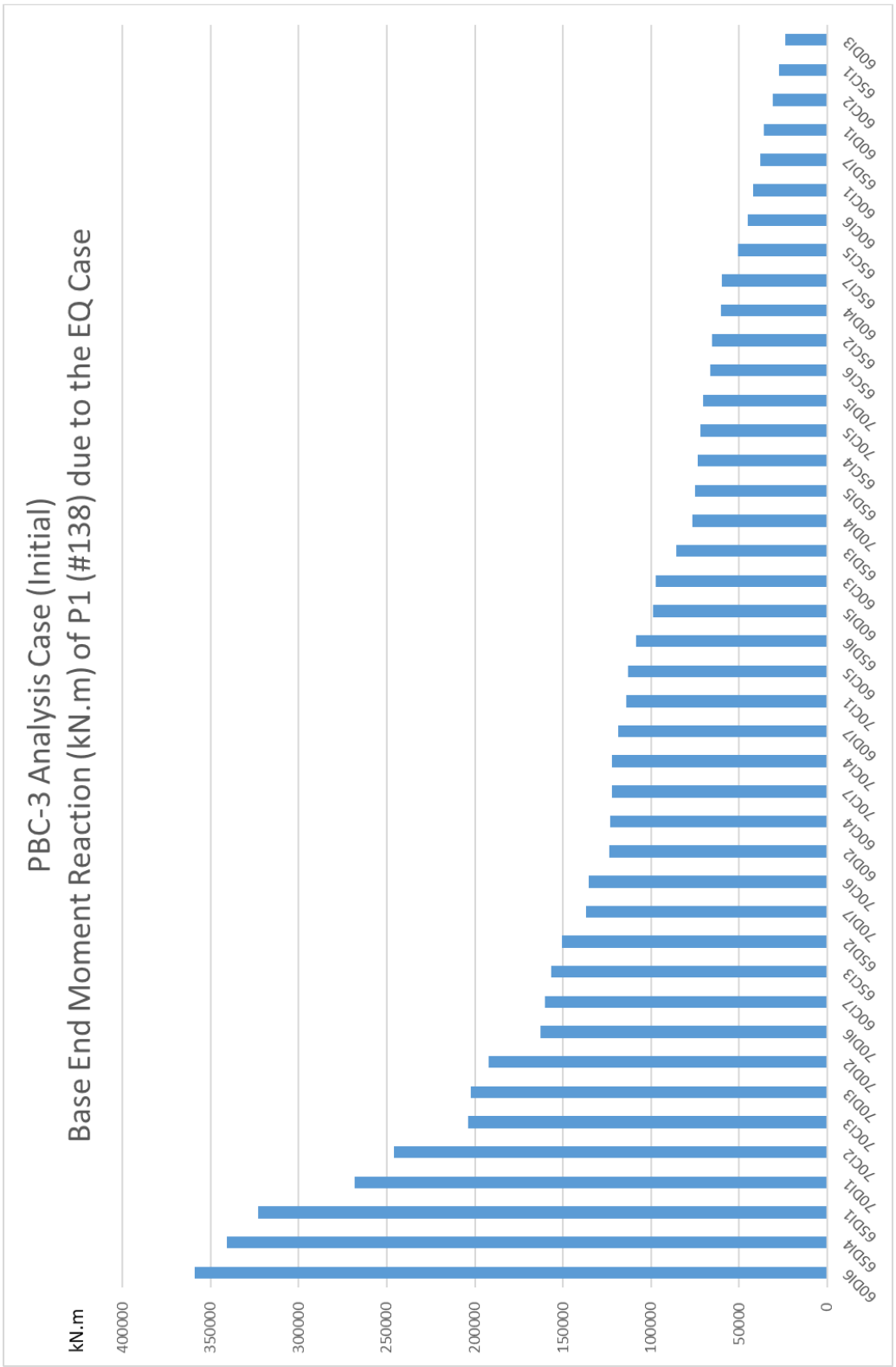

Figure 4.60. Base End Moment Reaction (kN.m) of P1 (#138) due to EQ Case

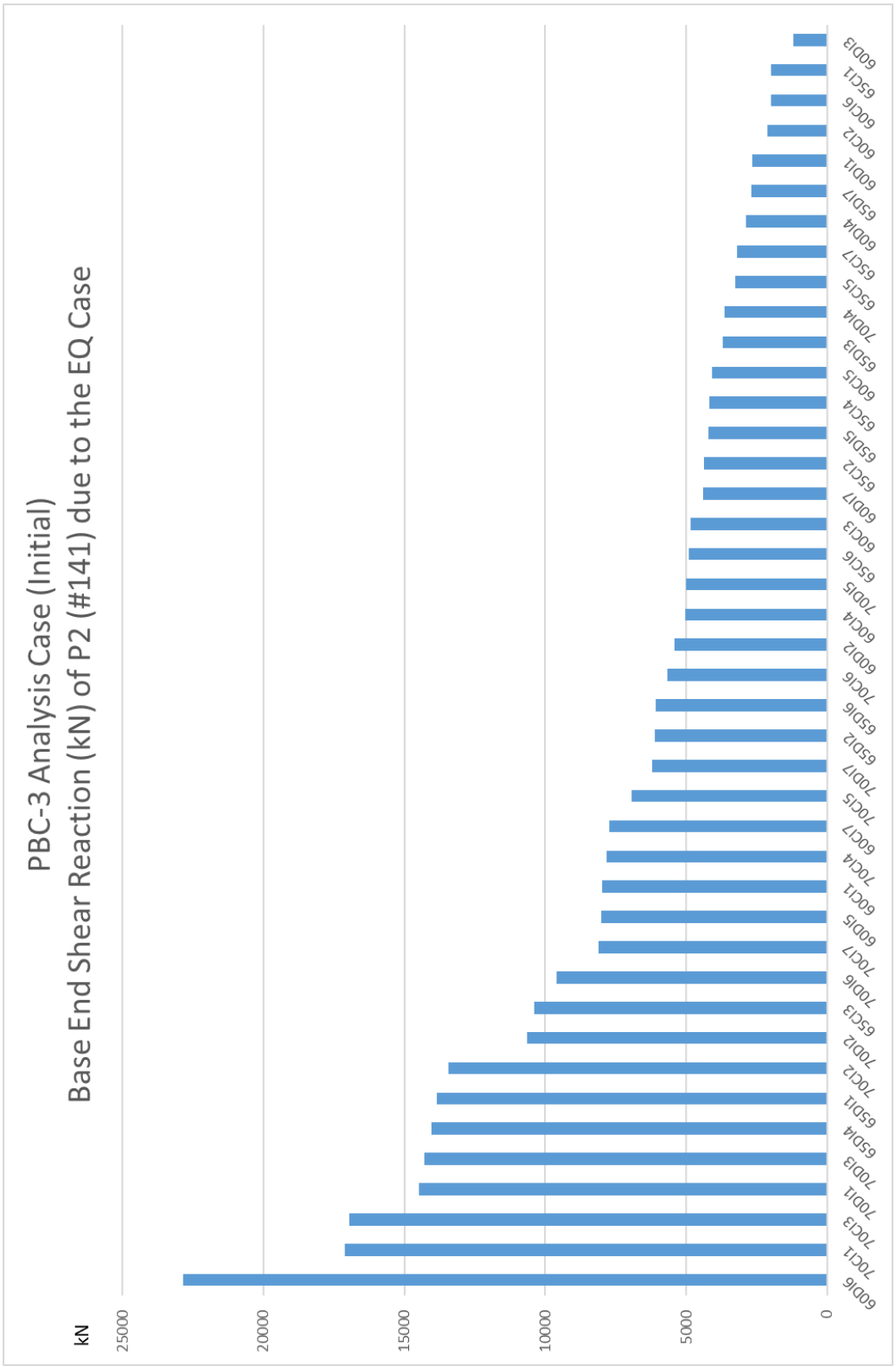

Figure 4.61. Base End Shear Reaction (kN) of P2 (#141) due to EQ Case

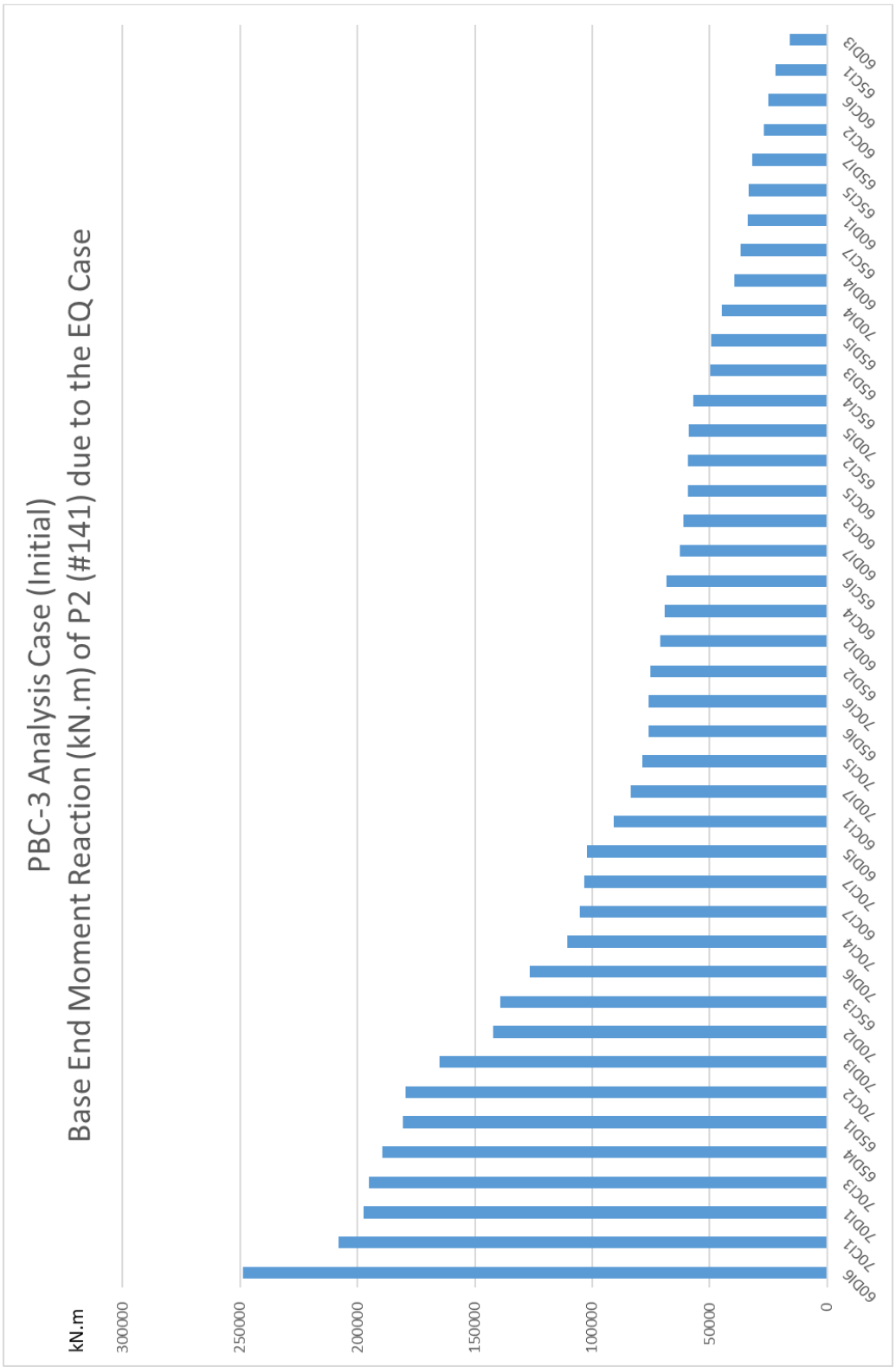

Figure 4.62. Base End Moment Reaction (kN.m) of P2 (#141) due to EQ Case

4.2.3.3. Specific Properties of the Structure (Iterated Stiffness)

Since relative displacements of three earthquake cases exceed the 10-centimeter limit, as done for the previous two analysis cases, stiffness values of bearings are iterated by generating some other analytical models to achieve the maximum relative displacement of bearings under any earthquake applied to the bridge within this study.

Final stiffness values of pot bearings standing upon the desired relative displacement limit are shown below in Figure 4.63 and Figure 4.64.

Results obtained from the structural analysis of the bridge via using bearings with specified properties are provided in part 4.2.3.4.

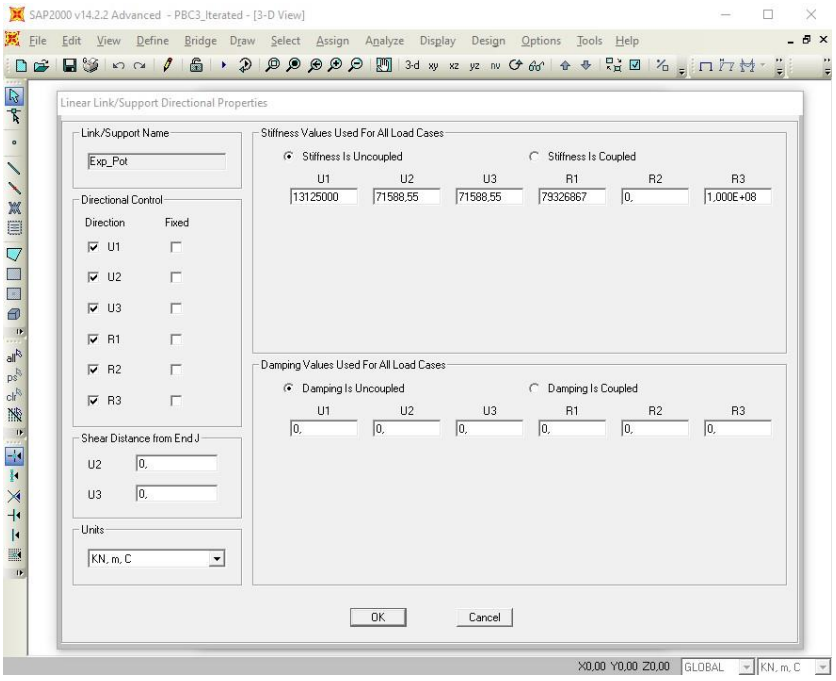

Figure 4.63. Stiffness Properties of Expansion Pot Bearings

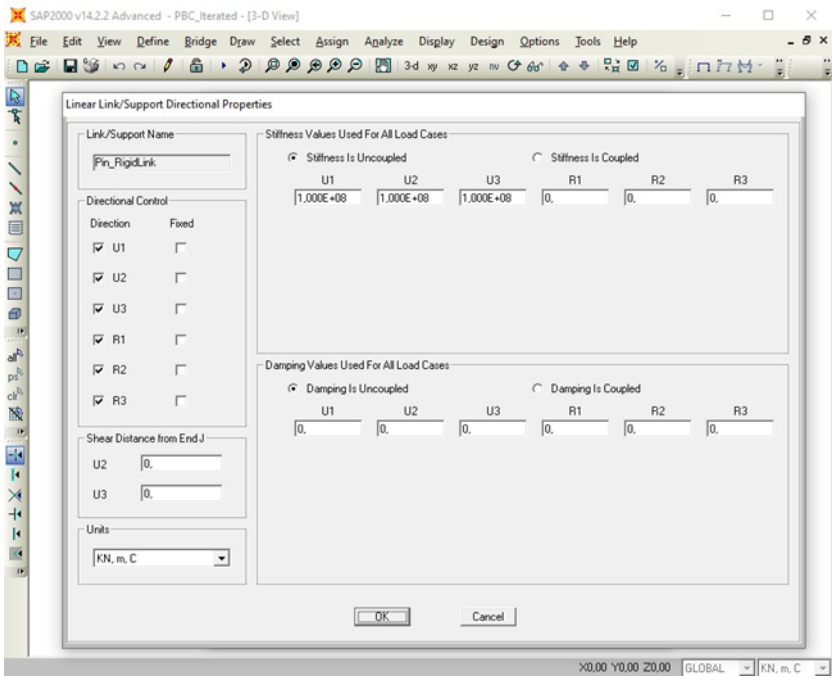

Figure 4.64. Stiffness Properties of Fixed Pot Bearings

4.2.3.4. Analysis Results of the Structure (Iterated Stiffness)

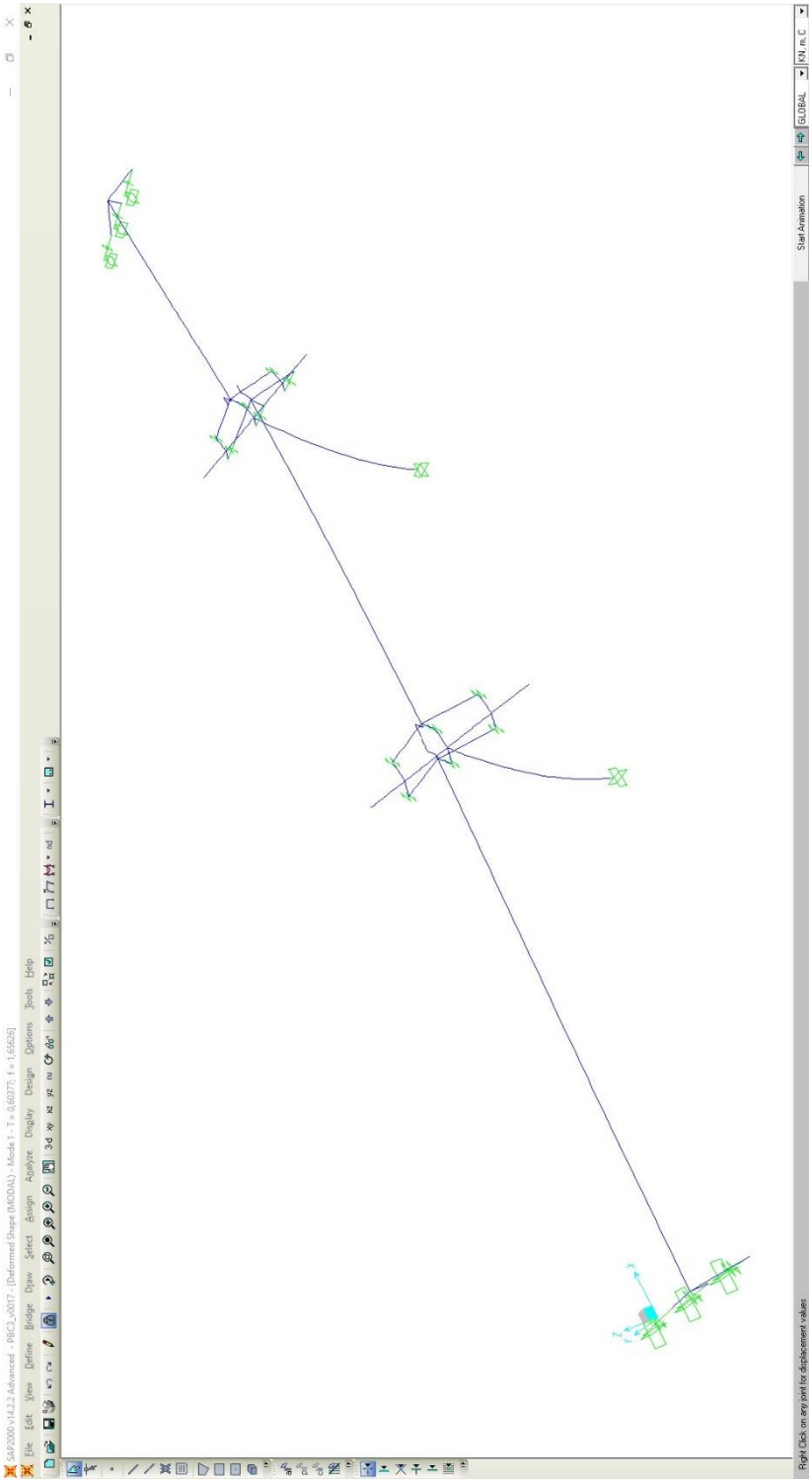

Figure 4.65. Shape and Period (T~=0,60s) of First Mode

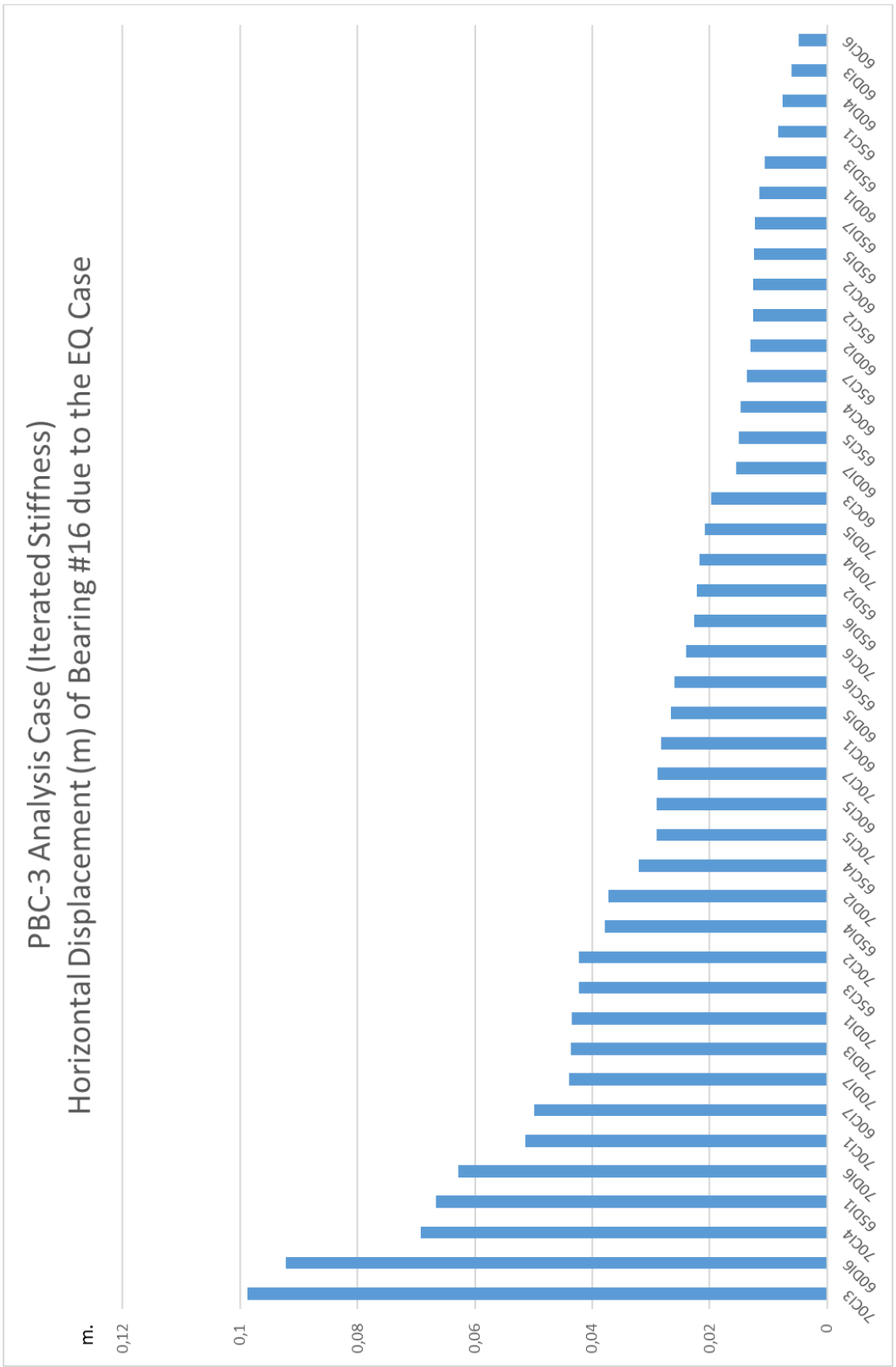

Figure 4.66. Horizontal Displacement (m) of Bearing #16 due to EQ Case (with iterated stiffness)

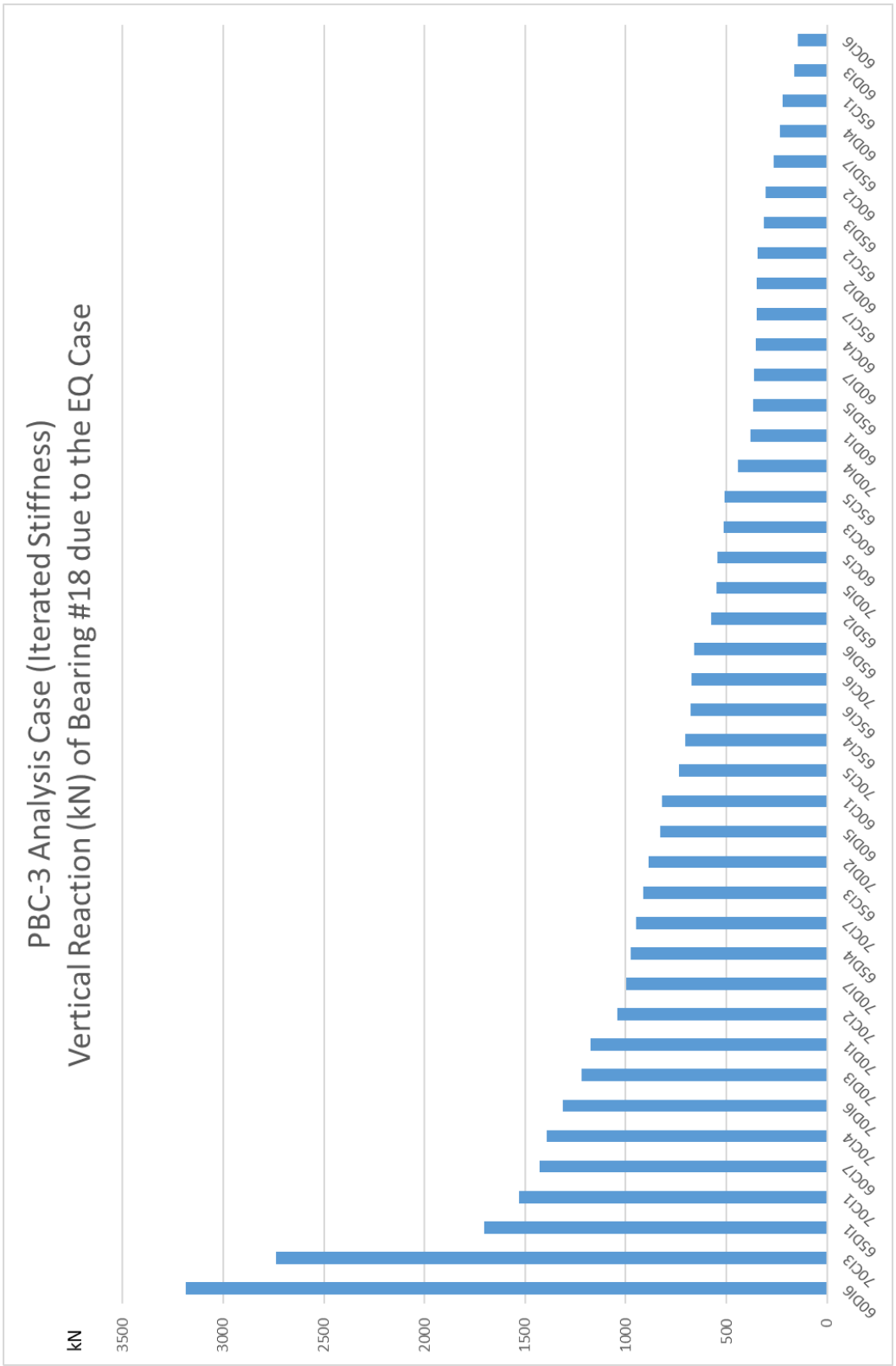

Figure 4.67. Vertical Reaction (kN) of Bearing #18 due to EQ Case (with iterated stiffness)

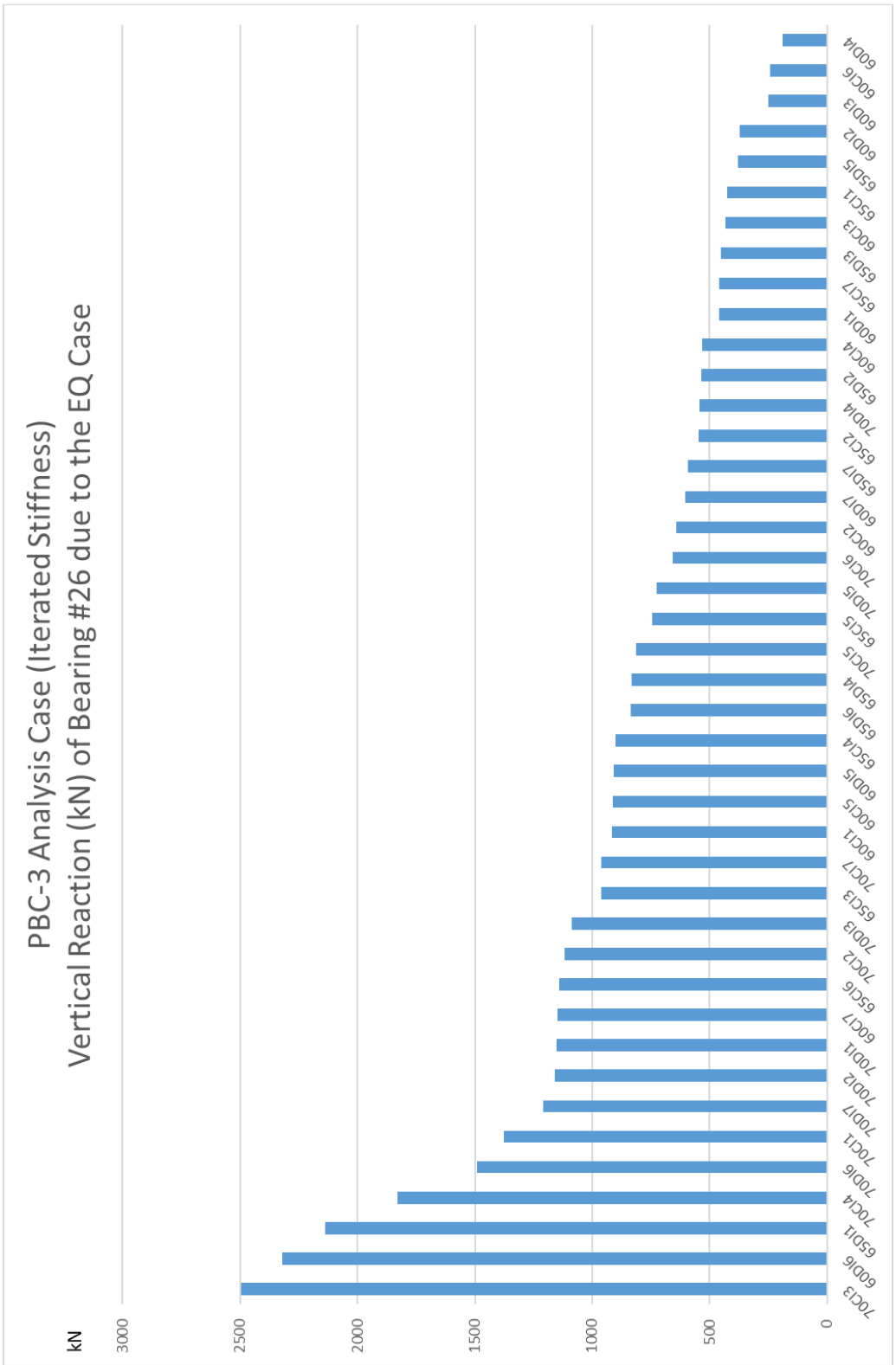

Figure 4.68. Vertical Reaction (kN) of Bearing #26 due to EQ Case (with iterated stiffness)

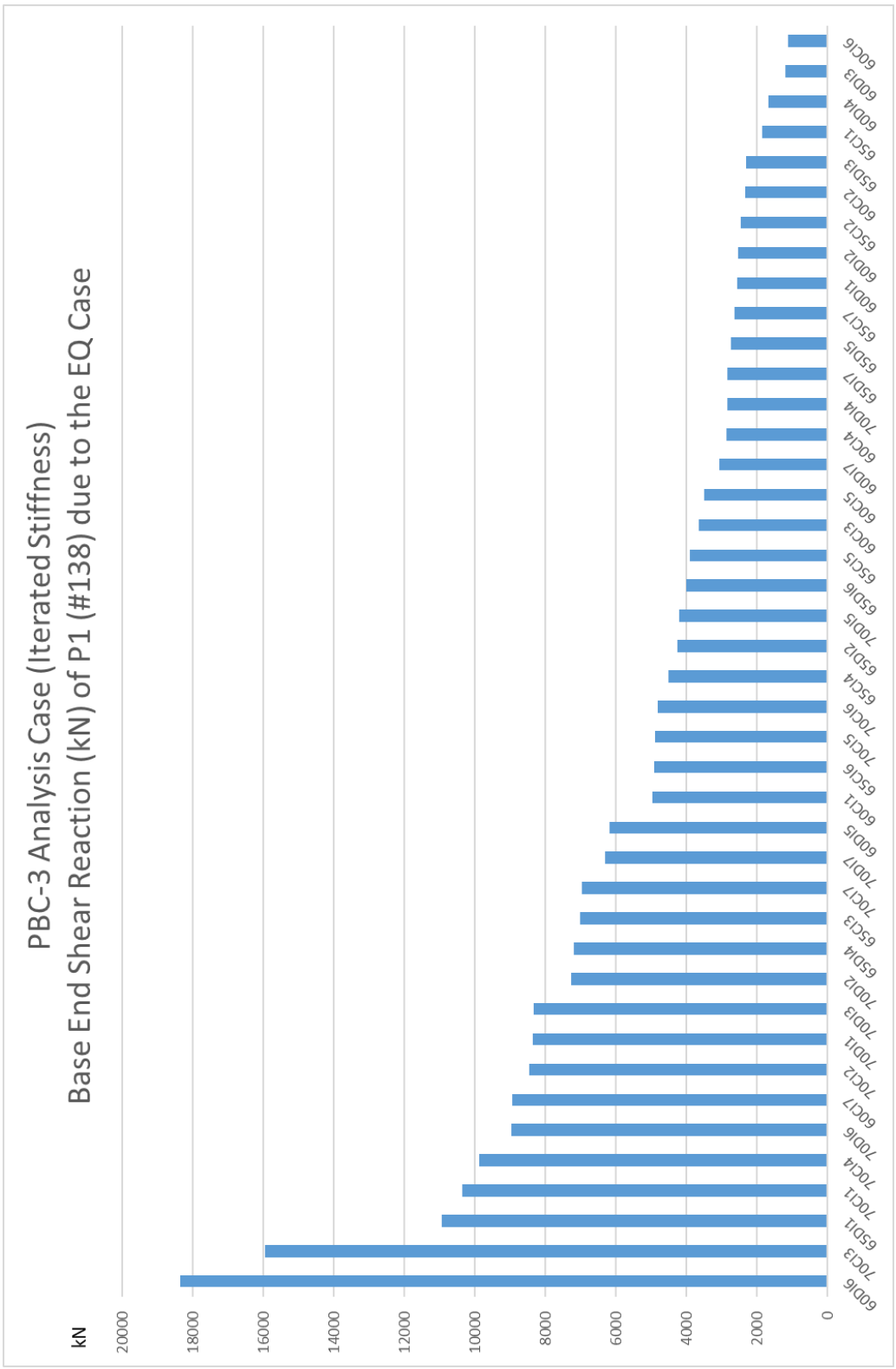

Figure 4.69. Base End Shear Reaction (kN) of P1 (#138) due to EQ Case (with iterated stiffness)

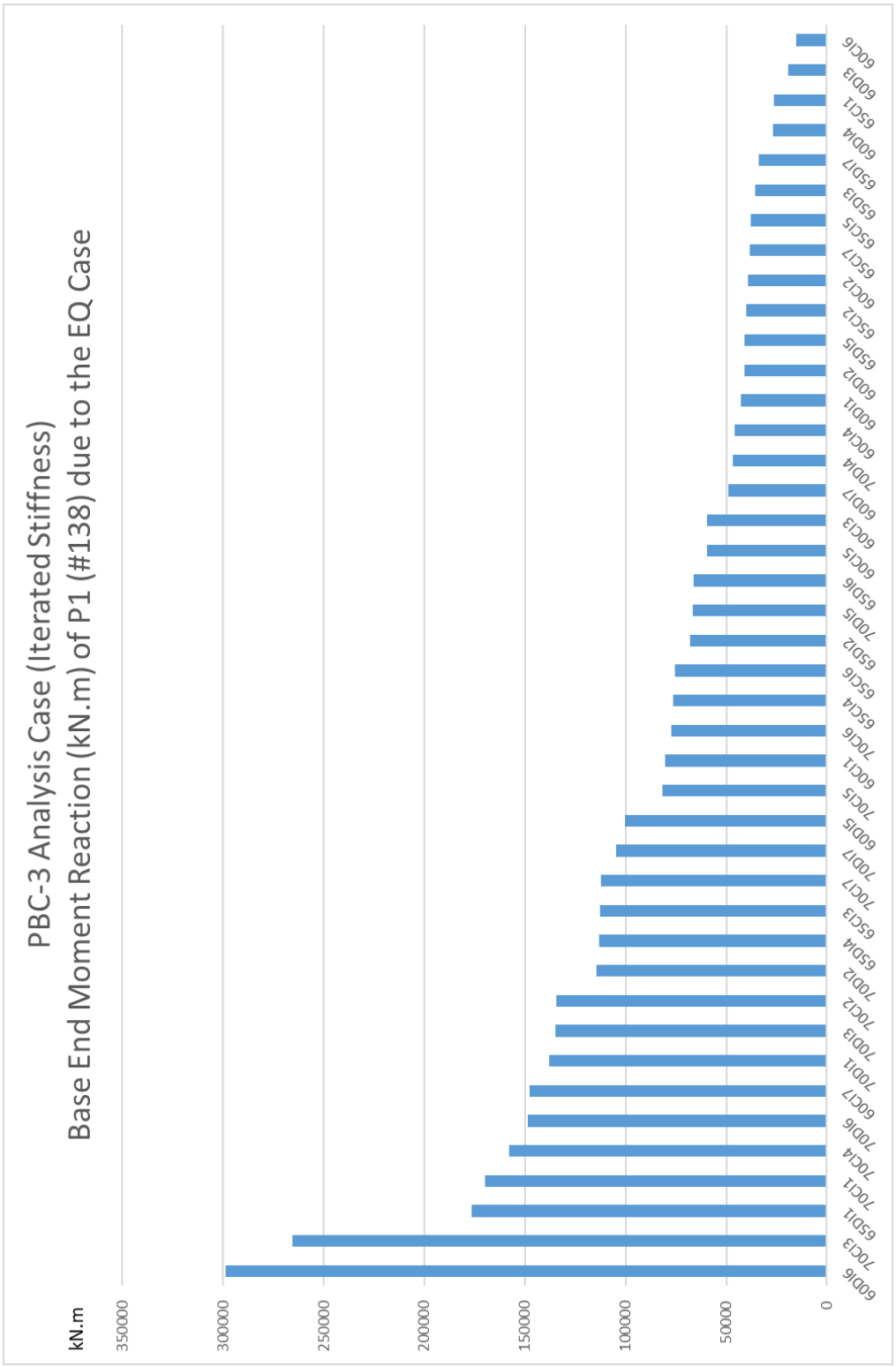

Figure 4.70. Base End Moment Reaction (kN.m) of P1 (#138) due to EQ Case (with iterated stiffness)

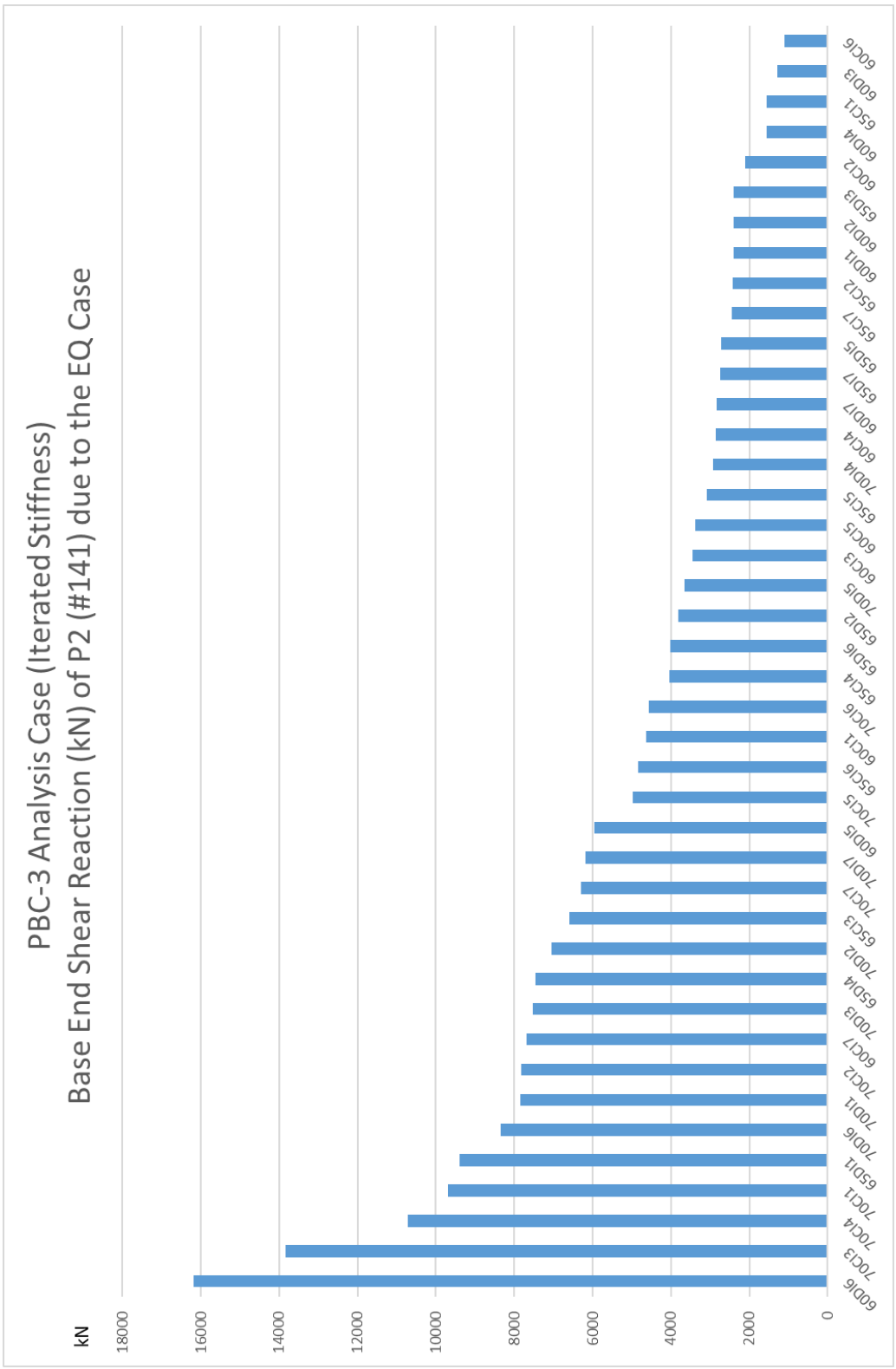

Figure 4.71. Base End Shear Reaction (kN) of P2 (#141) due to EQ Case (with iterated stiffness)

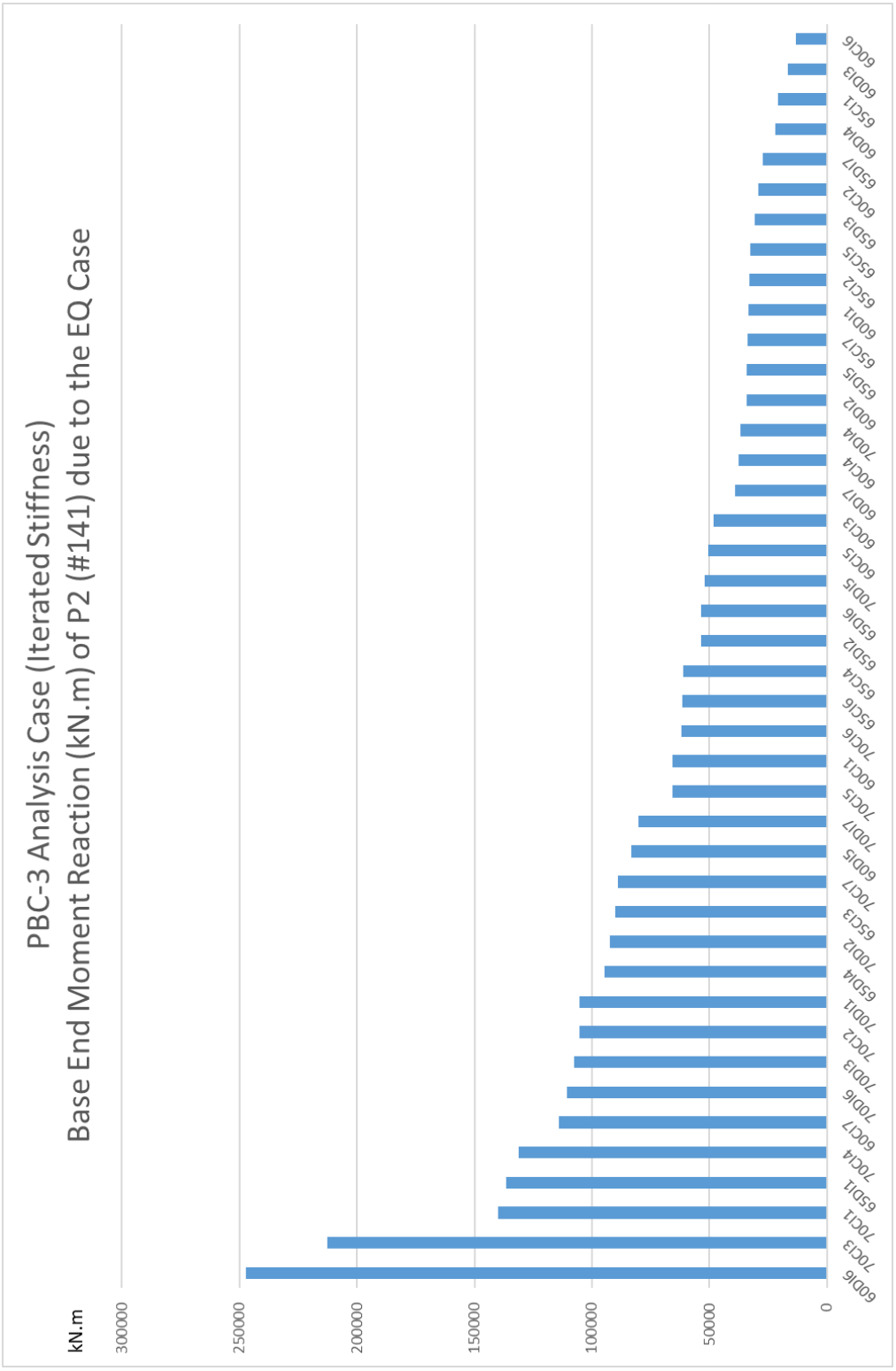

Figure 4.72. Base End Moment Reaction (kN.m) of P2 (#141) due to EQ Case (with iterated stiffness)

4.2.4. Response Spectra and Case Related Responses

In this part of the report, response spectra of ground motion data in horizontal direction 1 and periods of iterated analysis cases are provided. In Tables 4.1 and 4.2, periods of first modes for all three analysis cases are provided. In Figures from 4.73 to 4.78, response spectra of earthquake data in horizontal direction 1 are provided. In response spectrum graphs, dominant periods of the bridge for each analysis case are also added in order to see the effect of each earthquake ground motion separately. When the responses are examined, it is clear that for any period, each ground motion has a unique value of ground motion acceleration affecting the bridge formed. Whole response spectrum graphs of each earthquake data are provided in Appendix C for all directions (horizontal 1, horizontal 2 and vertical). In Figure 4.79, all responses of earthquakes for each analysis case and their periods are provided. In Figures 4.80, 4.81, and 4.82; acceleration responses of each earthquake were given for the periods of analysis cases EBC10-REF, EBC-3 and PBC-3, respectively.

Table 4.1. Periods for Dominant Modes of Initial Analysis Cases

Analysis Case Name - Initial	Period of First Mode (s)
EBC10-REF (Reference Case) (10 Elastomeric Bearing Used)	0,8447
EBC-3 (3 Elastomeric Bearing Used Case)	0,8429
PBC-3 (3 Pot Bearing Used Case)	1,3720

Table 4.2. Periods for Dominant Modes of Iterated Analysis Cases

Analysis Case Name - Iterated	Period of First Mode (s)
EBC10-REF (Reference Case) (10 Elastomeric Bearing Used)	0,6985
EBC-3 (3 Elastomeric Bearing Used Case)	0,6069
PBC-3 (3 Pot Bearing Used Case)	0,6038

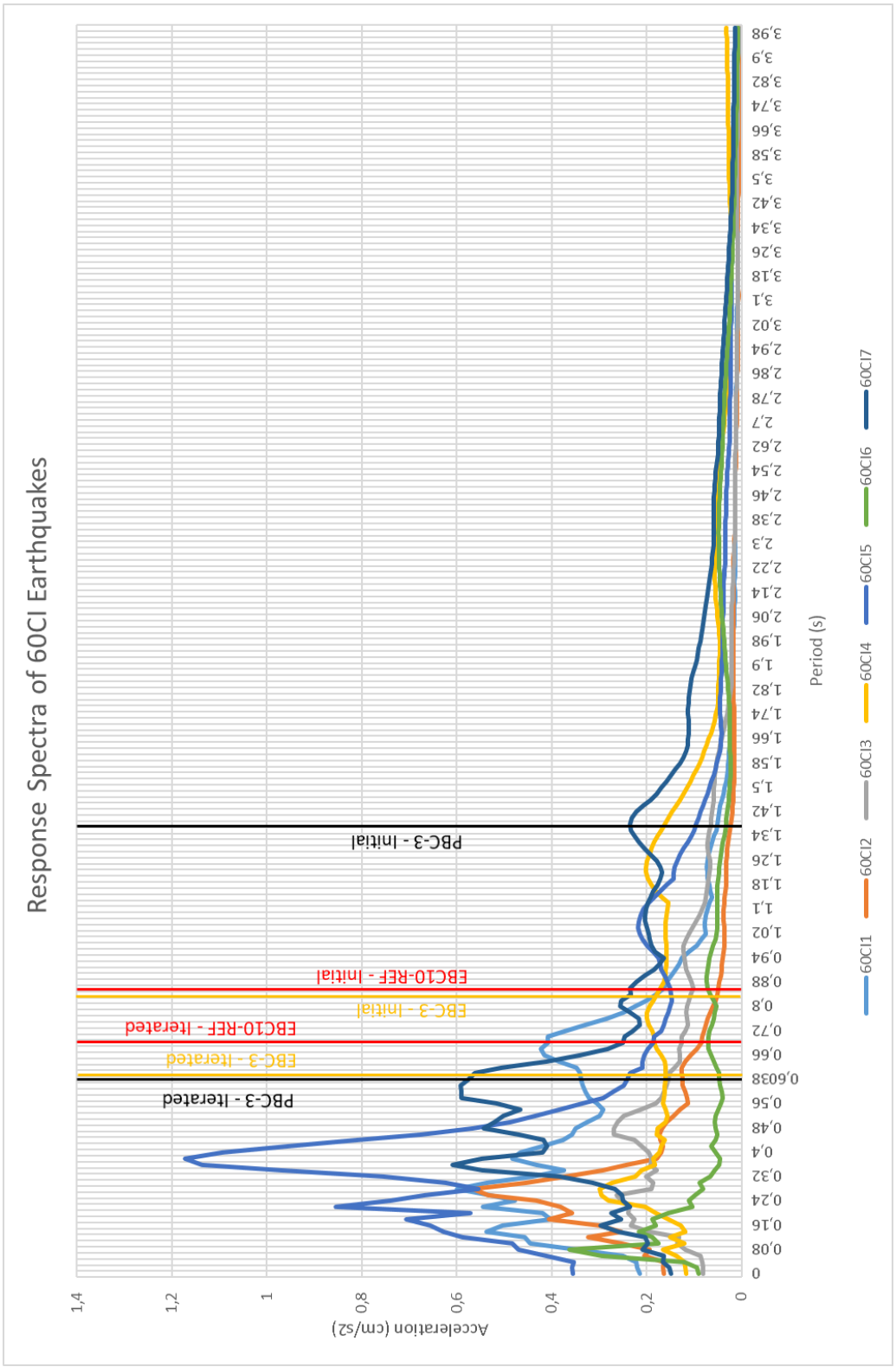

Figure 4.73. Response Spectra of 60CI Coded Earthquakes

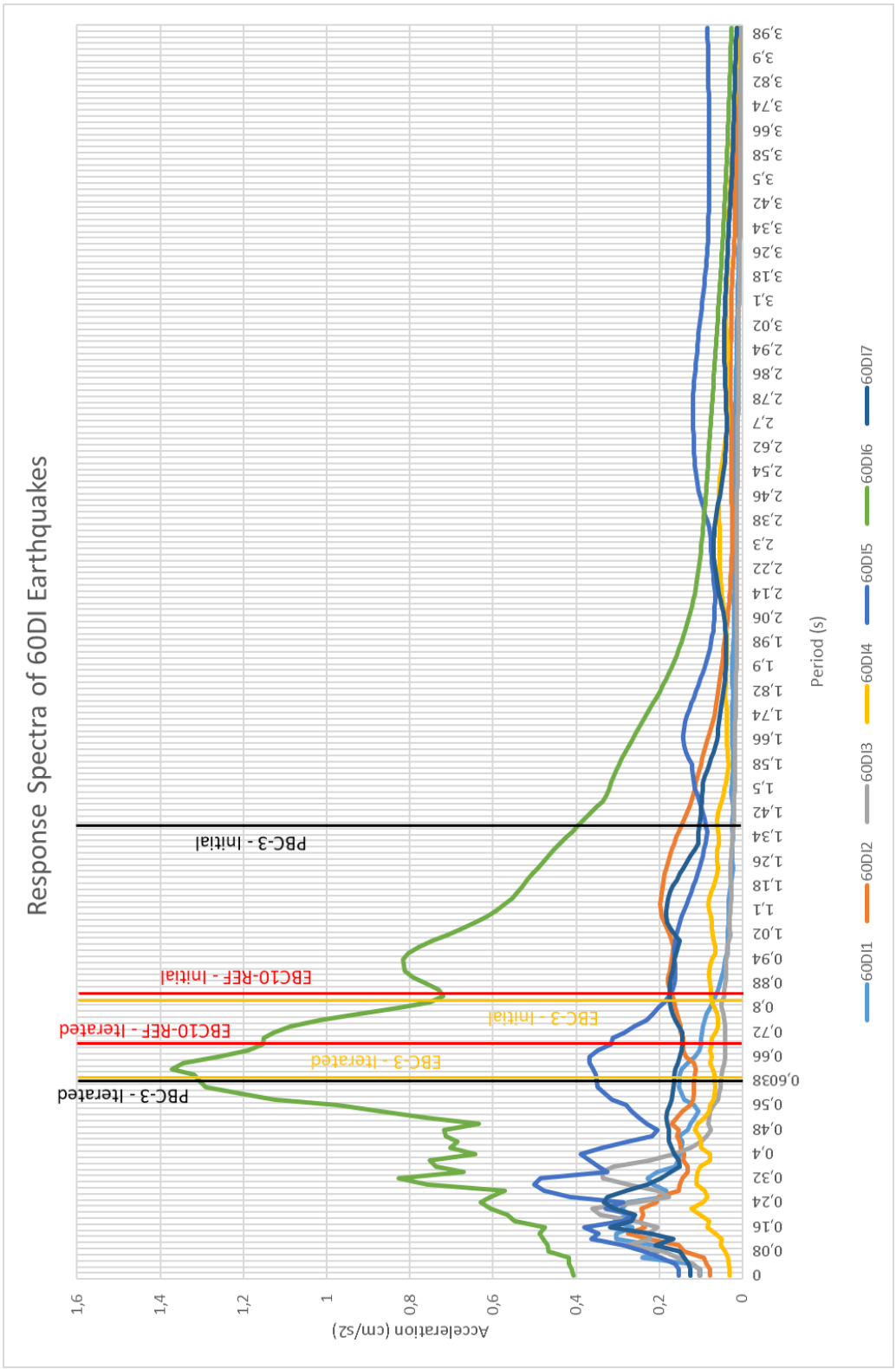

Figure 4.74. Response Spectra of 60DI Coded Earthquakes

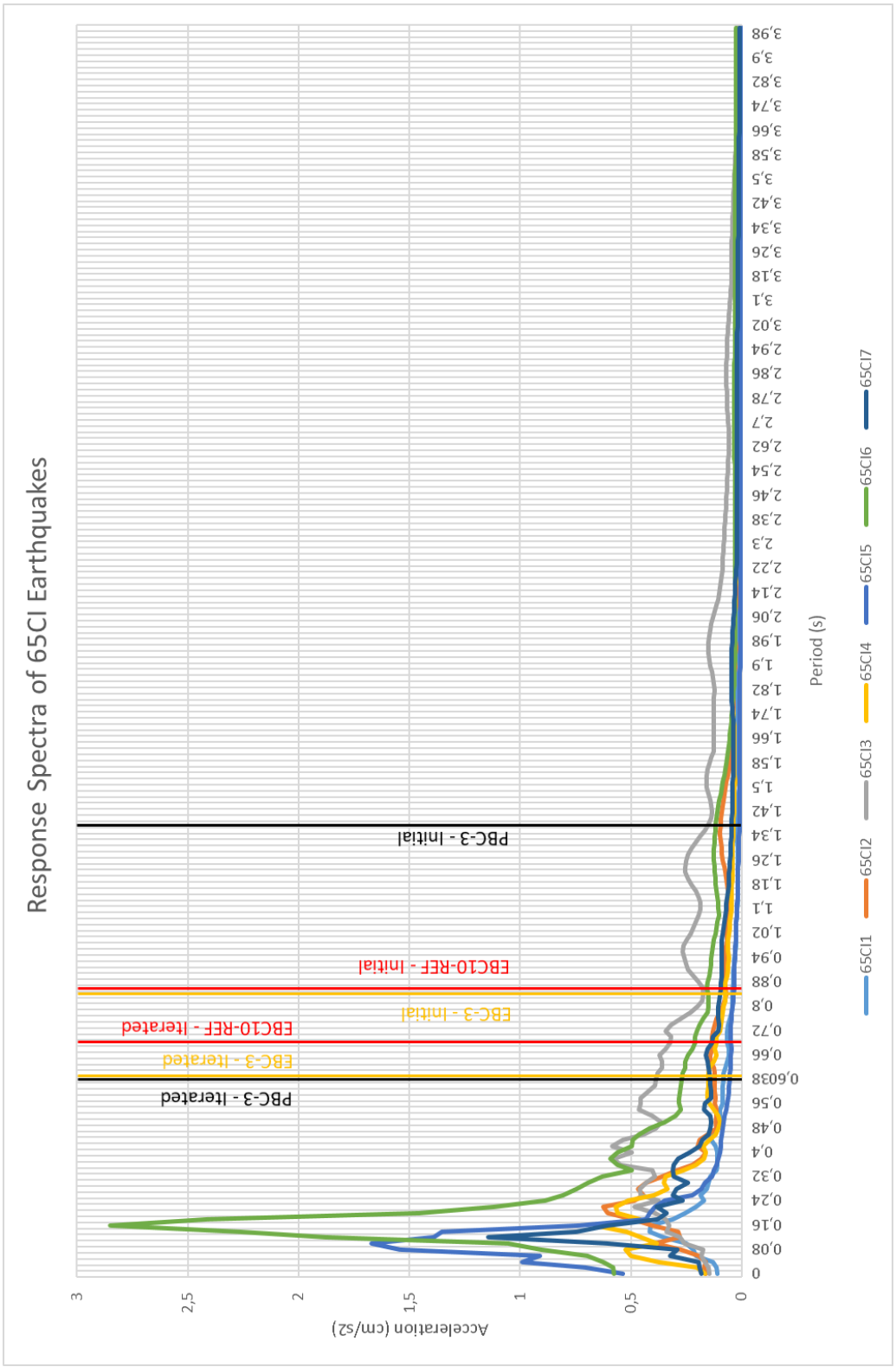

Figure 4.75. Response Spectra of 65CI Coded Earthquakes

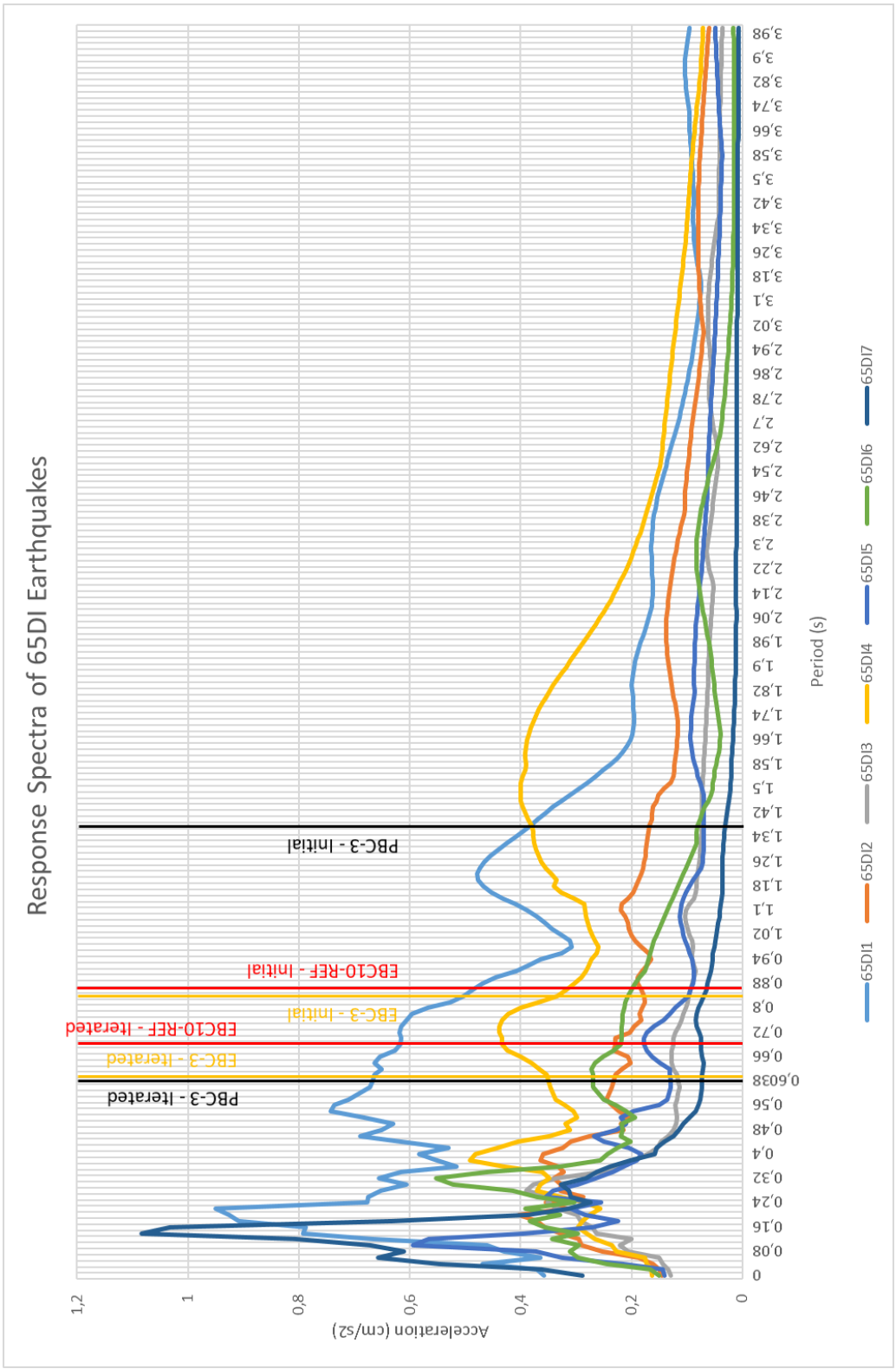

Figure 4.76. Response Spectra of 65DI Coded Earthquakes

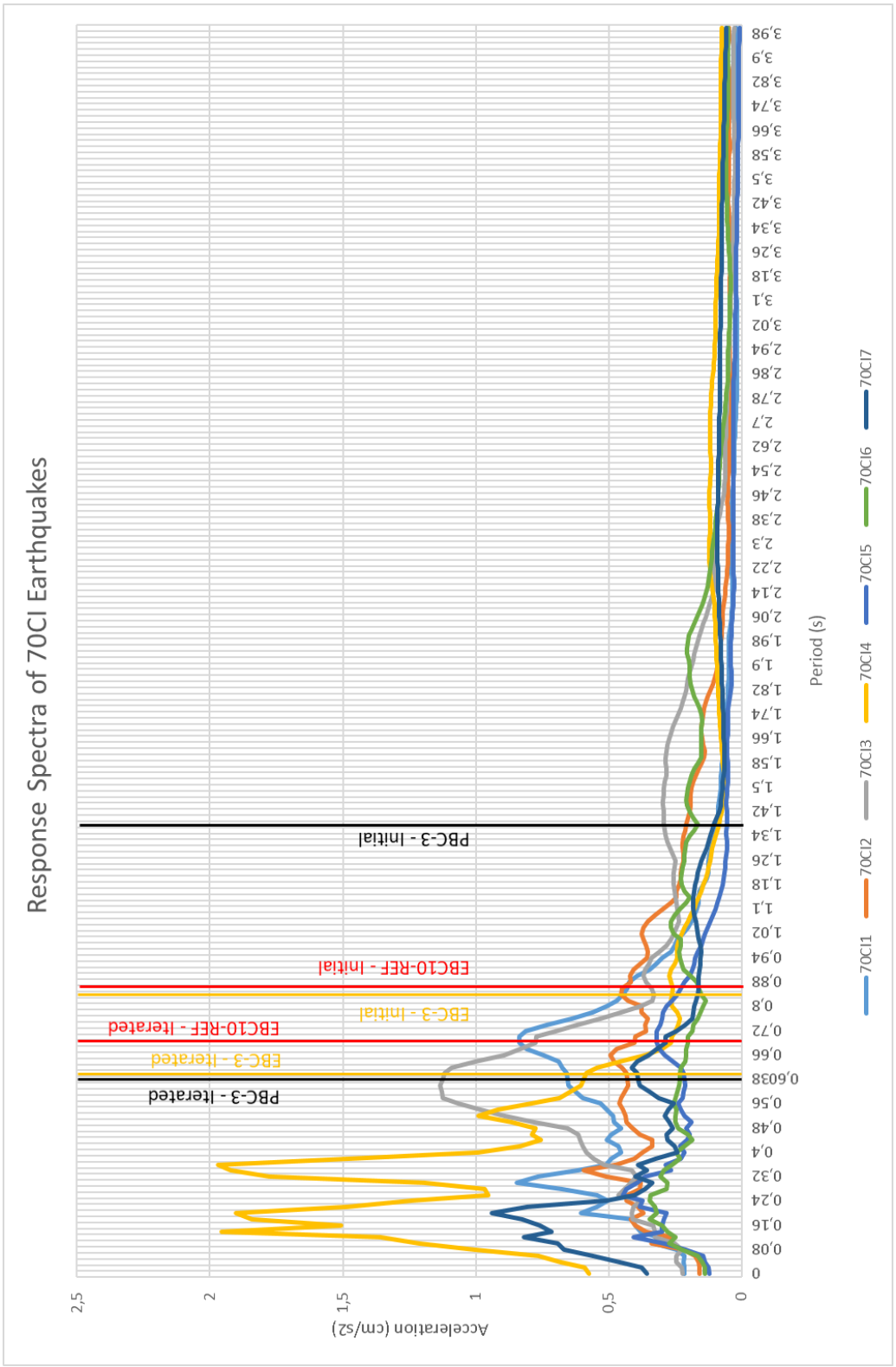

Figure 4.77. Response Spectra of 70CI Coded Earthquakes

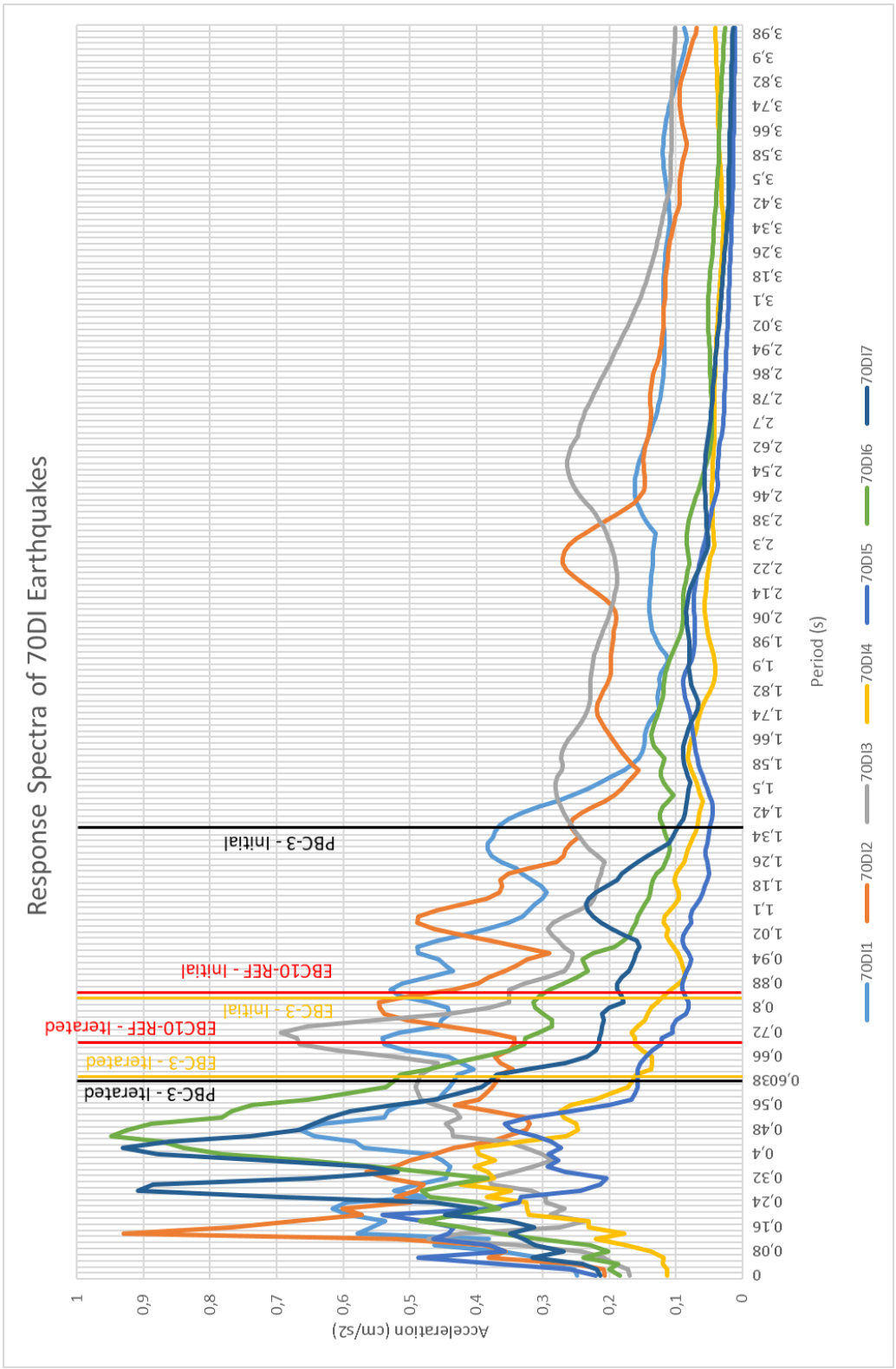

Figure 4.78. Response Spectra of 70DI Coded Earthquakes

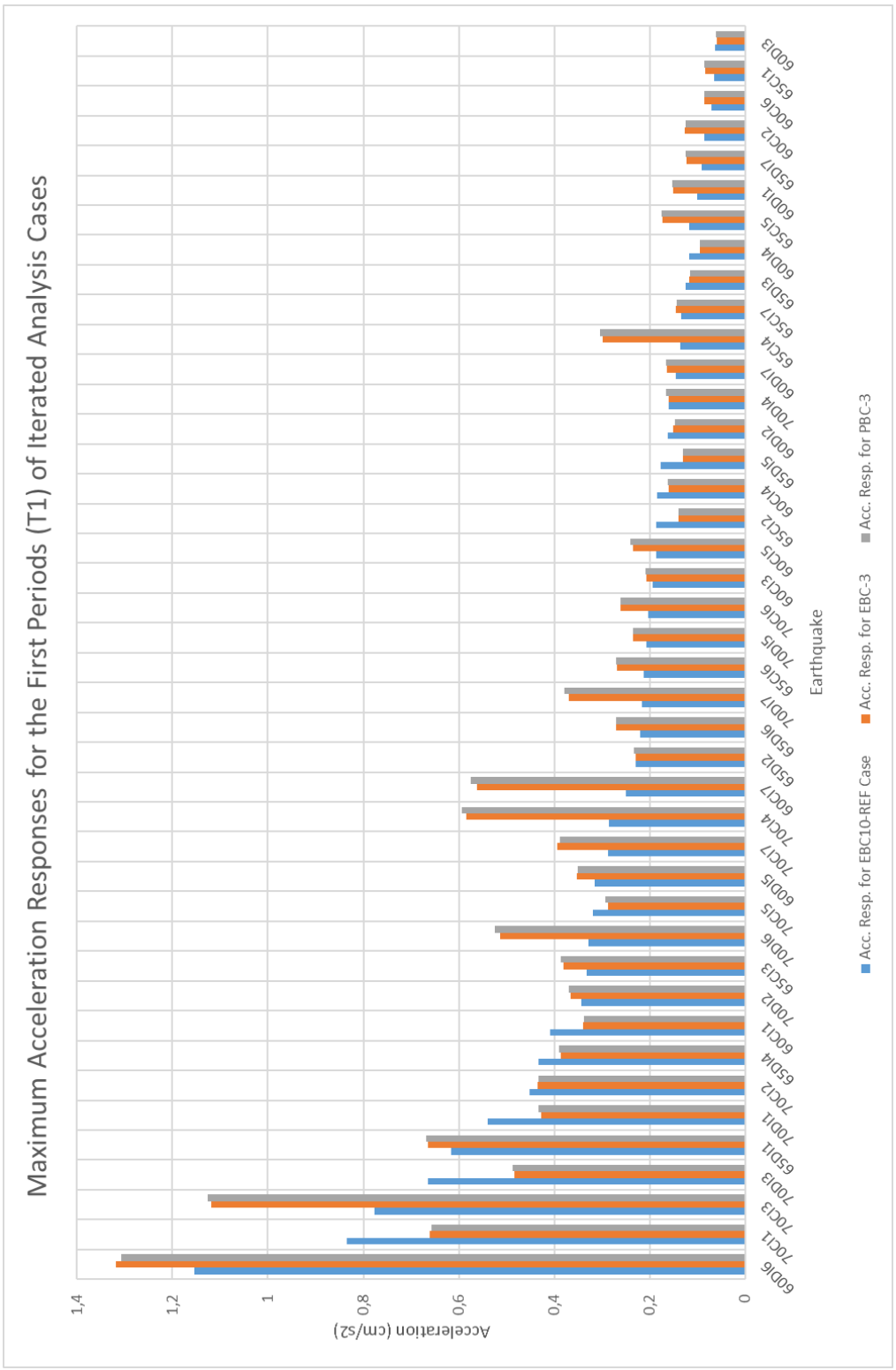

Figure 4.79. Maximum Acceleration Response for each Earthquake - For All Three Iterated Cases (EBC10-REF, EBC-3 and PBC-3)

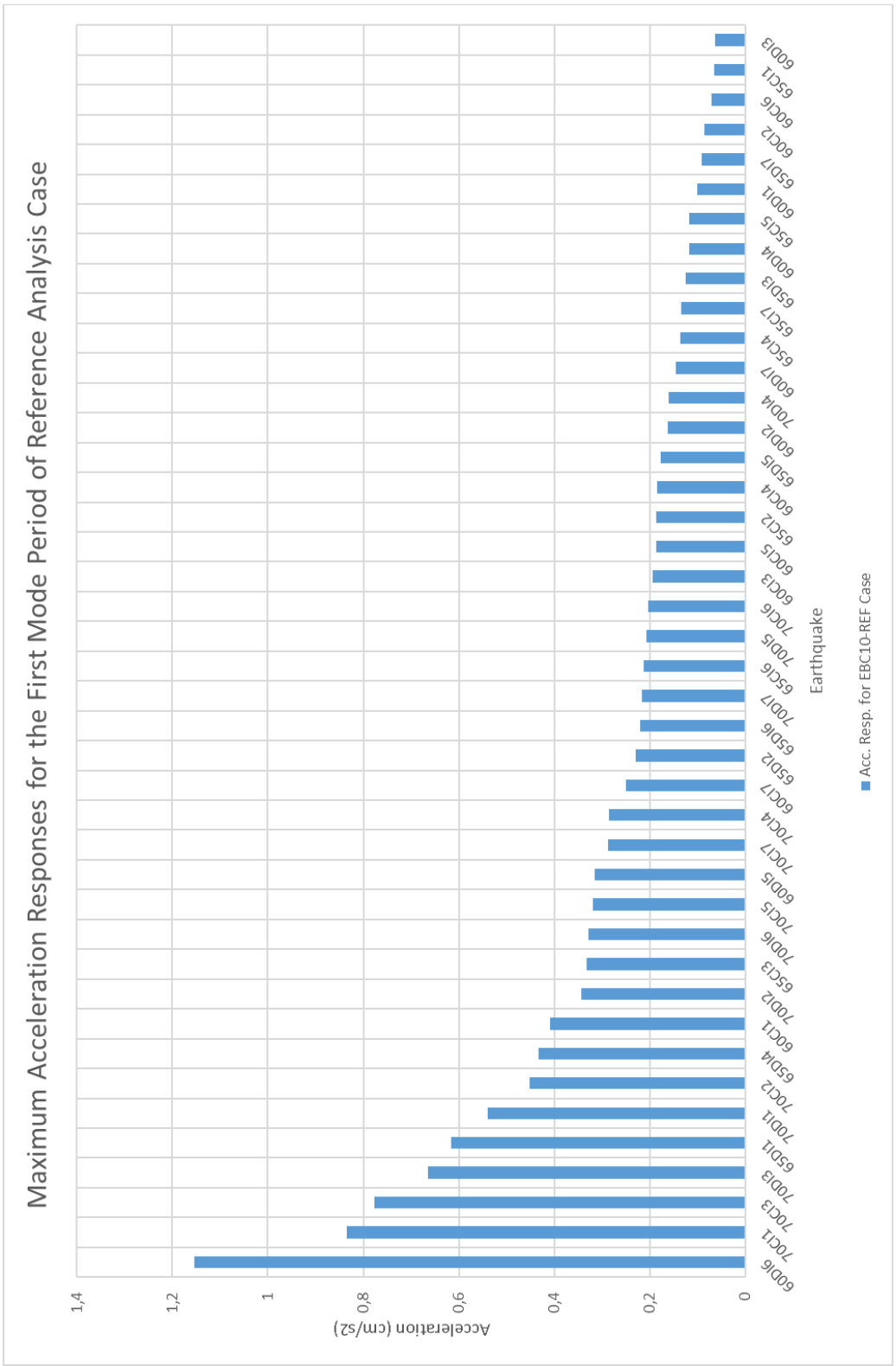

Figure 4.80. Maximum Acceleration Response for each Earthquake for EBC10-REF - Iterated

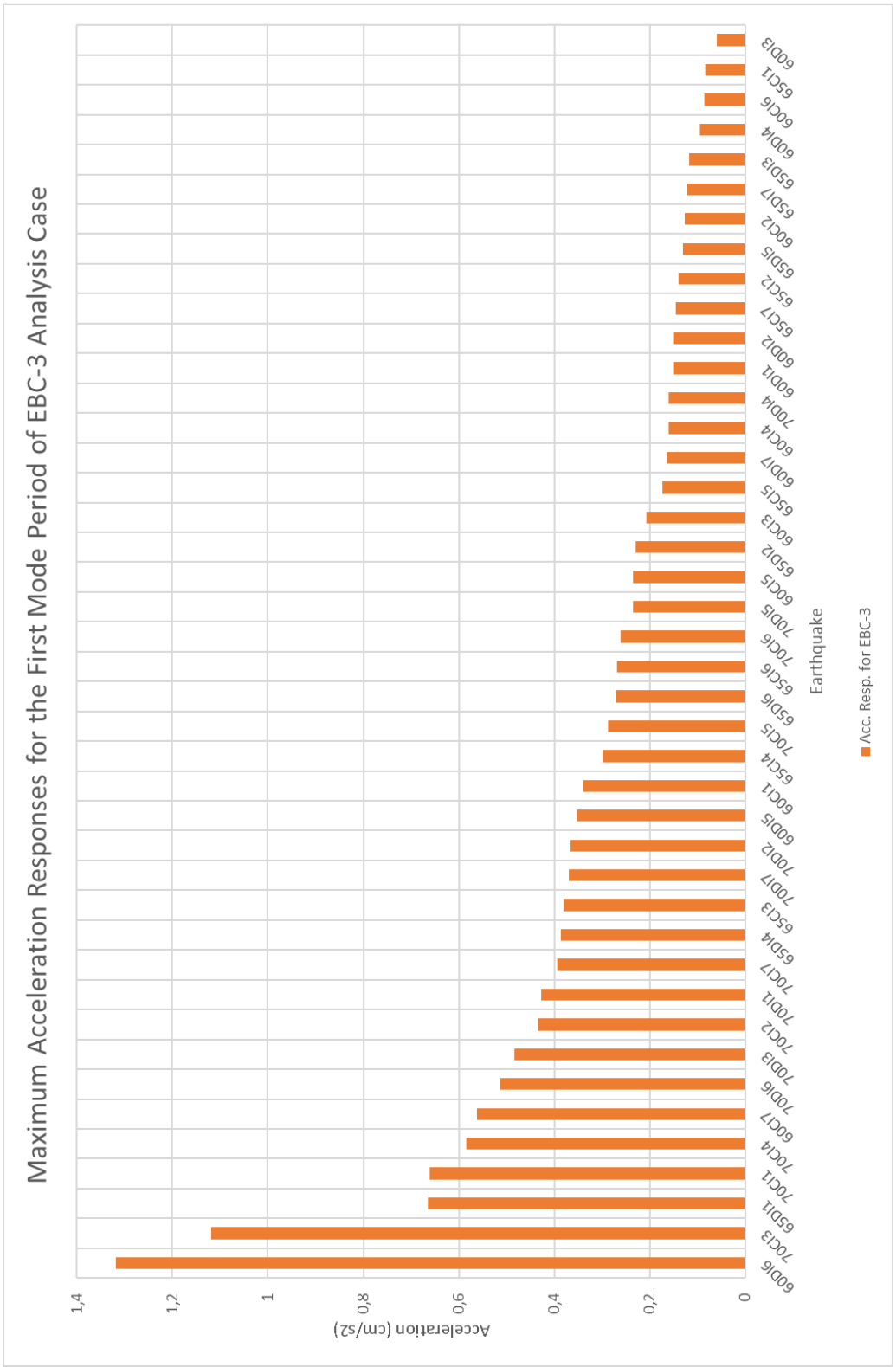

Figure 4.81. Maximum Acceleration Response for each Earthquake for EBC-3 - Iterated

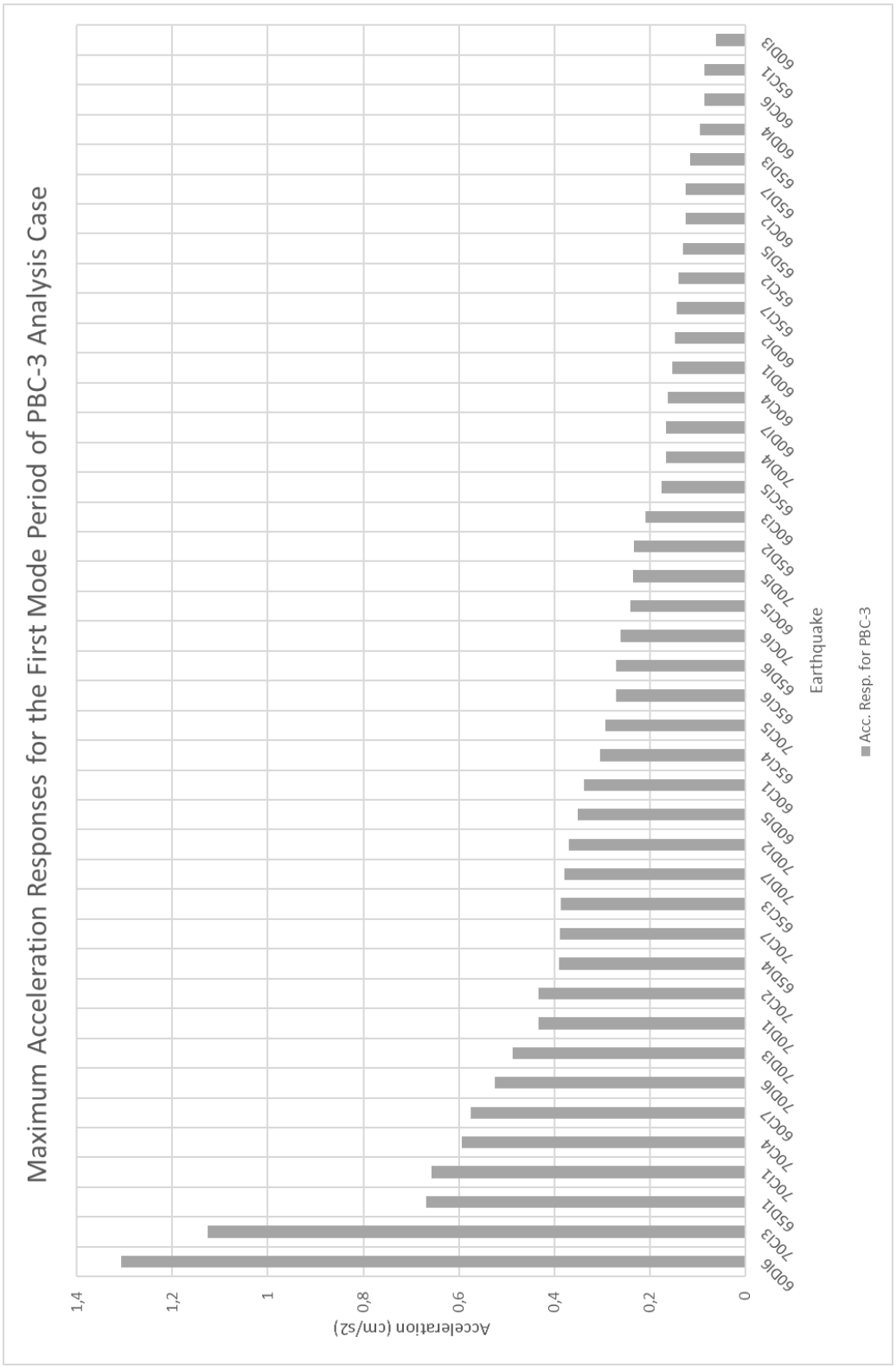

Figure 4.82. Maximum Acceleration Response for each Earthquake for PBC-3 – Iterated

4.2.5. Summary of the Results

For summarizing the results obtained from the analysis, consolidated graphs and very brief result tables are presented in this section. Consolidated graphs include all the results of all three analysis cases for either initial or iterated cases. They are provided in Figures 4.83, 4.84, 4.85, 4.86, 4.87 and 4.88.

Figure 4.83 shows all the results of bearings that have maximum deformations obtained in the initial structural situation of each case. Results given in the above-mentioned graphs show that elastomeric bearings have the same level of deformation and the pot bearing case has higher horizontal relative horizontal deformations since it was assumed to be free to move in horizontal directions.

Figure 4.84 displays the maximum vertical reactions exerted on bearings due to each applied earthquake ground motion. Figures 4.85, 4.86, 4.87 and 4.88 are the graphs for base end shear and moment results of piers for initially formed analytical structures of analysis cases EBC10-REF, EBC-3 and PBC-3.

The idea behind the iteration process is provided in a detailed way in previous parts of this section. Figures 4.89, 4.90, 4.91, 4.92, 4.93 and 4.94 show all the results of relative horizontal deformation, vertical reaction exerted on bearings, base-end shear and moment results of piers obtained in the structural situation with iterated stiffness for all three cases.

Very brief result tables of initial cases for relative deformations, vertical reactions on bearings, base end shear and moment reactions of piers 1 and 2 for each data group are provided in Tables 4.3, 4.4, 4.5, 4.6, 4.7 and 4.8.

In the same manner, the very brief result tables of iterated cases for relative deformations, vertical reactions on bearings, base end shear and moment reactions of piers 1 and 2 for each data group are provided in Tables 4.9, 4.10, 4.11, 4.12, 4.13 and 4.14.

4.2.5.1. Analysis Results of the Structure with Initial Stiffness

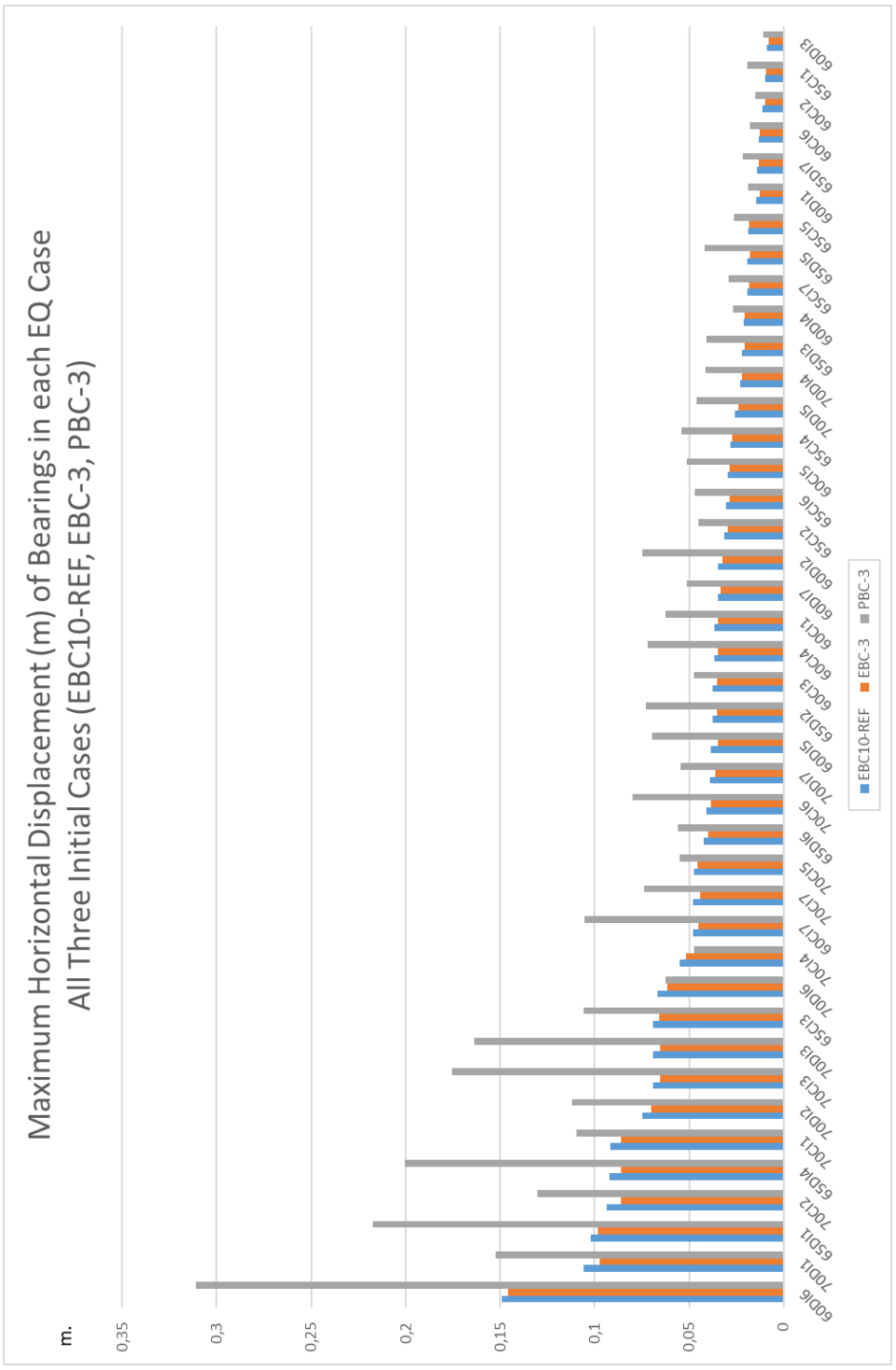

Figure 4.83. Maximum Horizontal Displacement (m) of Bearings in each EQ Case - All Three Initial Cases (EBC10-REF, EBC-3, PBC-3)

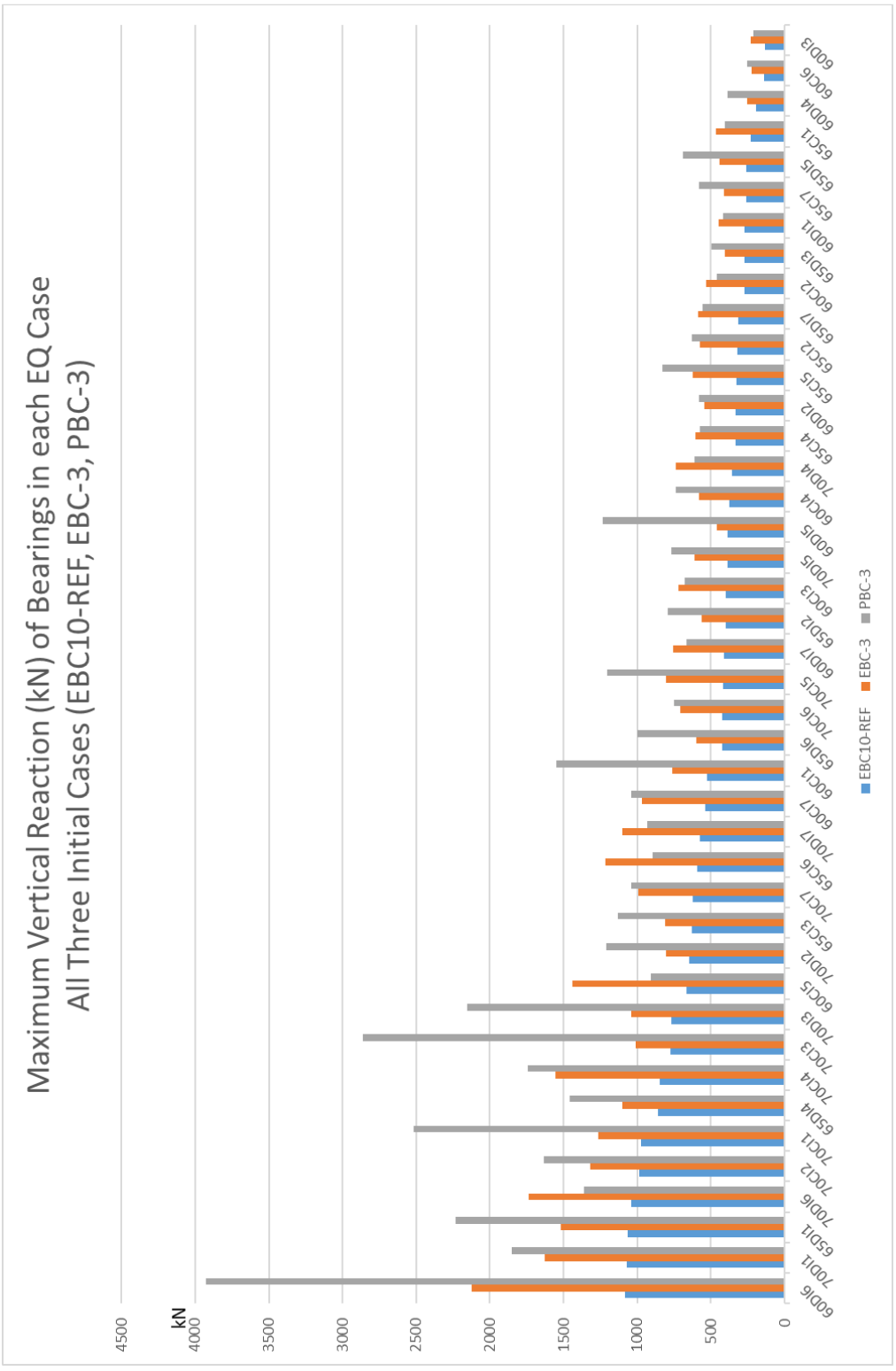

Figure 4.84. Maximum Vertical Reaction (kN) of Bearings in each EQ Case - All Three Initial Cases (EBC10-REF, EBC-3, PBC-3)

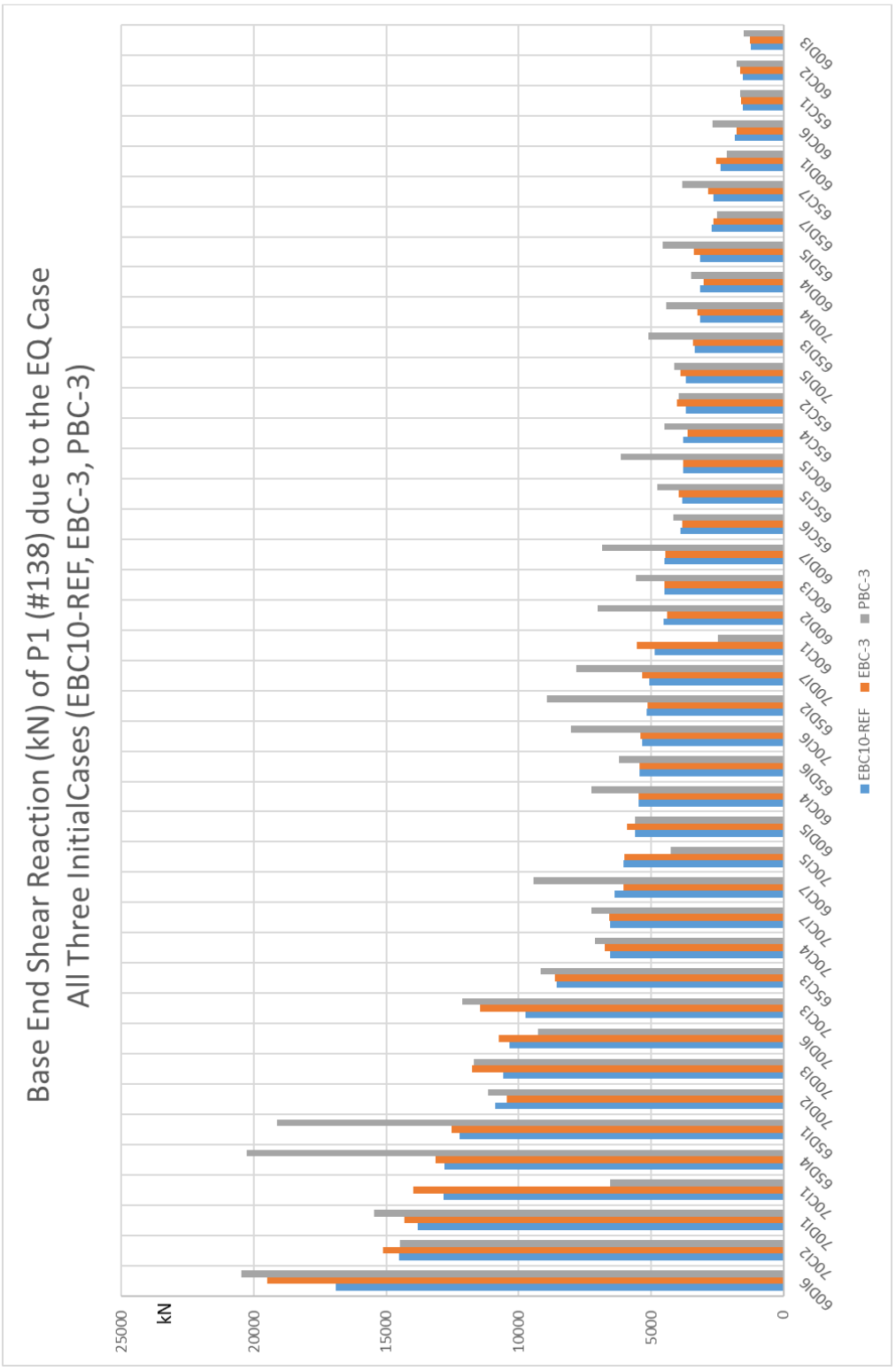

Figure 4.85. Base End Shear Reaction (kN) of P1 (#138) due to EQ Case - All Three Initial Cases (EBC10-REF, EBC-3, PBC-3)

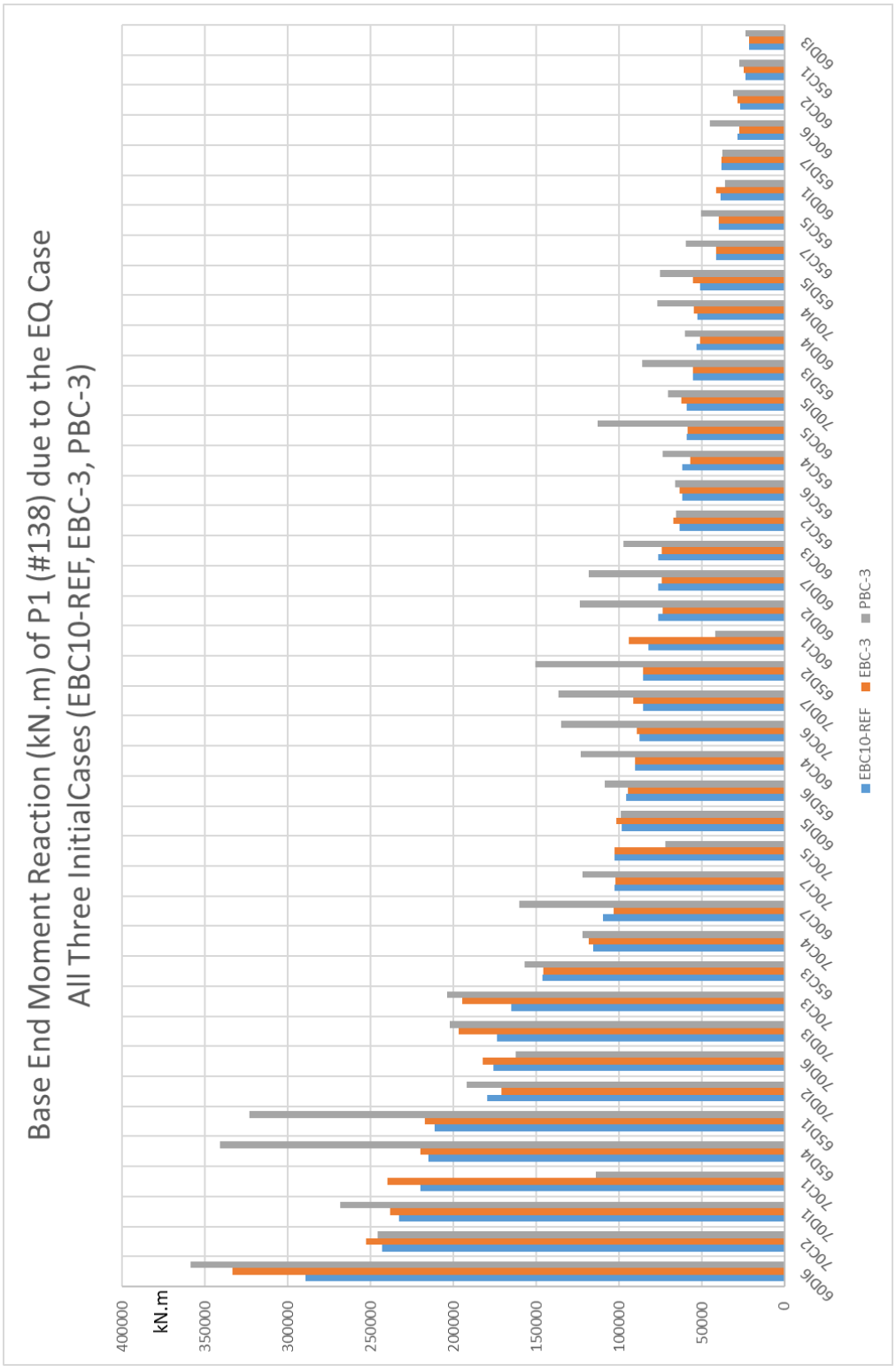

Figure 4.86. Base End Moment Reaction (kN.m) of P1 (#138) due to the EQ Case - All Three Initial Cases (EBC10-REF, EBC-3, PBC-3)

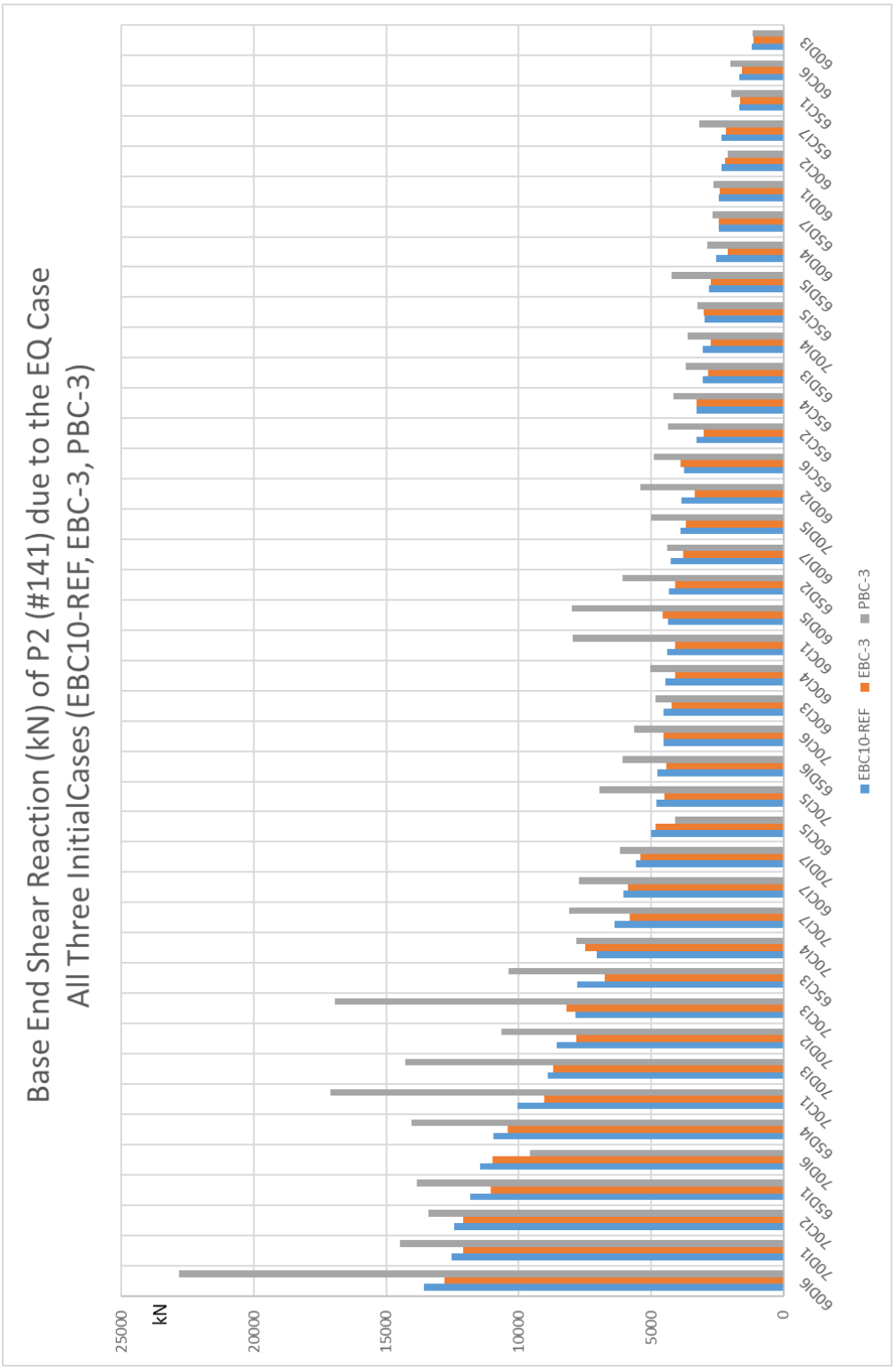

Figure 4.87. Base End Shear Reaction (kN) of P2 (#141) due to EQ Case - All Three Initial Cases (EBC10-REF, EBC-3, PBC-3)

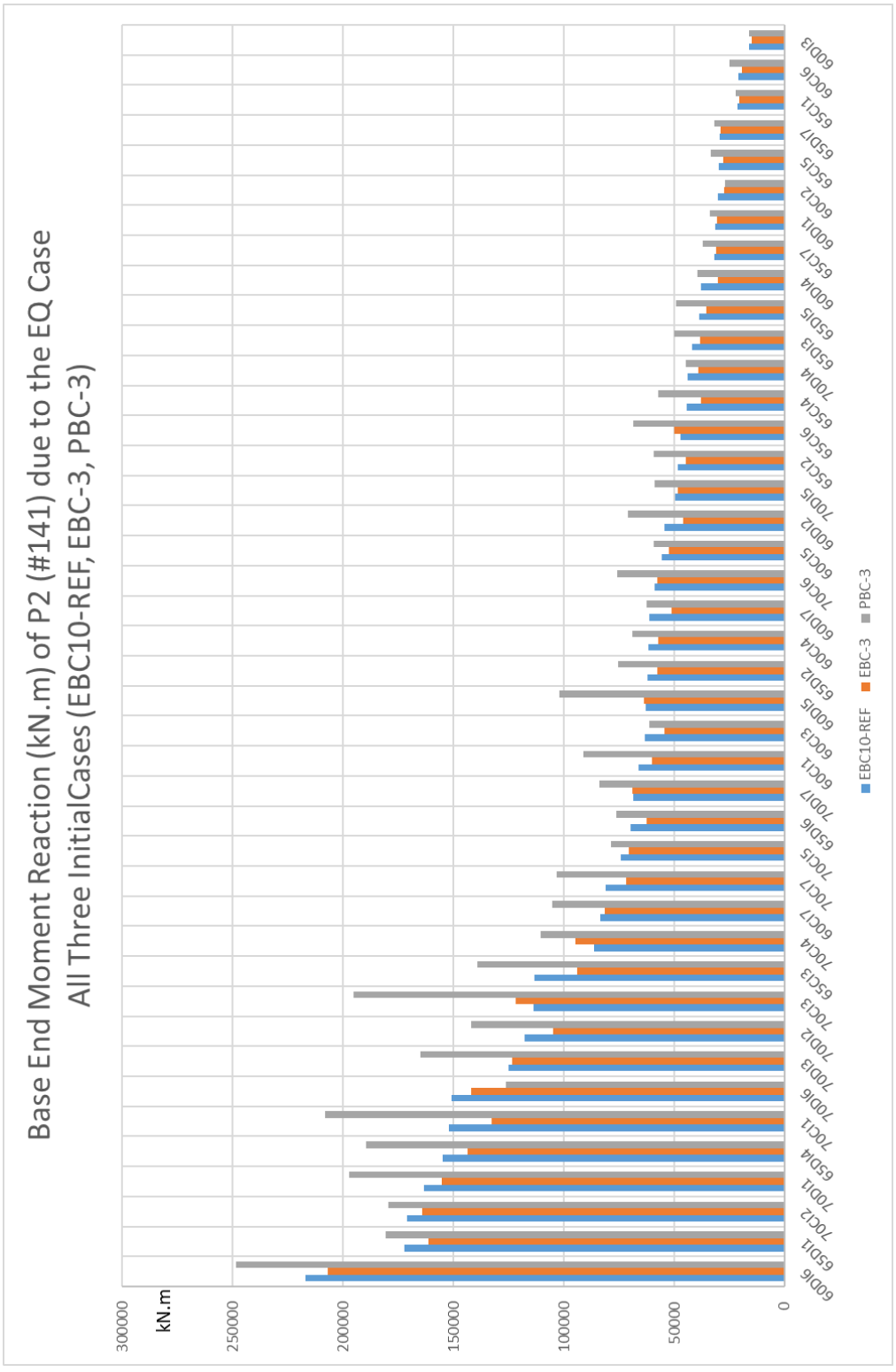

Figure 4.88. Base End Moment Reaction (kN.m) of P2 (#141) due to EQ Case - All Three Initial Cases (EBC10-REF, EBC-3, PBC-3)

4.2.5.2. Analysis Results of the Structure with Iterated Stiffness

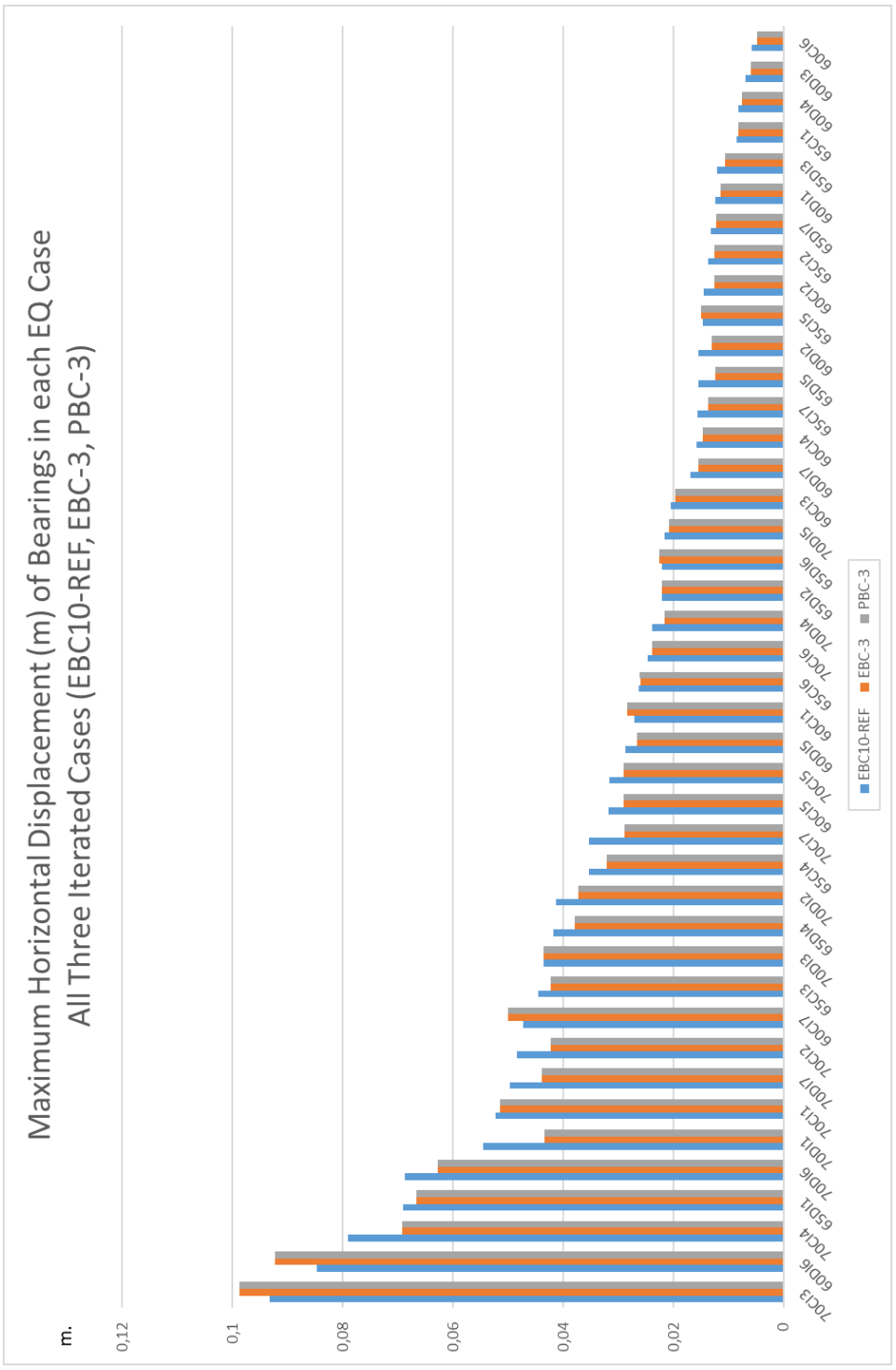

Figure 4.89. Maximum Horizontal Displacement (m) of Bearings in each EQ Case - All Three Iterated Cases (EBC10-REF, EBC-3, PBC-3)

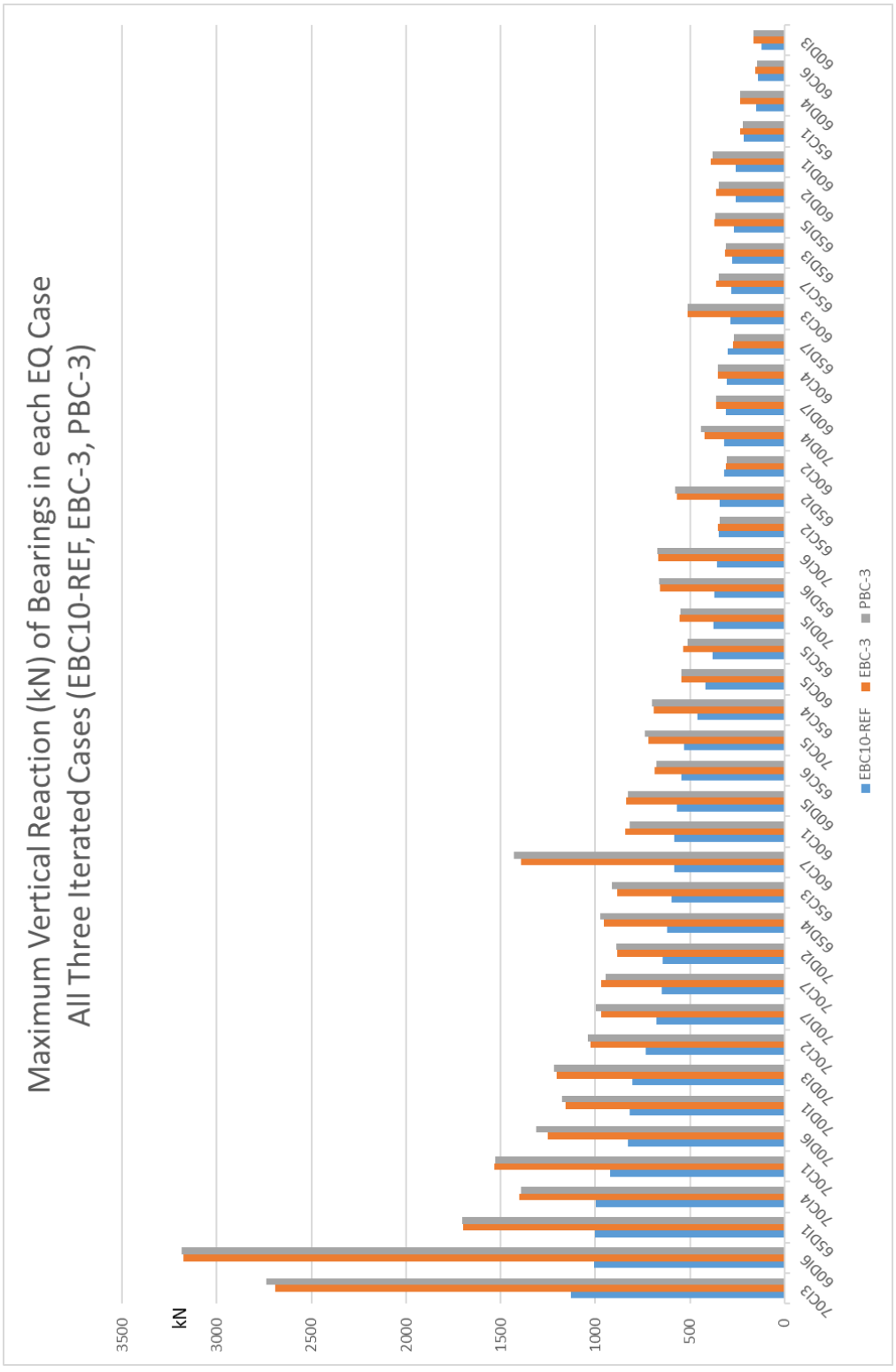

Figure 4.90. Maximum Vertical Reaction (kN) in Bearings in each EQ Case - All Three Iterated Cases (EBC10-REF, EBC-3, PBC-3)

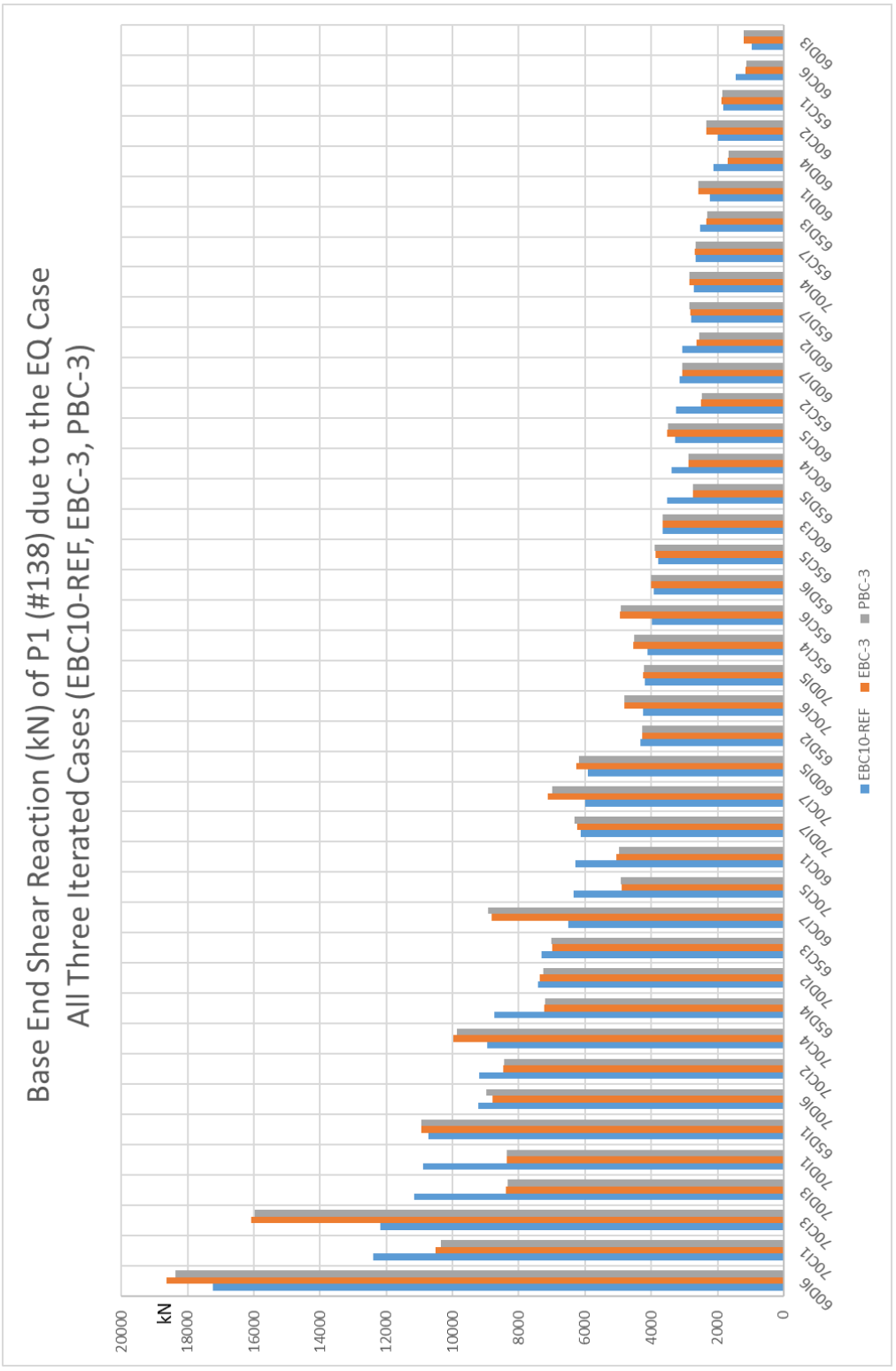

Figure 4.91. Base End Shear Reaction (kN) of P1 (#138) due to EQ Case - All Three Iterated Cases (EBC10-REF, EBC-3, PBC-3)

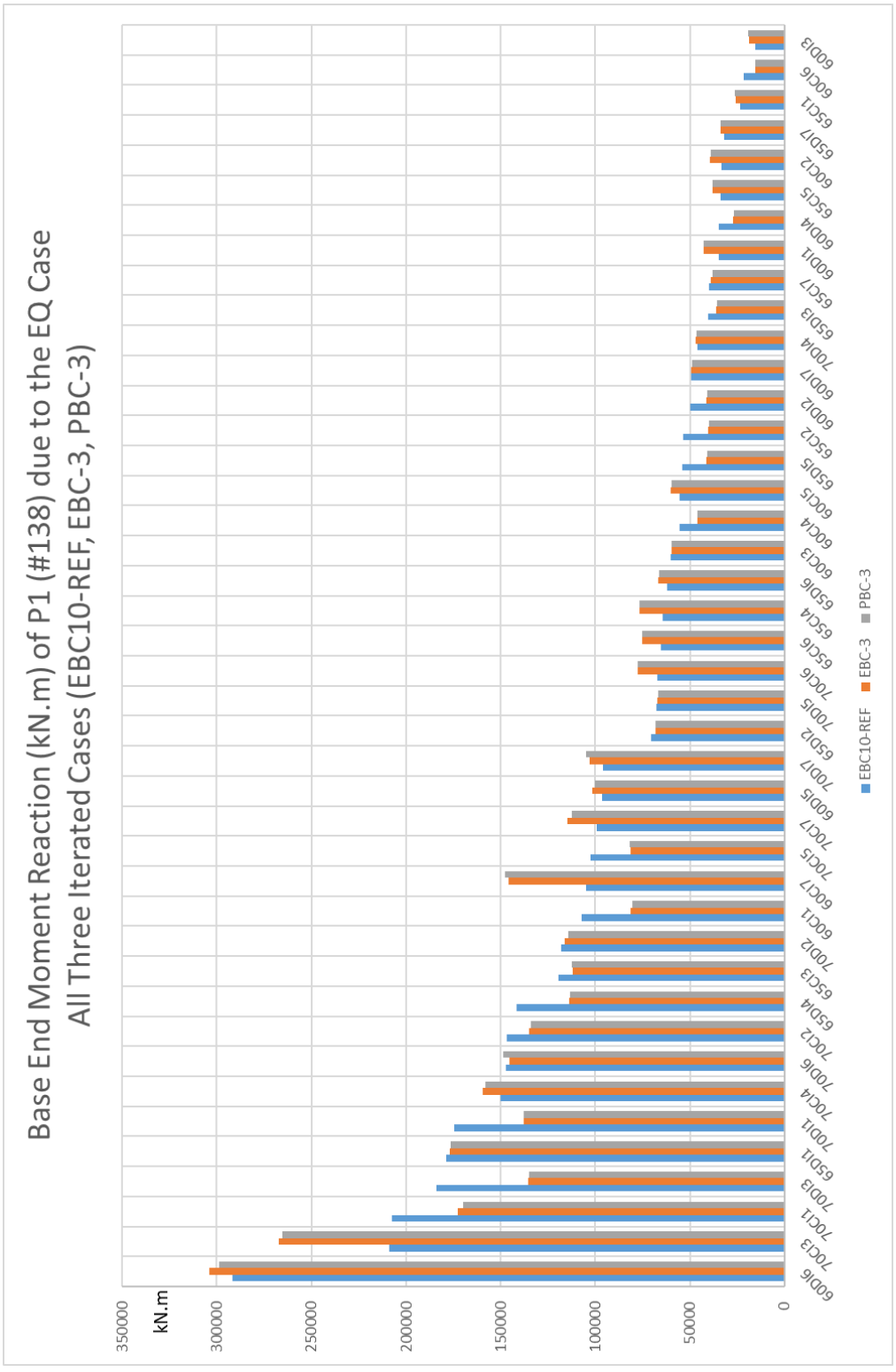

Figure 4.92. Base End Moment Reaction (kN.m) of P1 (#138) due to EQ Case - All Three Iterated Cases (EBC10-REF, EBC-3, PBC-3)

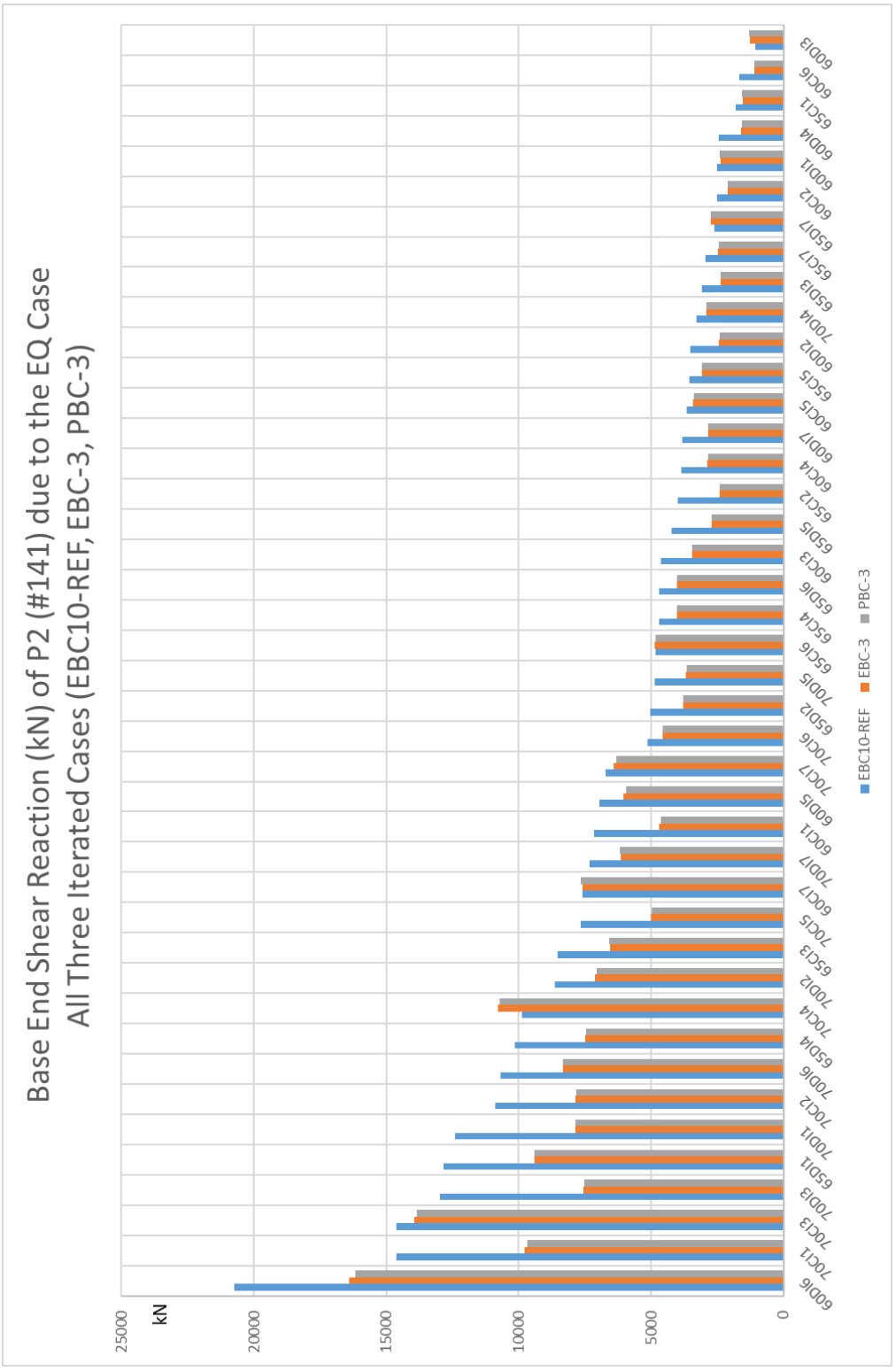

Figure 4.93. Base End Shear Reaction (kN) of P2 (#141) due to EQ Case - All Three Iterated Cases (EBC10-REF, EBC-3, PBC-3)

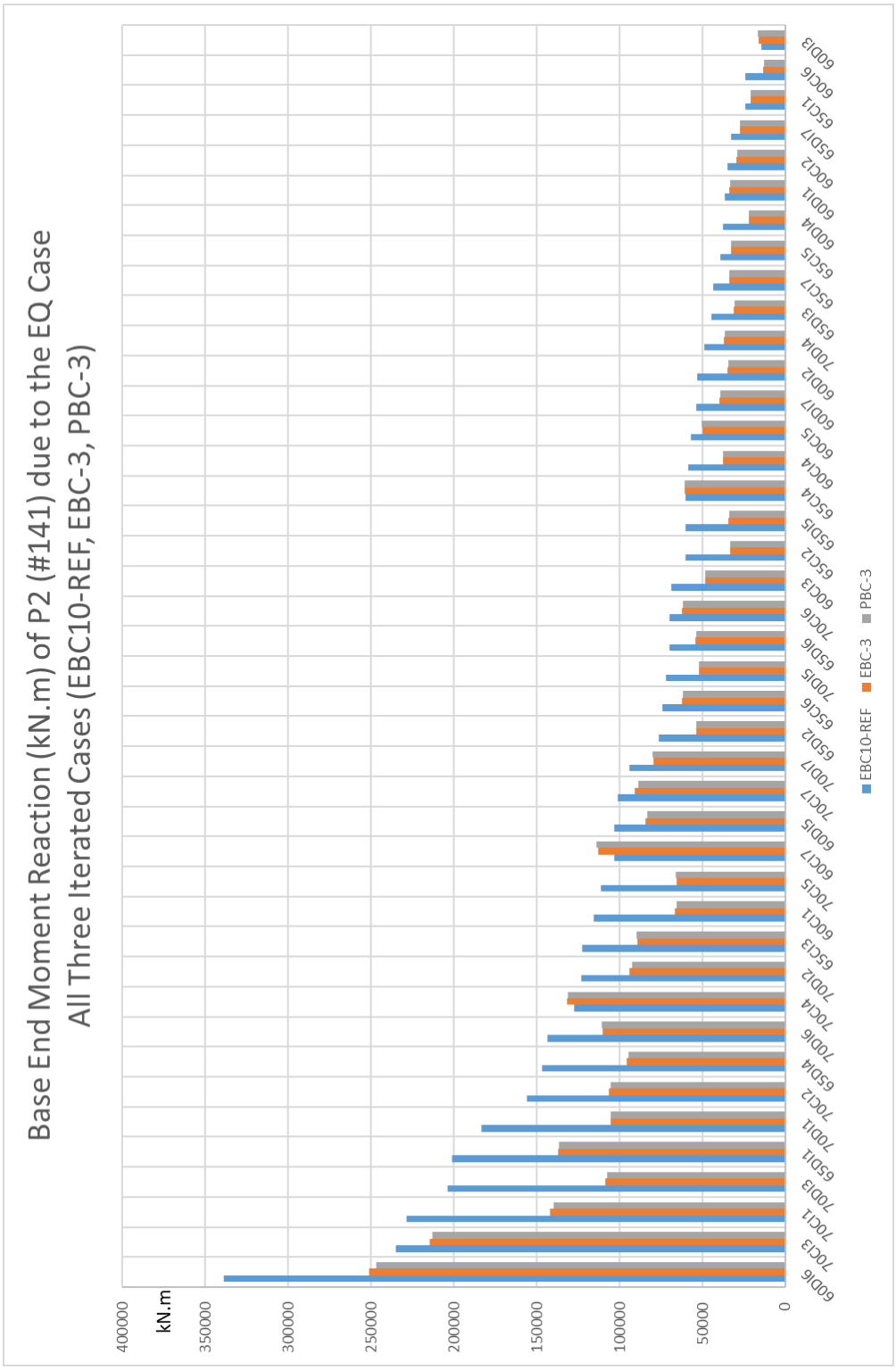

Figure 4.94. Base End Moment Reaction (kN.m) of P2 (#141) due to EQ Case - All Three Iterated Cases (EBC10-REF, EBC-3, PBC-3)

4.2.5.3. Summary Tables of Results with Initial Stiffness

Table 4.3. Summary Table for Maximum Relative Horizontal Deformations of Bearings for Each Data Group – Initial Analysis Cases

Relative Deformations of Bearings for Each Data Group - for Initial Analysis Cases

Number	Data Code	Magnitude	Soil Class	Analysis Case	Maximum Relative Deformation (mm)	Mean Value for Maximum Relative Deformations (mm)	Standard Deviation of Maximum Relative Deformations (mm)	Coefficient of Variation of Maximum Relative Deformations
1	60CI	6	C	EBC-10-REF	48,2	30,5	13,54	0,44
2	60CI	6	C	EBC-3	44,98	28,61	12,89	0,45
3	60CI	6	C	PBC-3	105,59	53,05	31,49	0,59
4	60DI	6	D	EBC-10-REF	149,32	43,18	48,13	1,11
5	60DI	6	D	EBC-3	145,82	41,15	47,34	1,15
6	60DI	6	D	PBC-3	310,96	80,44	104,63	1,30
7	65CI	7	C	EBC-10-REF	69,07	29,63	19,02	0,64
8	65CI	7	C	EBC-3	65,82	28,16	18,15	0,64
9	65CI	7	C	PBC-3	105,98	46,8	28,94	0,62
10	65DI	7	D	EBC-10-REF	102,24	47,16	35,79	0,76
11	65DI	7	D	EBC-3	98,23	44,48	34,17	0,77
12	65DI	7	D	PBC-3	217,41	93,07	80,88	0,87
13	70CI	7	C	EBC-10-REF	93,84	63,8	21,74	0,34
14	70CI	7	C	EBC-3	86,21	59,66	19,94	0,33
15	70CI	7	C	PBC-3	175,57	96,03	45,52	0,47
16	70DI	7	D	EBC-10-REF	105,75	57,84	29,90	0,52
17	70DI	7	D	EBC-3	97,53	53,82	27,62	0,51
18	70DI	7	D	PBC-3	163,61	90,27	51,78	0,57

Table 4.4. Summary Table for Maximum Vertical Reactions of Bearings for Each Data Group - Initial Analysis Cases

Vertical Reactions of Bearings for Each Data Group - for Initial Analysis Cases

Number	Data Code	Magnitude	Soil Class	Analysis Case	Maximum Vertical Reaciton (kN)	Mean Value for Maximum Vertical Reactions (kN)	Standard Deviation of Maximum Vertical Reactions (kN)	Mean + Standard Deviation (kN)	Coefficient of Variation of Maximum Vertical Reactions
1	60CI	6	C	EBC-10-REF	663,88	416,75	176,00	592,75	0,42
2	60CI	6	C	EBC-3	1439,03	745,97	382,85	1128,82	0,51
3	60CI	6	C	PBC-3	1546,53	803,25	420,23	1223,48	0,52
4	60DI	6	D	EBC-10-REF	1085,69	402	317,40	719,40	0,79
5	60DI	6	D	EBC-3	2123,71	687,93	657,82	1345,75	0,96
6	60DI	6	D	PBC-3	3928,81	1060,68	1305,69	2366,37	1,23
7	65CI	7	C	EBC-10-REF	631,04	385,19	160,43	545,62	0,42
8	65CI	7	C	EBC-3	1213,64	672,65	271,01	943,66	0,40
9	65CI	7	C	PBC-3	1131,35	721,46	244,34	965,80	0,34
10	65DI	7	D	EBC-10-REF	1065,51	513,55	318,51	832,06	0,62
11	65DI	7	D	EBC-3	1516,02	743,73	410,76	1154,49	0,55
12	65DI	7	D	PBC-3	2232,71	1031,72	621,35	1653,07	0,60
13	70CI	7	C	EBC-10-REF	984,35	721,53	239,51	961,04	0,33
14	70CI	7	C	EBC-3	1555,85	1093,4	300,42	1393,82	0,27
15	70CI	7	C	PBC-3	2863,85	1678,29	775,16	2453,45	0,46
16	70DI	7	D	EBC-10-REF	1073,95	693,45	287,17	980,62	0,41
17	70DI	7	D	EBC-3	1738,64	1093,92	438,06	1531,98	0,40
18	70DI	7	D	PBC-3	2156,55	1270,32	568,19	1838,51	0,45

Table 4.5. Summary Table for Maximum Base End Shear Reactions of P1 (#138) for Each Data Group - Initial Analysis Cases

Base End Shear Reactions of P1 (#138) for Each Data Group - for Initial Analysis Cases

Number	Data Code	Magnitude	Soil Class	Analysis Case	Maximum Shear Reaciton (kN)	Mean Value for Maximum Shear Reactions (kN)	Standard Deviation of Maximum Shear Reactions (kN)	Mean + Standard Deviation (kN)	Coefficient of Variation of Maximum Shear Reactions
1	60CI	6	C	EBC-10-REF	6374,26	4056,56	1805,52	5862,08	0,45
2	60CI	6	C	EBC-3	6056,33	4114,57	1805,41	5919,98	0,44
3	60CI	6	C	PBC-3	9435,82	5054,14	2841,67	7895,81	0,56
4	60DI	6	D	EBC-10-REF	16894,77	5475,7	5244,29	10719,99	0,96
5	60DI	6	D	EBC-3	19500,27	5874,73	6194,60	12069,33	1,05
6	60DI	6	D	PBC-3	20455,64	6724,57	6436,36	13160,93	0,96
7	65CI	7	C	EBC-10-REF	8579,23	4001,63	2197,99	6199,62	0,55
8	65CI	7	C	EBC-3	8628,81	4076	2183,84	6259,84	0,54
9	65CI	7	C	PBC-3	9159,23	4577,3	2264,90	6842,20	0,49
10	65DI	7	D	EBC-10-REF	12810,48	6418,01	4296,77	10714,78	0,67
11	65DI	7	D	EBC-3	13131,79	6537,21	4417,83	10955,04	0,68
12	65DI	7	D	PBC-3	20260,72	9530,68	7207,03	16737,71	0,76
13	70CI	7	C	EBC-10-REF	14509,51	8798,63	3640,89	12439,52	0,41
14	70CI	7	C	EBC-3	15140,54	9331,29	4095,99	13427,28	0,44
15	70CI	7	C	PBC-3	14494,35	8557,08	3523,97	12081,05	0,41
16	70DI	7	D	EBC-10-REF	13830,45	8225,04	4178,23	12403,27	0,51
17	70DI	7	D	EBC-3	14331,64	8541,83	4321,99	12863,82	0,51
18	70DI	7	D	PBC-3	15446,61	9137,56	4067,84	13205,40	0,45

Table 4.6. Summary Table for Maximum Base End Moment Reactions of P1 (#138) for Each Data Group - Initial Analysis Cases

Base End Moment Reactions of P1 (#138) for Each Data Group - for Initial Analysis Cases

Number	Data Code	Magnitude	Soil Class	Analysis Case	Maximum Moment Reaciton (kN.m)	Mean Value for Maximum Moment Reactions (kN.m)	Standard Deviation of Maximum Moment Reactions (kN.m)	Mean + Standard Deviation (kN.m)	Coefficient of Variation of Maximum Moment Reactions
1	60CI	6	C	EBC-10-REF	109751,18	67633,93	31145,42	98779,35	0,46
2	60CI	6	C	EBC-3	102992,11	68058,93	30931,31	98990,24	0,45
3	60CI	6	C	PBC-3	160334,2	87325,47	48926,12	136251,59	0,56
4	60DI	6	D	EBC-10-REF	289429,33	93473,87	90196,30	183670,17	0,96
5	60DI	6	D	EBC-3	333665,52	99500,78	106467,72	205968,50	1,07
6	60DI	6	D	PBC-3	358822,65	117150,21	113495,76	230645,97	0,97
7	65CI	7	C	EBC-10-REF	146106,2	62564,57	39705,73	102270,30	0,63
8	65CI	7	C	EBC-3	145680,1	62747,34	39511,58	102258,92	0,63
9	65CI	7	C	PBC-3	156874,11	71416,59	40561,66	111978,25	0,57
10	65DI	7	D	EBC-10-REF	215052,44	107463,23	74902,66	182365,89	0,70
11	65DI	7	D	EBC-3	219975,14	109400,43	76977,51	186377,94	0,70
12	65DI	7	D	PBC-3	340930,04	160195,03	122279,15	282474,18	0,76
13	70CI	7	C	EBC-10-REF	243037,05	148063,65	62330,05	210393,70	0,42
14	70CI	7	C	EBC-3	252737,19	157150,06	70192,61	227342,67	0,45
15	70CI	7	C	PBC-3	245965,9	144966,84	59266,94	204233,78	0,41
16	70DI	7	D	EBC-10-REF	232642,91	137067,22	70266,33	207333,55	0,51
17	70DI	7	D	EBC-3	238479,96	142382,25	72182,97	214565,22	0,51
18	70DI	7	D	PBC-3	268262,86	158437,73	70810,67	229248,40	0,45

Table 4.7. Summary Table for Maximum Base End Shear Reactions of P2 (#141) for Each Data Group - Initial Analysis Cases

Base End Shear Reactions of P2 (#141) for Each Data Group - for Initial Analysis Cases

Number	Data Code	Magnitude	Soil Class	Analysis Case	Maximum Shear Reaciton (kN)	Mean Value for Maximum Shear Reactions (kN)	Standard Deviation of Maximum Shear Reactions (kN)	Mean + Standard Deviation (kN)	Coefficient of Variation of Maximum Shear Reactions
1	60CI	6	C	EBC-10-REF	6039,18	4067,15	1525,02	5592,17	0,37
2	60CI	6	C	EBC-3	5882,07	3848,99	1488,11	5337,10	0,39
3	60CI	6	C	PBC-3	7971,28	4824,63	2386,38	7211,01	0,49
4	60DI	6	D	EBC-10-REF	13570,73	4609,51	4113,99	8723,50	0,89
5	60DI	6	D	EBC-3	12807	4317,64	3913,14	8230,78	0,91
6	60DI	6	D	PBC-3	22837,51	6770,27	7419,90	14190,17	1,10
7	65CI	7	C	EBC-10-REF	7810,02	3599,59	1982,57	5582,16	0,55
8	65CI	7	C	EBC-3	6756,75	3405,29	1651,35	5056,64	0,48
9	65CI	7	C	PBC-3	10397,9	4611,33	2726,39	7337,72	0,59
10	65DI	7	D	EBC-10-REF	11847	5748,92	3950,91	9699,83	0,69
11	65DI	7	D	EBC-3	11057,49	5441,66	3696,98	9138,64	0,68
12	65DI	7	D	PBC-3	14050,11	7247,6	4743,89	11991,49	0,65
13	70CI	7	C	EBC-10-REF	12429,98	7594,81	2835,23	10430,04	0,37
14	70CI	7	C	EBC-3	12095,45	7379,56	2727,60	10107,16	0,37
15	70CI	7	C	PBC-3	17121,33	10859,09	4865,18	15724,27	0,45
16	70DI	7	D	EBC-10-REF	12542,44	7715,46	3661,41	11376,87	0,47
17	70DI	7	D	EBC-3	12095,48	7359,29	3558,59	10917,88	0,48
18	70DI	7	D	PBC-3	14471,31	9118,03	4352,46	13470,49	0,48

Table 4.8. Summary Table for Maximum Base End Moment Reactions of P2 (#141) for Each Data Group - Initial Analysis Cases

Base End Moment Reactions of P2 (#141) for Each Data Group - for Initial Analysis Cases

Number	Data Code	Magnitude	Soil Class	Analysis Case	Maximum Moment Reaciton (kN.m)	Mean Value for Maximum Moment Reactions (kN.m)	Standard Deviation of Maximum Moment Reactions (kN.m)	Mean + Standard Deviation (kN.m)	Coefficient of Variation of Maximum Moment Reactions
1	60CI	6	C	EBC-10-REF	83608,56	54482,43	21718,76	76201,19	0,40
2	60CI	6	C	EBC-3	81452,97	50288,3	20963,58	71251,88	0,42
3	60CI	6	C	PBC-3	105283,1	62545,83	29935,73	92481,56	0,48
4	60DI	6	D	EBC-10-REF	216804,44	68612,73	67549,38	136162,11	0,98
5	60DI	6	D	EBC-3	206828,01	63281,53	65272,73	128554,26	1,03
6	60DI	6	D	PBC-3	248593,46	81929,69	78709,70	160639,39	0,96
7	65CI	7	C	EBC-10-REF	113200,01	47954,64	30467,27	78421,91	0,64
8	65CI	7	C	EBC-3	93819,53	43646,15	24276,29	67922,44	0,56
9	65CI	7	C	PBC-3	139271,76	59539,44	38792,07	98331,51	0,65
10	65DI	7	D	EBC-10-REF	172077,72	81201,3	58073,21	139274,51	0,72
11	65DI	7	D	EBC-3	161460,99	75466,11	54260,58	129726,69	0,72
12	65DI	7	D	PBC-3	189387,2	93169,3	64692,33	157861,63	0,69
13	70CI	7	C	EBC-10-REF	170958,75	105301,26	42153,02	147454,28	0,40
14	70CI	7	C	EBC-3	164179,11	101889,03	38970,69	140859,72	0,38
15	70CI	7	C	PBC-3	207989,08	135844,98	56538,68	192383,66	0,42
16	70DI	7	D	EBC-10-REF	163526,98	102704,33	48575,76	151280,09	0,47
17	70DI	7	D	EBC-3	155233,1	97437,53	46002,41	143439,94	0,47
18	70DI	7	D	PBC-3	197326,52	116904,26	56525,00	173429,26	0,48

4.2.5.4. Summary Tables of Results with Iterated Stiffness

Table 4.9. Summary Table for Maximum Relative Horizontal Deformations of Bearings for Each Data Group – Iterated Analysis Cases

Relative Deformations of Bearings for Each Data Group - for Iterated Analysis Cases

Number	Data Code	Magnitude	Soil Class	Analysis Case	Maximum Relative Deformation (mm)	Mean Value for Maximum Relative Deformations (mm)	Standard Deviation of Maximum Relative Deformations (mm)	Coefficient of Variation of Maximum Relative Deformations
1	60CI	6	C	EBC-10-REF	47,26	23,27	13,58	0,58
2	60CI	6	C	EBC-3	49,97	22,75	14,77	0,65
3	60CI	6	C	PBC-3	49,94	22,75	14,76	0,65
4	60DI	6	D	EBC-10-REF	84,72	24,75	27,40	1,11
5	60DI	6	D	EBC-3	92,27	24,63	30,58	1,24
6	60DI	6	D	PBC-3	92,25	24,63	30,57	1,24
7	65CI	7	C	EBC-10-REF	44,59	22,71	13,21	0,58
8	65CI	7	C	EBC-3	42,34	21,45	12,40	0,58
9	65CI	7	C	PBC-3	42,34	21,45	12,40	0,58
10	65DI	7	D	EBC-10-REF	69,08	27,99	20,71	0,74
11	65DI	7	D	EBC-3	66,66	26,38	20,11	0,76
12	65DI	7	D	PBC-3	66,64	26,38	20,11	0,76
13	70CI	7	C	EBC-10-REF	93,3	52,07	25,48	0,49
14	70CI	7	C	EBC-3	99,8	49,23	27,30	0,55
15	70CI	7	C	PBC-3	99,77	49,22	27,29	0,55
16	70DI	7	D	EBC-10-REF	68,65	43,33	16,63	0,38
17	70DI	7	D	EBC-3	62,79	39,07	14,51	0,37
18	70DI	7	D	PBC-3	62,8	39,07	14,51	0,37

Table 4.10. Summary Table for Maximum Vertical Reactions of Bearings for Each Data Group - Iterated Analysis Cases

Vertical Reactions of Bearings for Each Data Group - for Iterated Analysis Cases

Number	Data Code	Magnitude	Soil Class	Analysis Case	Maximum Vertical Reaciton (kN)	Mean Value for Maximum Vertical Reactions (kN)	Standard Deviation of Maximum Vertical Reactions (kN)	Mean + Standard Deviation (kN)	Coefficient of Variation of Maximum Vertical Reactions
1	60CI	6	C	EBC-10-REF	584,36	376,47	162,78	539,25	0,43
2	60CI	6	C	EBC-3	1390,87	586,26	415,79	1002,05	0,71
3	60CI	6	C	PBC-3	1147,8	689,25	317,84	1007,09	0,46
4	60DI	6	D	EBC-10-REF	1006,5	382,54	311,61	694,15	0,81
5	60DI	6	D	EBC-3	3174,16	789,7	1073,12	1862,82	1,36
6	60DI	6	D	PBC-3	2321,11	729,55	741,95	1471,50	1,02
7	65CI	7	C	EBC-10-REF	596,31	404,22	137,87	542,09	0,34
8	65CI	7	C	EBC-3	883,59	534,19	232,26	766,45	0,43
9	65CI	7	C	PBC-3	1140,82	739,95	274,51	1014,46	0,37
10	65DI	7	D	EBC-10-REF	1001,75	455,49	268,95	724,44	0,59
11	65DI	7	D	EBC-3	1697,01	691,43	502,64	1194,07	0,73
12	65DI	7	D	PBC-3	2138,57	823,64	605,68	1429,32	0,74
13	70CI	7	C	EBC-10-REF	1127,96	760,2	272,25	1032,45	0,36
14	70CI	7	C	EBC-3	2693,85	1287,68	698,26	1985,94	0,54
15	70CI	7	C	PBC-3	2495,93	1321,85	646,82	1968,67	0,49
16	70DI	7	D	EBC-10-REF	826,05	637,68	212,39	850,07	0,33
17	70DI	7	D	EBC-3	1253,28	920,97	324,63	1245,60	0,35
18	70DI	7	D	PBC-3	1489,68	1052,38	317,20	1369,58	0,30

Table 4.11. Summary Table for Maximum Base End Shear Reactions of P1 (#138) for Each Data Group - Iterated Analysis Cases

Base End Shear Reactions of P1 (#138) for Each Data Group - for Iterated Analysis Cases

Number	Data Code	Magnitude	Soil Class	Analysis Case	Maximum Shear Reaciton (kN)	Mean Value for Maximum Shear Reactions (kN)	Standard Deviation of Maximum Shear Reactions (kN)	Mean + Standard Deviation (kN)	Coefficient of Variation of Maximum Shear Reactions
1	60CI	6	C	EBC-10-REF	6514,5	3797,75	1946,68	5744,43	0,51
2	60CI	6	C	EBC-3	8827,49	3917,94	2477,36	6395,30	0,63
3	60CI	6	C	PBC-3	8936,18	3914,31	2513,87	6428,18	0,64
4	60DI	6	D	EBC-10-REF	17228,32	4953,65	5624,27	10577,92	1,14
5	60DI	6	D	EBC-3	18627,87	5155,37	6159,28	11314,65	1,19
6	60DI	6	D	PBC-3	18371,54	5088,24	6071,71	11159,95	1,19
7	65CI	7	C	EBC-10-REF	7300,24	3842,08	1724,99	5567,07	0,45
8	65CI	7	C	EBC-3	6983,57	3914,38	1758,82	5673,20	0,45
9	65CI	7	C	PBC-3	7029,82	3908,5	1777,16	5685,66	0,45
10	65DI	7	D	EBC-10-REF	10724,4	5220,88	3193,00	8413,88	0,61
11	65DI	7	D	EBC-3	10940,54	4909,06	3127,46	8036,52	0,64
12	65DI	7	D	PBC-3	10935,37	4899,03	3123,71	8022,74	0,64
13	70CI	7	C	EBC-10-REF	12402,78	8471,83	3121,02	11592,85	0,37
14	70CI	7	C	EBC-3	16072,31	8840,95	3896,68	12737,63	0,44
15	70CI	7	C	PBC-3	15968,82	8765,16	3860,40	12625,56	0,44
16	70DI	7	D	EBC-10-REF	11169,13	7396,23	3251,43	10647,66	0,44
17	70DI	7	D	EBC-3	8805,42	6605,39	2286,63	8892,02	0,35
18	70DI	7	D	PBC-3	8975,32	6619,82	2314,08	8933,90	0,35

Table 4.12. Summary Table for Maximum Base End Moment Reactions of P1 (#138) for Each Data Group - Iterated Analysis Cases

Base End Moment Reactions of P1 (#138) for Each Data Group - for Iterated Analysis Cases

Number	Data Code	Magnitude	Soil Class	Analysis Case	Maximum Moment Reaciton (kN.m)	Mean Value for Maximum Moment Reactions (kN.m)	Standard Deviation of Maximum Moment Reactions (kN.m)	Mean + Standard Deviation (kN.m)	Coefficient of Variation of Maximum Moment Reactions
1	60CI	6	C	EBC-10-REF	107290,05	62604,21	32805,17	95409,38	0,52
2	60CI	6	C	EBC-3	145911,54	64131,71	41430,27	105561,98	0,65
3	60CI	6	C	PBC-3	147704,03	64024,99	42069,06	106094,05	0,66
4	60DI	6	D	EBC-10-REF	291708,59	81762,77	95918,92	177681,69	1,17
5	60DI	6	D	EBC-3	303837,31	83614,95	100660,49	184275,44	1,20
6	60DI	6	D	PBC-3	298731,14	82496,15	98848,35	181344,50	1,20
7	65CI	7	C	EBC-10-REF	119408,36	57217,74	31542,04	88759,78	0,55
8	65CI	7	C	EBC-3	111817,02	58194,22	30642,34	88836,56	0,53
9	65CI	7	C	PBC-3	112575,92	58138,4	30941,05	89079,45	0,53
10	65DI	7	D	EBC-10-REF	178882,74	82790,76	55521,31	138312,07	0,67
11	65DI	7	D	EBC-3	176838,56	76767,06	52125,21	128892,27	0,68
12	65DI	7	D	PBC-3	176667,91	76335,17	52186,83	128522,00	0,68
13	70CI	7	C	EBC-10-REF	208696,79	140336,09	54391,47	194727,56	0,39
14	70CI	7	C	EBC-3	267246,17	143972,48	65213,60	209186,08	0,45
15	70CI	7	C	PBC-3	265345,4	142699,12	64531,62	207230,74	0,45
16	70DI	7	D	EBC-10-REF	184067,23	119125,3	52575,69	171700,99	0,44
17	70DI	7	D	EBC-3	145358,35	107442,39	37649,08	145091,47	0,35
18	70DI	7	D	PBC-3	148598,47	107729,88	38267,12	145997,00	0,36

Table 4.13. Summary Table for Maximum Base End Shear Reactions of P2 (#141) for Each Data Group - Iterated Analysis Cases

Base End Shear Reactions of P2 (#141) for Each Data Group - for Iterated Analysis Cases

Number	Data Code	Magnitude	Soil Class	Analysis Case	Maximum Shear Reaciton (kN)	Mean Value for Maximum Shear Reactions (kN)	Standard Deviation of Maximum Shear Reactions (kN)	Mean + Standard Deviation (kN)	Coefficient of Variation of Maximum Shear Reactions
1	60CI	6	C	EBC-10-REF	7599,5	4444,96	2227,20	6672,16	0,50
2	60CI	6	C	EBC-3	7594,84	3612,46	2086,45	5698,91	0,58
3	60CI	6	C	PBC-3	7676,37	3600,73	2111,66	5712,39	0,59
4	60DI	6	D	EBC-10-REF	20741,77	5870,92	6804,39	12675,31	1,16
5	60DI	6	D	EBC-3	16399,05	4717,1	5381,52	10098,62	1,14
6	60DI	6	D	PBC-3	16174,51	4664,41	5301,52	9965,93	1,14
7	65CI	7	C	EBC-10-REF	8533,98	4344,78	2120,30	6465,08	0,49
8	65CI	7	C	EBC-3	6538,45	3570,1	1708,56	5278,66	0,48
9	65CI	7	C	PBC-3	6585,09	3568,9	1719,87	5288,77	0,48
10	65DI	7	D	EBC-10-REF	12841,91	6095,25	3866,03	9961,28	0,63
11	65DI	7	D	EBC-3	9415,25	4663,3	2718,79	7382,09	0,58
12	65DI	7	D	PBC-3	9402,03	4652,3	2709,43	7361,73	0,58
13	70CI	7	C	EBC-10-REF	14627,24	9938,22	3724,62	13662,84	0,37
14	70CI	7	C	EBC-3	13958,23	8337,88	3389,31	11727,19	0,41
15	70CI	7	C	PBC-3	13846,43	8274,38	3362,14	11636,52	0,41
16	70DI	7	D	EBC-10-REF	12978,49	8590,94	3691,97	12282,91	0,43
17	70DI	7	D	EBC-3	8343,21	6240,28	2119,40	8359,68	0,34
18	70DI	7	D	PBC-3	8346,78	6219,78	2121,86	8341,64	0,34

Table 4.14. Summary Table for Maximum Base End Moment Reactions of P2 (#141) for Each Data Group - Iterated Analysis Cases

Base End Moment Reactions of P2 (#141) for Each Data Group - for Iterated Analysis Cases

Number	Data Code	Magnitude	Soil Class	Analysis Case	Maximum Moment Reaciton (kN.m)	Mean Value for Maximum Moment Reactions (kN.m)	Standard Deviation of Maximum Moment Reactions (kN.m)	Mean + Standard Deviation (kN.m)	Coeffient of Variation of Maximum Moment Reactions
1	60CI	6	C	EBC-10-REF	115553,56	65964,59	33528,96	99493,55	0,51
2	60CI	6	C	EBC-3	112966,78	51215,7	32004,00	83219,70	0,62
3	60CI	6	C	PBC-3	114184,84	51186,46	32415,97	83602,43	0,63
4	60DI	6	D	EBC-10-REF	338575,04	91082,17	112482,03	203564,20	1,23
5	60DI	6	D	EBC-3	251190,01	68876,61	83322,95	152199,56	1,21
6	60DI	6	D	PBC-3	247056,22	67927,73	81881,38	149809,11	1,21
7	65CI	7	C	EBC-10-REF	122516,8	60619,58	31839,52	92459,10	0,53
8	65CI	7	C	EBC-3	89501,12	47698,29	24007,16	71705,45	0,50
9	65CI	7	C	PBC-3	89994,6	47602,08	24183,78	71785,86	0,51
10	65DI	7	D	EBC-10-REF	200951,47	90200,88	61001,57	151202,45	0,68
11	65DI	7	D	EBC-3	137018,44	61893,06	40455,08	102348,14	0,65
12	65DI	7	D	PBC-3	136628,15	61577,18	40230,87	101808,05	0,65
13	70CI	7	C	EBC-10-REF	235193,93	146970,31	63515,58	210485,89	0,43
14	70CI	7	C	EBC-3	214696	116198,46	52905,81	169104,27	0,46
15	70CI	7	C	PBC-3	212709,85	115153	52305,17	167458,17	0,45
16	70DI	7	D	EBC-10-REF	203768,56	124127,46	56946,96	181074,42	0,46
17	70DI	7	D	EBC-3	110188,61	83814,6	29019,74	112834,34	0,35
18	70DI	7	D	PBC-3	110621,79	83588,23	29074,27	112662,50	0,35

CHAPTER 5

COMPARISON CHARTS OF ANALYSIS RESULTS

All the results, gathered from the analysis done in three cases, stated in a detailed way in Chapter 4. The comparisons and discussions are made in this section. This study has 1.512 separate sets of results. These sets of results can be compared upon numerous parameters; however, the magnitude of an earthquake, type of soil class and the bearing type and formation will be the basic comparison parameters in this study. As mentioned before; in the bridge formed for analysis cases 1 and 2, elastomeric bearings were used and in case 3, pot bearings were used.

Initially, it was assumed that elastomeric bearings have stiffness in the longitudinal direction of the bridge arising from their material properties and dimensions while assuming pot bearings have no stiffness in the specified direction. And in iterated cases, bearings have the spring stiffness coefficients for limiting the maximum relative deformation up to 10 centimeters.

Comparison graphs based on magnitude are generated by showing the results of the analysis in the same soil type and the same analysis case. For example, Figure 5.13 shows the comparison of results based on magnitudes; 6.0, 6.5 and 7.0 in soil type C for analysis case EBC10-REF (Elastomeric Bearing under each Beam). Figures 5.14, 5.15, 5.16, 5.17 and 5.18 also show the comparison of results based on magnitude.

In section 5.4, comparison graphs based on soil class is given. Earthquake magnitude and analysis case is set to be the same and the soil type is changing for this comparison. For instance, Figure 5.19 shows the results based on soil types ZC and ZD for magnitude 6.0 and analysis case EBC10-REF. Figures 5.20, 5.21, 5.22, 5.23, 5.24, 5.25, 5.26 and 5.27 also show the comparison based on soil class of other sets of results.

Section 5.5 includes the graphs generated for the comparison based on the bearing type and their formations. For this comparison process, magnitude and soil type are set to be same and analysis cases are changing. As an example, Figure 5.28 shows the results of initial analysis cases; EBC10-REF, EBC-3, and PBC-3 on ZC soil type with a magnitude of 6.0. Figures 5.29, 5.30, 5.31, 5.32, and 5.33 include the comparison graphs of other data for the initial analysis sets. In the same manner, Figures 5.34, 5.35, 5.36, 5.37, 5.38 and 5.39 include the graphs for comparison process based on bearing types and formations for the iterated analysis sets.

5.1. Comparison Based on Magnitude

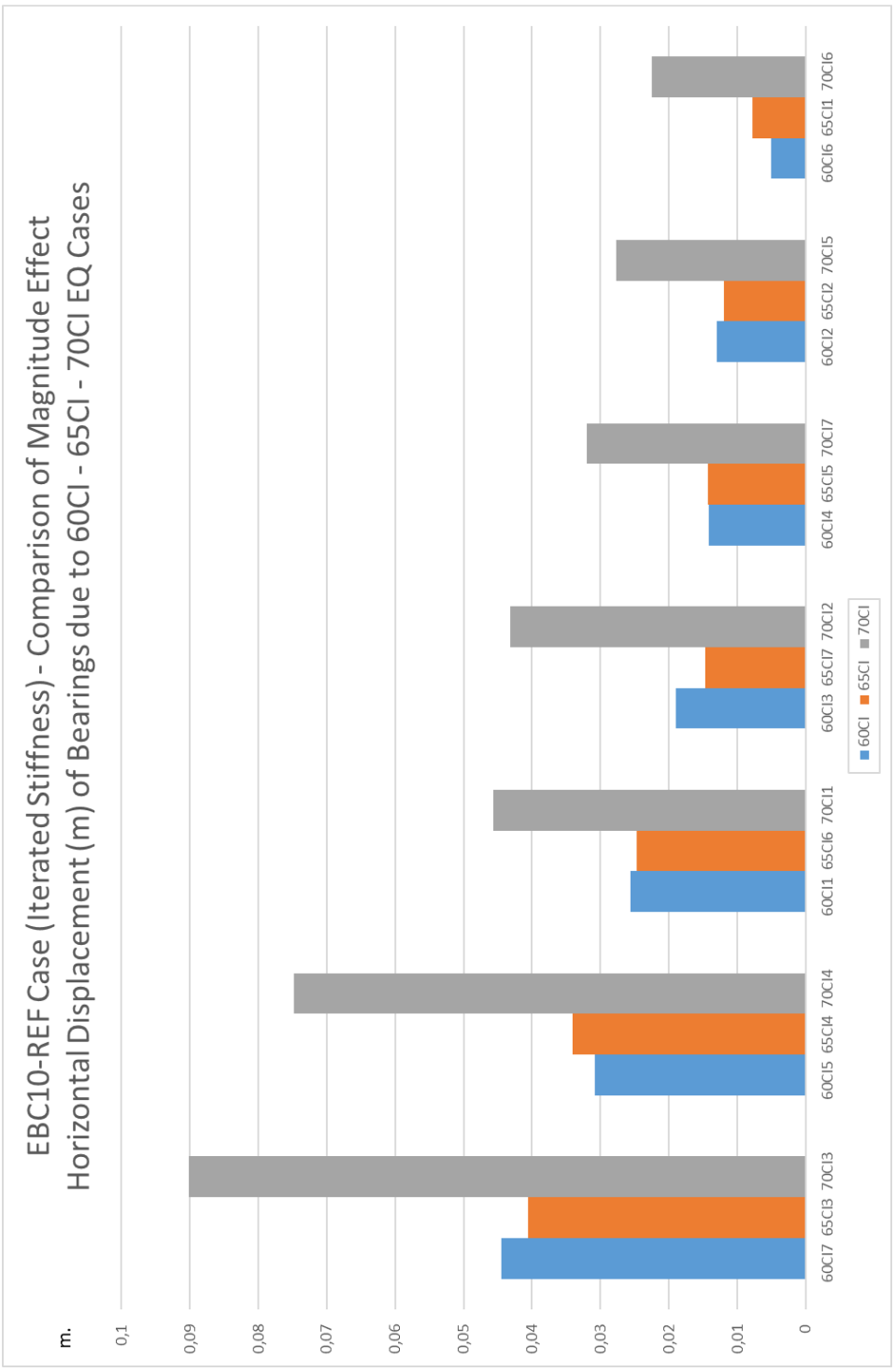

Figure 5.1. EBC10-REF Case (Iterated Stiffness) - Comparison of Magnitude Effect - Horizontal Displacement (m) of Bearings due to 60CI - 65CI - 70CI EQ Cases

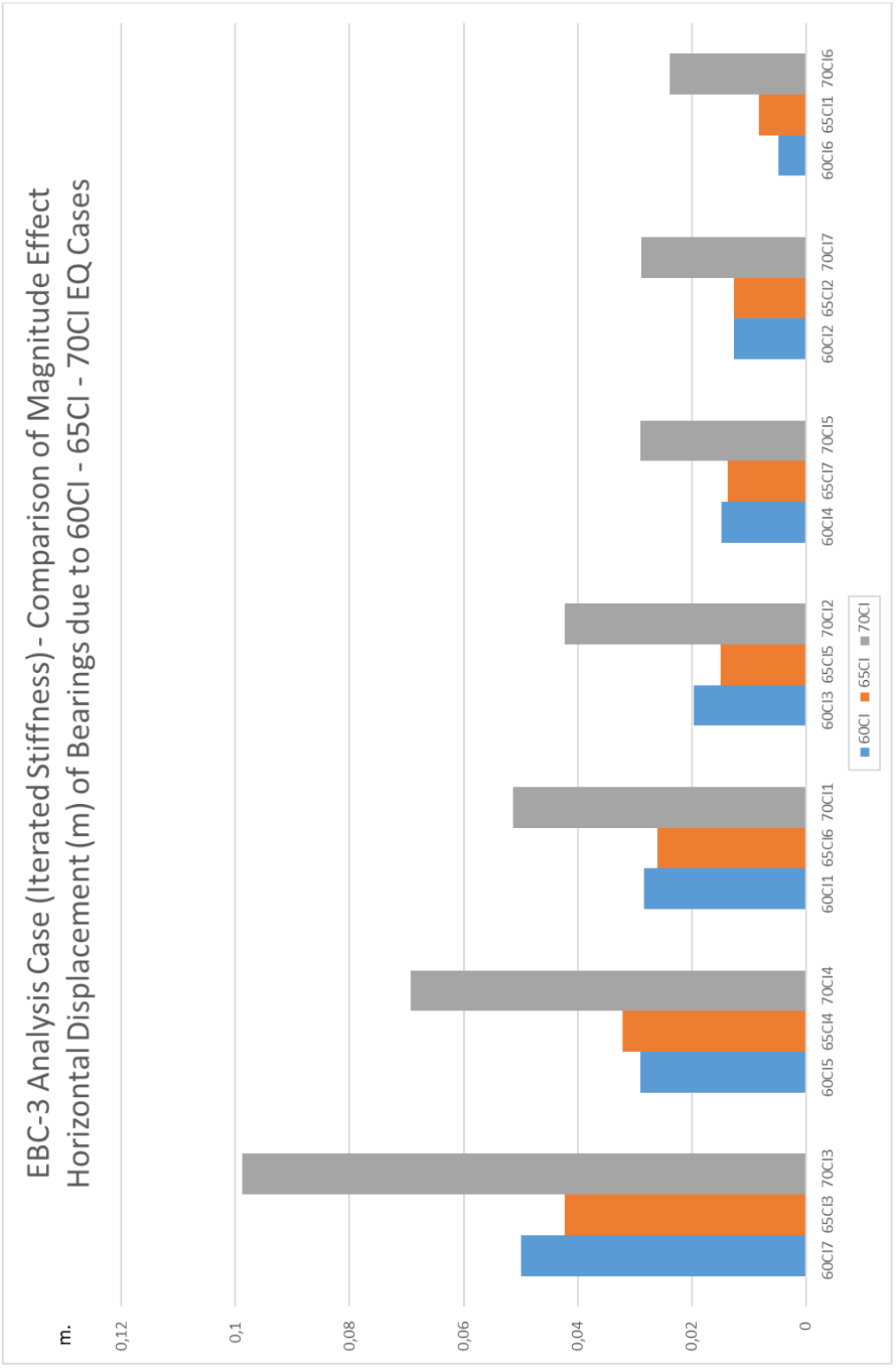

Figure 5.2. EBC-3 Case (Iterated Stiffness) - Comparison of Magnitude Effect - Horizontal Displacement (m) of Bearings due to 60CI - 65CI - 70CI EQ Cases

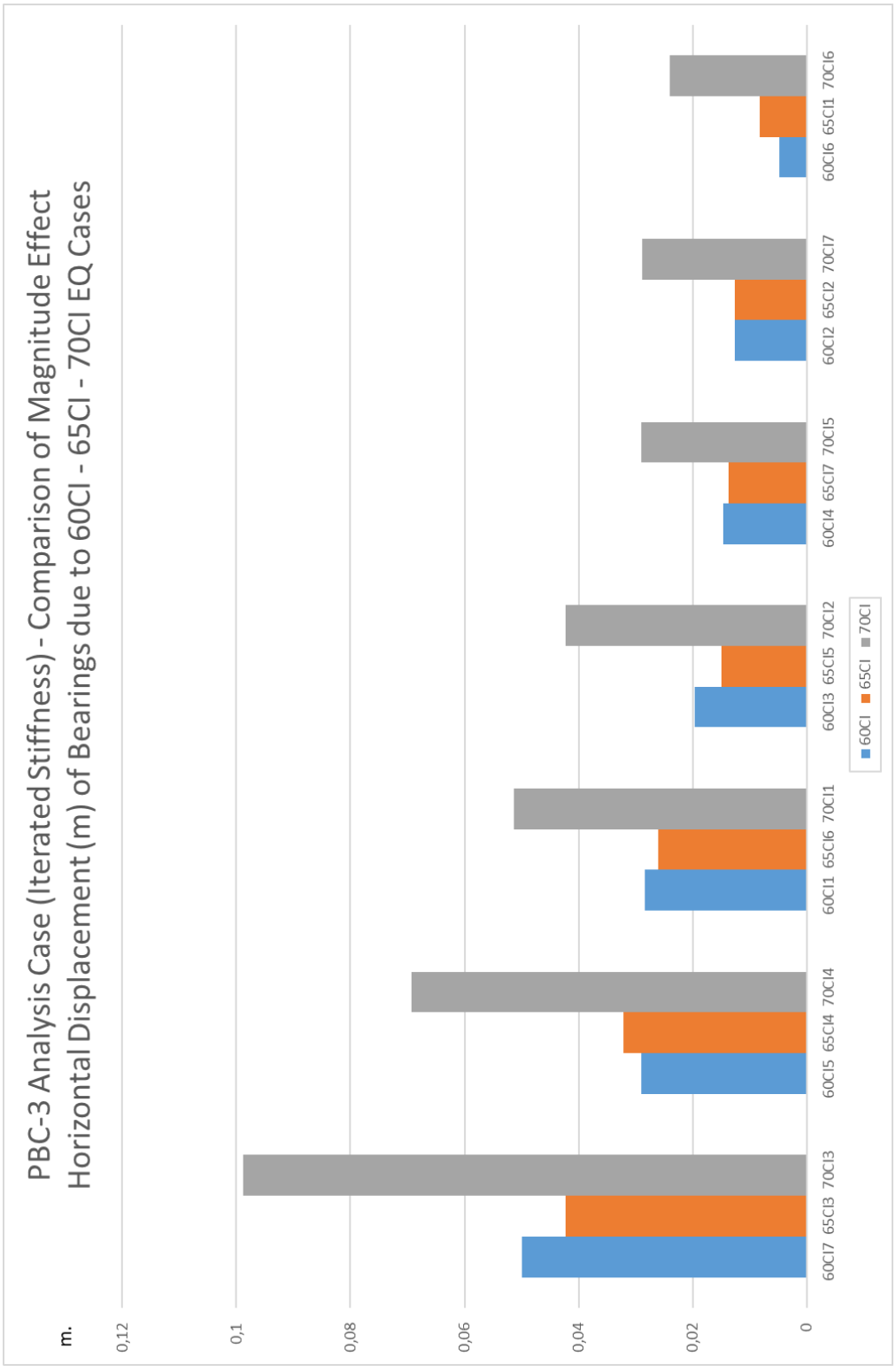

Figure 5.3. PBC-3 Case (Iterated Stiffness) - Comparison of Magnitude Effect - Horizontal Displacement (m) of Bearings due to 60CI - 65CI - 70CI EQ Cases

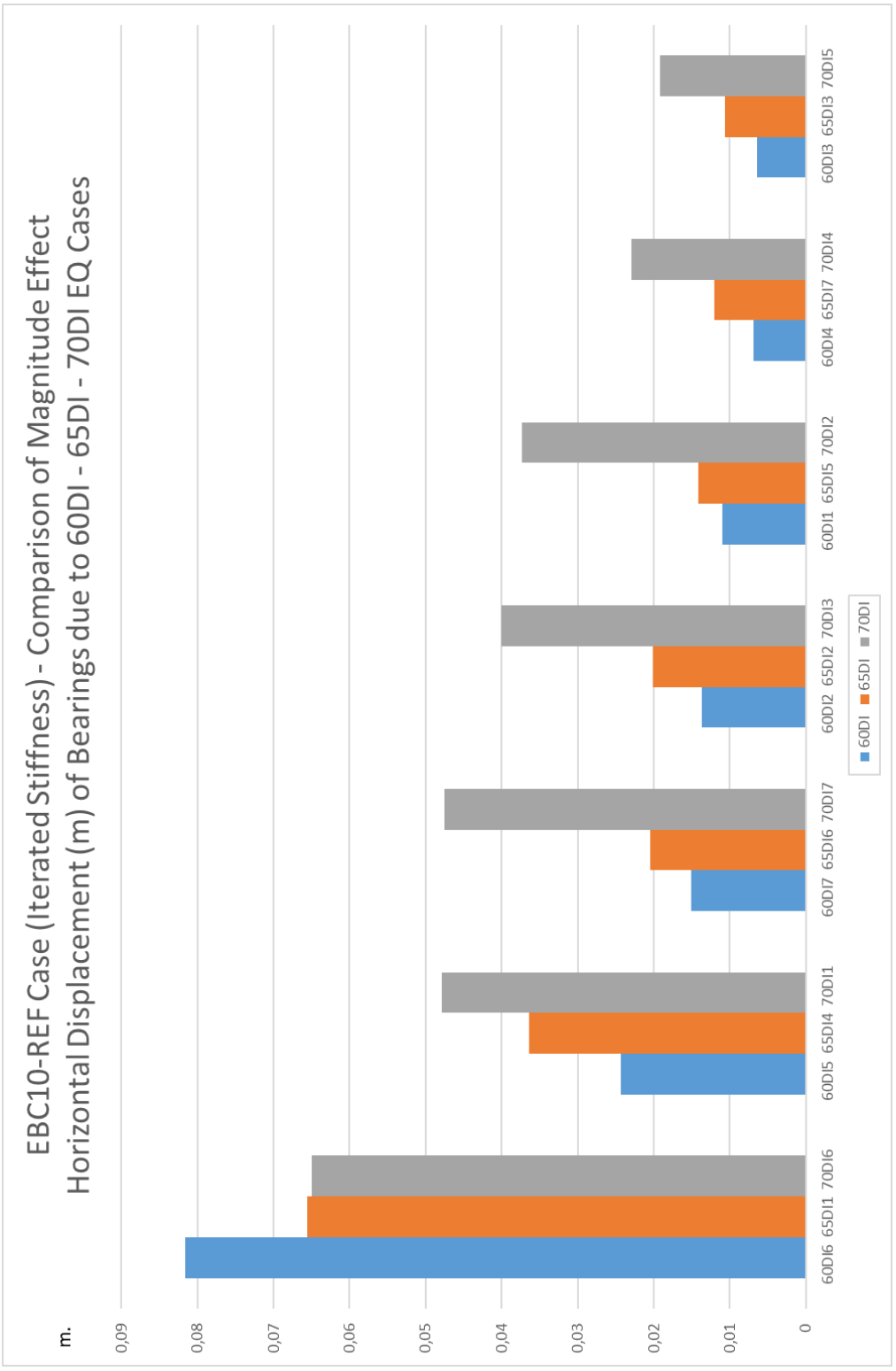

Figure 5.4. EBC10-REF Case (Iterated Stiffness) - Comparison of Magnitude Effect - Horizontal Displacement (m) of Bearings due to 60DI - 65DI - 70DI EQ Cases

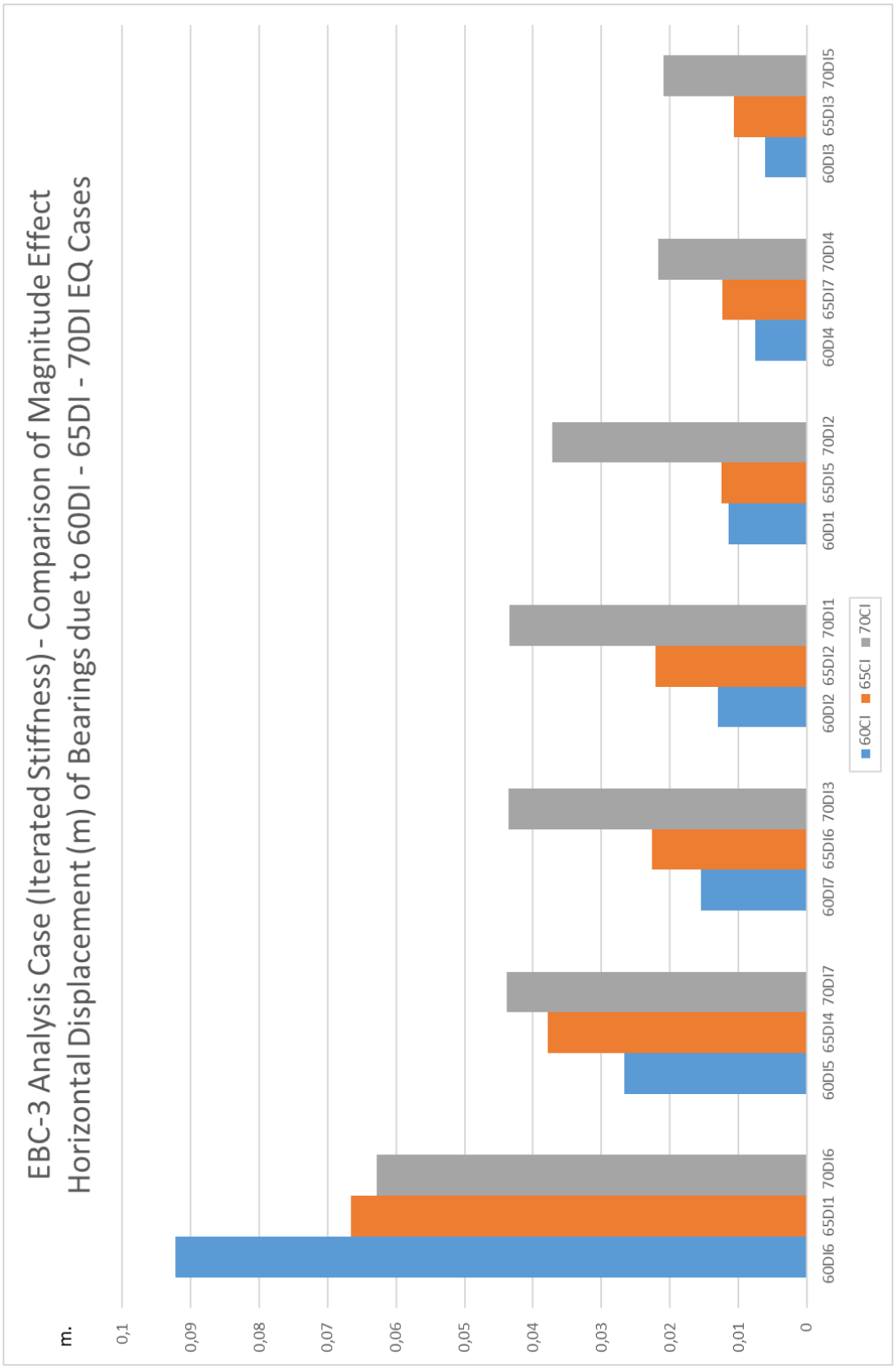

Figure 5.5. EBC-3 Case (Iterated Stiffness) - Comparison of Magnitude Effect - Horizontal Displacement (m) of Bearings due to 60DI - 65DI - 70DI EQ Cases

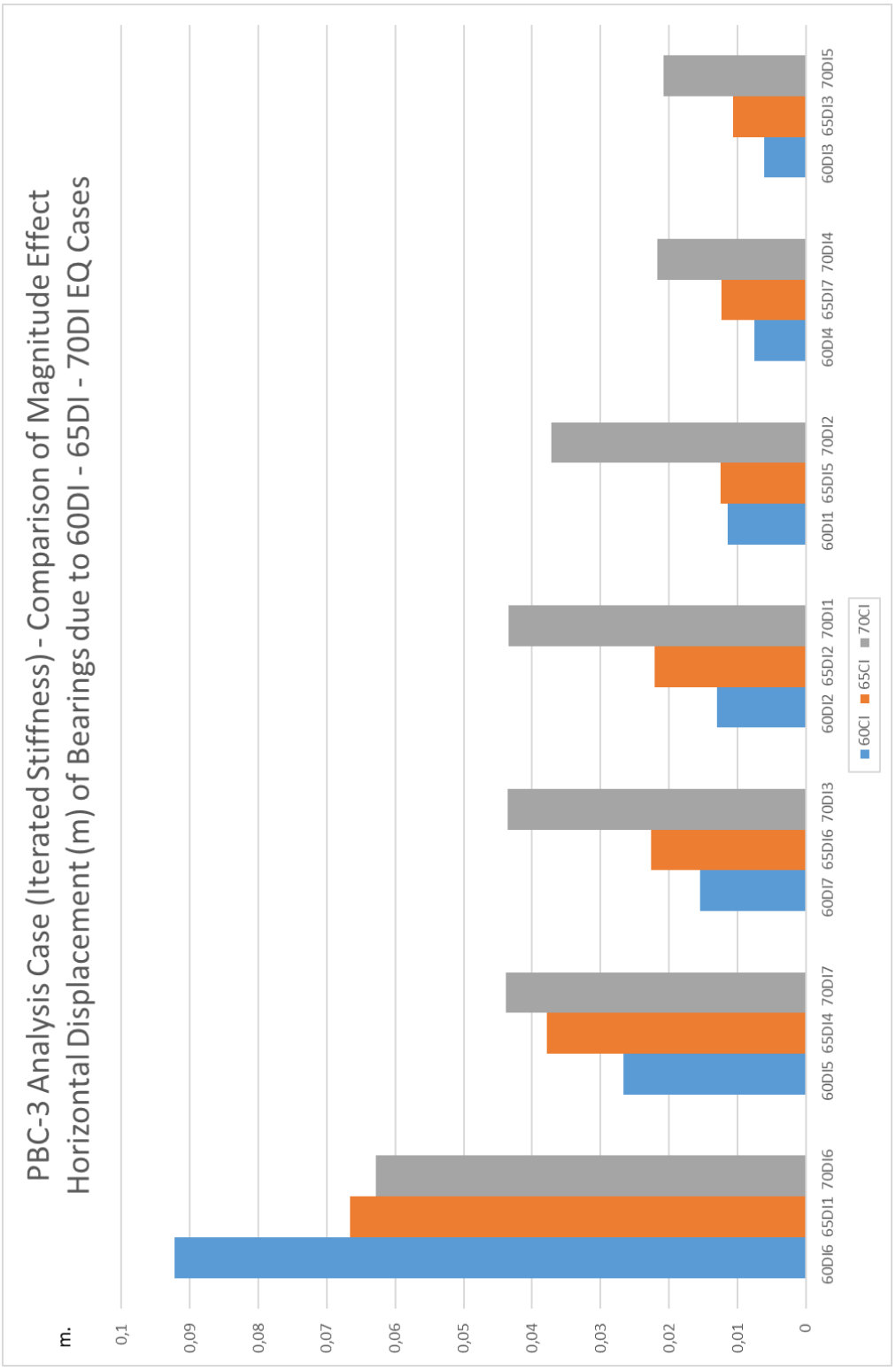

Figure 5.6. PBC-3 Case (Iterated Stiffness) - Comparison of Magnitude Effect - Horizontal Displacement (m) of Bearings due to 60DI - 65DI - 70DI EQ Cases

5.2. Comparison Based on Soil Class

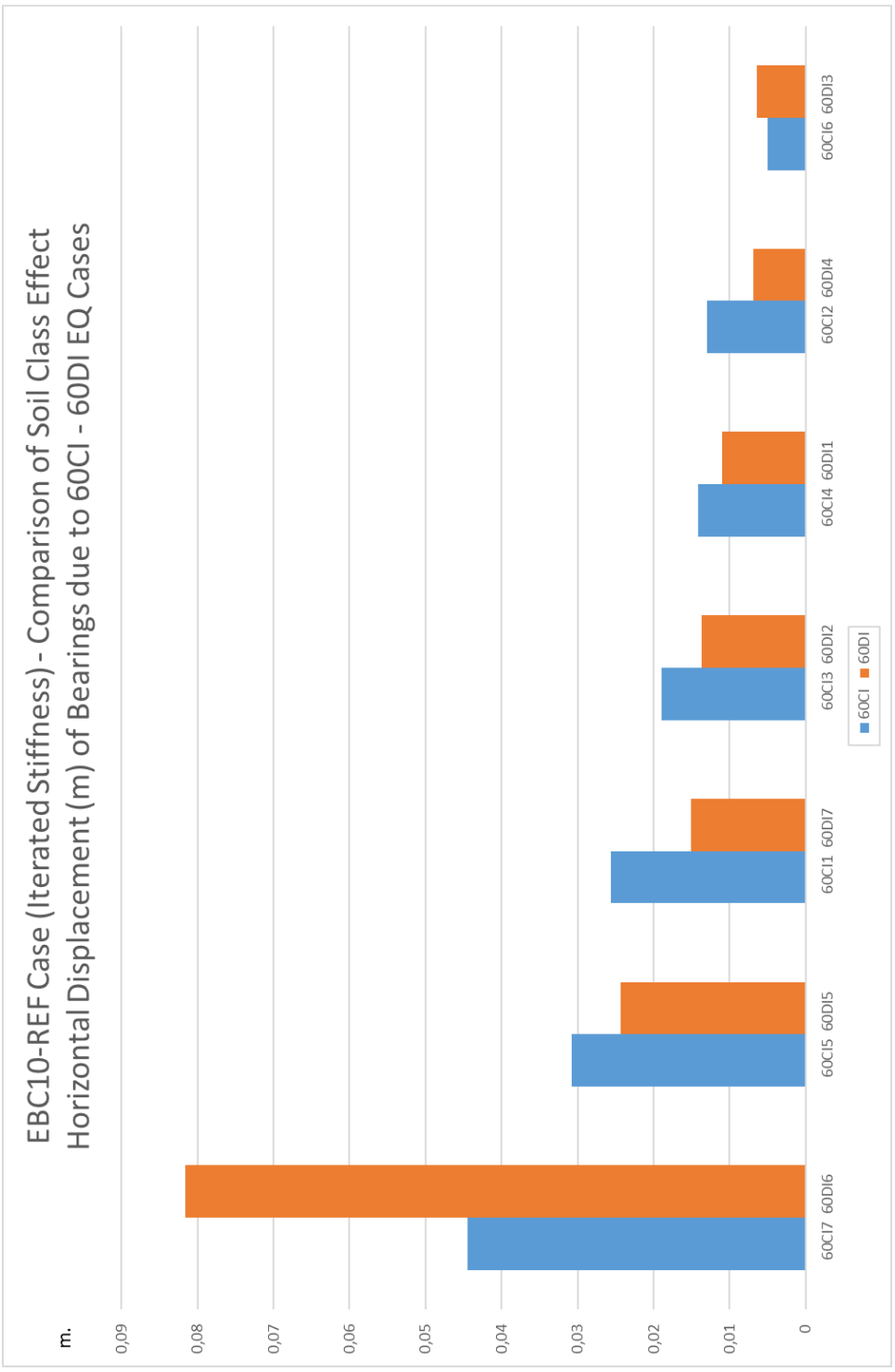

Figure 5.7. EBC10-REF Case (Iterated Stiffness) - Comparison of Soil Class Effect - Horizontal Displacement (m) of Bearings due to 60CI - 60DI EQ Cases

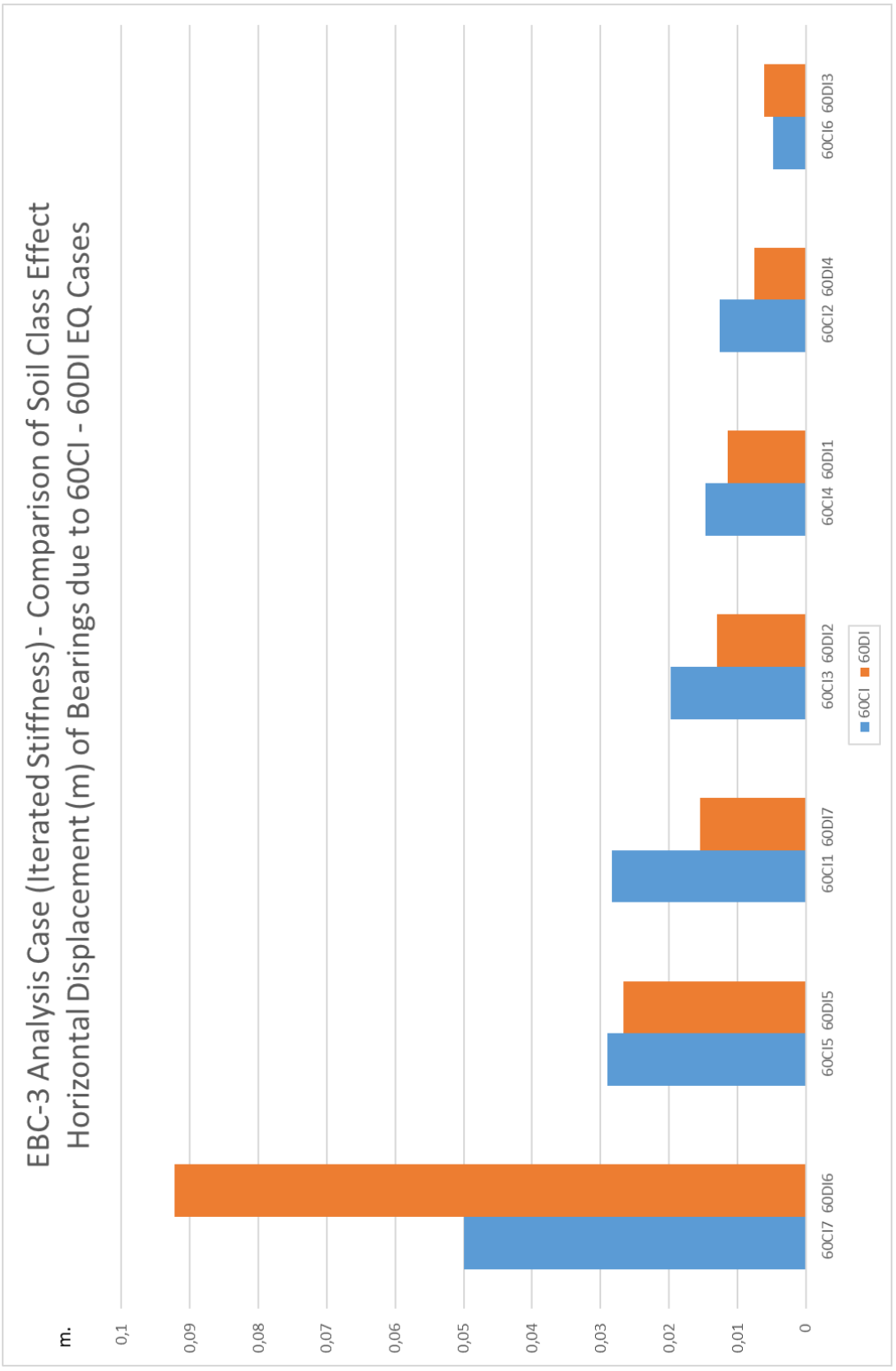

Figure 5.8. EBC-3 Case (Iterated Stiffness) - Comparison of Soil Class Effect - Horizontal Displacement (m) of Bearings due to 60CI - 60DI EQ Cases

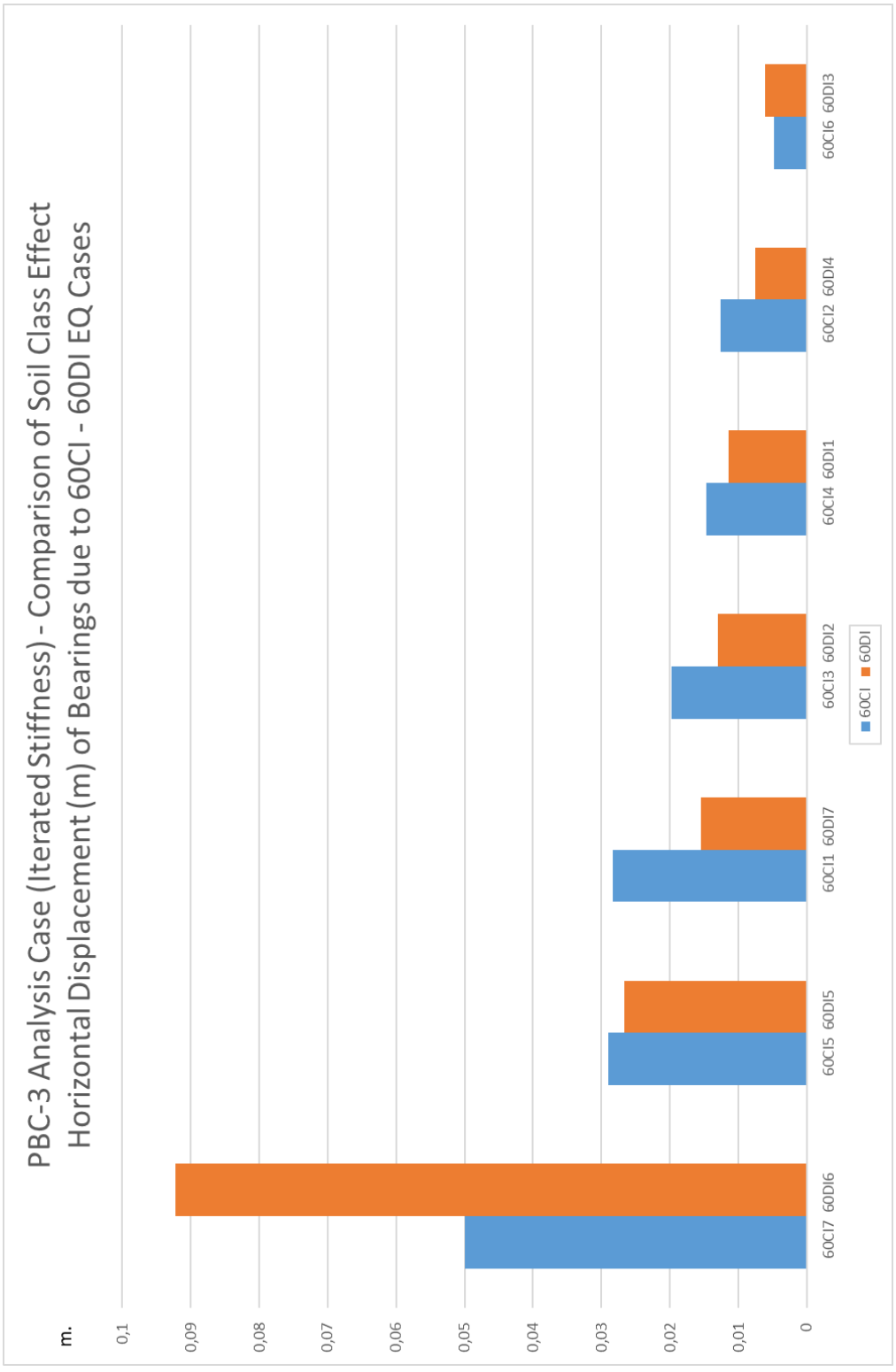

Figure 5.9. PBC-3 Case (Iterated Stiffness) - Comparison of Soil Class Effect - Horizontal Displacement (m) of Bearings due to 60CI - 60DI EQ Cases

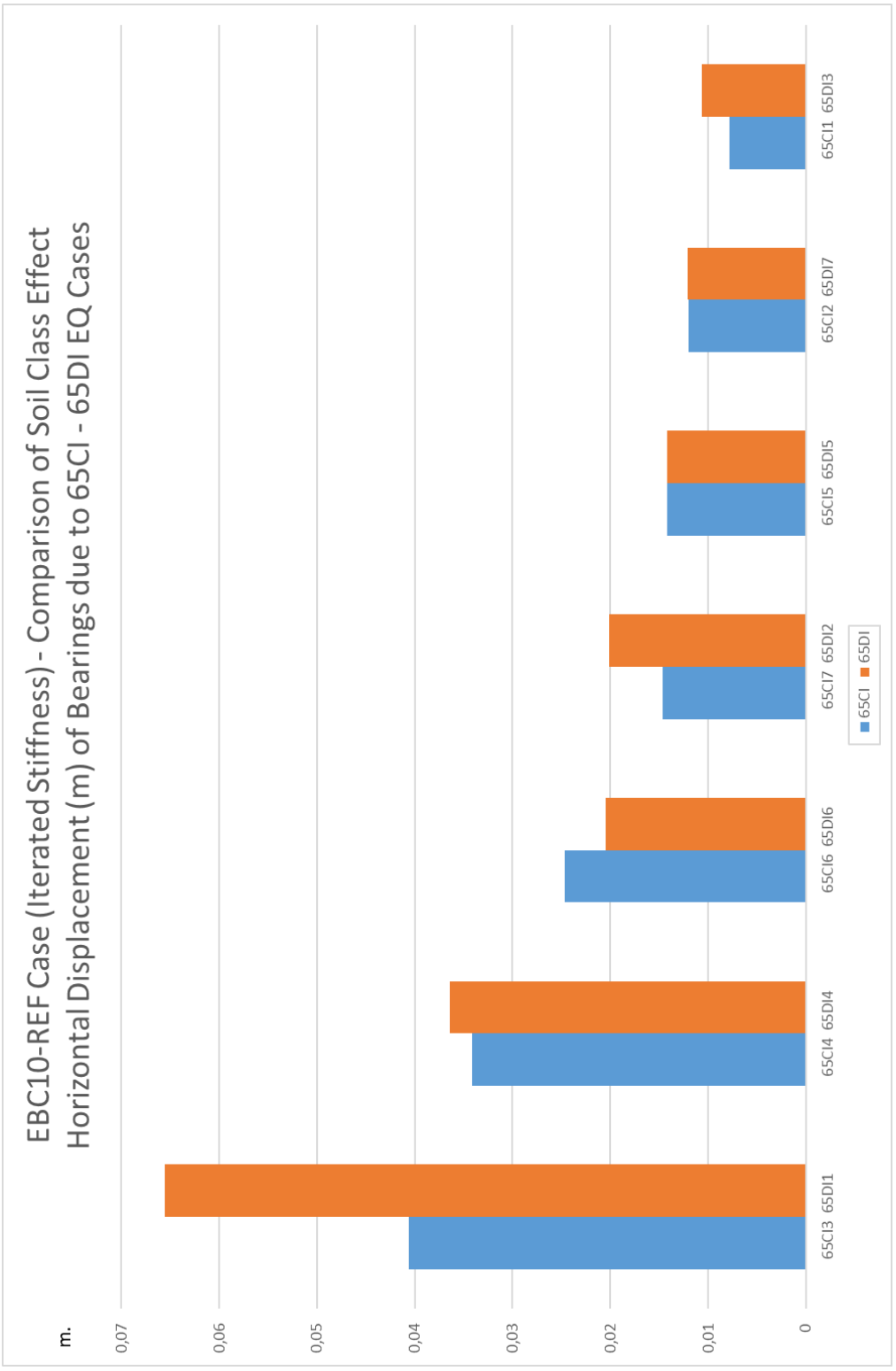

Figure 5.10. EBC10-REF Case (Iterated Stiffness) - Comparison of Soil Class Effect - Horizontal Displacement (m) of Bearings due to 65CI - 65DI EQ Cases

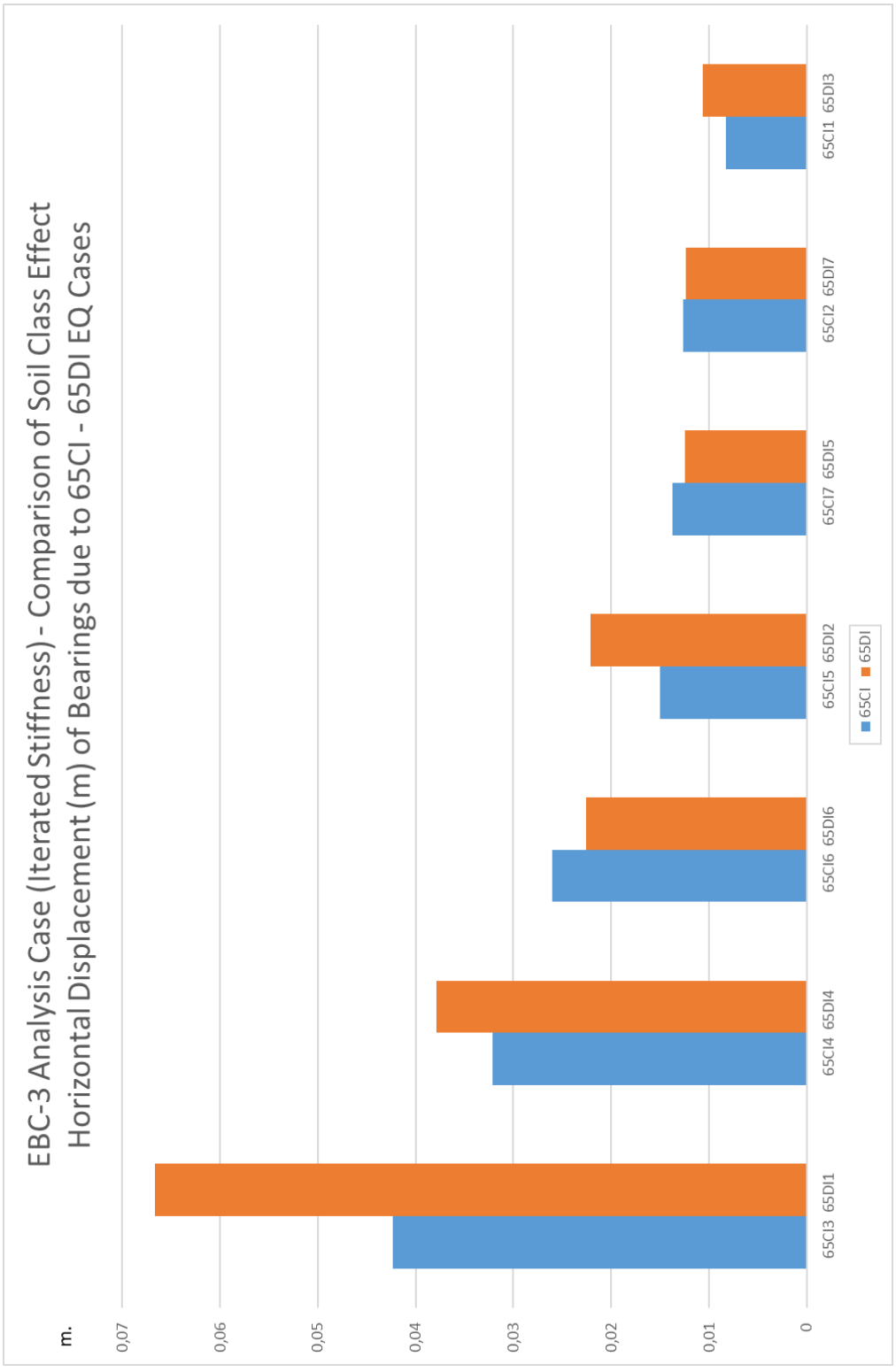

Figure 5.11. EBC-3 Case (Iterated Stiffness) - Comparison of Soil Class Effect - Horizontal Displacement (m) of Bearings due to 65CI - 65DI EQ Cases

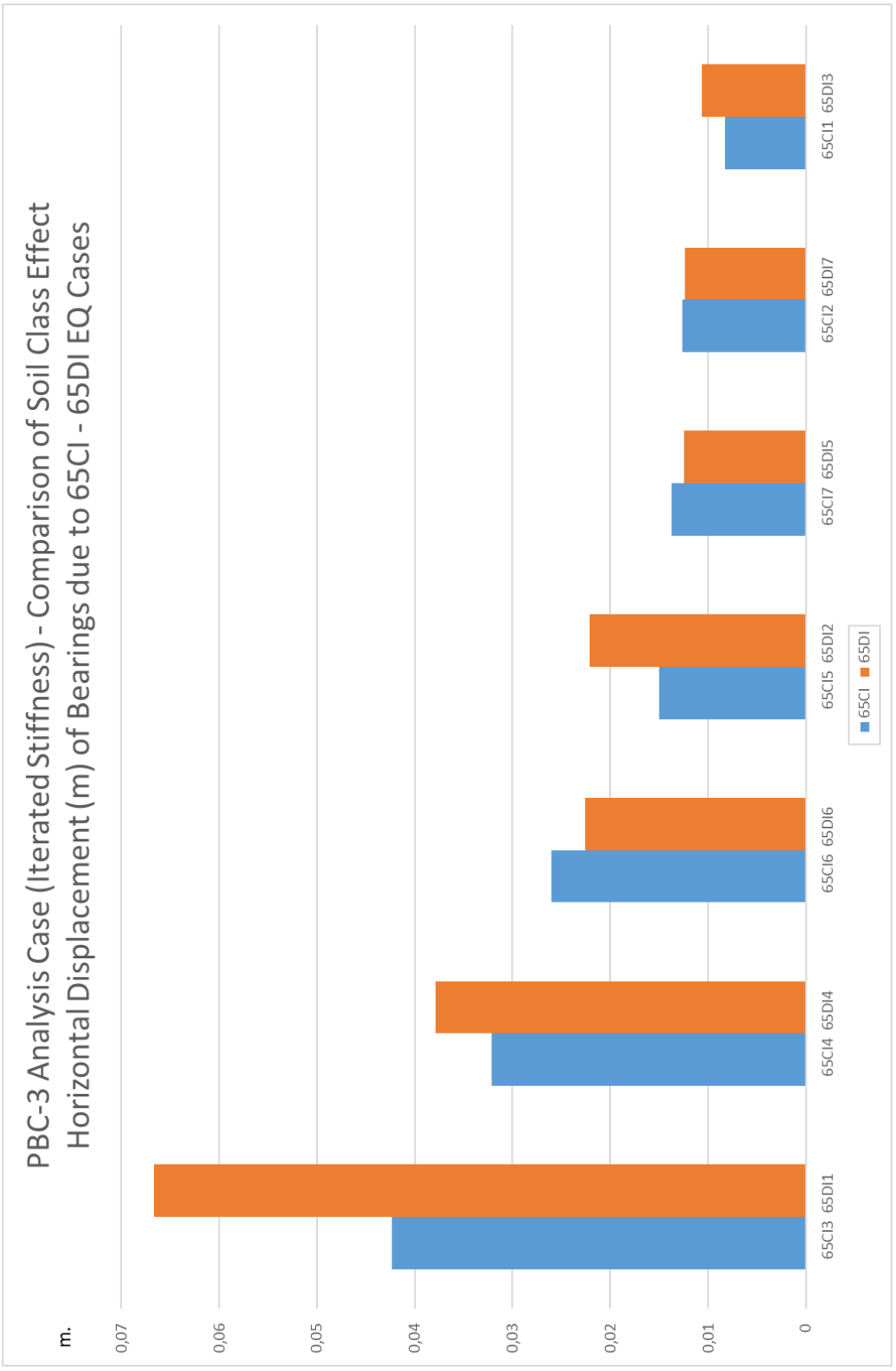

Figure 5.12. PBC-3 Case (Iterated Stiffness) - Comparison of Soil Class Effect - Horizontal Displacement (m) of Bearings due to 65CI - 65DI EQ Cases

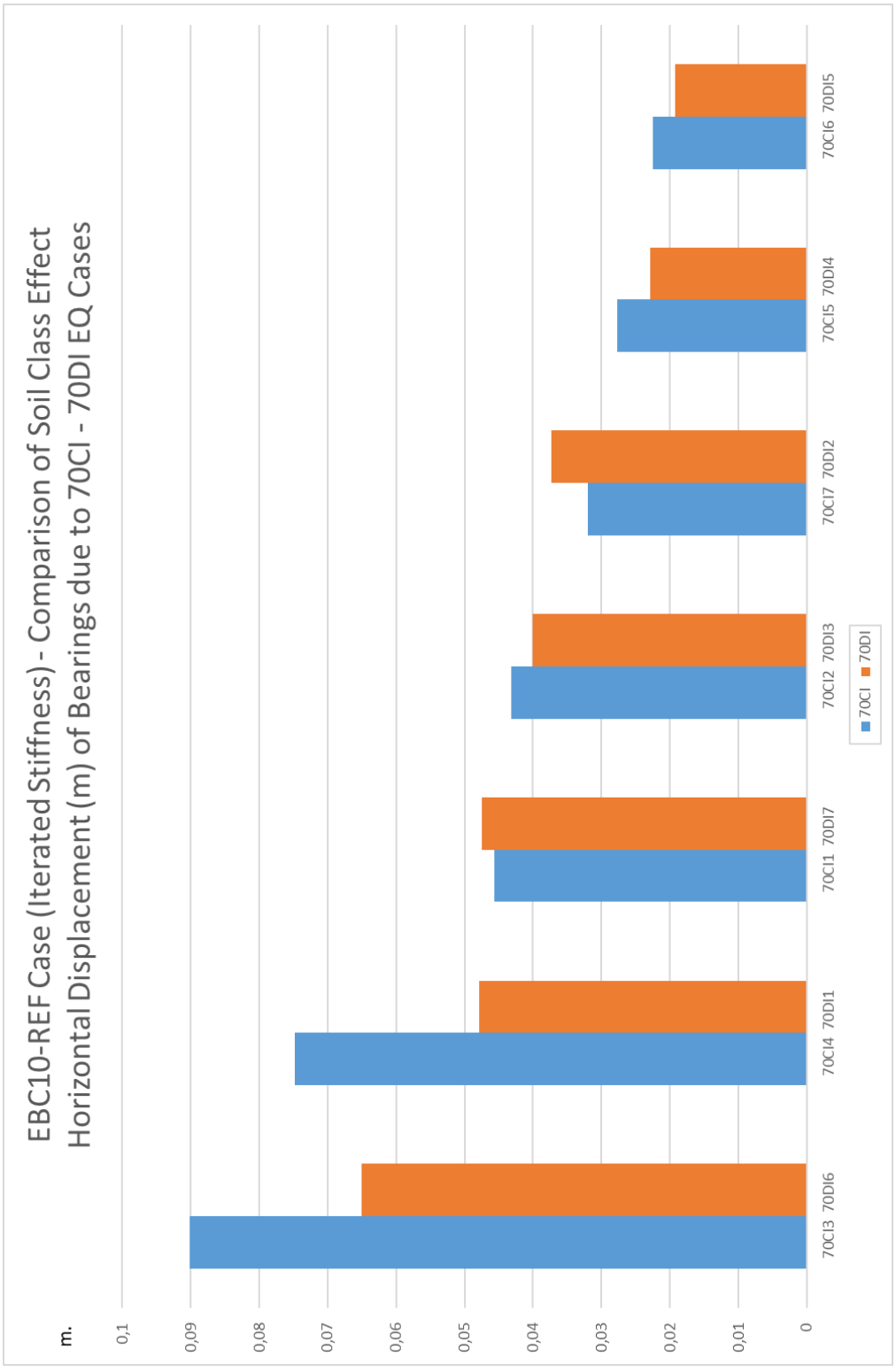

Figure 5.13. EBC10-REF Case (Iterated Stiffness) - Comparison of Soil Class Effect - Horizontal Displacement (m) of Bearings due to 70CI - 70DI EQ Cases

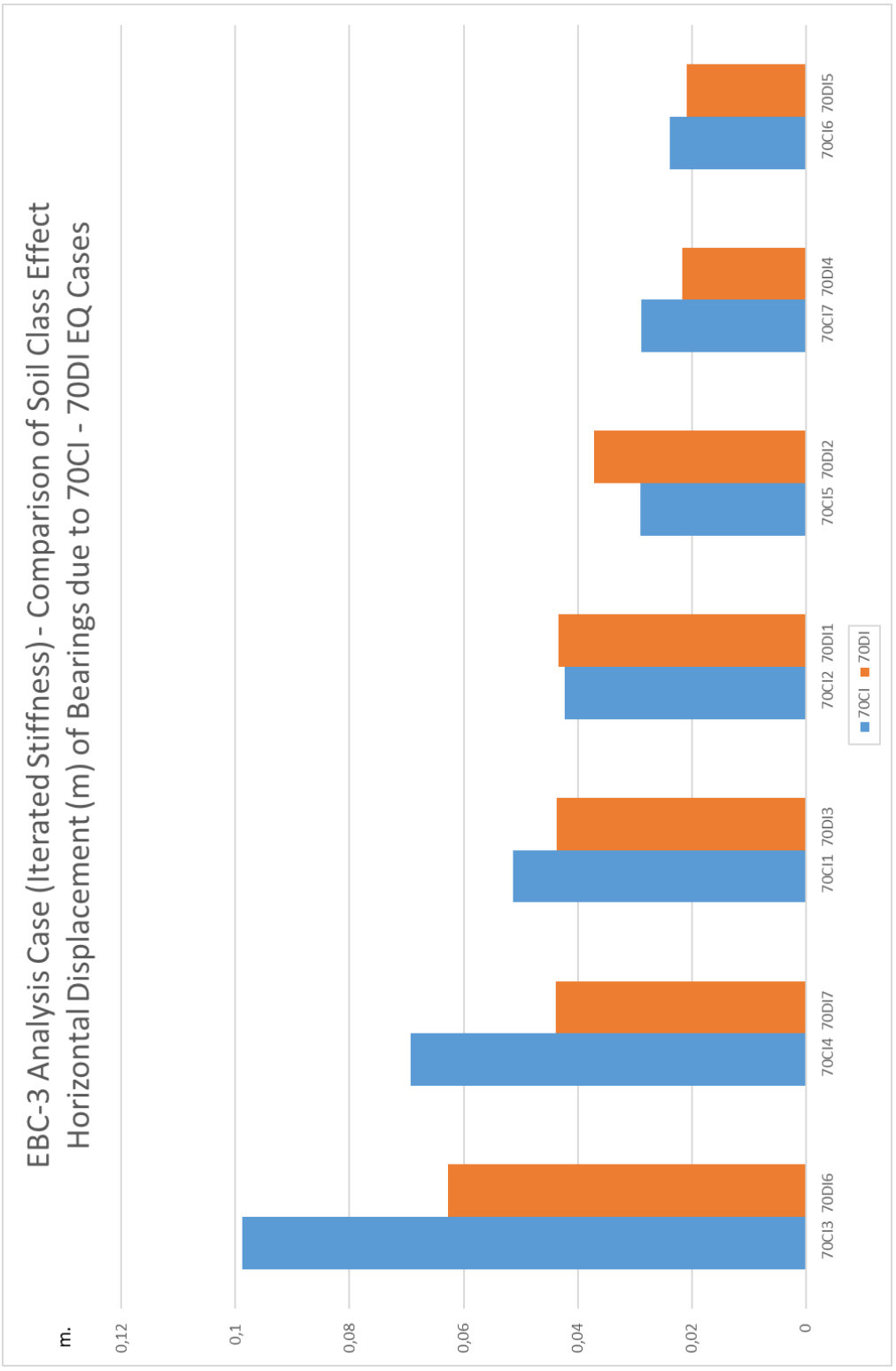

Figure 5.14. EBC-3 Case (Iterated Stiffness) - Comparison of Soil Class Effect - Horizontal Displacement (m) of Bearings due to 70CI - 70DI EQ Cases

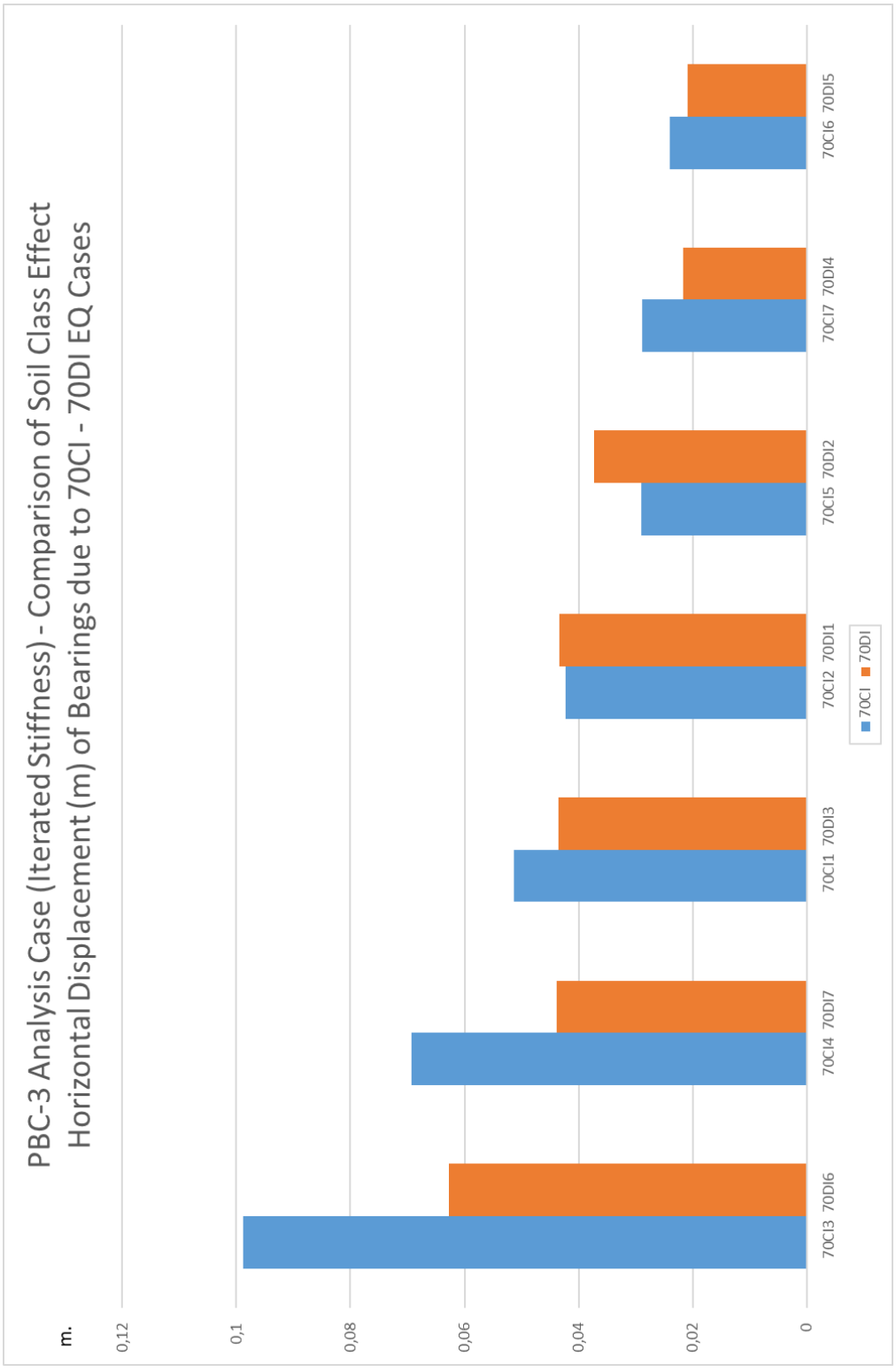

Figure 5.15. PBC-3 Case (Iterated Stiffness) - Comparison of Soil Class Effect - Horizontal Displacement (m) of Bearings due to 70CI - 70DI EQ Cases

5.3. Comparison Based on Bearing Type and Formation

5.3.1. Comparison Based on Bearing Type and Formation (Initial Case)

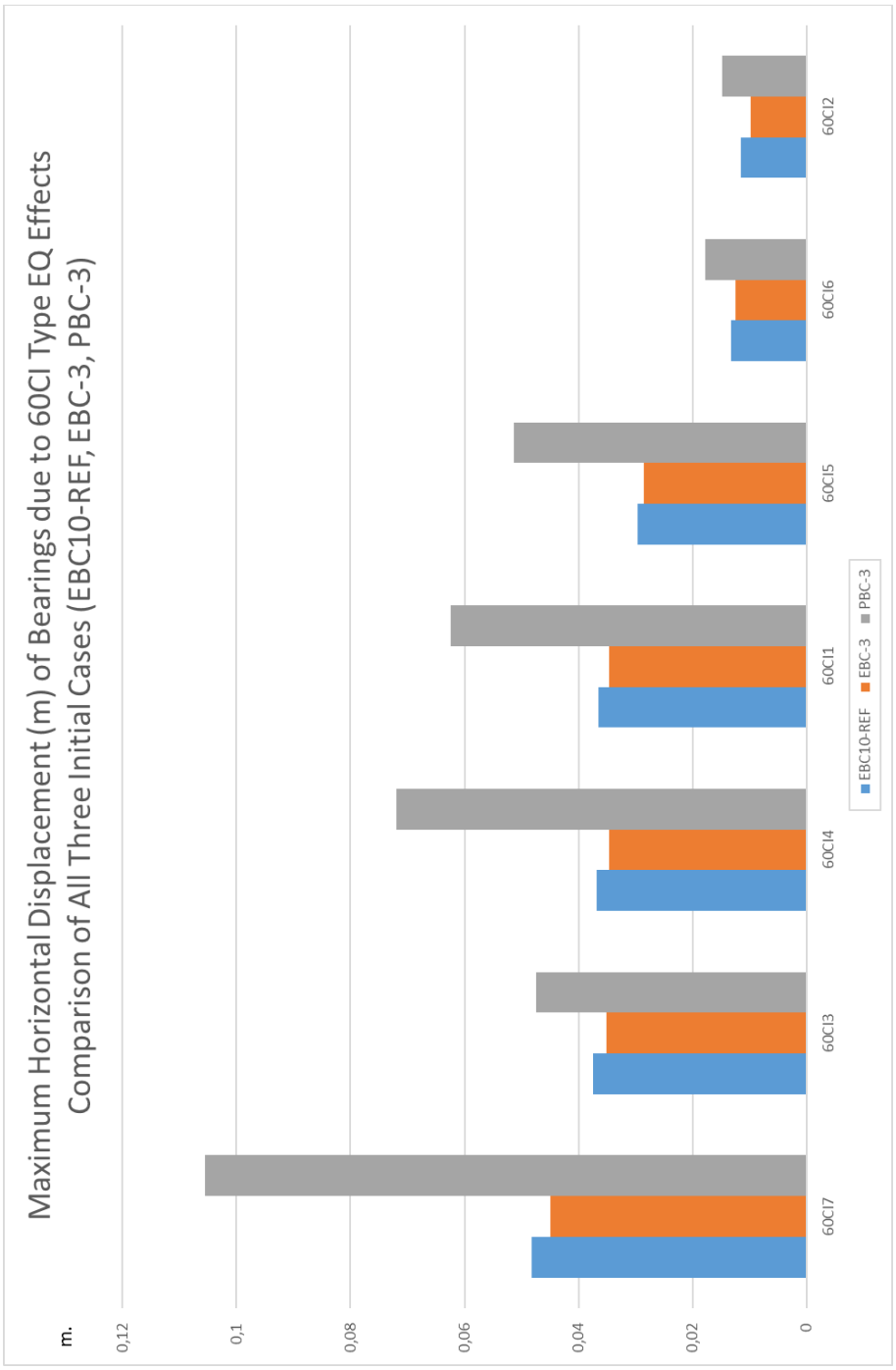

Figure 5.16. Maximum Horizontal Displacement of Bearings due to 60CI Type EQ Effects - Comparison of All Three Initial Cases (EBC10-REF, EBC-3, PBC-3)

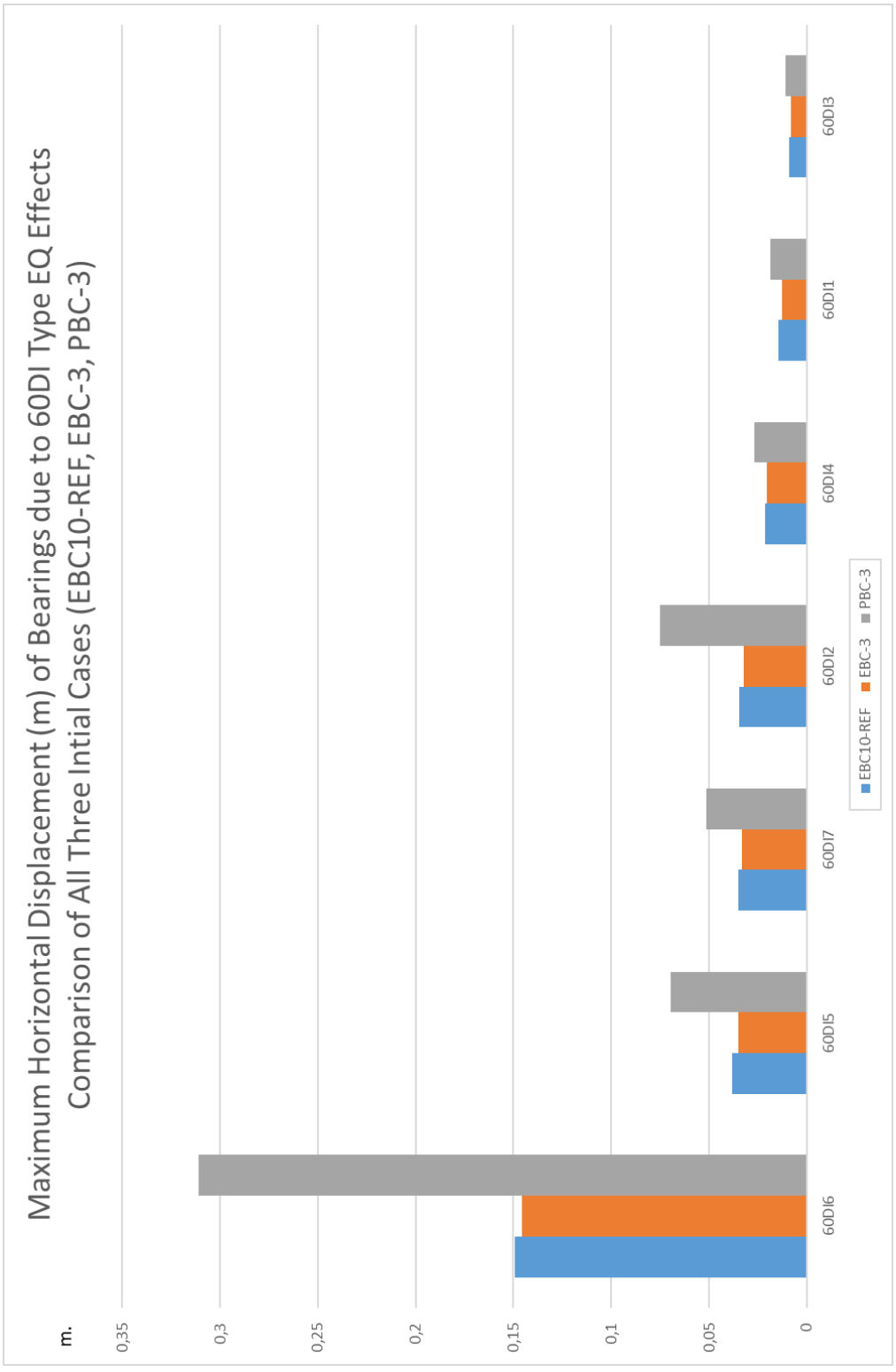

Figure 5.17. Maximum Horizontal Displacement of Bearings due to 60DI Type EQ Effects - Comparison of All Three Initial Cases (EBC10-REF, EBC-3, PBC-3)

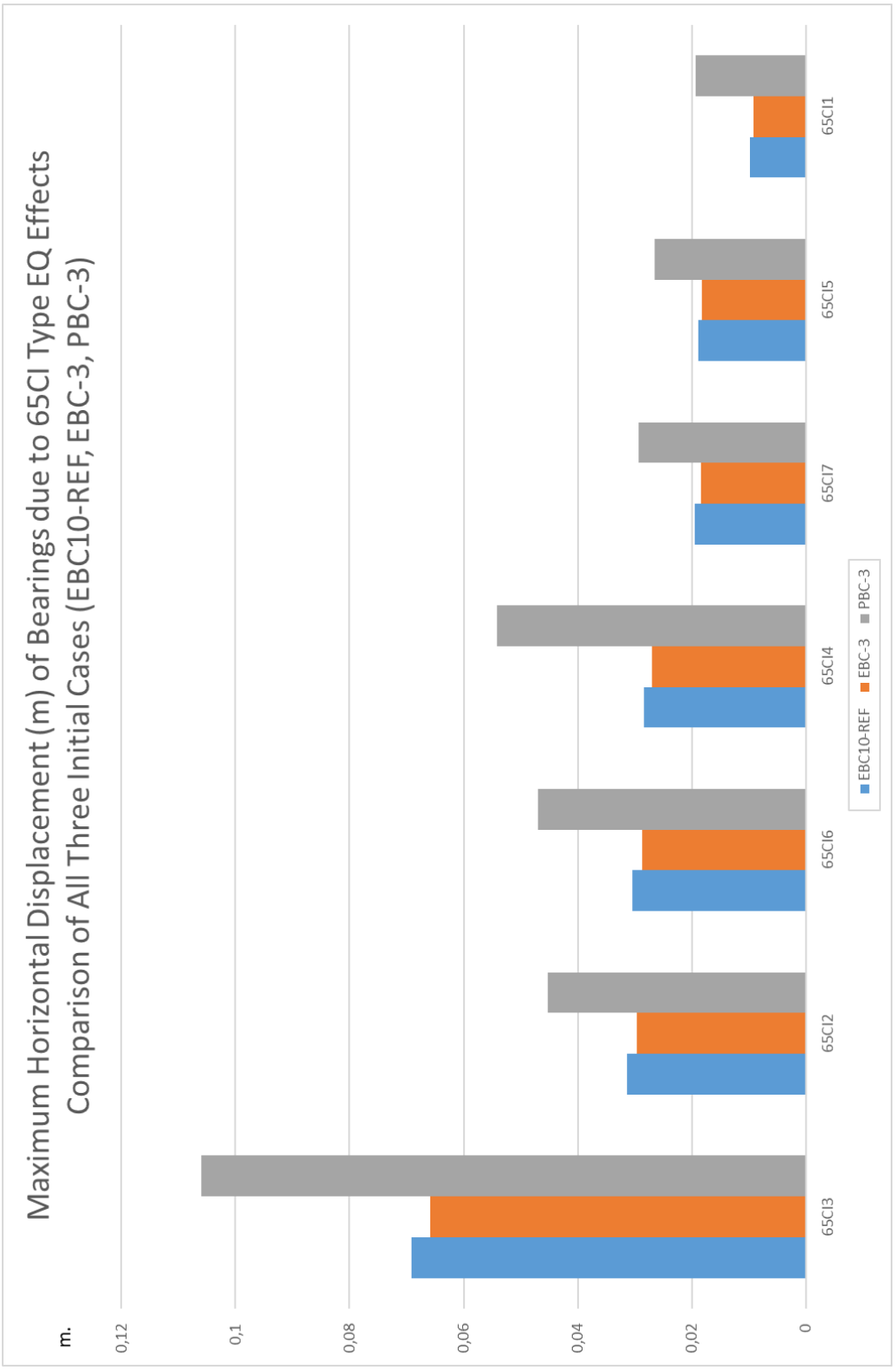

Figure 5.18. Maximum Horizontal Displacement of Bearings due to 65CI Type EQ Effects - Comparison of All Three Initial Cases (EBC10-REF, EBC-3, PBC-3)

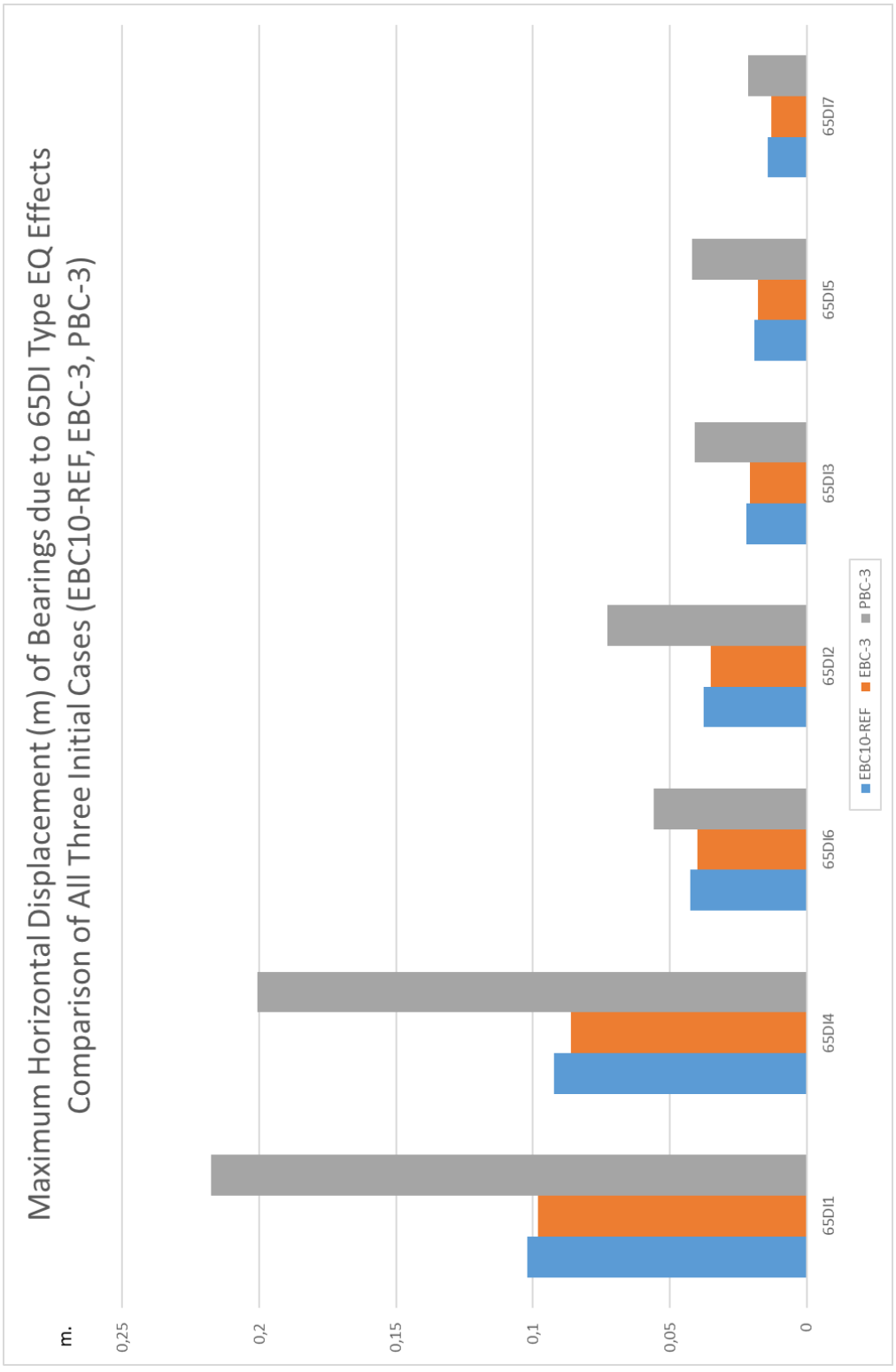

Figure 5.19. Maximum Horizontal Displacement of Bearings due to 65DI Type EQ Effects - Comparison of All Three Initial Cases (EBC10-REF, EBC-3, PBC-3)

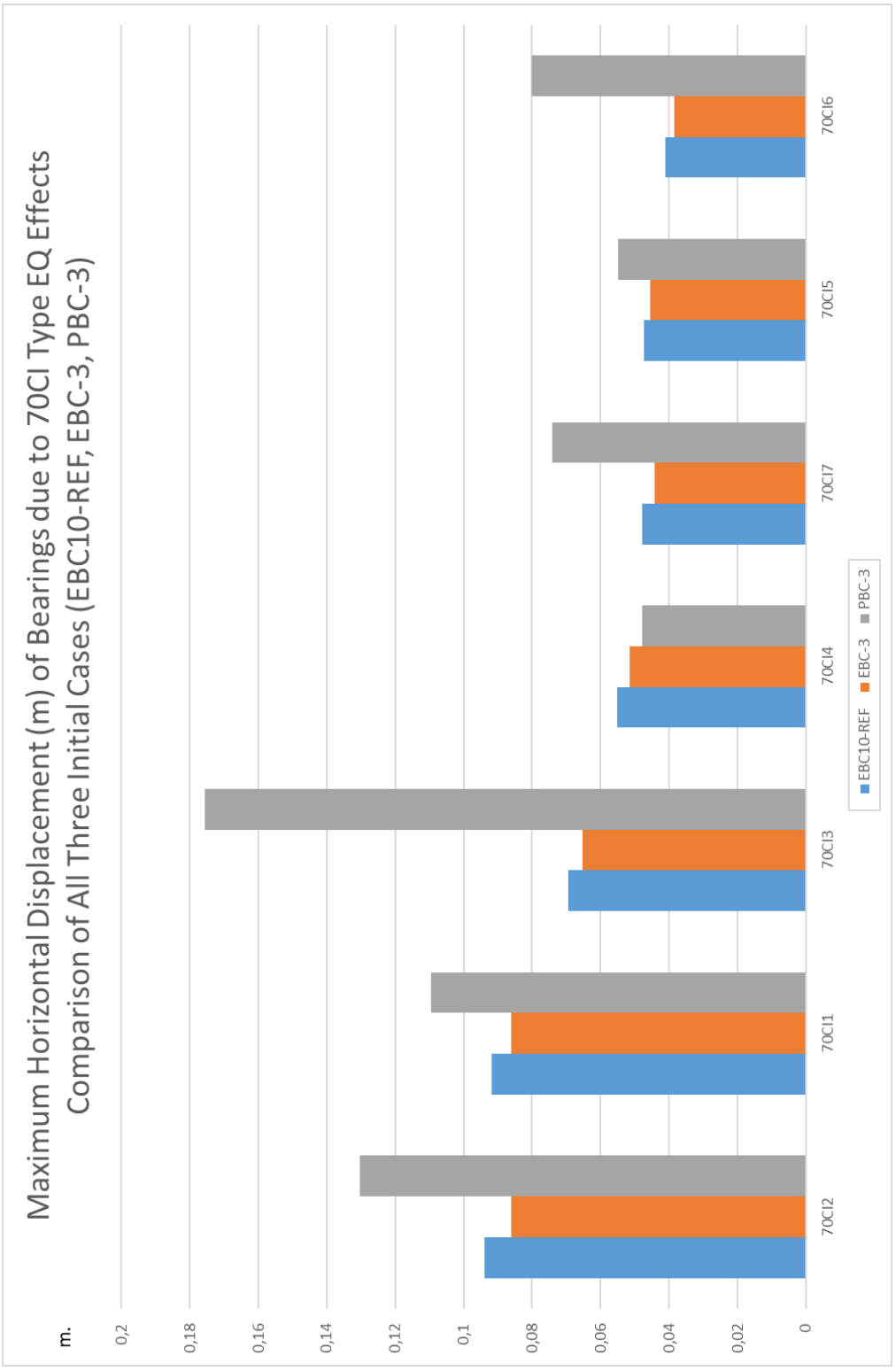

Figure 5.20. Maximum Horizontal Displacement of Bearings due to 70CI Type EQ Effects - Comparison of All Three Initial Cases (EBC10-REF, EBC-3, PBC-3)

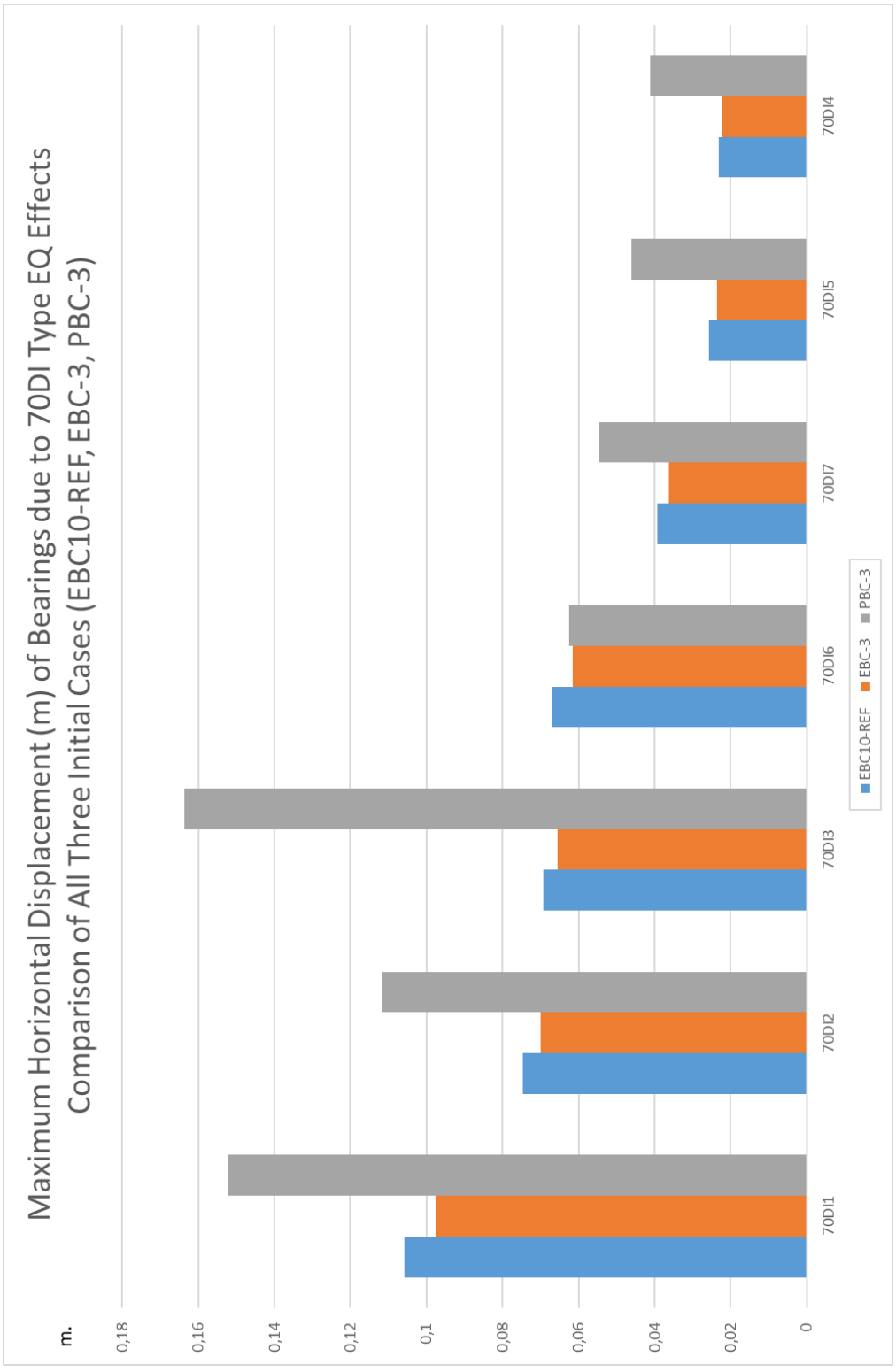

Figure 5.21. Maximum Horizontal Displacement of Bearings due to 70DI Type EQ Effects - Comparison of All Three Iterated Cases (EBC10-REF, EBC-3, PBC-3)

5.3.2. Comparison Based on Bearing Type and Formation (Iterated Case)

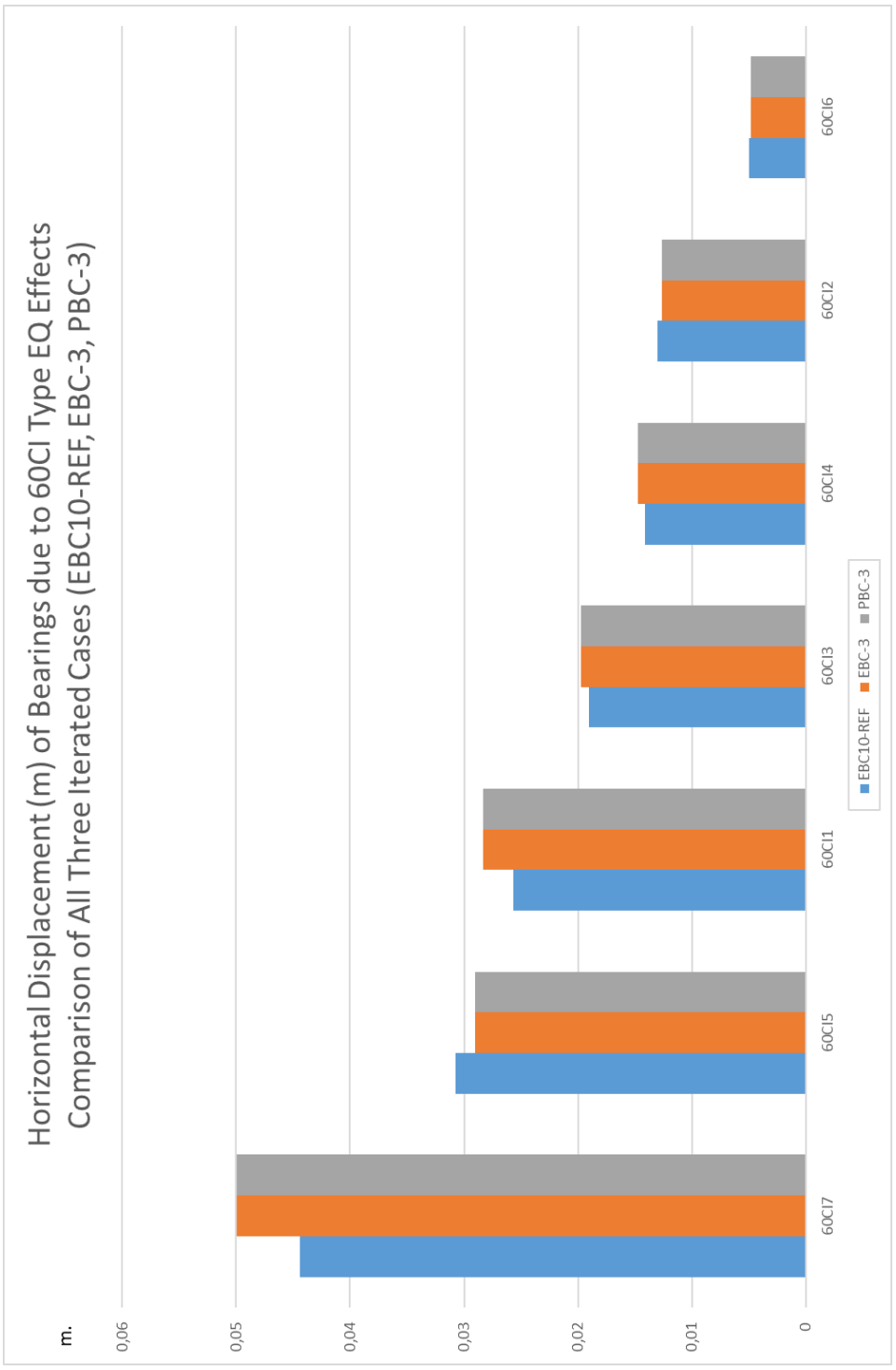

Figure 5.22. Maximum Horizontal Displacement of Bearings due to 60CI Type EQ Effects - Comparison of All Three Iterated Cases (EBC10-REF, EBC-3, PBC-3)

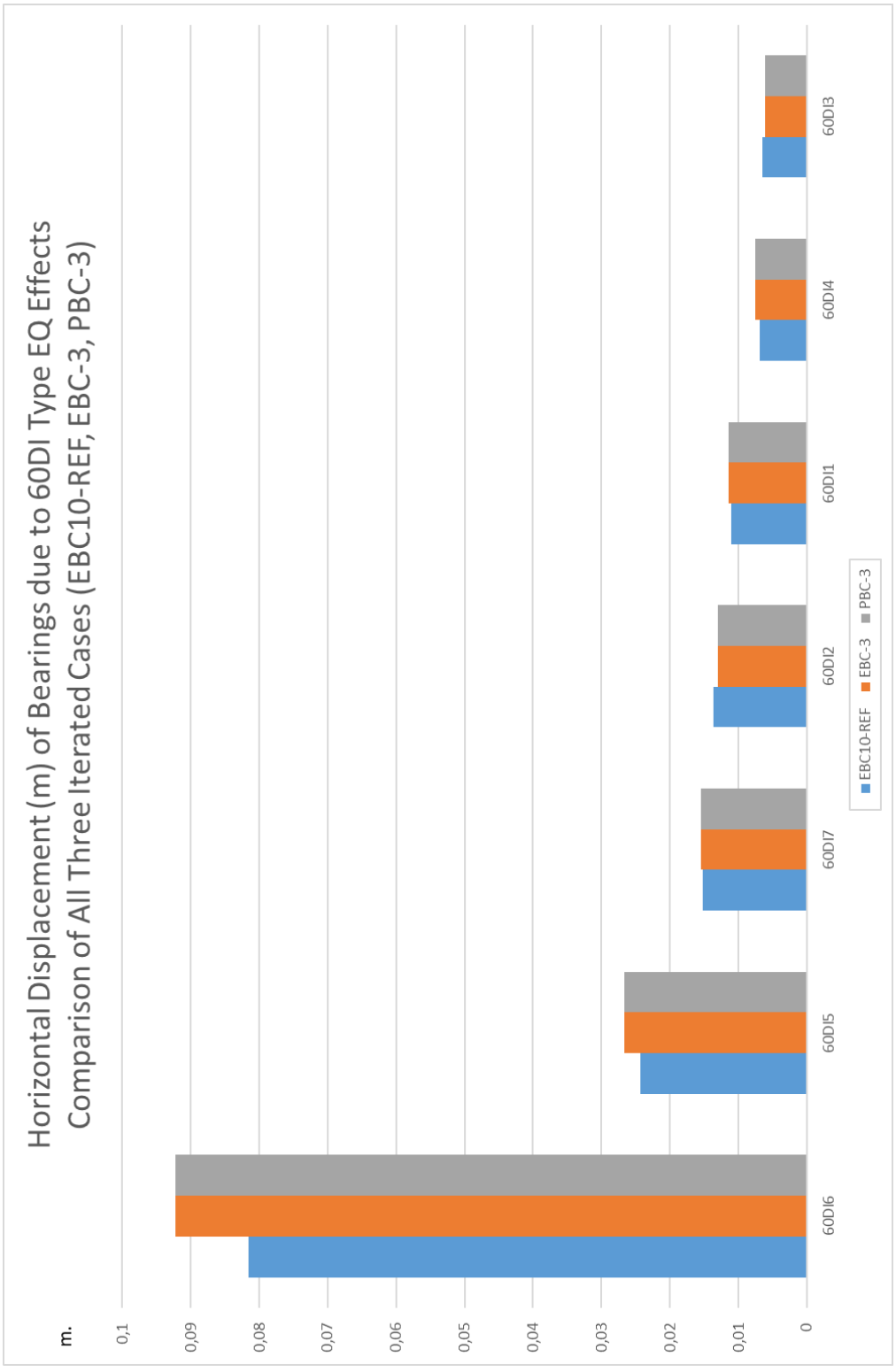

Figure 5.23. Maximum Horizontal Displacement of Bearings due to 60DI Type EQ Effects - Comparison of All Three Iterated Cases (EBC10-REF, EBC-3, PBC-3)

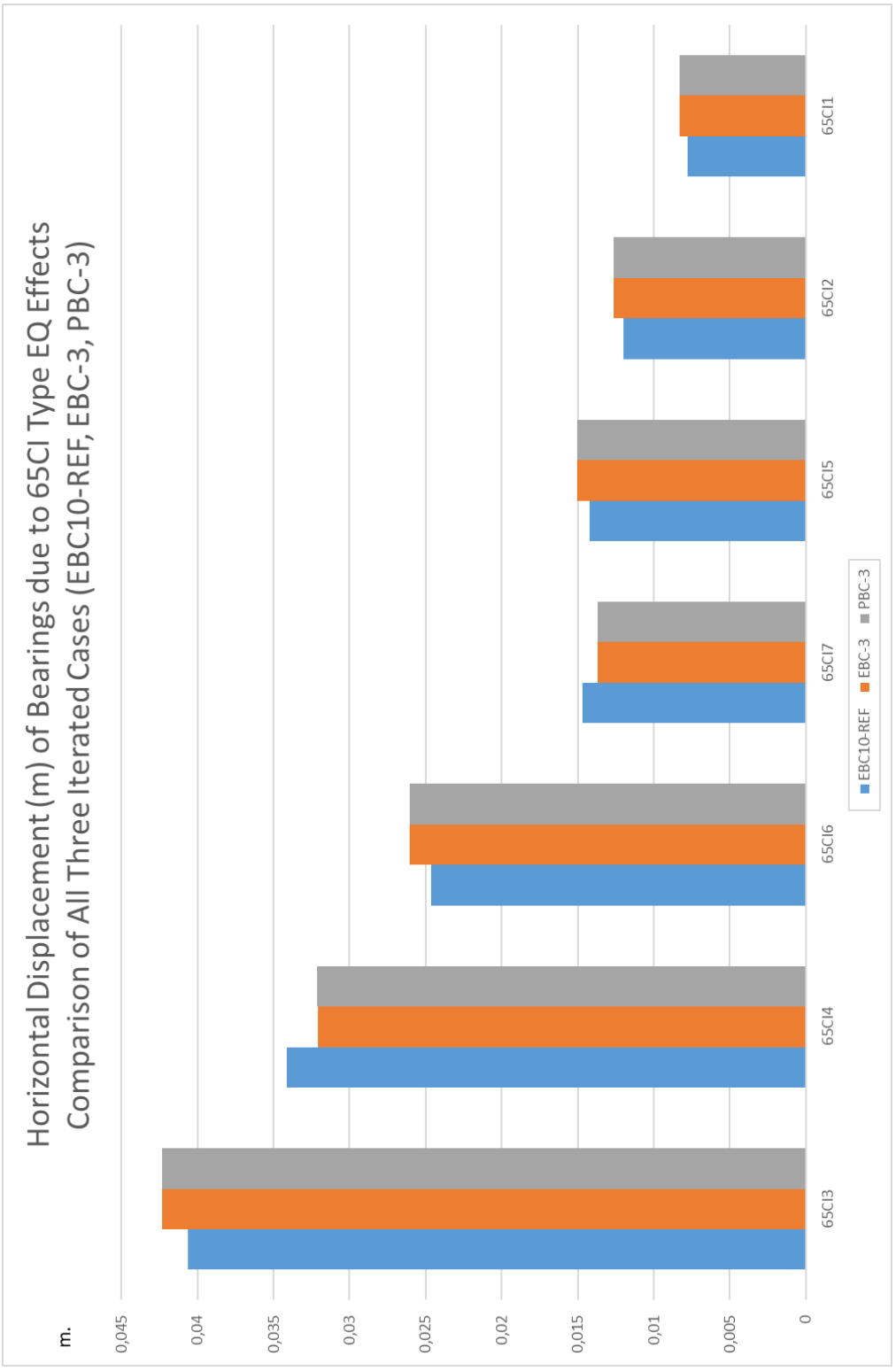

Figure 5.24. Maximum Horizontal Displacement of Bearings due to 65CI Type EQ Effects - Comparison of All Three Iterated Cases (EBC10-REF, EBC-3, PBC-3)

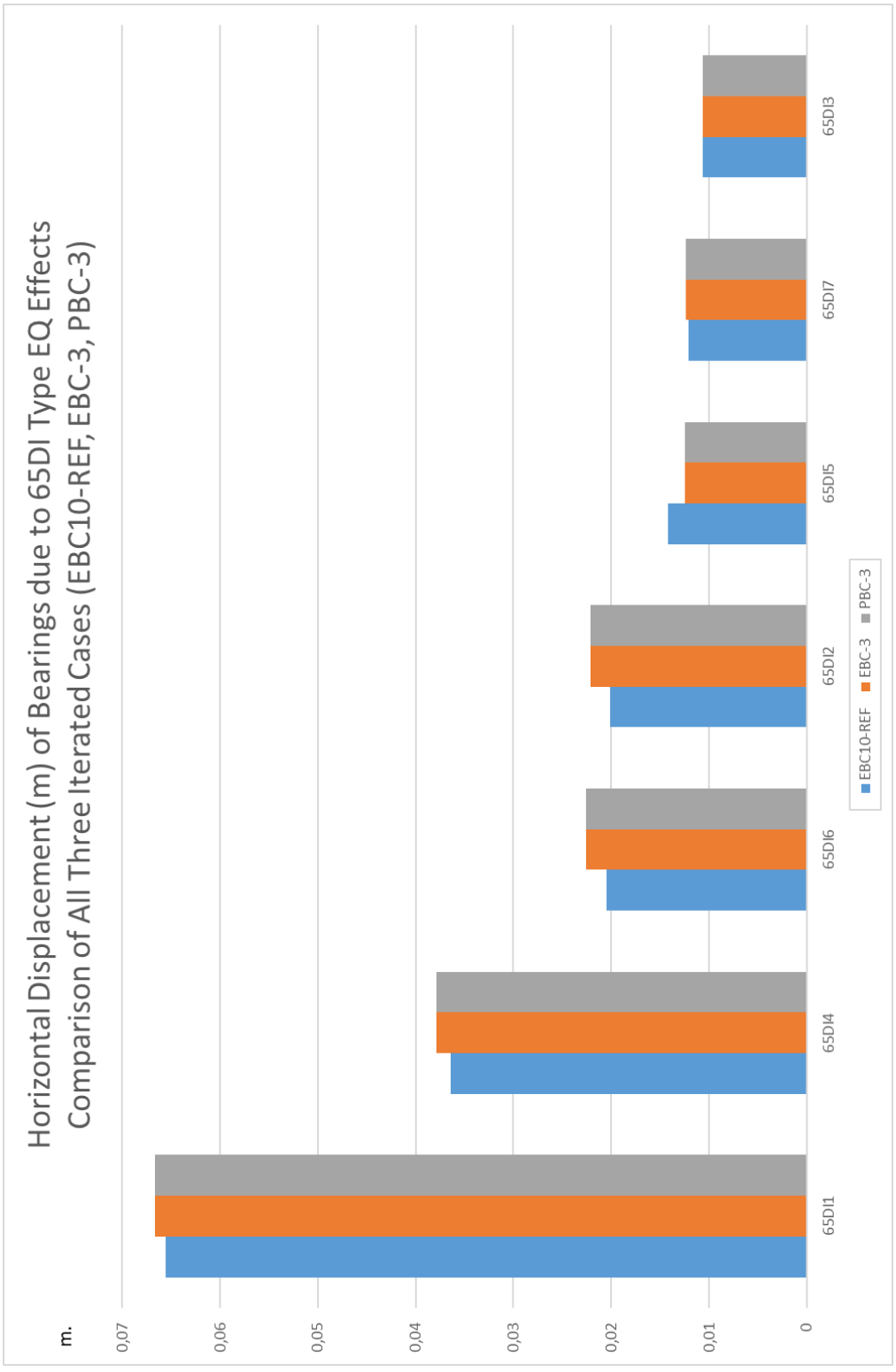

Figure 5.25. Maximum Horizontal Displacement of Bearings due to 65DI Type EQ Effects - Comparison of All Three Iterated Cases (EBC10-REF, EBC-3, PBC-3)

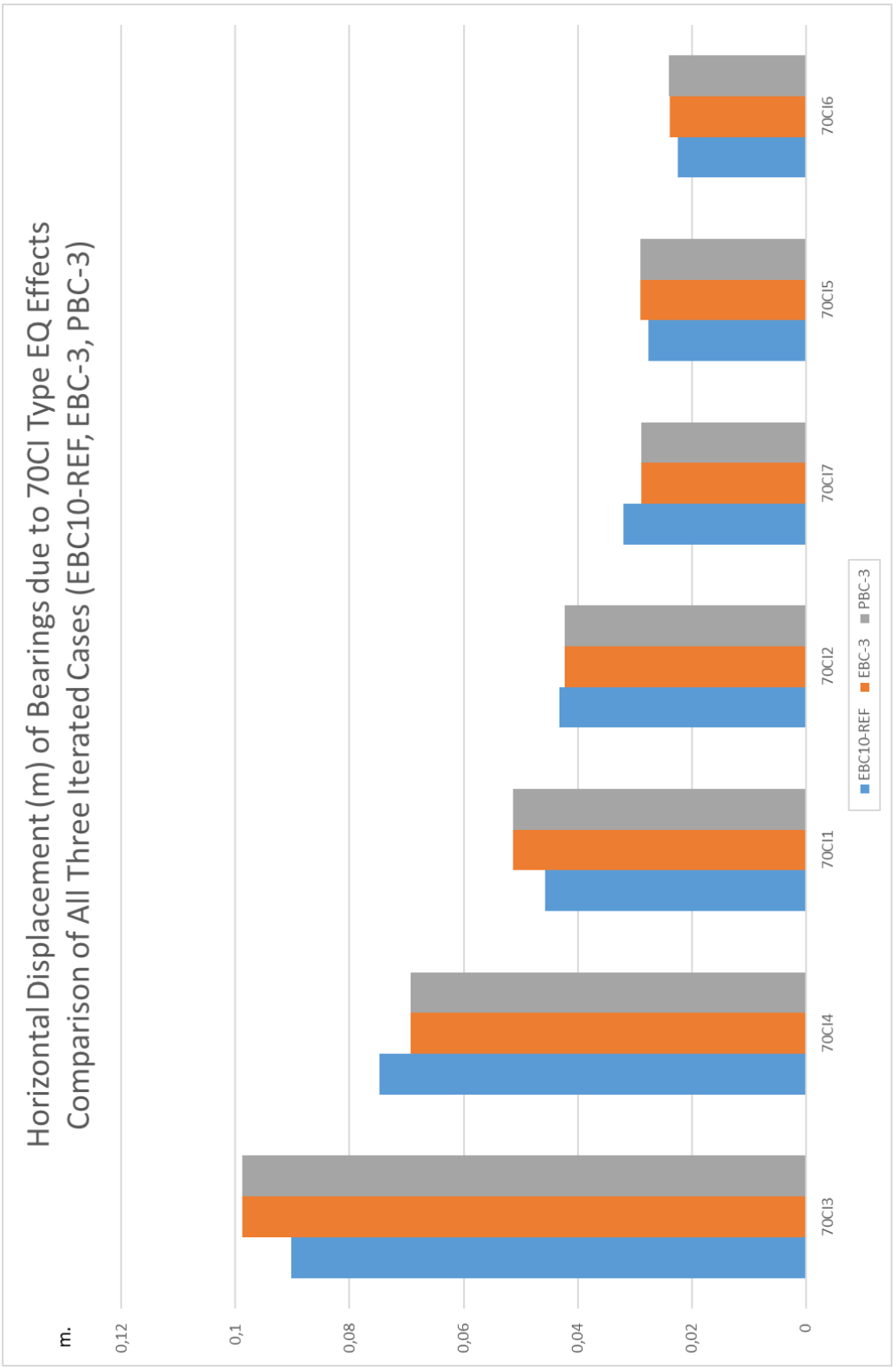

Figure 5.26. Maximum Horizontal Displacement of Bearings due to 70CI Type EQ Effects - Comparison of All Three Iterated Cases (EBC10-REF, EBC-3, PBC-3)

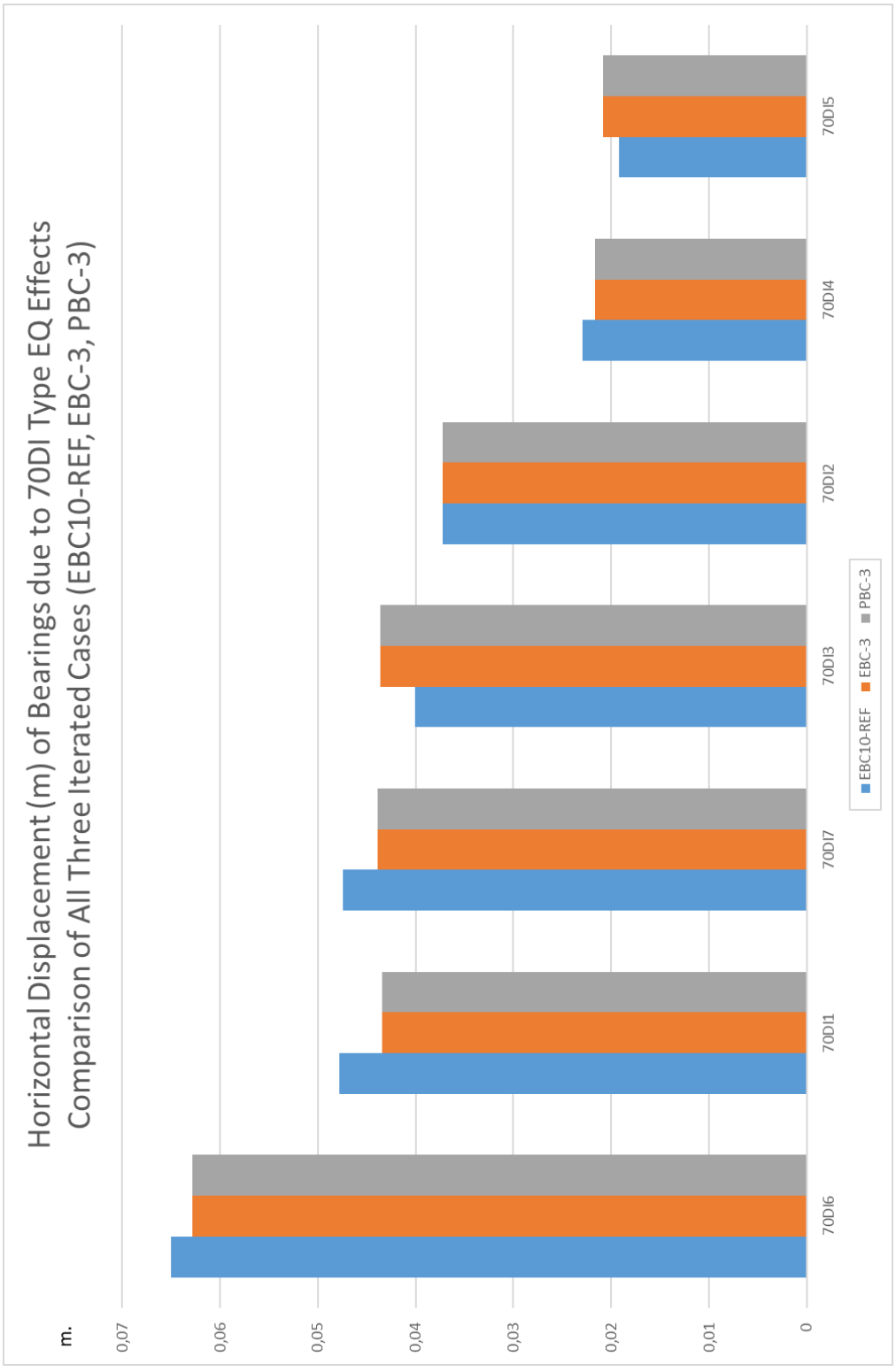

Figure 5.27. Maximum Horizontal Displacement of Bearings due to 70DI Type EQ Effects - Comparison of All Three Iterated Cases (EBC10-REF, EBC-3, PBC-3)

CHAPTER 6

CONCLUSION

6.1. Summary

The need for high-speed railway lines is increasing all over the world. Therefore, the need for design and construction of these lines is increasing. In order to integrate the technological advancements with the design stage and new construction materials more academic researches are being done today than in the past. Some of these academic researches are trying to understand the behavior of devices used against earthquake effects.

Logical inferences done from the results obtained from this study are valid only for the case of using the ground motions selected and used within this study. Even if it is stated so within the text of this study, results and inferences obtained from this study cannot be generalized without any further investigation.

In this study, bearings used in bridges over high-speed railway lines are compared regarding the effect of forty-two separate earthquake ground motions. Two hundred and ten ground motion records for forty-two separate earthquakes are used as the input for the analysis software.

In this study, a typical and symmetrical high-speed railway bridge is taken into consideration. Elastomeric and pot bearings have been investigated. They are used as bearing devices. Two different soil class and three different earthquake magnitude ranges were specified to filter the ground motion data gathered from the PEER database. Three different analysis cases were investigated by changing the number and type of bearings. Case 1 named “Reference Analysis Case (EBC10-REF)”, has ten elastomeric bearings under each row at one-end. Case 2 named “Elastomeric Bearing Case (EBC-3)” has three elastomeric bearings and case 3, named “Pot Bearing Case

(PBC-3)", has 3 pot bearings under each row at one-end. Each analysis case has two steps for analysis; "Initial" and "Iterated". In the initial case, the gap between girders allows movement and in the "Iterated" case, spring-stiffness coefficients of bearings were increased to simulate the gap closing to ten centimeters. 84 analyses were made for each model of analysis case, and totally 252 analyses were conducted for this study. After doing those analyses, 1.512 sets of results were collected, examined and compared throughout this study.

For structural analysis, version v14.2.2 of Sap2000 software has been used. Linear direct integration time history analysis was used. The results of the analyses are given in sections 4 and 5.

6.2. Conclusions

In the known literature, comparison of the response of bridges with elastomeric bearing and pot bearing has not been studied in detail. The aim of this study is to provide o comparison between the earthquake responses of the elastomeric and pot bearings used in bridges over high-speed railways.

This study reveals that the effects of earthquakes cannot be directly predicted via examining the magnitude, soil class, and bearing types solely. Comparison graphs, provided in section 5, show some earthquakes having less magnitude than another earthquake can have more effect on the bridge. In the same manner among earthquakes having the nearly same magnitude, the one in soil class ZC was affected more than from the one in soil class ZD. When just the soil class types are considered, this situation may be regarded as an unusual situation.

Ground motion data are usually recorded during an earthquake at a station. Ground motion data may include some soil amplification occurred during that earthquake. If the soil amplification occurred, the ground motion data of earthquakes, which has the same magnitudes, can generate different ground motion accelerations. (Tezcan et al.,

2002) studied the soil amplification of Avcılar district, which is located in İstanbul, during the earthquake that occurred on 17 August 1999 in Golcuk, Kocaeli. In the article of the study mentioned in the previous sentence, it is stated that soil amplification can trigger higher effects on the region that is affected by an earthquake.

In the same manner, seismic amplification can also be an answer to the unusual situation stated above. If seismic amplification occurs, the effect of an earthquake on a structure will be higher than the effect on any other structure. The study, (Ateş, 2017) is an example of the seismic amplification that occurs during an earthquake due to the matching of the dominant periods of structures and the period of the earthquake.

Moreover, the situation, pointed above, would not be an unusual situation when response spectra of ground motion records are examined. Response spectra show that each earthquake has unique characteristics including various ground motion acceleration values for various periods. The similarity of the descending order of the earthquakes between Figure 4.76 and Figures from 4.18 to 4.24 shows the parallelism of the results and response spectra of ground motion data. In the same manner, Figure 4.77 and Figures from 4.41 to 4.46 has a similar order of earthquakes and results. Besides, Figure 4.78 and Figures from 4.62 to 4.67 support the same similarity. For example, for the specific case in Figure 5.16 in this study, 60DI6 generates the highest horizontal relative deformations on bearings. Congruently, according to the Response Spectrum Graphs, 60DI6 is the earthquake generating the highest ground motion acceleration regarding the period of the bridge used in this study. This subject is proved during (Akray & Caner, 2019) which is an ongoing Master's Degree Thesis study which is being conducted by Ayhan Akray as the student, Prof. Dr. Alp Caner as the advisor and the Prof. Dr. Ayşen Dener Akkaya as the Co-Advisor.

By examining the results obtained throughout this study, it is understood that; elastomeric bearings and pot bearings typically do not change the earthquake response of the bridge except in some cases. When Figures 5.1, 5.2, 5.3., 5.4, 5.5 and 5.6 are analyzed, it is observed that the results of some cases obtained in the initial pot bearing

analysis case (PBC-3 – Initial) are relatively much higher than the results obtained for the same cases in the other two initial analysis cases (EBC10-REF and EBC-3). This situation has been observed within the results of approximately 15 earthquake ground motion effects. When the horizontal displacements are not limited, the maximum and average displacements in the pot bearing case are higher than the other cases, as provided in the Table 4.2. After iterating the spring-stiffness coefficients of bearings for limiting the displacements to 10 centimeters, the behavior of three analysis cases gets similar to each other. When the analysis cases are compared to each other by taking the Table 4.3 into account, it is observed that the relative horizontal deformations, standard deviations and the coefficient of variations of data groups of results show a parallel trend.

Both types of bearings shall be used in high-speed railway bridges, however, pot bearing selection may yield higher substructural forces in some cases when compared to the elastomeric bearings used cases. Besides, economical aspects, durability, and material properties are some other deterministic concerns for bearing selection for a bridge over high-speed railways.

When earthquake ground motions are taken into consideration, the response spectrum of the ground motion records is an efficient parameter in addition to the magnitude and soil class, which are important parameters for earthquake-related studies.

6.3. Suggestions for Future Studies

This study may be a footstep for many other pieces of research and studies including but of course not limited to the list stated below:

- This study can be repeated by increasing bearing types including spherical bearings.

- A comparison between the rail-structure interaction and earthquake effects can be handled by using the results of this study. By doing that, the question: “Shall we protect the rail or the infrastructure?” shall be answered.

- A prototype of the bridge can be formed and real experiments can be made on laboratory conditions.

REFERENCES

https://earthquake.usgs.gov/learn/topics/keeping_track.php

AASHTO LRFD Bridge Design Specifications, U.S. Customary and SI Units, Fourth Edition, 2007.

Adagunodo, T. A., & Sunmonu, L. A. (2015). Earthquake : A terrifying of all natural phenomena, (January 2015), 4–11.

Lee, J., & Green, R. A. (2008). An Empirical Earthquake Arias Intensity Relationship For The An Empirical Earthquake Arias Intensity Relationship, (March).

Marioni, A. (2006). Bearing systems for high speed railway bridges, (September), 17–21.

Yu, Z., Li, H., Wei, B., Jiang, L., & Mao, J. (2018). Numerical analysis on longitudinal seismic responses of high-speed railway bridges isolated by friction pendulum bearings. Journal of Vibroengineering, 20(4), 1748–1760. https://doi.org/10.21595/jve.2017.18557

Tang, H., Wang, H., Zhou, B., & Chen, L. (2011). Study on seismic isolation of high-speed railway bridge fabricated lead rubber bearings. Applied Mechanics and

Materials, 80–81, 409–413. https://doi.org/10.4028/www.scientific.net/AMM.80-81.409

Zou, S., Wenliuhan, H., & Zhou, F. (2019). Shaking table test of a high-speed railway bridge with a new isolation system. Engineering Structures, 196(June), 109315. https://doi.org/10.1016/j.engstruct.2019.109315

Ülker-kaustell, M. (2017). Dynamic behaviour of pot bearings A preliminary study, (December).

Ancheta, T. D., Bozorgnia, Y., Chiou, B. S.-J., Stewart, J. P., Boore, D. M., Graves, R. W., … Atkinson, G. M. (2012). PEER NGA-West2 Database : A Database of Ground Motions Recorded in Shallow Crustal Earthquakes in Active Tectonic. 15th World Conference on Earthquake Engineering, 6.

Seismosignal 2016, Earthquake Software for Signal Processing of Strong-Motion data Help System, Seismosoft Earthquake Engineering Software Solutions. https://seismosoft.com/wp-content/uploads/prods/lib/SeismoSignal.chm

AASHTO Standard Specifications for Highway Bridges, Seventeenth Edition, 2002

https://www.bridgebearing.org/bridgebearing/pot-bearing.html

Sap2000 (v14.2.2). Integrated Software for Structural Analysis & Design, Knowledge Base, Computers and Structures Inc. California, USA. https://wiki.csiamerica.com/display/SAP2000/Home

Tezcan, S. S., Kaya, E., Engin Bal, I., & Özdemir, Z. (2002). Seismic amplification at Avcilar, Istanbul. Engineering Structures, 24(5), 661–667. https://doi.org/10.1016/S0141-0296(02)00002-0

Ateş A., Evaluation Of Seismic Amplification On Earthquake Damages Of Reinforced Concrete Structures Due To 12 November Duzce Earthquake 1999 In Duzce, Turkey, [in:] Journal of Current Construction Issues. Civil Engineering Present Problems, Innovative Solutions - Optimization in Business and Engineering, ed. Jarosław Górecki, BGJ Consulting, 2017.

Akray, A. Caner, A. (2019). Evaluation of Intensity Measures for Ground Motion Selection to be Used in the Analysis of Highway Flyover Bridge (Unpublished Master's Thesis). Middle East Technical University, Ankara, Turkey.

APPENDICES

A. APPENDIX A - Acceleration, Velocity and Displacement Graphs

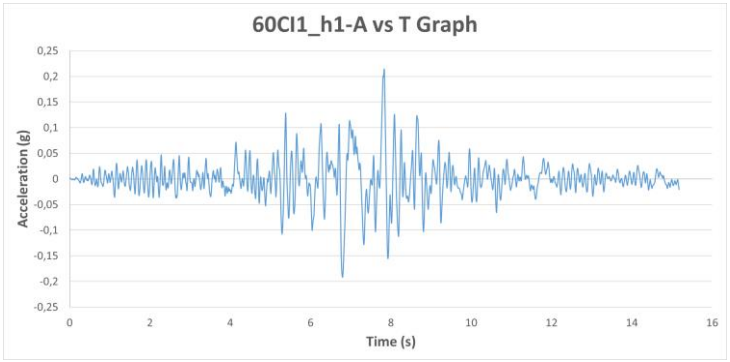

Figure A.1. Acceleration vs Time Graph of Ground Motion named 60CI1_h1

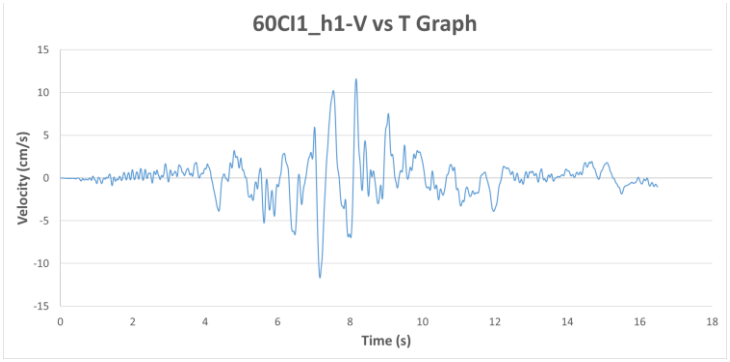

Figure A.2. Velocity vs Time Graph of Ground Motion named 60CI1_h1

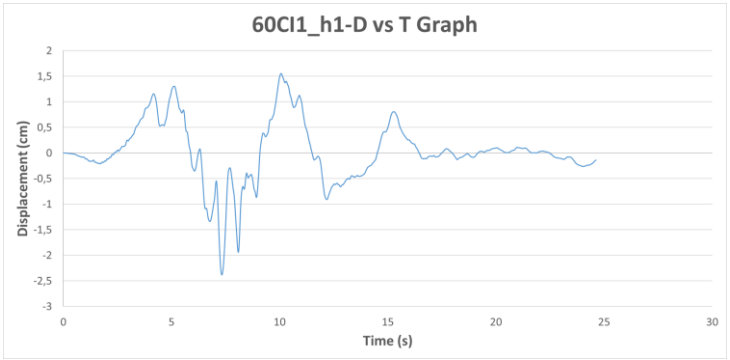

Figure A.3. Displacement vs Time Graph of Ground Motion named 60CI1_h1

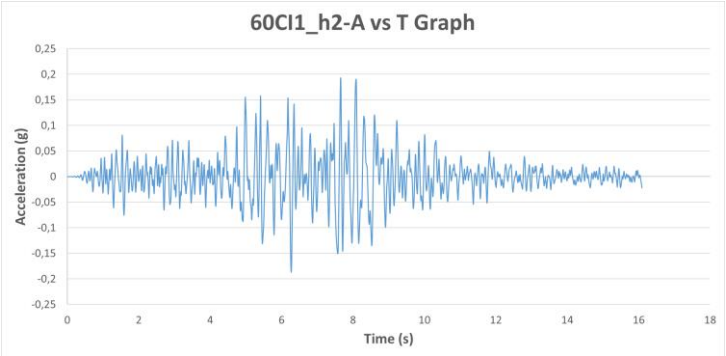

Figure A.4. Acceleration vs Time Graph of Ground Motion named 60CI1_h2

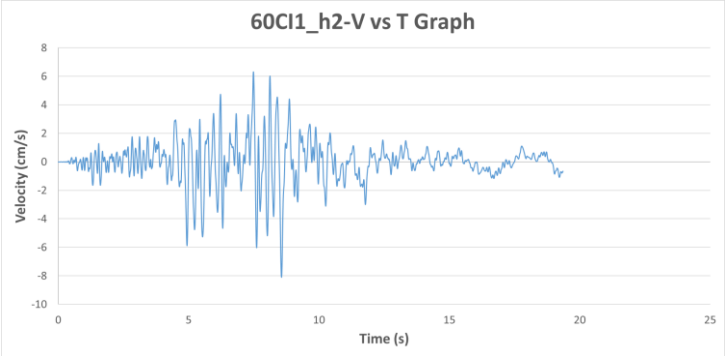

Figure A.5. Velocity vs Time Graph of Ground Motion named 60CI1_h2

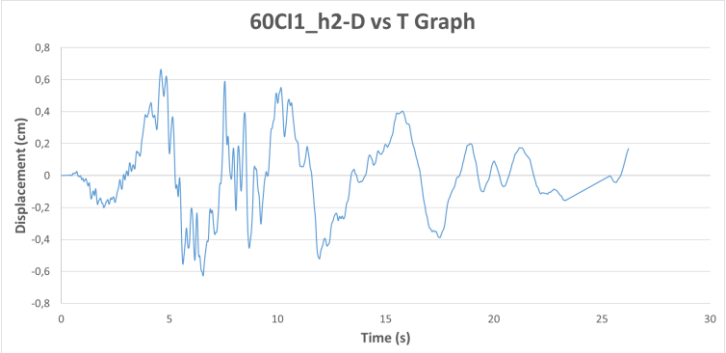

Figure A.6. Displacement vs Time Graph of Ground Motion named 60CI1_h2

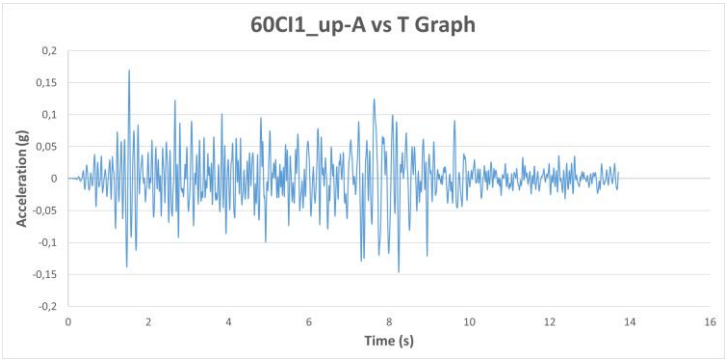

Figure A.7. Acceleration vs Time Graph of Ground Motion named 60CI1_up

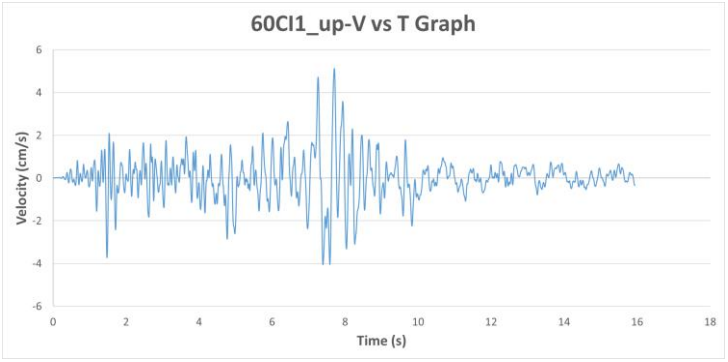

Figure A.8. Velocity vs Time Graph of Ground Motion named 60CI1_up

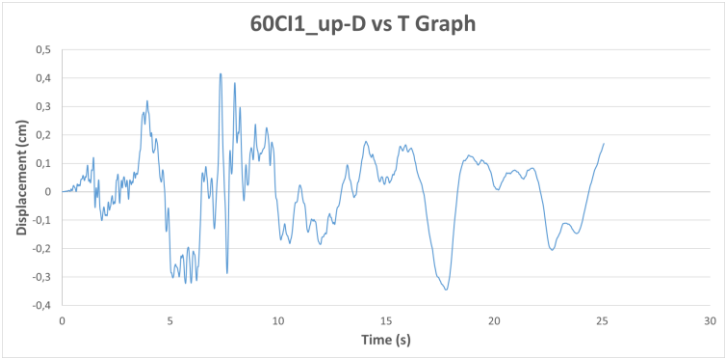

Figure A.9. Displacement vs Time Graph of Ground Motion named 60CI1_up

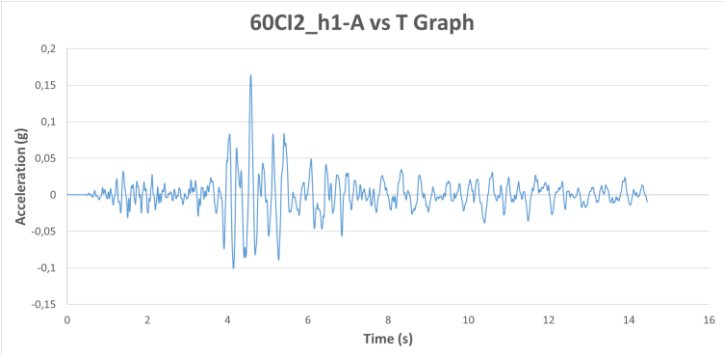

Figure A.10. Acceleration vs Time Graph of Ground Motion named 60CI2_h1

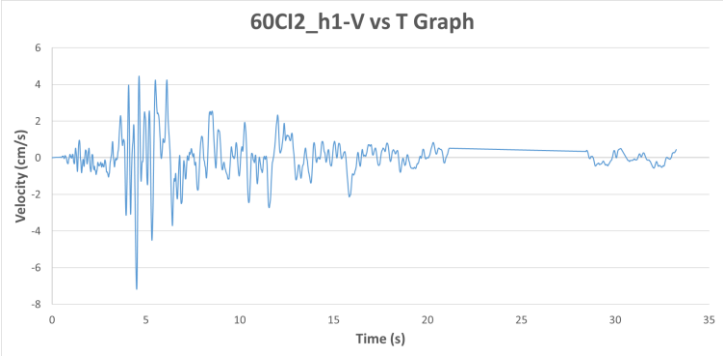

Figure A.11. Velocity vs Time Graph of Ground Motion named 60CI2_h1

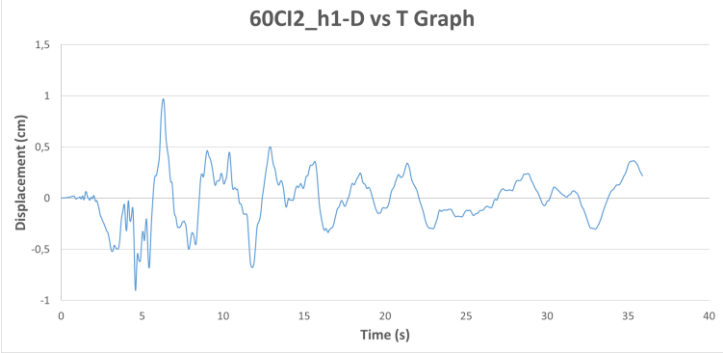

Figure A.12. Displacement vs Time Graph of Ground Motion named 60CI2_h1

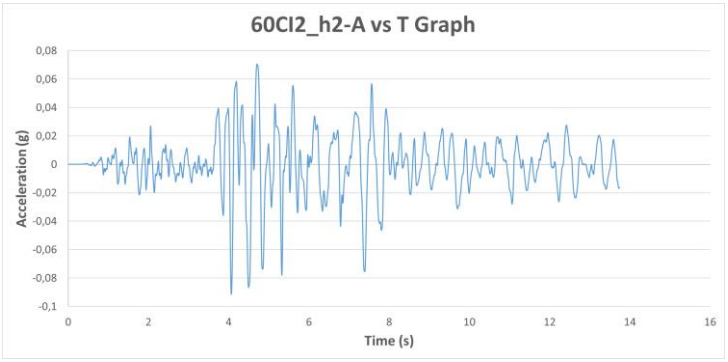

Figure A.13. Acceleration vs Time Graph of Ground Motion named 60CI2_h2

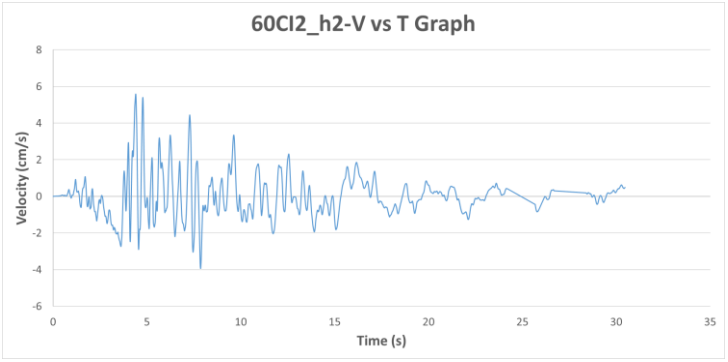

Figure A.14. Velocity vs Time Graph of Ground Motion named 60CI2_h2

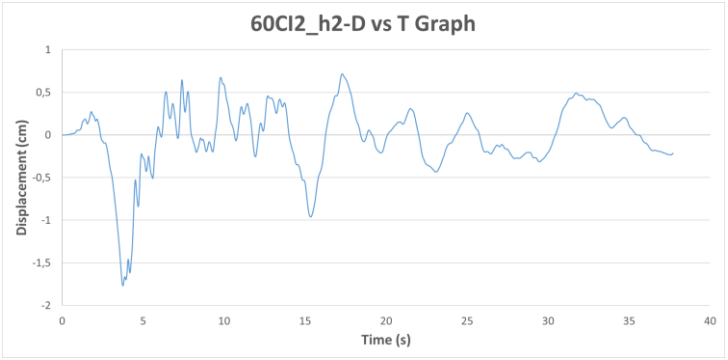

Figure A.15. Displacement vs Time Graph of Ground Motion named 60CI2_h2

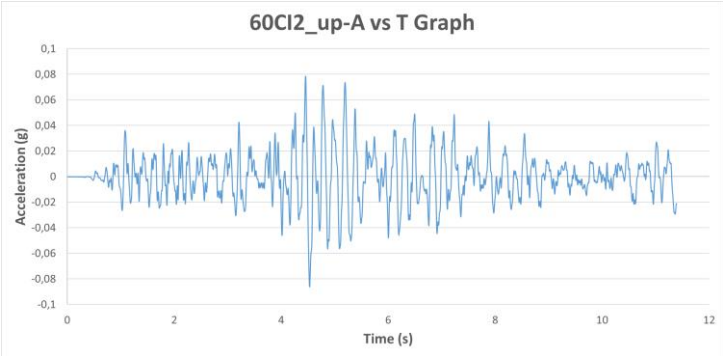

Figure A.16. Acceleration vs Time Graph of Ground Motion named 60CI2_up

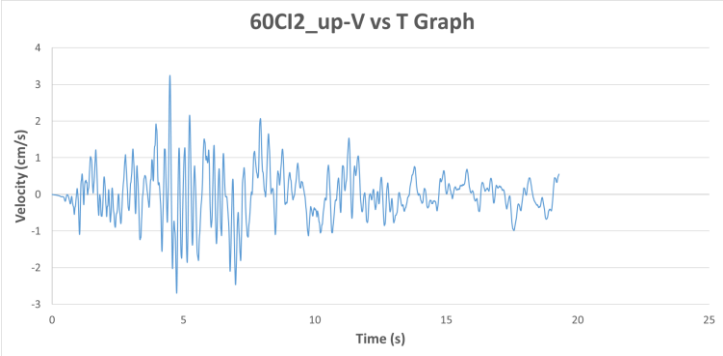

Figure A.17. Velocity vs Time Graph of Ground Motion named 60CI2_up

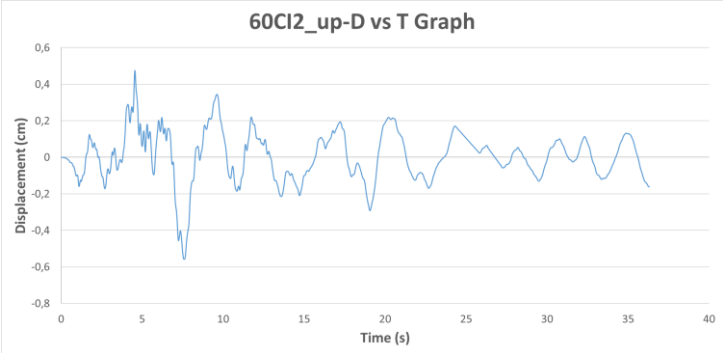

Figure A.18. Displacement vs Time Graph of Ground Motion named 60CI2_up

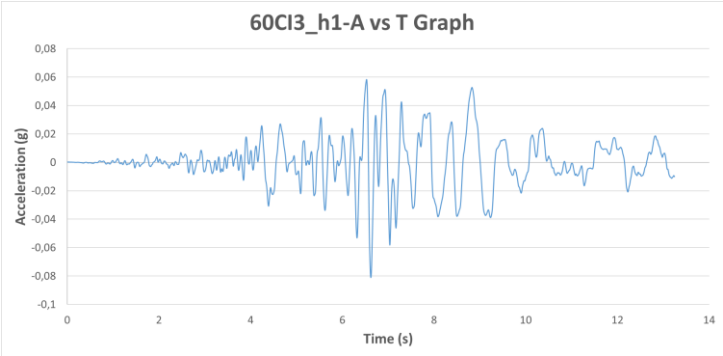

Figure A.19. Acceleration vs Time Graph of Ground Motion named 60CI3_h1

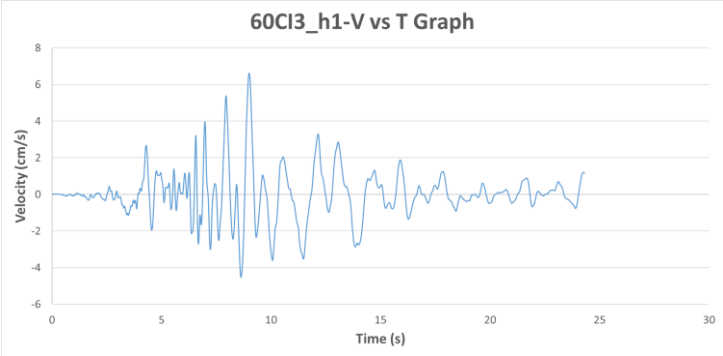

Figure A.20. Velocity vs Time Graph of Ground Motion named 60CI3_h1

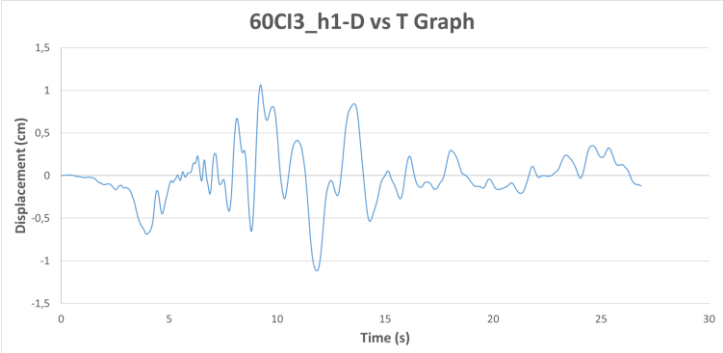

Figure A.21. Displacement vs Time Graph of Ground Motion named 60CI3_h1

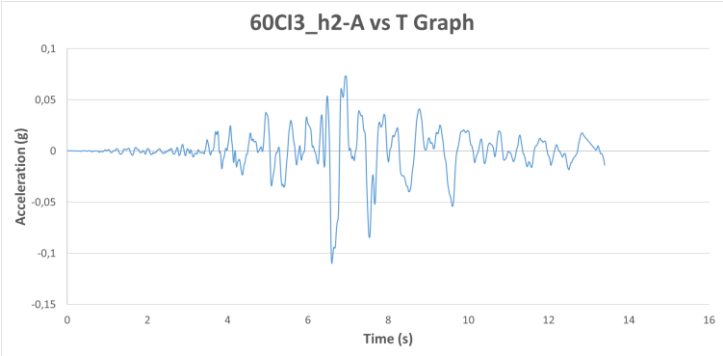

Figure A.22. Acceleration vs Time Graph of Ground Motion named 60CI3_h2

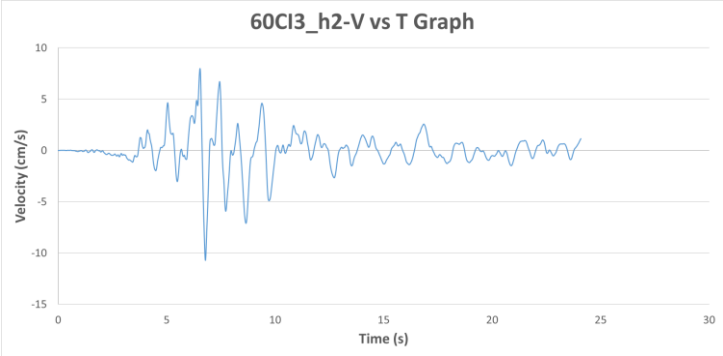

Figure A.23. Velocity vs Time Graph of Ground Motion named 60CI3_h2

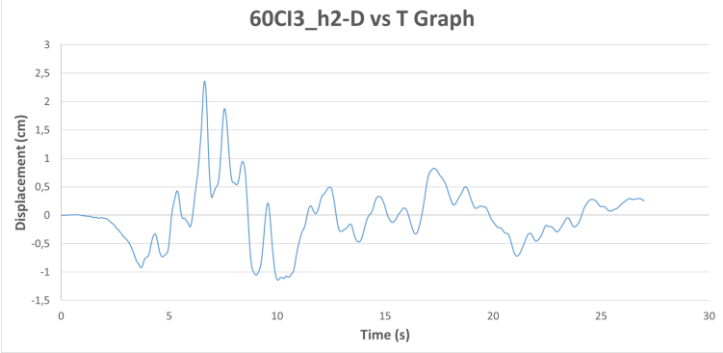

Figure A.24. Displacement vs Time Graph of Ground Motion named 60CI3_h2

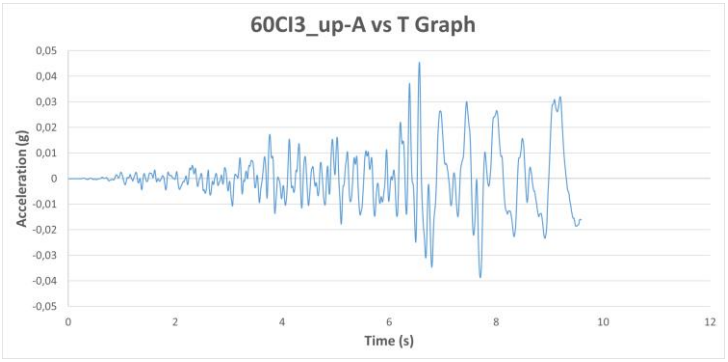

Figure A.25. Acceleration vs Time Graph of Ground Motion named 60CI3_up

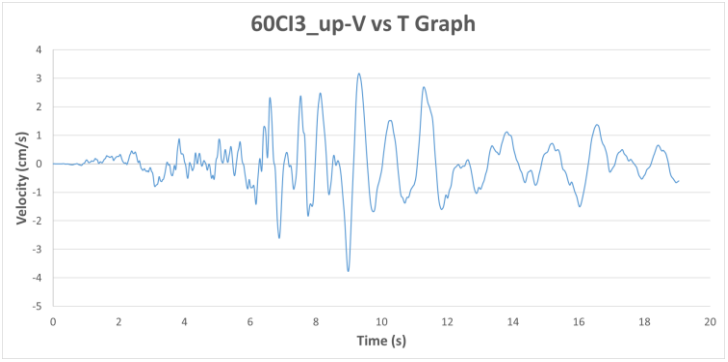

Figure A.26. Velocity vs Time Graph of Ground Motion named 60CI3_up

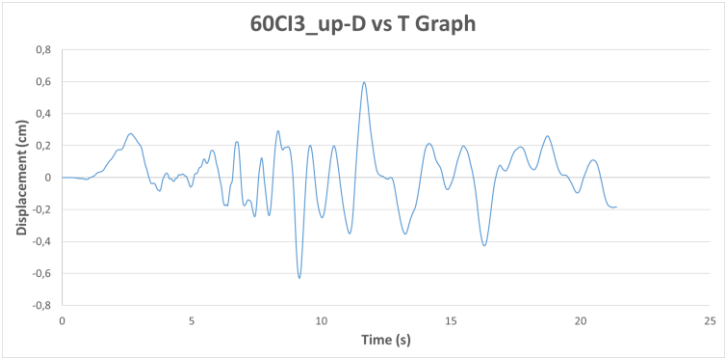

Figure A.27. Displacement vs Time Graph of Ground Motion named 60CI3_up

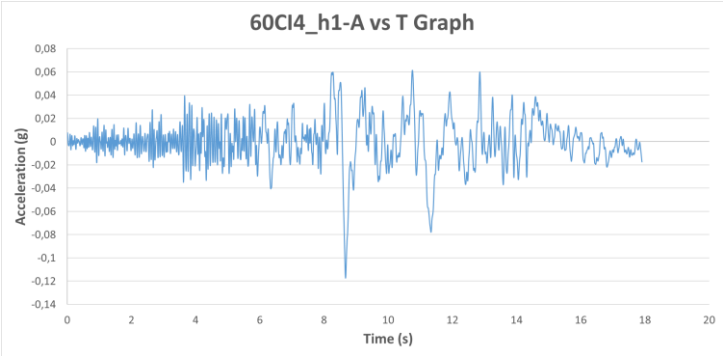

Figure A.28. Acceleration vs Time Graph of Ground Motion named 60CI4_h1

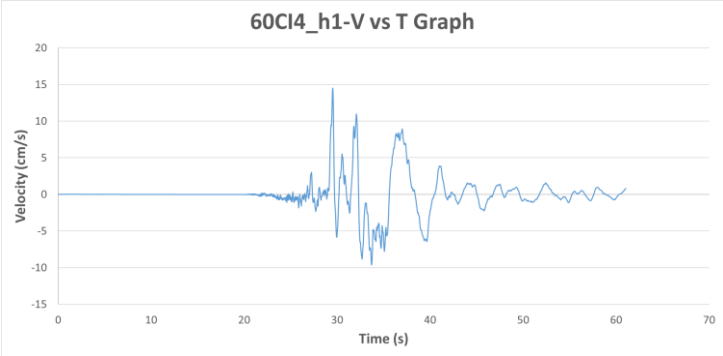

Figure A.29. Velocity vs Time Graph of Ground Motion named 60CI4_h1

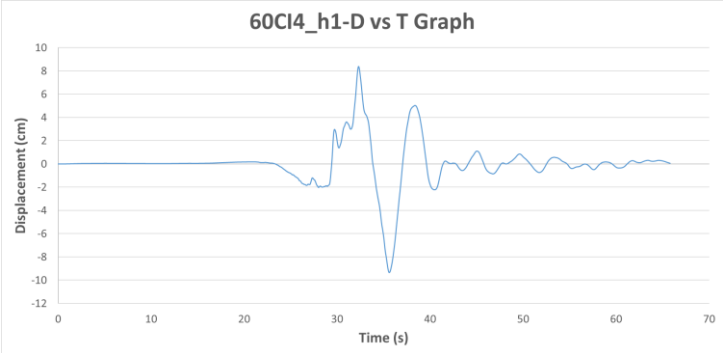

Figure A.30. Displacement vs Time Graph of Ground Motion named 60CI4_h1

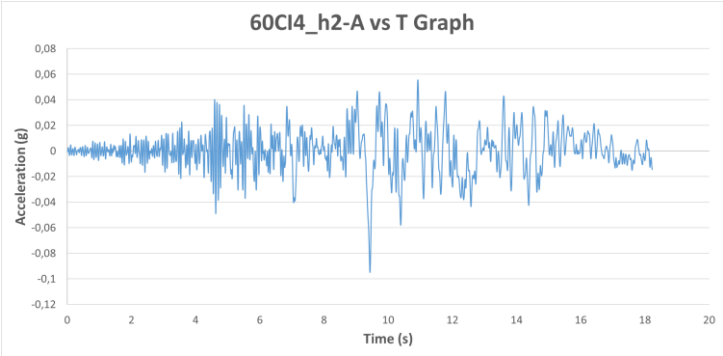

Figure A.31. Acceleration vs Time Graph of Ground Motion named 60CI4_h2

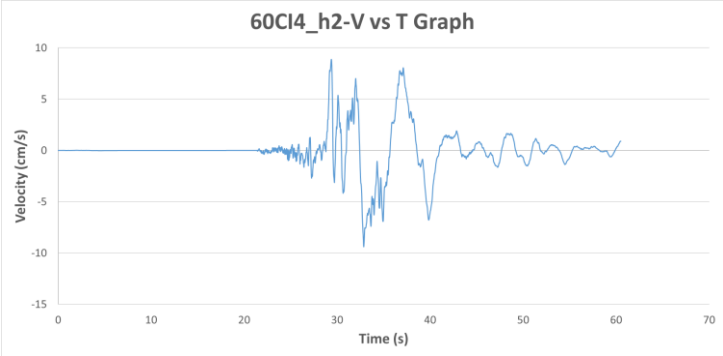

Figure A.32. Velocity vs Time Graph of Ground Motion named 60CI4_h2

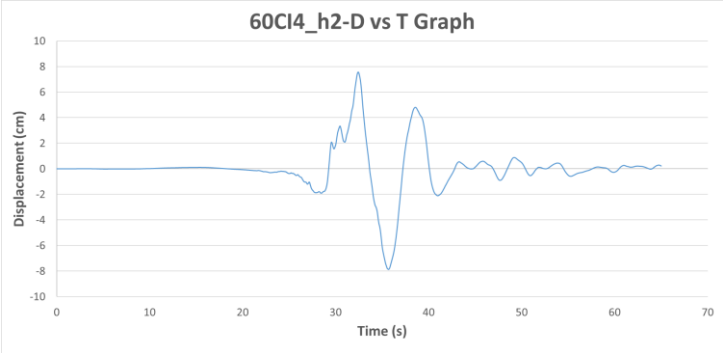

Figure A.33. Displacement vs Time Graph of Ground Motion named 60CI4_h2

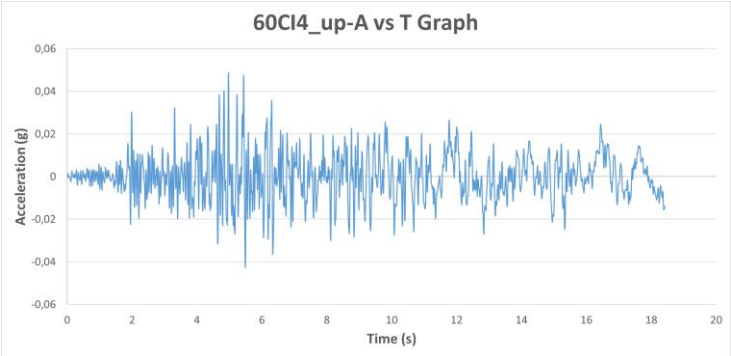

Figure A.34. Acceleration vs Time Graph of Ground Motion named 60CI4_up

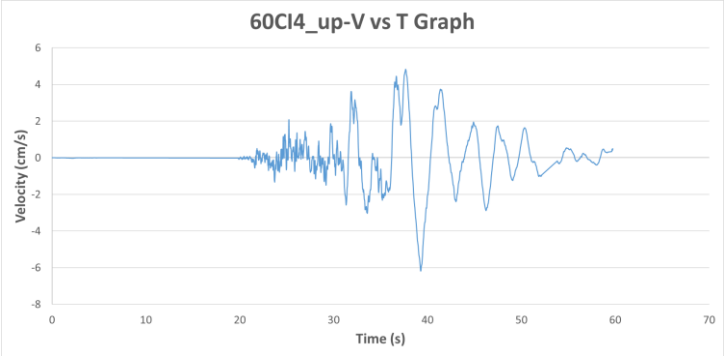

Figure A.35. Velocity vs Time Graph of Ground Motion named 60CI4_up

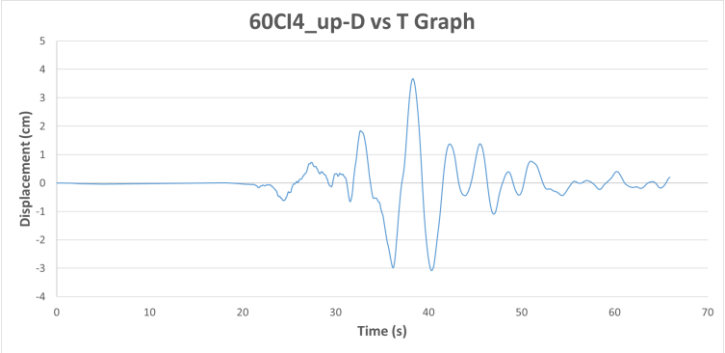

Figure A.36. Displacement vs Time Graph of Ground Motion named 60CI4_up

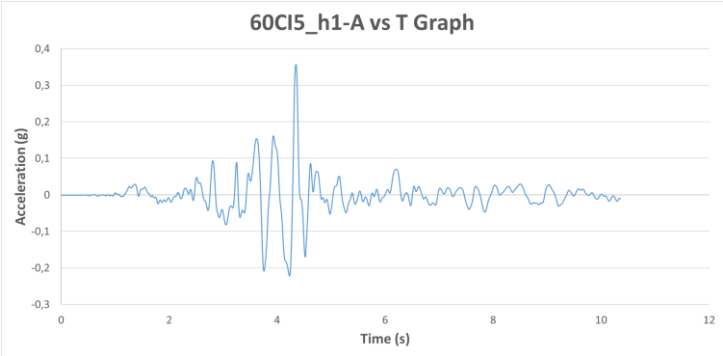

Figure A.37. Acceleration vs Time Graph of Ground Motion named 60CI5_h1

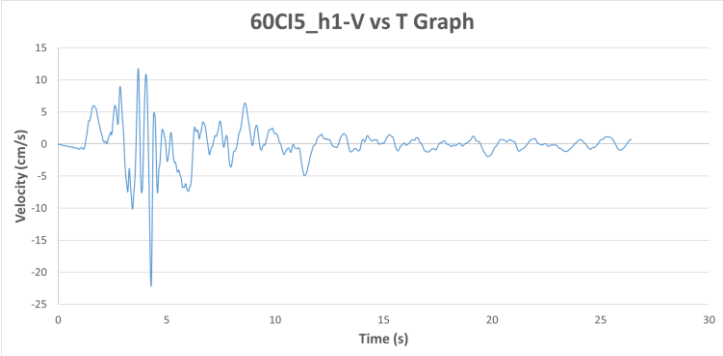

Figure A.38. Velocity vs Time Graph of Ground Motion named 60CI5_h1

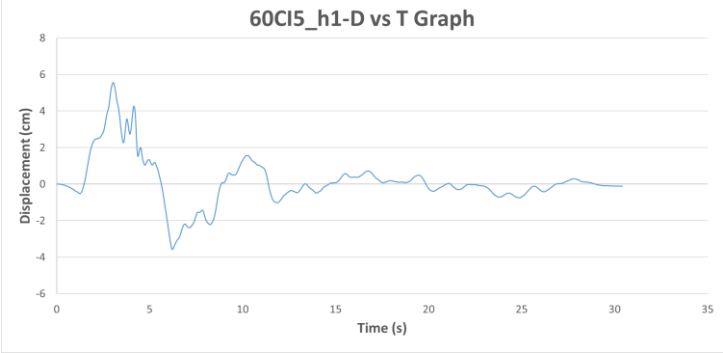

Figure A.39. Displacement vs Time Graph of Ground Motion named 60CI5_h1

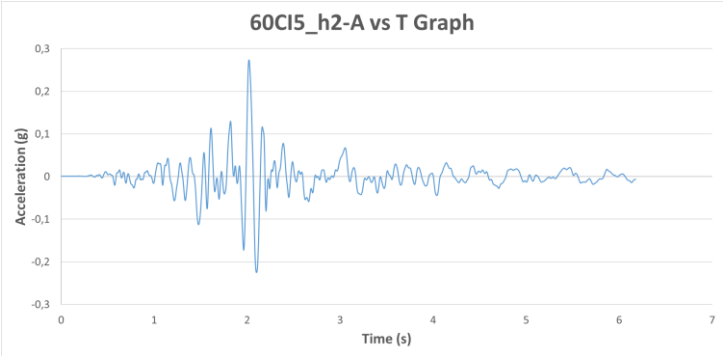

Figure A.40. Acceleration vs Time Graph of Ground Motion named 60CI5_h2

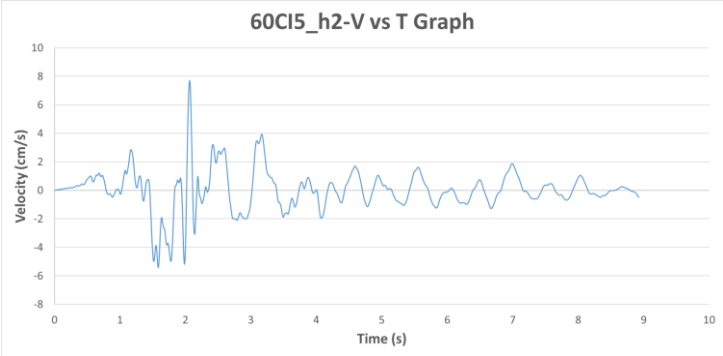

Figure A.41. Velocity vs Time Graph of Ground Motion named 60CI5_h2

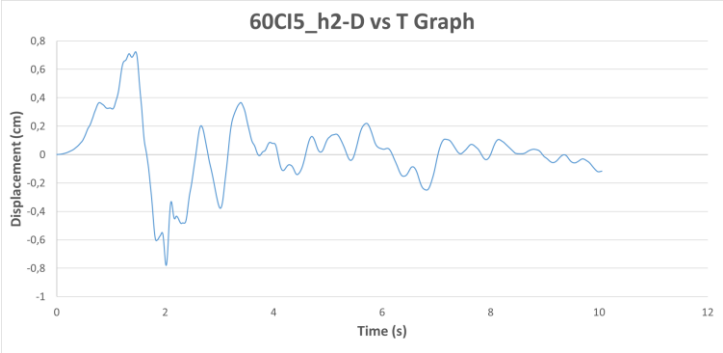

Figure A.42. Displacement vs Time Graph of Ground Motion named 60CI5_h2

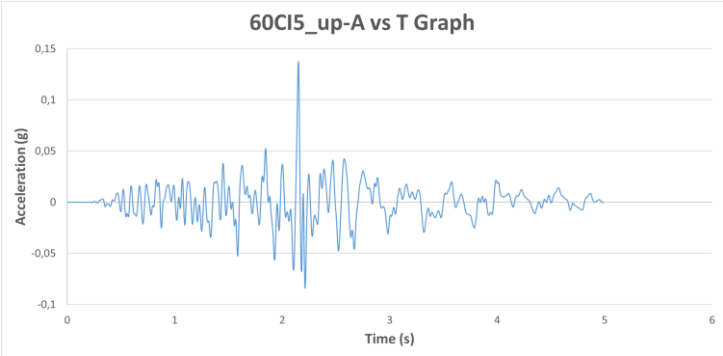

Figure A.43. Acceleration vs Time Graph of Ground Motion named 60CI5_up

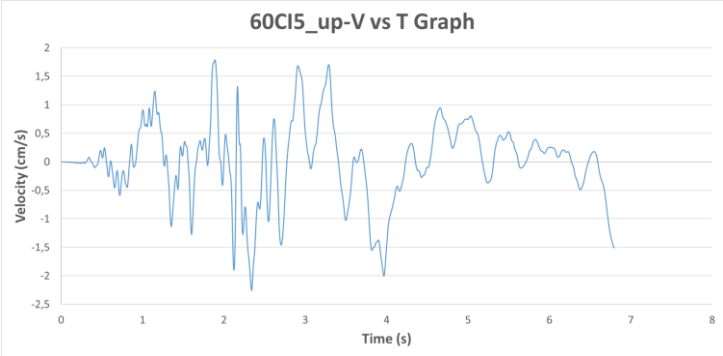

Figure A.44. Velocity vs Time Graph of Ground Motion named 60CI5_up

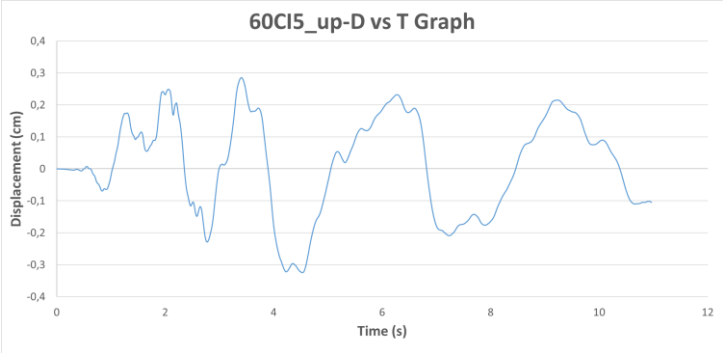

Figure A.45. Displacement vs Time Graph of Ground Motion named 60CI5_up

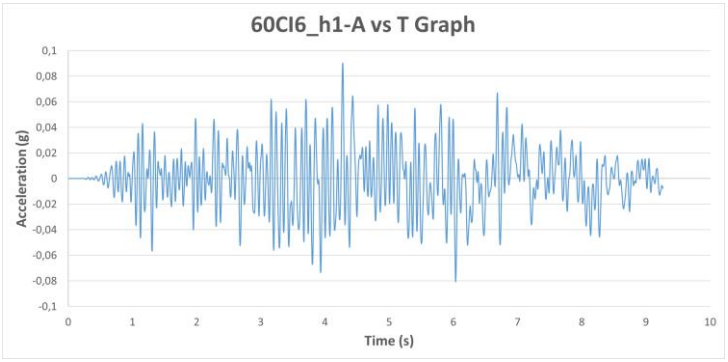

Figure A.46. Acceleration vs Time Graph of Ground Motion named 60CI6_h1

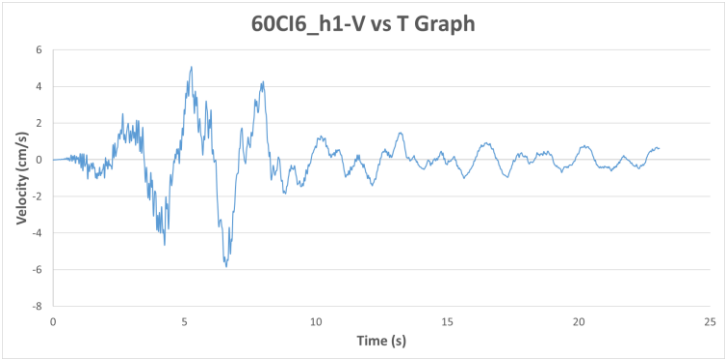

Figure A.47. Velocity vs Time Graph of Ground Motion named 60CI6_h1

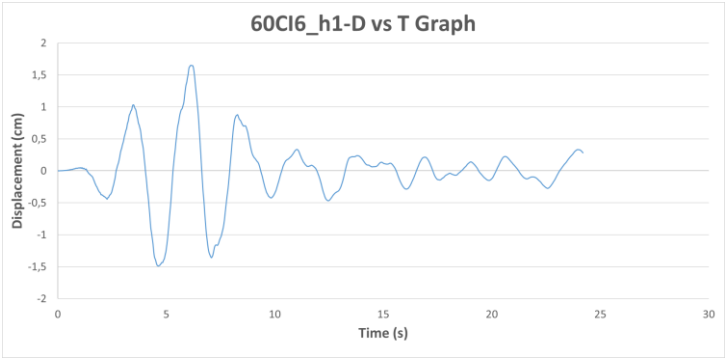

Figure A.48. Displacement vs Time Graph of Ground Motion named 60CI6_h1

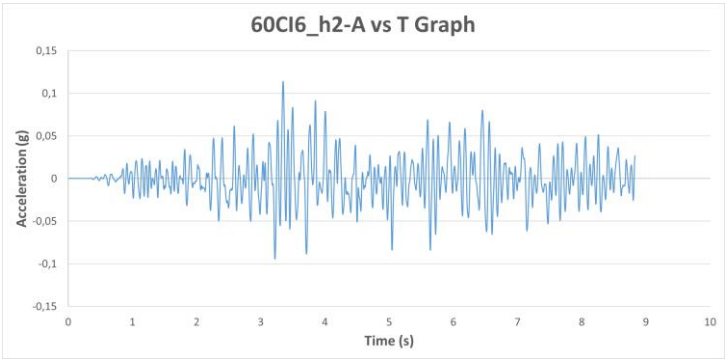

Figure A.49. Acceleration vs Time Graph of Ground Motion named 60CI6_h2

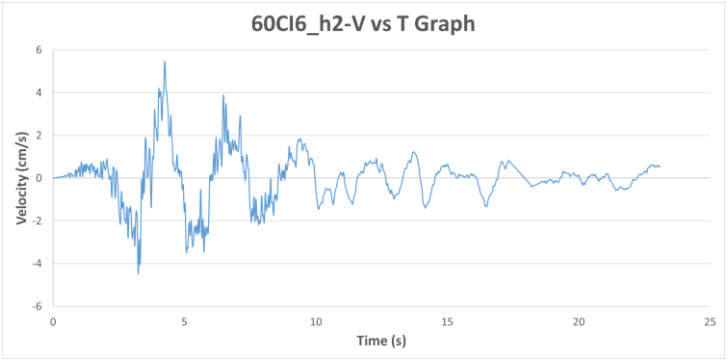

Figure A.50. Velocity vs Time Graph of Ground Motion named 60CI6_h2

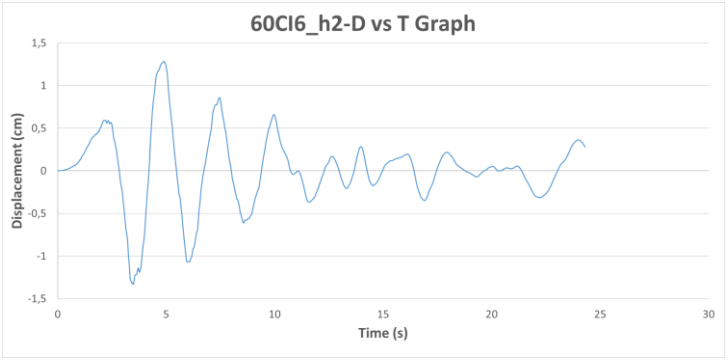

Figure A.51. Displacement vs Time Graph of Ground Motion named 60CI6_h2

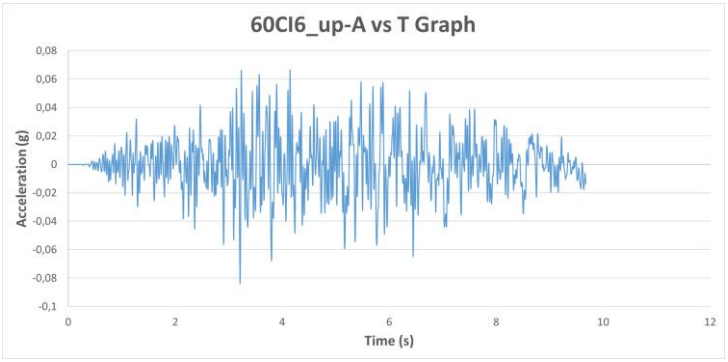

Figure A.52. Acceleration vs Time Graph of Ground Motion named 60CI6_up

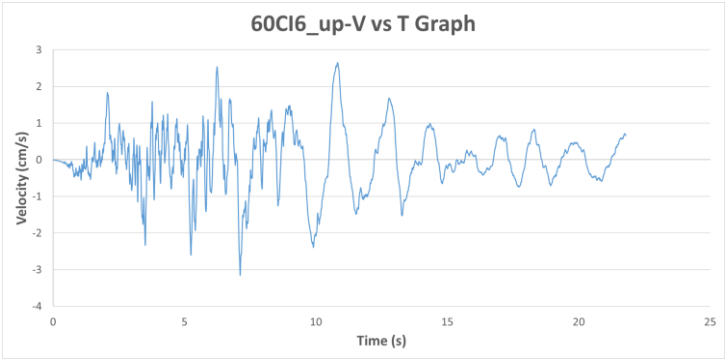

Figure A.53. Velocity vs Time Graph of Ground Motion named 60CI6_up

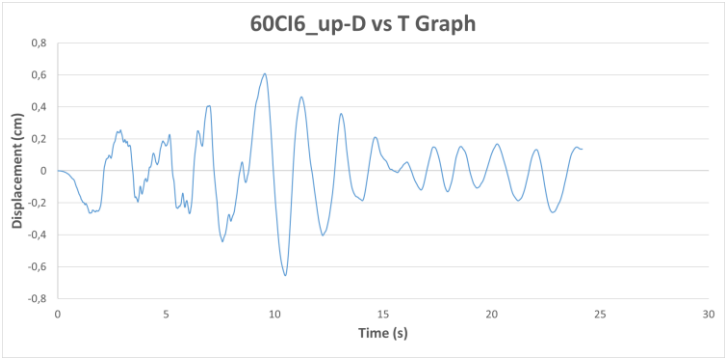

Figure A.54. Displacement vs Time Graph of Ground Motion named 60CI6_up

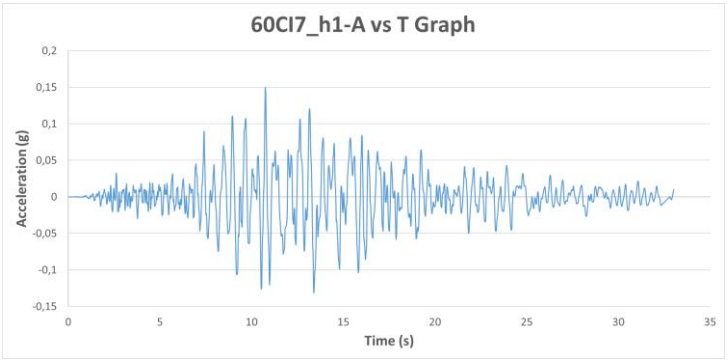

Figure A.55. Acceleration vs Time Graph of Ground Motion named 60CI7_h1

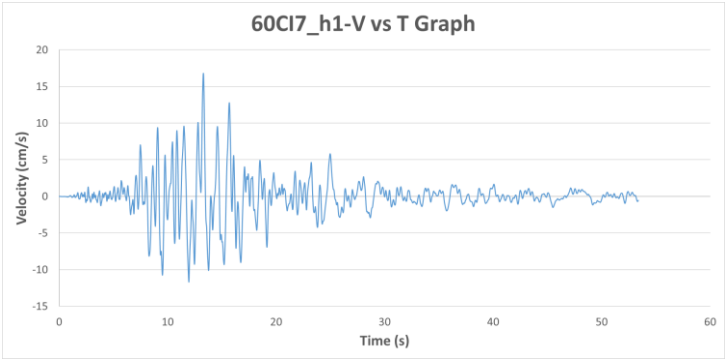

Figure A.56. Velocity vs Time Graph of Ground Motion named 60CI7_h1

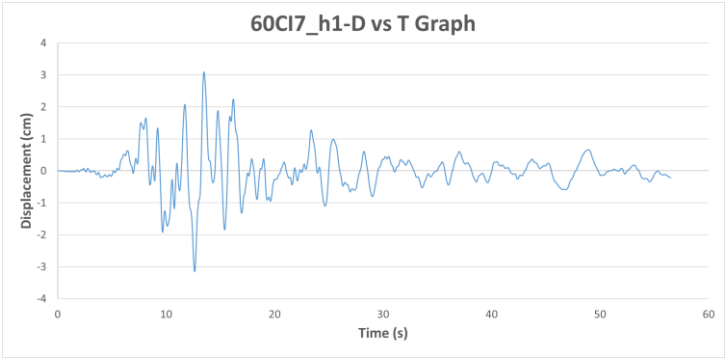

Figure A.57. Displacement vs Time Graph of Ground Motion named 60CI7_h1

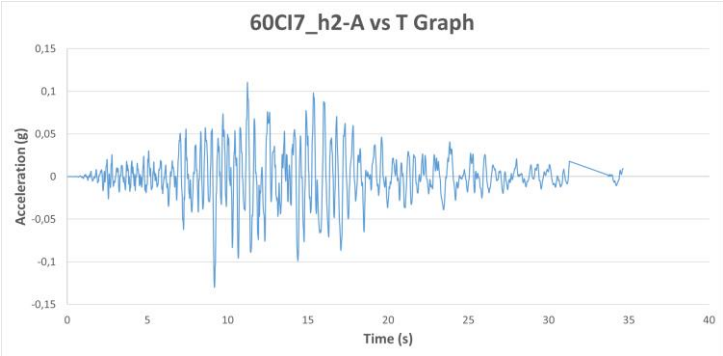

Figure A.58. Acceleration vs Time Graph of Ground Motion named 60CI7_h2

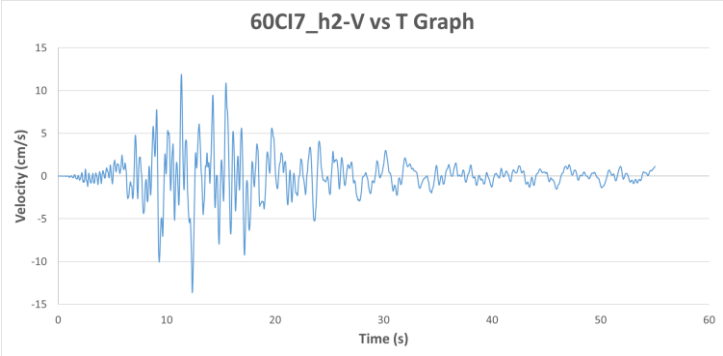

Figure A.59. Velocity vs Time Graph of Ground Motion named 60CI7_h2

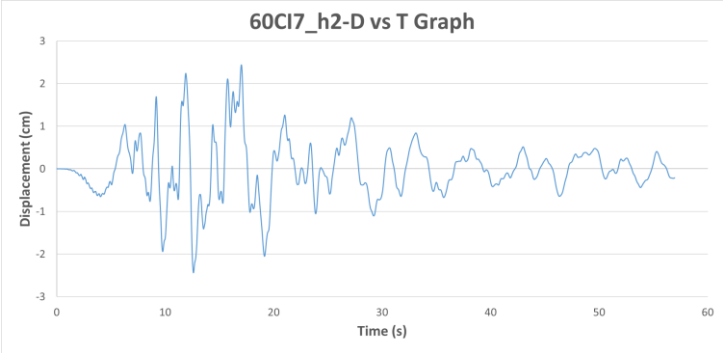

Figure A.60. Displacement vs Time Graph of Ground Motion named 60CI7_h2

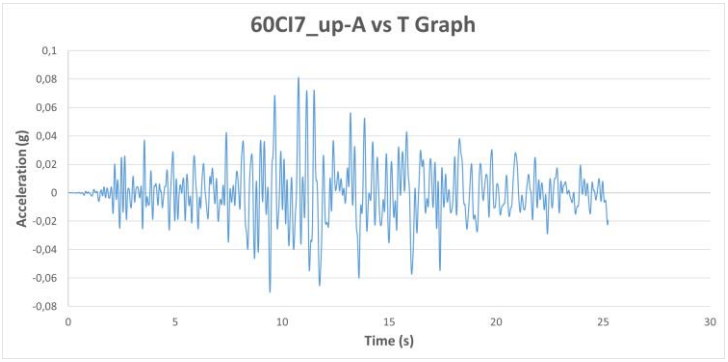

Figure A.61. Acceleration vs Time Graph of Ground Motion named 60CI7_up

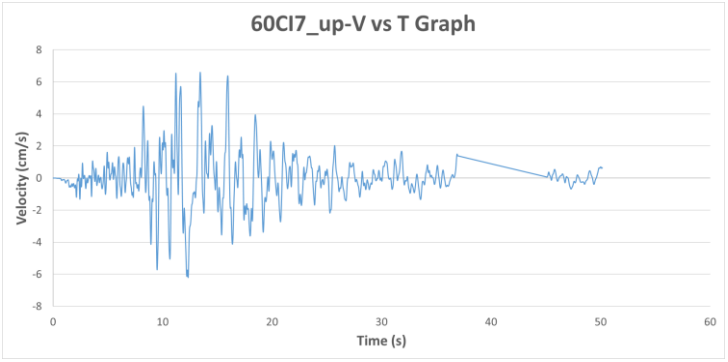

Figure A.62. Velocity vs Time Graph of Ground Motion named 60CI7_up

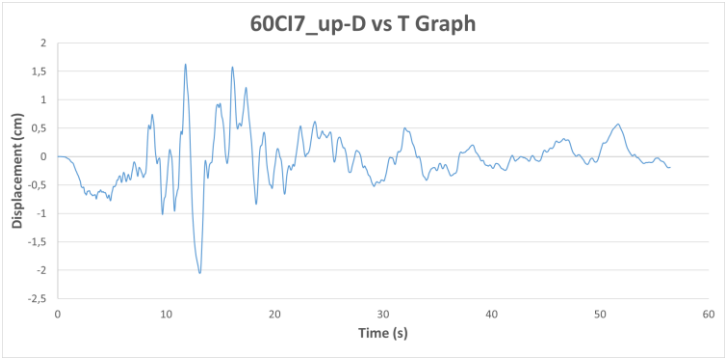

Figure A.63. Displacement vs Time Graph of Ground Motion named 60CI7_up

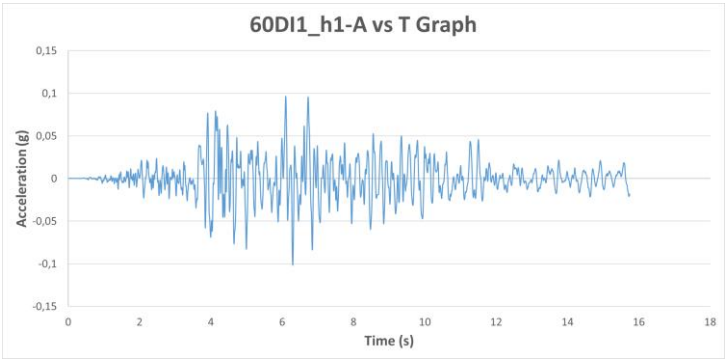

Figure A.64. Acceleration vs Time Graph of Ground Motion named 60DI1_h1

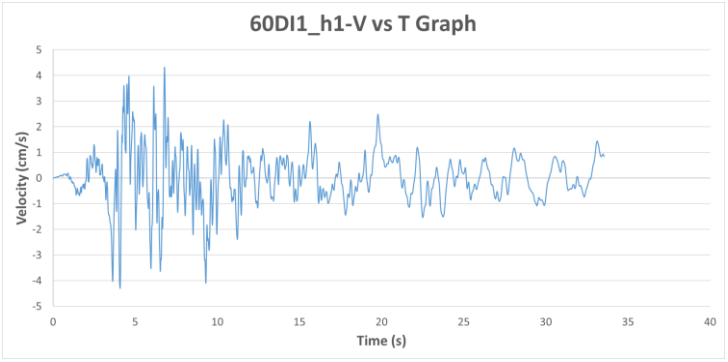

Figure A.65. Velocity vs Time Graph of Ground Motion named 60DI1_h1

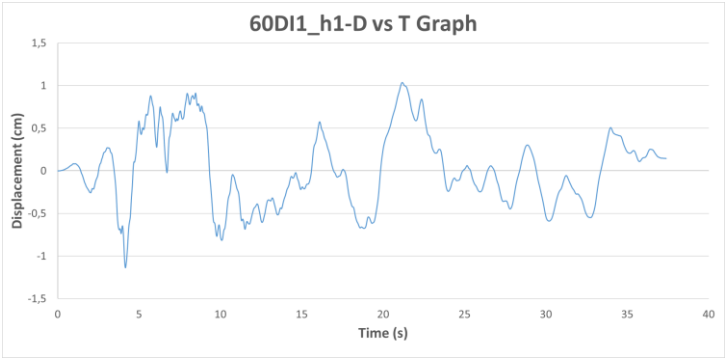

Figure A.66. Displacement vs Time Graph of Ground Motion named 60DI1_h1

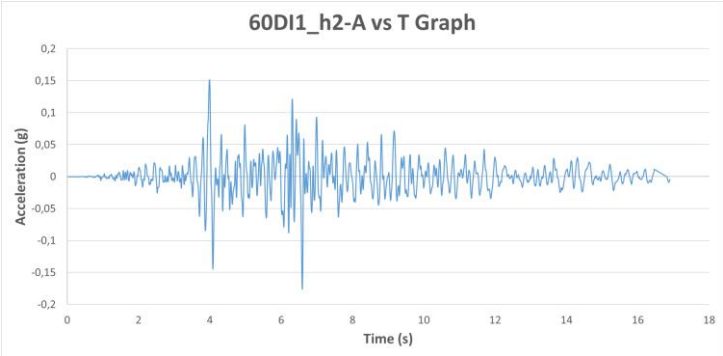

Figure A.67. Acceleration vs Time Graph of Ground Motion named 60DI1_h2

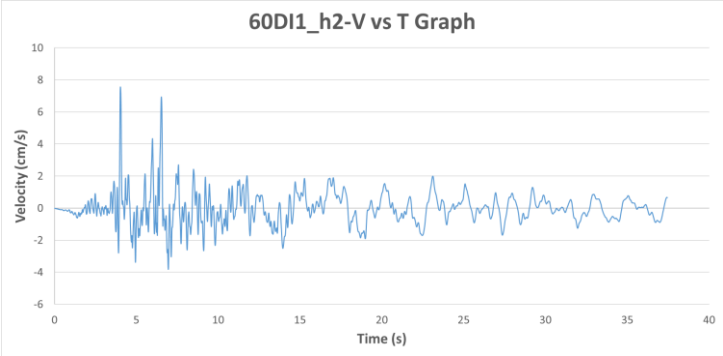

Figure A.68. Velocity vs Time Graph of Ground Motion named 60DI1_h2

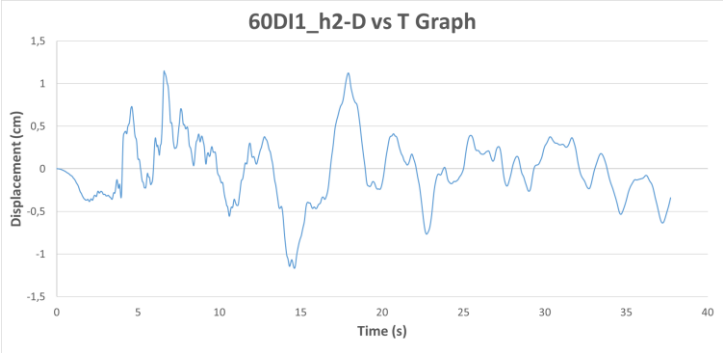

Figure A.69. Displacement vs Time Graph of Ground Motion named 60DI1_h2

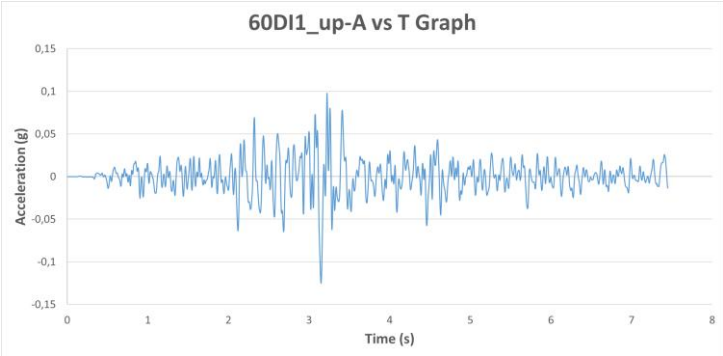

Figure A.70. Acceleration vs Time Graph of Ground Motion named 60DI1_up

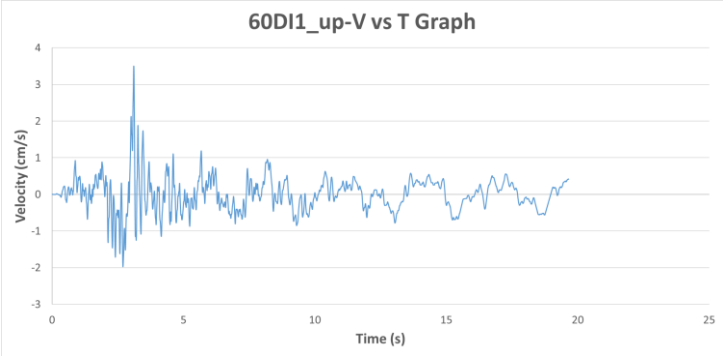

Figure A.71. Velocity vs Time Graph of Ground Motion named 60DI1_up

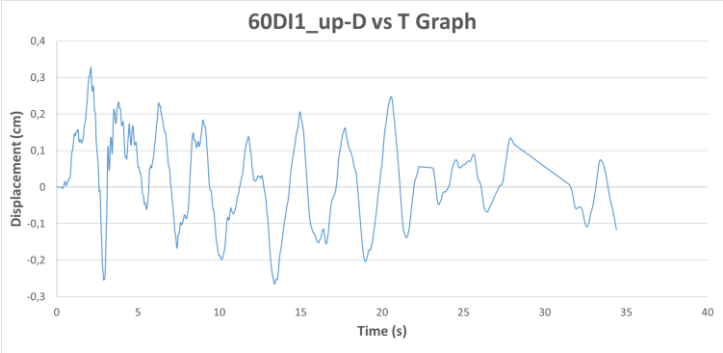

Figure A.72. Displacement vs Time Graph of Ground Motion named 60DI1_up

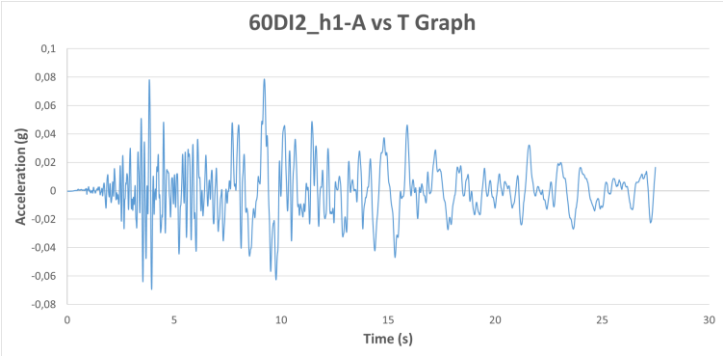

Figure A.73. Acceleration vs Time Graph of Ground Motion named 60DI2_h1

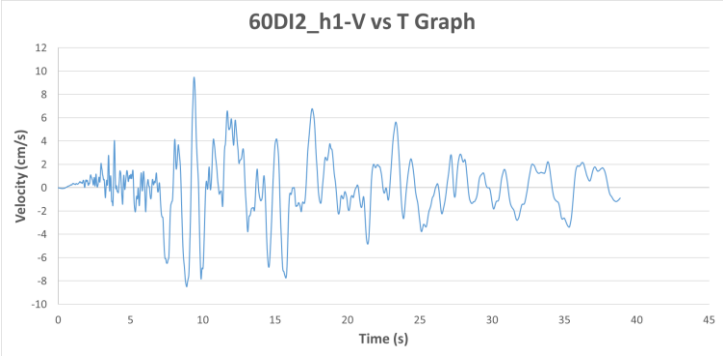

Figure A.74. Velocity vs Time Graph of Ground Motion named 60DI2_h1

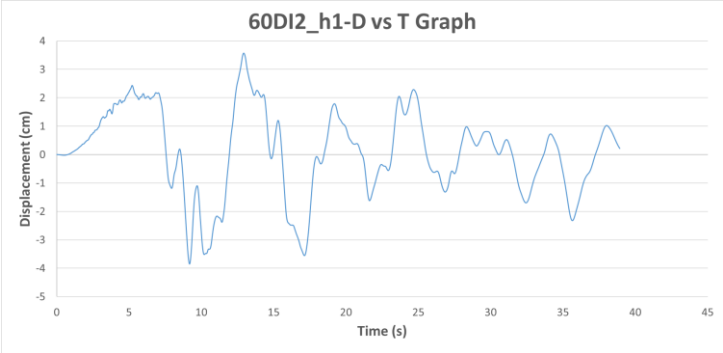

Figure A.75. Displacement vs Time Graph of Ground Motion named 60DI2_h1

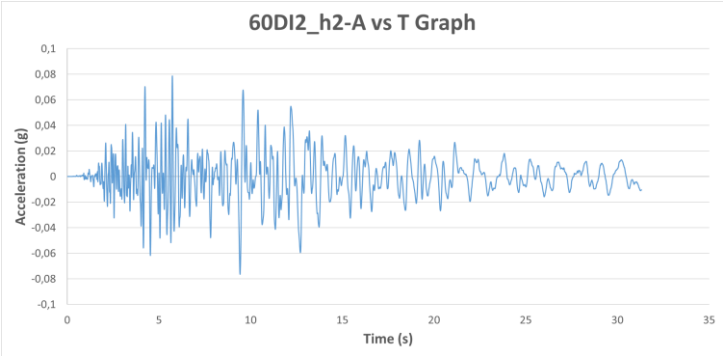

Figure A.76. Acceleration vs Time Graph of Ground Motion named 60DI2_h2

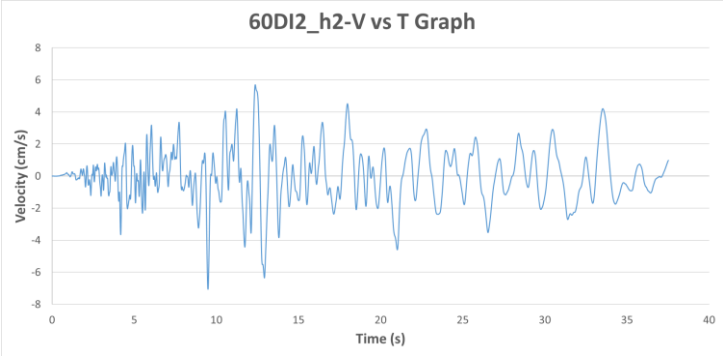

Figure A.77. Velocity vs Time Graph of Ground Motion named 60DI2_h2

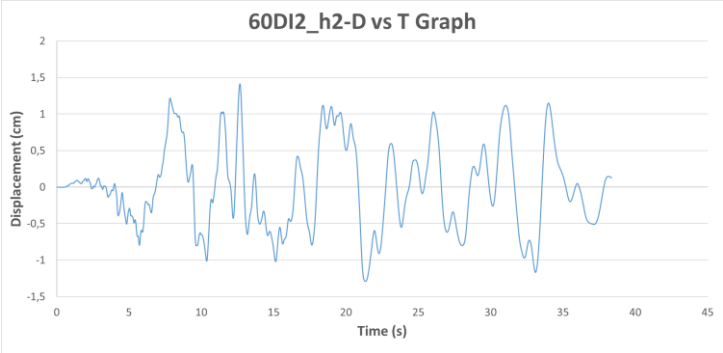

Figure A.78. Displacement vs Time Graph of Ground Motion named 60DI2_h2

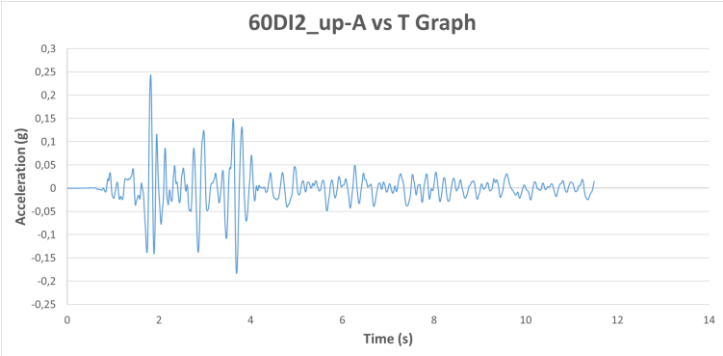

Figure A.79. Acceleration vs Time Graph of Ground Motion named 60DI2_up

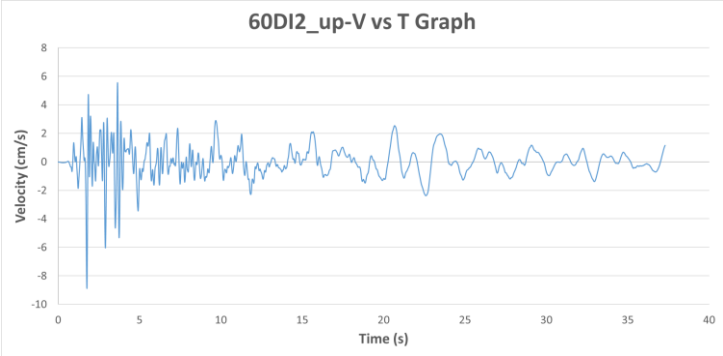

Figure A.80. Velocity vs Time Graph of Ground Motion named 60DI2_up

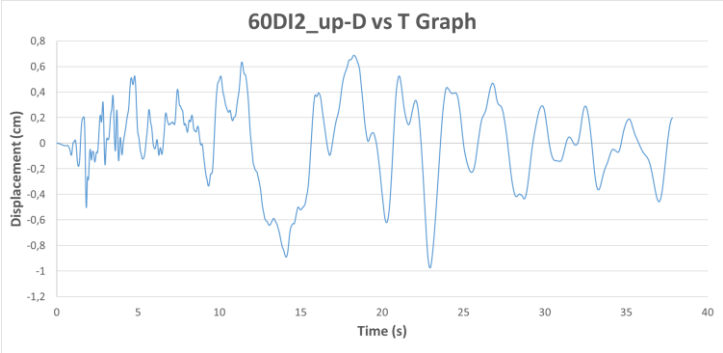

Figure A.81. Displacement vs Time Graph of Ground Motion named 60DI2_up

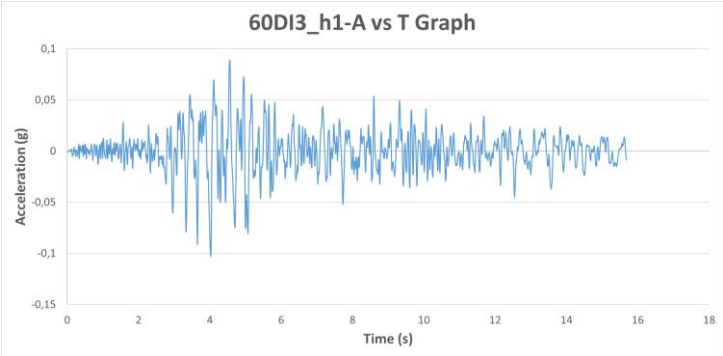

Figure A.82. Acceleration vs Time Graph of Ground Motion named 60DI3_h1

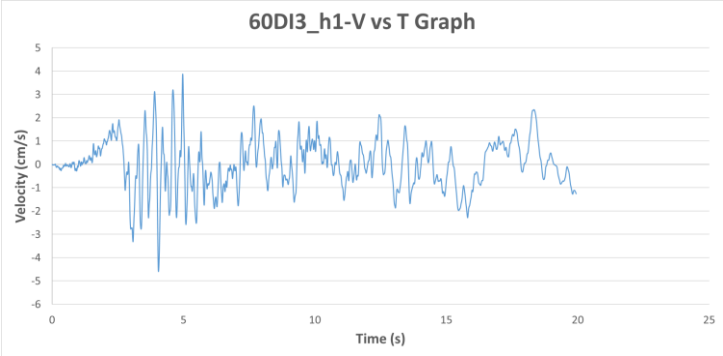

Figure A.83. Velocity vs Time Graph of Ground Motion named 60DI3_h1

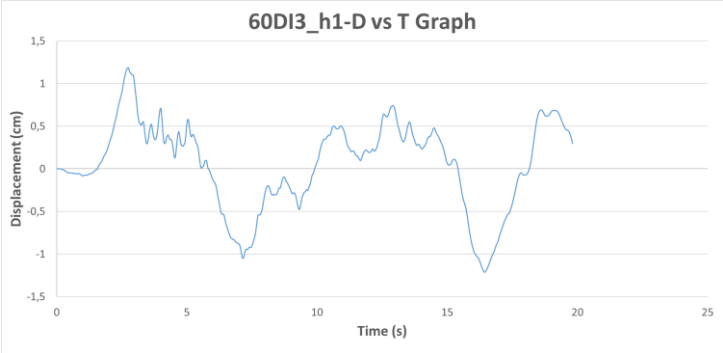

Figure A.84. Displacement vs Time Graph of Ground Motion named 60DI3_h1

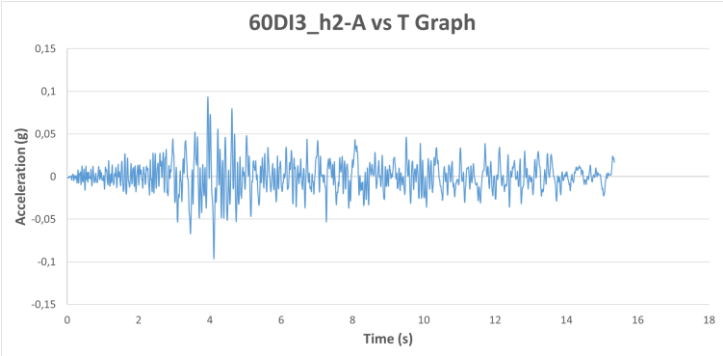

Figure A.85. Acceleration vs Time Graph of Ground Motion named 60DI3_h2

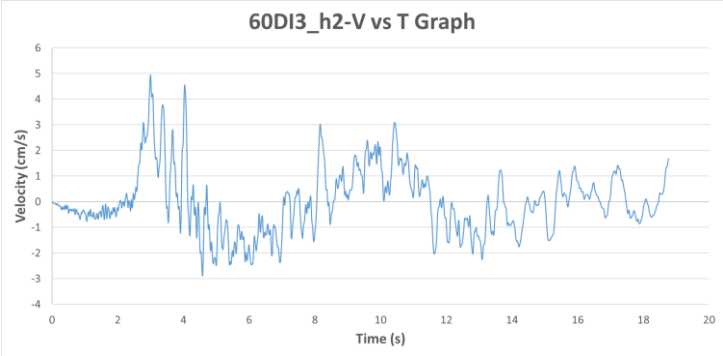

Figure A.86. Velocity vs Time Graph of Ground Motion named 60DI3_h2

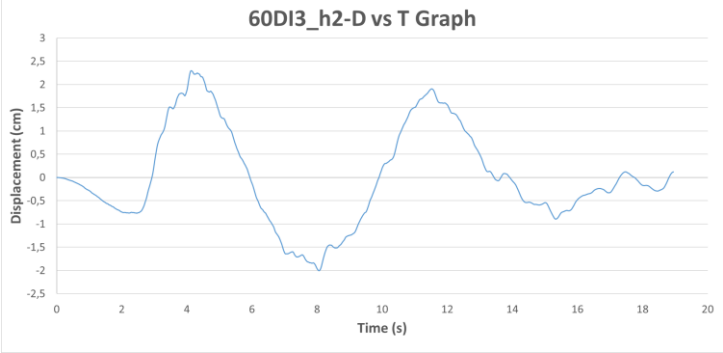

Figure A.87. Displacement vs Time Graph of Ground Motion named 60DI3_h2

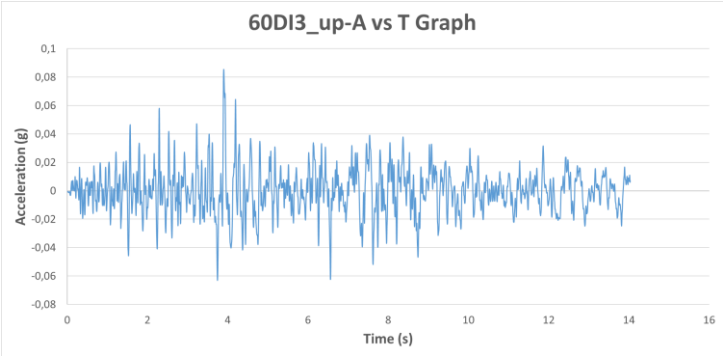

Figure A.88. Acceleration vs Time Graph of Ground Motion named 60DI3_up

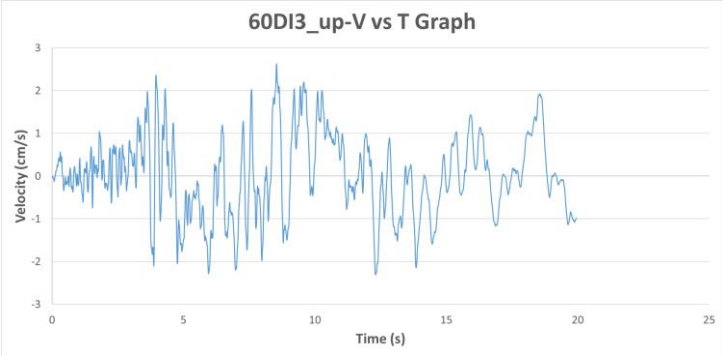

Figure A.89. Velocity vs Time Graph of Ground Motion named 60DI3_up

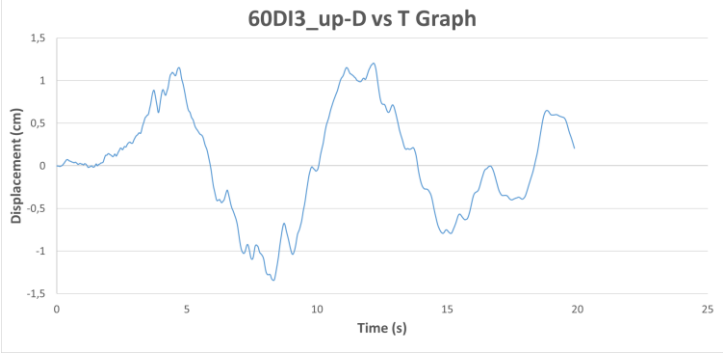

Figure A.90. Displacement vs Time Graph of Ground Motion named 60DI3_up

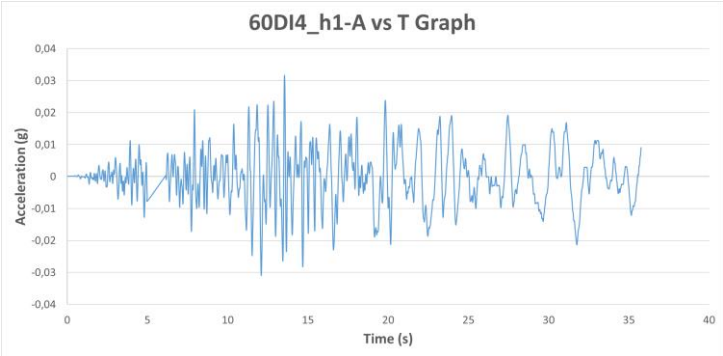

Figure A.91. Acceleration vs Time Graph of Ground Motion named 60DI4_h1

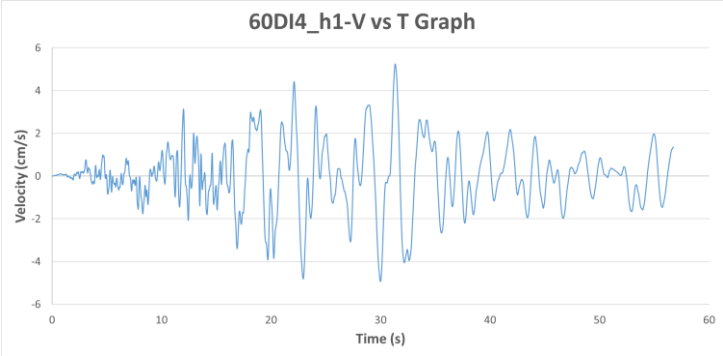

Figure A.92. Velocity vs Time Graph of Ground Motion named 60DI4_h1

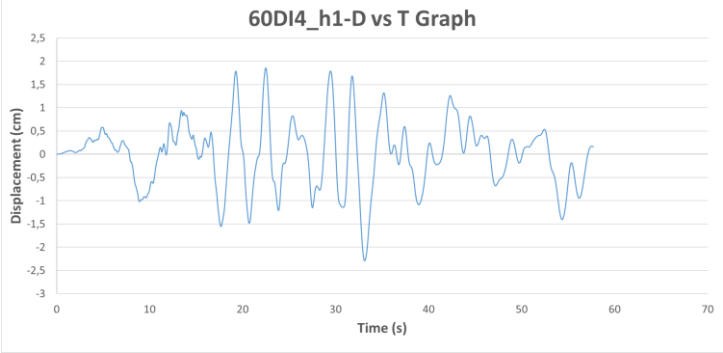

Figure A.93. Displacement vs Time Graph of Ground Motion named 60DI4_h1

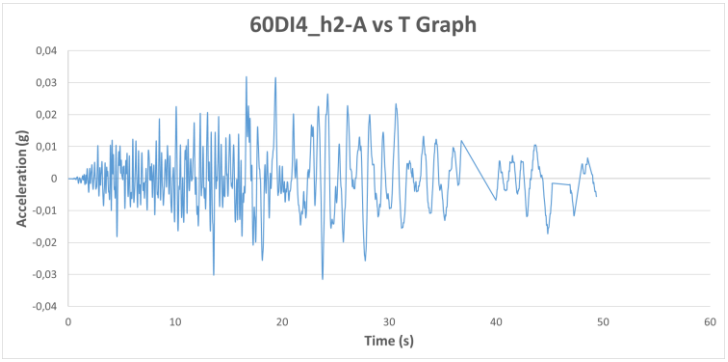

Figure A.94. Acceleration vs Time Graph of Ground Motion named 60DI4_h2

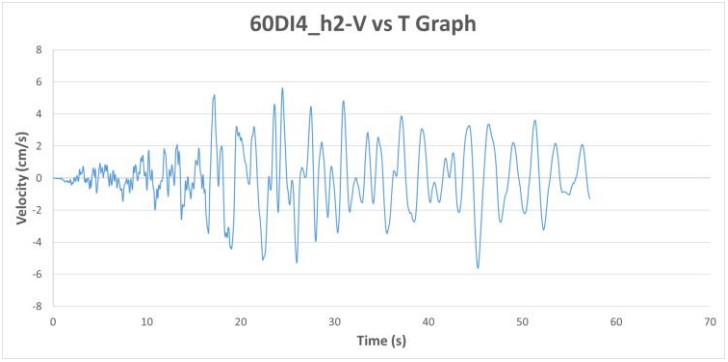

Figure A.95. Velocity vs Time Graph of Ground Motion named 60DI4_h2

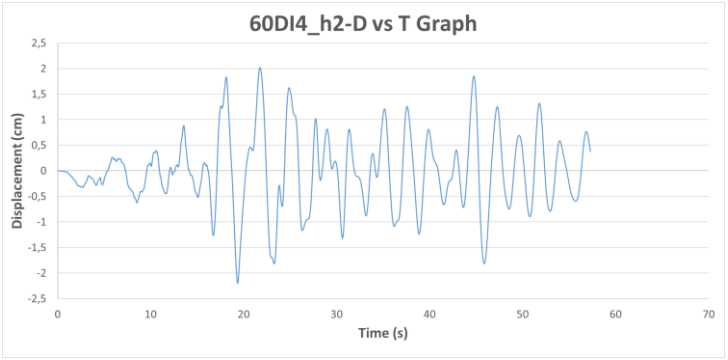

Figure A.96. Displacement vs Time Graph of Ground Motion named 60DI4_h2

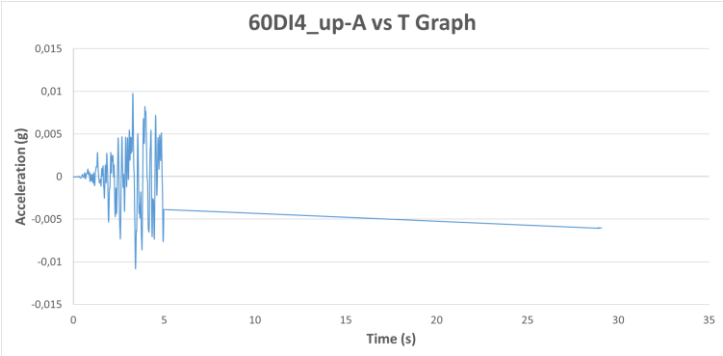

Figure A.97. Acceleration vs Time Graph of Ground Motion named 60DI4_up

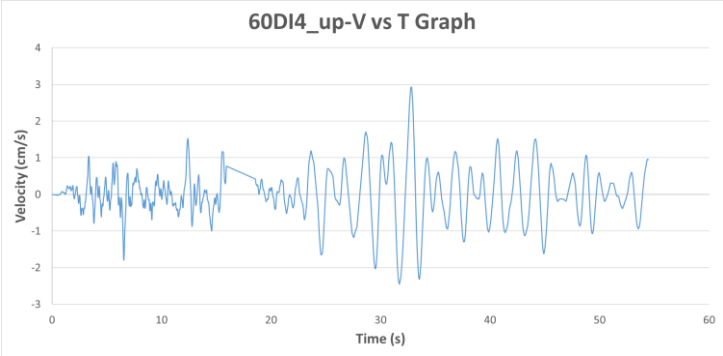

Figure A.98. Velocity vs Time Graph of Ground Motion named 60DI4_up

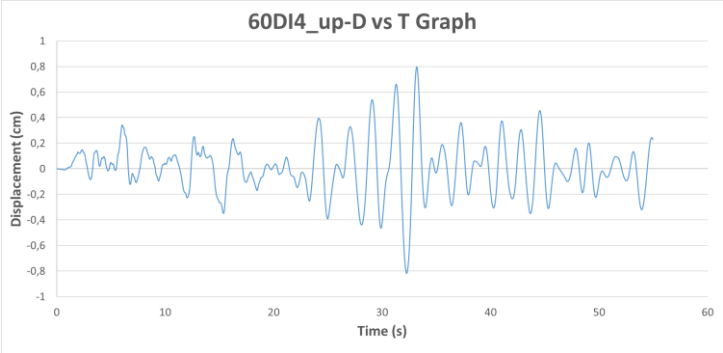

Figure A.99. Displacement vs Time Graph of Ground Motion named 60DI4_up

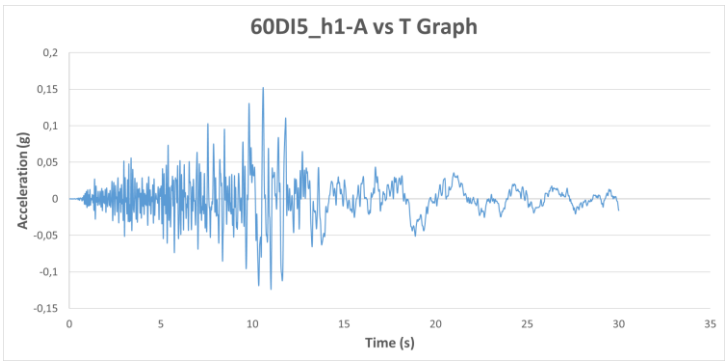

Figure A.100. Acceleration vs Time Graph of Ground Motion named 60DI5_h1

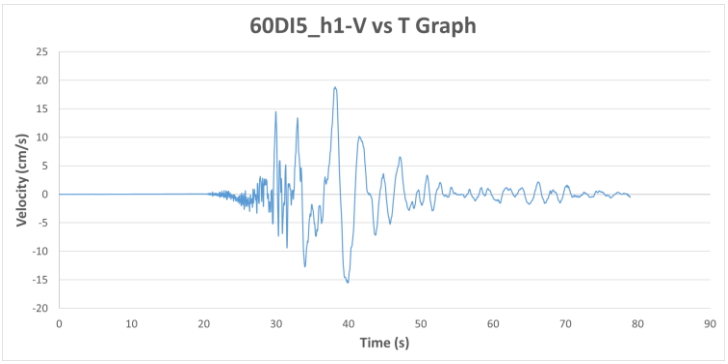

Figure A.101. Velocity vs Time Graph of Ground Motion named 60DI5_h1

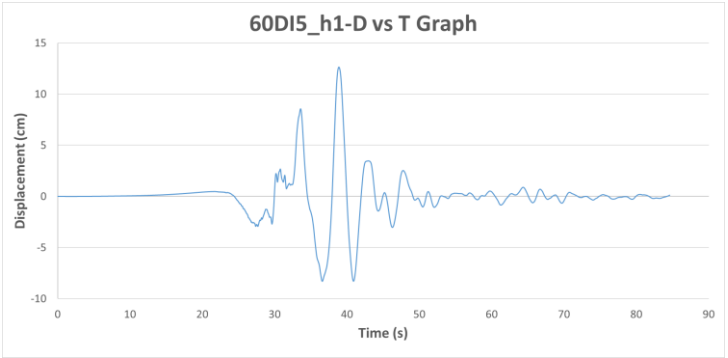

Figure A.102. Displacement vs Time Graph of Ground Motion named 60DI5_h1

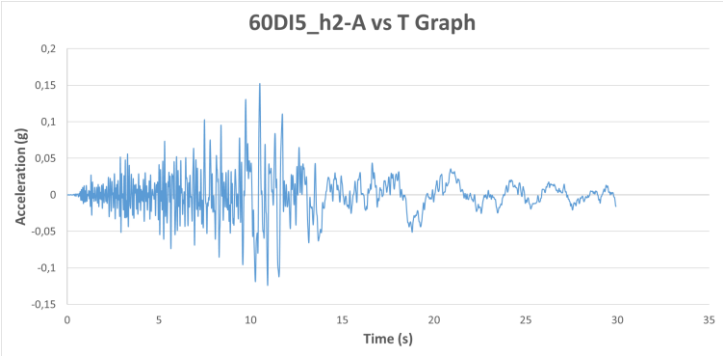

Figure A.103. Acceleration vs Time Graph of Ground Motion named 60DI5_h2

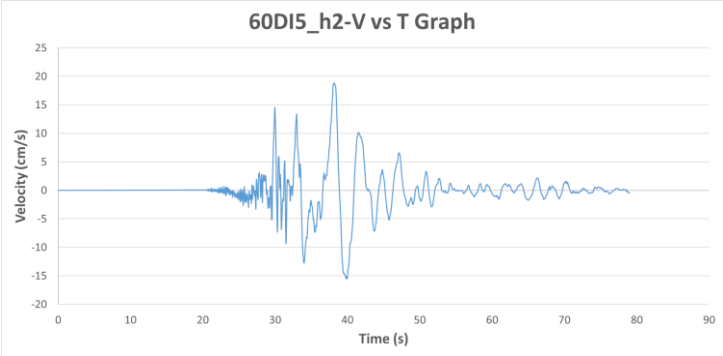

Figure A.104. Velocity vs Time Graph of Ground Motion named 60DI5_h2

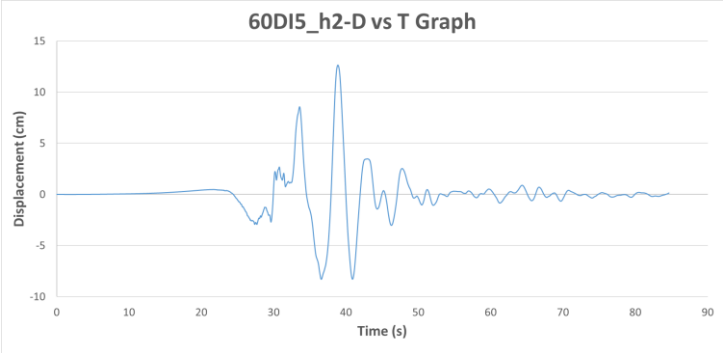

Figure A.105. Displacement vs Time Graph of Ground Motion named 60DI5_h2

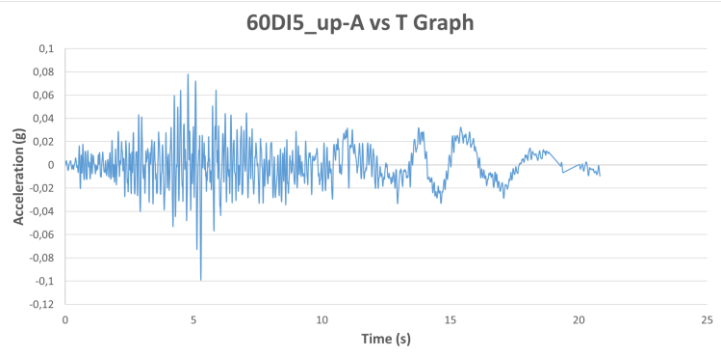

Figure A.106. Acceleration vs Time Graph of Ground Motion named 60DI5_up

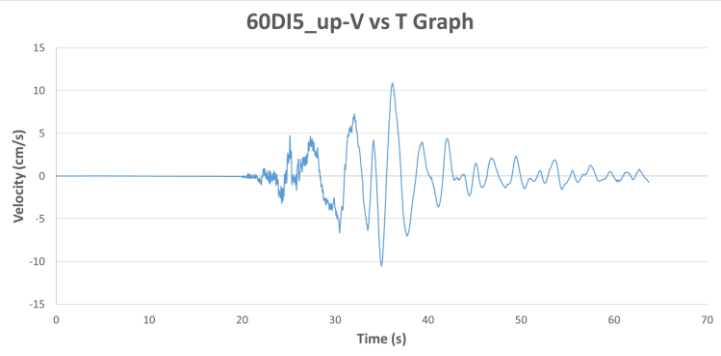

Figure A.107. Velocity vs Time Graph of Ground Motion named 60DI5_up

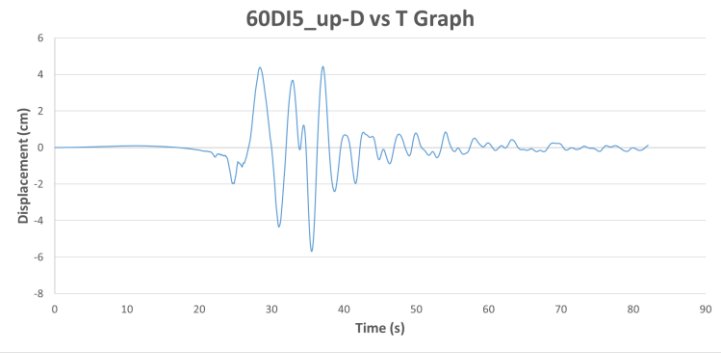

Figure A.108. Displacement vs Time Graph of Ground Motion named 60DI5_up

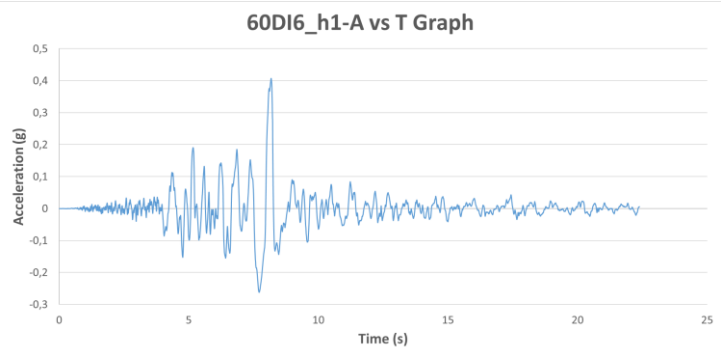

Figure A.109. Acceleration vs Time Graph of Ground Motion named 60DI6_h1

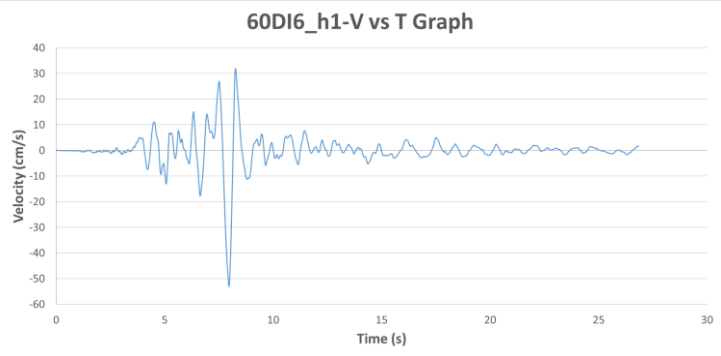

Figure A.110. Velocity vs Time Graph of Ground Motion named 60DI6_h1

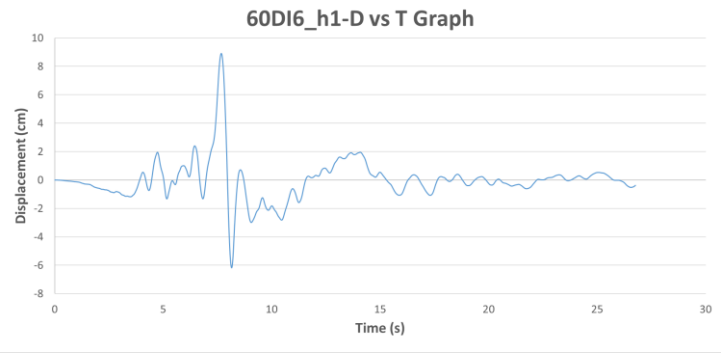

Figure A.111. Displacement vs Time Graph of Ground Motion named 60DI6_h1

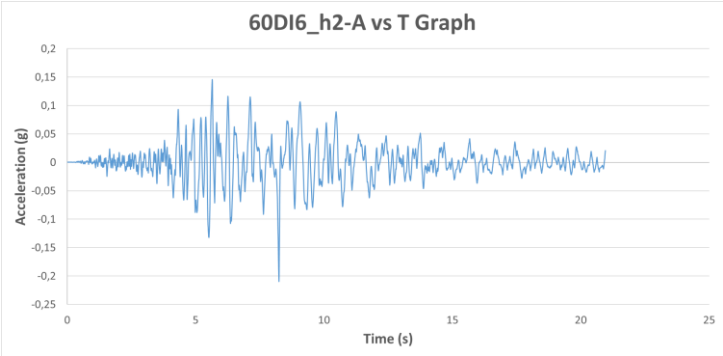

Figure A.112. Acceleration vs Time Graph of Ground Motion named 60DI6_h2

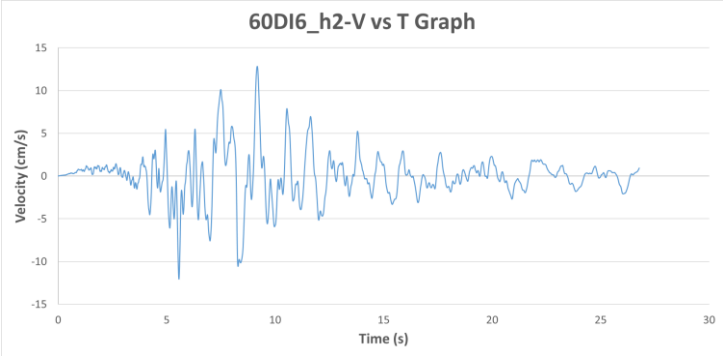

Figure A.113. Velocity vs Time Graph of Ground Motion named 60DI6_h2

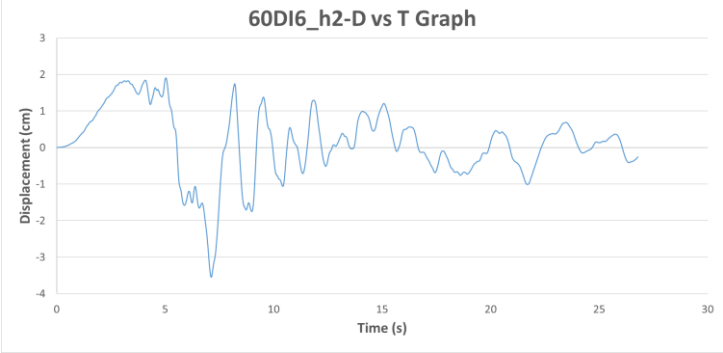

Figure A.114. Displacement vs Time Graph of Ground Motion named 60DI6_h2

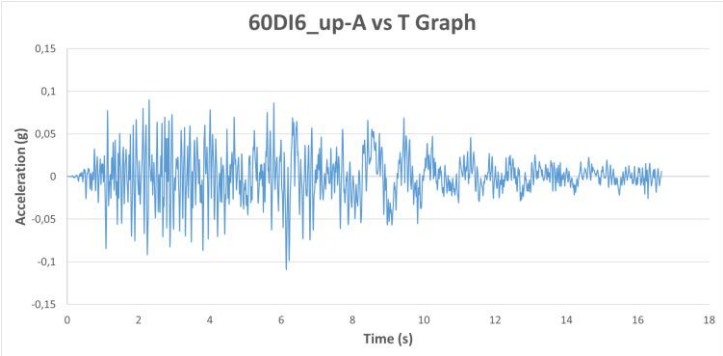

Figure A.115. Acceleration vs Time Graph of Ground Motion named 60DI6_up

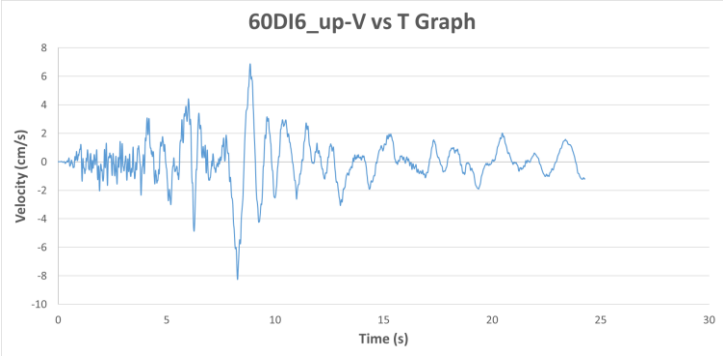

Figure A.116. Velocity vs Time Graph of Ground Motion named 60DI6_up

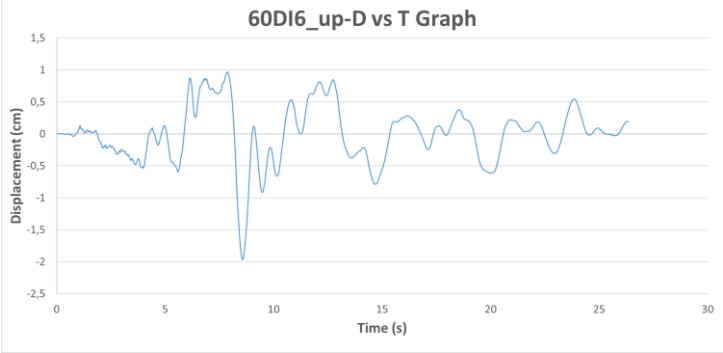

Figure A.117. Displacement vs Time Graph of Ground Motion named 60DI6_up

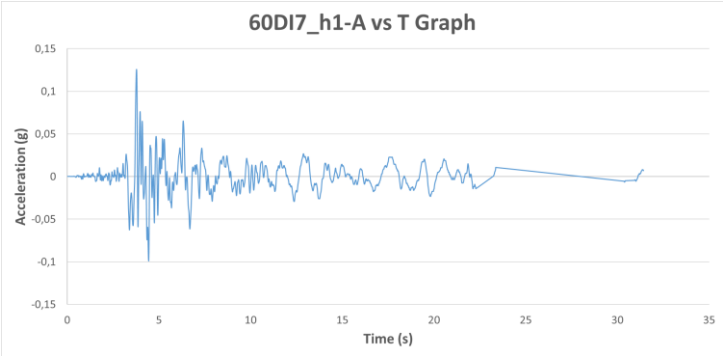

Figure A.118. Acceleration vs Time Graph of Ground Motion named 60DI7_h1

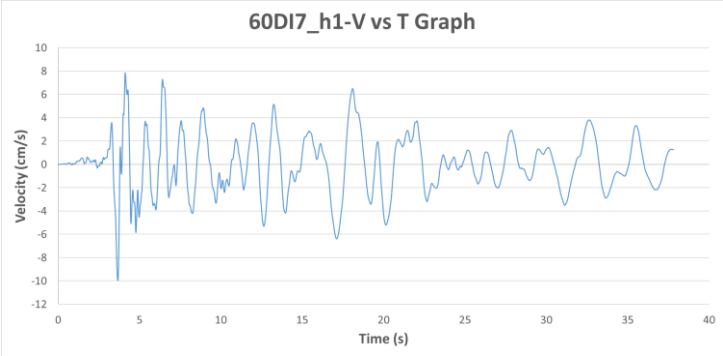

Figure A.119. Velocity vs Time Graph of Ground Motion named 60DI7_h1

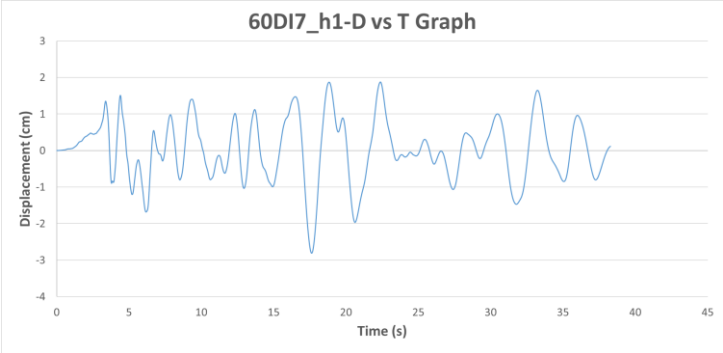

Figure A.120. Displacement vs Time Graph of Ground Motion named 60DI7_h1

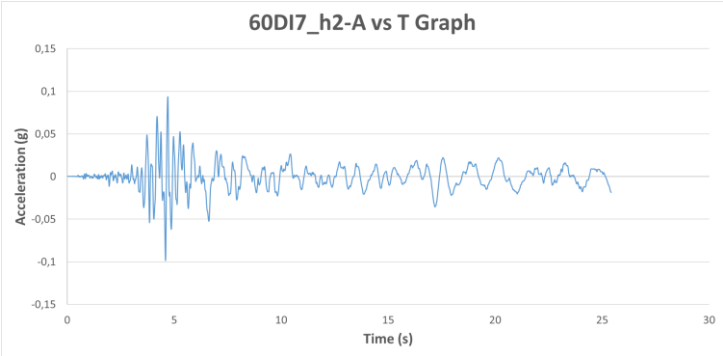

Figure A.121. Acceleration vs Time Graph of Ground Motion named 60DI7_h2

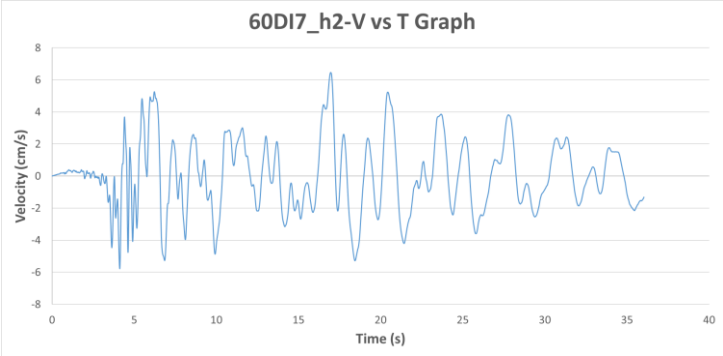

Figure A.122. Velocity vs Time Graph of Ground Motion named 60DI7_h2

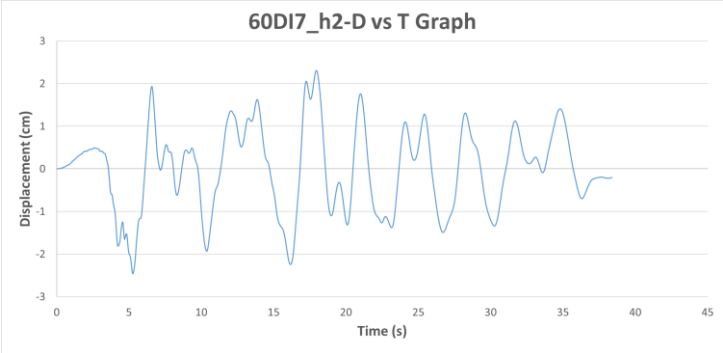

Figure A.123. Displacement vs Time Graph of Ground Motion named 60DI7_h2

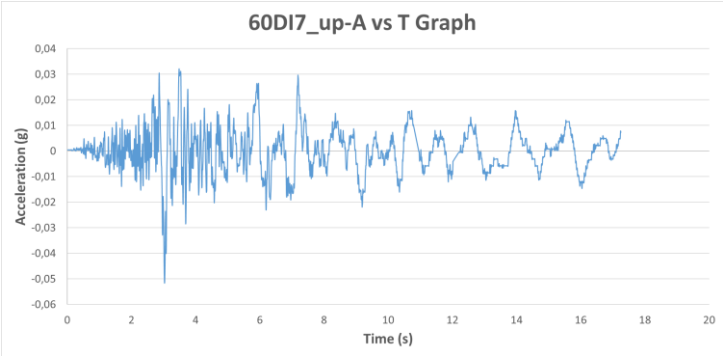

Figure A.124. Acceleration vs Time Graph of Ground Motion named 60DI7_up

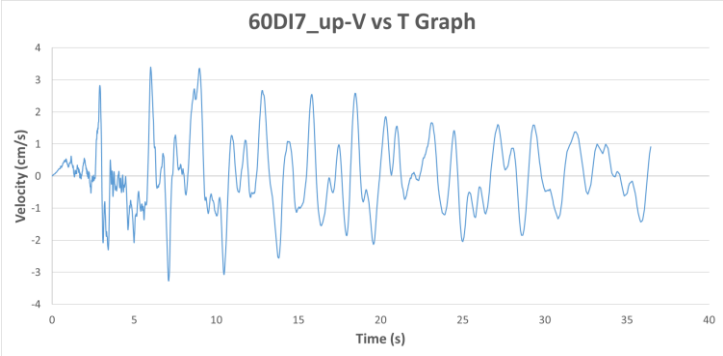

Figure A.125. Velocity vs Time Graph of Ground Motion named 60DI7_up

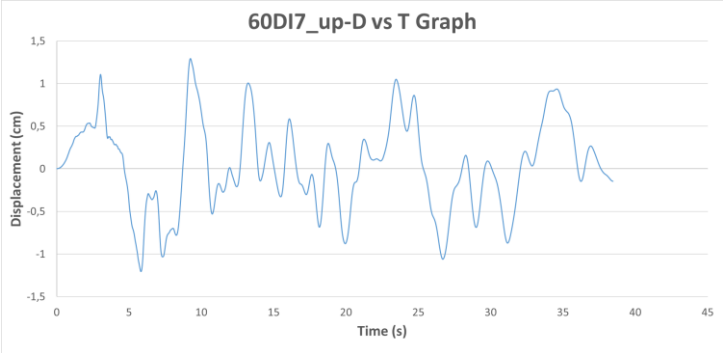

Figure A.126. Displacement vs Time Graph of Ground Motion named 60DI7_up

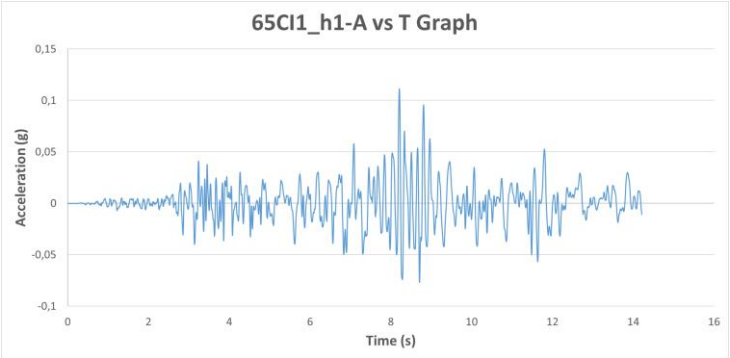

Figure A.127. Acceleration vs Time Graph of Ground Motion named 65CI1_h1

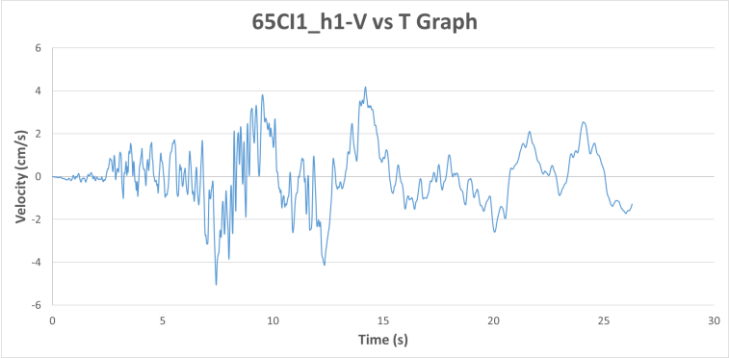

Figure A.128. Velocity vs Time Graph of Ground Motion named 65CI1_h1

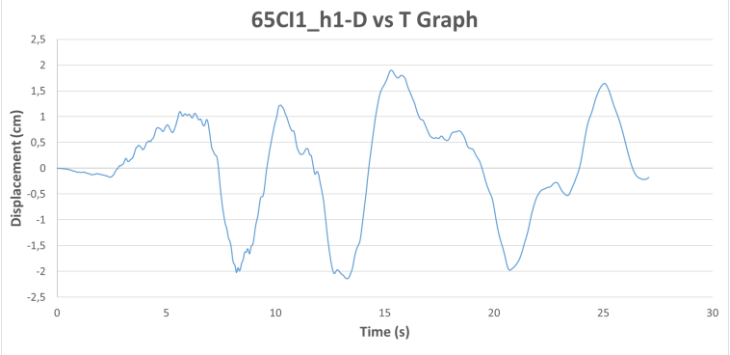

Figure A.129. Displacement vs Time Graph of Ground Motion named 65CI1_h1

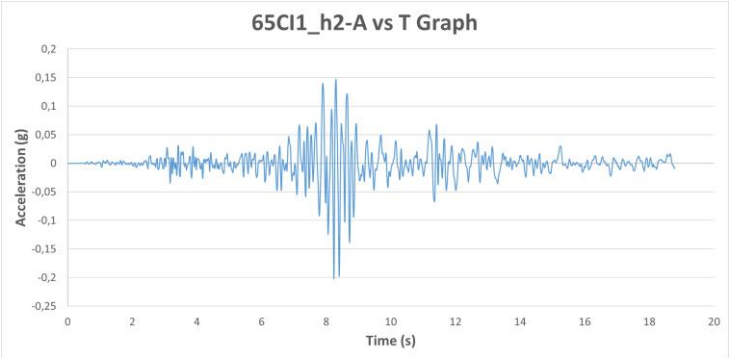

Figure A.130. Acceleration vs Time Graph of Ground Motion named 65CI1_h2

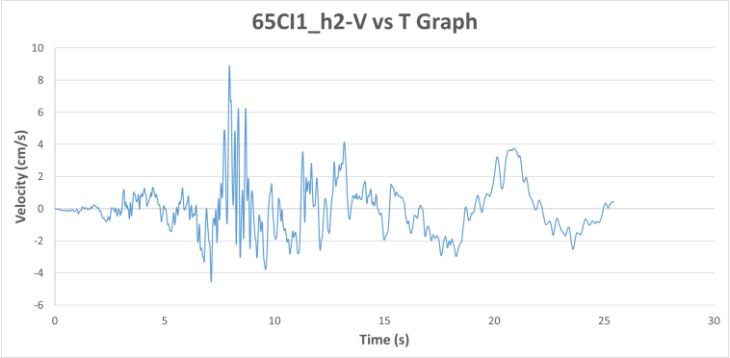

Figure A.131. Velocity vs Time Graph of Ground Motion named 65CI1_h2

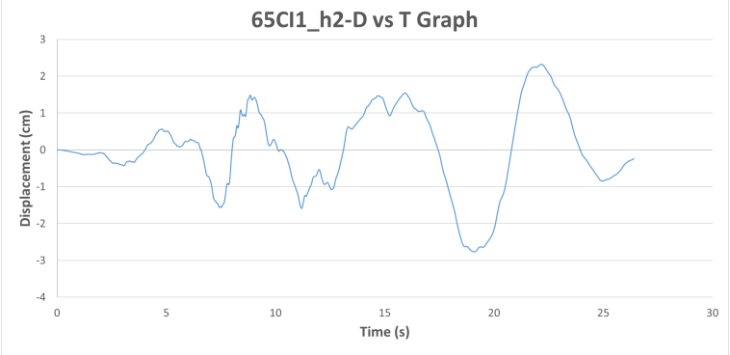

Figure A.132. Displacement vs Time Graph of Ground Motion named 65CI1_h2

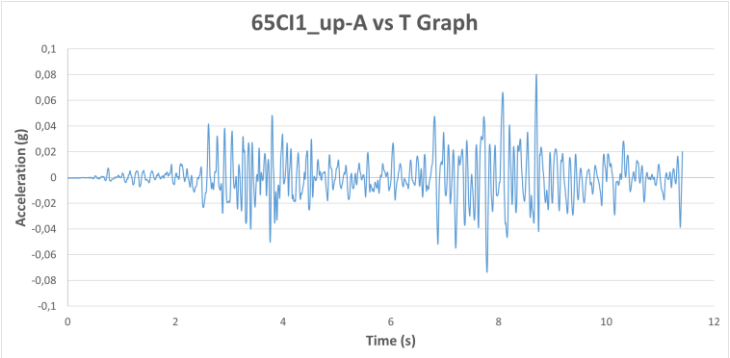

Figure A.133. Acceleration vs Time Graph of Ground Motion named 65CI1_up

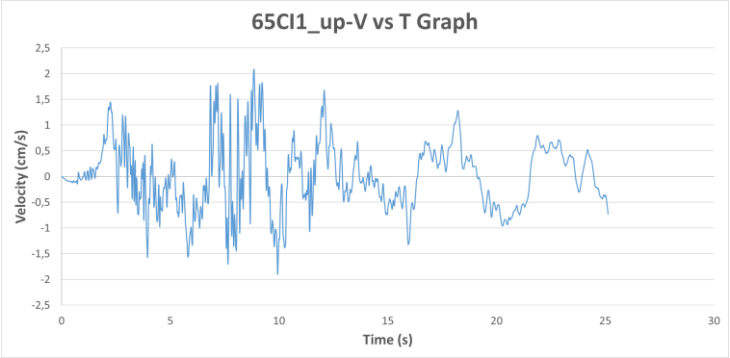

Figure A.134. Velocity vs Time Graph of Ground Motion named 65CI1_up

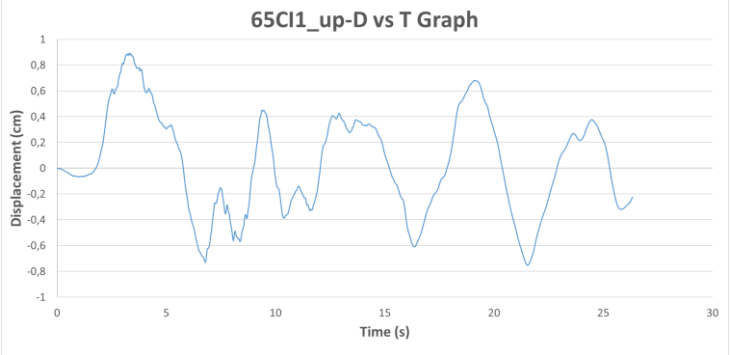

Figure A.135. Displacement vs Time Graph of Ground Motion named 65CI1_up

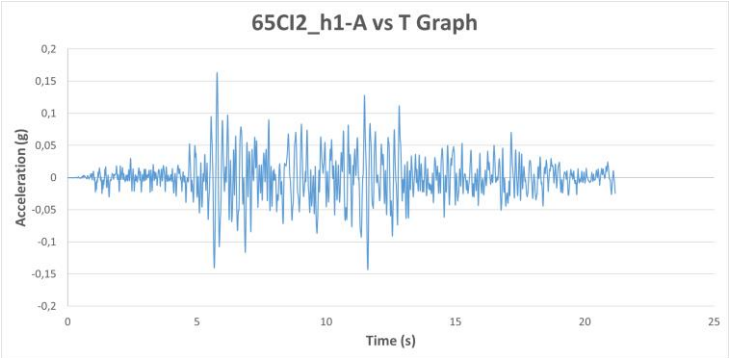

Figure A.136. Acceleration vs Time Graph of Ground Motion named 65CI2_h1

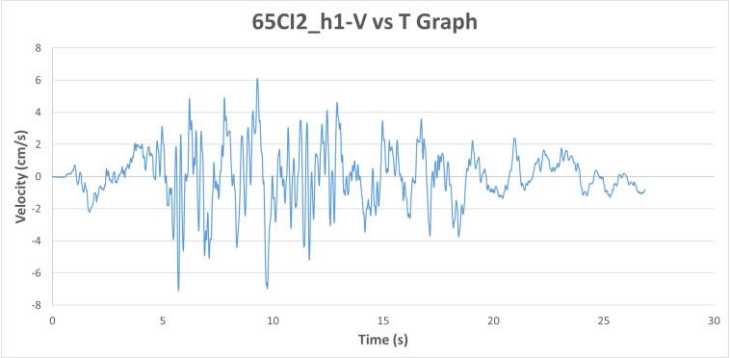

Figure A.137. Velocity vs Time Graph of Ground Motion named 65CI2_h1

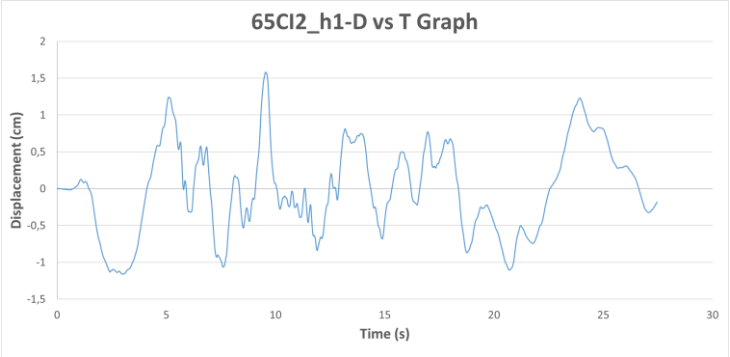

Figure A.138. Displacement vs Time Graph of Ground Motion named 65CI2_h1

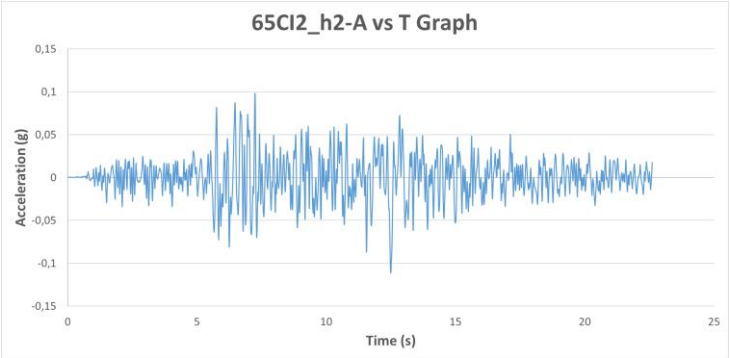

Figure A.139. Acceleration vs Time Graph of Ground Motion named 65CI2_h2

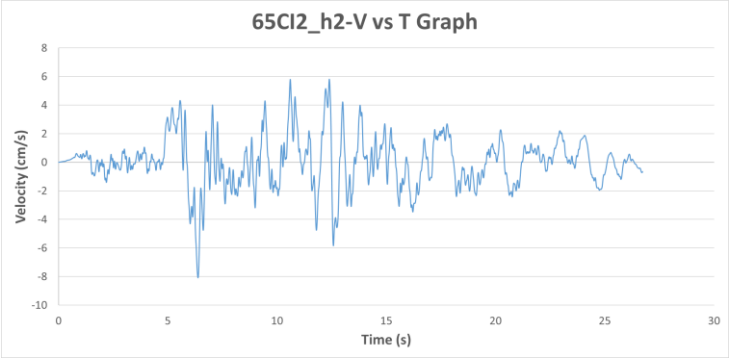

Figure A.140. Velocity vs Time Graph of Ground Motion named 65CI2_h2

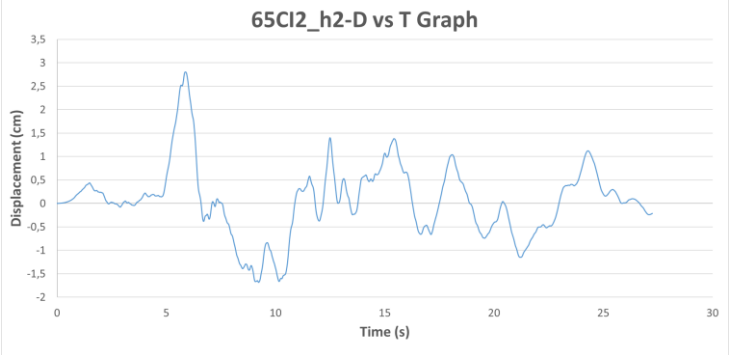

Figure A.141. Displacement vs Time Graph of Ground Motion named 65CI2_h2

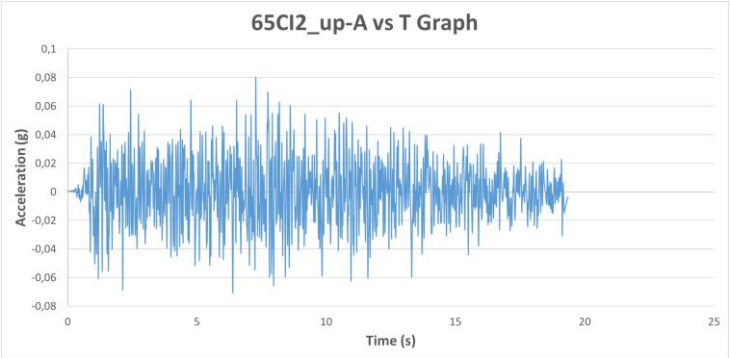

Figure A.142. Acceleration vs Time Graph of Ground Motion named 65CI2_up

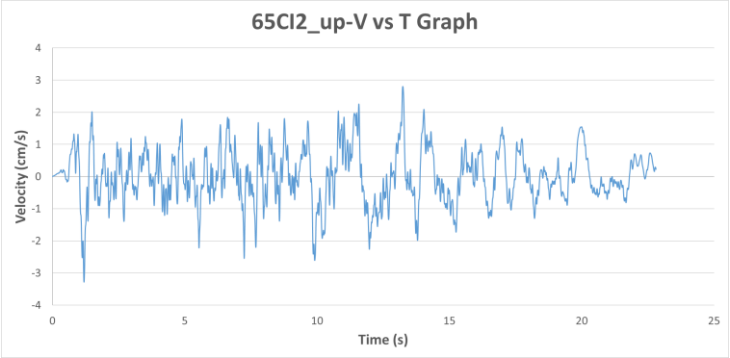

Figure A.143. Velocity vs Time Graph of Ground Motion named 65CI2_up

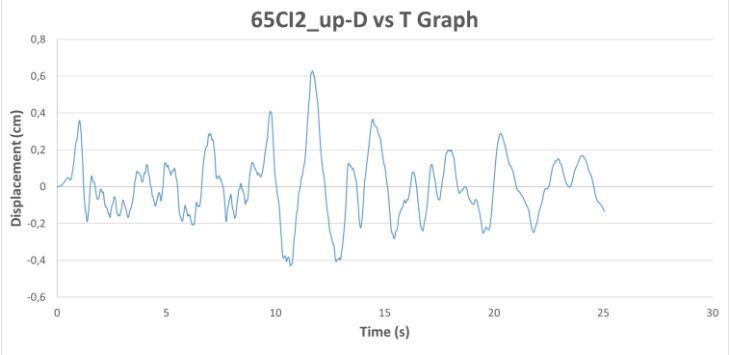

Figure A.144. Displacement vs Time Graph of Ground Motion named 65CI2_up

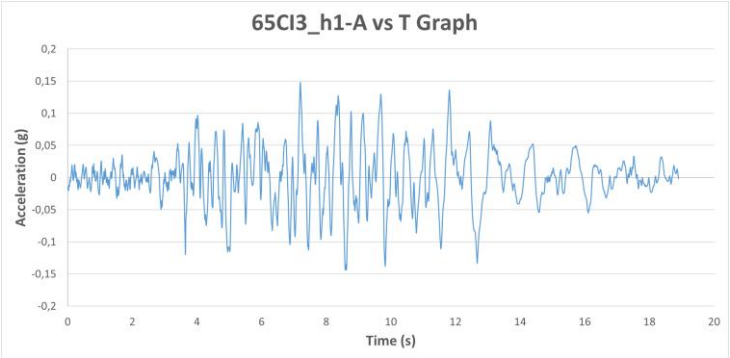

Figure A.145. Acceleration vs Time Graph of Ground Motion named 65CI3_h1

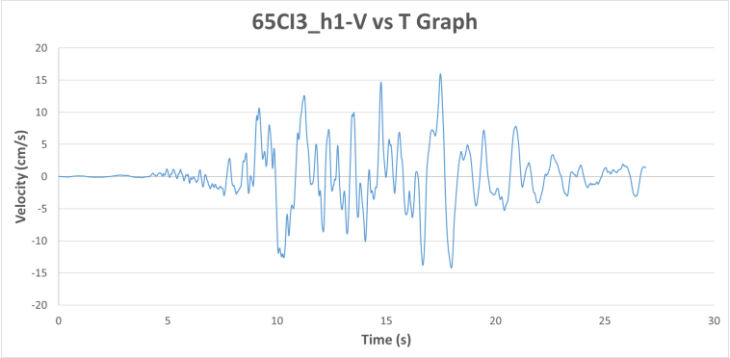

Figure A.146. Velocity vs Time Graph of Ground Motion named 65CI3_h1

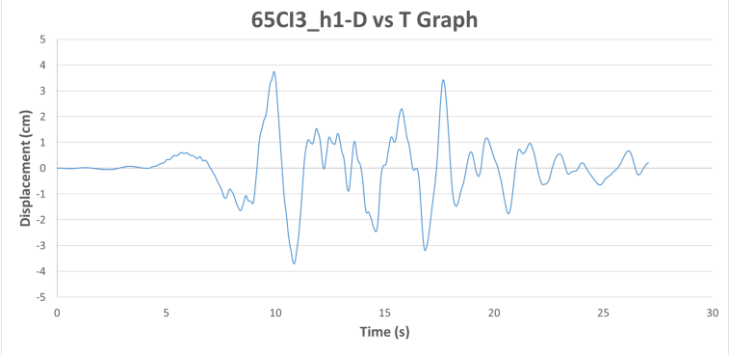

Figure A.147. Displacement vs Time Graph of Ground Motion named 65CI3_h1

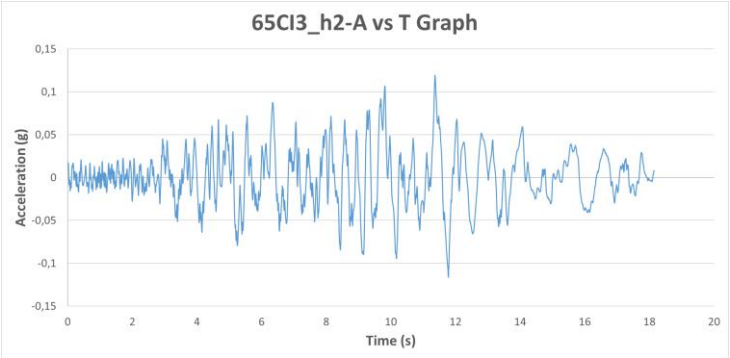

Figure A.148. Acceleration vs Time Graph of Ground Motion named 65CI3_h2

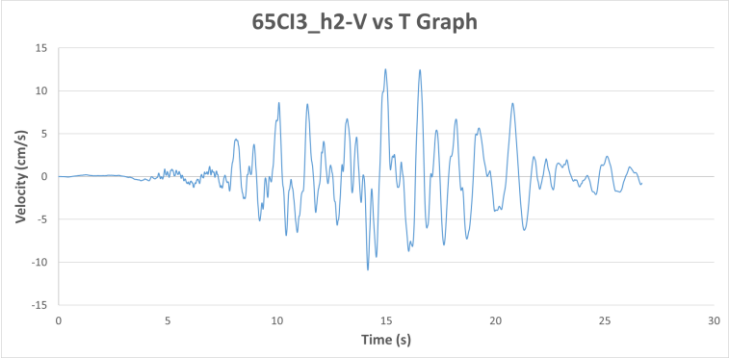

Figure A.149. Velocity vs Time Graph of Ground Motion named 65CI3_h2

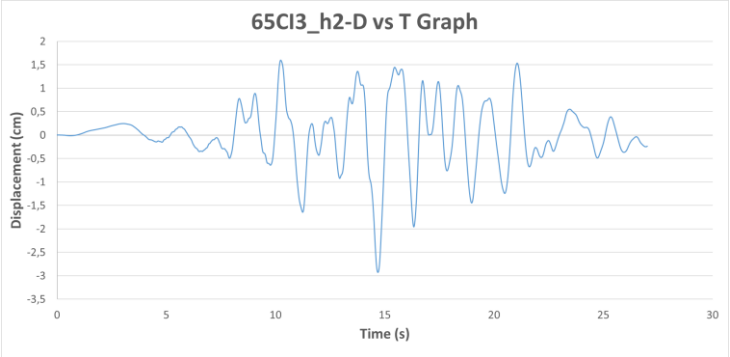

Figure A.150. Displacement vs Time Graph of Ground Motion named 65CI3_h2

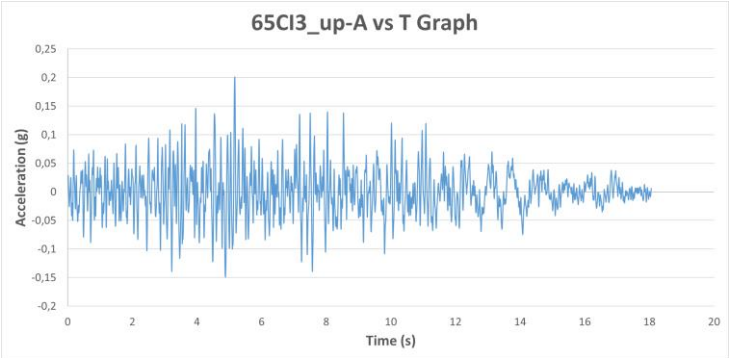

Figure A.151. Acceleration vs Time Graph of Ground Motion named 65CI3_up

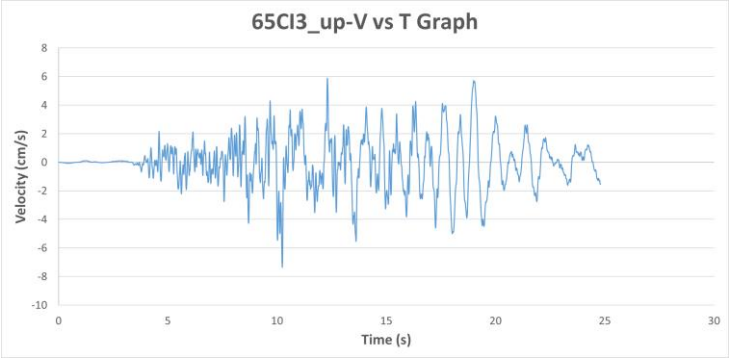

Figure A.152. Velocity vs Time Graph of Ground Motion named 65CI3_up

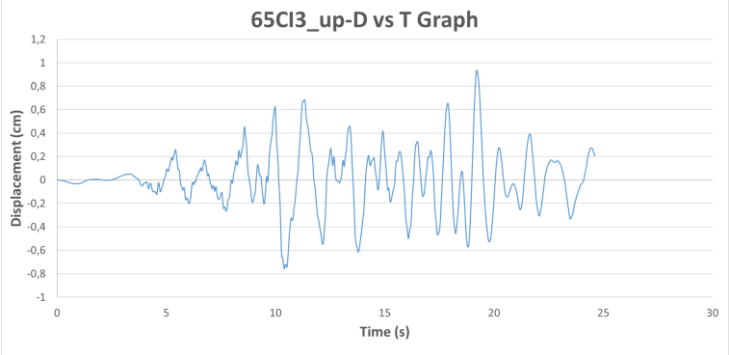

Figure A.153. Displacement vs Time Graph of Ground Motion named 65CI3_up

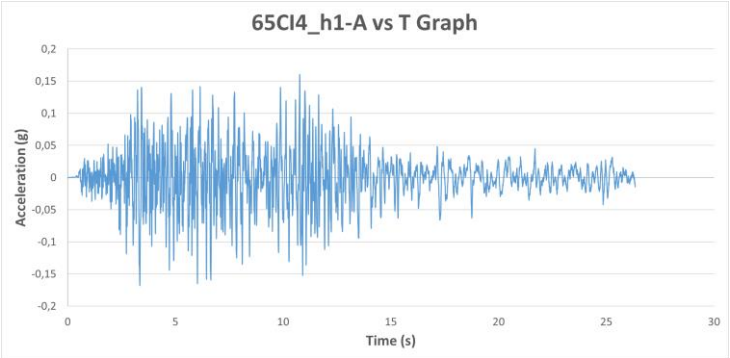

Figure A.154. Acceleration vs Time Graph of Ground Motion named 65CI4_h1

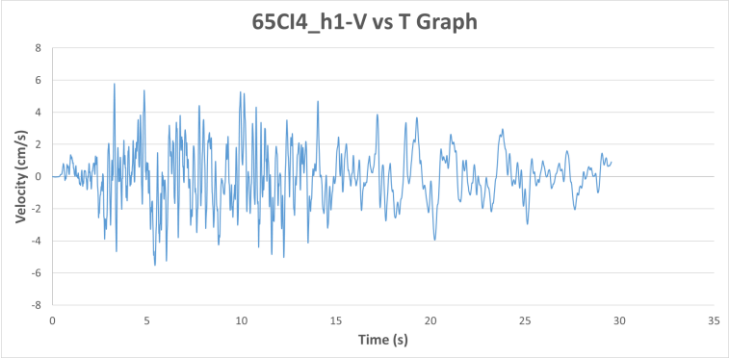

Figure A.155. Velocity vs Time Graph of Ground Motion named 65CI4_h1

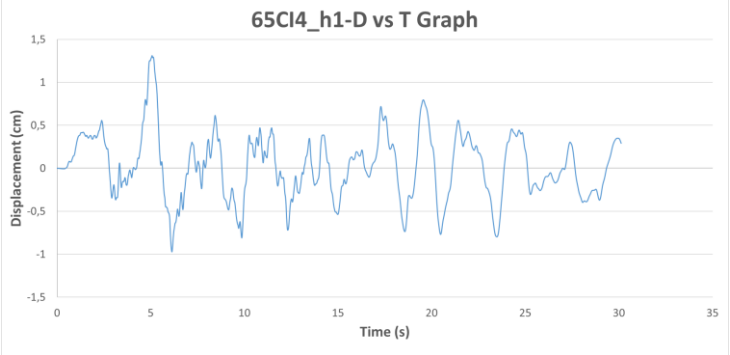

Figure A.156. Displacement vs Time Graph of Ground Motion named 65CI4_h1

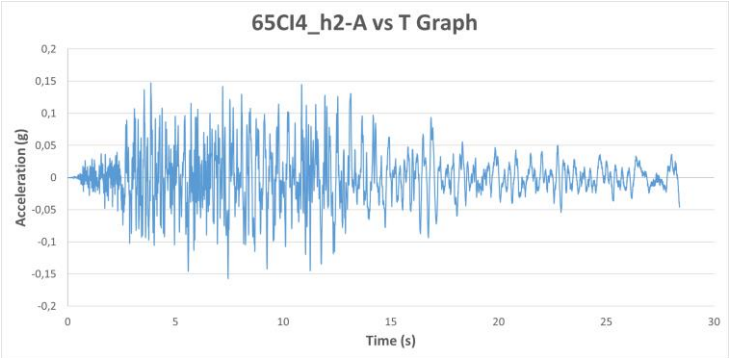

Figure A.157. Acceleration vs Time Graph of Ground Motion named 65CI4_h2

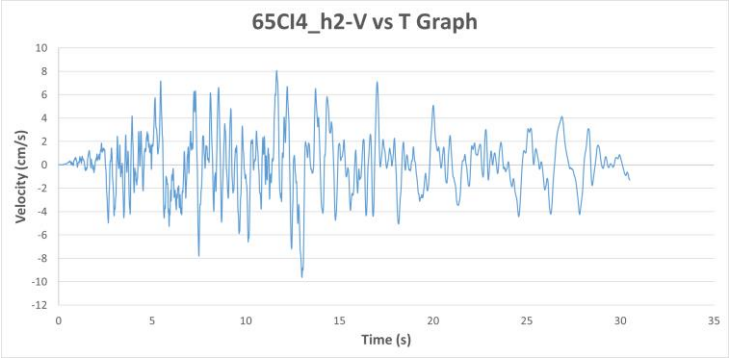

Figure A.158. Velocity vs Time Graph of Ground Motion named 65CI4_h2

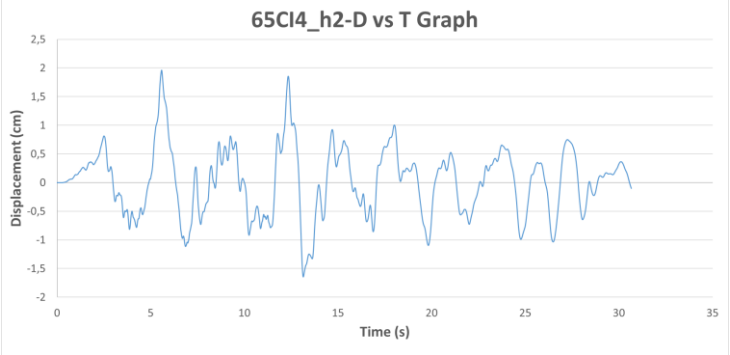

Figure A.159. Displacement vs Time Graph of Ground Motion named 65CI4_h2

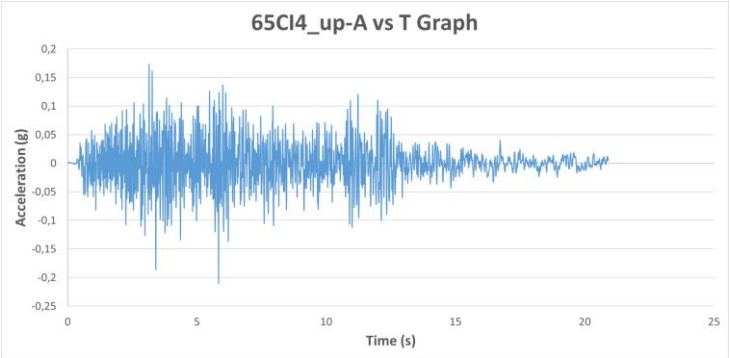

Figure A.160. Acceleration vs Time Graph of Ground Motion named 65CI4_up

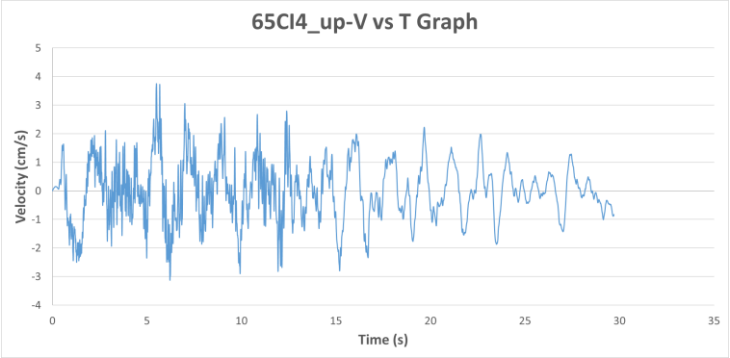

Figure A.161. Velocity vs Time Graph of Ground Motion named 65CI4_up

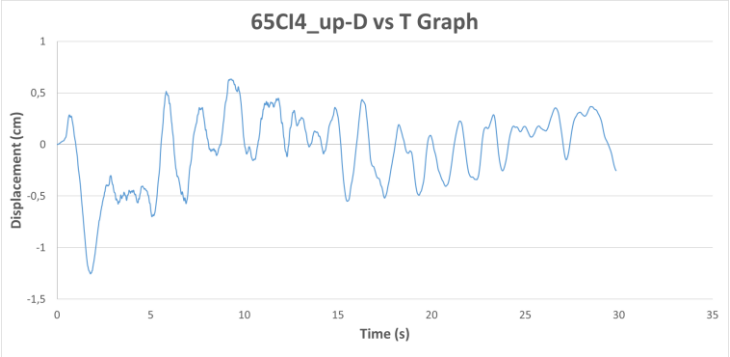

Figure A.162. Displacement vs Time Graph of Ground Motion named 65CI4_up

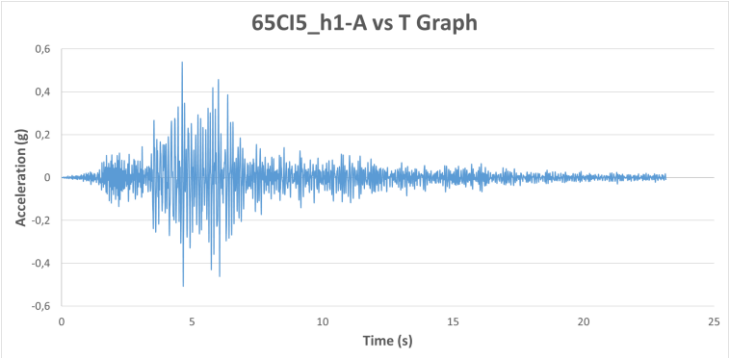

Figure A.163. Acceleration vs Time Graph of Ground Motion named 65CI5_h1

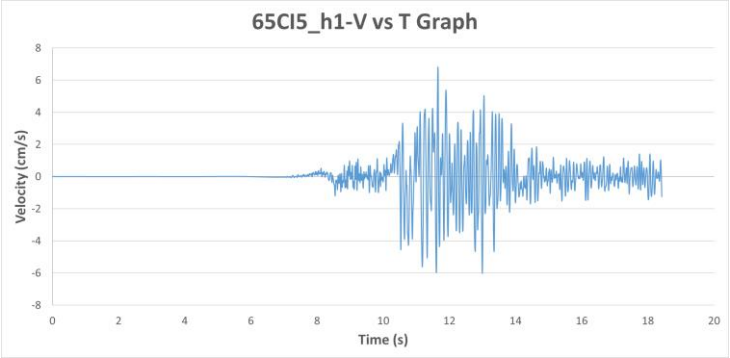

Figure A.164. Velocity vs Time Graph of Ground Motion named 65CI5_h1

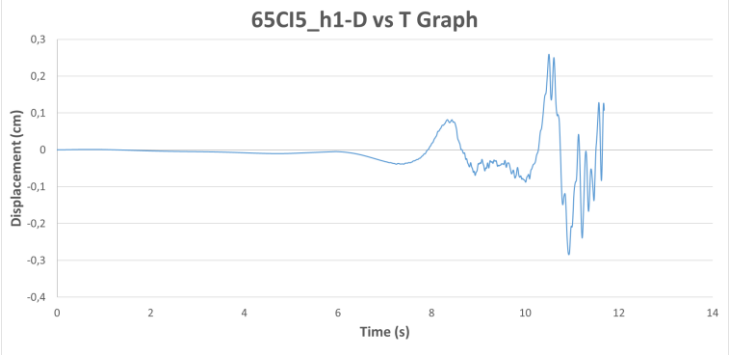

Figure A.165. Displacement vs Time Graph of Ground Motion named 65CI5_h1

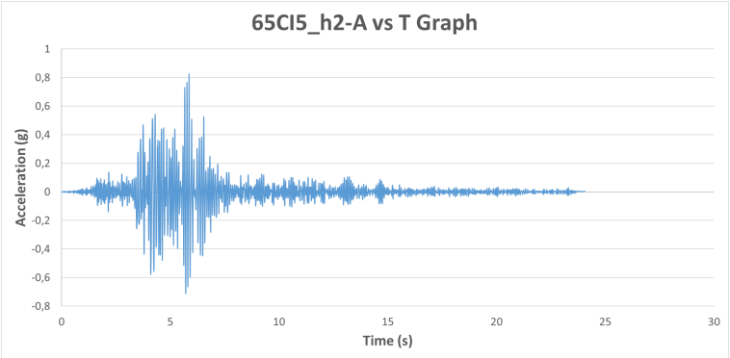

Figure A.166. Acceleration vs Time Graph of Ground Motion named 65CI5_h2

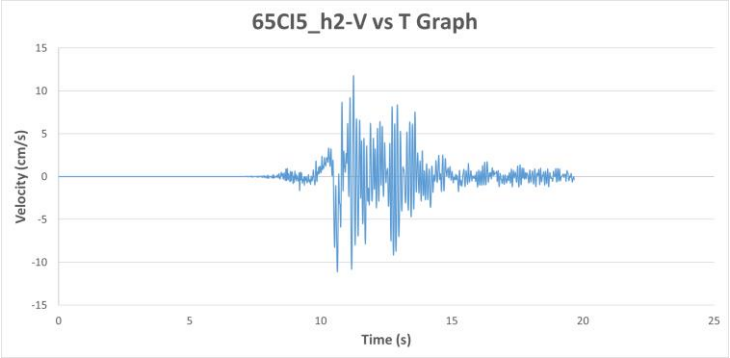

Figure A.167. Velocity vs Time Graph of Ground Motion named 65CI5_h2

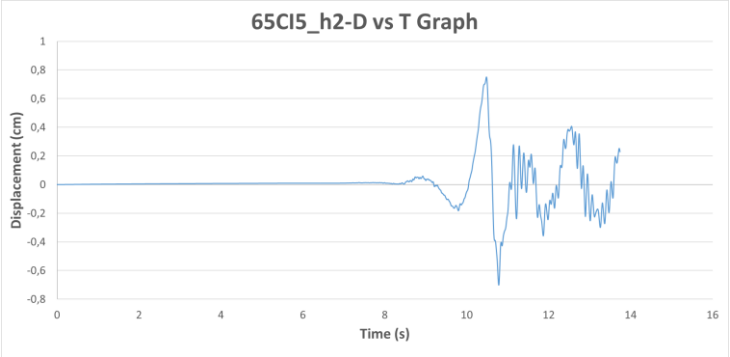

Figure A.168. Displacement vs Time Graph of Ground Motion named 65CI5_h2

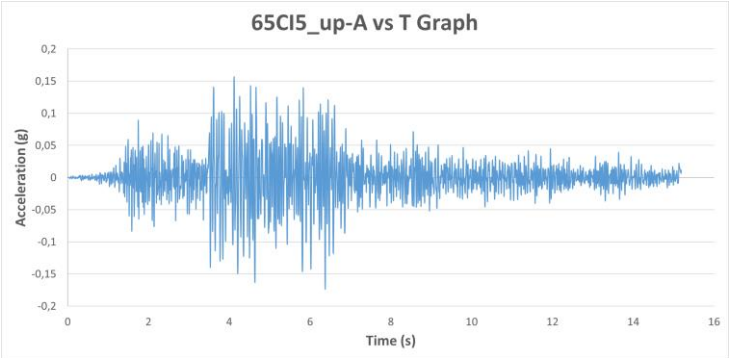

Figure A.169. Acceleration vs Time Graph of Ground Motion named 65CI5_up

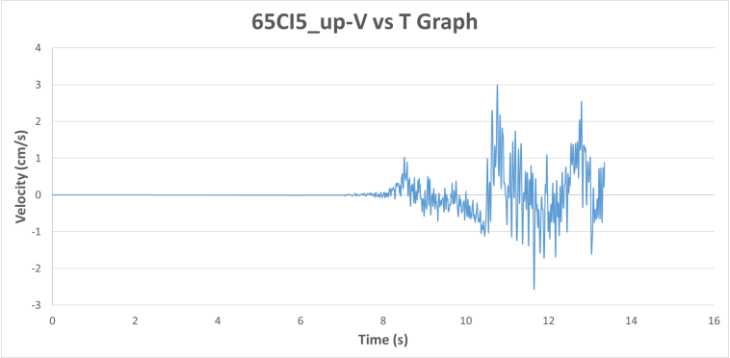

Figure A.170. Velocity vs Time Graph of Ground Motion named 65CI5_up

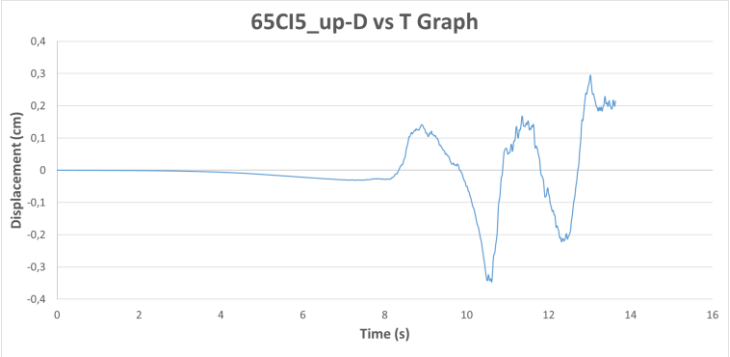

Figure A.171. Displacement vs Time Graph of Ground Motion named 65CI5_up

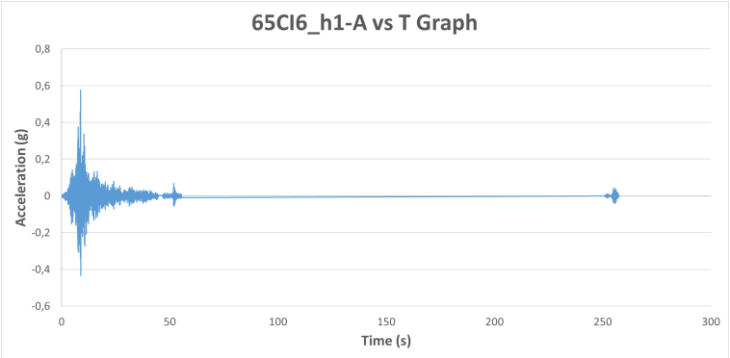

Figure A.172. Acceleration vs Time Graph of Ground Motion named 65CI6_h1

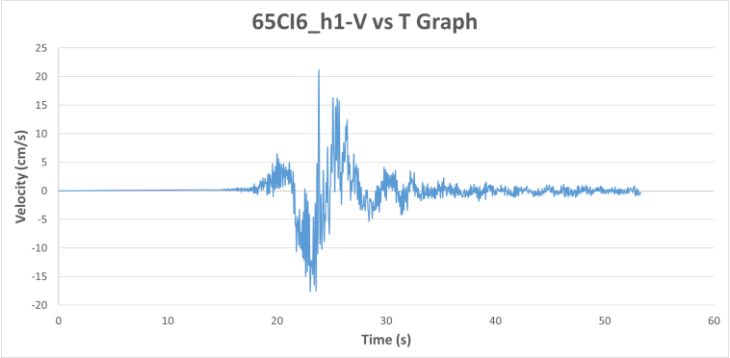

Figure A.173. Velocity vs Time Graph of Ground Motion named 65CI6_h1

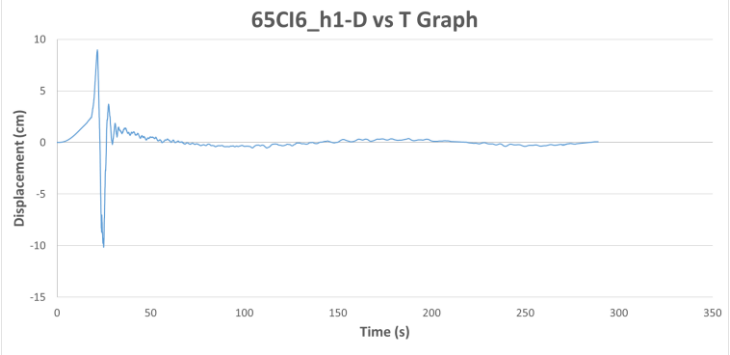

Figure A.174. Displacement vs Time Graph of Ground Motion named 65CI6_h1

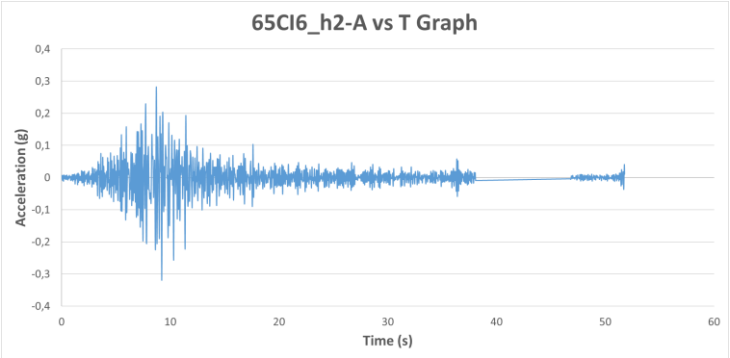

Figure A.175. Acceleration vs Time Graph of Ground Motion named 65CI6_h2

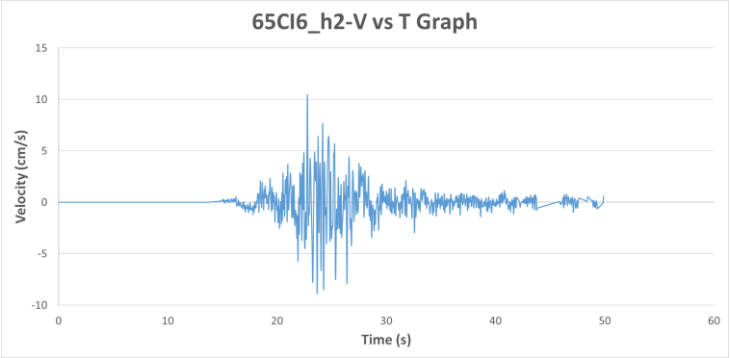

Figure A.176. Velocity vs Time Graph of Ground Motion named 65CI6_h2

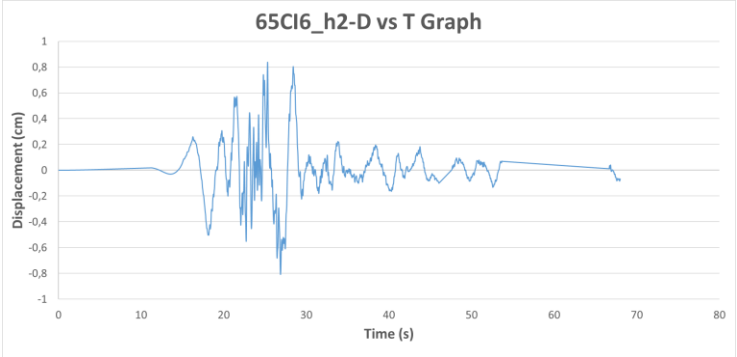

Figure A.177. Displacement vs Time Graph of Ground Motion named 65CI6_h2

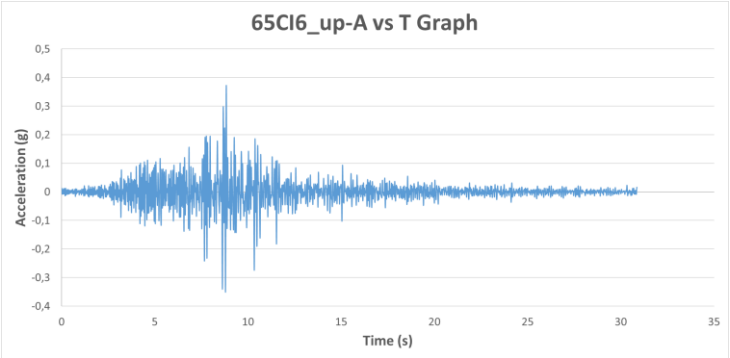

Figure A.178. Acceleration vs Time Graph of Ground Motion named 65CI6_up

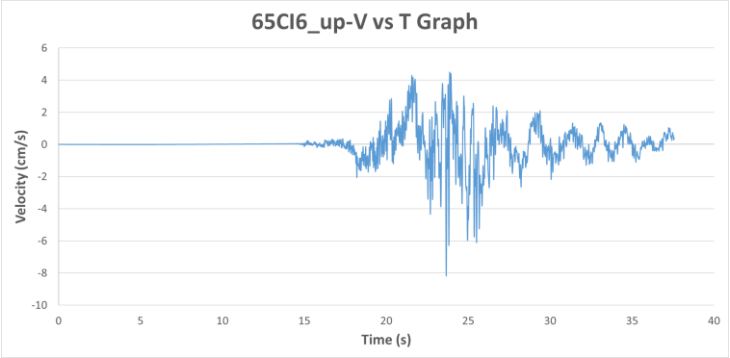

Figure A.179. Velocity vs Time Graph of Ground Motion named 65CI6_up

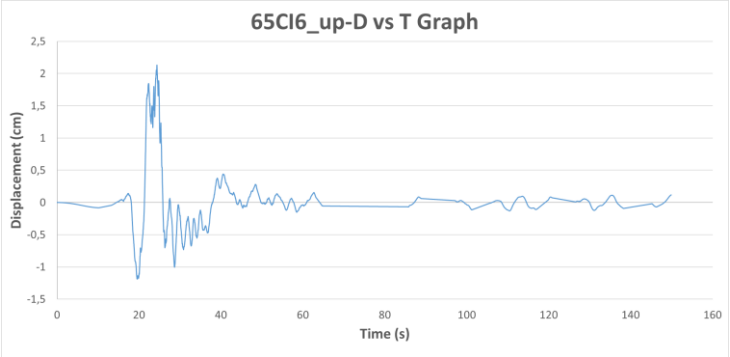

Figure A.180. Displacement vs Time Graph of Ground Motion named 65CI6_up

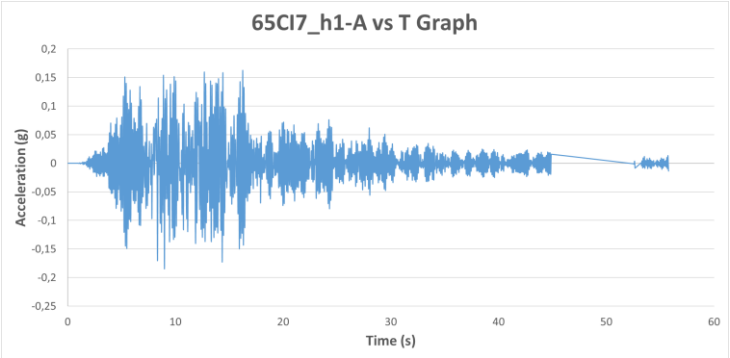

Figure A.181. Acceleration vs Time Graph of Ground Motion named 65CI7_h1

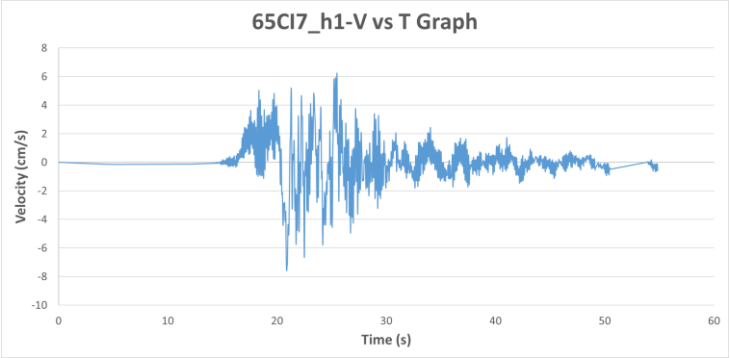

Figure A.182. Velocity vs Time Graph of Ground Motion named 65CI7_h1

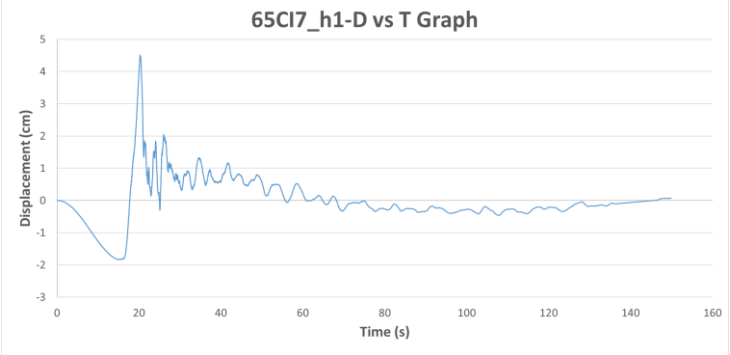

Figure A.183. Displacement vs Time Graph of Ground Motion named 65CI7_h1

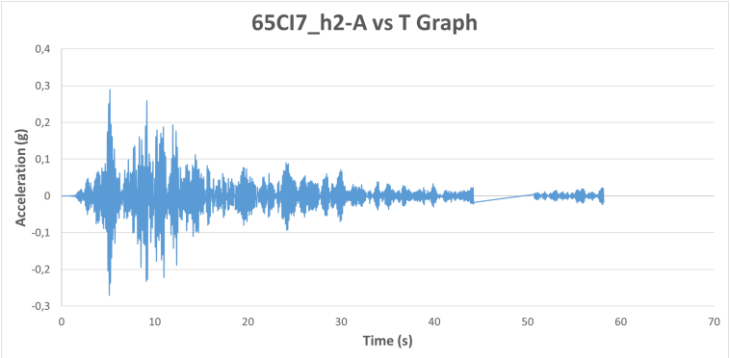

Figure A.184. Acceleration vs Time Graph of Ground Motion named 65CI7_h2

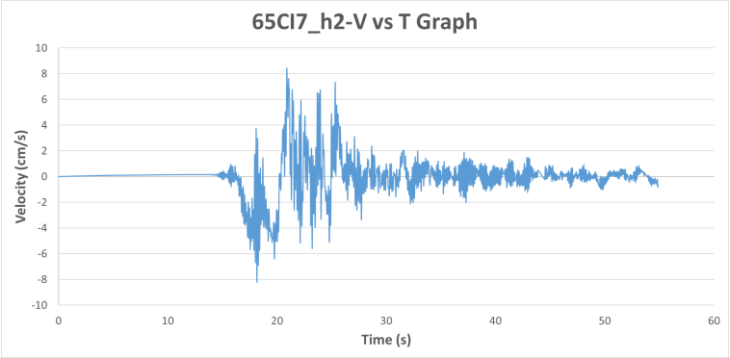

Figure A.185. Velocity vs Time Graph of Ground Motion named 65CI7_h2

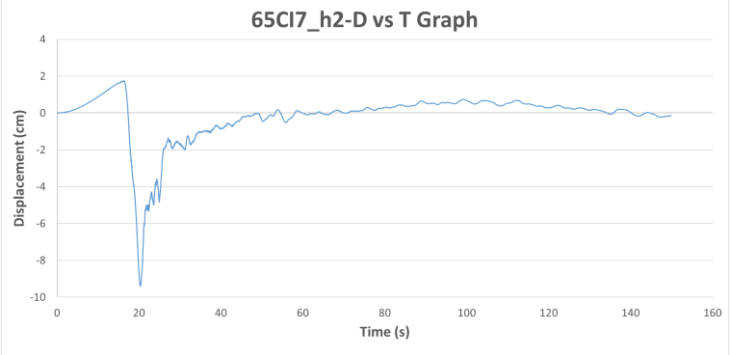

Figure A.186. Displacement vs Time Graph of Ground Motion named 65CI7_h2

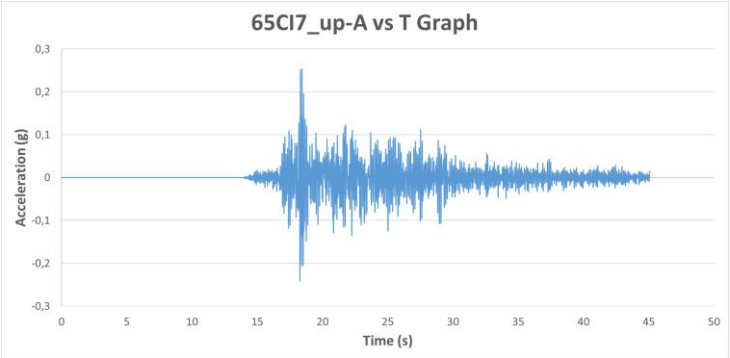

Figure A.187. Acceleration vs Time Graph of Ground Motion named 65CI7_up

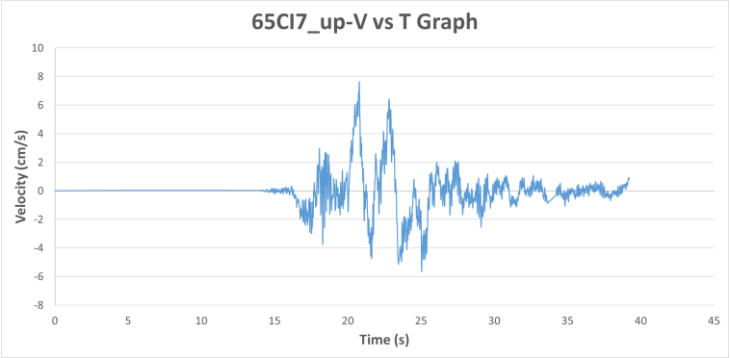

Figure A.188. Velocity vs Time Graph of Ground Motion named 65CI7_up

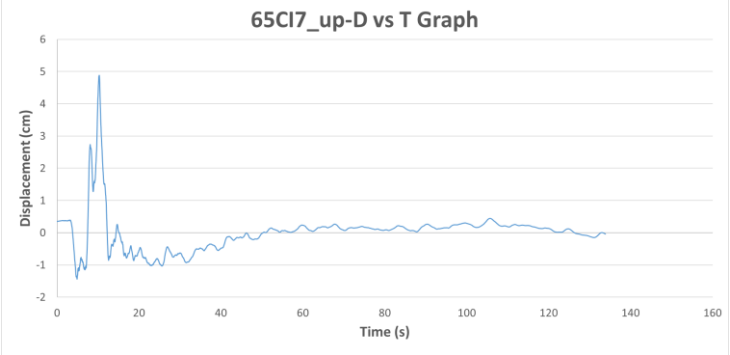

Figure A.189. Displacement vs Time Graph of Ground Motion named 65CI7_up

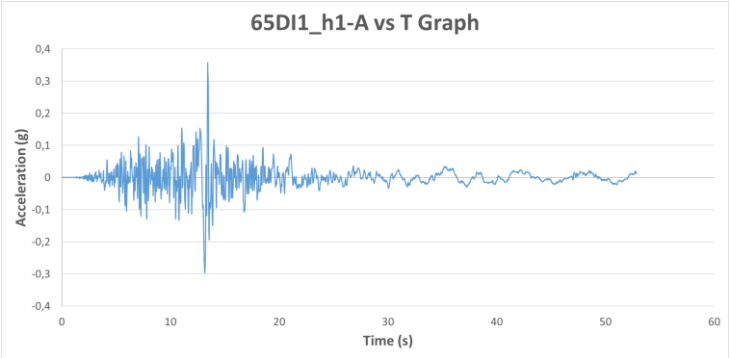

Figure A.190. Acceleration vs Time Graph of Ground Motion named 65DI1_h1

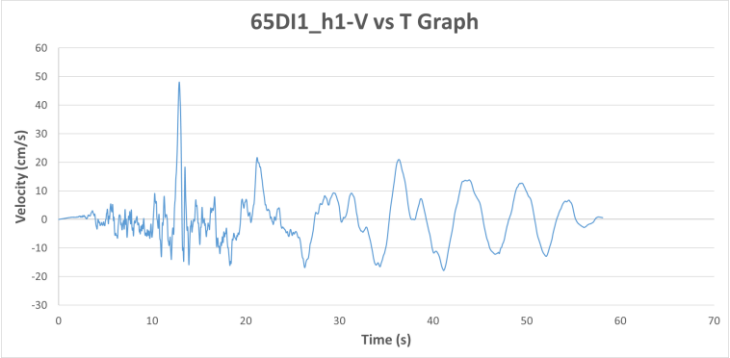

Figure A.191. Velocity vs Time Graph of Ground Motion named 65DI1_h1

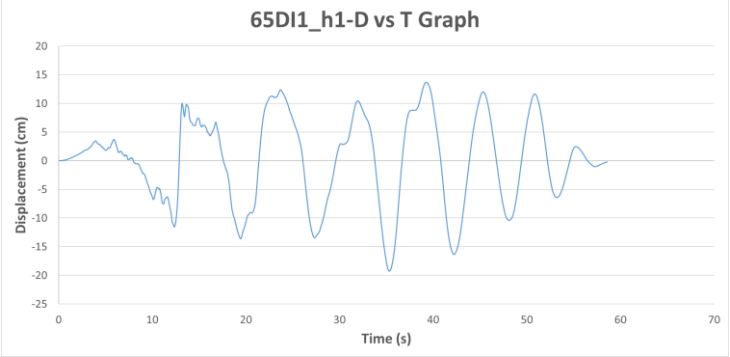

Figure A.192. Displacement vs Time Graph of Ground Motion named 65DI1_h1

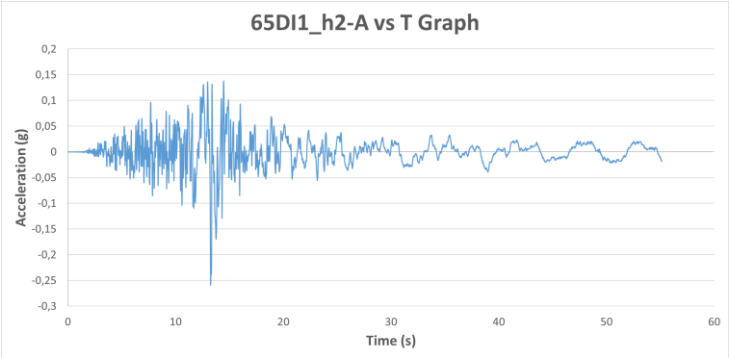

Figure A.193. Acceleration vs Time Graph of Ground Motion named 65DI1_h2

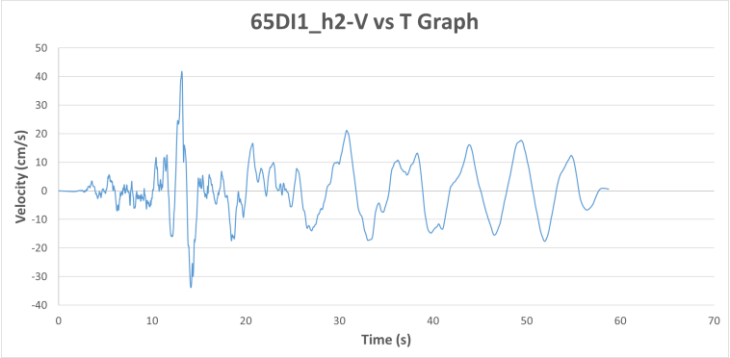

Figure A.194. Velocity vs Time Graph of Ground Motion named 65DI1_h2

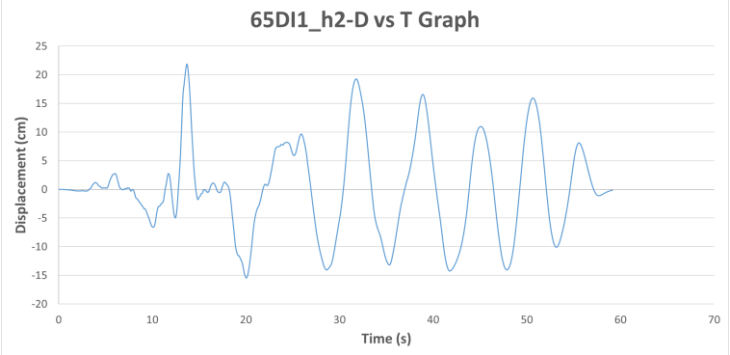

Figure A.195. Displacement vs Time Graph of Ground Motion named 65DI1_h2

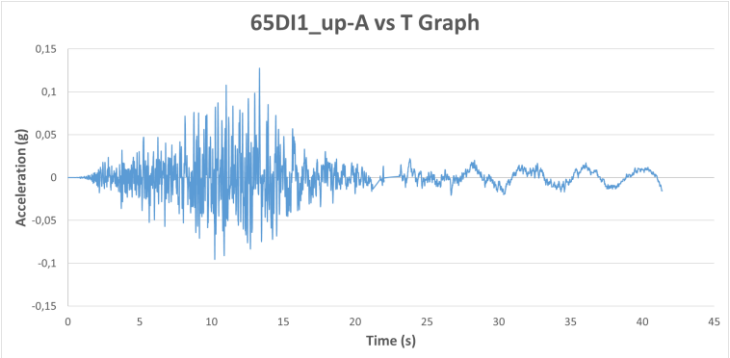

Figure A.196. Acceleration vs Time Graph of Ground Motion named 65DI1_up

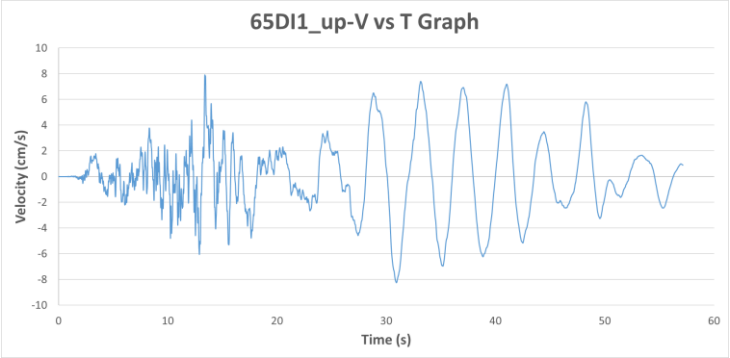

Figure A.197. Velocity vs Time Graph of Ground Motion named 65DI1_up

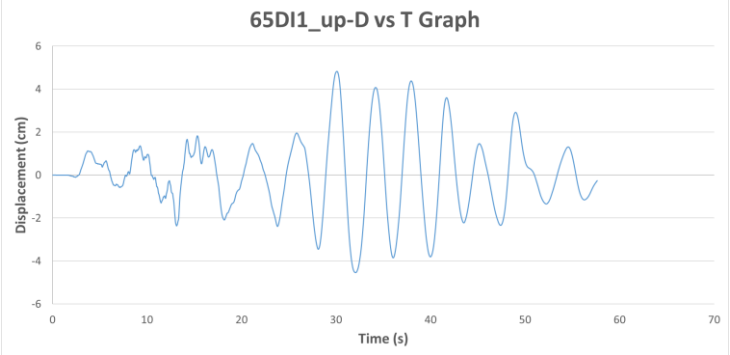

Figure A.198. Displacement vs Time Graph of Ground Motion named 65DI1_up

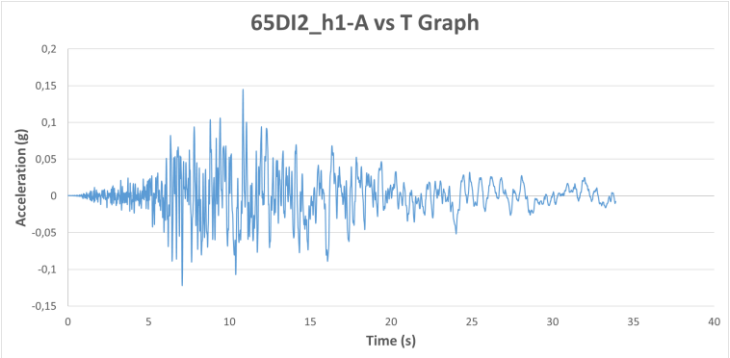

Figure A.199. Acceleration vs Time Graph of Ground Motion named 65DI2_h1

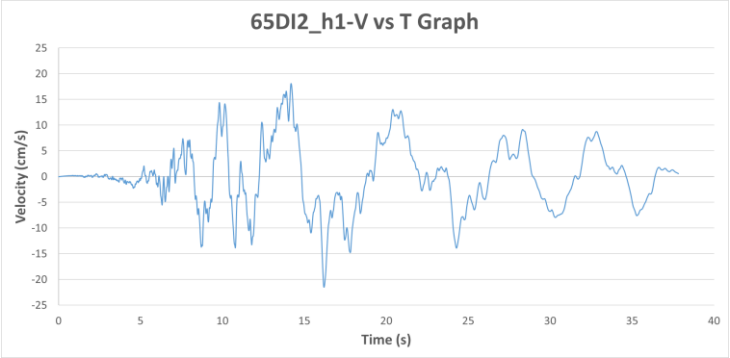

Figure A.200. Velocity vs Time Graph of Ground Motion named 65DI2_h1

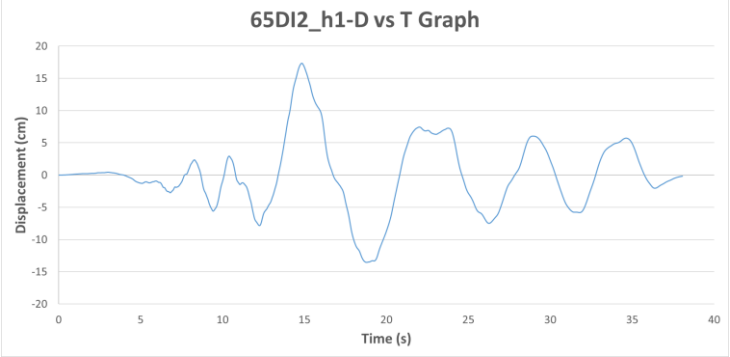

Figure A.201. Displacement vs Time Graph of Ground Motion named 65DI2_h1

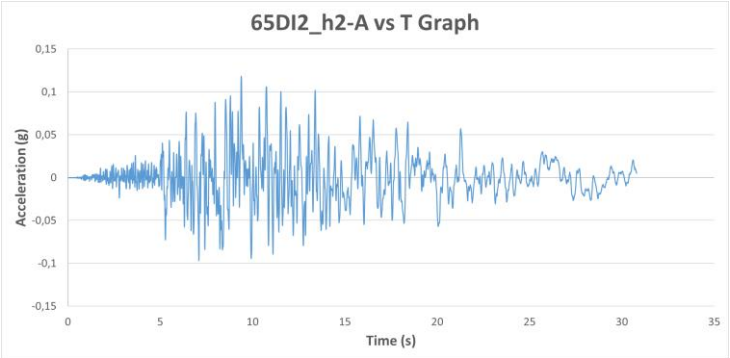

Figure A.202. Acceleration vs Time Graph of Ground Motion named 65DI2_h2

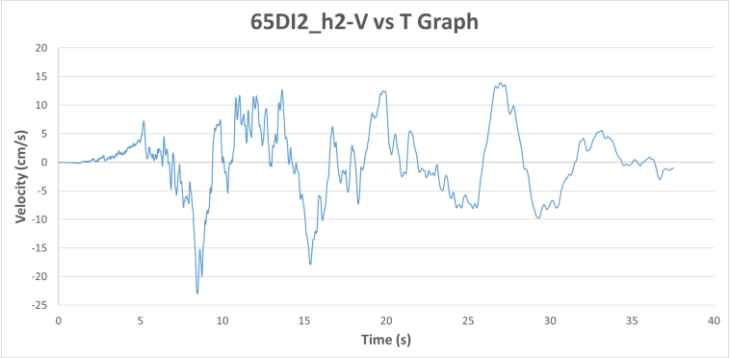

Figure A.203. Velocity vs Time Graph of Ground Motion named 65DI2_h2

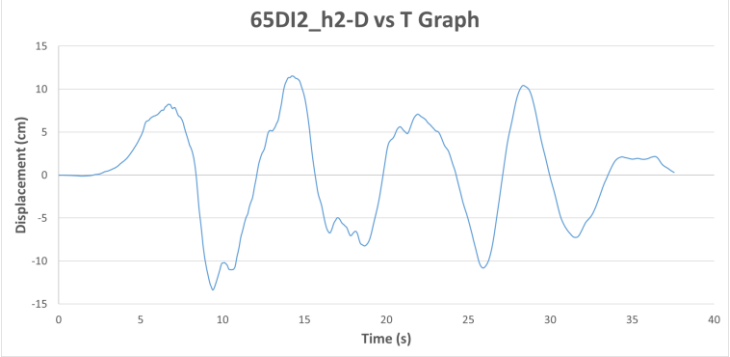

Figure A.204. Displacement vs Time Graph of Ground Motion named 65DI2_h2

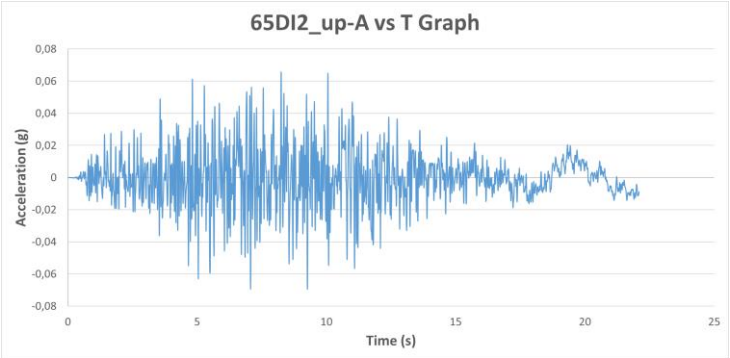

Figure A.205. Acceleration vs Time Graph of Ground Motion named 65DI2_up

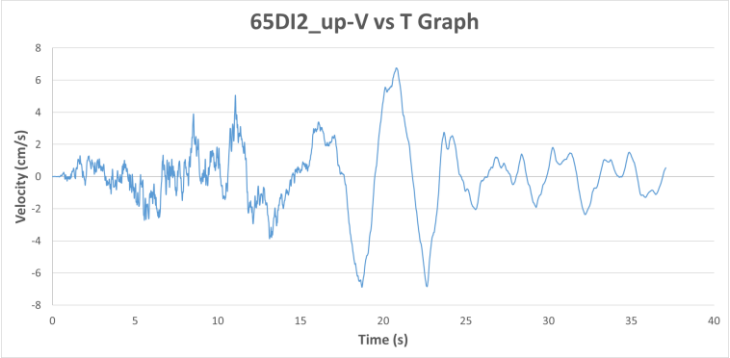

Figure A.206. Velocity vs Time Graph of Ground Motion named 65DI2_up

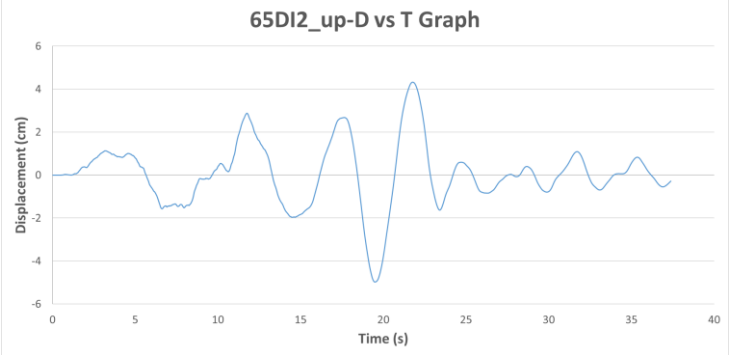

Figure A.207. Displacement vs Time Graph of Ground Motion named 65DI2_up

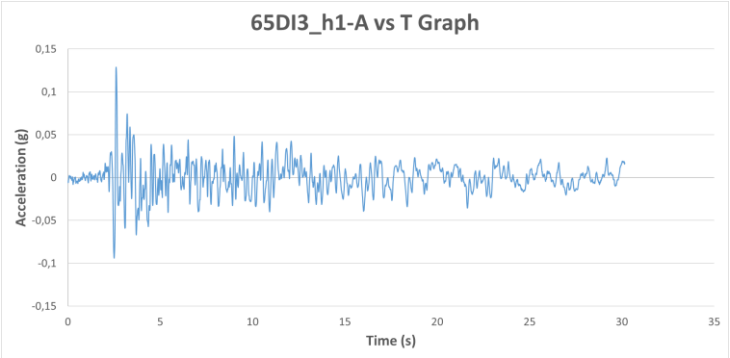

Figure A.208. Acceleration vs Time Graph of Ground Motion named 65DI3_h1

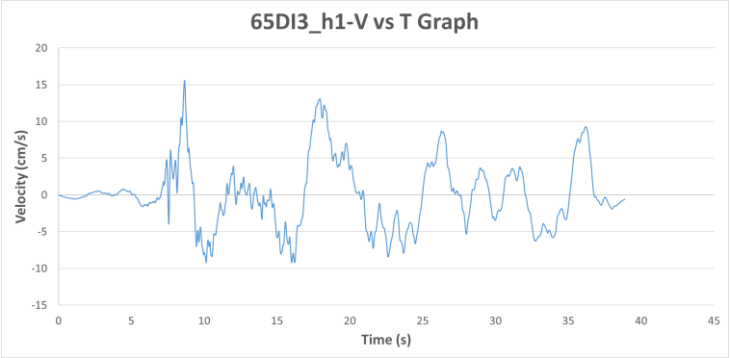

Figure A.209. Velocity vs Time Graph of Ground Motion named 65DI3_h1

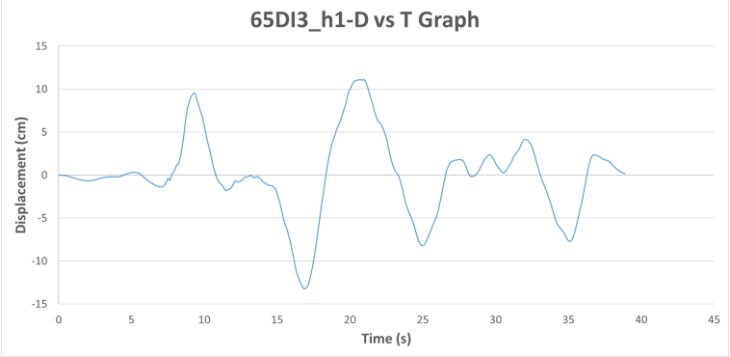

Figure A.210. Displacement vs Time Graph of Ground Motion named 65DI3_h1

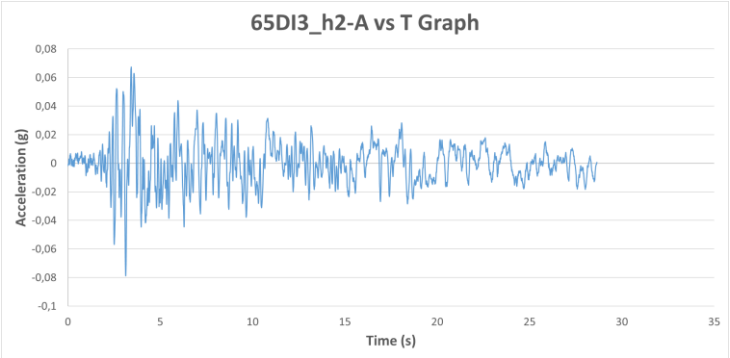

Figure A.211. Acceleration vs Time Graph of Ground Motion named 65DI3_h2

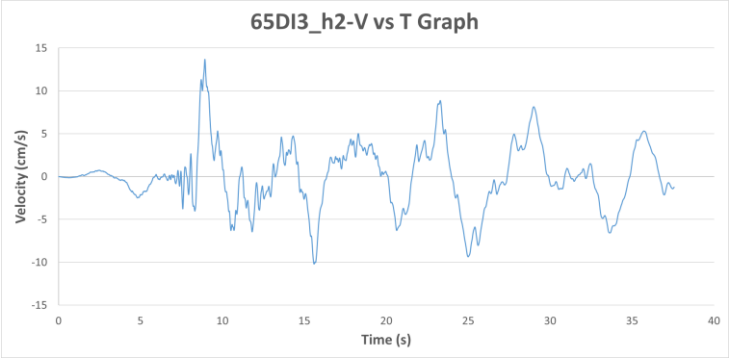

Figure A.212. Velocity vs Time Graph of Ground Motion named 65DI3_h2

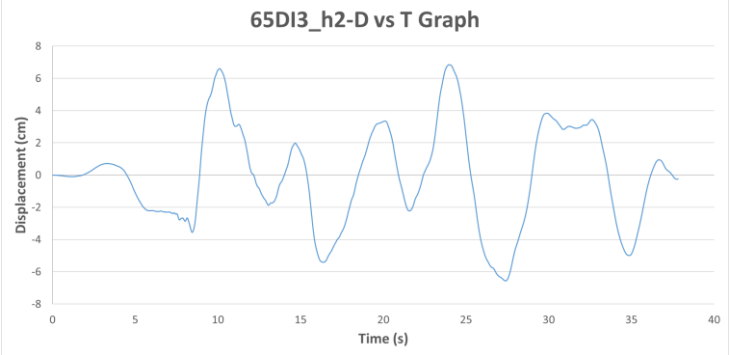

Figure A.213. Displacement vs Time Graph of Ground Motion named 65DI3_h2

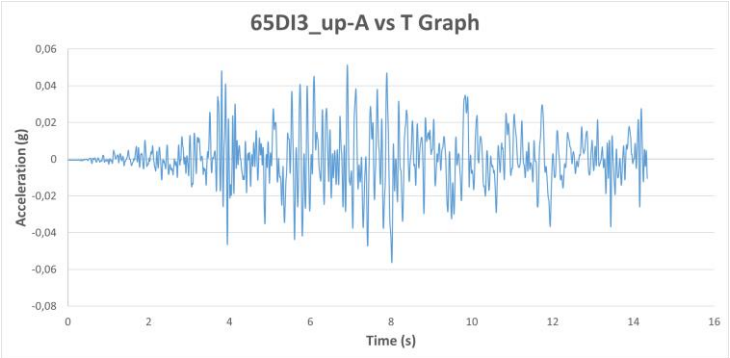

Figure A.214. Acceleration vs Time Graph of Ground Motion named 65DI3_up

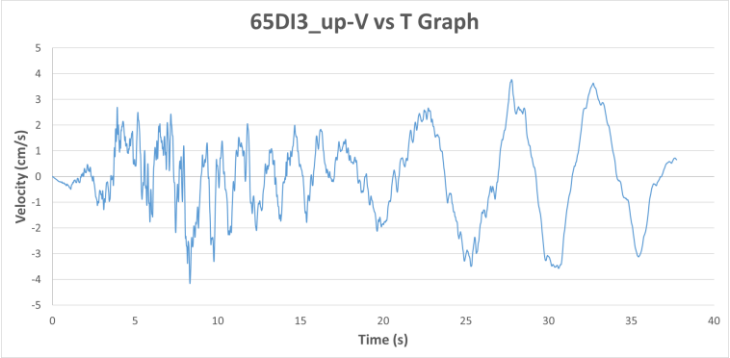

Figure A.215. Velocity vs Time Graph of Ground Motion named 65DI3_up

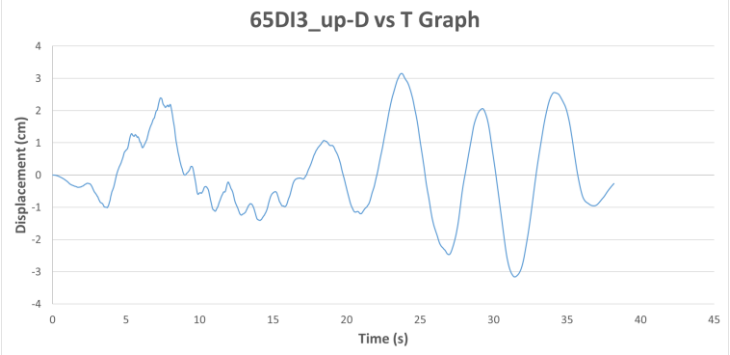

Figure A.216. Displacement vs Time Graph of Ground Motion named 65DI3_up

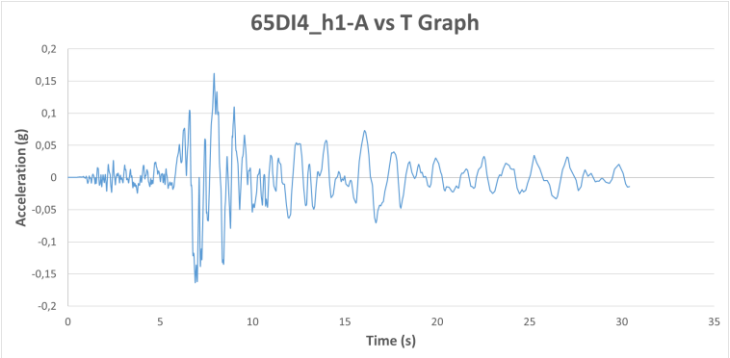

Figure A.217. Acceleration vs Time Graph of Ground Motion named 65DI4_h1

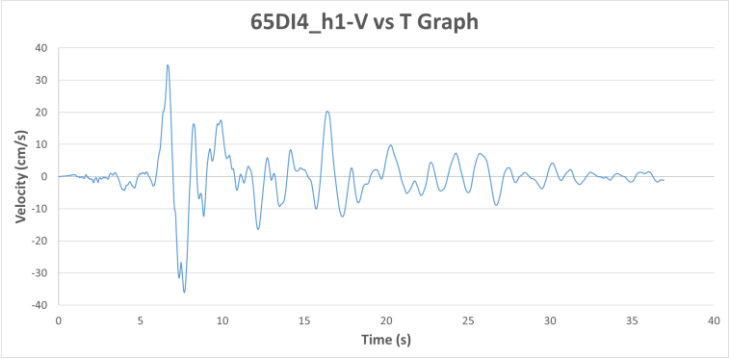

Figure A.218. Velocity vs Time Graph of Ground Motion named 65DI4_h1

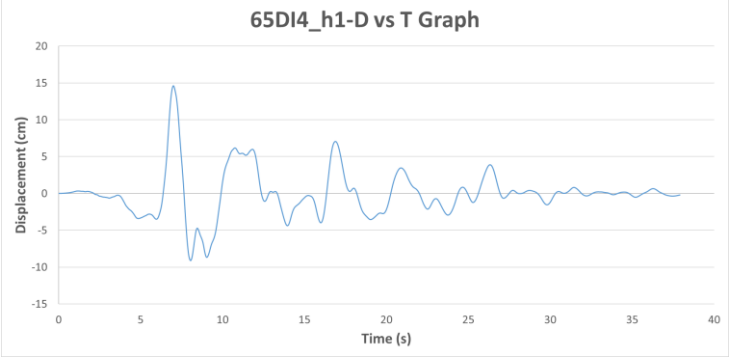

Figure A.219. Displacement vs Time Graph of Ground Motion named 65DI4_h1

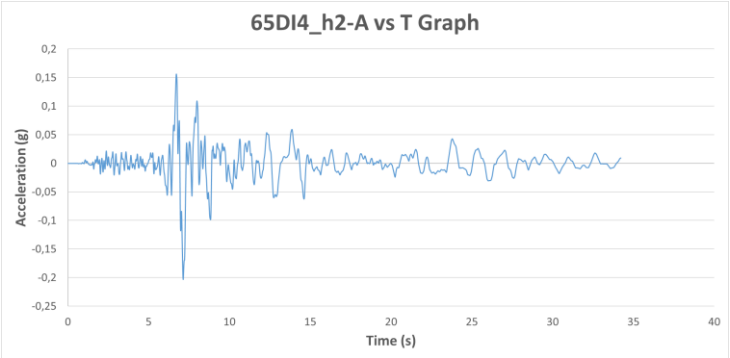

Figure A.220. Acceleration vs Time Graph of Ground Motion named 65DI4_h2

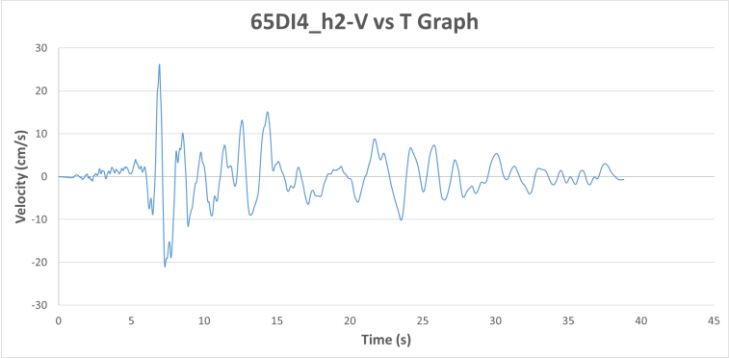

Figure A.221. Velocity vs Time Graph of Ground Motion named 65DI4_h2

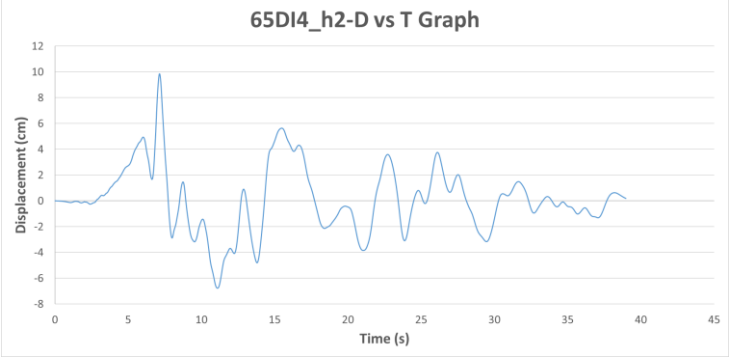

Figure A.222. Displacement vs Time Graph of Ground Motion named 65DI4_h2

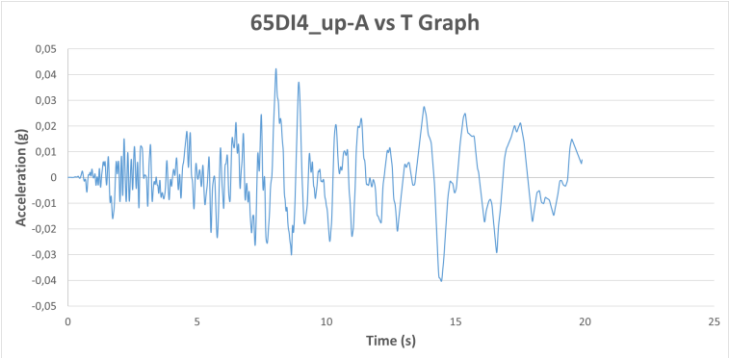

Figure A.223. Acceleration vs Time Graph of Ground Motion named 65DI4_up

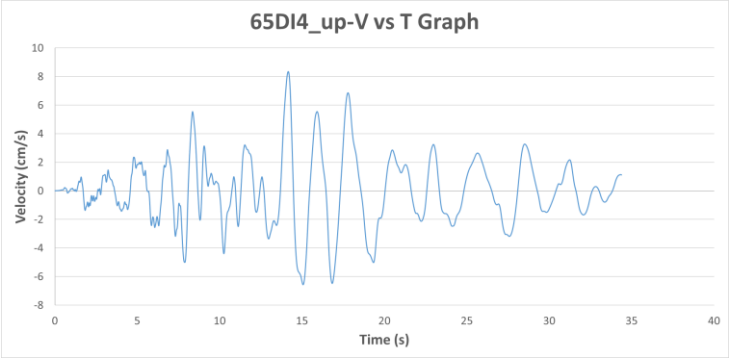

Figure A.224. Velocity vs Time Graph of Ground Motion named 65DI4_up

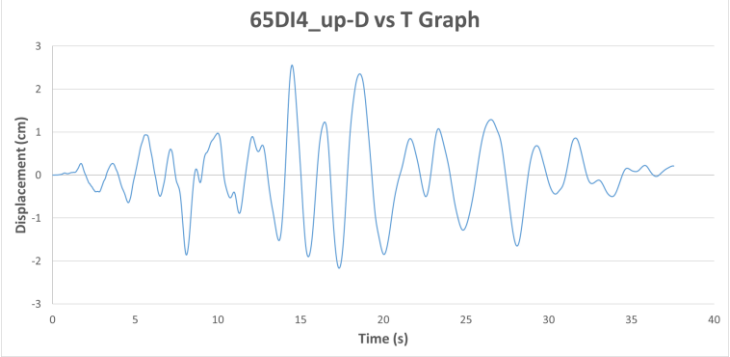

Figure A.225. Displacement vs Time Graph of Ground Motion named 65DI4_up

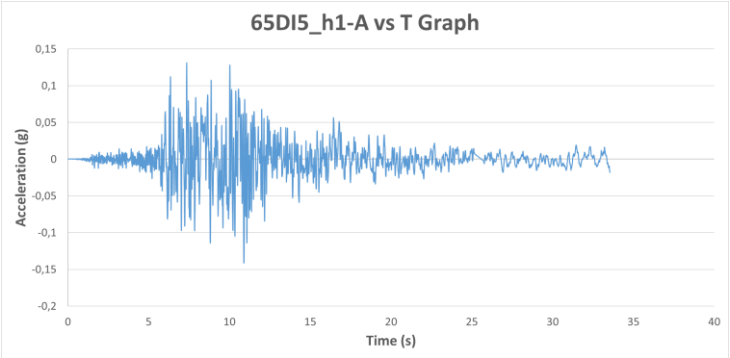

Figure A.226. Acceleration vs Time Graph of Ground Motion named 65DI5_h1

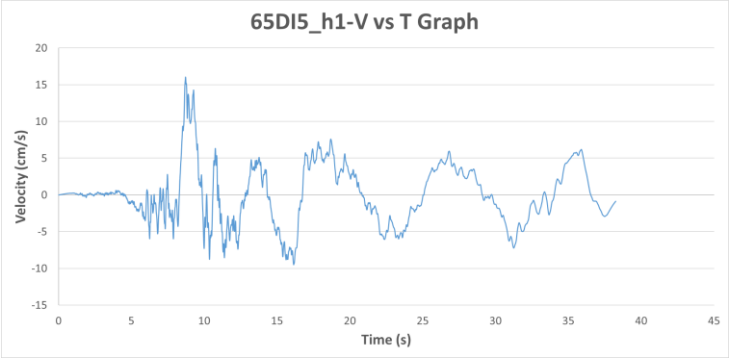

Figure A.227. Velocity vs Time Graph of Ground Motion named 65DI5_h1

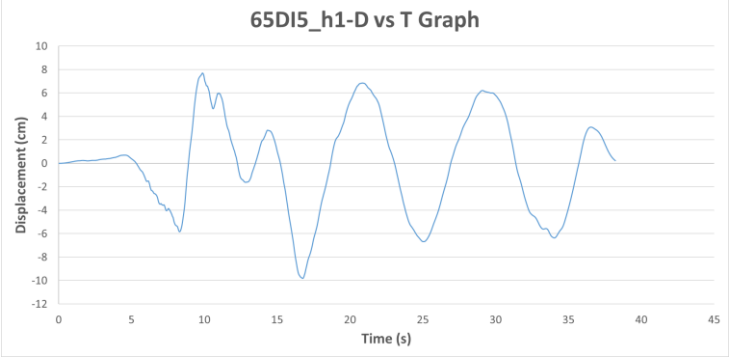

Figure A.228. Displacement vs Time Graph of Ground Motion named 65DI5_h1

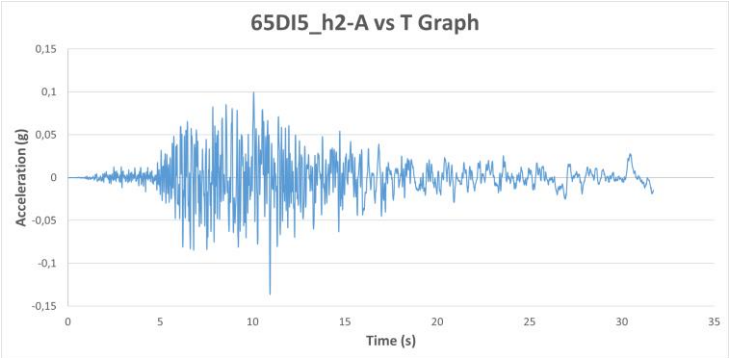

Figure A.229. Acceleration vs Time Graph of Ground Motion named 65DI5_h2

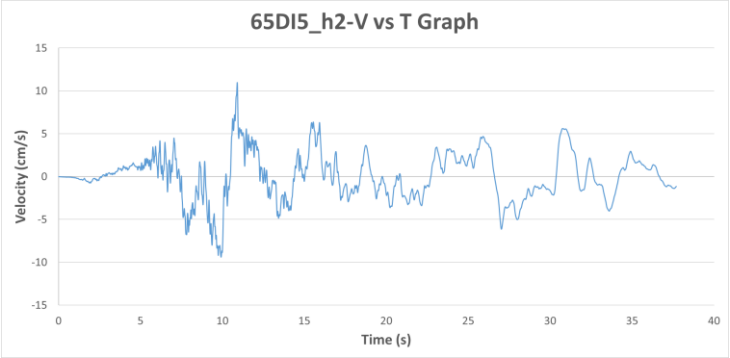

Figure A.230. Velocity vs Time Graph of Ground Motion named 65DI5_h2

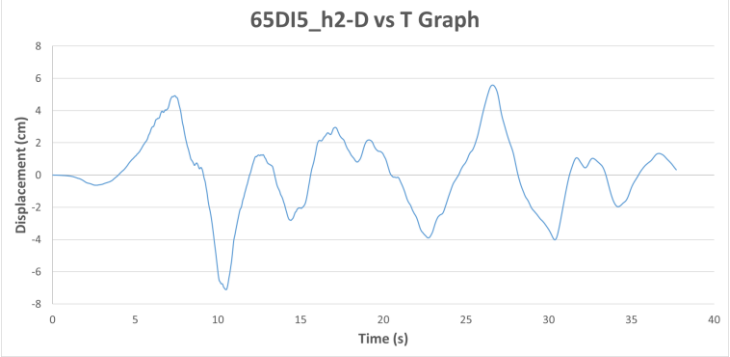

Figure A.231. Displacement vs Time Graph of Ground Motion named 65DI5_h2

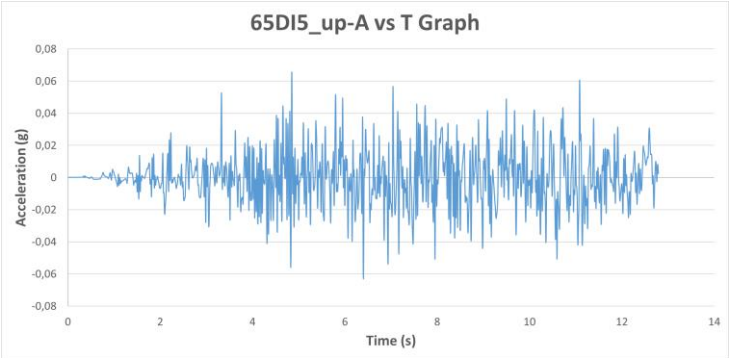

Figure A.232. Acceleration vs Time Graph of Ground Motion named 65DI5_up

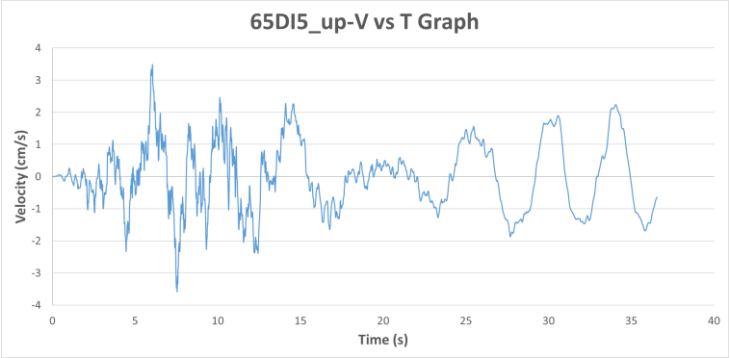

Figure A.233. Velocity vs Time Graph of Ground Motion named 65DI5_up

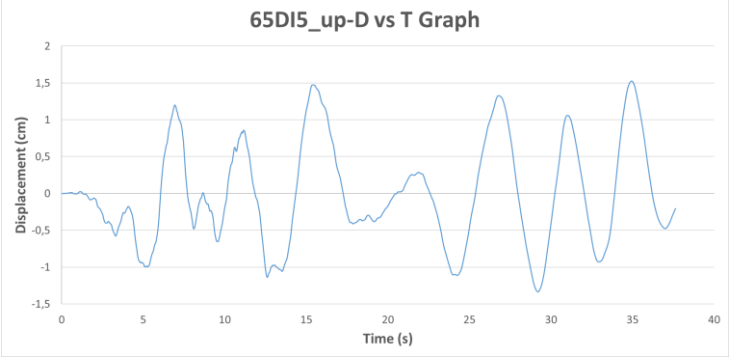

Figure A.234. Displacement vs Time Graph of Ground Motion named 65DI5_up

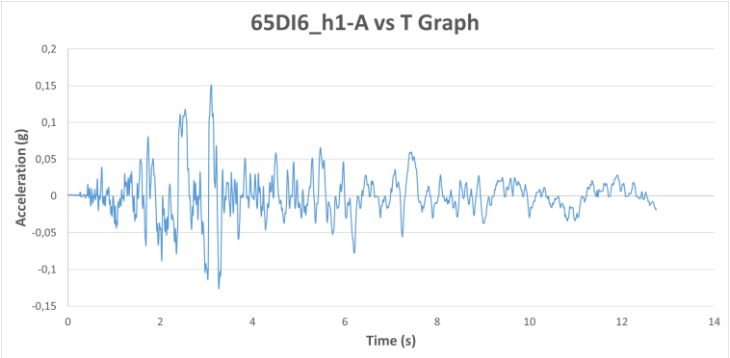

Figure A.235. Acceleration vs Time Graph of Ground Motion named 65DI6_h1

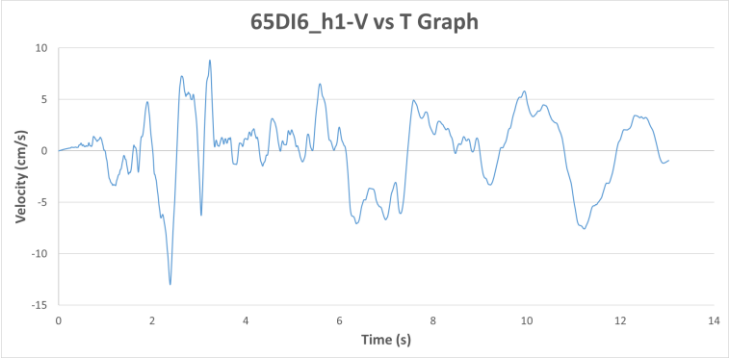

Figure A.236. Velocity vs Time Graph of Ground Motion named 65DI6_h1

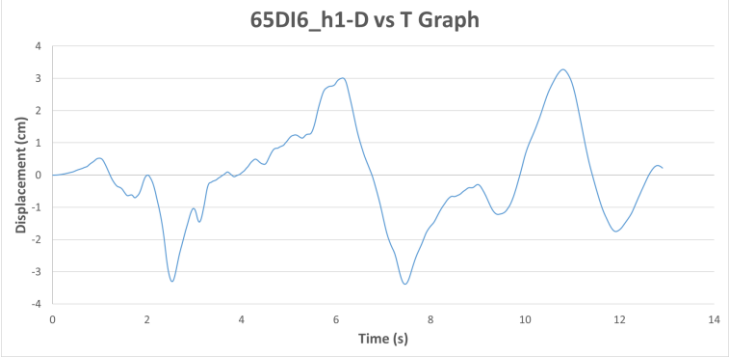

Figure A.237. Displacement vs Time Graph of Ground Motion named 65DI6_h1

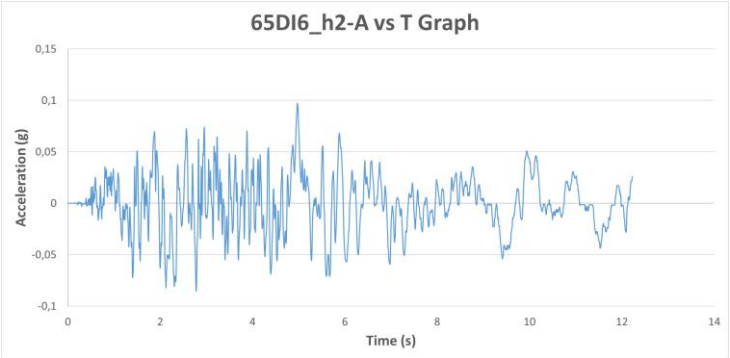

Figure A.238. Acceleration vs Time Graph of Ground Motion named 65DI6_h2

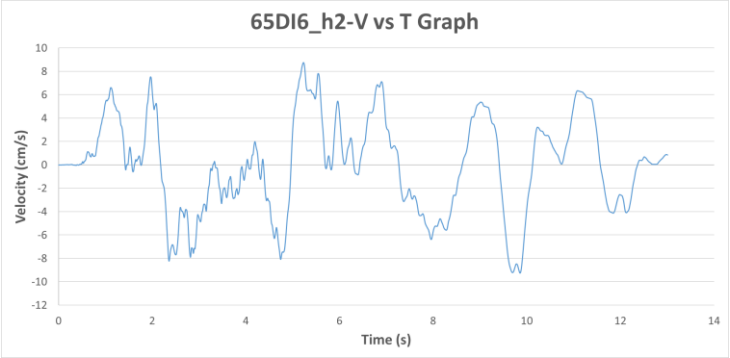

Figure A.239. Velocity vs Time Graph of Ground Motion named 65DI6_h2

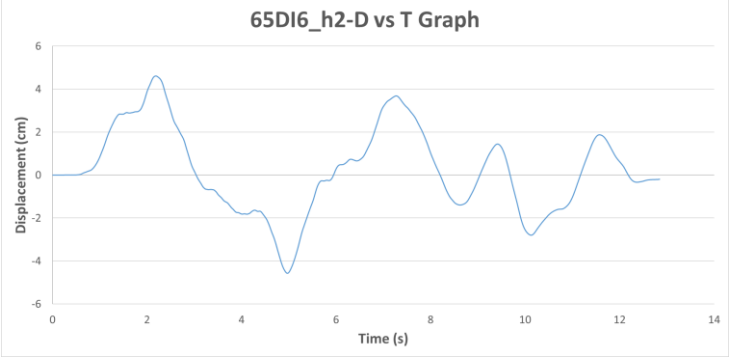

Figure A.240. Displacement vs Time Graph of Ground Motion named 65DI6_h2

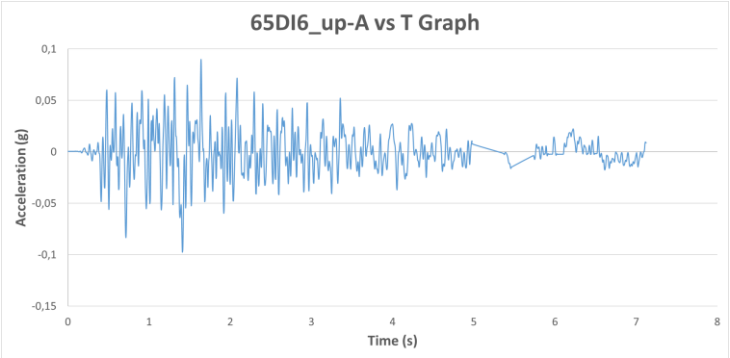

Figure A.241. Acceleration vs Time Graph of Ground Motion named 65DI6_up

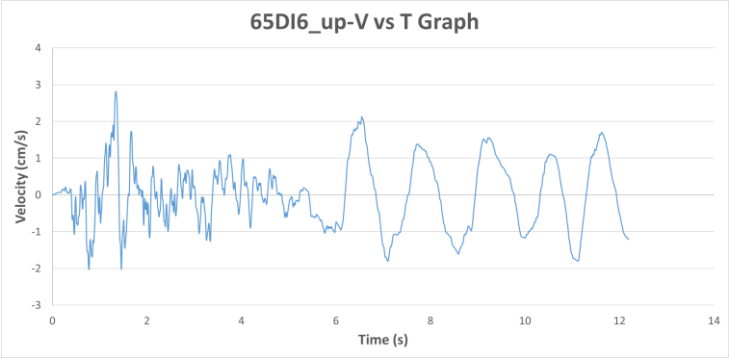

Figure A.242. Velocity vs Time Graph of Ground Motion named 65DI6_up

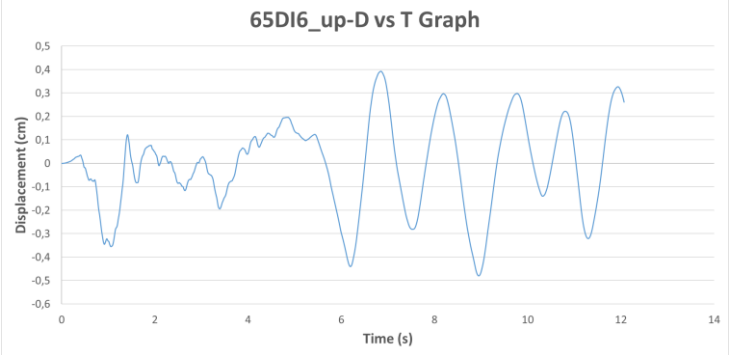

Figure A.243. Displacement vs Time Graph of Ground Motion named 65DI6_up

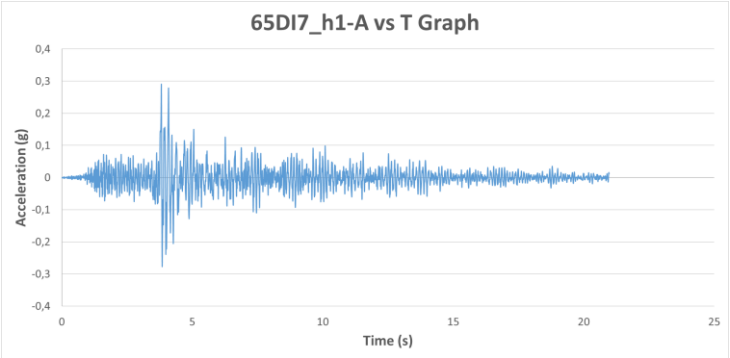

Figure A.244. Acceleration vs Time Graph of Ground Motion named 65DI7_h1

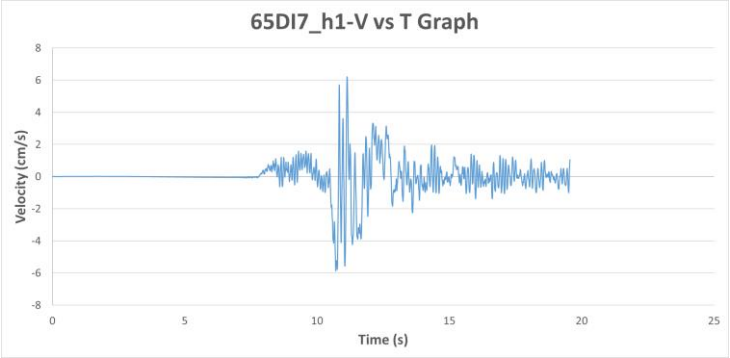

Figure A.245. Velocity vs Time Graph of Ground Motion named 65DI7_h1

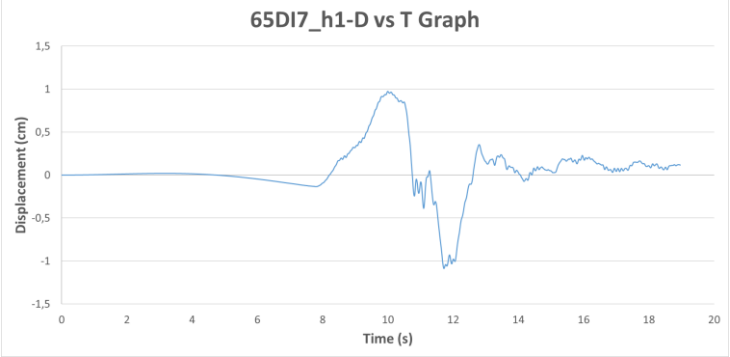

Figure A.246. Displacement vs Time Graph of Ground Motion named 65DI7_h1

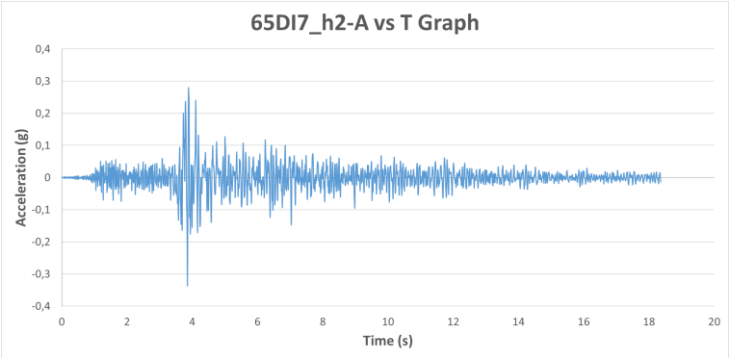

Figure A.247. Acceleration vs Time Graph of Ground Motion named 65DI7_h2

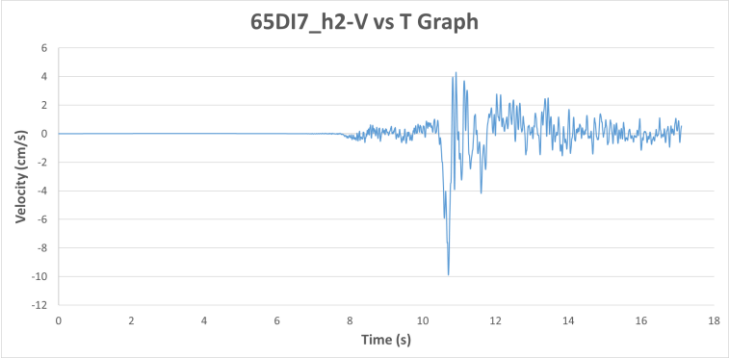

Figure A.248. Velocity vs Time Graph of Ground Motion named 65DI7_h2

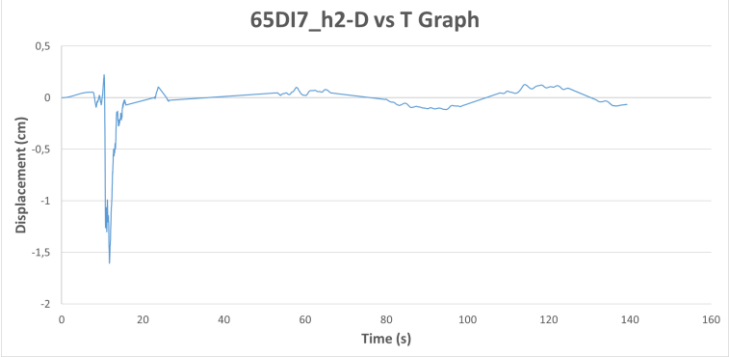

Figure A.249. Displacement vs Time Graph of Ground Motion named 65DI7_h2

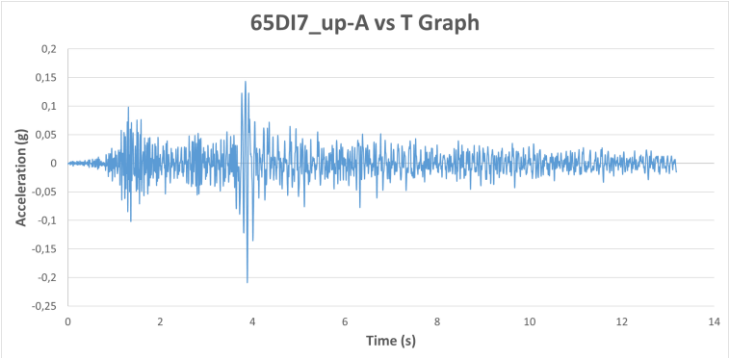

Figure A.250. Acceleration vs Time Graph of Ground Motion named 65DI7_up

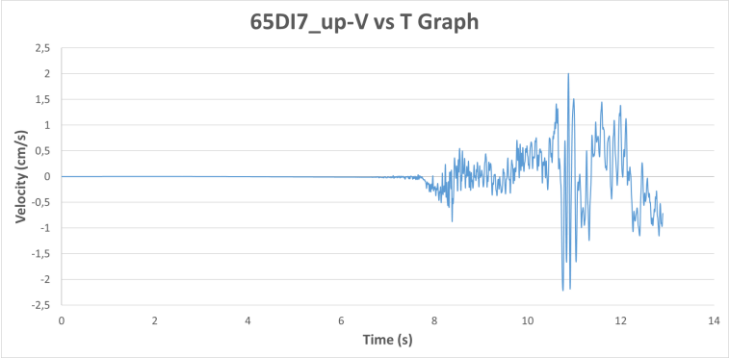

Figure A.251. Velocity vs Time Graph of Ground Motion named 65DI7_up

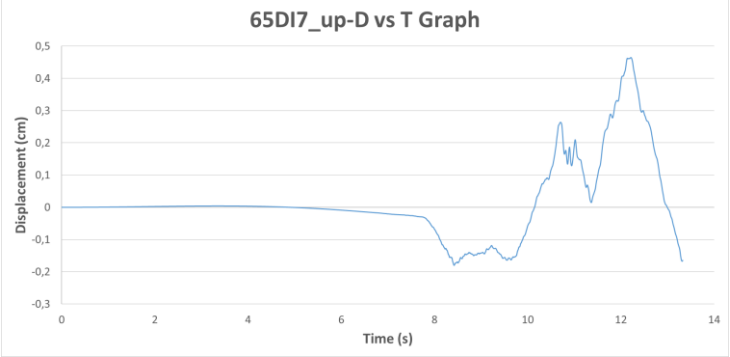

Figure A.252. Displacement vs Time Graph of Ground Motion named 65DI7_up

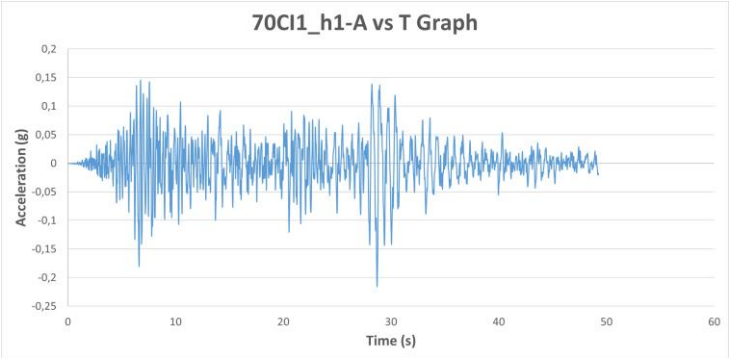

Figure A.253. Acceleration vs Time Graph of Ground Motion named 70CI1_h1

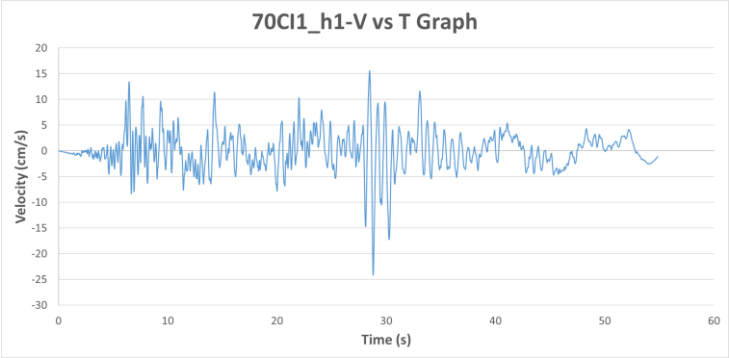

Figure A.254. Velocity vs Time Graph of Ground Motion named 70CI1_h1

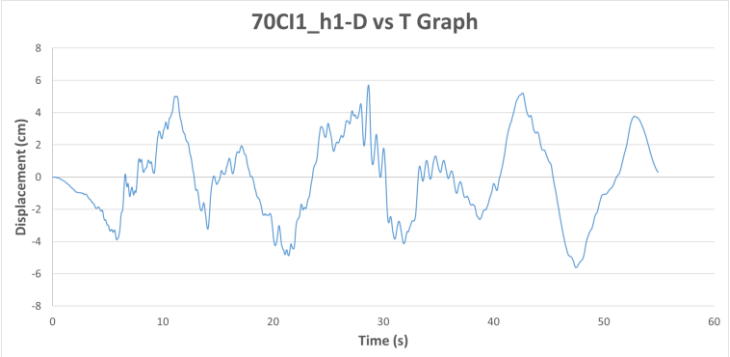

Figure A.255. Displacement vs Time Graph of Ground Motion named 70CI1_h1

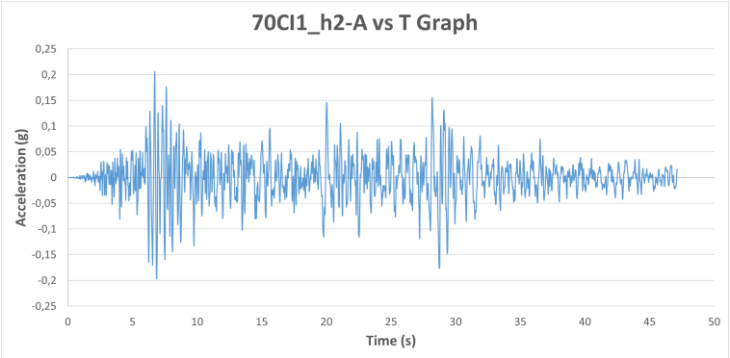

Figure A.256. Acceleration vs Time Graph of Ground Motion named 70CI1_h2

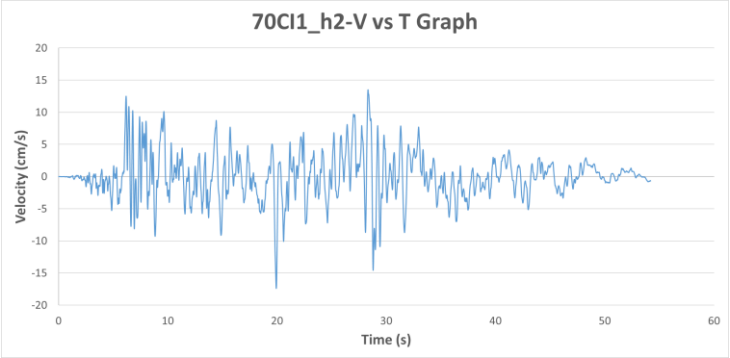

Figure A.257. Velocity vs Time Graph of Ground Motion named 70CI1_h2

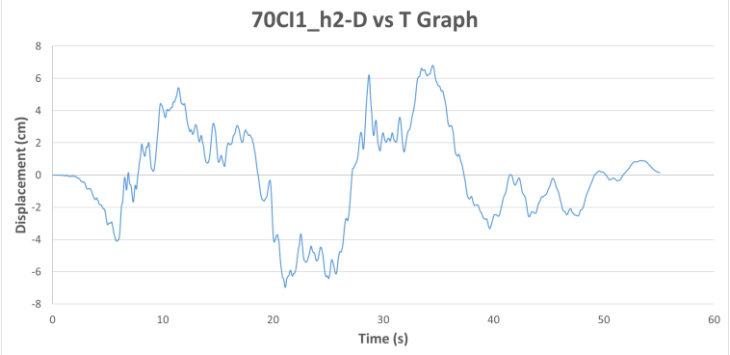

Figure A.258. Displacement vs Time Graph of Ground Motion named 70CI1_h2

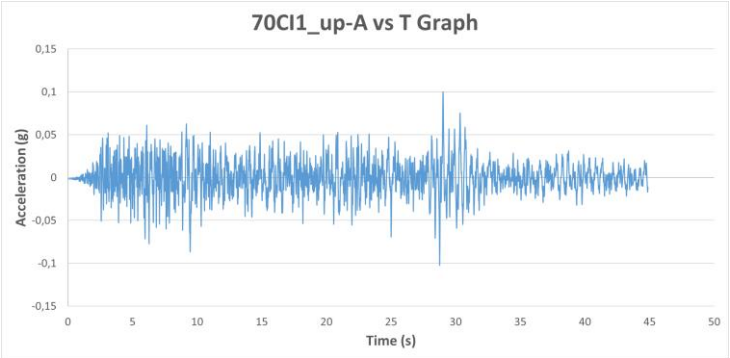

Figure A.259. Acceleration vs Time Graph of Ground Motion named 70CI1_up

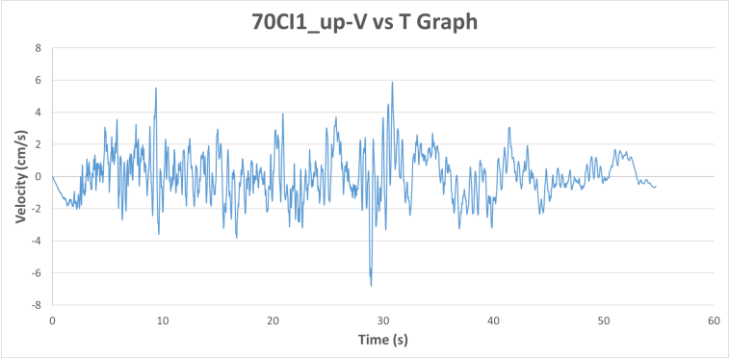

Figure A.260. Velocity vs Time Graph of Ground Motion named 70CI1_up

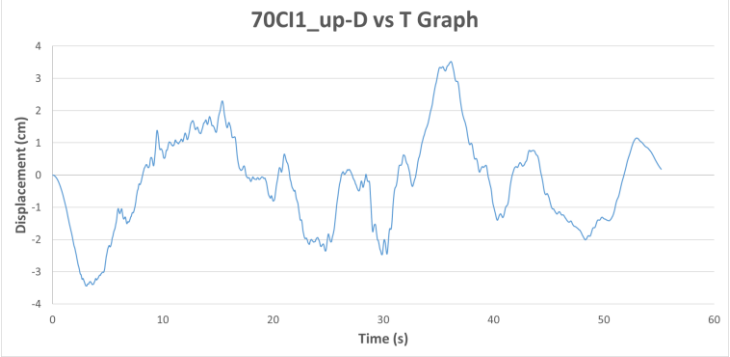

Figure A.261. Displacement vs Time Graph of Ground Motion named 70CI1_up

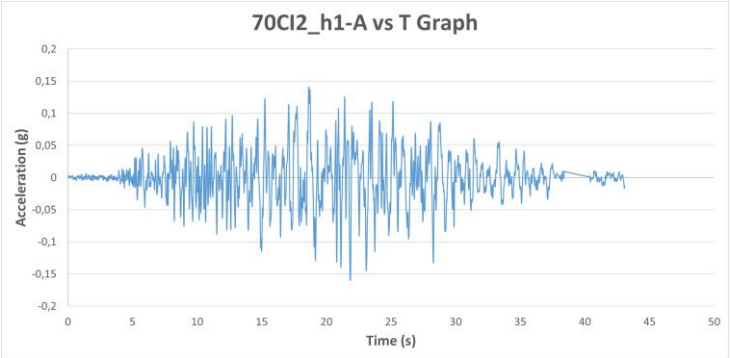

Figure A.262. Acceleration vs Time Graph of Ground Motion named 70CI2_h1

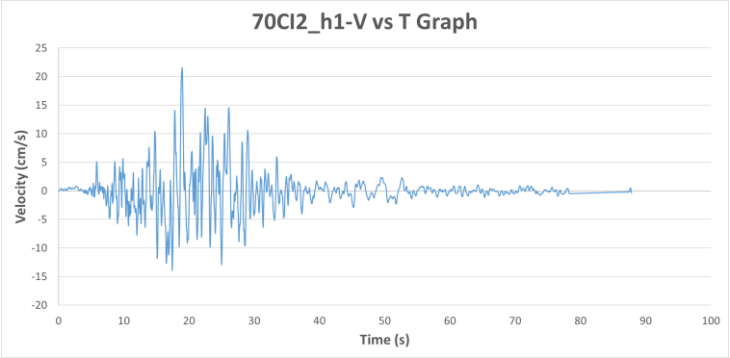

Figure A.263. Velocity vs Time Graph of Ground Motion named 70CI2_h1

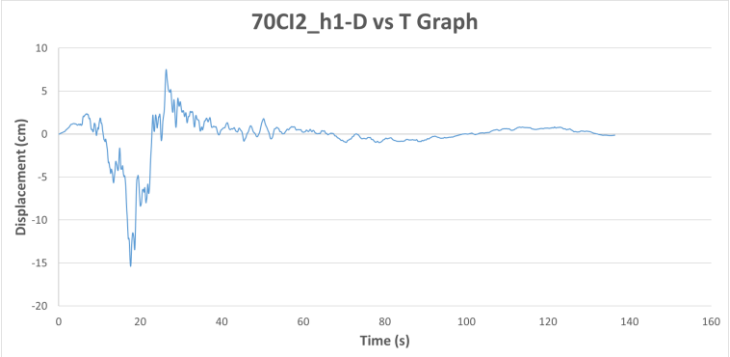

Figure A.264. Displacement vs Time Graph of Ground Motion named 70CI2_h1

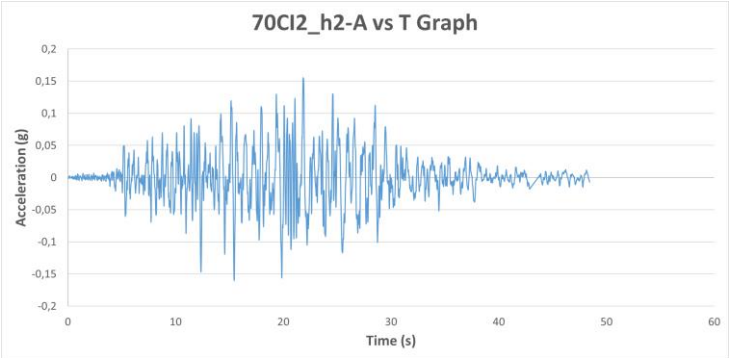

Figure A.265. Acceleration vs Time Graph of Ground Motion named 70CI2_h2

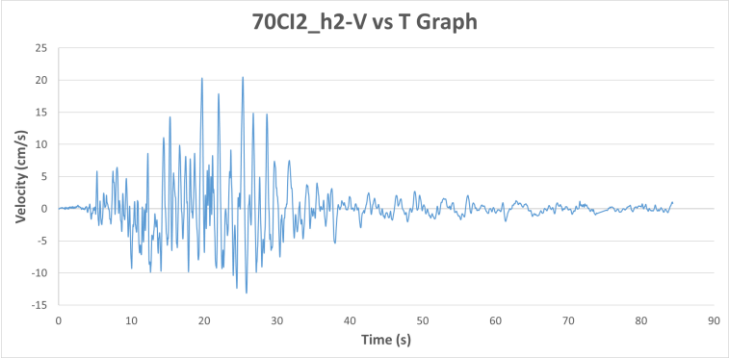

Figure A.266. Velocity vs Time Graph of Ground Motion named 70CI2_h2

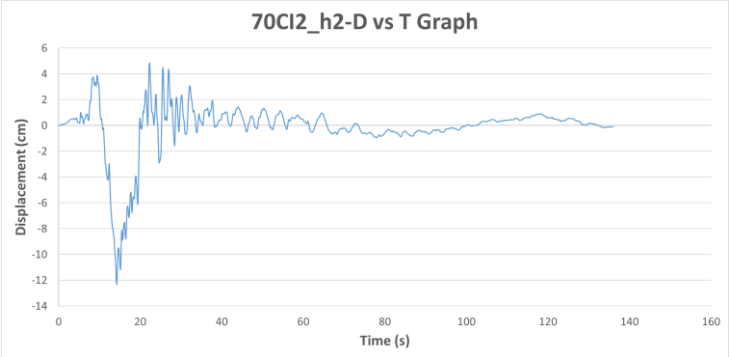

Figure A.267. Displacement vs Time Graph of Ground Motion named 70CI2_h2

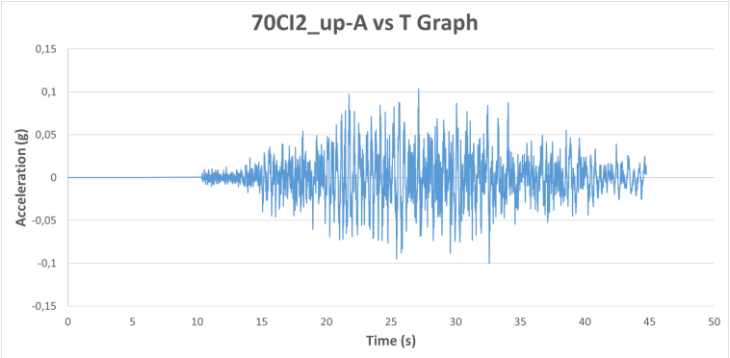

Figure A.268. Acceleration vs Time Graph of Ground Motion named 70CI2_up

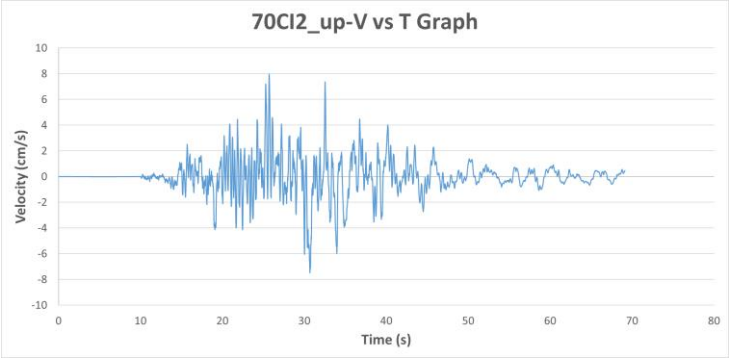

Figure A.269. Velocity vs Time Graph of Ground Motion named 70CI2_up

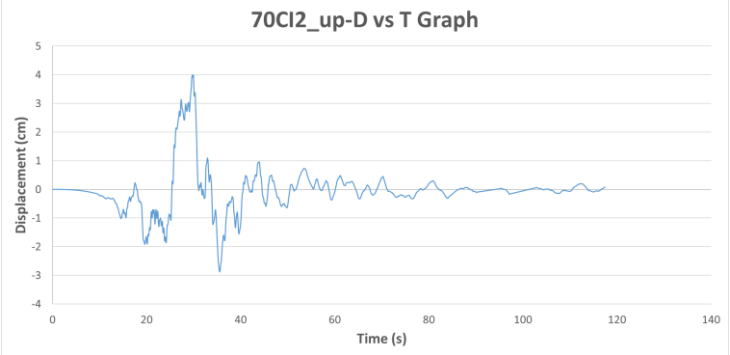

Figure A.270. Displacement vs Time Graph of Ground Motion named 70CI2_up

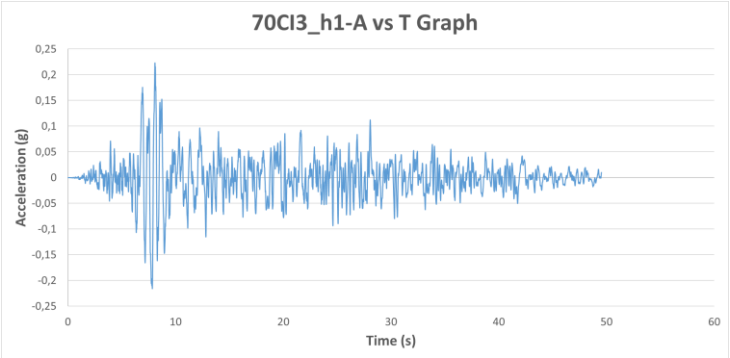

Figure A.271. Acceleration vs Time Graph of Ground Motion named 70CI3_h1

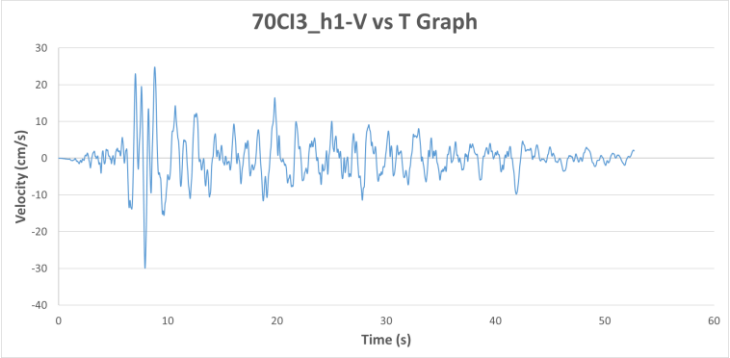

Figure A.272. Velocity vs Time Graph of Ground Motion named 70CI3_h1

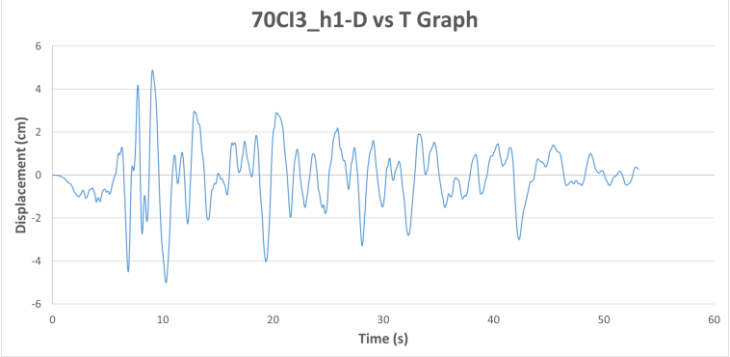

Figure A.273. Displacement vs Time Graph of Ground Motion named 70CI3_h1

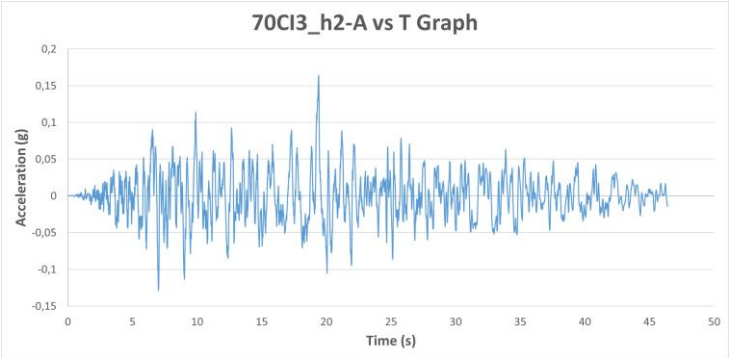

Figure A.274. Acceleration vs Time Graph of Ground Motion named 70CI3_h2

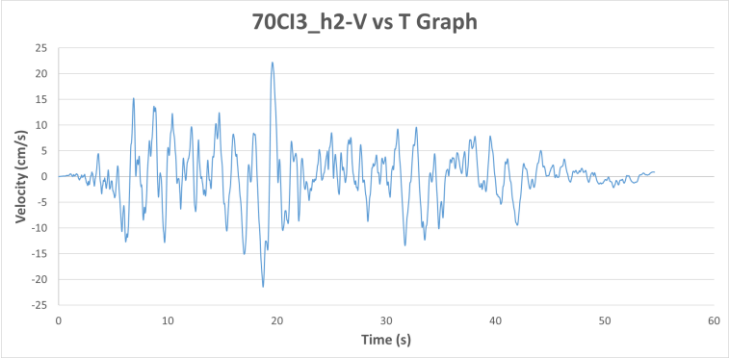

Figure A.275. Velocity vs Time Graph of Ground Motion named 70CI3_h2

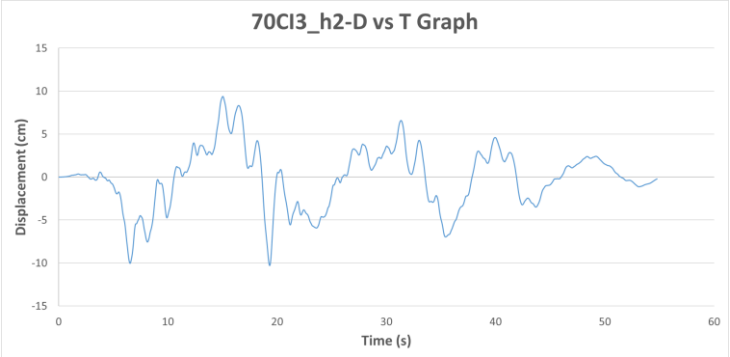

Figure A.276. Displacement vs Time Graph of Ground Motion named 70CI3_h2

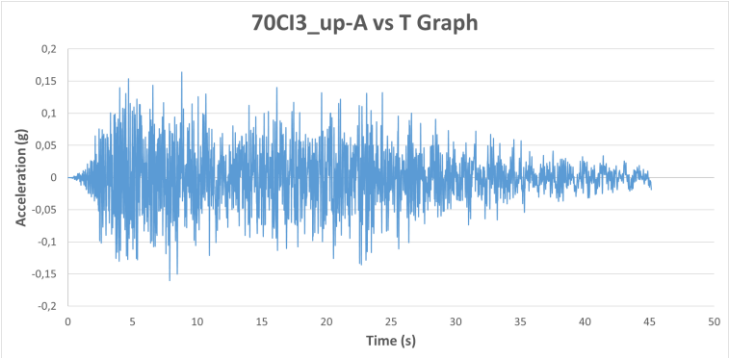

Figure A.277. Acceleration vs Time Graph of Ground Motion named 70CI3_up

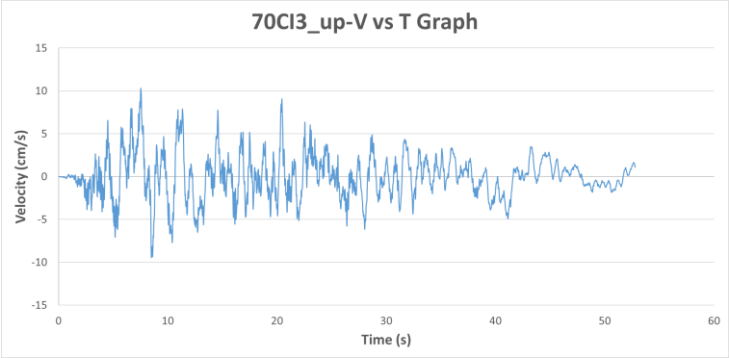

Figure A.278. Velocity vs Time Graph of Ground Motion named 70CI3_up

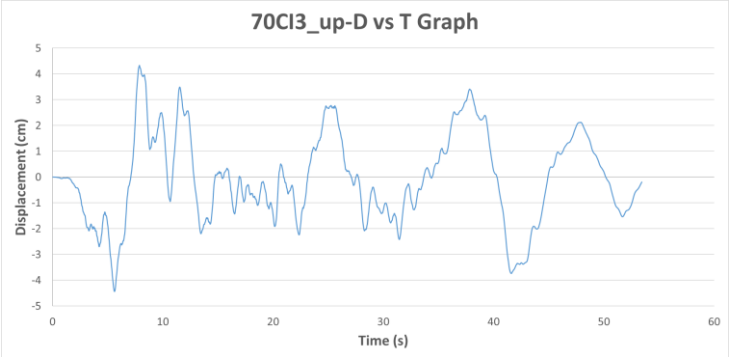

Figure A.279. Displacement vs Time Graph of Ground Motion named 70CI3_up

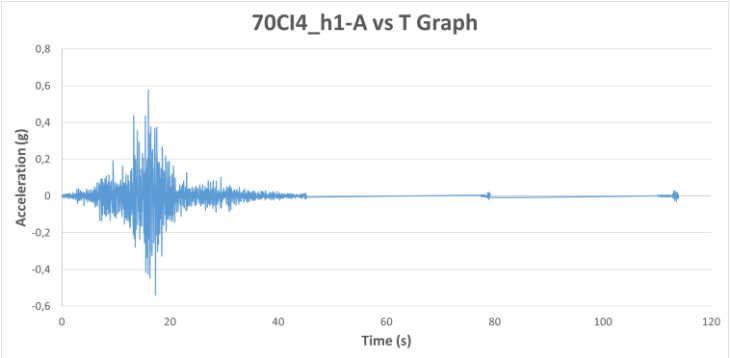

Figure A.280. Acceleration vs Time Graph of Ground Motion named 70CI4_h1

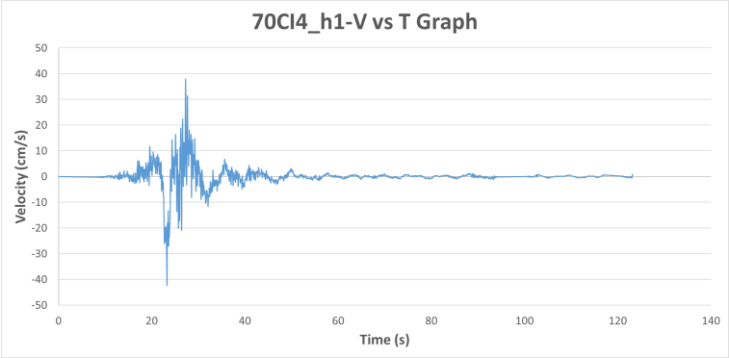

Figure A.281. Velocity vs Time Graph of Ground Motion named 70CI4_h1

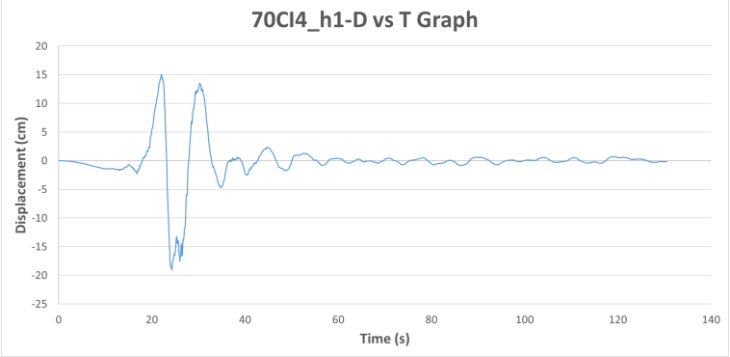

Figure A.282. Displacement vs Time Graph of Ground Motion named 70CI4_h1

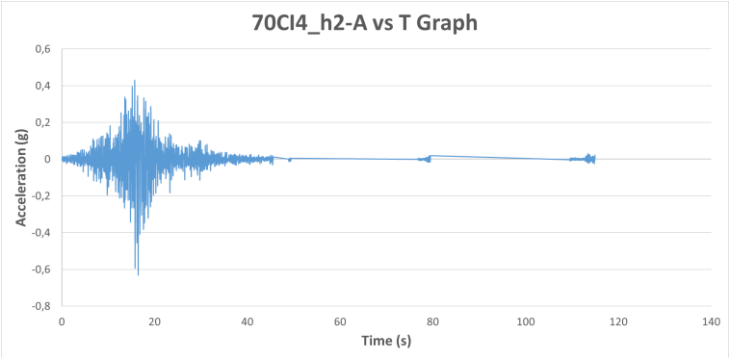

Figure A.283. Acceleration vs Time Graph of Ground Motion named 70CI4_h2

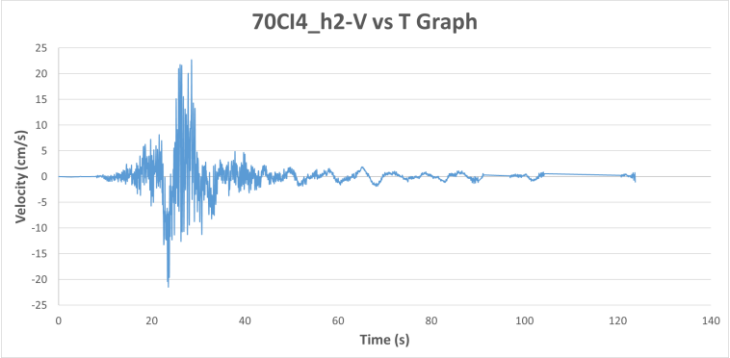

Figure A.284. Velocity vs Time Graph of Ground Motion named 70CI4_h2

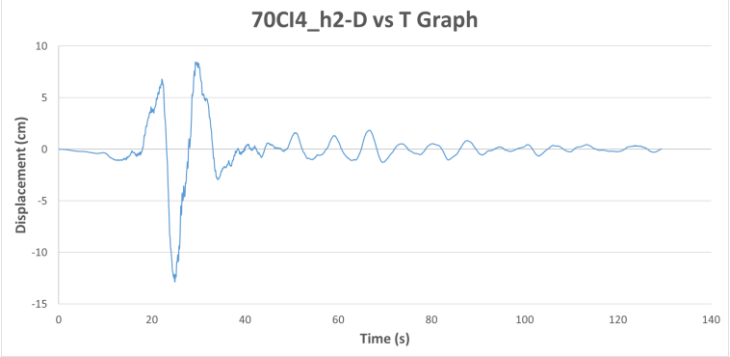

Figure A.285. Displacement vs Time Graph of Ground Motion named 70CI4_h2

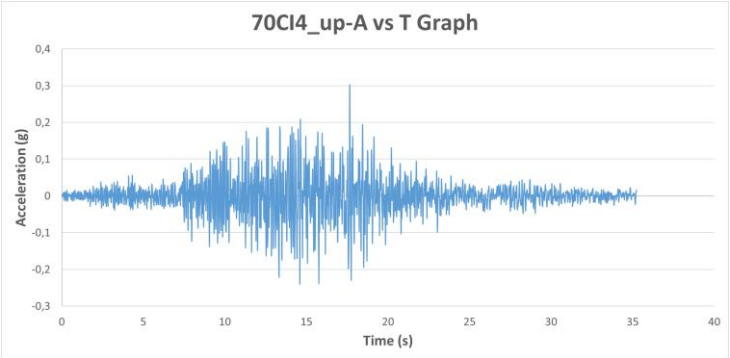

Figure A.286. Acceleration vs Time Graph of Ground Motion named 70CI4_up

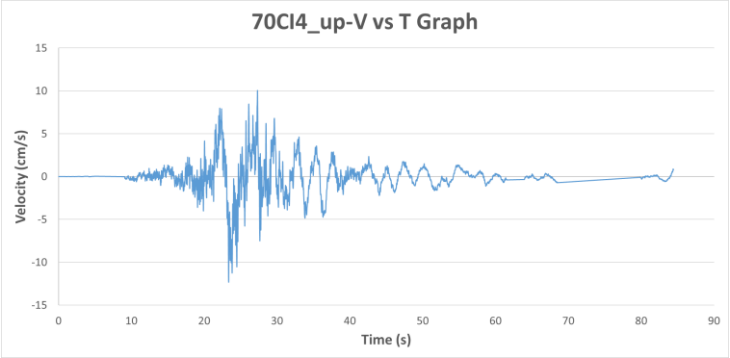

Figure A.287. Velocity vs Time Graph of Ground Motion named 70CI4_up

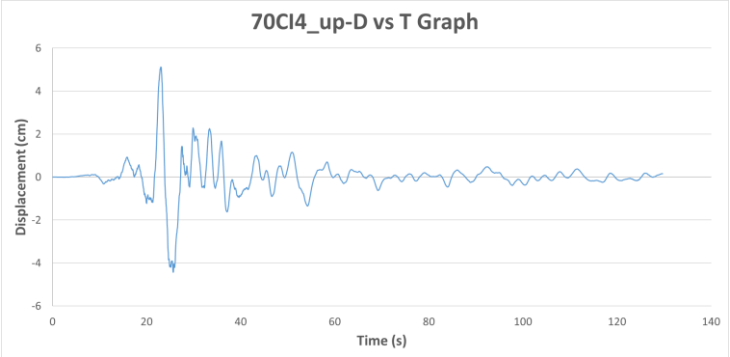

Figure A.288. Displacement vs Time Graph of Ground Motion named 70CI4_up

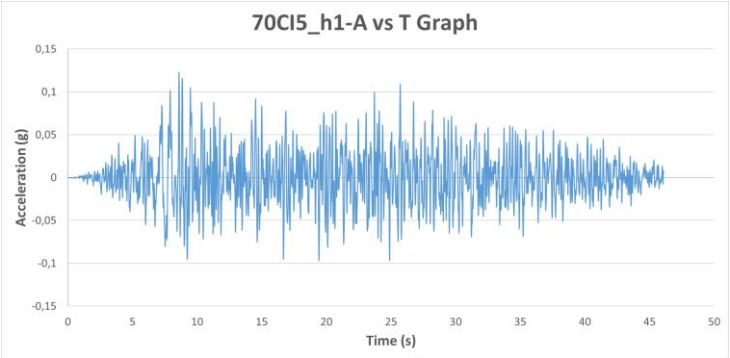

Figure A.289. Acceleration vs Time Graph of Ground Motion named 70CI5_h1

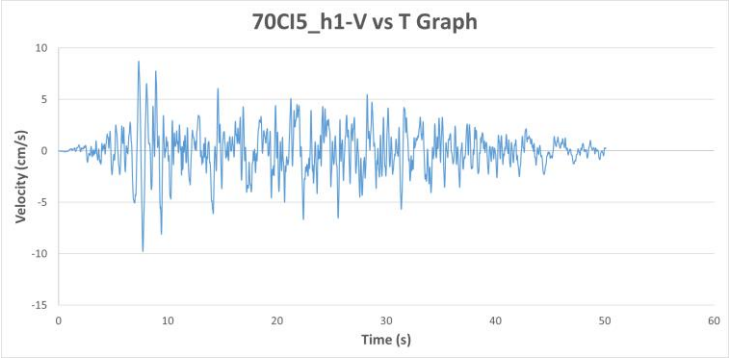

Figure A.290. Velocity vs Time Graph of Ground Motion named 70CI5_h1

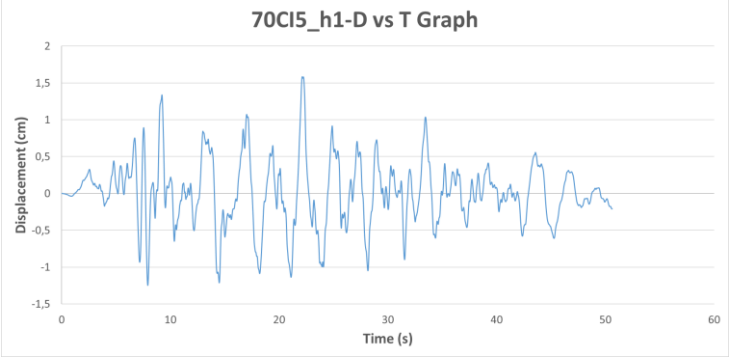

Figure A.291. Displacement vs Time Graph of Ground Motion named 70CI5_h1

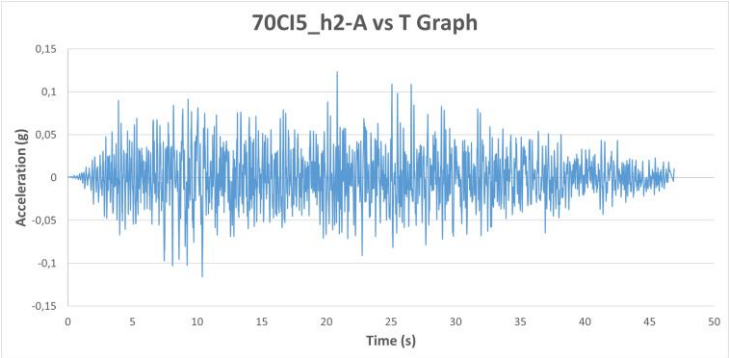

Figure A.292. Acceleration vs Time Graph of Ground Motion named 70CI5_h2

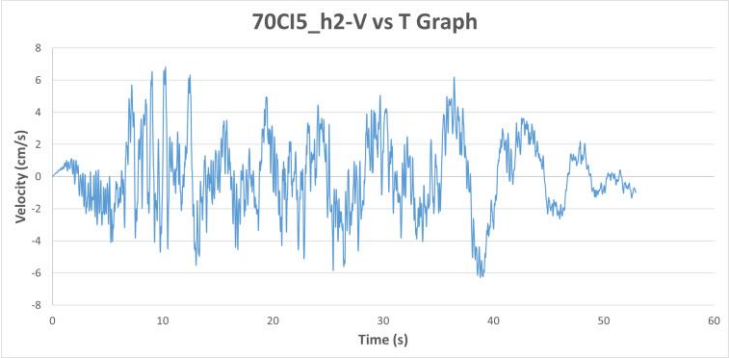

Figure A.293. Velocity vs Time Graph of Ground Motion named 70CI5_h2

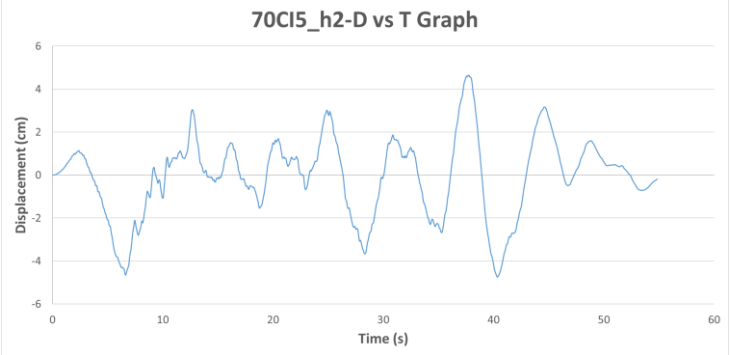

Figure A.294. Displacement vs Time Graph of Ground Motion named 70CI5_h2

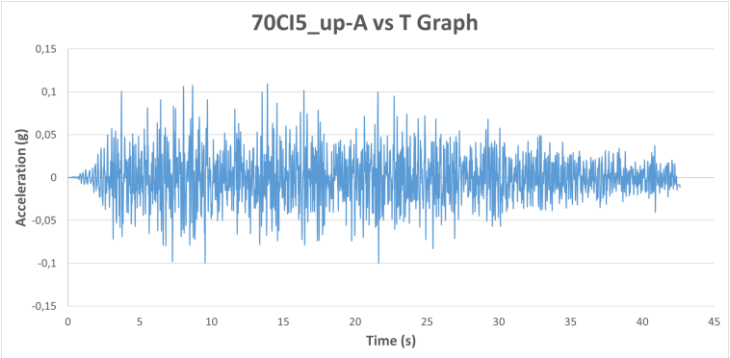

Figure A.295. Acceleration vs Time Graph of Ground Motion named 70CI5_up

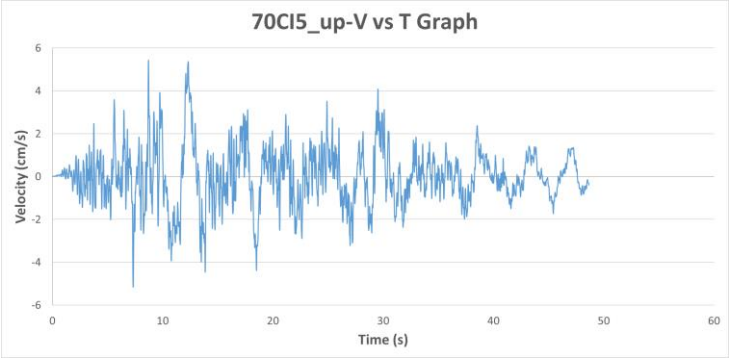

Figure A.296. Velocity vs Time Graph of Ground Motion named 70CI5_up

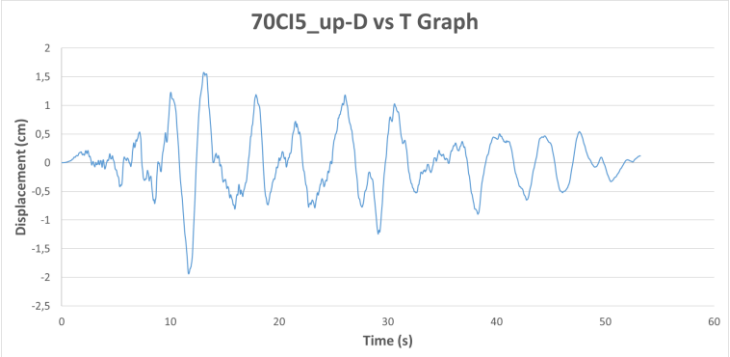

Figure A.297. Displacement vs Time Graph of Ground Motion named 70CI5_up

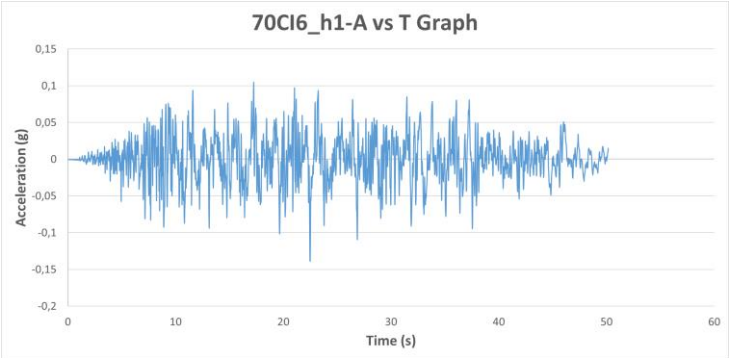

Figure A.298. Acceleration vs Time Graph of Ground Motion named 70CI6_h1

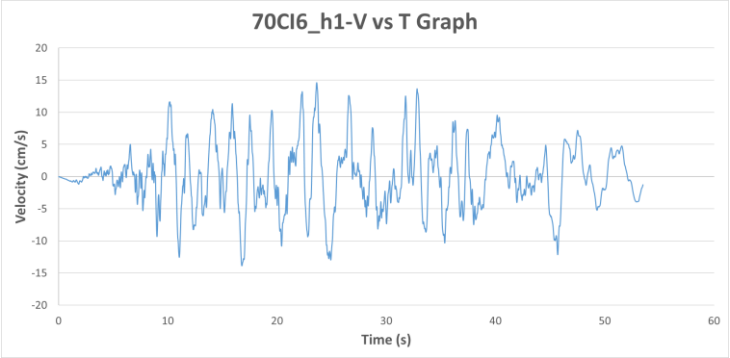

Figure A.299. Velocity vs Time Graph of Ground Motion named 70CI6_h1

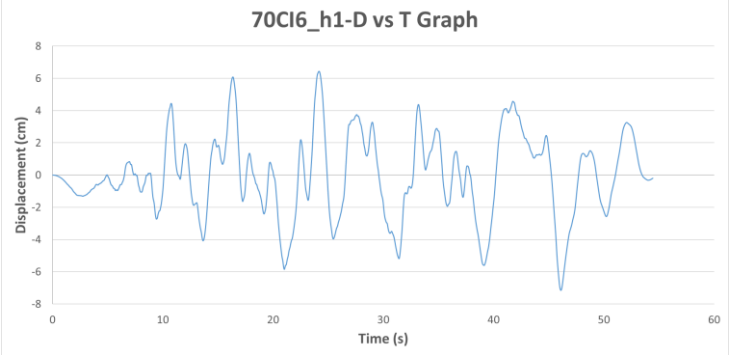

Figure A.300. Displacement vs Time Graph of Ground Motion named 70CI6_h1

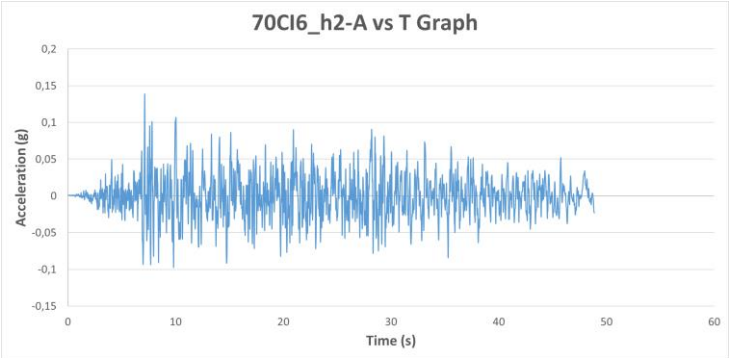

Figure A.301. Acceleration vs Time Graph of Ground Motion named 70CI6_h2

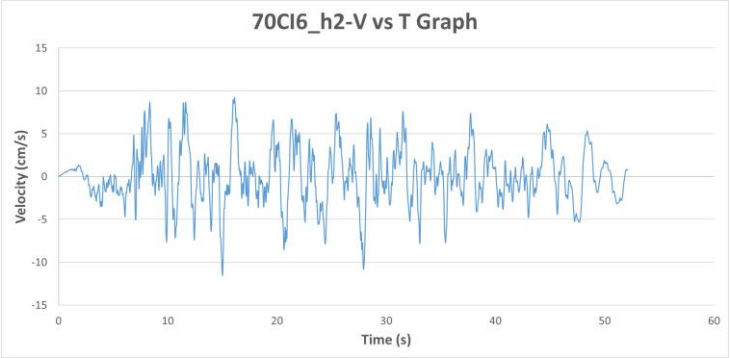

Figure A.302. Velocity vs Time Graph of Ground Motion named 70CI6_h2

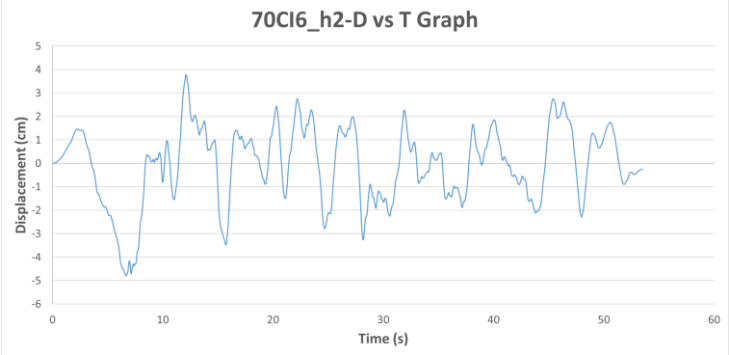

Figure A.303. Displacement vs Time Graph of Ground Motion named 70CI6_h2

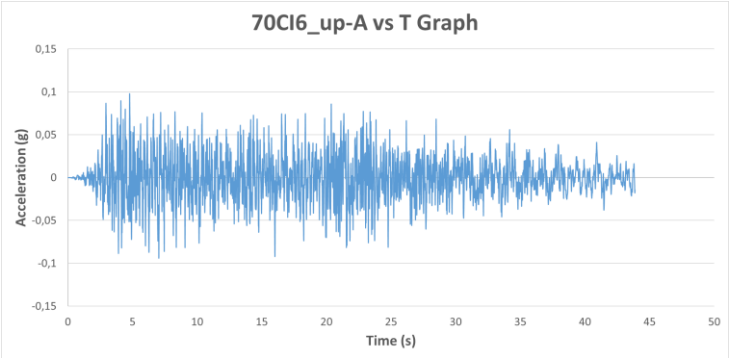

Figure A.304. Acceleration vs Time Graph of Ground Motion named 70CI6_up

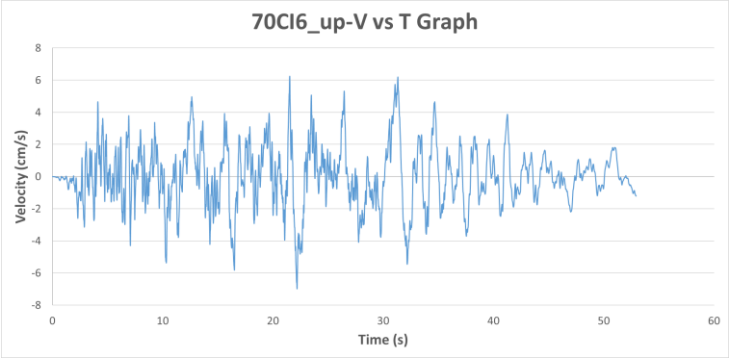

Figure A.305. Velocity vs Time Graph of Ground Motion named 70CI6_up

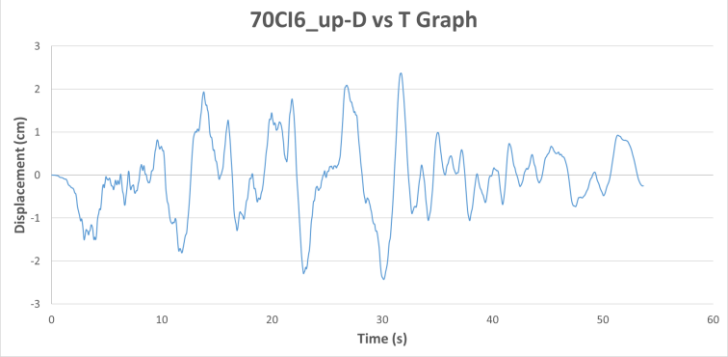

Figure A.306. Displacement vs Time Graph of Ground Motion named 70CI6_up

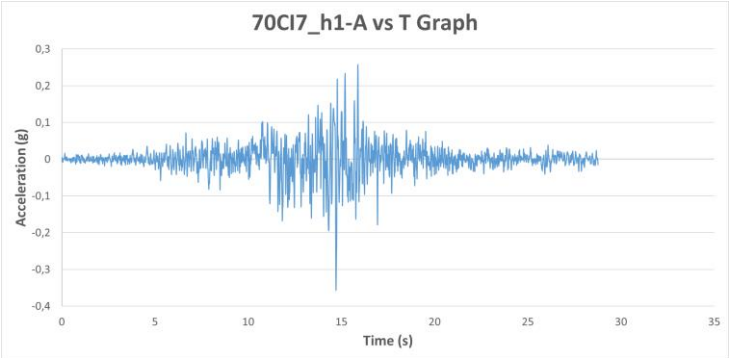

Figure A.307. Acceleration vs Time Graph of Ground Motion named 70CI7_h1

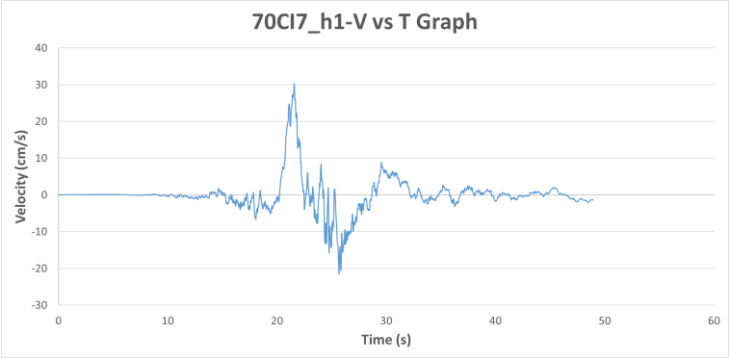

Figure A.308. Velocity vs Time Graph of Ground Motion named 70CI7_h1

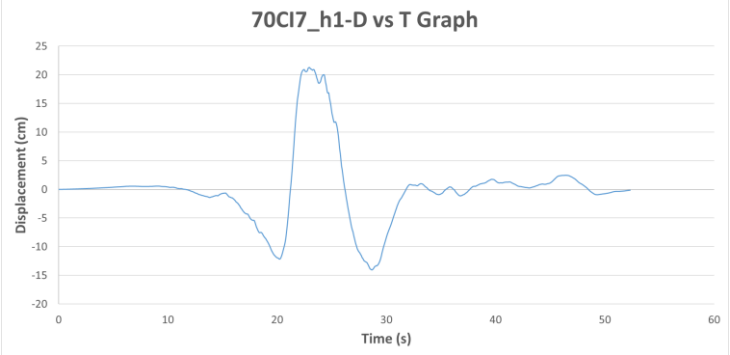

Figure A.309. Displacement vs Time Graph of Ground Motion named 70CI7_h1

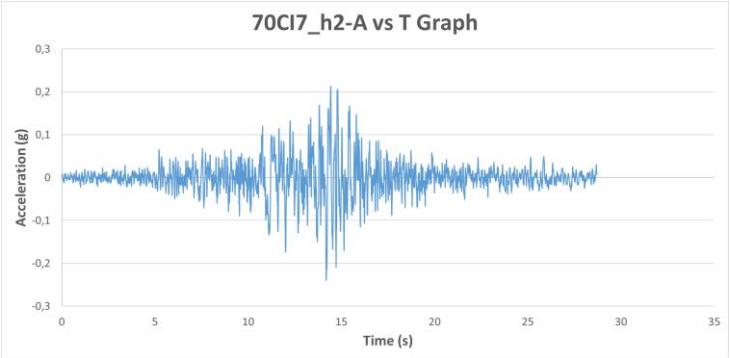

Figure A.310. Acceleration vs Time Graph of Ground Motion named 70CI7_h2

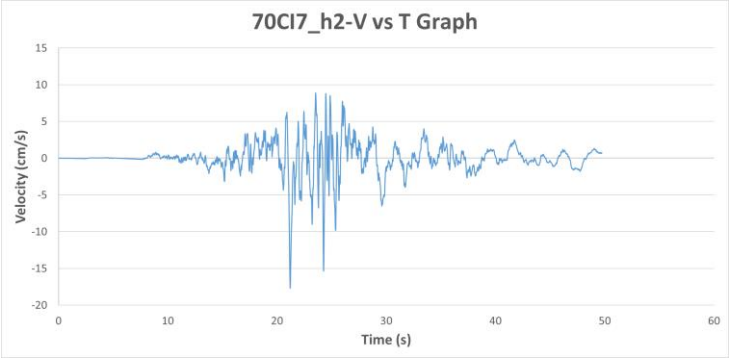

Figure A.311. Velocity vs Time Graph of Ground Motion named 70CI7_h2

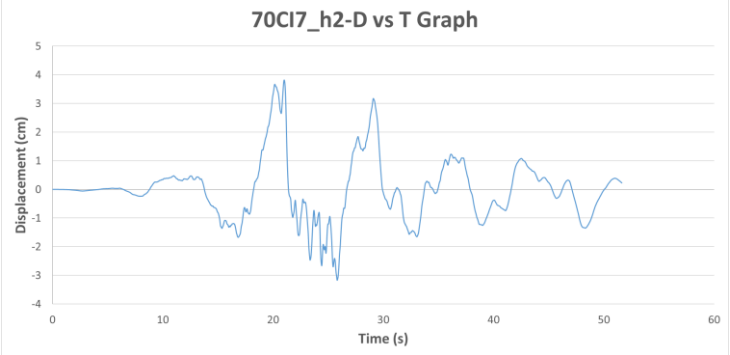

Figure A.312. Displacement vs Time Graph of Ground Motion named 70CI7_h2

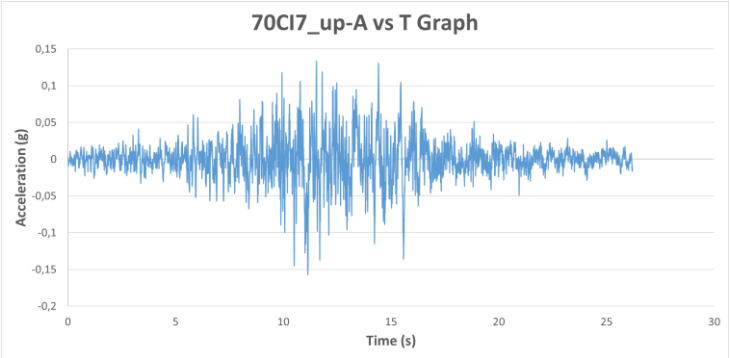

Figure A.313. Acceleration vs Time Graph of Ground Motion named 70CI7_up

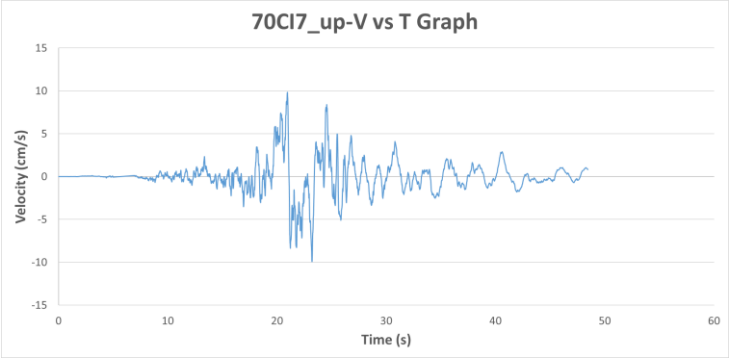

Figure A.314. Velocity vs Time Graph of Ground Motion named 70CI7_up

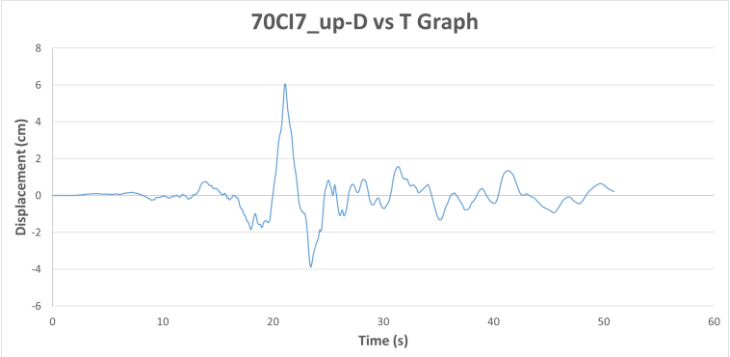

Figure A.315. Displacement vs Time Graph of Ground Motion named 70CI7_up

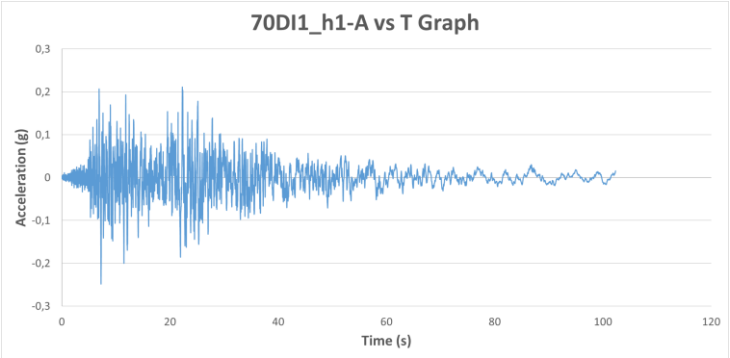

Figure A.316. Acceleration vs Time Graph of Ground Motion named 70DI1_h1

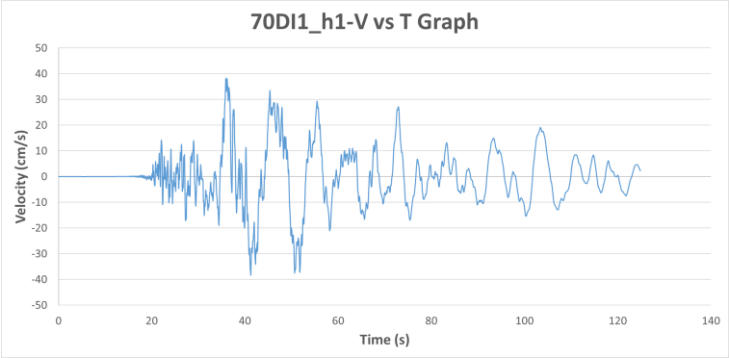

Figure A.317. Velocity vs Time Graph of Ground Motion named 70DI1_h1

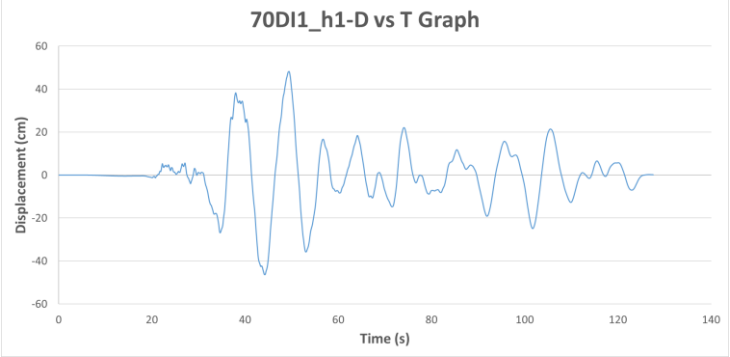

Figure A.318. Displacement vs Time Graph of Ground Motion named 70DI1_h1

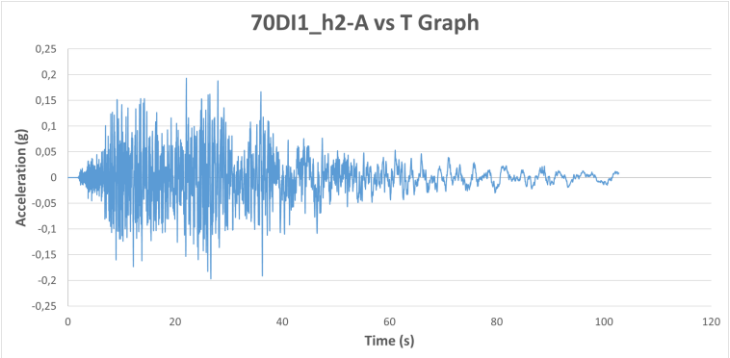

Figure A.319. Acceleration vs Time Graph of Ground Motion named 70DI1_h2

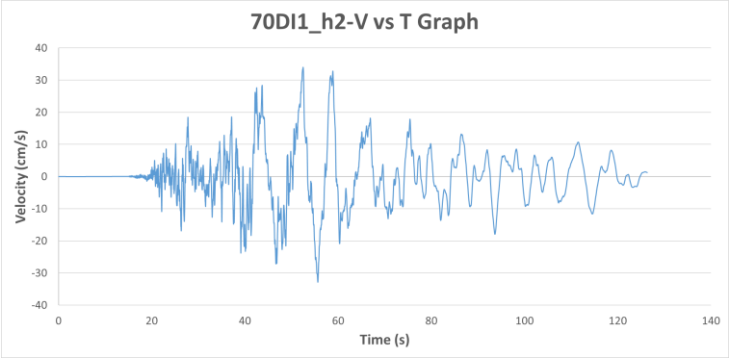

Figure A.320. Velocity vs Time Graph of Ground Motion named 70DI1_h2

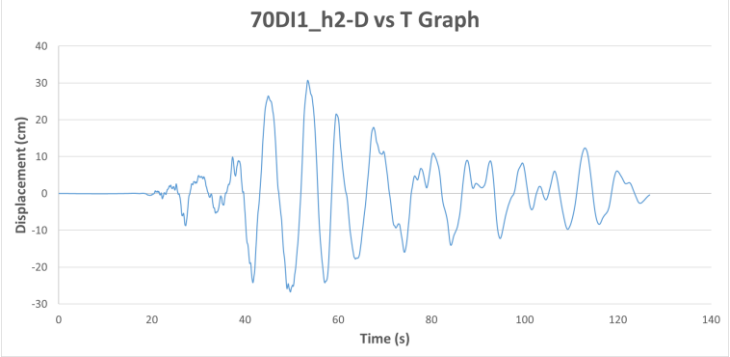

Figure A.321. Displacement vs Time Graph of Ground Motion named 70DI1_h2

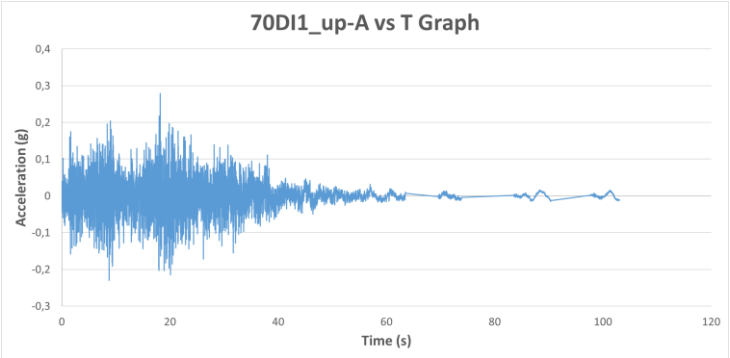

Figure A.322. Acceleration vs Time Graph of Ground Motion named 70DI1_up

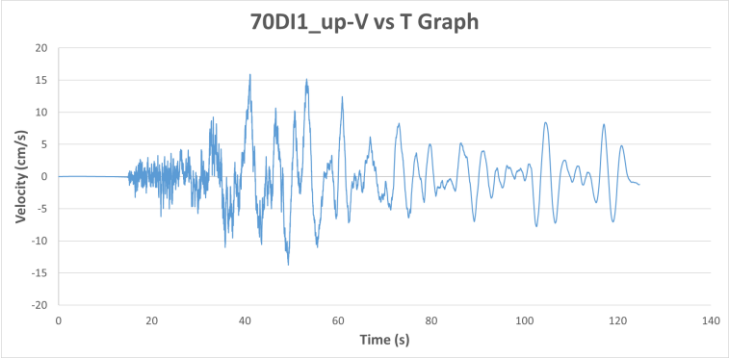

Figure A.323. Velocity vs Time Graph of Ground Motion named 70DI1_up

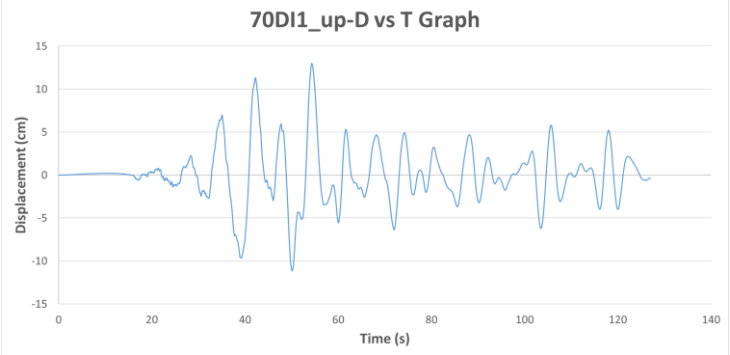

Figure A.324. Displacement vs Time Graph of Ground Motion named 70DI1_up

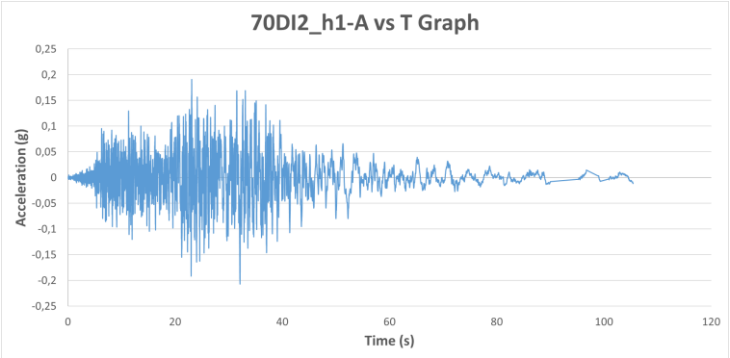

Figure A.325. Acceleration vs Time Graph of Ground Motion named 70DI2_h1

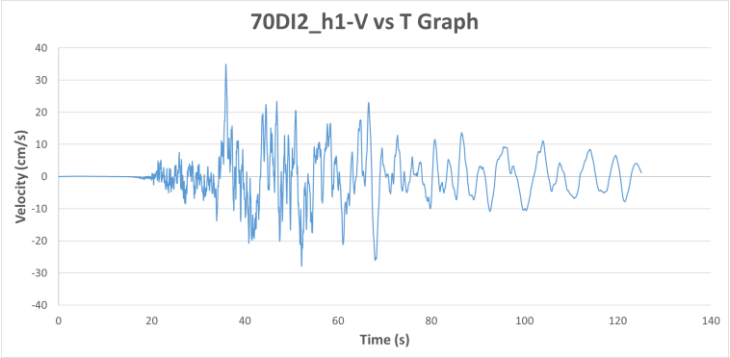

Figure A.326. Velocity vs Time Graph of Ground Motion named 70DI2_h1

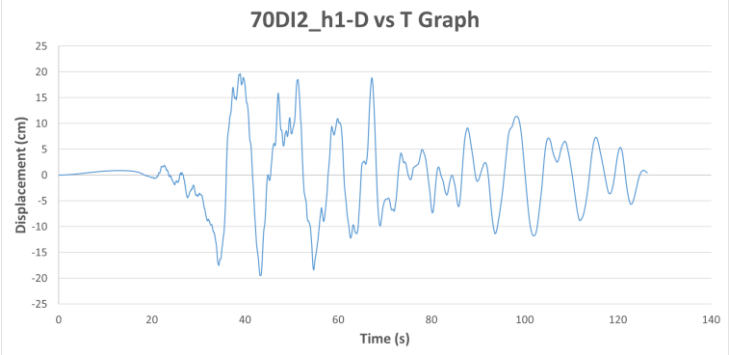

Figure A.327. Displacement vs Time Graph of Ground Motion named 70DI2_h1

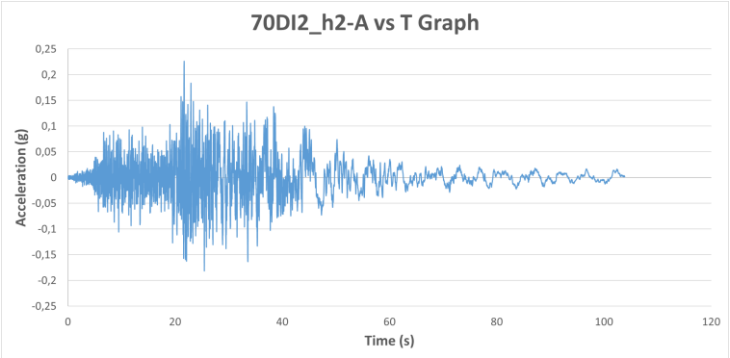

Figure A.328. Acceleration vs Time Graph of Ground Motion named 70DI2_h2

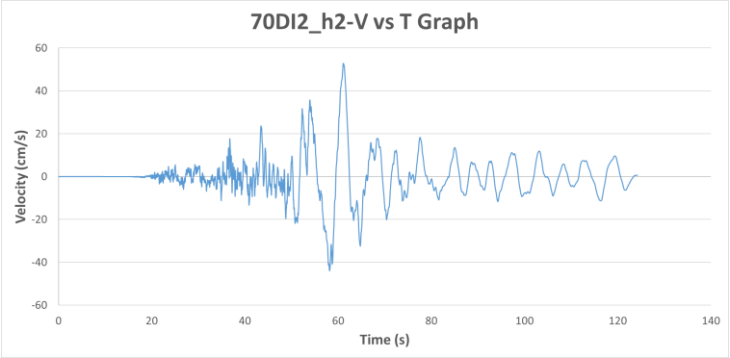

Figure A.329. Velocity vs Time Graph of Ground Motion named 70DI2_h2

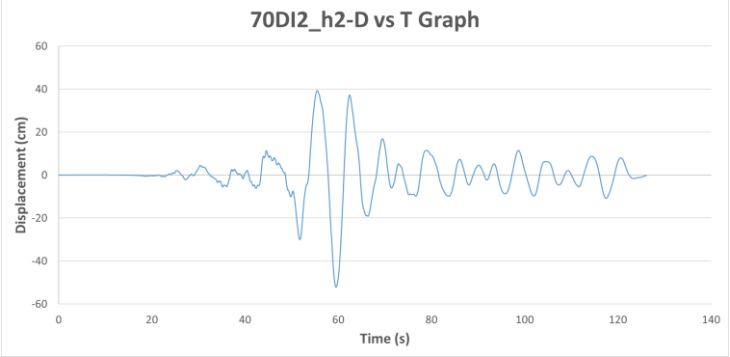

Figure A.330. Displacement vs Time Graph of Ground Motion named 70DI2_h2

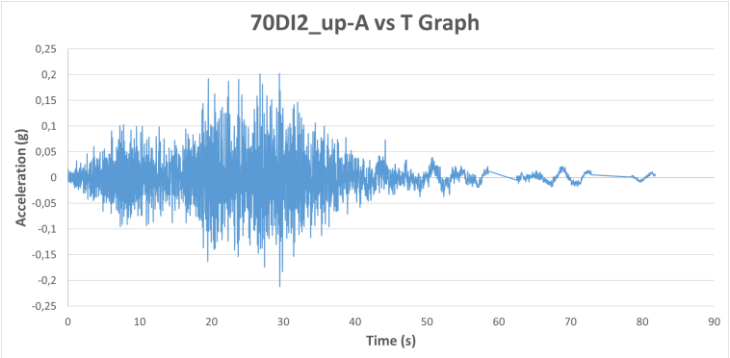

Figure A.331. Acceleration vs Time Graph of Ground Motion named 70DI2_up

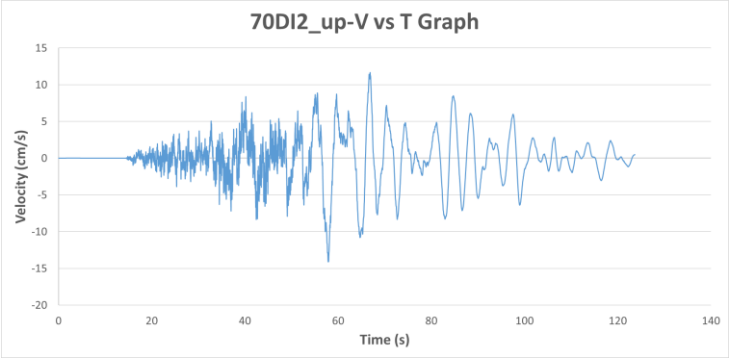

Figure A.332. Velocity vs Time Graph of Ground Motion named 70DI2_up

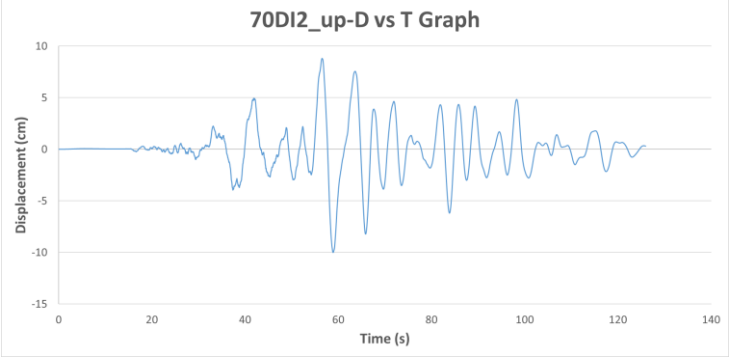

Figure A.333. Displacement vs Time Graph of Ground Motion named 70DI2_up

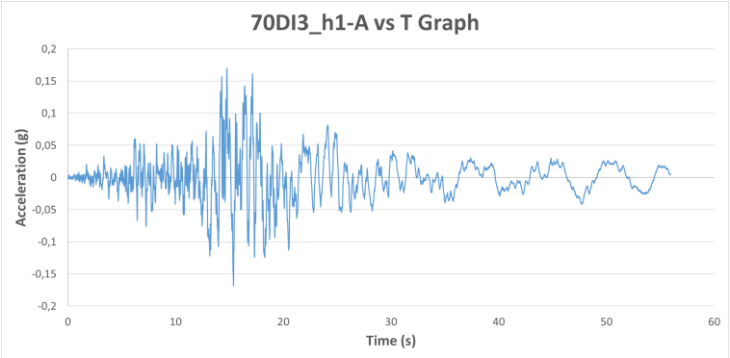

Figure A.334. Acceleration vs Time Graph of Ground Motion named 70DI3_h1

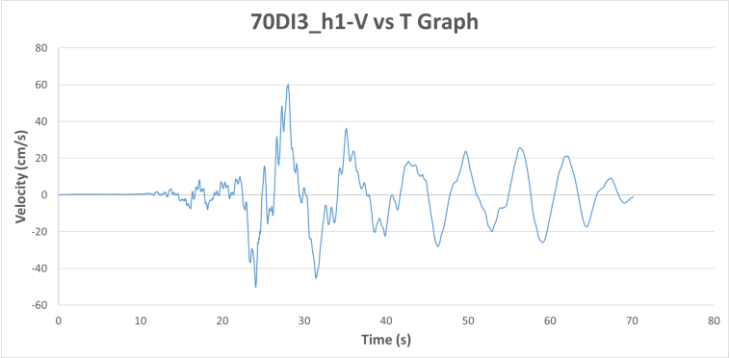

Figure A.335. Velocity vs Time Graph of Ground Motion named 70DI3_h1

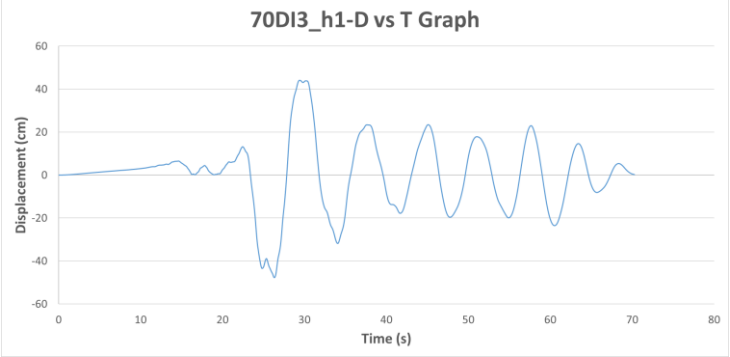

Figure A.336. Displacement vs Time Graph of Ground Motion named 70DI3_h1

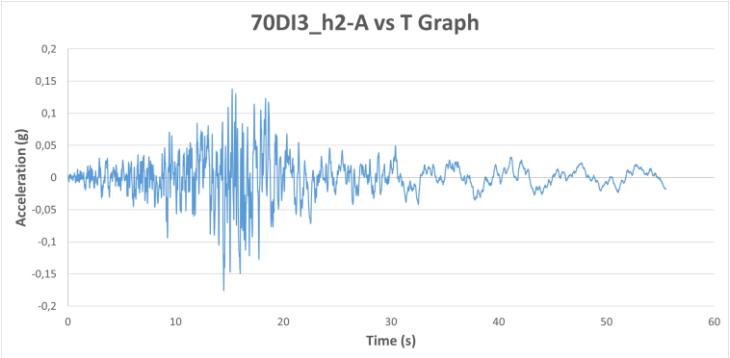

Figure A.337. Acceleration vs Time Graph of Ground Motion named 70DI3_h2

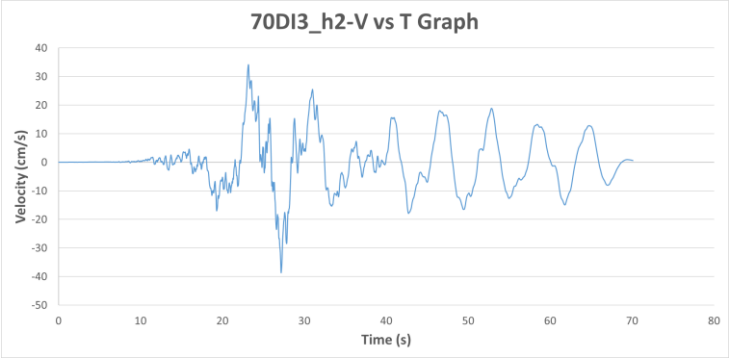

Figure A.338. Velocity vs Time Graph of Ground Motion named 70DI3_h2

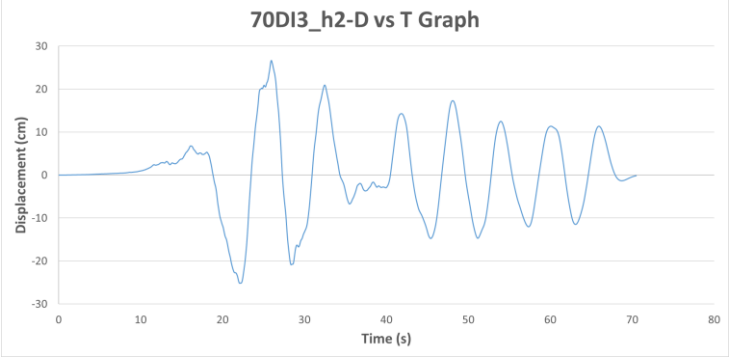

Figure A.339. Displacement vs Time Graph of Ground Motion named 70DI3_h2

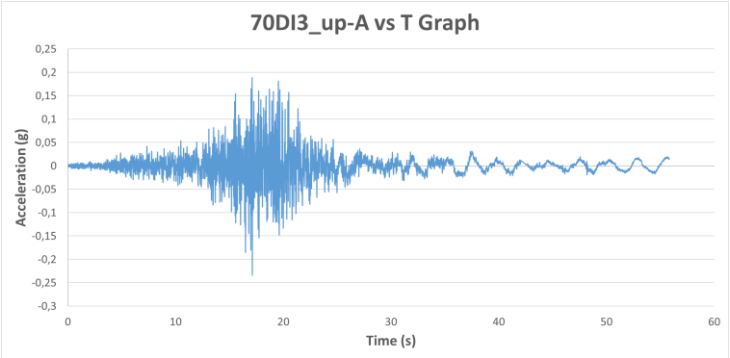

Figure A.340. Acceleration vs Time Graph of Ground Motion named 70DI3_up

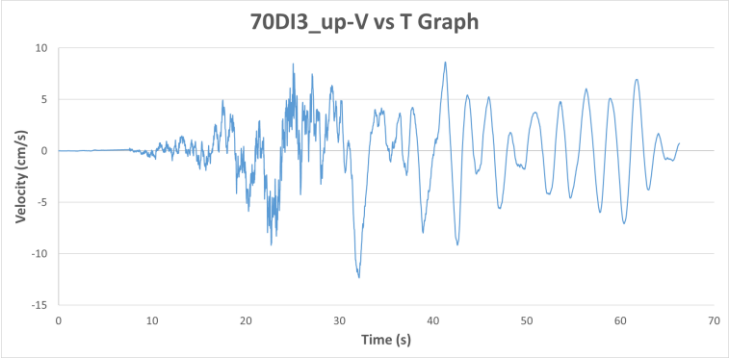

Figure A.341. Velocity vs Time Graph of Ground Motion named 70DI3_up

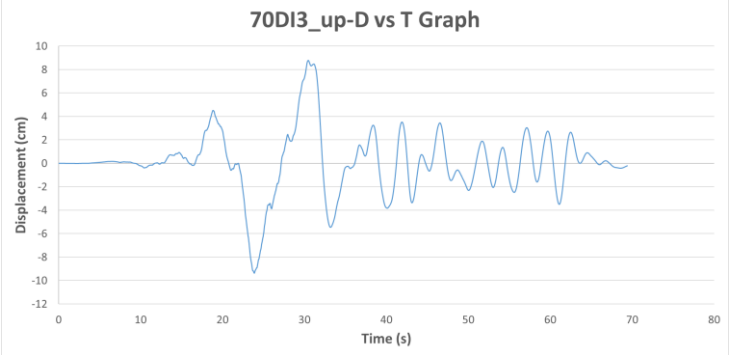

Figure A.342. Displacement vs Time Graph of Ground Motion named 70DI3_up

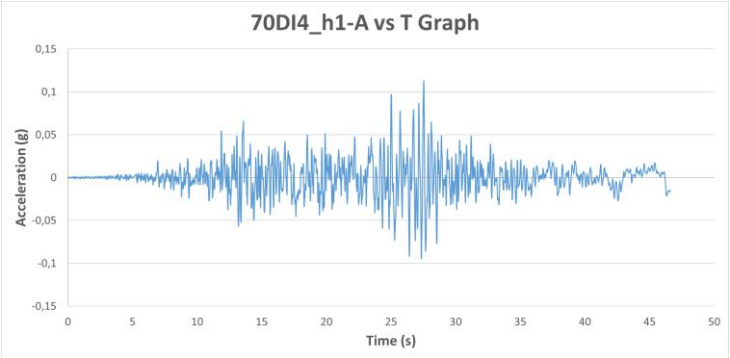

Figure A.343. Acceleration vs Time Graph of Ground Motion named 70DI4_h1

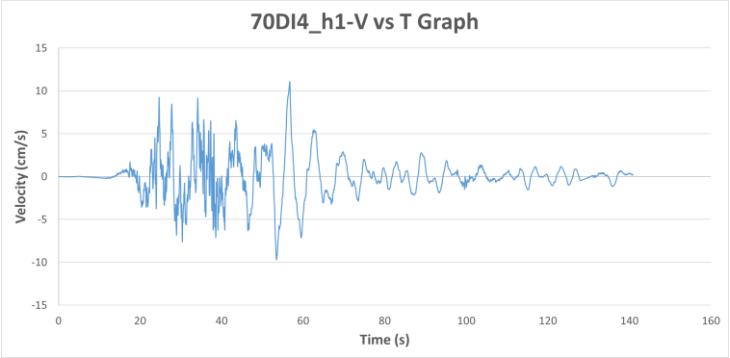

Figure A.344. Velocity vs Time Graph of Ground Motion named 70DI4_h1

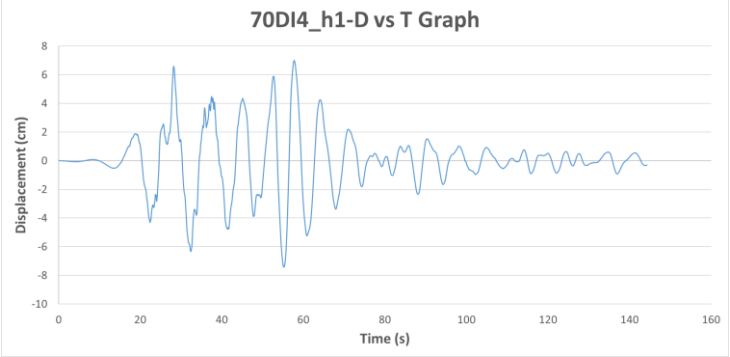

Figure A.345. Displacement vs Time Graph of Ground Motion named 70DI4_h1

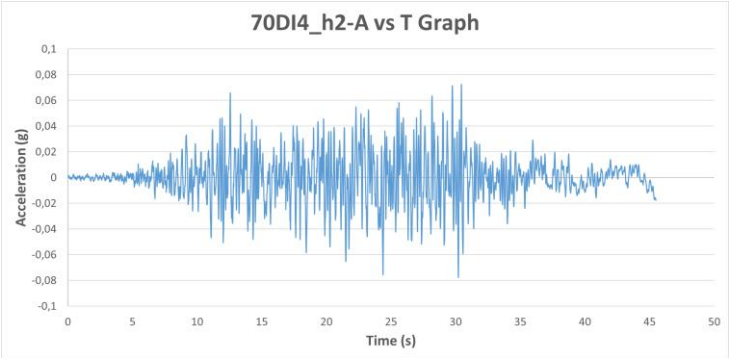

Figure A.346. Acceleration vs Time Graph of Ground Motion named 70DI4_h2

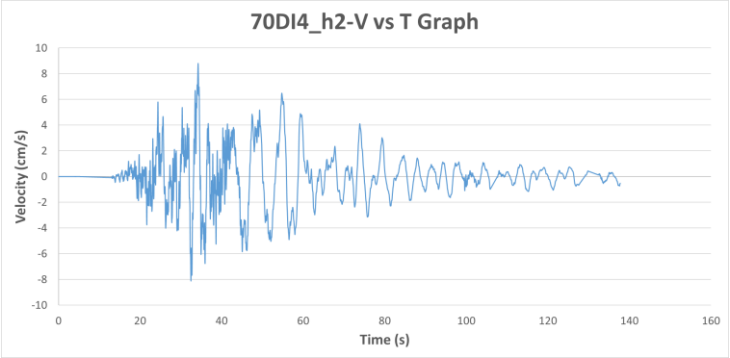

Figure A.347. Velocity vs Time Graph of Ground Motion named 70DI4_h2

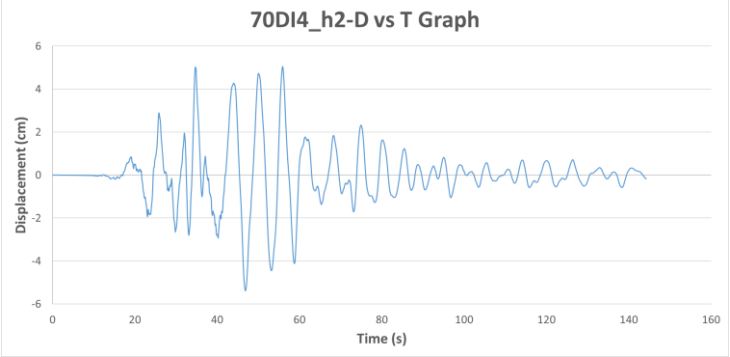

Figure A.348. Displacement vs Time Graph of Ground Motion named 70DI4_h2

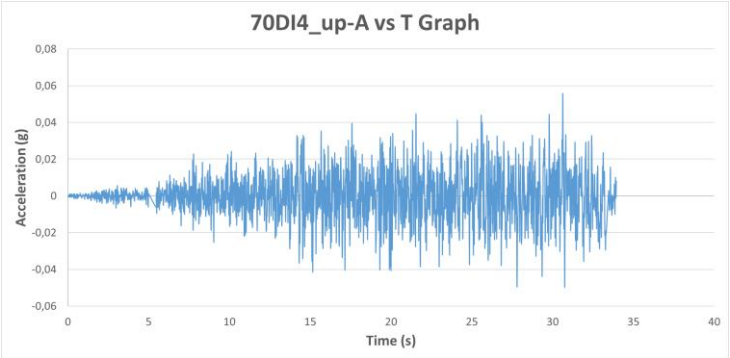

Figure A.349. Acceleration vs Time Graph of Ground Motion named 70DI4_up

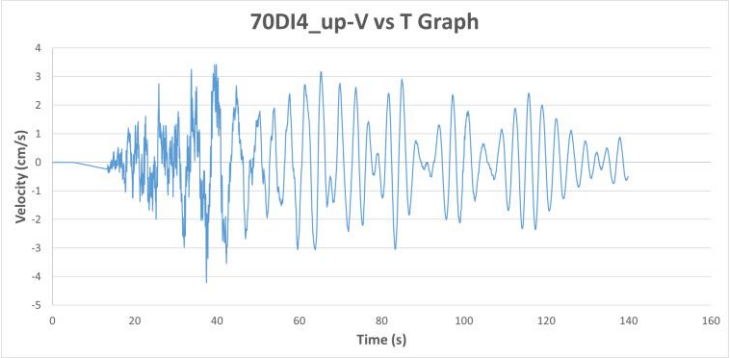

Figure A.350. Velocity vs Time Graph of Ground Motion named 70DI4_up

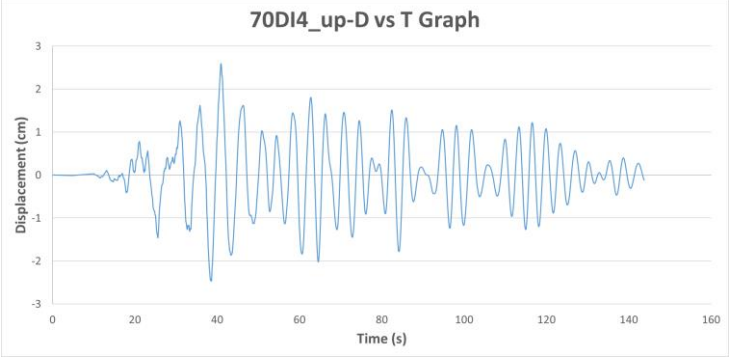

Figure A.351. Displacement vs Time Graph of Ground Motion named 70DI4_up

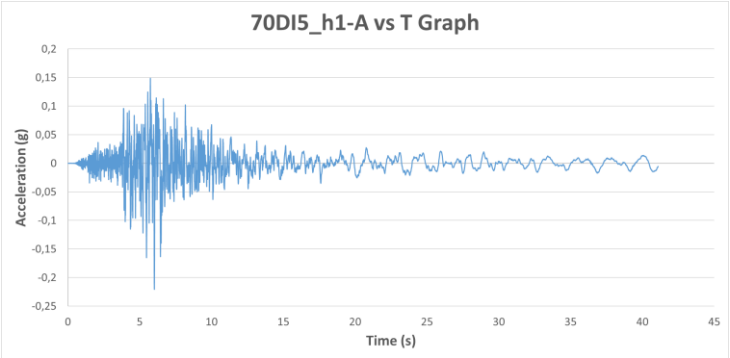

Figure A.352. Acceleration vs Time Graph of Ground Motion named 70DI5_h1

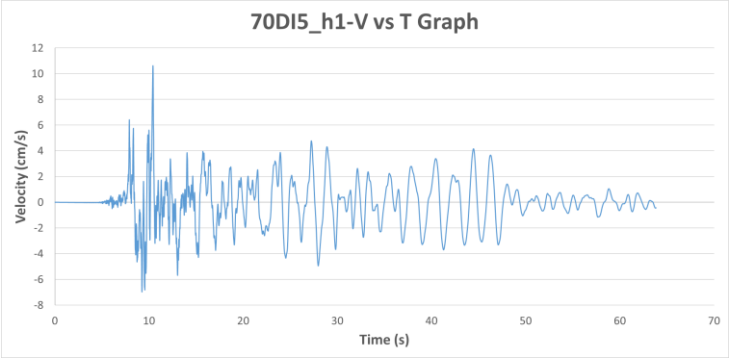

Figure A.353. Velocity vs Time Graph of Ground Motion named 70DI5_h1

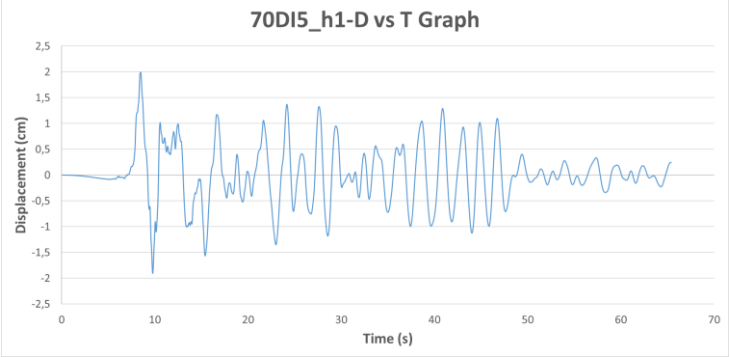

Figure A.354. Displacement vs Time Graph of Ground Motion named 70DI5_h1

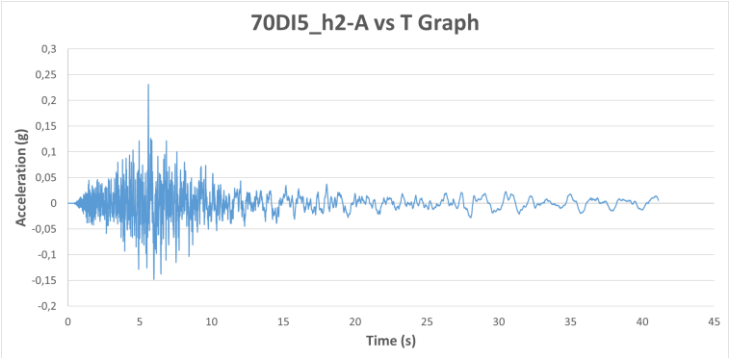

Figure A.355 Acceleration vs Time Graph of Ground Motion named 70DI5_h2

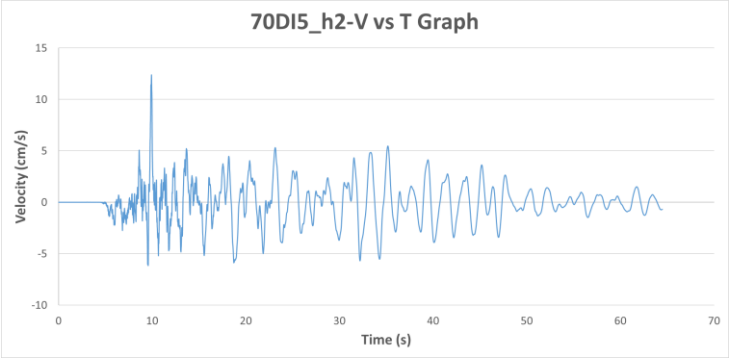

Figure A.356. Velocity vs Time Graph of Ground Motion named 70DI5_h2

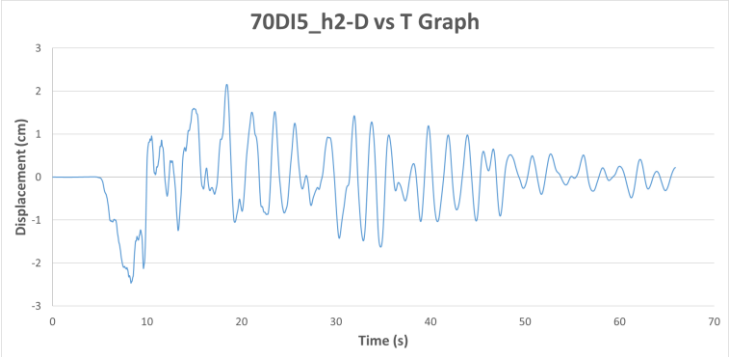

Figure A.357. Displacement vs Time Graph of Ground Motion named 70DI5_h2

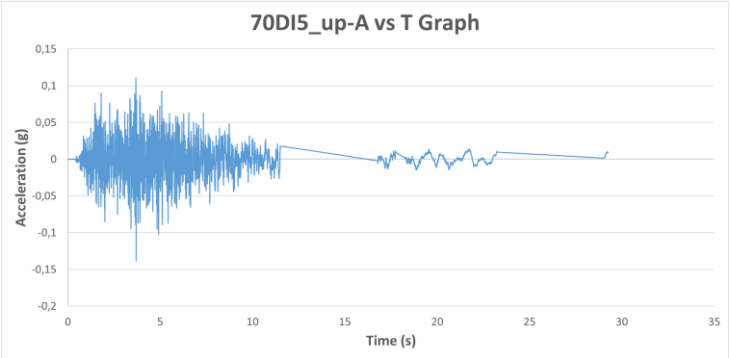

Figure A.358. Acceleration vs Time Graph of Ground Motion named 70DI5_up

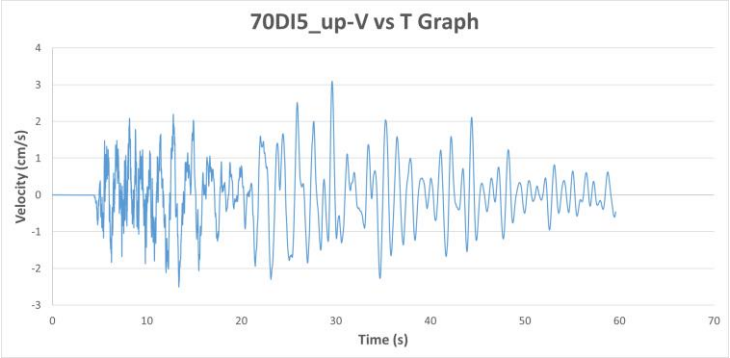

Figure A.359. Velocity vs Time Graph of Ground Motion named 70DI5_up

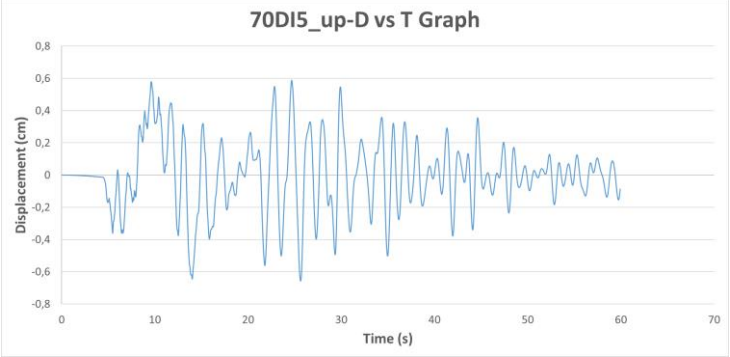

Figure A.360. Displacement vs Time Graph of Ground Motion named 70DI5_up

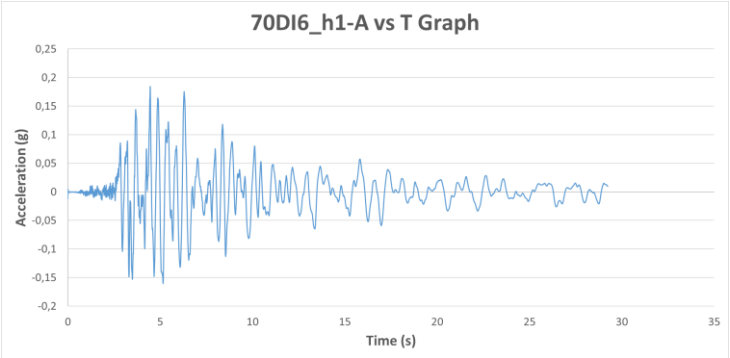

Figure A.361. Acceleration vs Time Graph of Ground Motion named 70DI6_h1

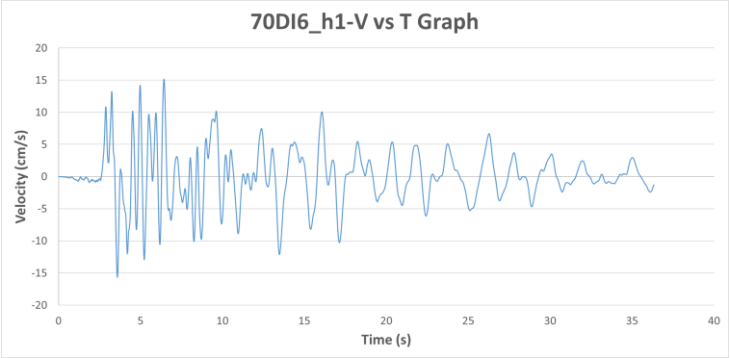

Figure A.362. Velocity vs Time Graph of Ground Motion named 70DI6_h1

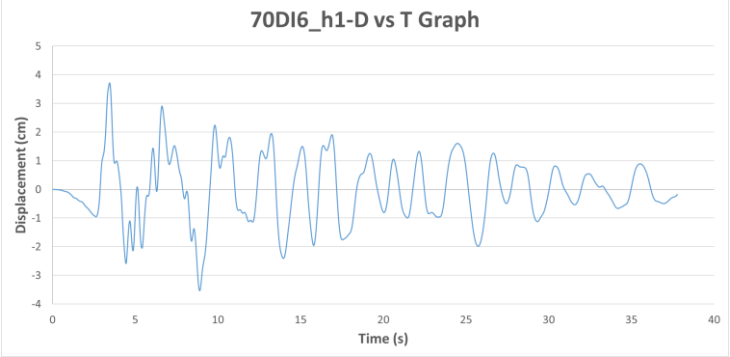

Figure A.363. Displacement vs Time Graph of Ground Motion named 70DI6_h1

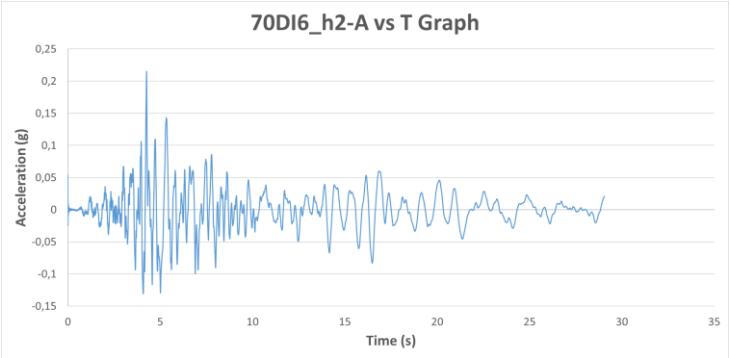

Figure A.364. Acceleration vs Time Graph of Ground Motion named 70DI6_h2

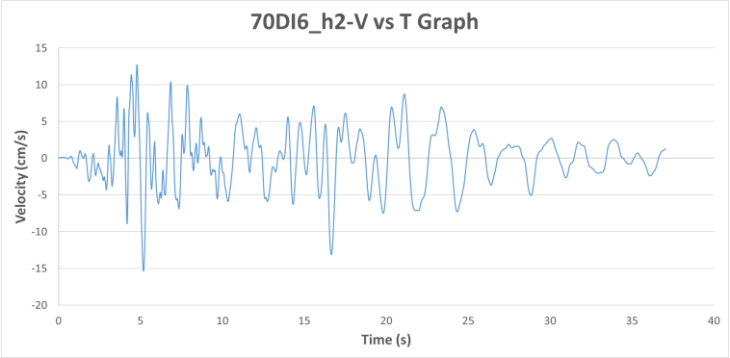

Figure A.365. Velocity vs Time Graph of Ground Motion named 70DI6_h2

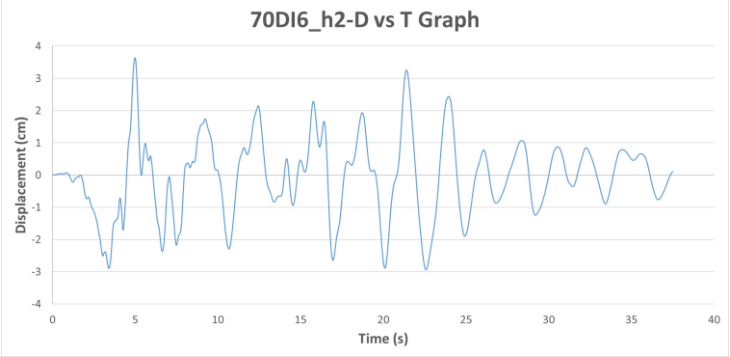

Figure A.366. Displacement vs Time Graph of Ground Motion named 70DI6_h2

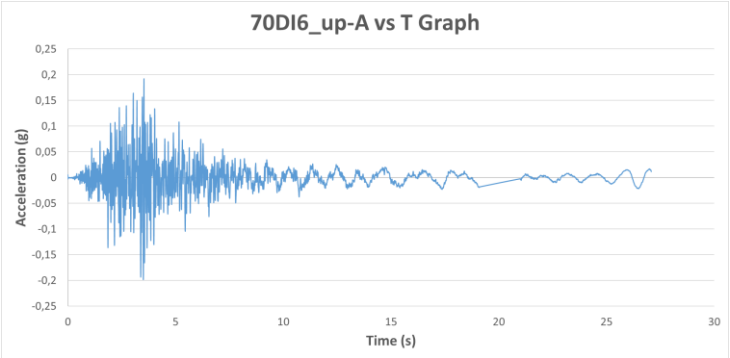

Figure A.367. Acceleration vs Time Graph of Ground Motion named 70DI6_up

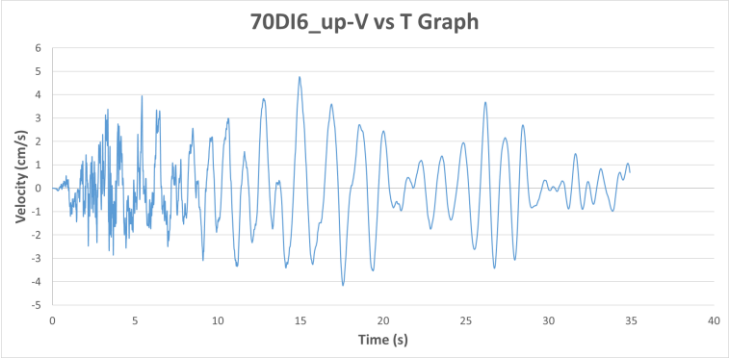

Figure A.368. Velocity vs Time Graph of Ground Motion named 70DI6_up

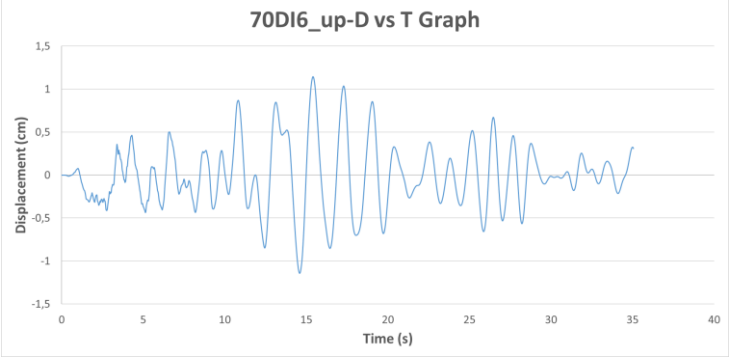

Figure A.369. Displacement vs Time Graph of Ground Motion named 70DI6_up

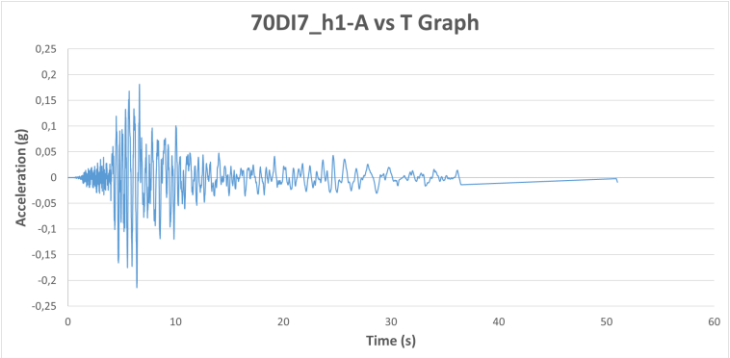

Figure A.370. Acceleration vs Time Graph of Ground Motion named 70DI7_h1

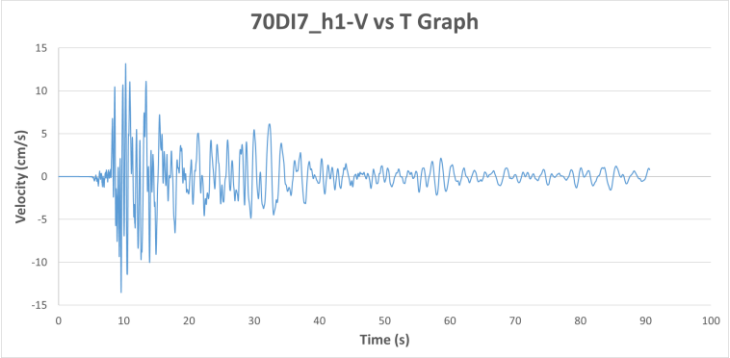

Figure A.371. Velocity vs Time Graph of Ground Motion named 70DI7_h1

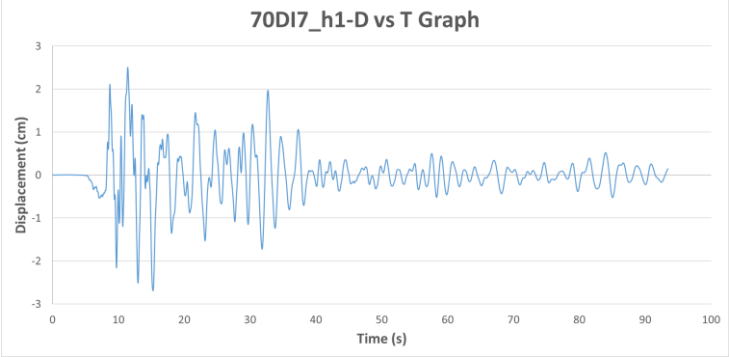

Figure A.372. Displacement vs Time Graph of Ground Motion named 70DI7_h1

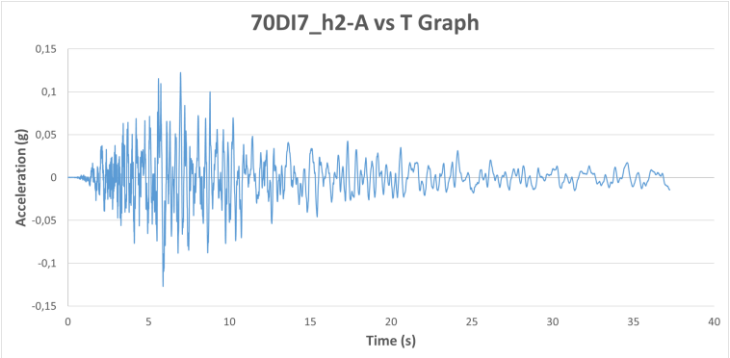

Figure A.373. Acceleration vs Time Graph of Ground Motion named 70DI7_h2

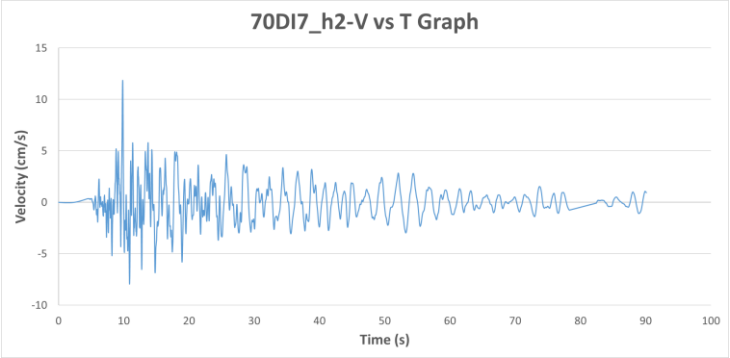

Figure A.374. Velocity vs Time Graph of Ground Motion named 70DI7_h2

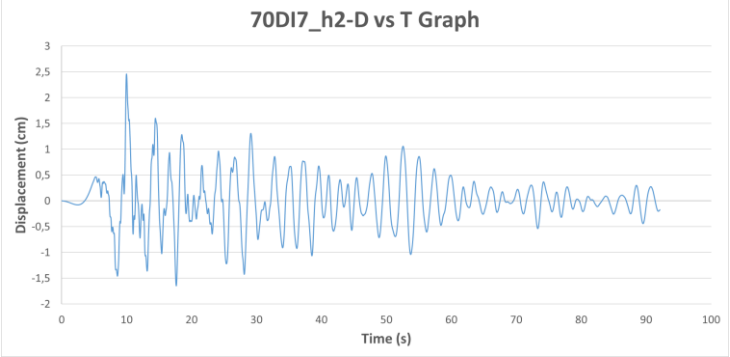

Figure A.375. Displacement vs Time Graph of Ground Motion named 70DI7_h2

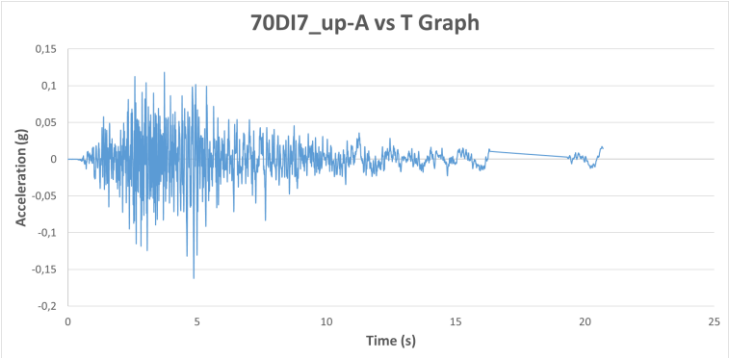

Figure A.376. Acceleration vs Time Graph of Ground Motion named 70DI7_up

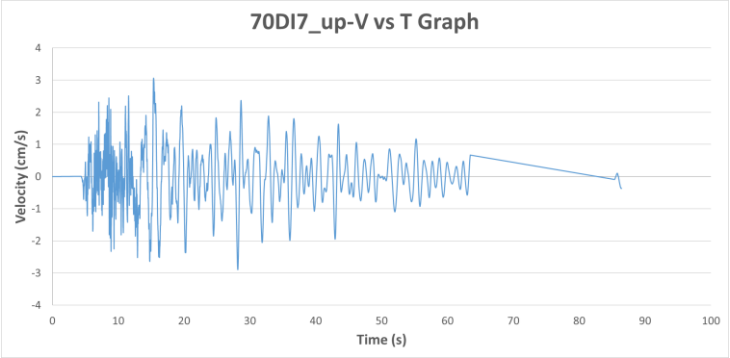

Figure A.377. Velocity vs Time Graph of Ground Motion named 70DI7_up

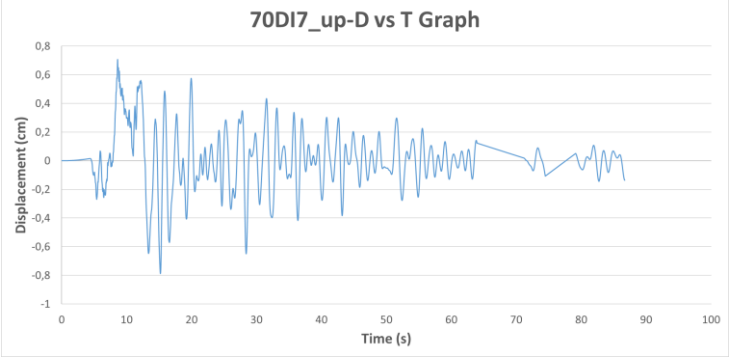

Figure A.378. Displacement vs Time Graph of Ground Motion named 70DI7_up

B. APPENDIX B – Fourier Amplitude Spectra Graphs

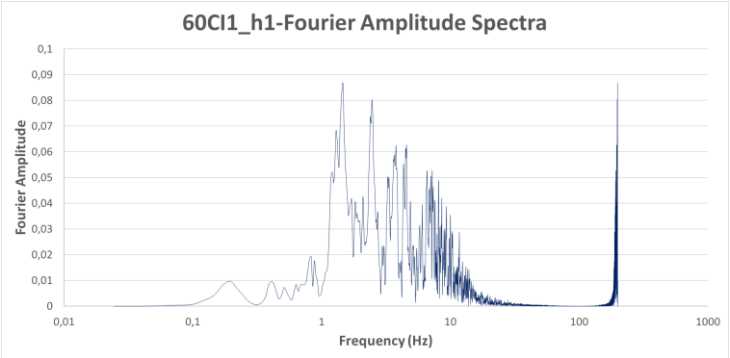

Figure B.1. Fourier Amplitude Spectra Graph of Ground Motion named 60CI1_h1

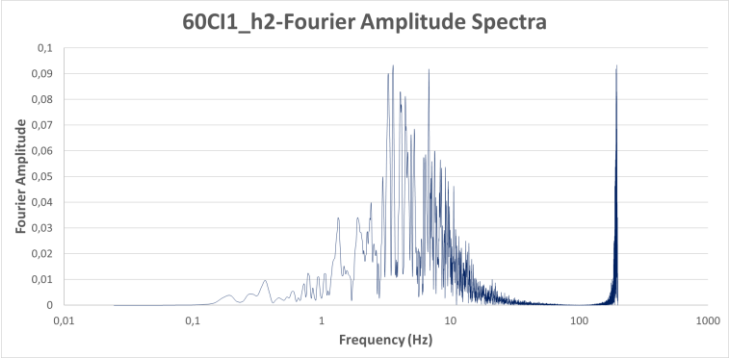

Figure B.2. Fourier Amplitude Spectra Graph of Ground Motion named 60CI1_h2

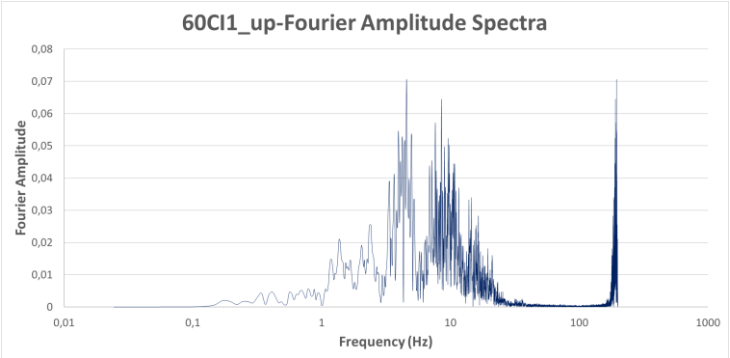

Figure B.3. Fourier Amplitude Spectra Graph of Ground Motion named 60CI1_up

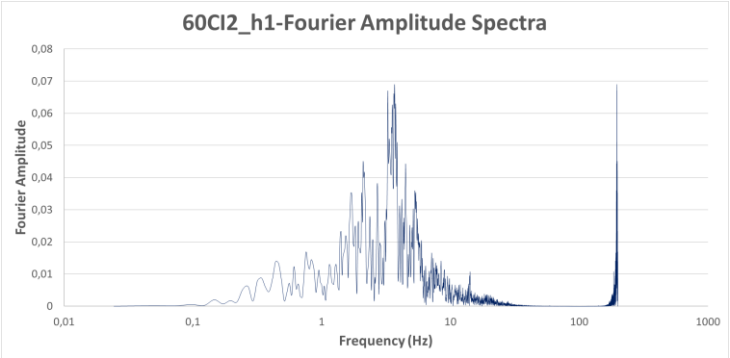

Figure B.4. Fourier Amplitude Spectra Graph of Ground Motion named 60CI2_h1

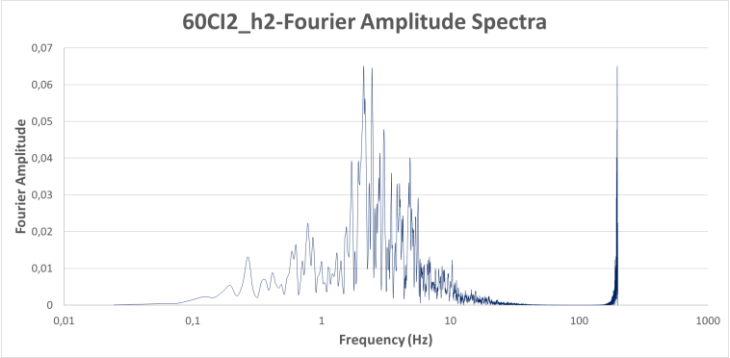

Figure B.5. Fourier Amplitude Spectra Graph of Ground Motion named 60CI2_h2

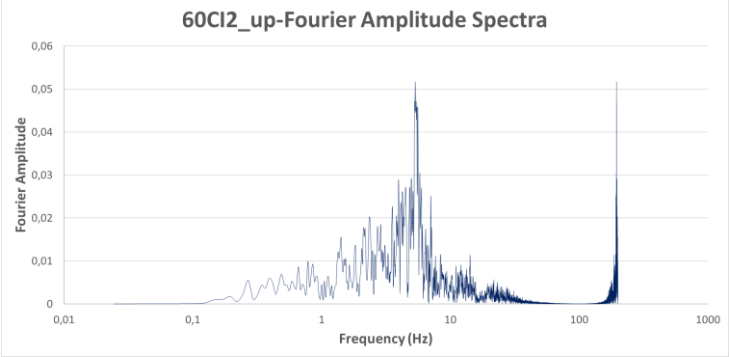

Figure B.6. Fourier Amplitude Spectra Graph of Ground Motion named 60CI2_up

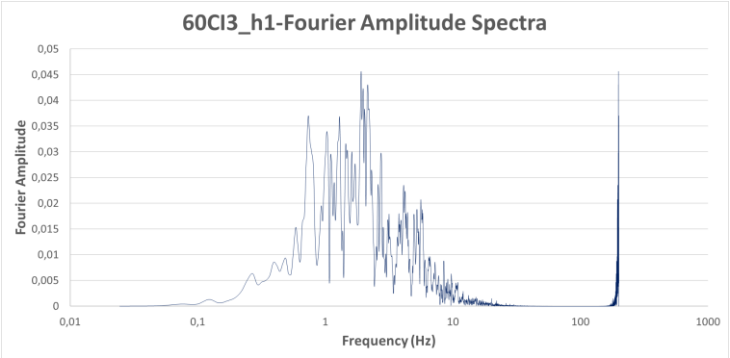

Figure B.7. Fourier Amplitude Spectra Graph of Ground Motion named 60CI3_h1

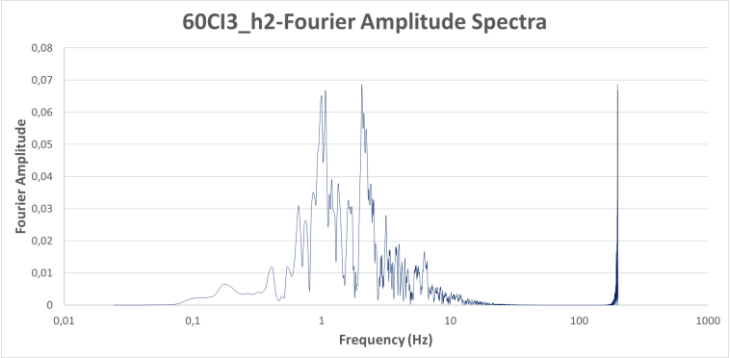

Figure B.8. Fourier Amplitude Spectra Graph of Ground Motion named 60CI3_h2

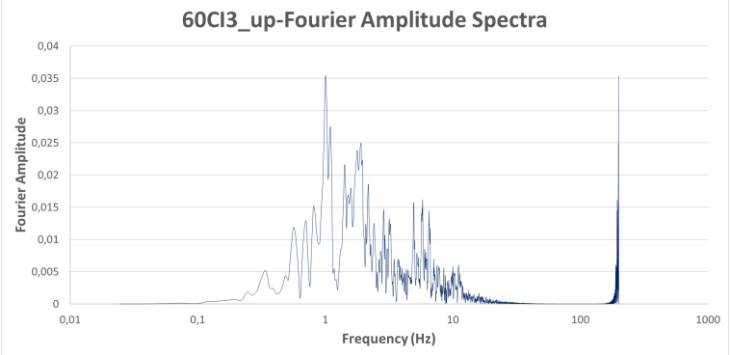

Figure B.9. Fourier Amplitude Spectra Graph of Ground Motion named 60CI3_up

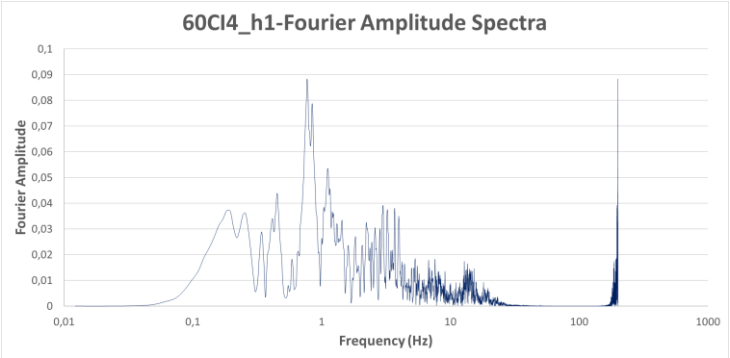

Figure B.10. Fourier Amplitude Spectra Graph of Ground Motion named 60CI4_h1

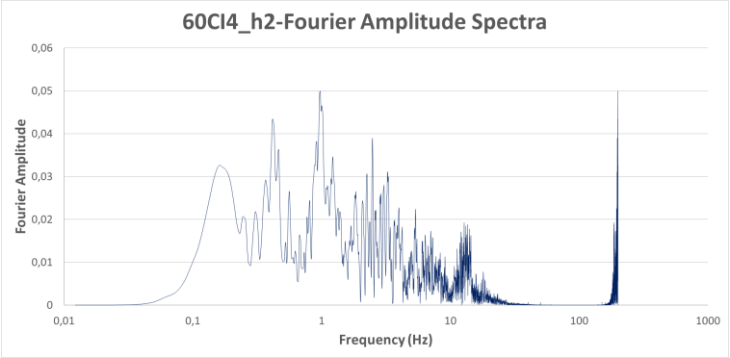

Figure B.11. Fourier Amplitude Spectra Graph of Ground Motion named 60CI4_h2

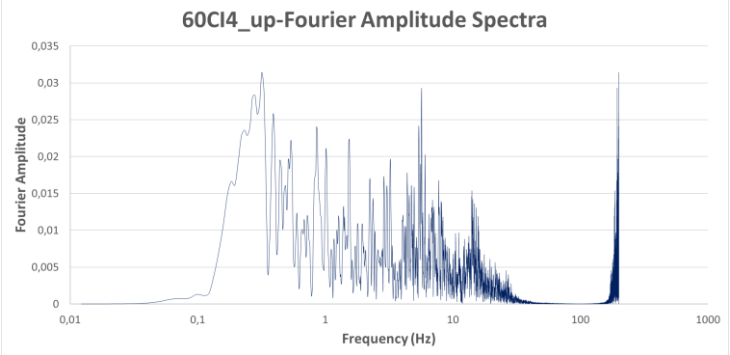

Figure B.12. Fourier Amplitude Spectra Graph of Ground Motion named 60CI4_up

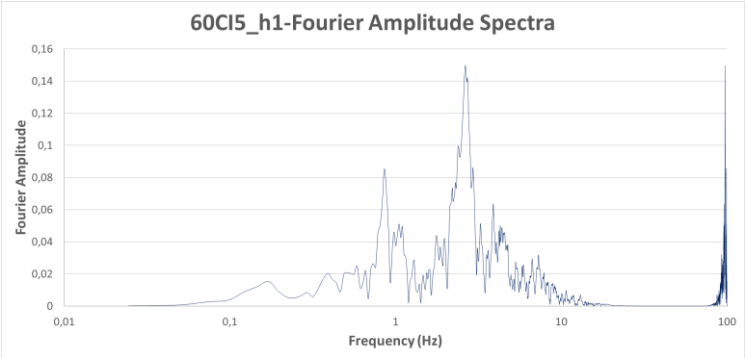

Figure B.13. Fourier Amplitude Spectra Graph of Ground Motion named 60CI5_h1

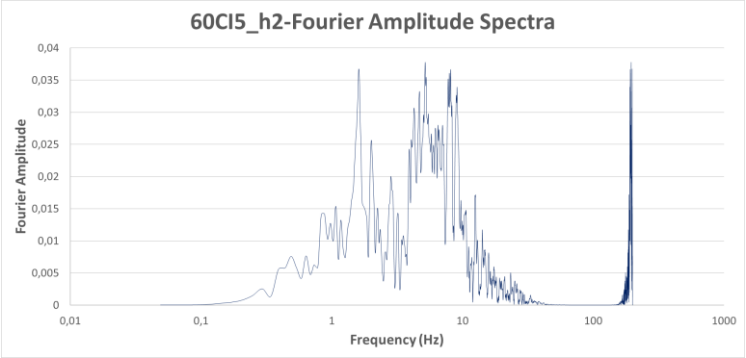

Figure B.14. Fourier Amplitude Spectra Graph of Ground Motion named 60CI5_h2

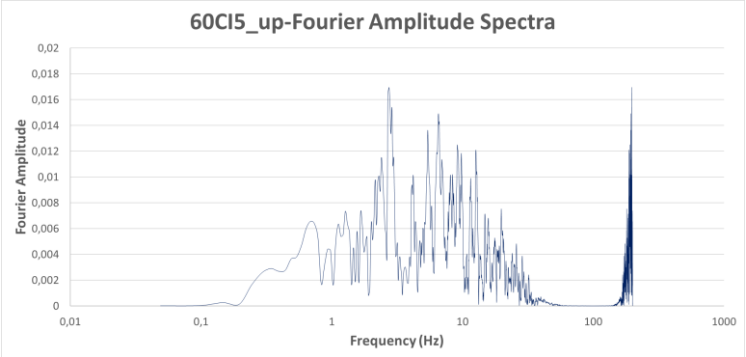

Figure B.15. Fourier Amplitude Spectra Graph of Ground Motion named 60CI5_up

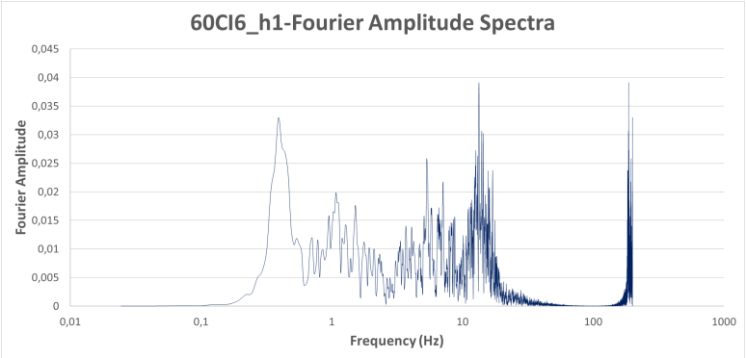

Figure B.16. Fourier Amplitude Spectra Graph of Ground Motion named 60CI6_h1

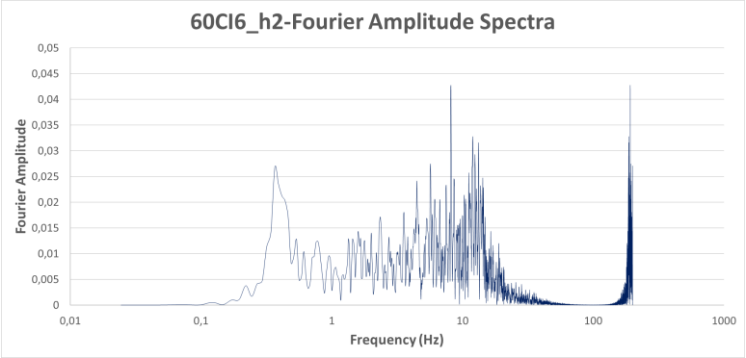

Figure B.17. Fourier Amplitude Spectra Graph of Ground Motion named 60CI6_h2

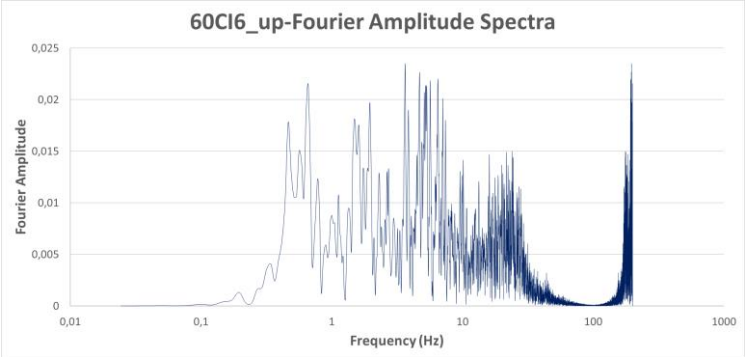

Figure B.18. Fourier Amplitude Spectra Graph of Ground Motion named 60CI6_up

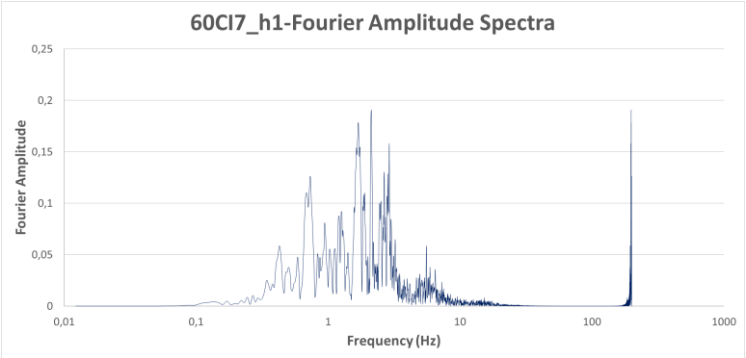

Figure B.19. Fourier Amplitude Spectra Graph of Ground Motion named 60CI7_h1

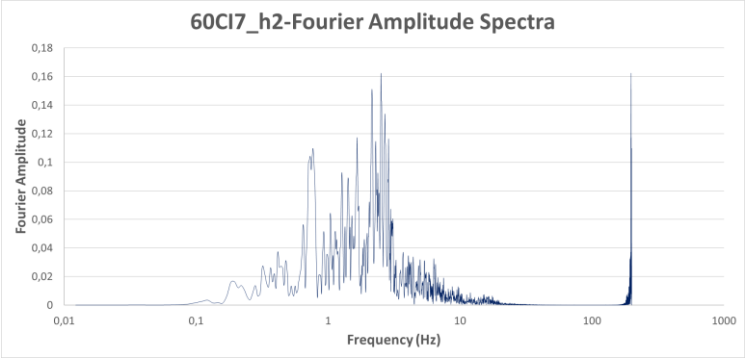

Figure B.20. Fourier Amplitude Spectra Graph of Ground Motion named 60CI7_h2

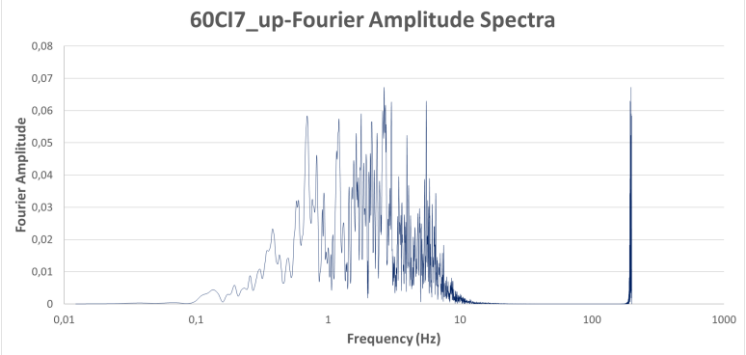

Figure B.21. Fourier Amplitude Spectra Graph of Ground Motion named 60CI7_up

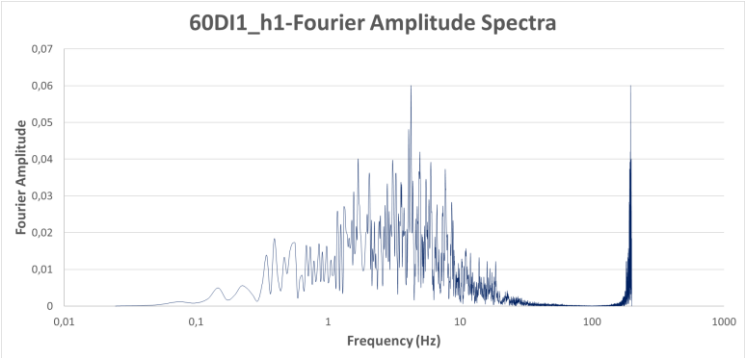

Figure B.22. Fourier Amplitude Spectra Graph of Ground Motion named 60DI1_h1

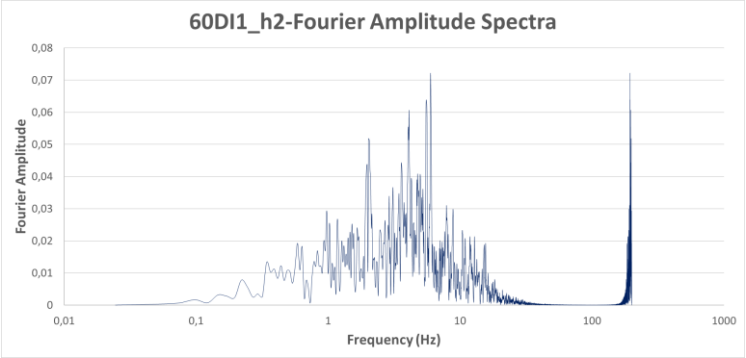

Figure B.23. Fourier Amplitude Spectra Graph of Ground Motion named 60DI1_h2

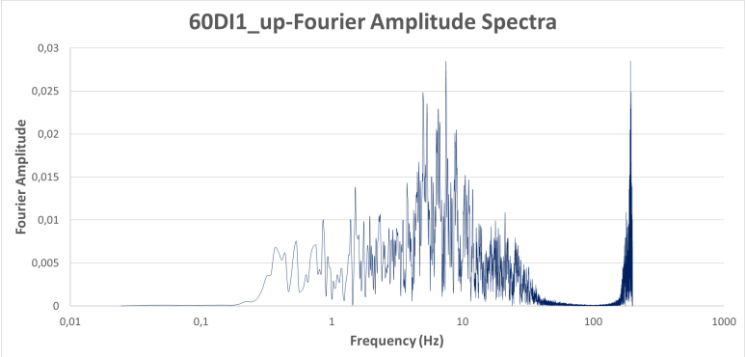

Figure B.24. Fourier Amplitude Spectra Graph of Ground Motion named 60DI1_up

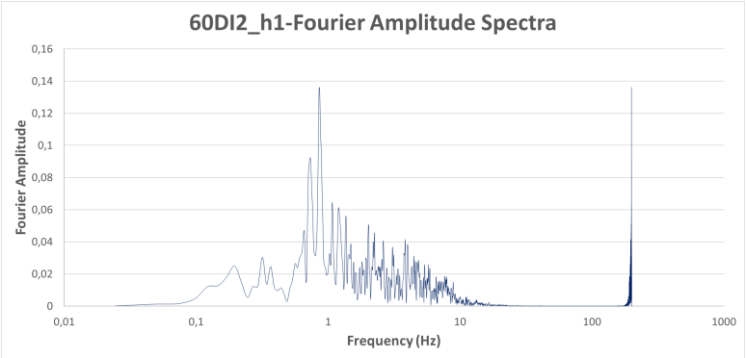

Figure B.25. Fourier Amplitude Spectra Graph of Ground Motion named 60DI2_h1

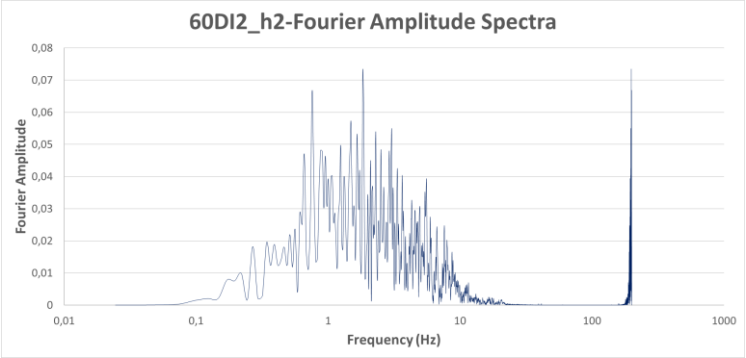

Figure B.26. Fourier Amplitude Spectra Graph of Ground Motion named 60DI2_h2

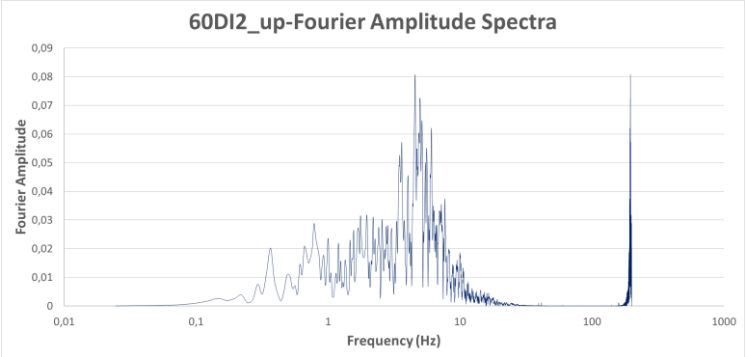

Figure B.27. Fourier Amplitude Spectra Graph of Ground Motion named 60DI2_up

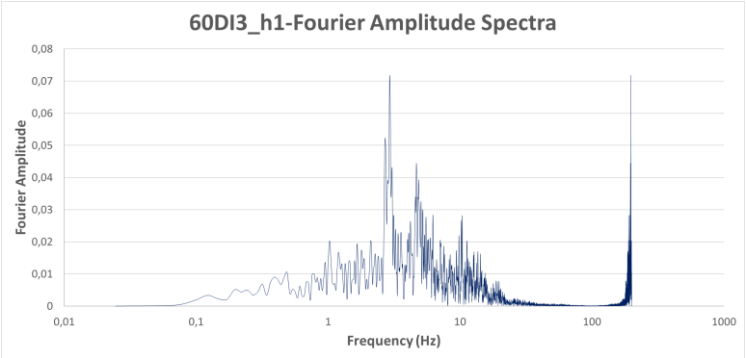

Figure B.28. Fourier Amplitude Spectra Graph of Ground Motion named 60DI3_h1

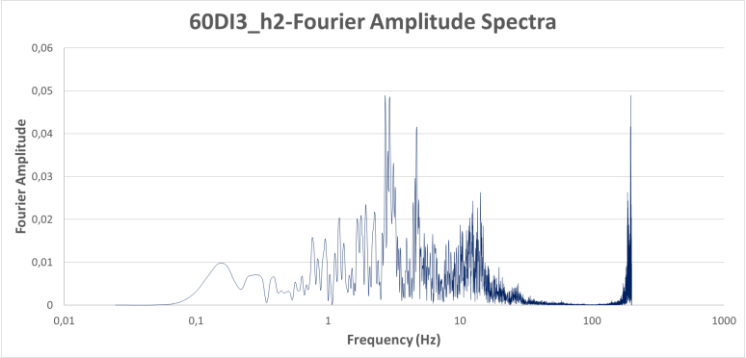

Figure B.29. Fourier Amplitude Spectra Graph of Ground Motion named 60DI3_h2

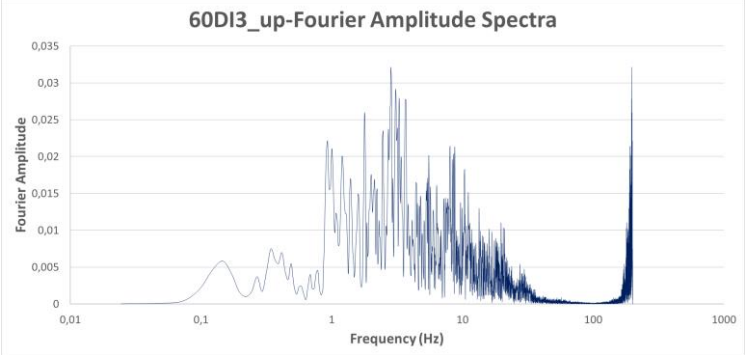

Figure B.30. Fourier Amplitude Spectra Graph of Ground Motion named 60DI3_up

3

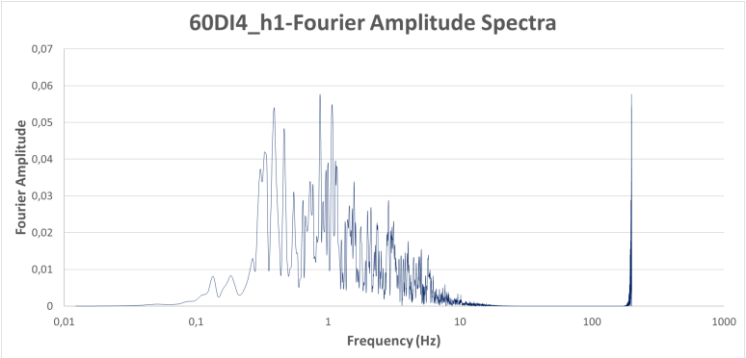

Figure B.31. Fourier Amplitude Spectra Graph of Ground Motion named 60DI4_h1

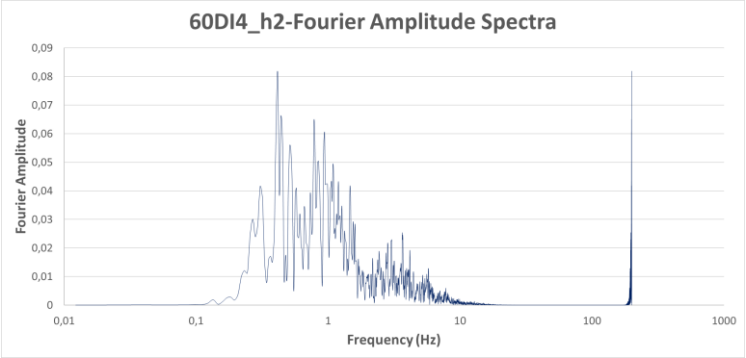

Figure B.32. Fourier Amplitude Spectra Graph of Ground Motion named 60DI4_h2

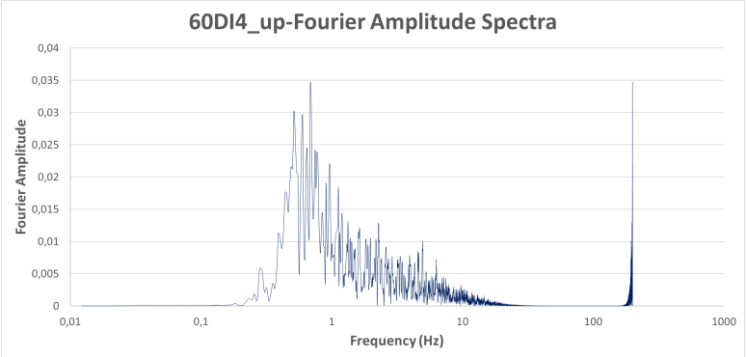

Figure B.33. Fourier Amplitude Spectra Graph of Ground Motion named 60DI4_up

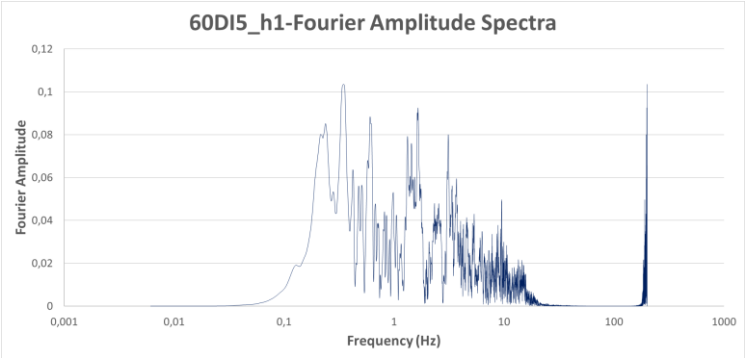

Figure B.34. Fourier Amplitude Spectra Graph of Ground Motion named 60DI5_h1

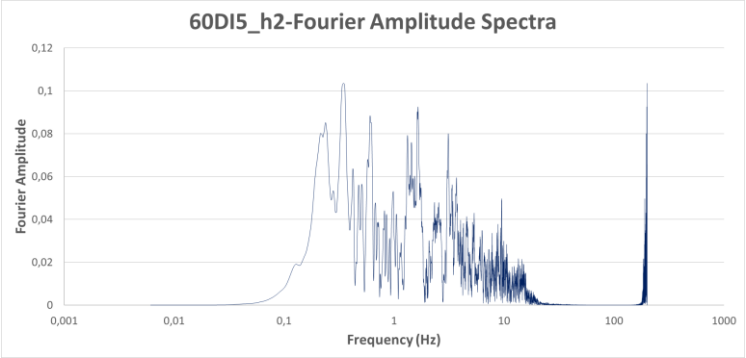

Figure B.35. Fourier Amplitude Spectra Graph of Ground Motion named 60DI5_h2

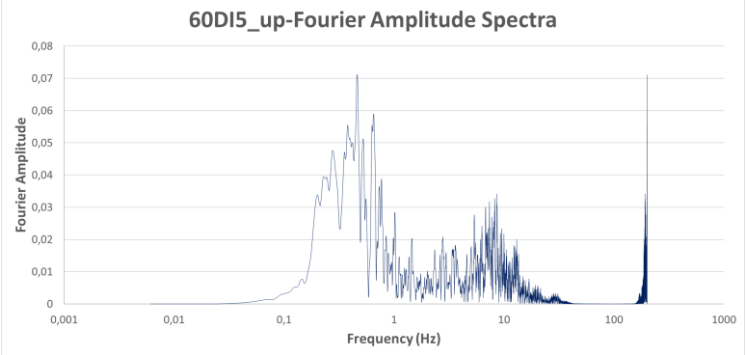

Figure B.36. Fourier Amplitude Spectra Graph of Ground Motion named 60DI5_up

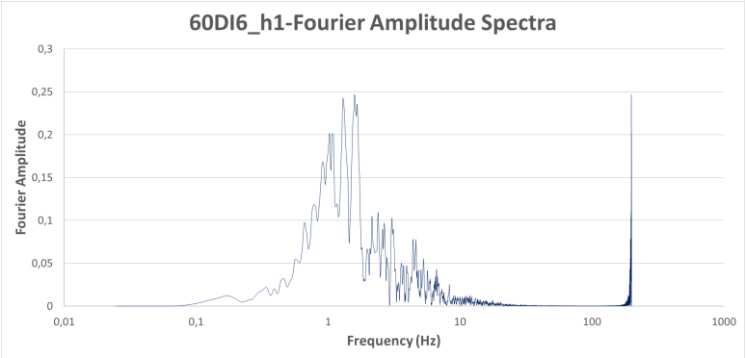

Figure B.37. Fourier Amplitude Spectra Graph of Ground Motion named 60DI6_h1

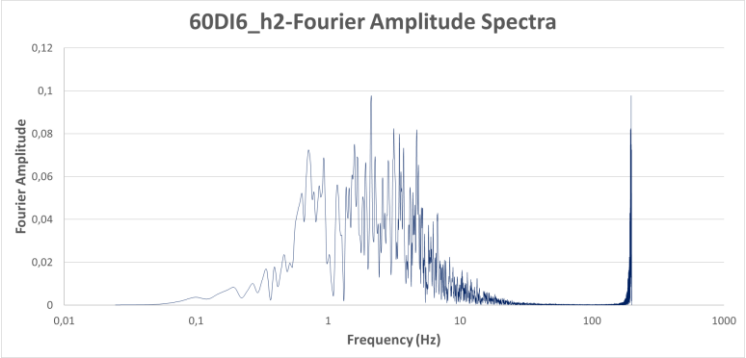

Figure B.38. Fourier Amplitude Spectra Graph of Ground Motion named 60DI6_h2

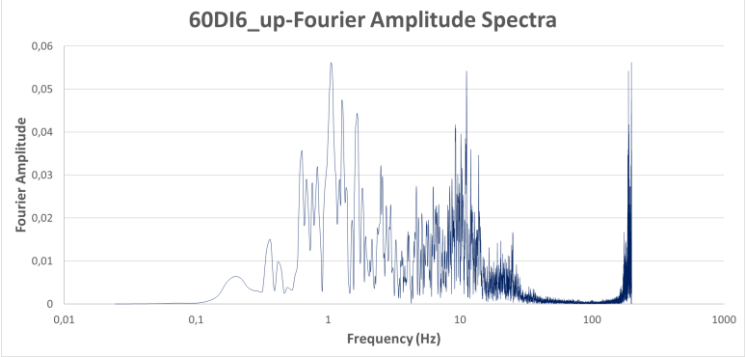

Figure B.39. Fourier Amplitude Spectra Graph of Ground Motion named 60DI6_up

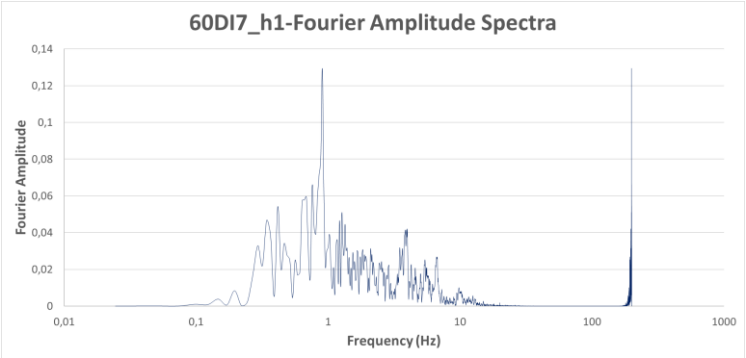

Figure B.40. Fourier Amplitude Spectra Graph of Ground Motion named 60DI7_h1

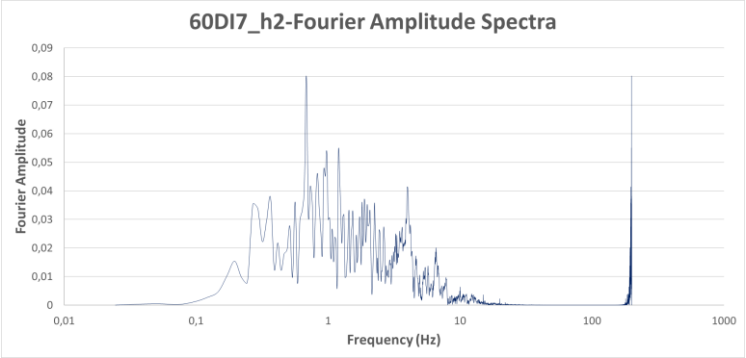

Figure B.41. Fourier Amplitude Spectra Graph of Ground Motion named 60DI7_h2

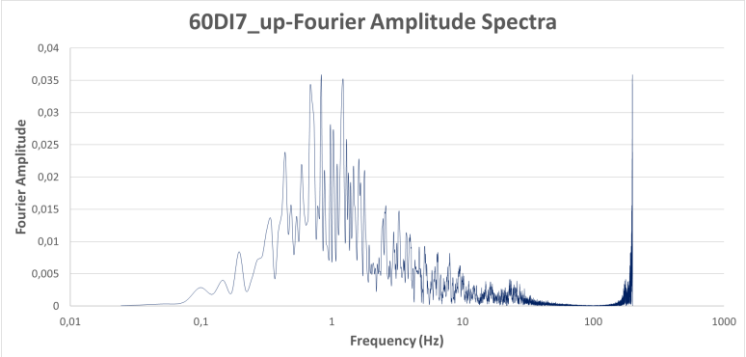

Figure B.42. Fourier Amplitude Spectra Graph of Ground Motion named 60DI7_up

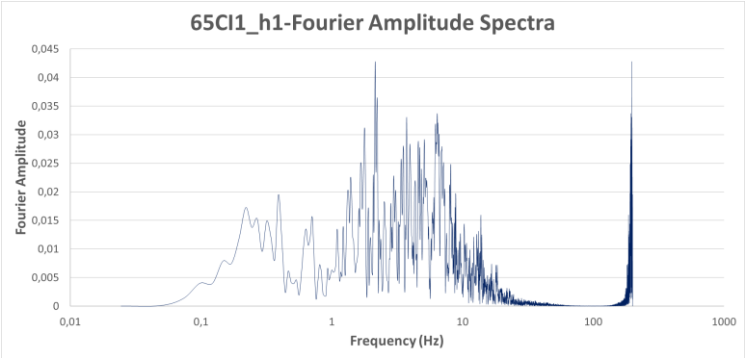

Figure B.43. Fourier Amplitude Spectra Graph of Ground Motion named 65CI1_h1

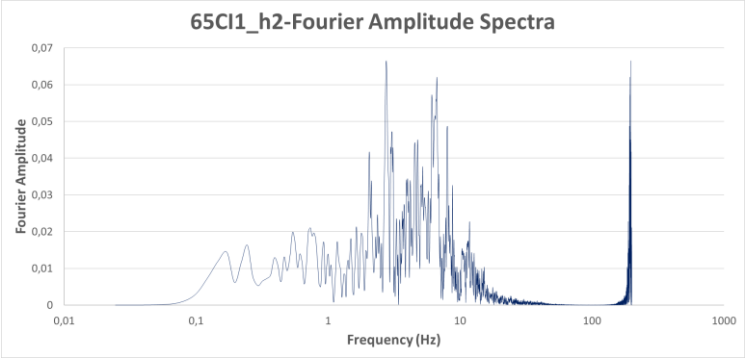

Figure B.44. Fourier Amplitude Spectra Graph of Ground Motion named 65CI1_h2

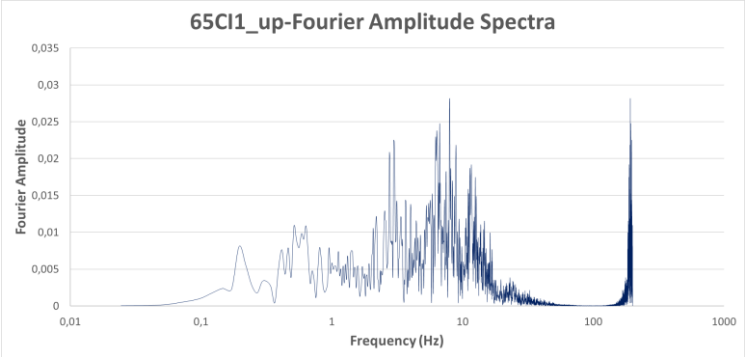

Figure B.45. Fourier Amplitude Spectra Graph of Ground Motion named 65CI1_up

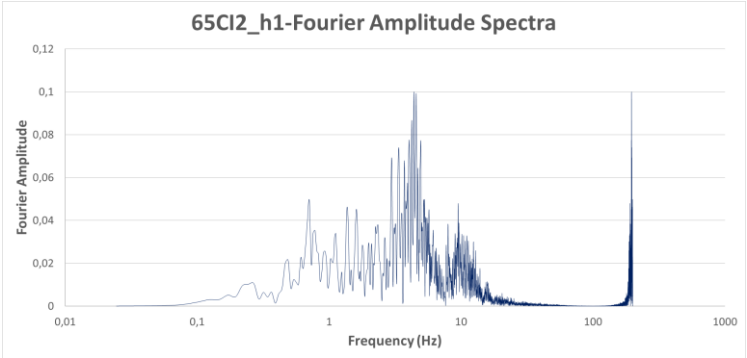

Figure B.46. Fourier Amplitude Spectra Graph of Ground Motion named 65CI2_h1

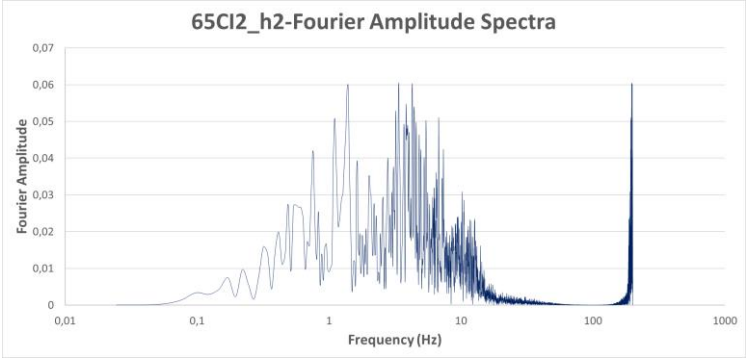

Figure B.47. Fourier Amplitude Spectra Graph of Ground Motion named 65CI2_h2

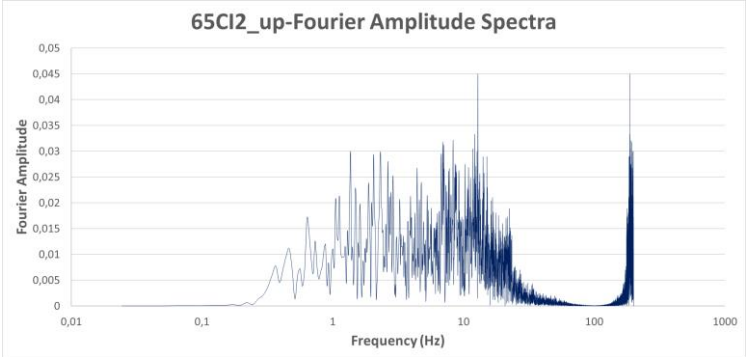

Figure B.48. Fourier Amplitude Spectra Graph of Ground Motion named 65CI2_up

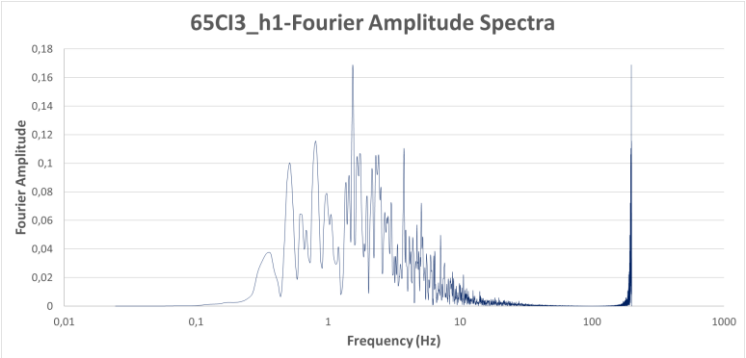

Figure B.49. Fourier Amplitude Spectra Graph of Ground Motion named 65CI3_h1

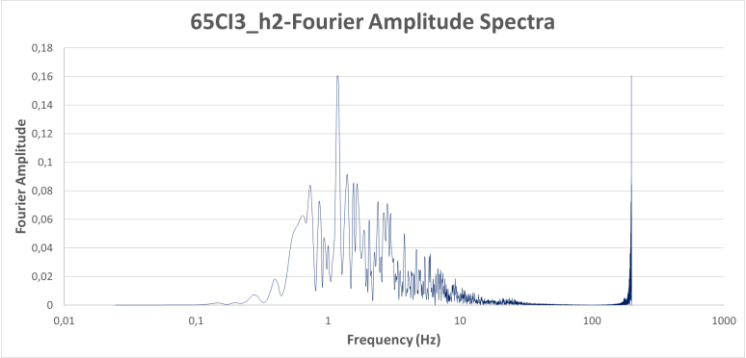

Figure B.50. Fourier Amplitude Spectra Graph of Ground Motion named 65CI3_h2

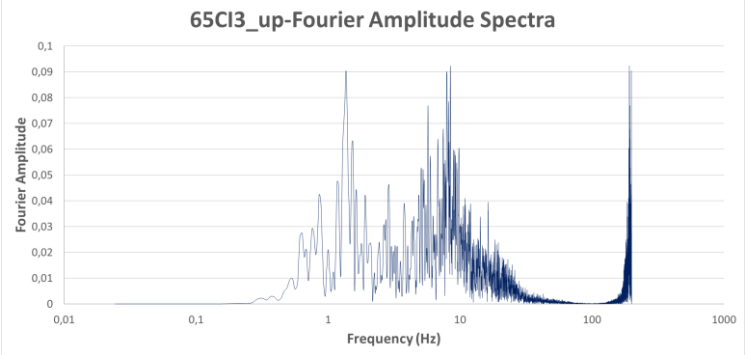

Figure B.51. Fourier Amplitude Spectra Graph of Ground Motion named 65CI3_up

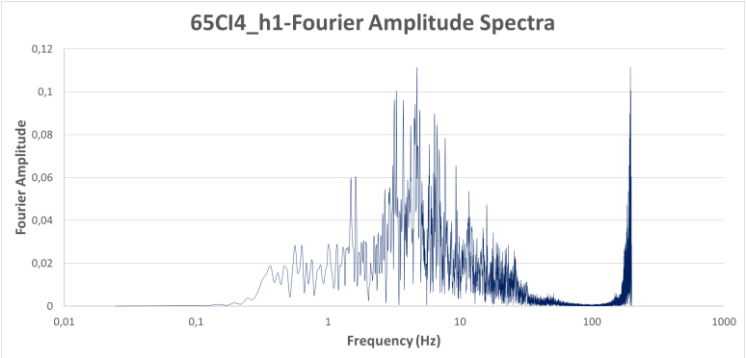

Figure B.52. Fourier Amplitude Spectra Graph of Ground Motion named 65CI4_h1

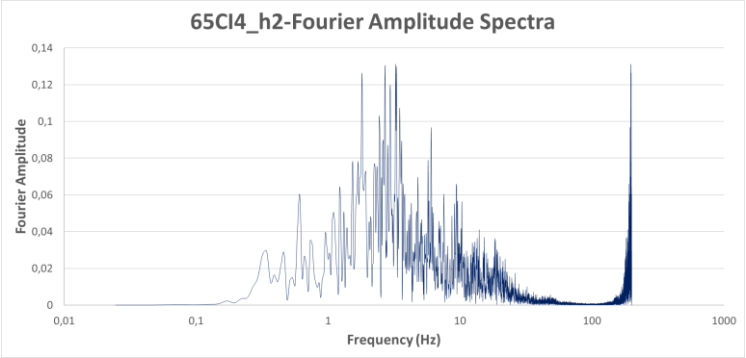

Figure B.53. Fourier Amplitude Spectra Graph of Ground Motion named 65CI4_h2

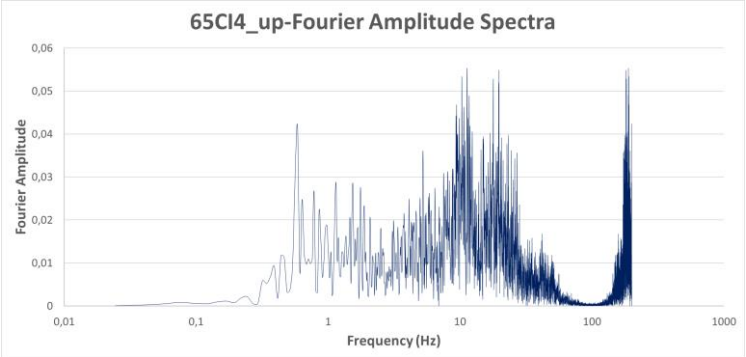

Figure B.54. Fourier Amplitude Spectra Graph of Ground Motion named 65CI4_up

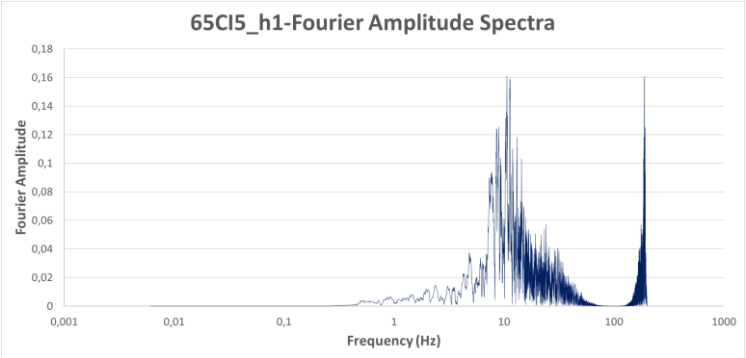

Figure B.55. Fourier Amplitude Spectra Graph of Ground Motion named 65CI5_h1

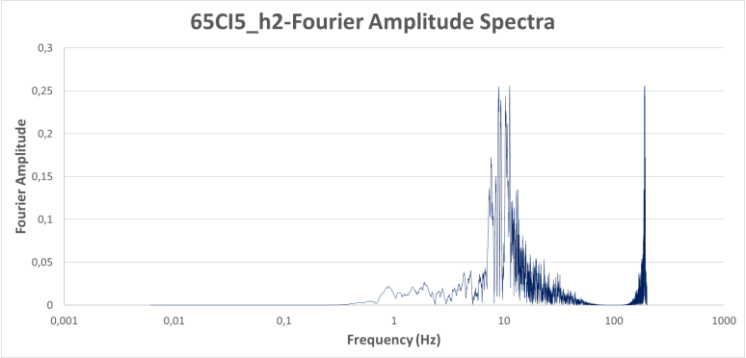

Figure B.56. Fourier Amplitude Spectra Graph of Ground Motion named 65CI5_h2

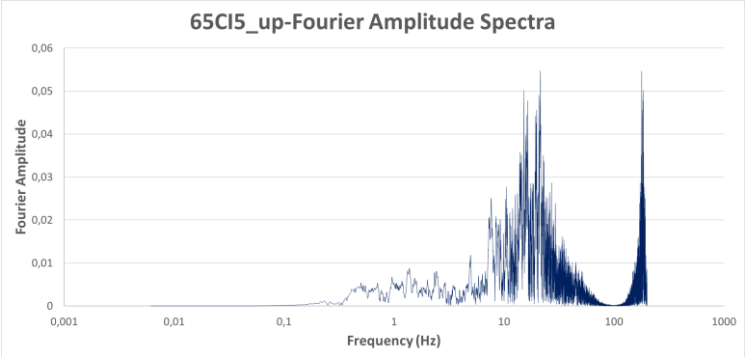

Figure B.57. Fourier Amplitude Spectra Graph of Ground Motion named 65CI5_up

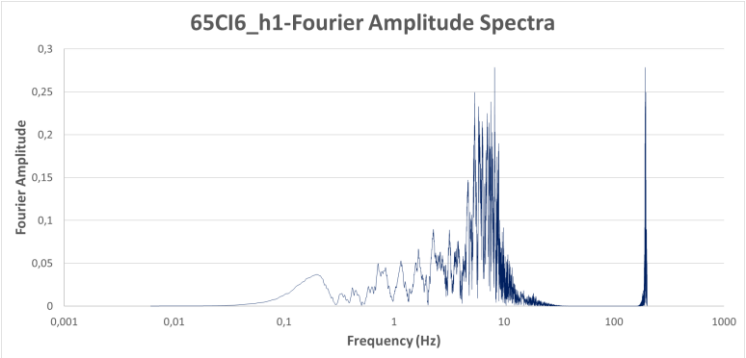

Figure B.58. Fourier Amplitude Spectra Graph of Ground Motion named 65CI6_h1

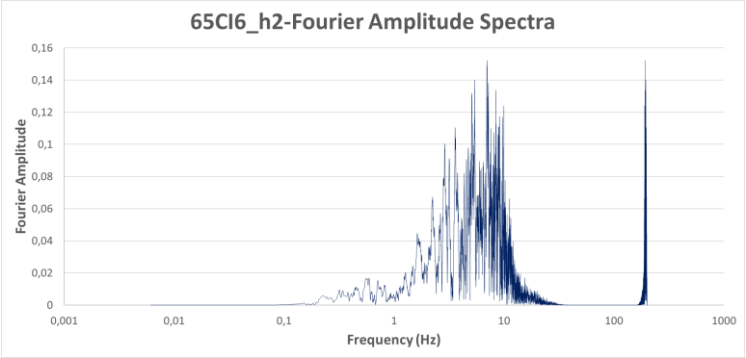

Figure B.59. Fourier Amplitude Spectra Graph of Ground Motion named 65CI6_h2

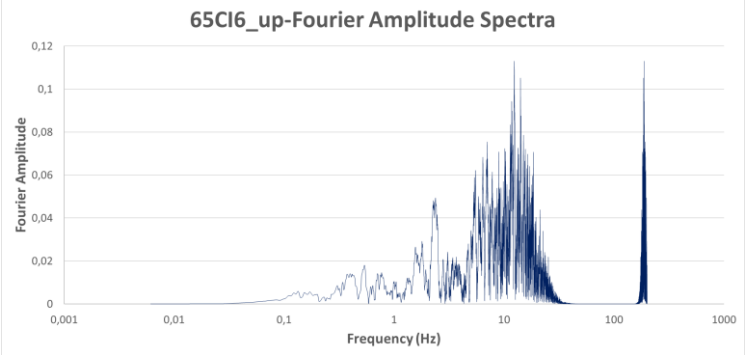

Figure B.60. Fourier Amplitude Spectra Graph of Ground Motion named 65CI6_up

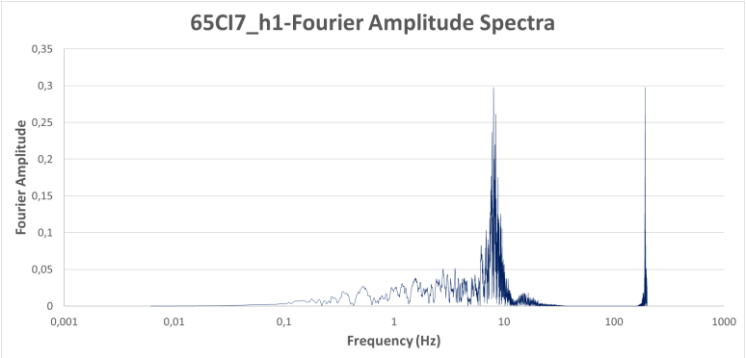

Figure B.61. Fourier Amplitude Spectra Graph of Ground Motion named 65CI7_h1

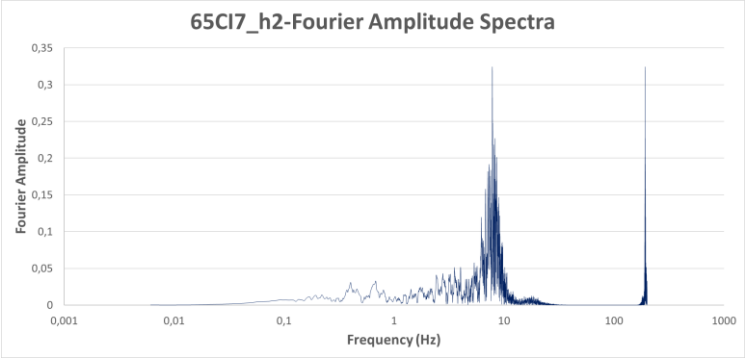

Figure B.62. Fourier Amplitude Spectra Graph of Ground Motion named 65CI7_h2

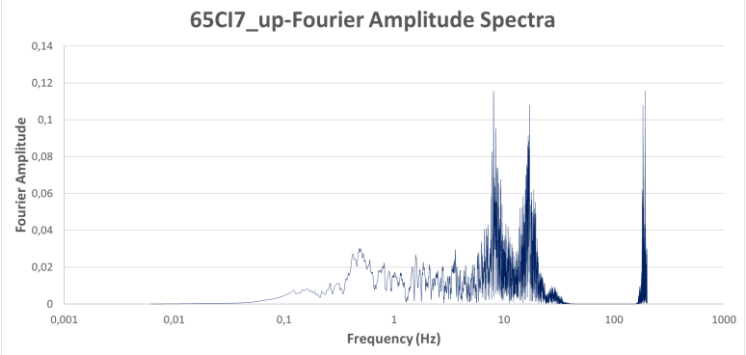

Figure B.63. Fourier Amplitude Spectra Graph of Ground Motion named 65CI7_up

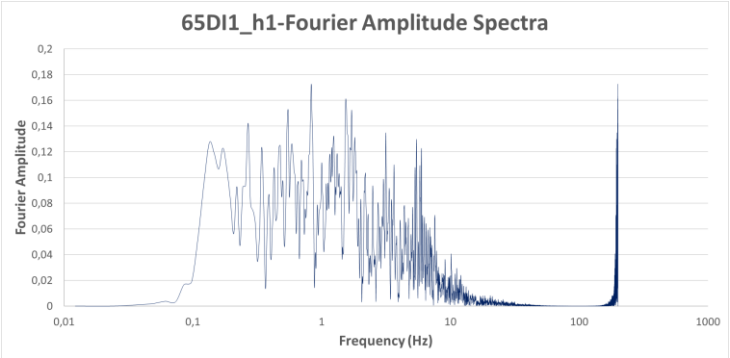

Figure B.64. Fourier Amplitude Spectra Graph of Ground Motion named 65DI1_h1

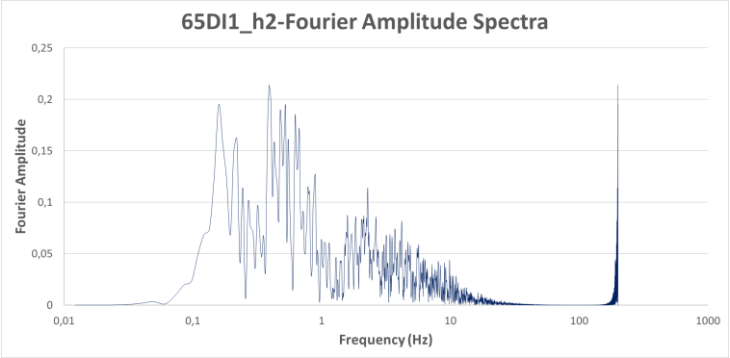

Figure B65. Fourier Amplitude Spectra Graph of Ground Motion named 65DI1_h2

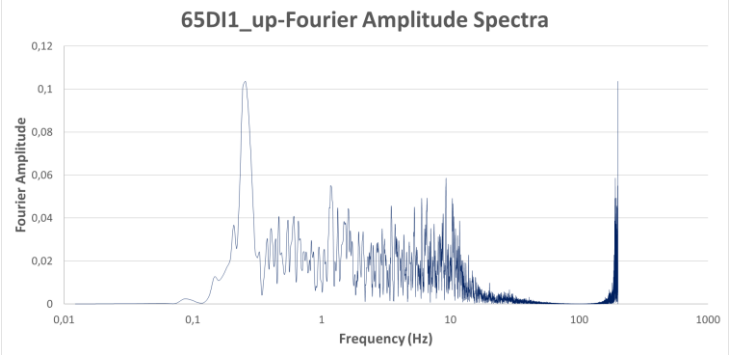

Figure B.66. Fourier Amplitude Spectra Graph of Ground Motion named 65DI1_up

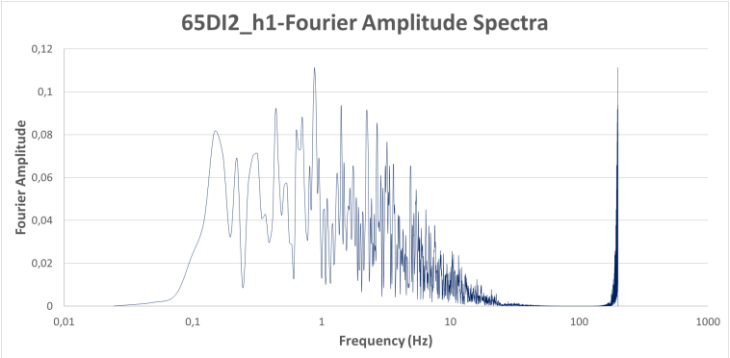

Figure B.67. Fourier Amplitude Spectra Graph of Ground Motion named 65DI2_h1

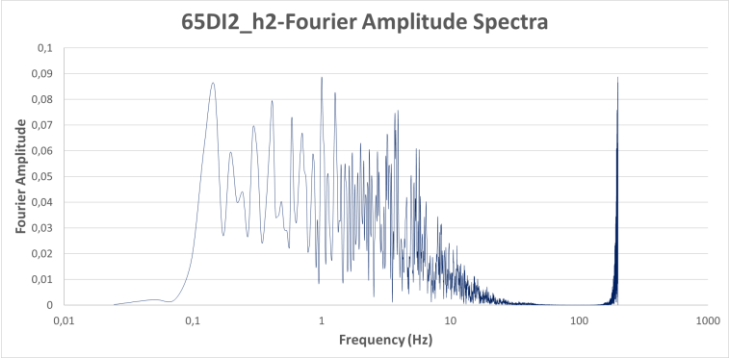

Figure B.68. Fourier Amplitude Spectra Graph of Ground Motion named 65DI2_h2

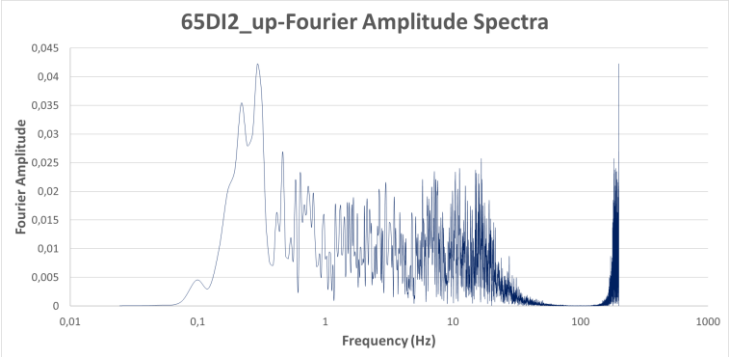

Figure B.69. Fourier Amplitude Spectra Graph of Ground Motion named 65DI2_up

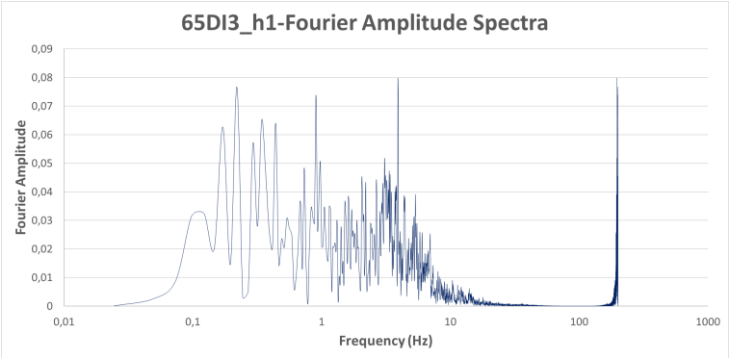

Figure B.70. Fourier Amplitude Spectra Graph of Ground Motion named 65DI3_h1

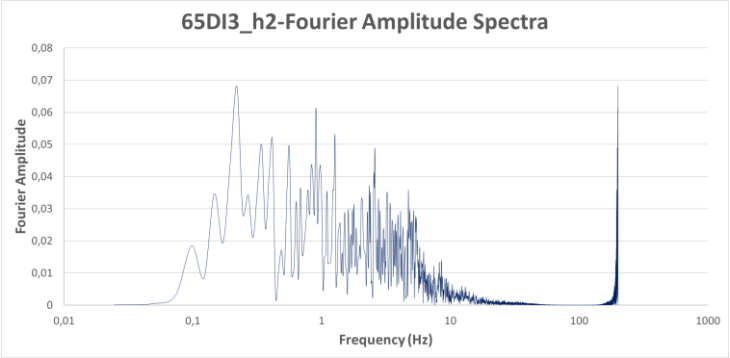

Figure B.71. Fourier Amplitude Spectra Graph of Ground Motion named 65DI3_h2

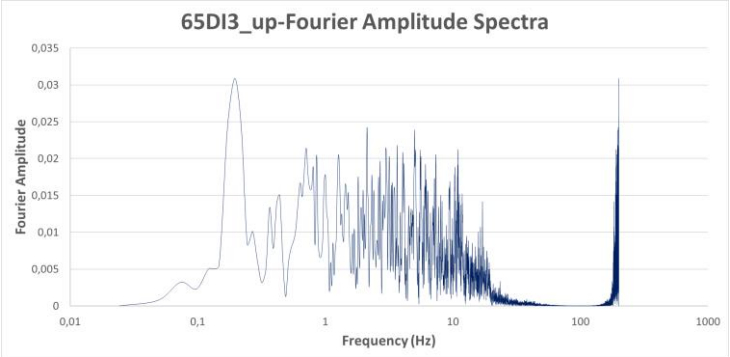

Figure B.72. Fourier Amplitude Spectra Graph of Ground Motion named 65DI3_up

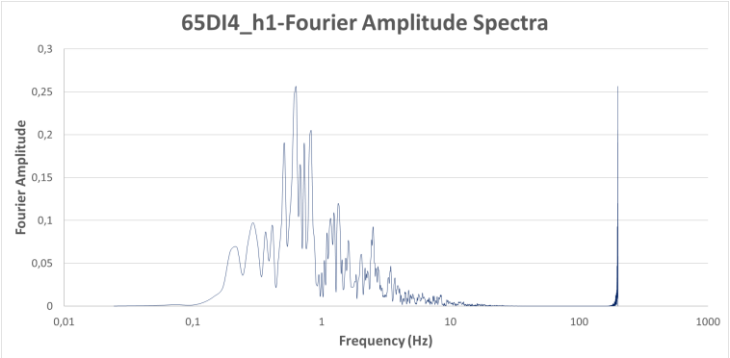

Figure B.73. Fourier Amplitude Spectra Graph of Ground Motion named 65DI4_h1

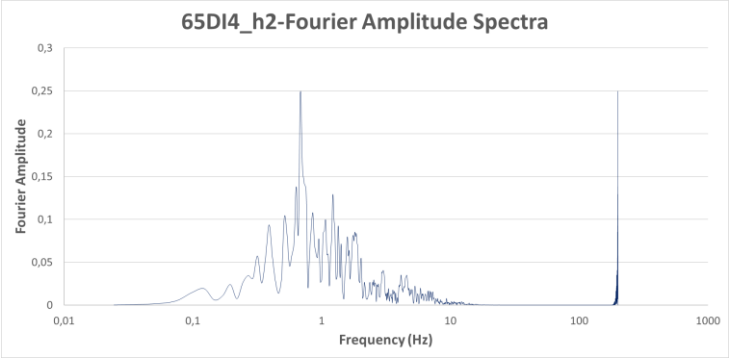

Figure B.74. Fourier Amplitude Spectra Graph of Ground Motion named 65DI4_h2

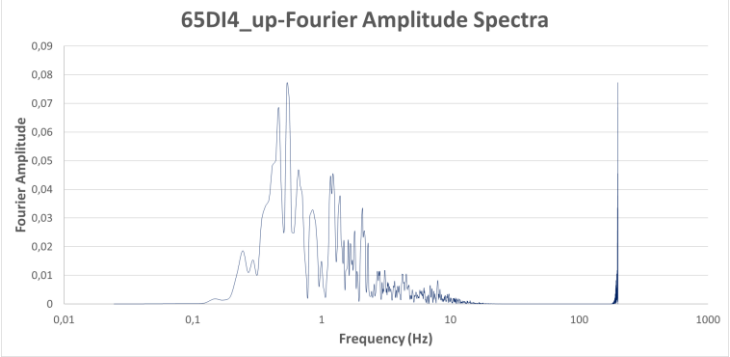

Figure B.75. Fourier Amplitude Spectra Graph of Ground Motion named 65DI4_up

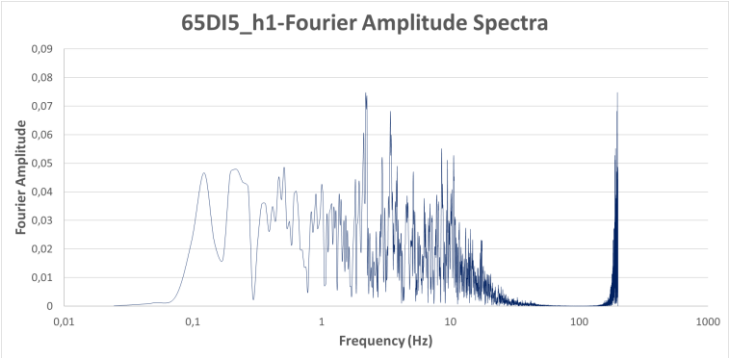

Figure B.76. Fourier Amplitude Spectra Graph of Ground Motion named 65DI5_h1

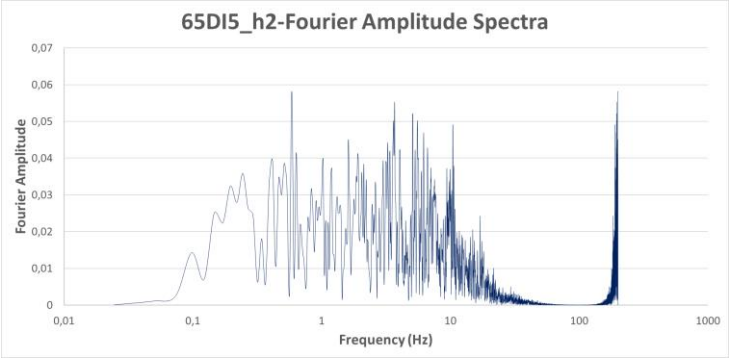

Figure B.77. Fourier Amplitude Spectra Graph of Ground Motion named 65DI5_h2

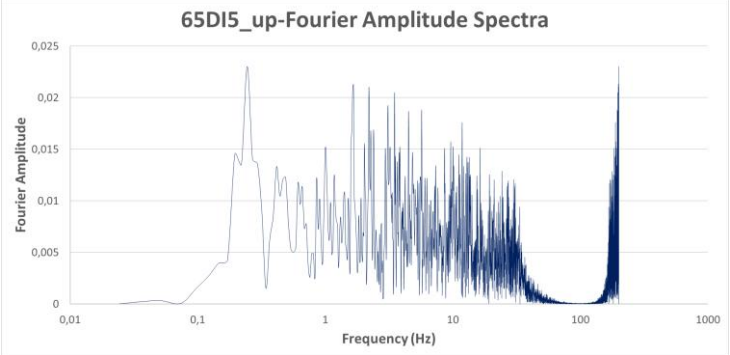

Figure B.78. Fourier Amplitude Spectra Graph of Ground Motion named 65DI5_up

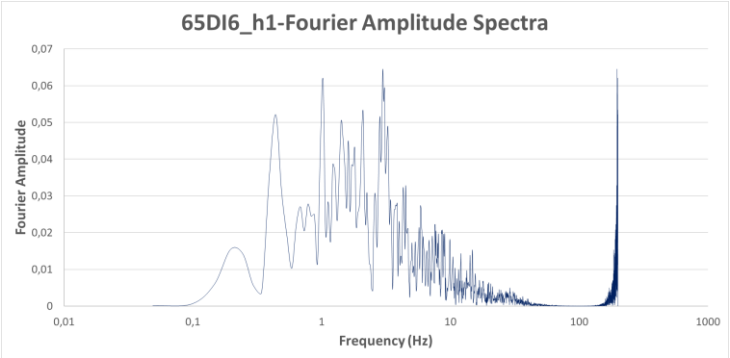

Figure B.79. Fourier Amplitude Spectra Graph of Ground Motion named 65DI6_h1

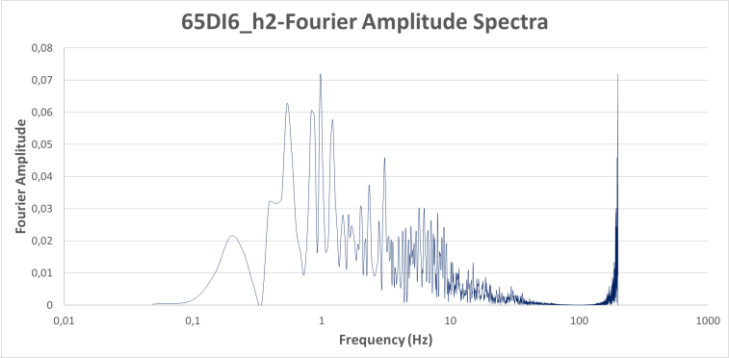

Figure B.80. Fourier Amplitude Spectra Graph of Ground Motion named 65DI6_h2

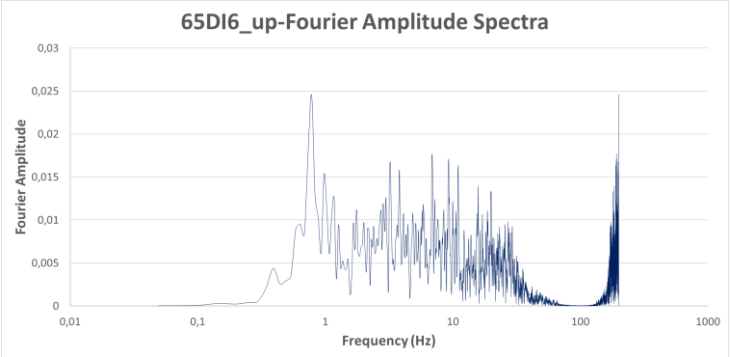

Figure B.81. Fourier Amplitude Spectra Graph of Ground Motion named 65DI6_up

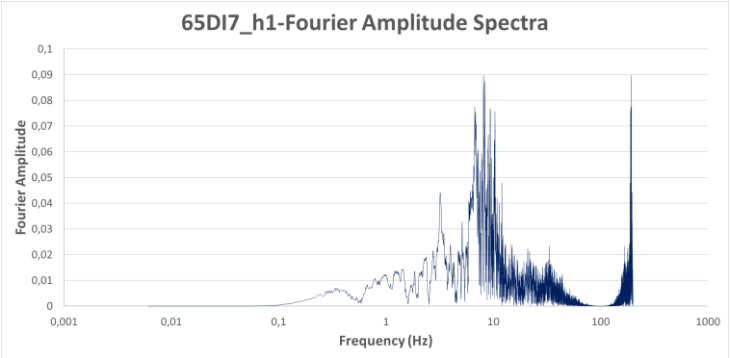

Figure B.82. Fourier Amplitude Spectra Graph of Ground Motion named 65DI7_h1

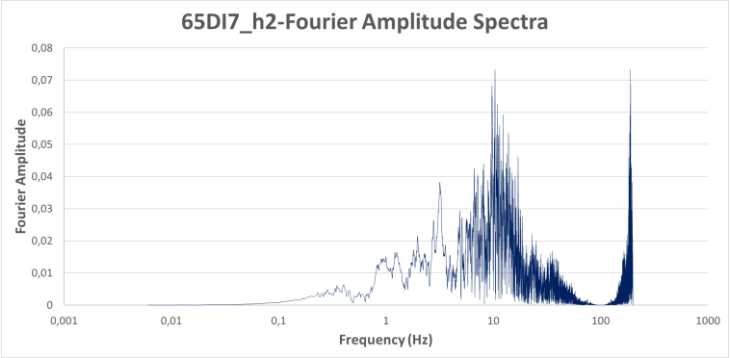

Figure B.83. Fourier Amplitude Spectra Graph of Ground Motion named 65DI7_h2

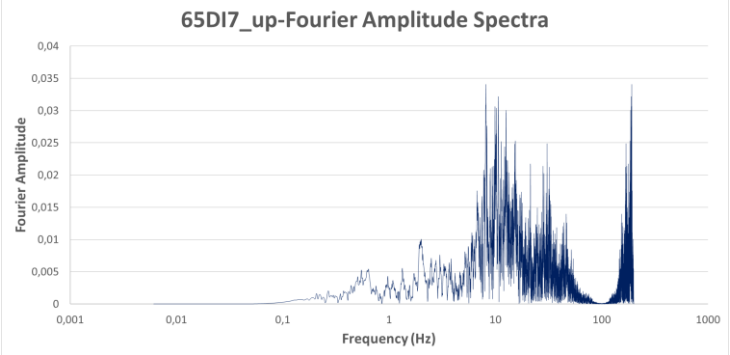

Figure B.84. Fourier Amplitude Spectra Graph of Ground Motion named 65DI7_up

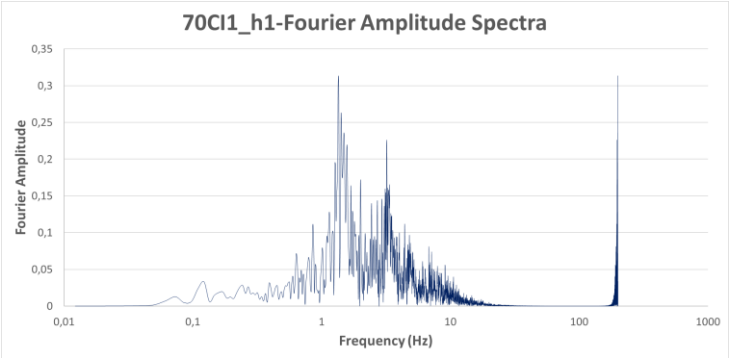

Figure B.85. Fourier Amplitude Spectra Graph of Ground Motion named 70CI1_h1

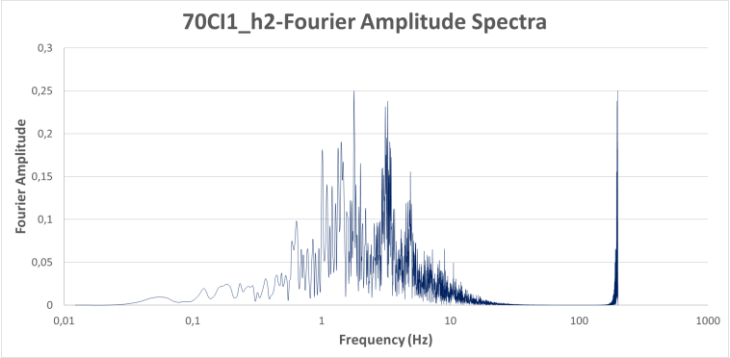

Figure B.86. Fourier Amplitude Spectra Graph of Ground Motion named 70CI1_h2

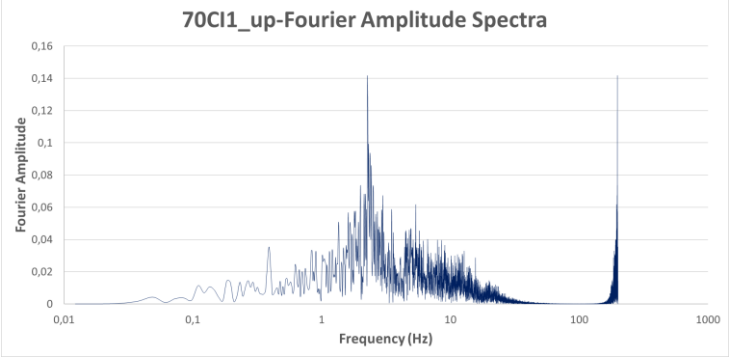

Figure B.87. Fourier Amplitude Spectra Graph of Ground Motion named 70CI1_up

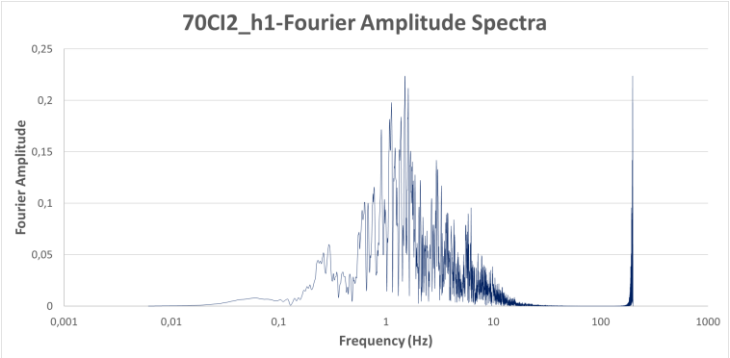

Figure B.88. Fourier Amplitude Spectra Graph of Ground Motion named 70CI2_h1

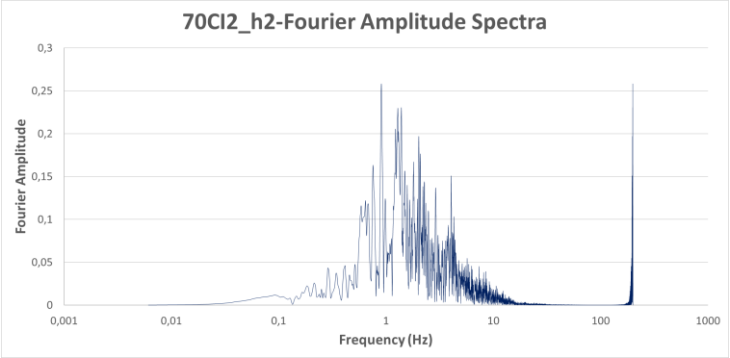

Figure B.89. Fourier Amplitude Spectra Graph of Ground Motion named 70CI2_h2

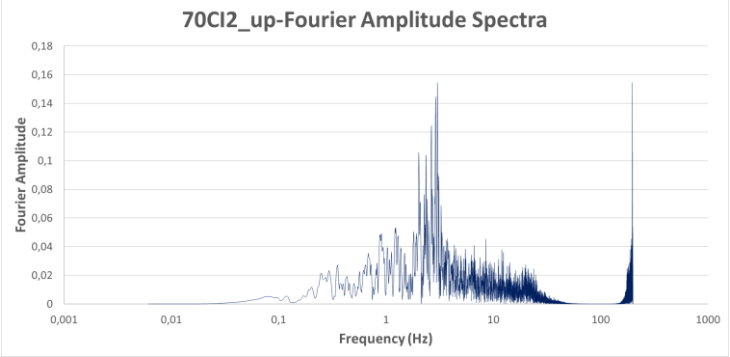

Figure B.90. Fourier Amplitude Spectra Graph of Ground Motion named 70CI2_up

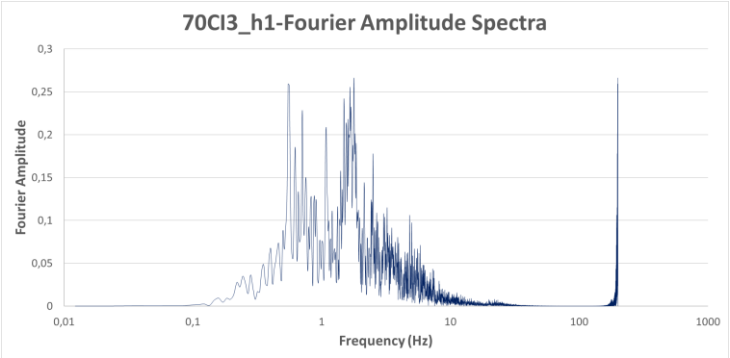

Figure B.91. Fourier Amplitude Spectra Graph of Ground Motion named 70CI3_h1

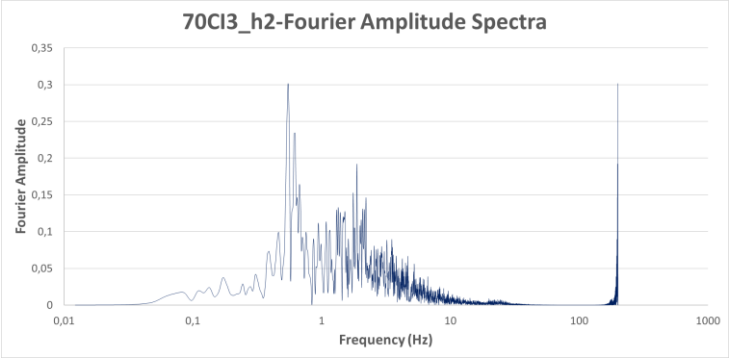

Figure B.92. Fourier Amplitude Spectra Graph of Ground Motion named 70CI3_h2

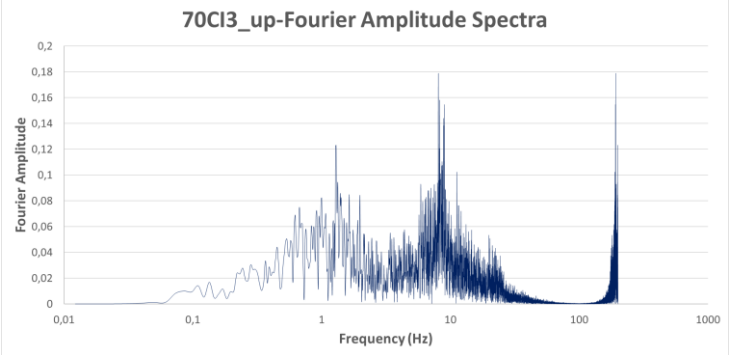

Figure B.93. Fourier Amplitude Spectra Graph of Ground Motion named 70CI3_up

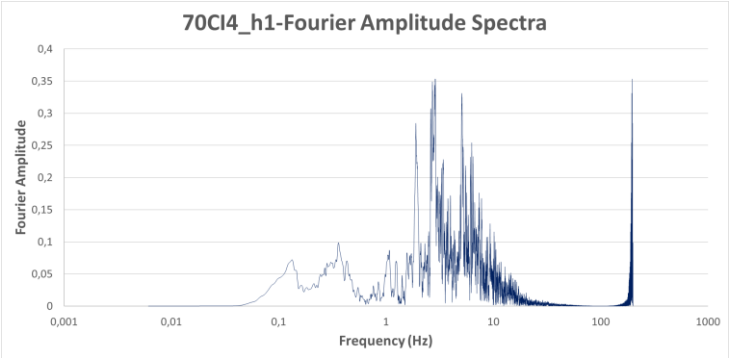

Figure B.94. Fourier Amplitude Spectra Graph of Ground Motion named 70CI4_h1

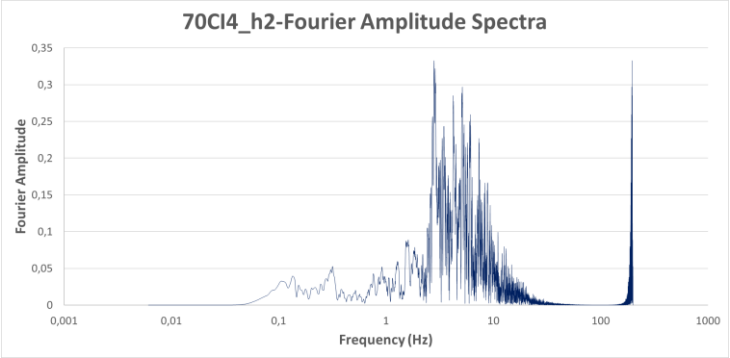

Figure B.95. Fourier Amplitude Spectra Graph of Ground Motion named 70CI4_h2

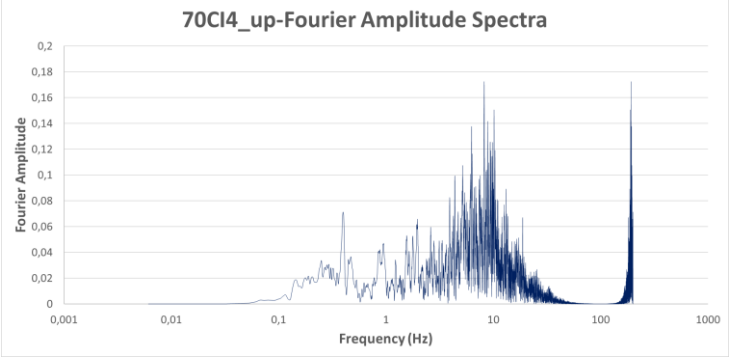

Figure B.96. Fourier Amplitude Spectra Graph of Ground Motion named 70CI4_up

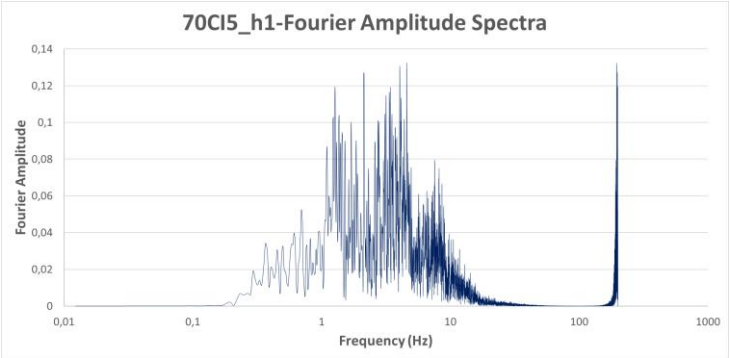

Figure B.97. Fourier Amplitude Spectra Graph of Ground Motion named 70CI5_h1

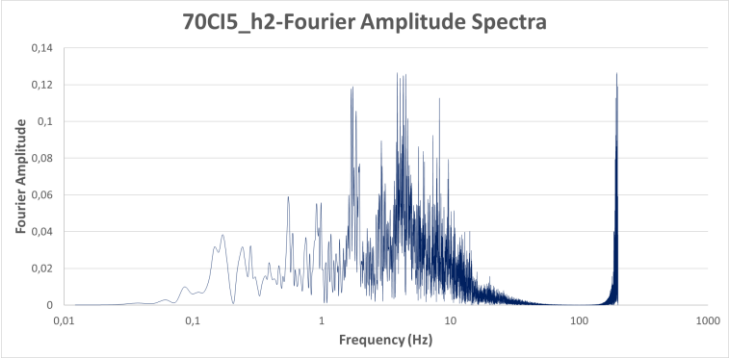

Figure B.98. Fourier Amplitude Spectra Graph of Ground Motion named 70CI5_h2

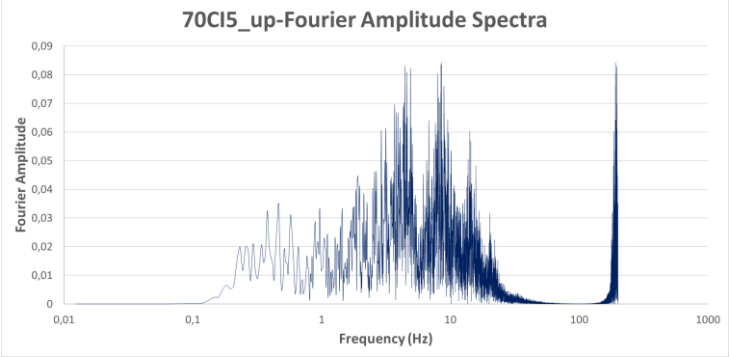

Figure B.99. Fourier Amplitude Spectra Graph of Ground Motion named 70CI5_up

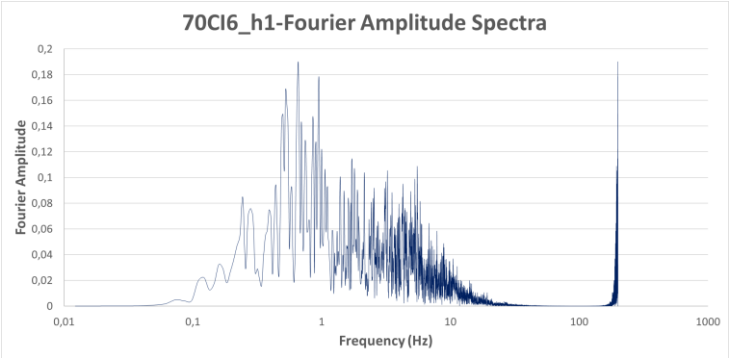

Figure B.100. Fourier Amplitude Spectra Graph of Ground Motion named 70CI6_h1

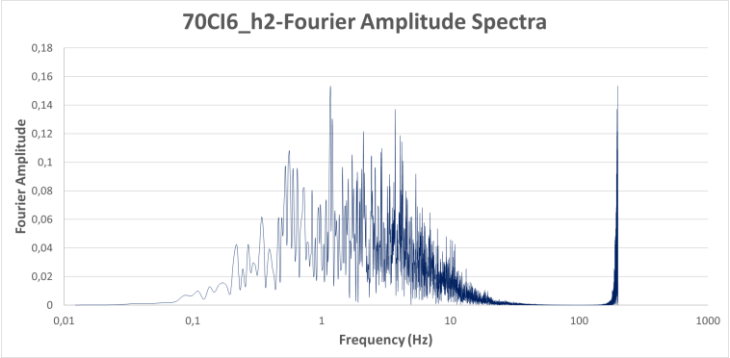

Figure B.101. Fourier Amplitude Spectra Graph of Ground Motion named 70CI6_h2

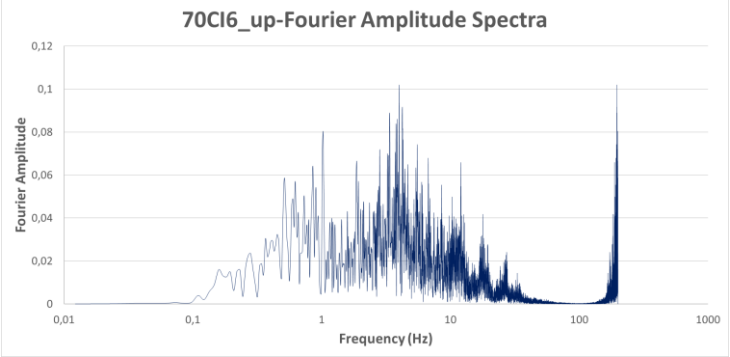

Figure B.102. Fourier Amplitude Spectra Graph of Ground Motion named 70CI6_up

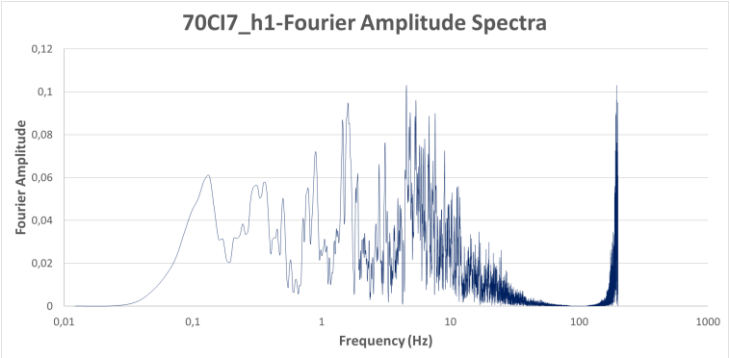

Figure B.103. Fourier Amplitude Spectra Graph of Ground Motion named 70CI7_h1

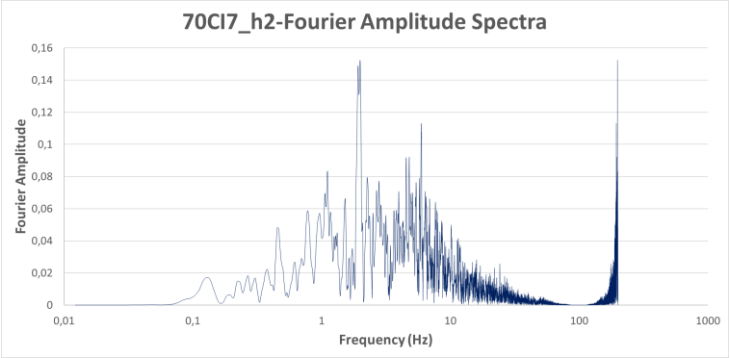

Figure B.104. Fourier Amplitude Spectra Graph of Ground Motion named 70CI7_h2

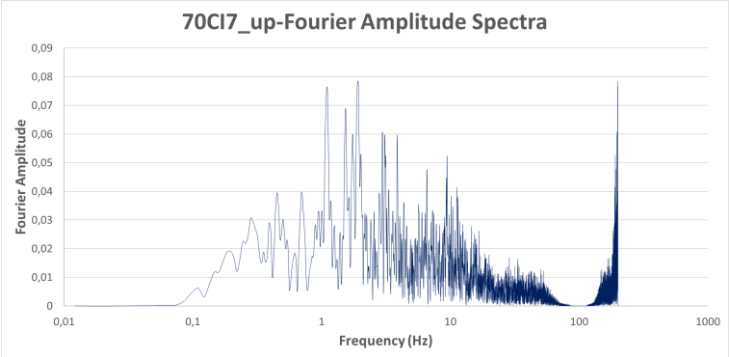

Figure B.105. Fourier Amplitude Spectra Graph of Ground Motion named 70CI7_up

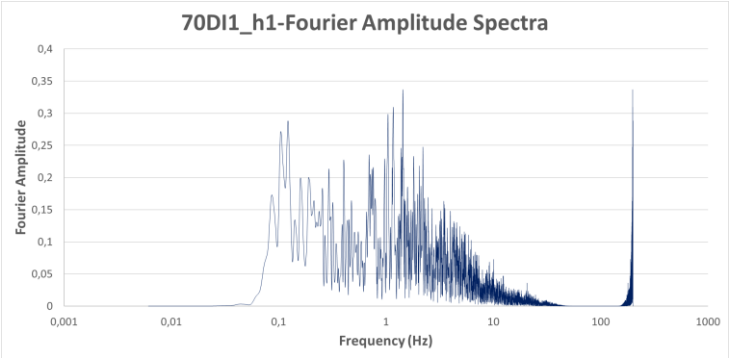

Figure B.106. Fourier Amplitude Spectra Graph of Ground Motion named 70DI1_h1

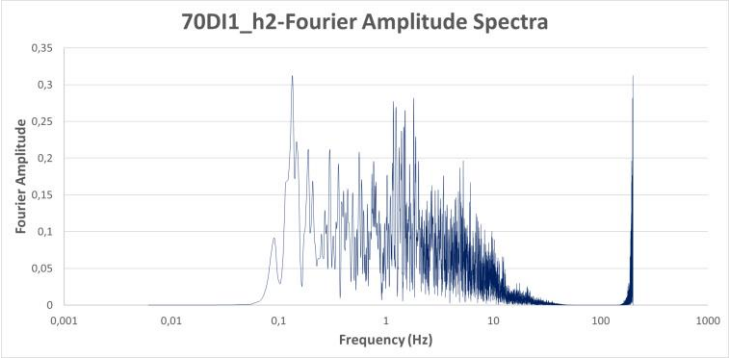

Figure B.107. Fourier Amplitude Spectra Graph of Ground Motion named 70DI1_h2

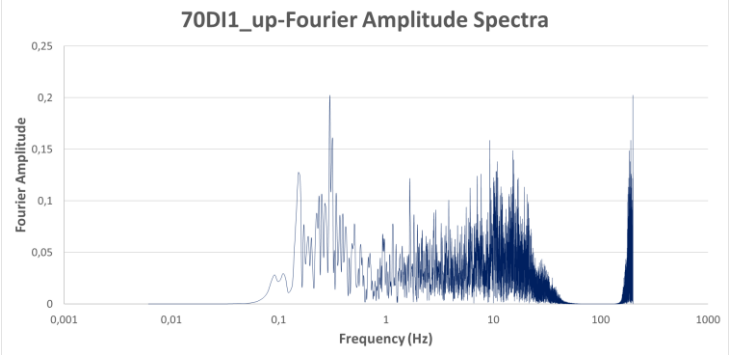

Figure B.108. Fourier Amplitude Spectra Graph of Ground Motion named 70DI1_up

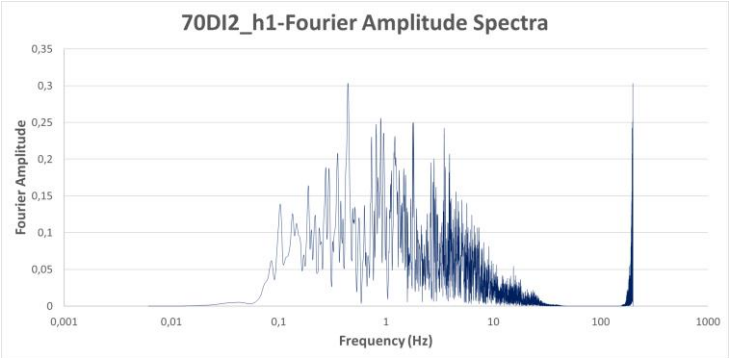

Figure B.109. Fourier Amplitude Spectra Graph of Ground Motion named 70DI2_h1

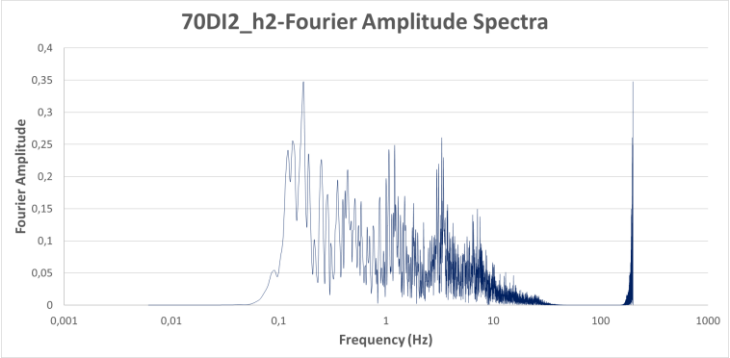

Figure B.110. Fourier Amplitude Spectra Graph of Ground Motion named 70DI2_h2

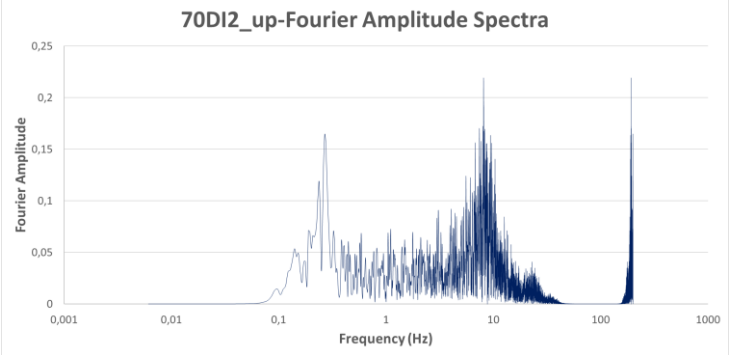

Figure B.111. Fourier Amplitude Spectra Graph of Ground Motion named 70DI2_up

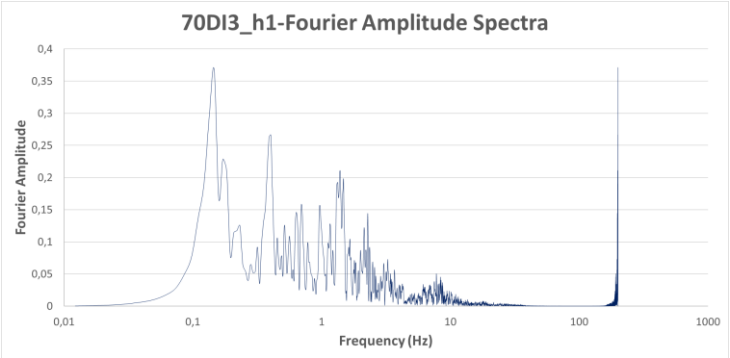

Figure B.112. Fourier Amplitude Spectra Graph of Ground Motion named 70DI3_h1

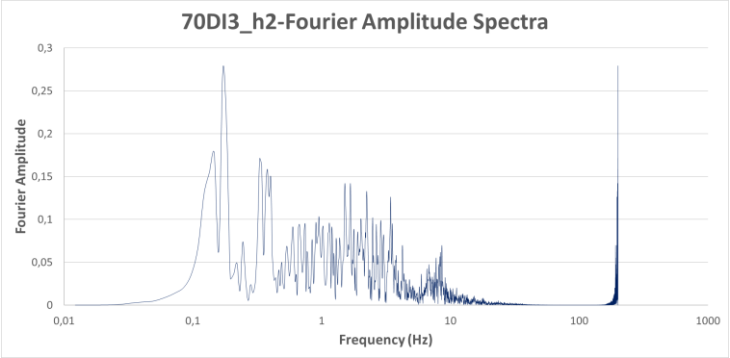

Figure B.113. Fourier Amplitude Spectra Graph of Ground Motion named 70DI3_h2

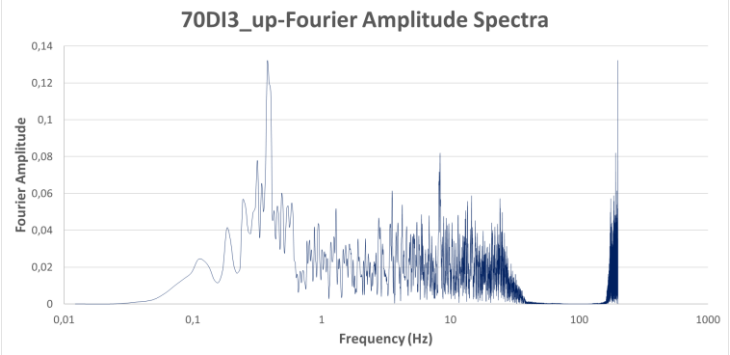

Figure B.114. Fourier Amplitude Spectra Graph of Ground Motion named 70DI3_up

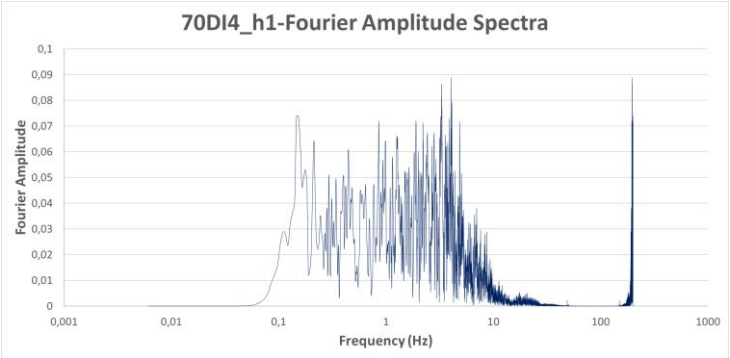

Figure B.115. Fourier Amplitude Spectra Graph of Ground Motion named 70DI4_h1

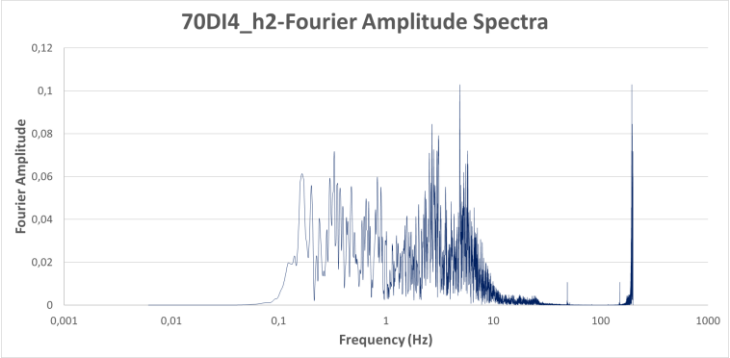

Figure B.116. Fourier Amplitude Spectra Graph of Ground Motion named 70DI4_h2

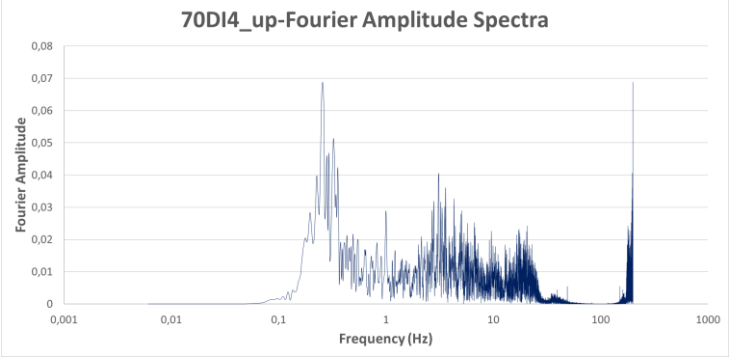

Figure B.117. Fourier Amplitude Spectra Graph of Ground Motion named 70DI4_up

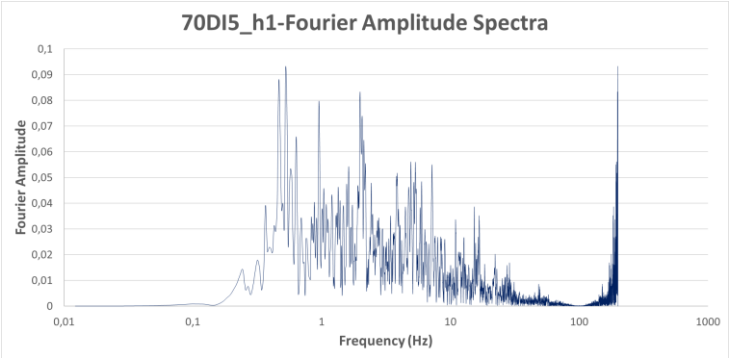

Figure B.118. Fourier Amplitude Spectra Graph of Ground Motion named 70DI5_h1

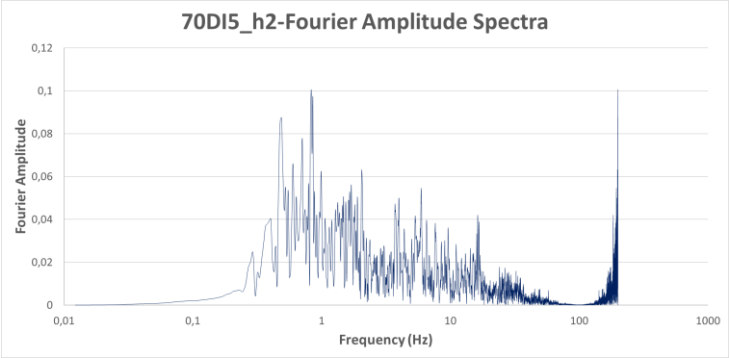

Figure B.119. Fourier Amplitude Spectra Graph of Ground Motion named 70DI5_h2

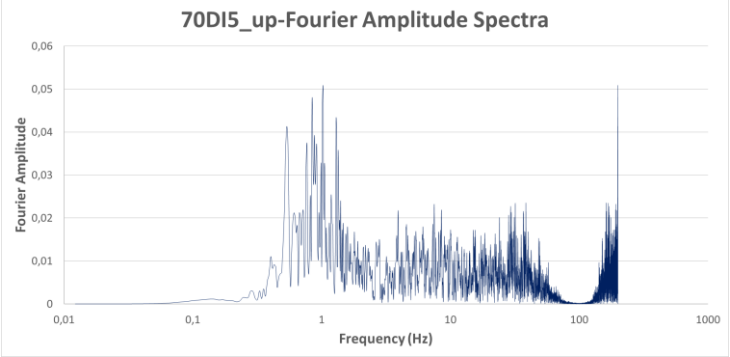

Figure B.120. Fourier Amplitude Spectra Graph of Ground Motion named 70DI5_up

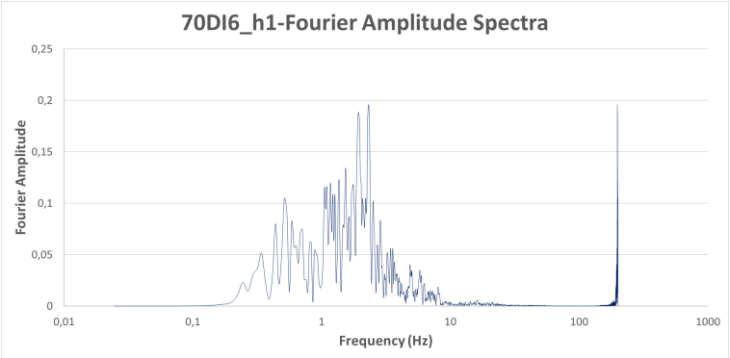

Figure B.121. Fourier Amplitude Spectra Graph of Ground Motion named 70DI6_h1

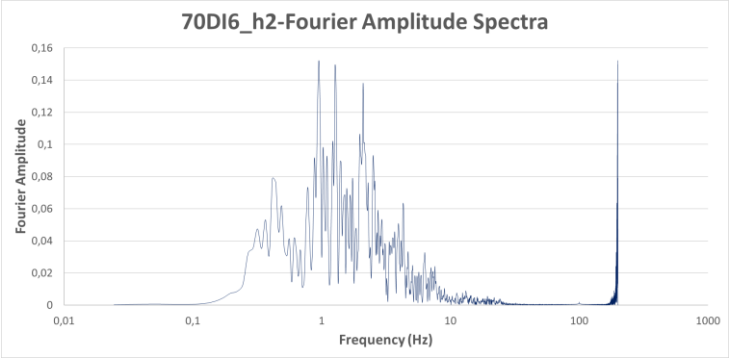

Figure B.122. Fourier Amplitude Spectra Graph of Ground Motion named 70DI6_h2

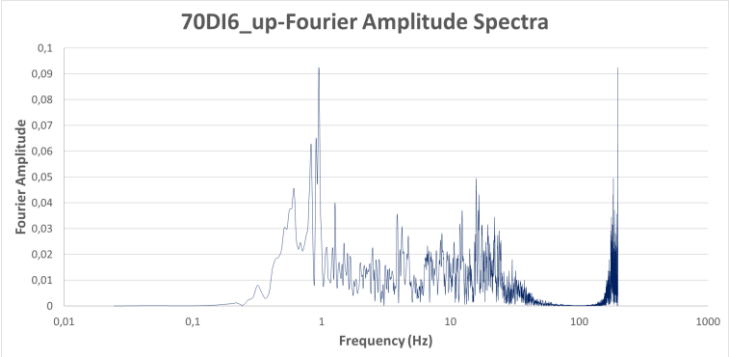

Figure B.123. Fourier Amplitude Spectra Graph of Ground Motion named 70DI6_up

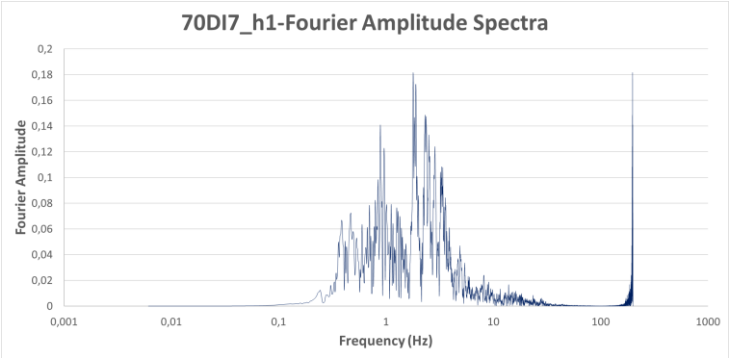

Figure B.124. Fourier Amplitude Spectra Graph of Ground Motion named 70DI7_h1

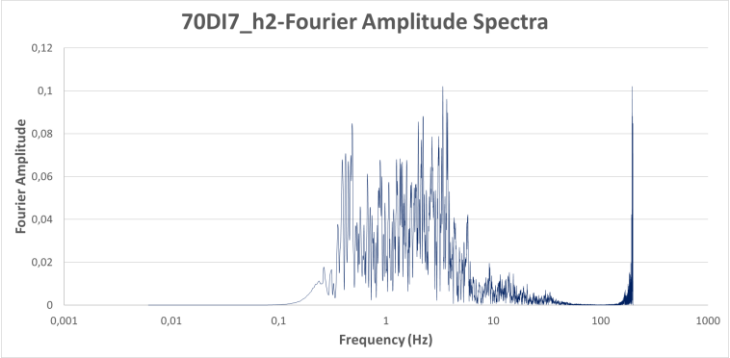

Figure B.125. Fourier Amplitude Spectra Graph of Ground Motion named 70DI7_h2

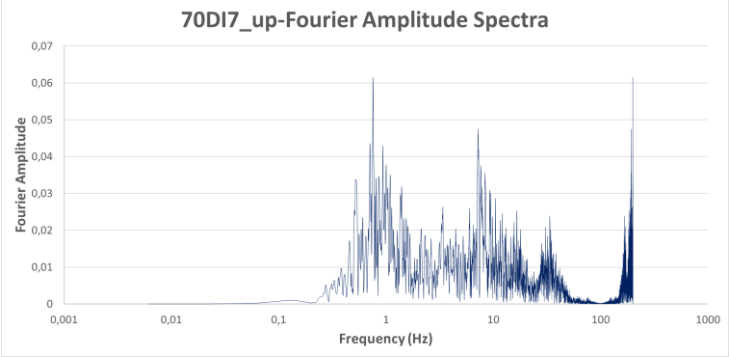

Figure B.126. Fourier Amplitude Spectra Graph of Ground Motion named 70DI7_up

C. APPENDIX C – Response Spectrum Graphs

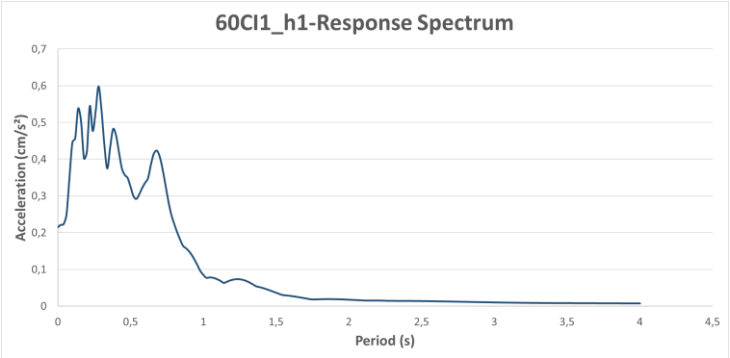

Figure C.1. Response Spectrum Graph of Ground Motion named 60CI1_h1

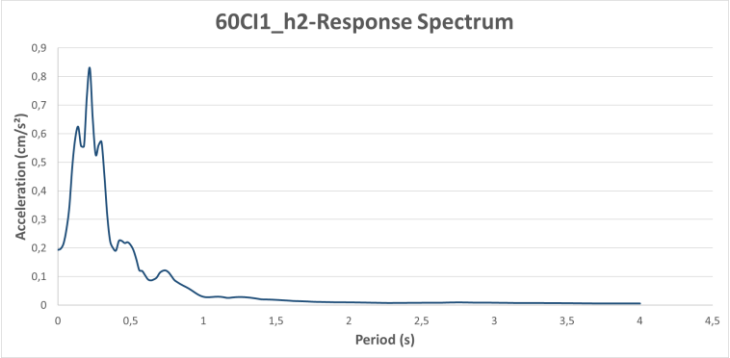

Figure C.2. Response Spectrum Graph of Ground Motion named 60CI1_h2

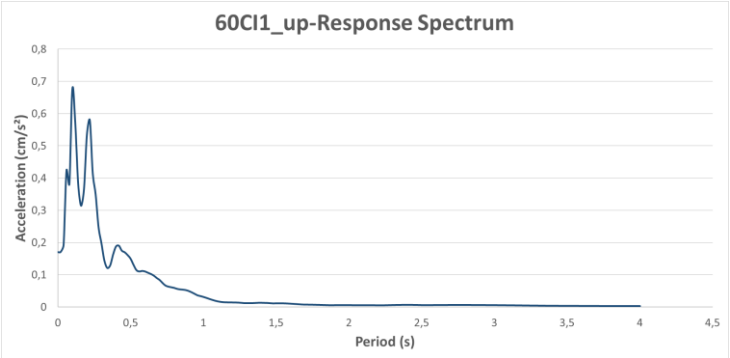

Figure C.3. Response Spectrum Graph of Ground Motion named 60CI1_up

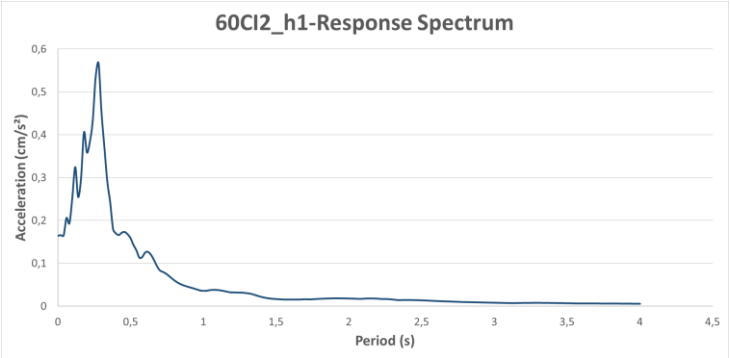

Figure C.4. Response Spectrum Graph of Ground Motion named 60CI2_h1

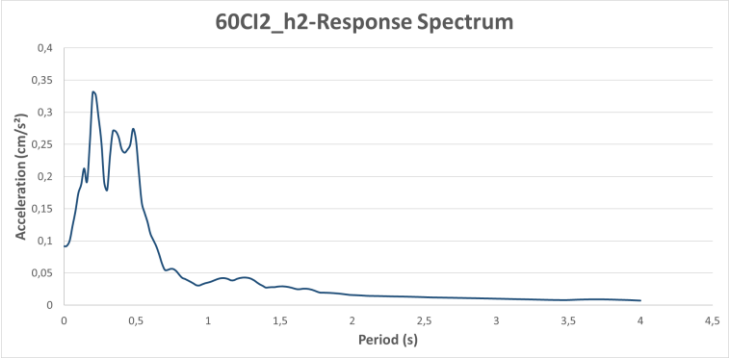

Figure C.5. Response Spectrum Graph of Ground Motion named 60CI2_h2

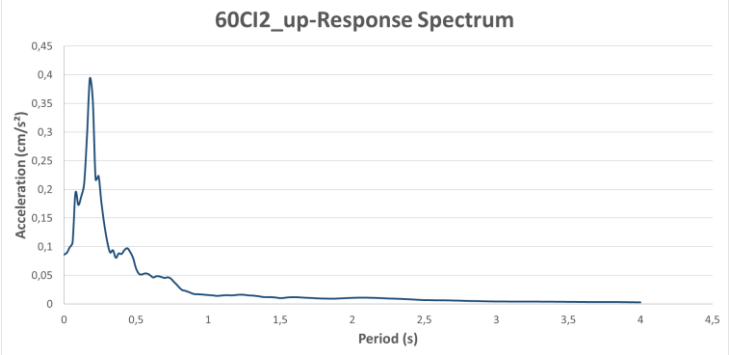

Figure C.6. Response Spectrum Graph of Ground Motion named 60CI2_up

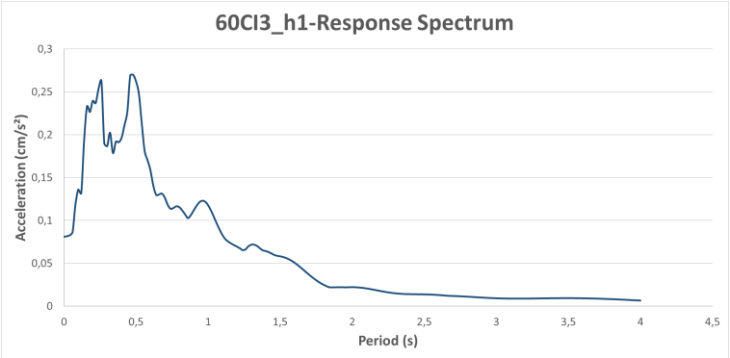

Figure C.7. Response Spectrum Graph of Ground Motion named 60CI3_h1

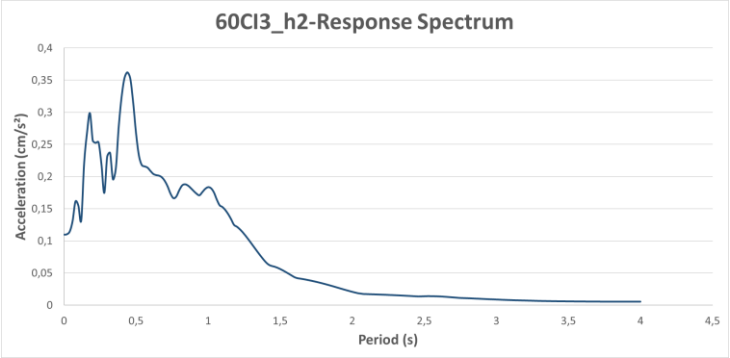

Figure C.8. Response Spectrum Graph of Ground Motion named 60CI3_h2

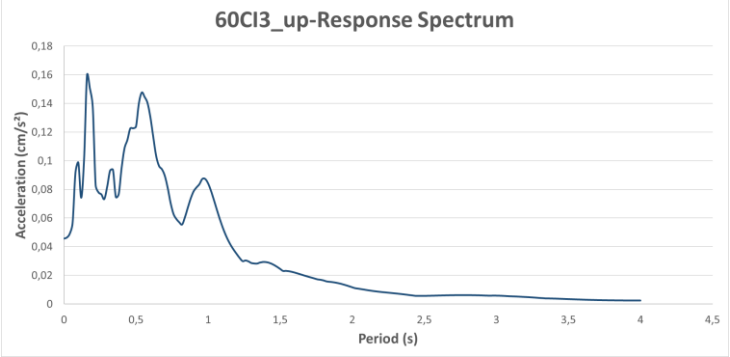

Figure C.9. Response Spectrum Graph of Ground Motion named 60CI3_up

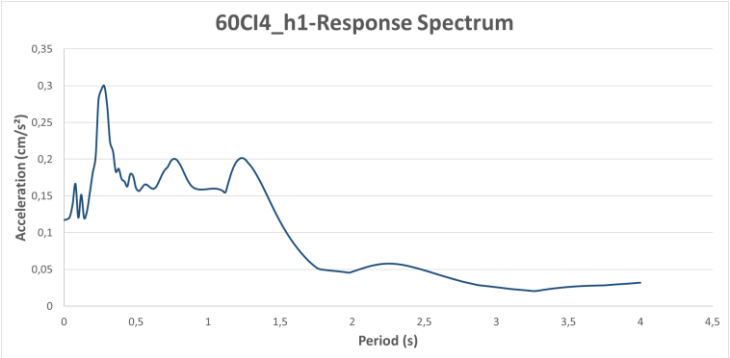

Figure C.10. Response Spectrum Graph of Ground Motion named 60CI4_h1

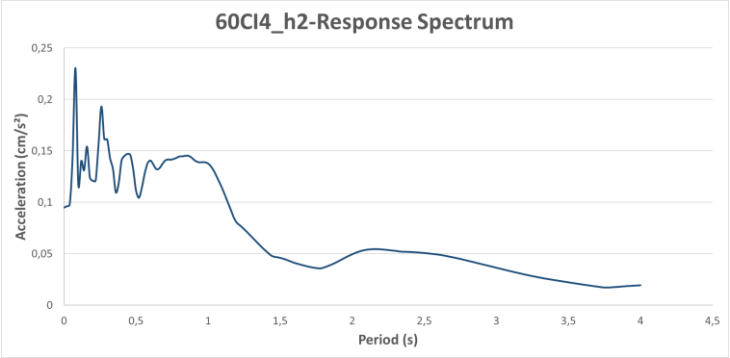

Figure C.11. Response Spectrum Graph of Ground Motion named 60CI4_h2

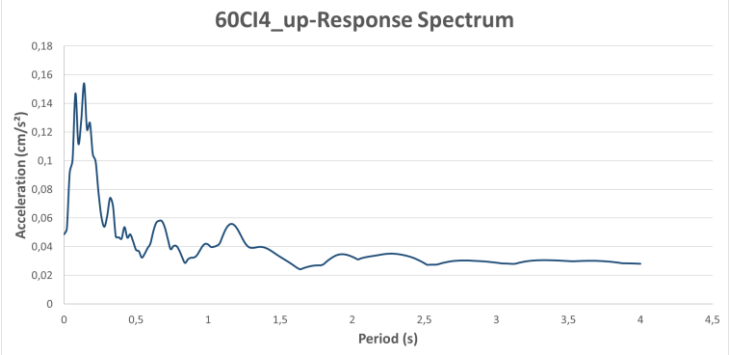

Figure C.12. Response Spectrum Graph of Ground Motion named 60CI4_up

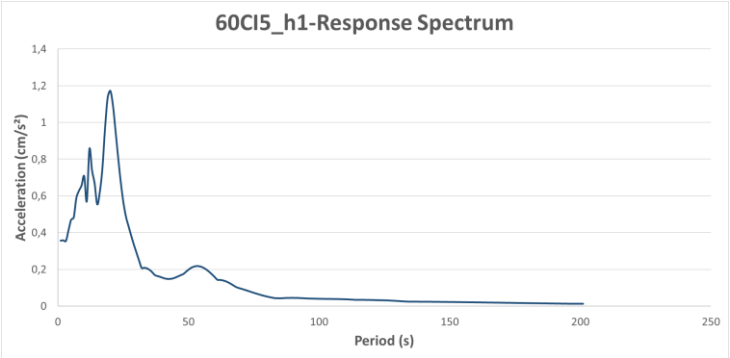

Figure C.13. Response Spectrum Graph of Ground Motion named 60CI5_h1

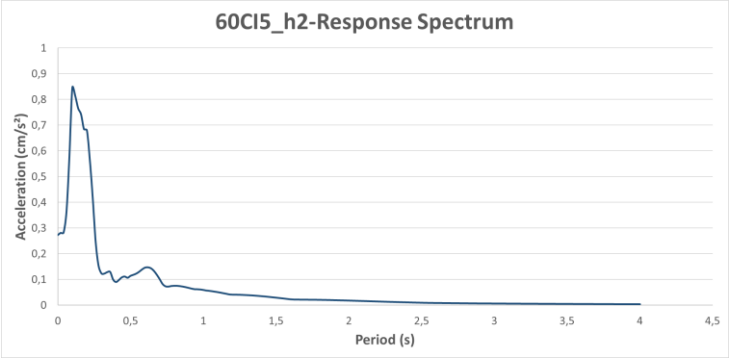

Figure C.14. Response Spectrum Graph of Ground Motion named 60CI5_h2

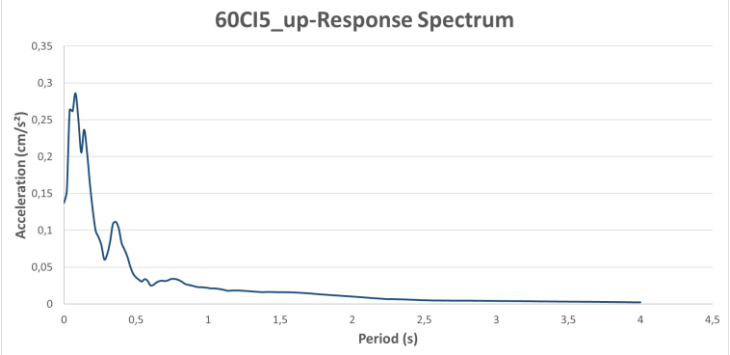

Figure C.15. Response Spectrum Graph of Ground Motion named 60CI5_up

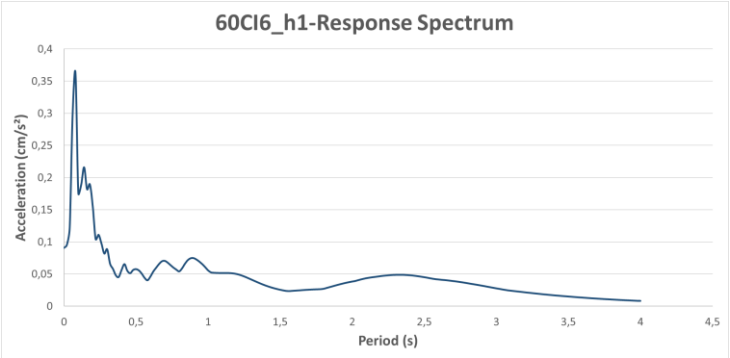

Figure C.16. Response Spectrum Graph of Ground Motion named 60CI6_h1

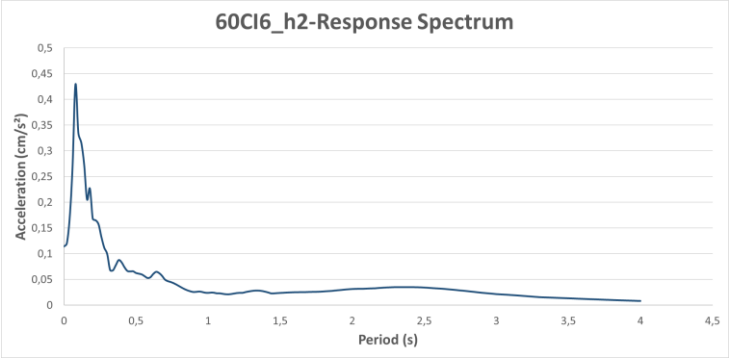

Figure C.17. Response Spectrum Graph of Ground Motion named 60CI6_h2

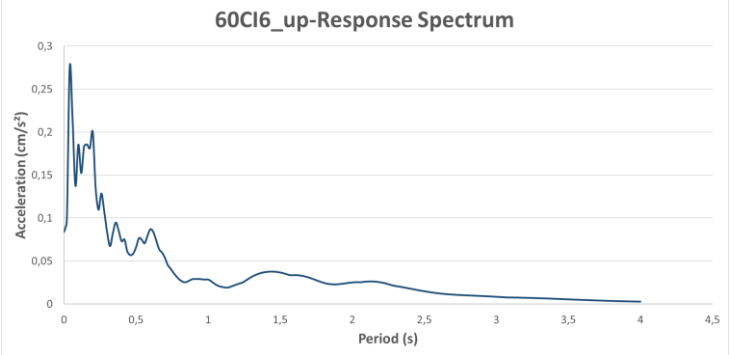

Figure C.18. Response Spectrum Graph of Ground Motion named 60CI6_up

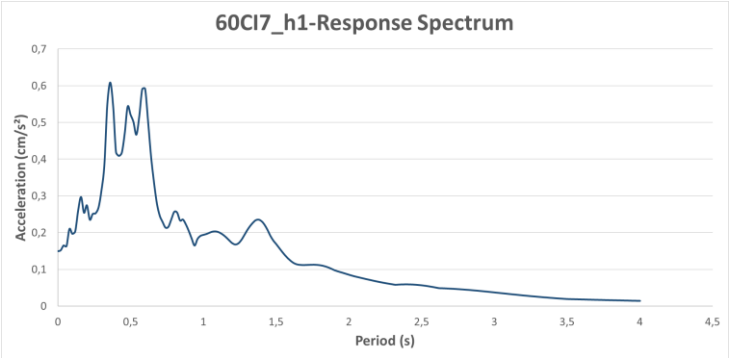

Figure C.19. Response Spectrum Graph of Ground Motion named 60CI7_h1

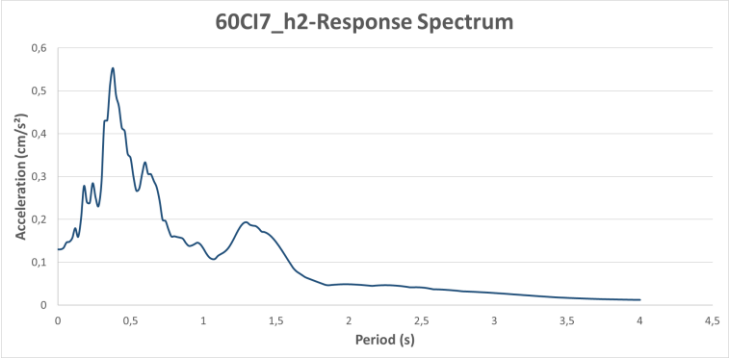

Figure C.20. Response Spectrum Graph of Ground Motion named 60CI7_h2

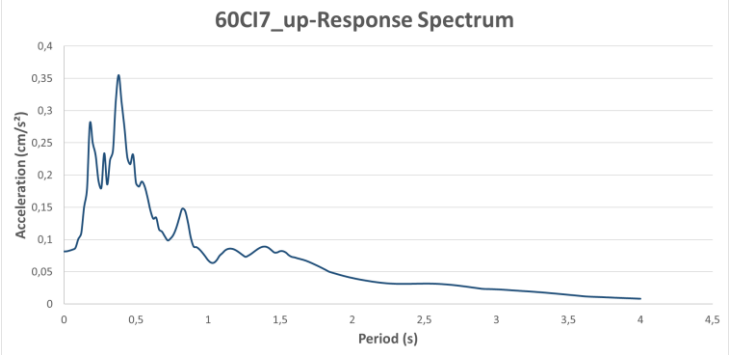

Figure C.21. Response Spectrum Graph of Ground Motion named 60CI7_up

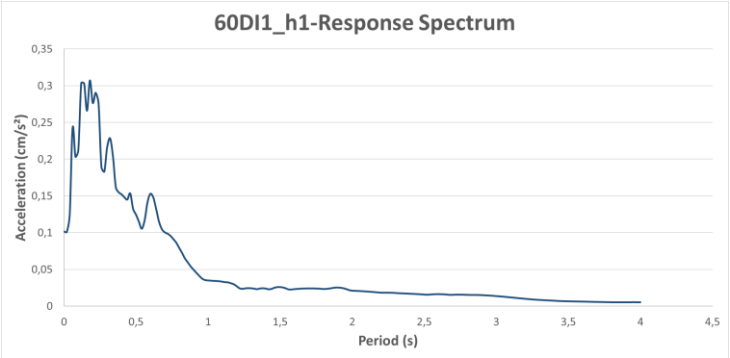

Figure C.22. Response Spectrum Graph of Ground Motion named 60DI1_h1

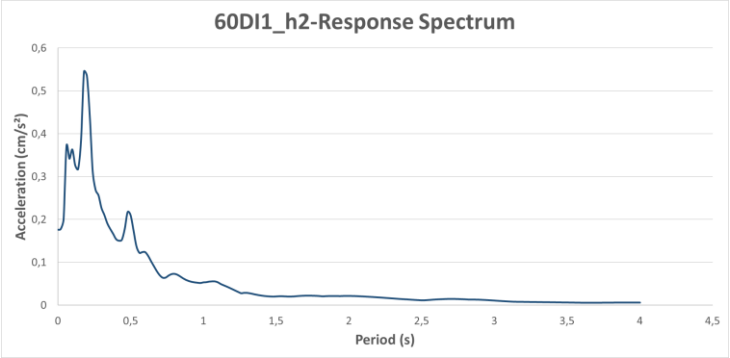

Figure C.23. Response Spectrum Graph of Ground Motion named 60DI1_h2

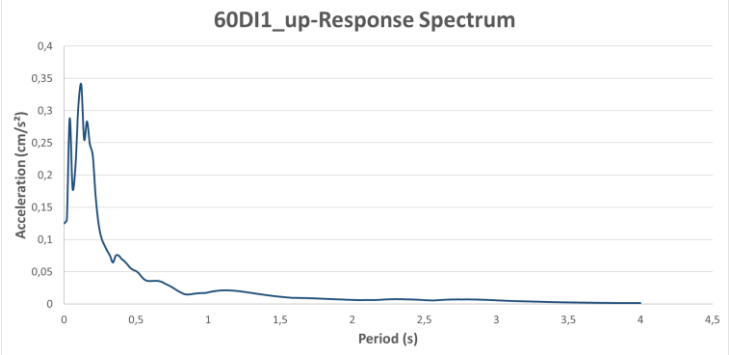

Figure C.24. Response Spectrum Graph of Ground Motion named 60DI1_up

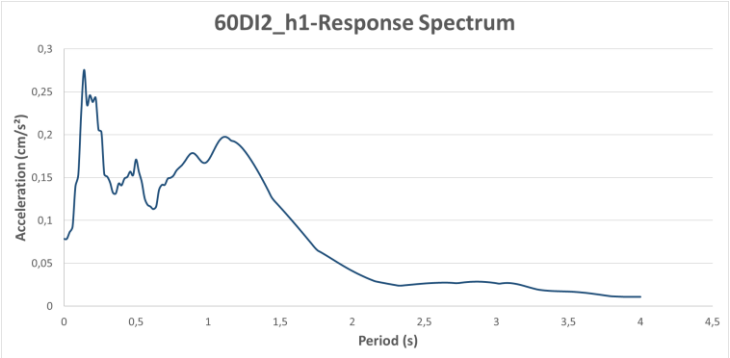

Figure C.25. Response Spectrum Graph of Ground Motion named 60DI2_h1

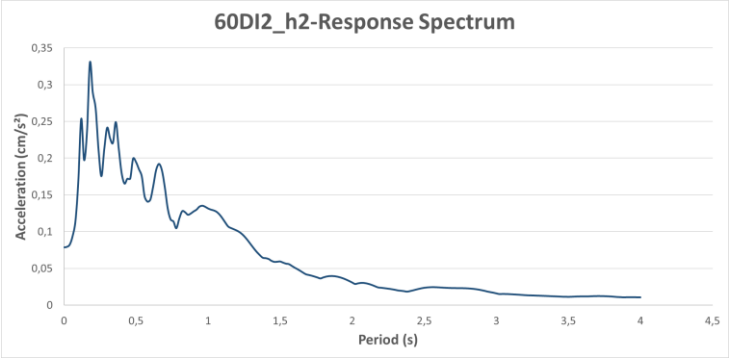

Figure C.26. Response Spectrum Graph of Ground Motion named 60DI2_h2

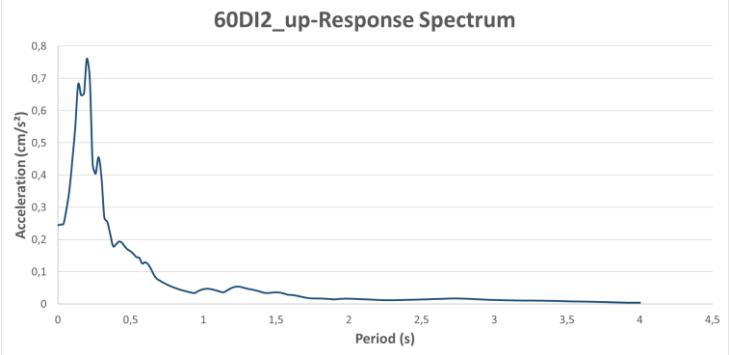

Figure C.27. Response Spectrum Graph of Ground Motion named 60DI2_up

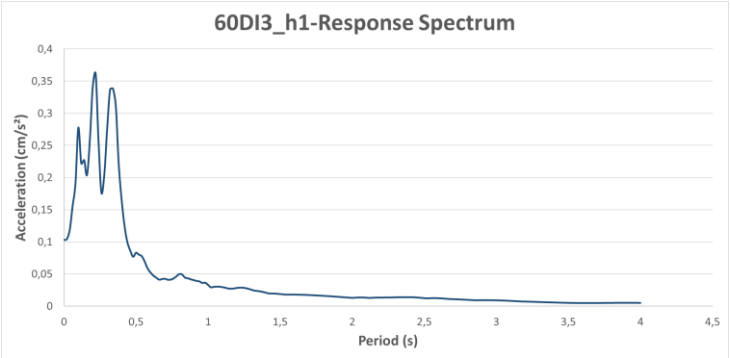

Figure C.28. Response Spectrum Graph of Ground Motion named 60DI3_h1

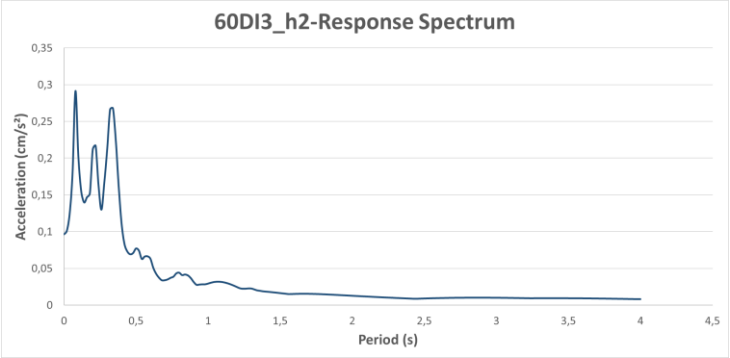

Figure C.29. Response Spectrum Graph of Ground Motion named 60DI3_h2

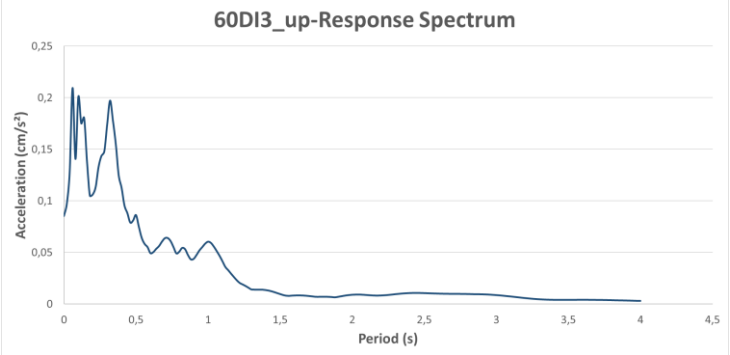

Figure C.30. Response Spectrum Graph of Ground Motion named 60DI3_up

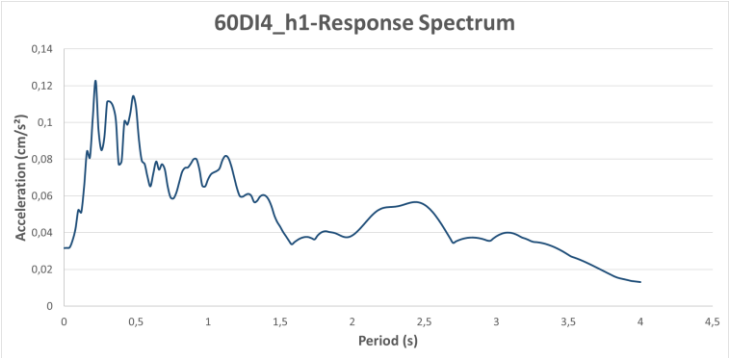

Figure C.31. Response Spectrum Graph of Ground Motion named 60DI4_h1

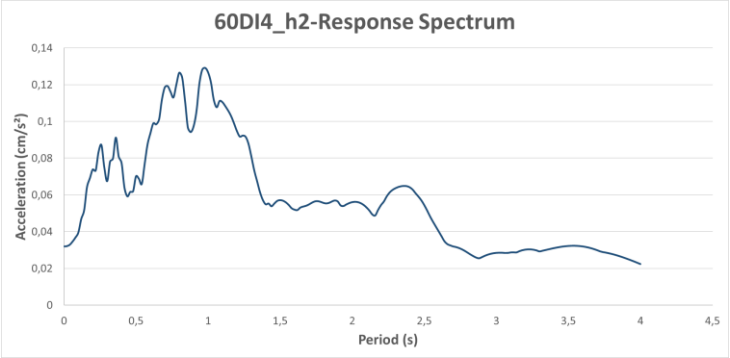

Figure C.32. Response Spectrum Graph of Ground Motion named 60DI4_h2

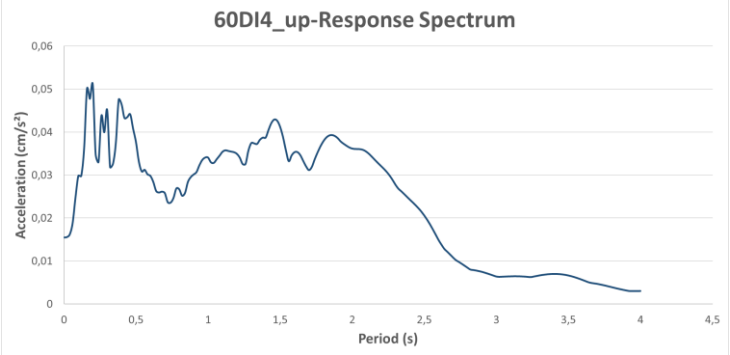

Figure C.33. Response Spectrum Graph of Ground Motion named 60DI4_up

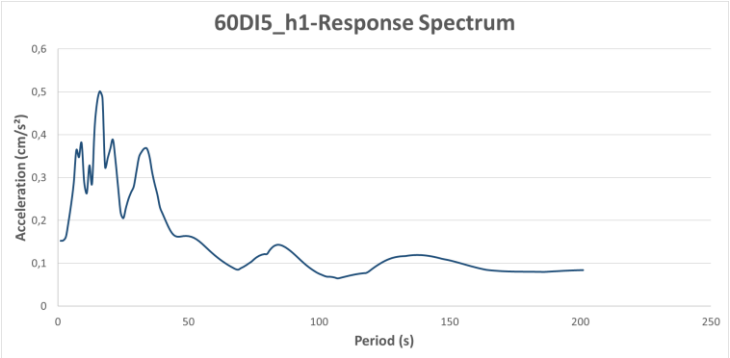

Figure C.34. Response Spectrum Graph of Ground Motion named 60DI5_h1

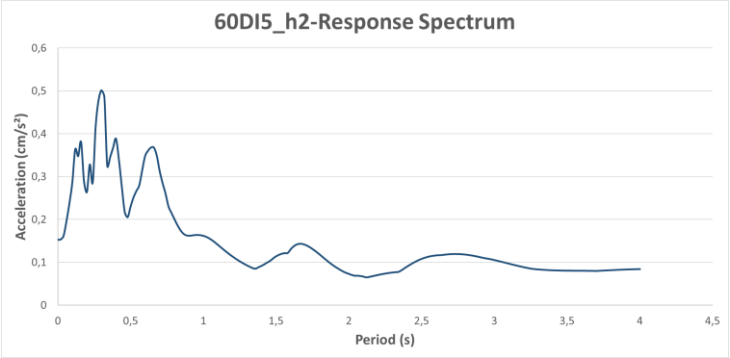

Figure C.35. Response Spectrum Graph of Ground Motion named 60DI5_h2

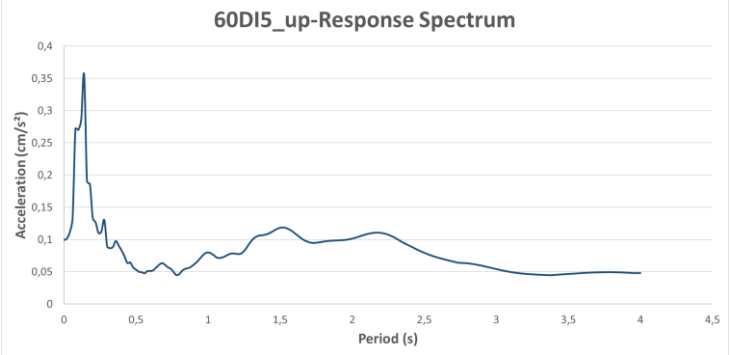

Figure C.36. Response Spectrum Graph of Ground Motion named 60DI5_up

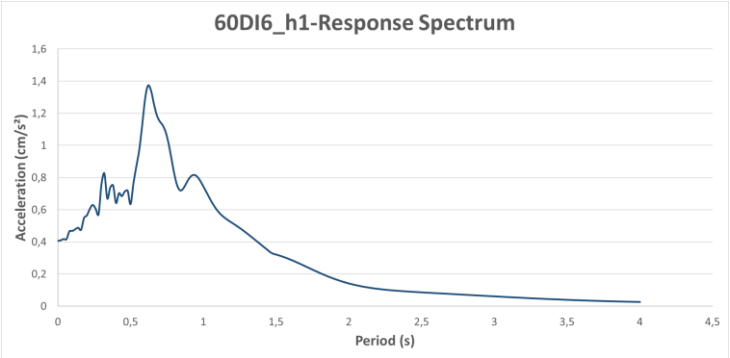

Figure C.37. Response Spectrum Graph of Ground Motion named 60DI6_h1

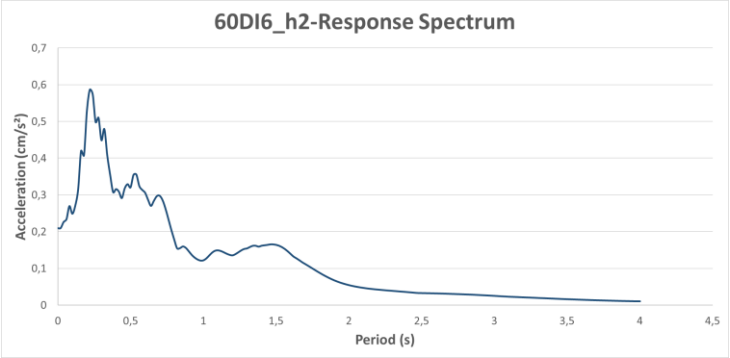

Figure C.38. Response Spectrum Graph of Ground Motion named 60DI6_h2

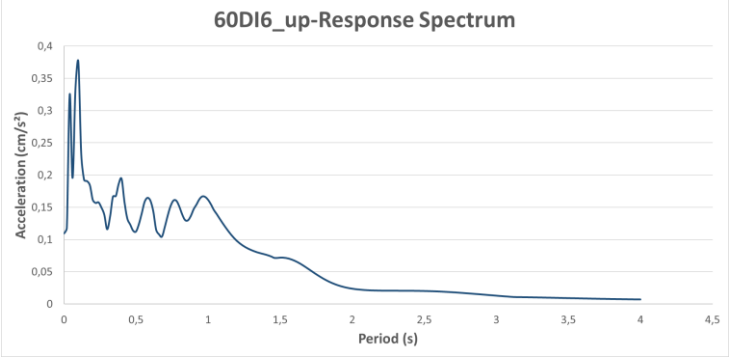

Figure C.39. Response Spectrum Graph of Ground Motion named 60DI6_up

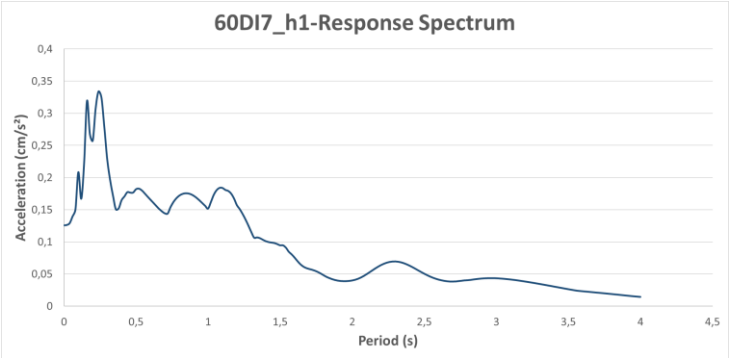

Figure C.40. Response Spectrum Graph of Ground Motion named 60DI7_h1

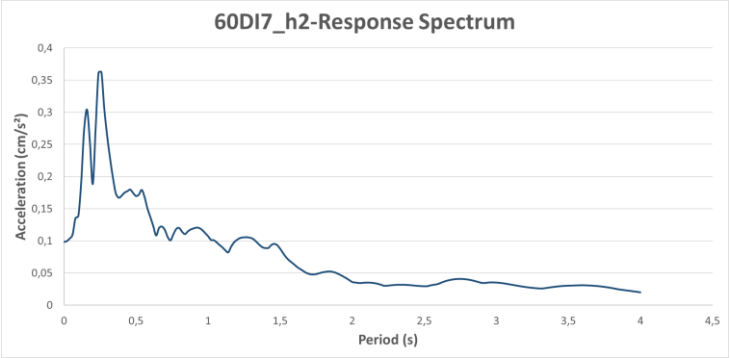

Figure C.41. Response Spectrum Graph of Ground Motion named 60DI7_h2

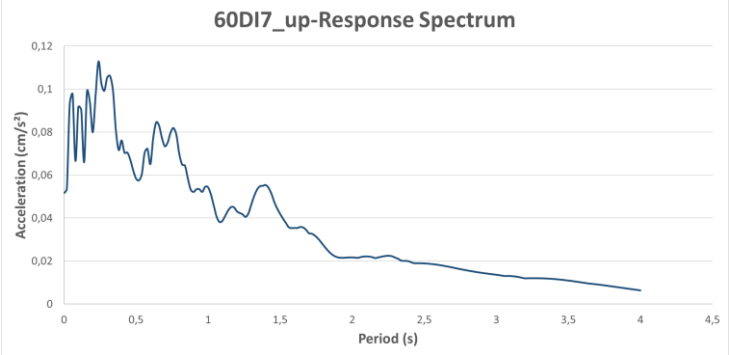

Figure C.42. Response Spectrum Graph of Ground Motion named 60DI7_up

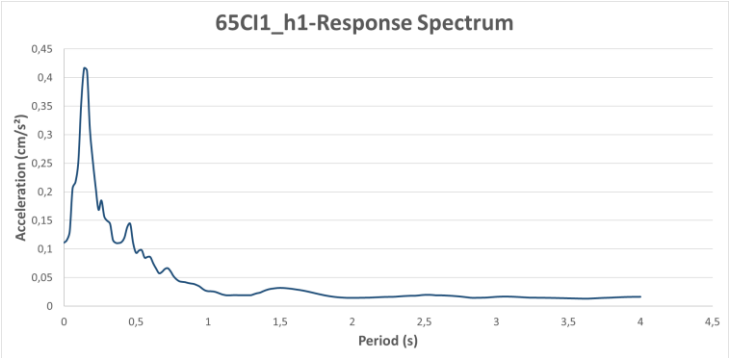

Figure C.43. Response Spectrum Graph of Ground Motion named 65CI1_h1

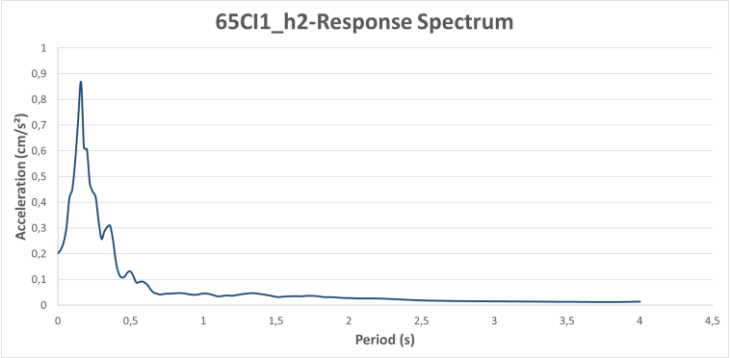

Figure C.44. Response Spectrum Graph of Ground Motion named 65CI1_h2

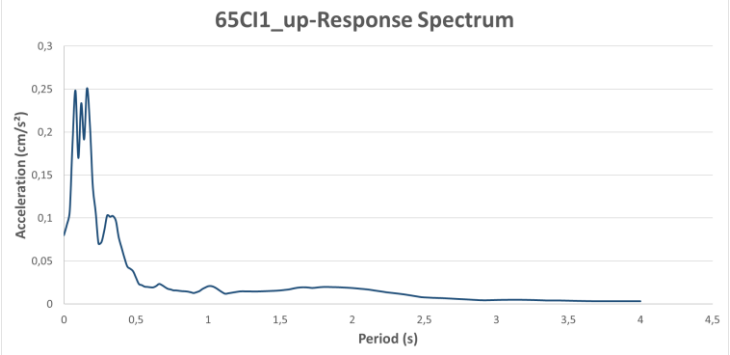

Figure C.45. Response Spectrum Graph of Ground Motion named 65CI1_up

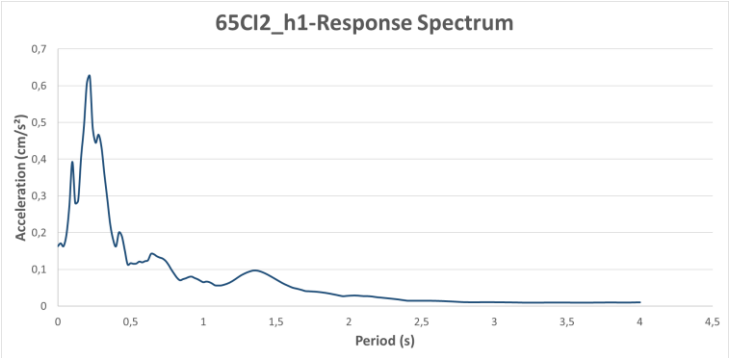

Figure C.46. Response Spectrum Graph of Ground Motion named 65CI2_h1

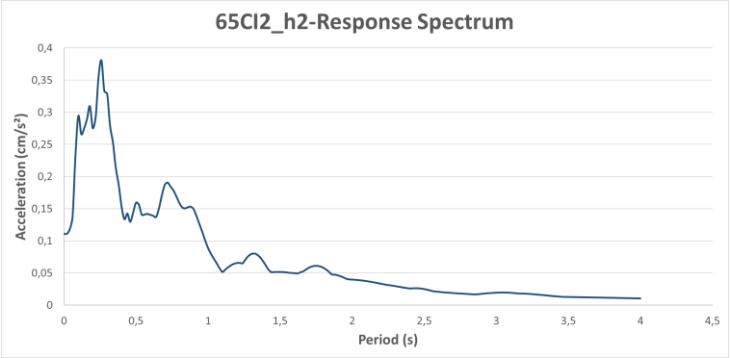

Figure C.47. Response Spectrum Graph of Ground Motion named 65CI2_h2

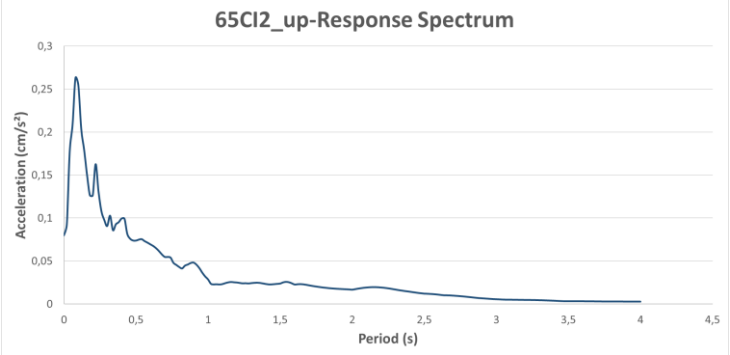

Figure C.48. Response Spectrum Graph of Ground Motion named 65CI2_up

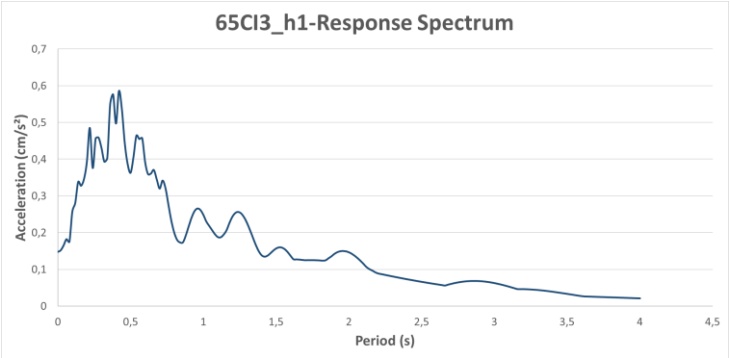

Figure C.49. Response Spectrum Graph of Ground Motion named 65CI3_h1

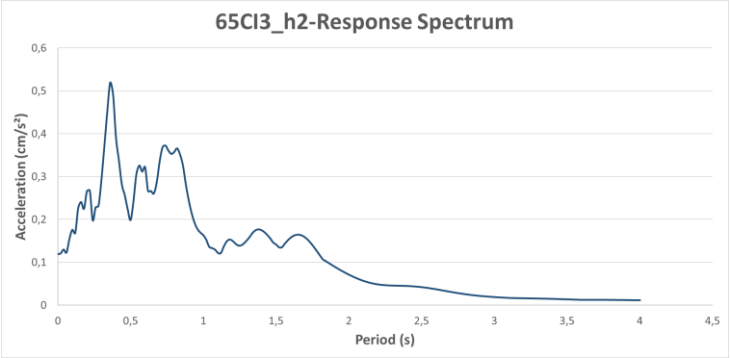

Figure C.50. Response Spectrum Graph of Ground Motion named 65CI3_h2

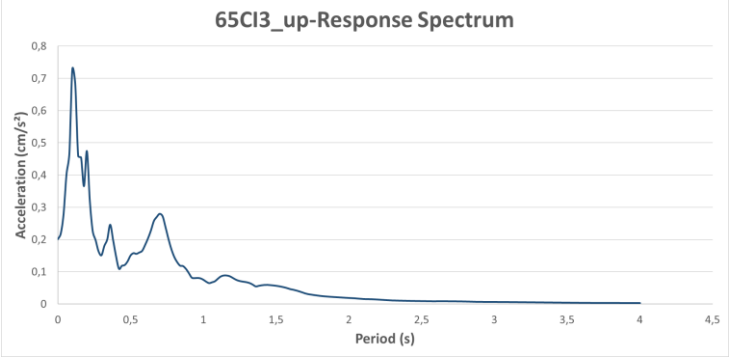

Figure C.51. Response Spectrum Graph of Ground Motion named 65CI3_up

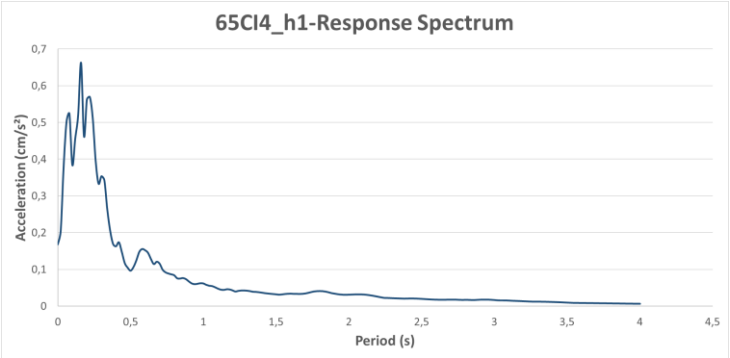

Figure C.52. Response Spectrum Graph of Ground Motion named 65CI4_h1

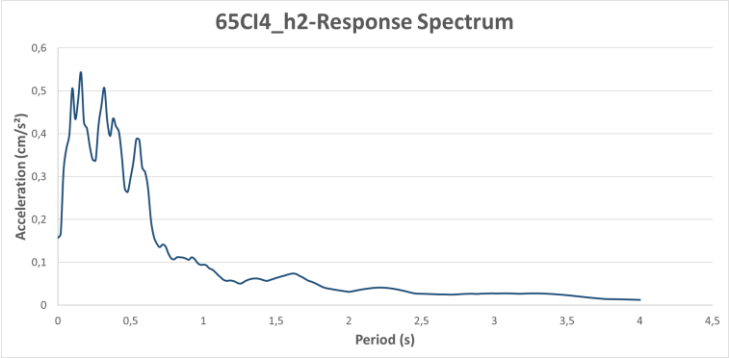

Figure C.53. Response Spectrum Graph of Ground Motion named 65CI4_h2

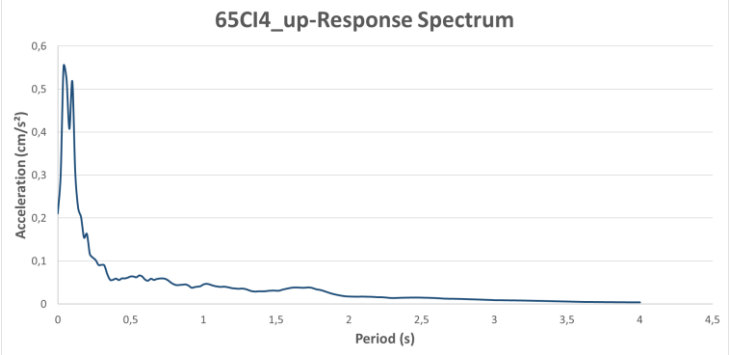

Figure C.54. Response Spectrum Graph of Ground Motion named 65CI4_up

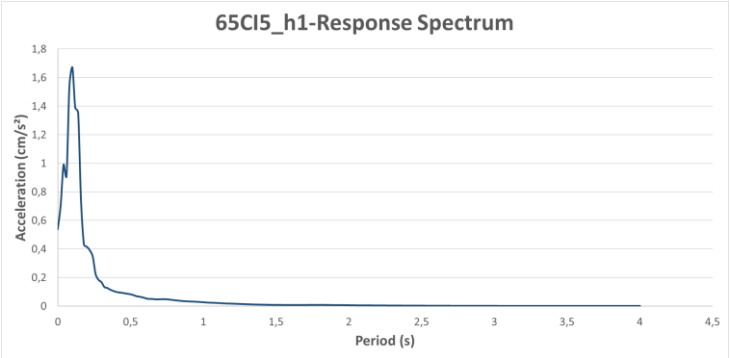

Figure C.55. Response Spectrum Graph of Ground Motion named 65CI5_h1

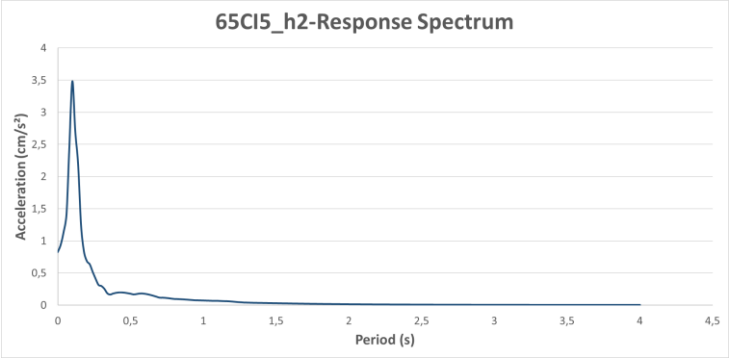

Figure C.56. Response Spectrum Graph of Ground Motion named 65CI5_h2

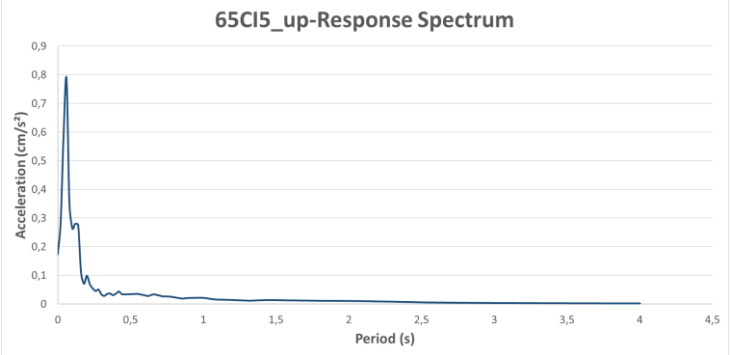

Figure C.57. Response Spectrum Graph of Ground Motion named 65CI5_up

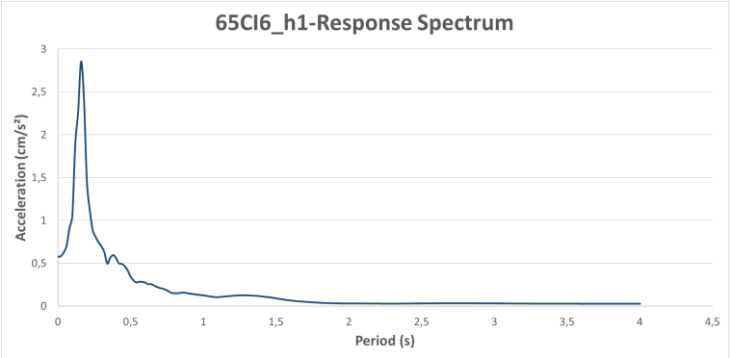

Figure C.58. Response Spectrum Graph of Ground Motion named 65CI6_h1

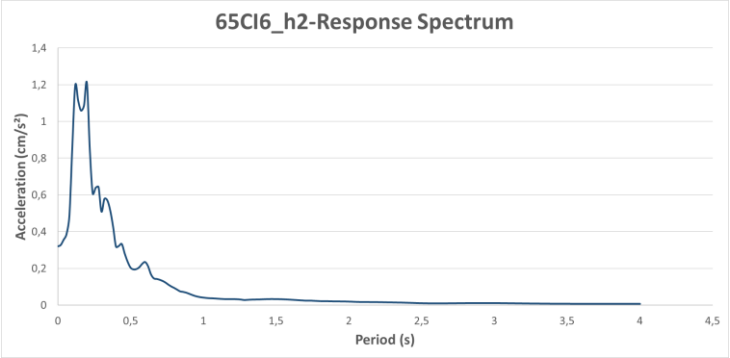

Figure C.59. Response Spectrum Graph of Ground Motion named 65CI6_h2

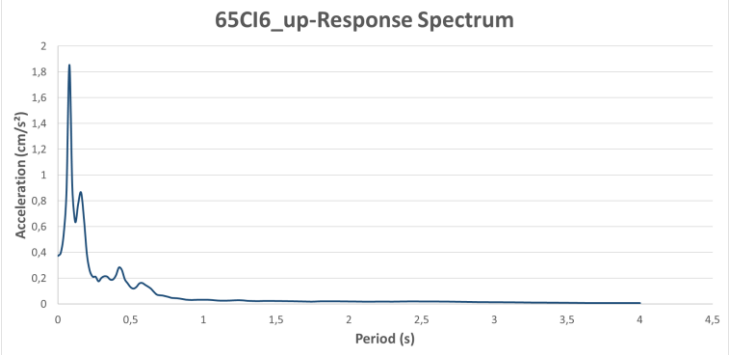

Figure C.60. Response Spectrum Graph of Ground Motion named 65CI6_up

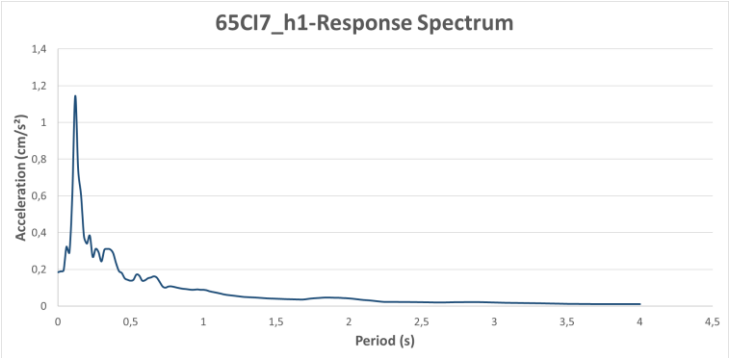

Figure C.61. Response Spectrum Graph of Ground Motion named 65CI7_h1

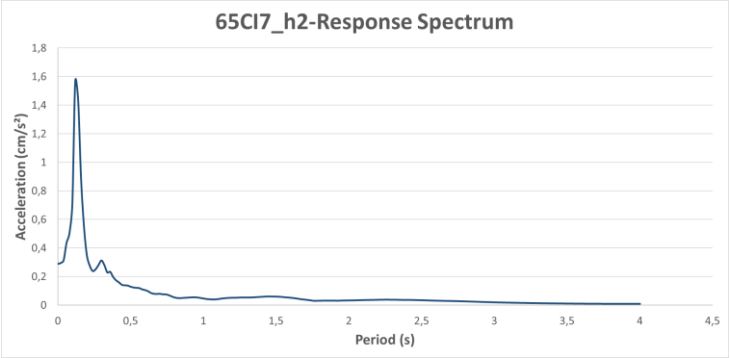

Figure C.62. Response Spectrum Graph of Ground Motion named 65CI7_h2

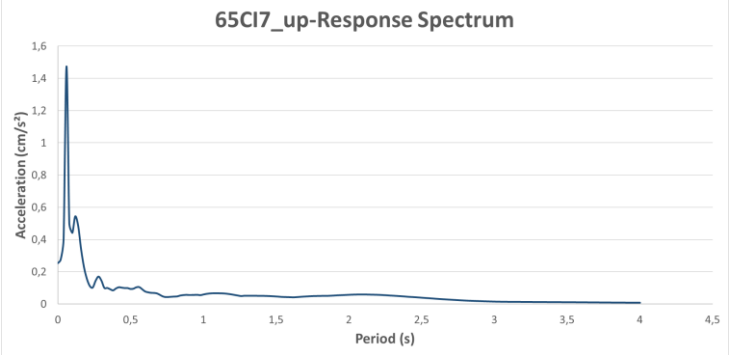

Figure C.63. Response Spectrum Graph of Ground Motion named 65CI7_up

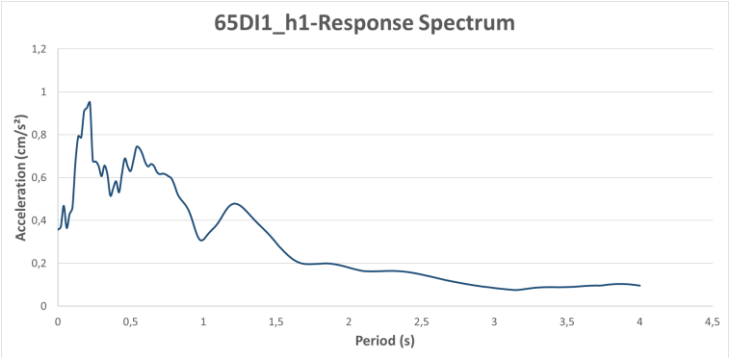

Figure C.64. Response Spectrum Graph of Ground Motion named 65DI1_h1

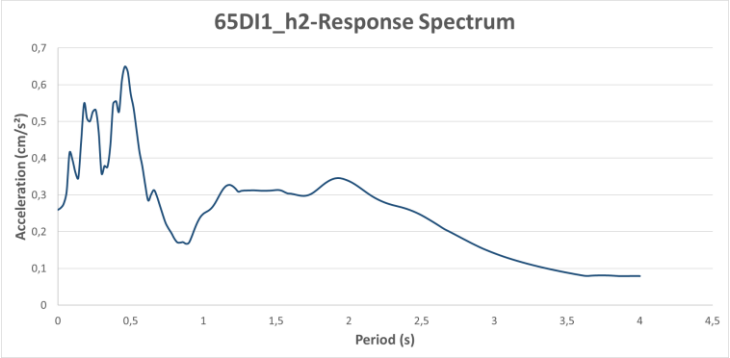

Figure C.65. Response Spectrum Graph of Ground Motion named 65DI1_h2

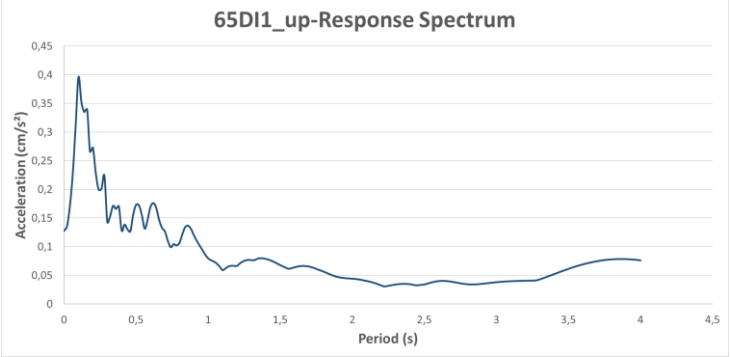

Figure C.66. Response Spectrum Graph of Ground Motion named 65DI1_up

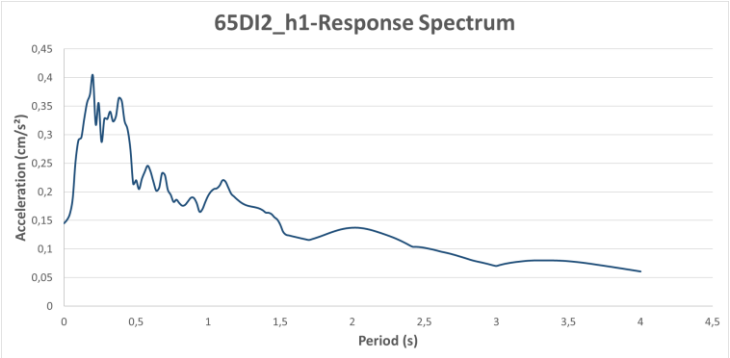

Figure C.67. Response Spectrum Graph of Ground Motion named 65DI2_h1

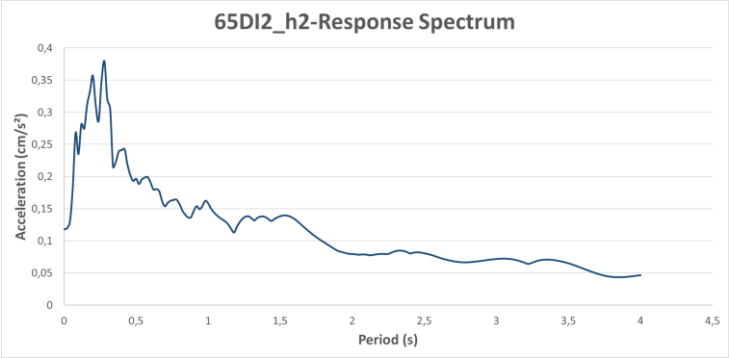

Figure C.68. Response Spectrum Graph of Ground Motion named 65DI2_h2

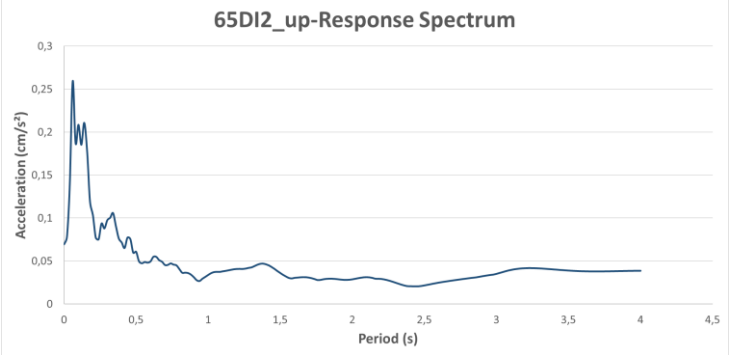

Figure C.69. Response Spectrum Graph of Ground Motion named 65DI2_up

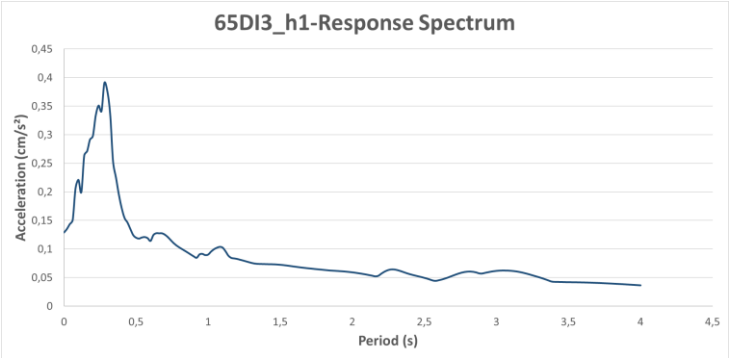

Figure C.70. Response Spectrum Graph of Ground Motion named 65DI3_h1

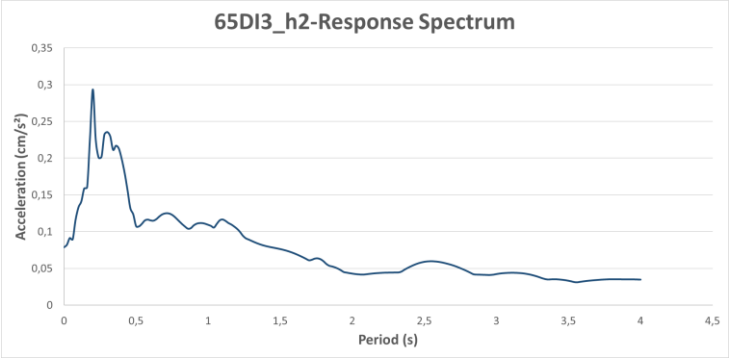

Figure C.71. Response Spectrum Graph of Ground Motion named 65DI3_h2

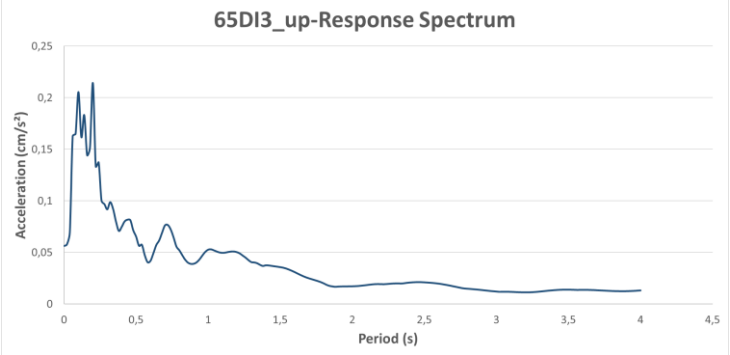

Figure C.72. Response Spectrum Graph of Ground Motion named 65DI3_up

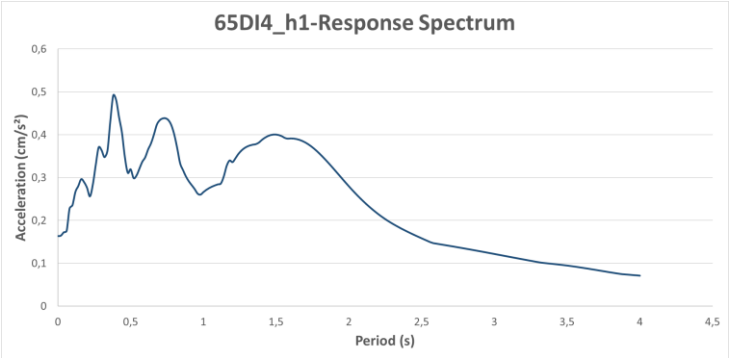

Figure C.73. Response Spectrum Graph of Ground Motion named 65DI4_h1

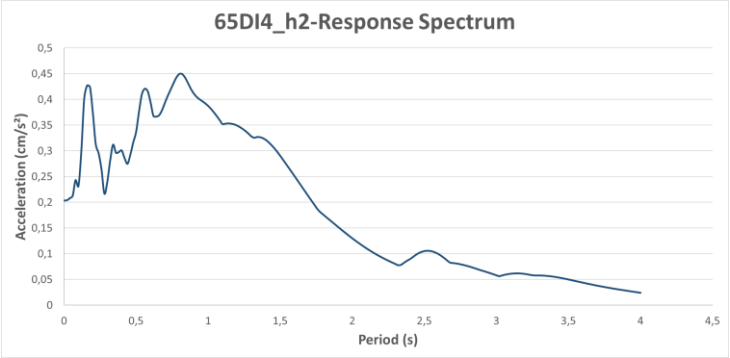

Figure C.74. Response Spectrum Graph of Ground Motion named 65DI4_h2

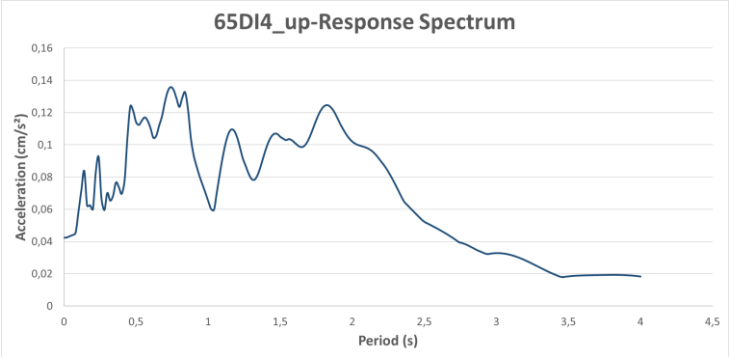

Figure C.75. Response Spectrum Graph of Ground Motion named 65DI4_up

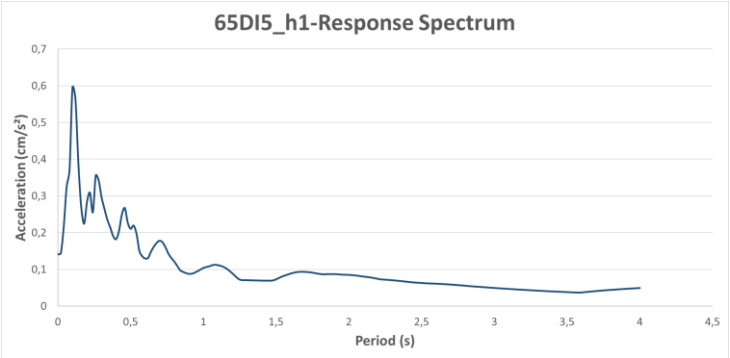

Figure C.76. Response Spectrum Graph of Ground Motion named 65DI5_h1

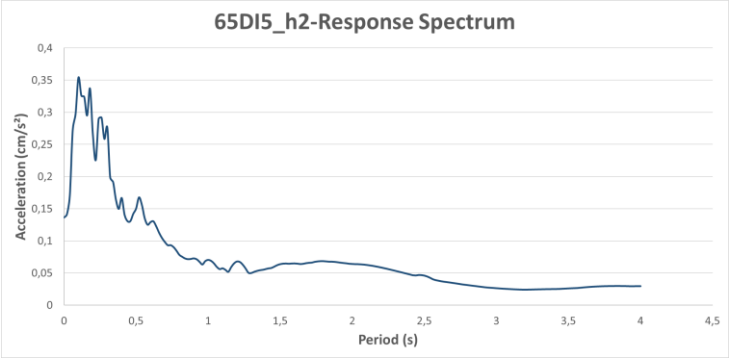

Figure C.77. Response Spectrum Graph of Ground Motion named 65DI5_h2

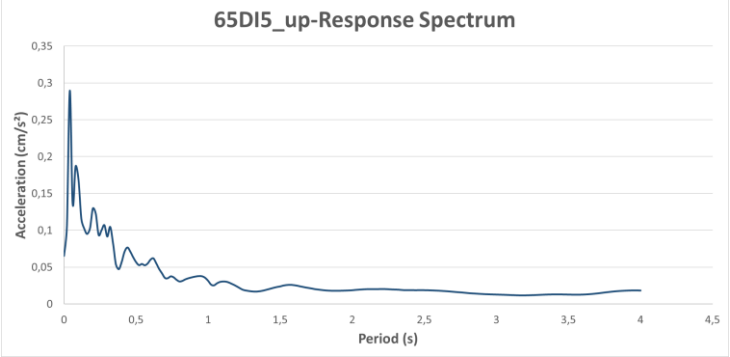

Figure C.78. Response Spectrum Graph of Ground Motion named 65DI5_up

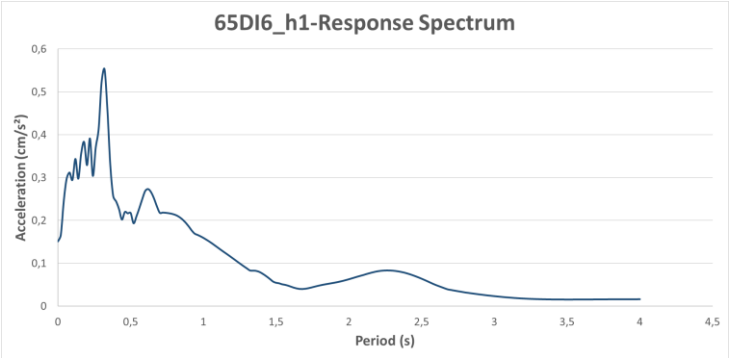

Figure C.79. Response Spectrum Graph of Ground Motion named 65DI6_h1

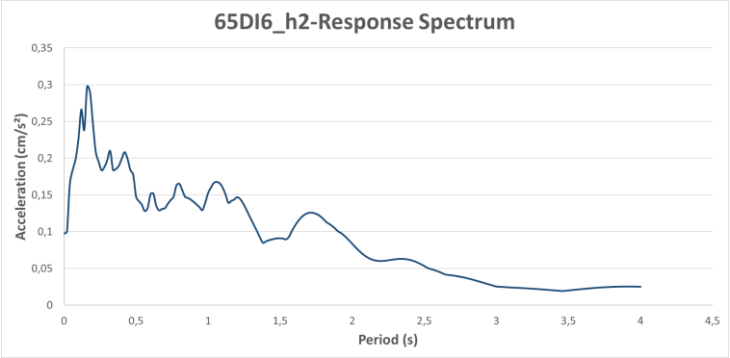

Figure C.80. Response Spectrum Graph of Ground Motion named 65DI6_h2

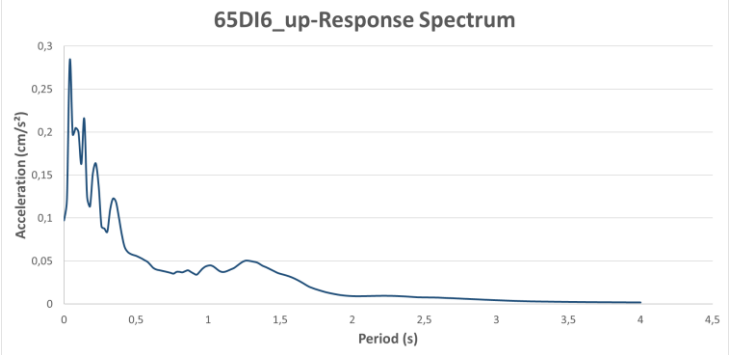

Figure C.81. Response Spectrum Graph of Ground Motion named 65DI6_up

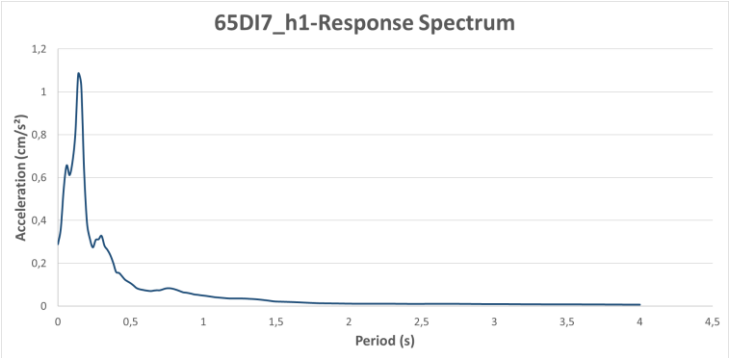

Figure C.82. Response Spectrum Graph of Ground Motion named 65DI7_h1

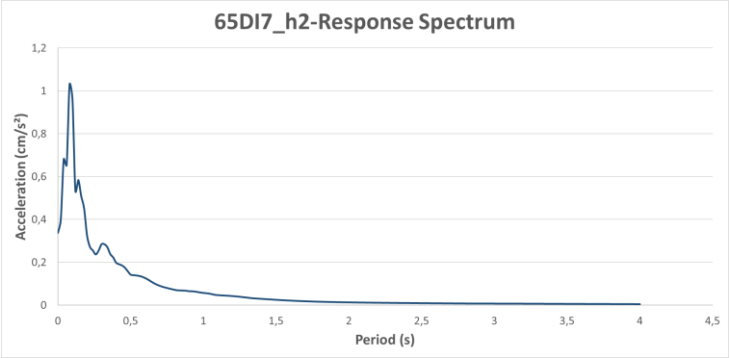

Figure C.83. Response Spectrum Graph of Ground Motion named 65DI7_h2

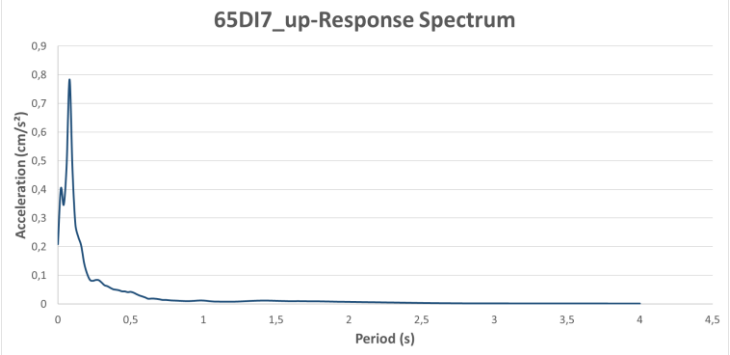

Figure C.84. Response Spectrum Graph of Ground Motion named 65DI7_up

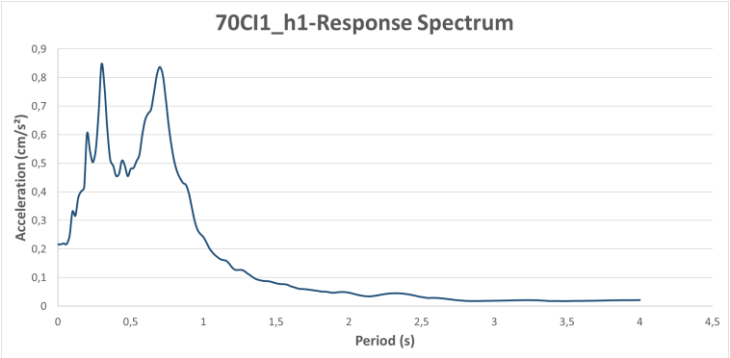

Figure C.85. Response Spectrum Graph of Ground Motion named 70CI1_h1

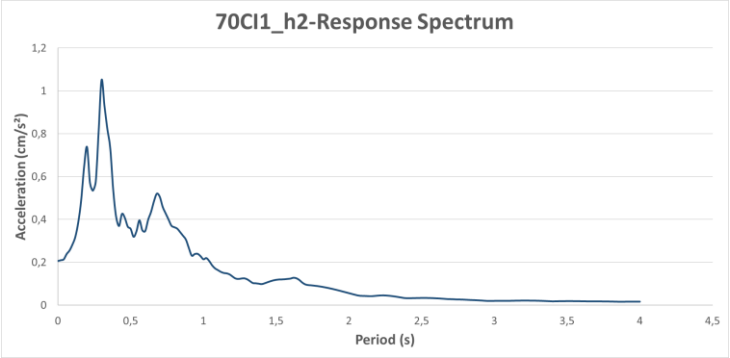

Figure C.86. Response Spectrum Graph of Ground Motion named 70CI1_h2

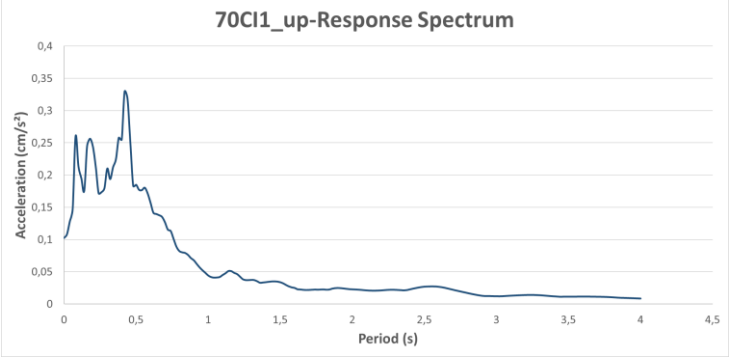

Figure C.87. Response Spectrum Graph of Ground Motion named 70CI1_up

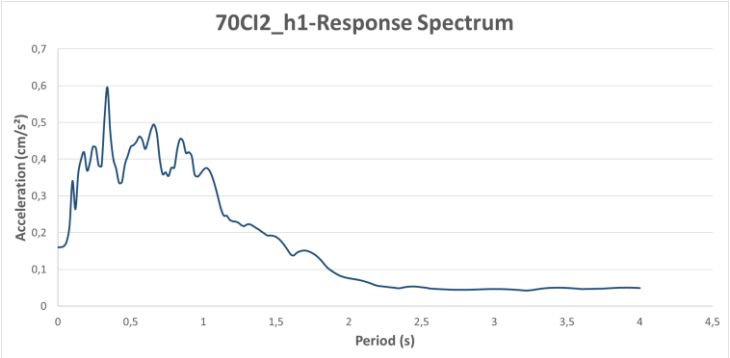

Figure C.88. Response Spectrum Graph of Ground Motion named 70CI2_h1

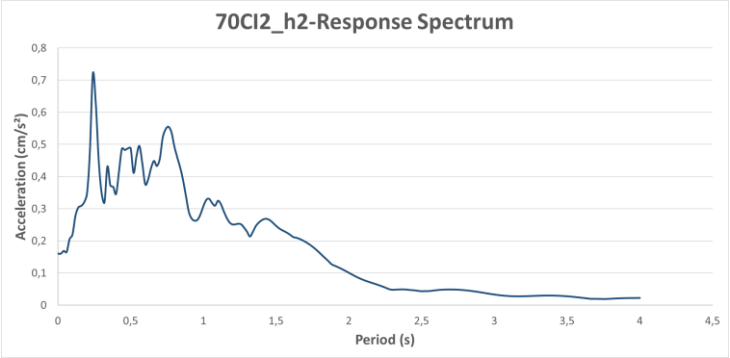

Figure C.89. Response Spectrum Graph of Ground Motion named 70CI2_h2

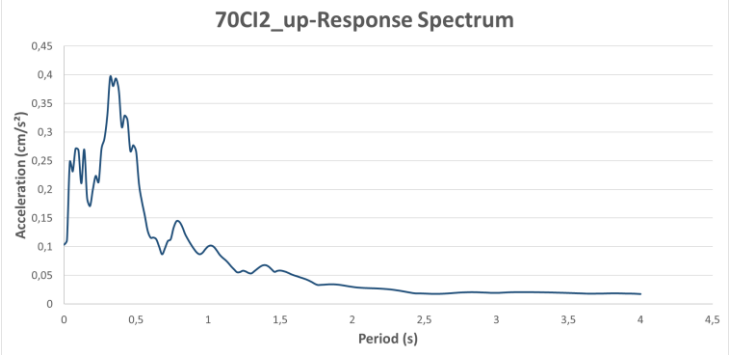

Figure C.90. Response Spectrum Graph of Ground Motion named 70CI2_up

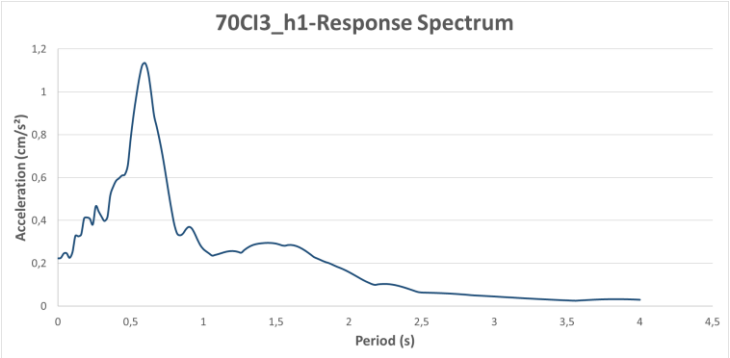

Figure C.91. Response Spectrum Graph of Ground Motion named 70CI3_h1

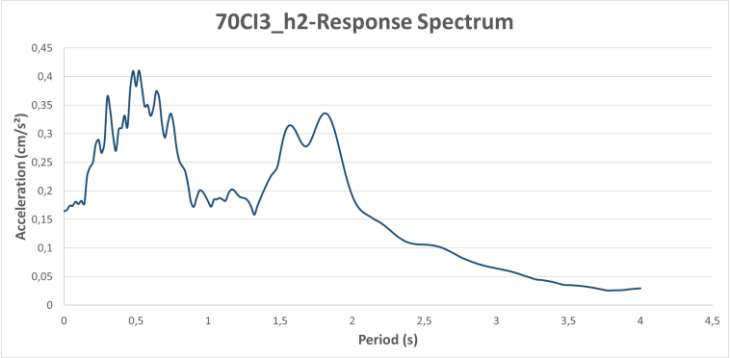

Figure C.92. Response Spectrum Graph of Ground Motion named 70CI3_h2

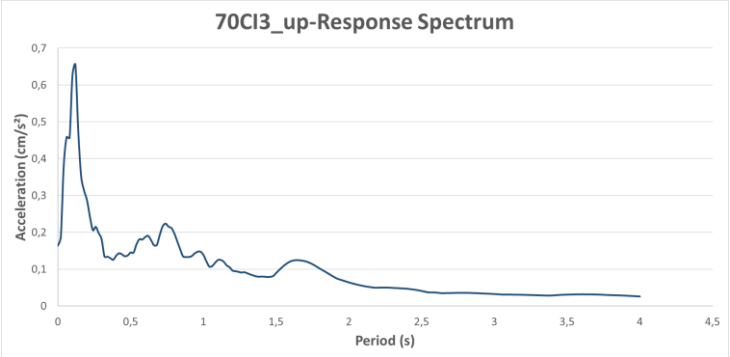

Figure C.93. Response Spectrum Graph of Ground Motion named 70CI3_up

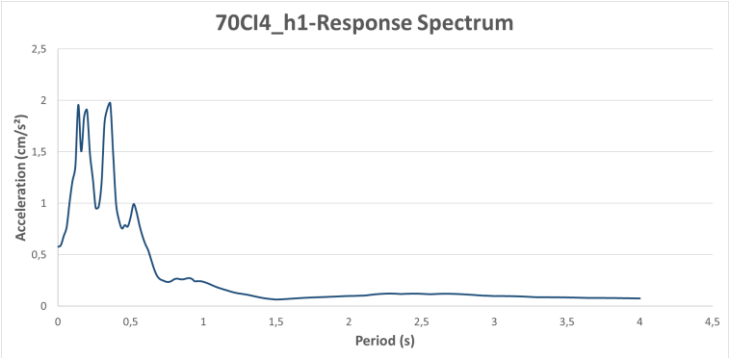

Figure C.94. Response Spectrum Graph of Ground Motion named 70CI4_h1

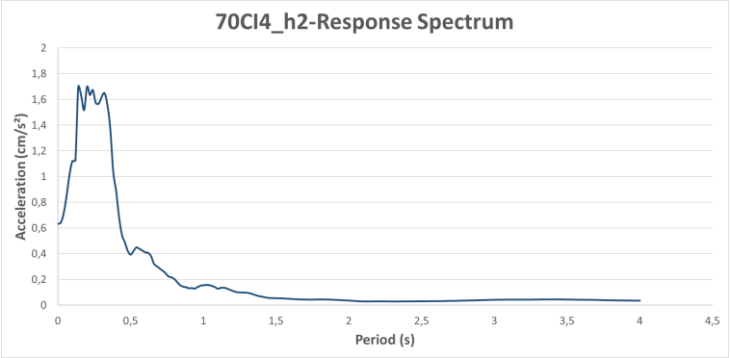

Figure C.95. Response Spectrum Graph of Ground Motion named 70CI4_h2

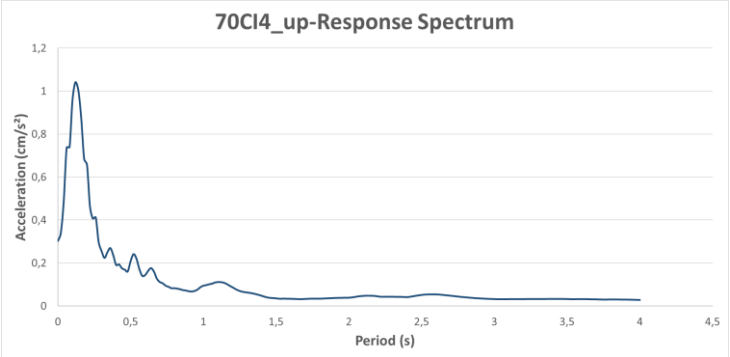

Figure C.96. Response Spectrum Graph of Ground Motion named 70CI4_up

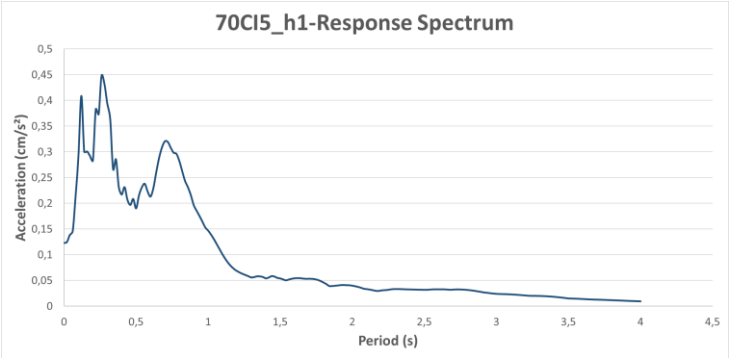

Figure C.97. Response Spectrum Graph of Ground Motion named 70CI5_h1

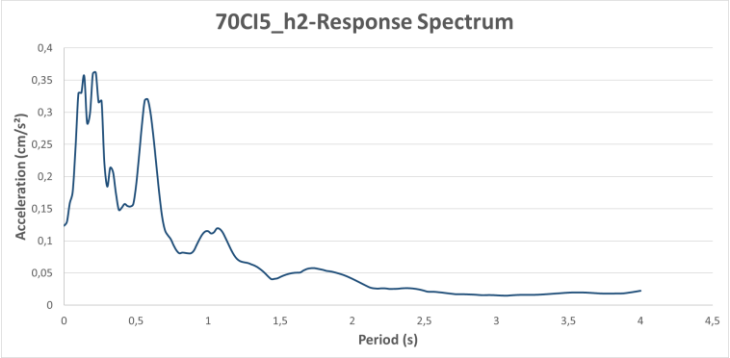

Figure C.98. Response Spectrum Graph of Ground Motion named 70CI5_h2

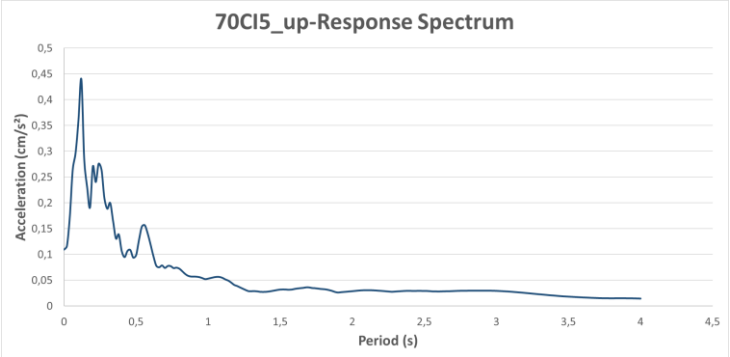

Figure C.99. Response Spectrum Graph of Ground Motion named 70CI5_up

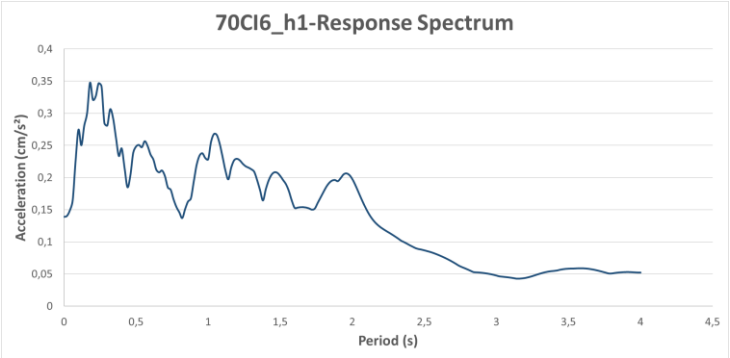

Figure C.100. Response Spectrum Graph of Ground Motion named 70CI6_h1

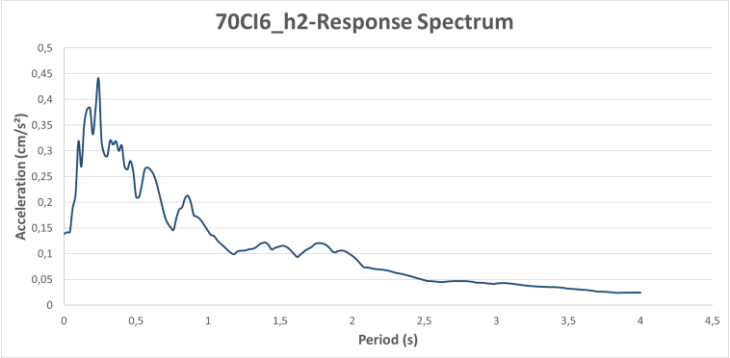

Figure C.101. Response Spectrum Graph of Ground Motion named 70CI6_h2

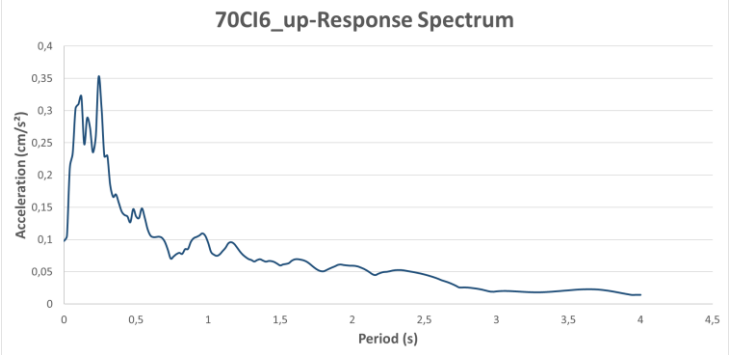

Figure C.102. Response Spectrum Graph of Ground Motion named 70CI6_up

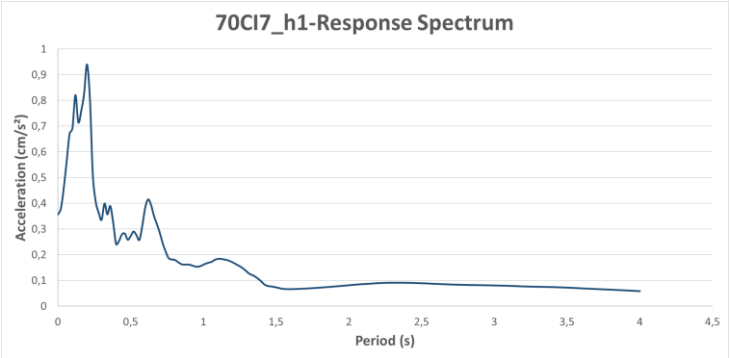

Figure C.103. Response Spectrum Graph of Ground Motion named 70CI7_h1

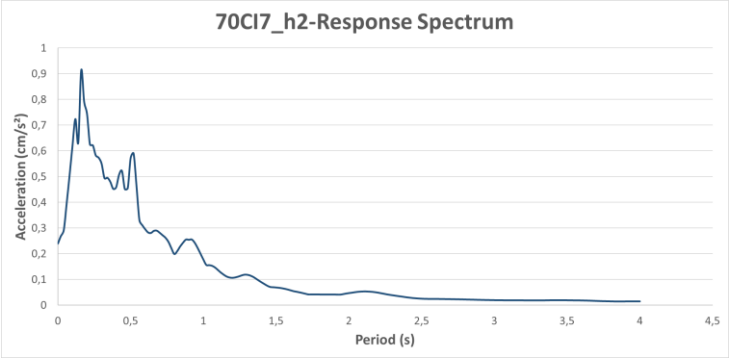

Figure C.104. Response Spectrum Graph of Ground Motion named 70CI7_h2

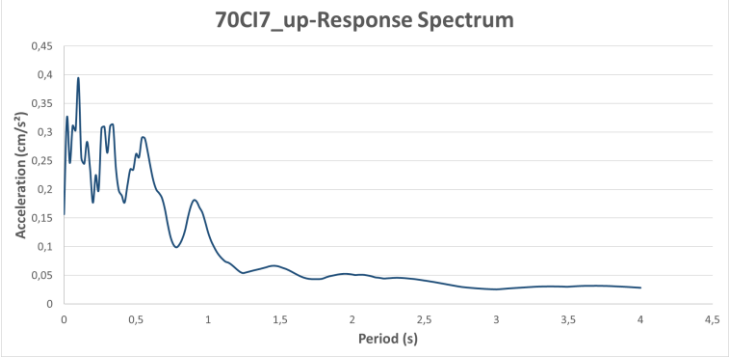

Figure C.105. Response Spectrum Graph of Ground Motion named 70CI7_up

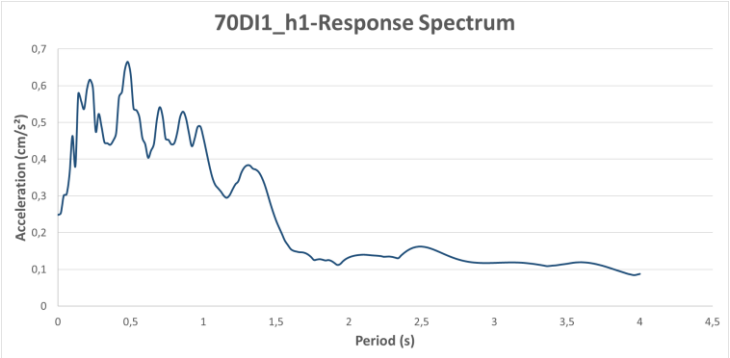

Figure C.106. Response Spectrum Graph of Ground Motion named 70DI1_h1

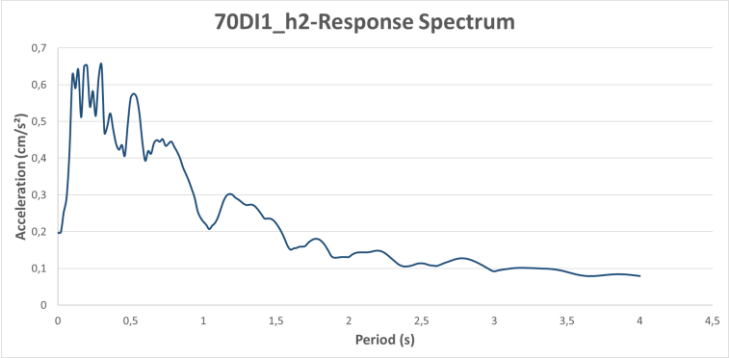

Figure C.107. Response Spectrum Graph of Ground Motion named 70DI1_h2

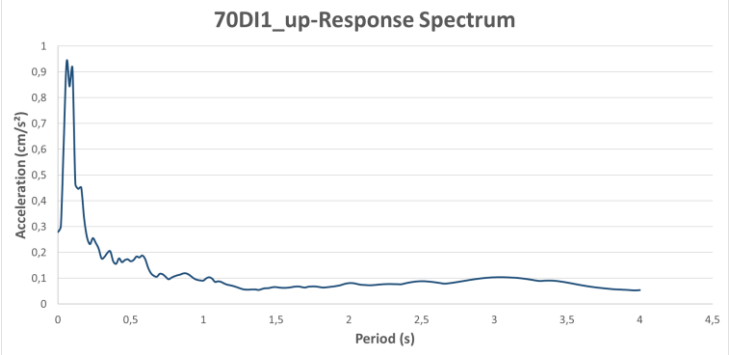

Figure C.108. Response Spectrum Graph of Ground Motion named 70DI1_up

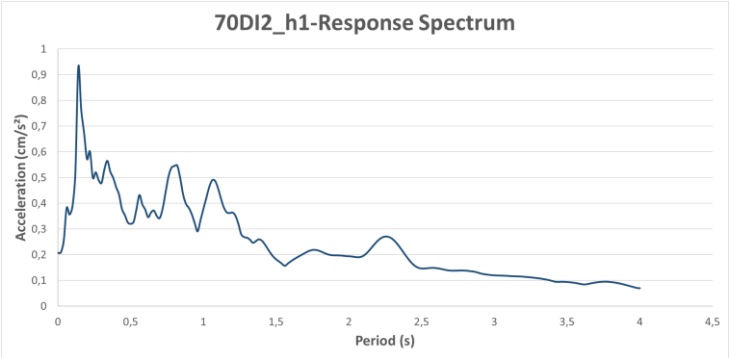

Figure C.109. Response Spectrum Graph of Ground Motion named 70DI2_h1

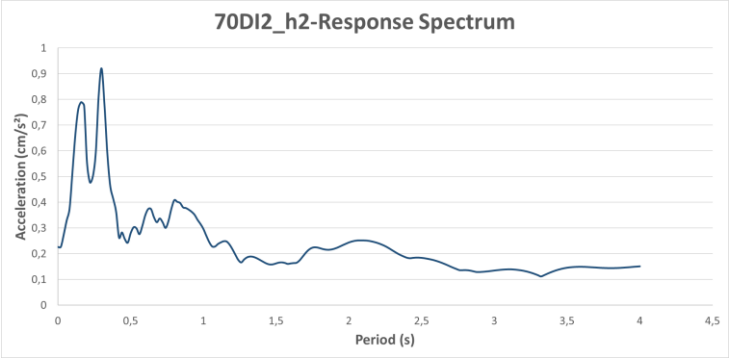

Figure C.110. Response Spectrum Graph of Ground Motion named 70DI2_h2

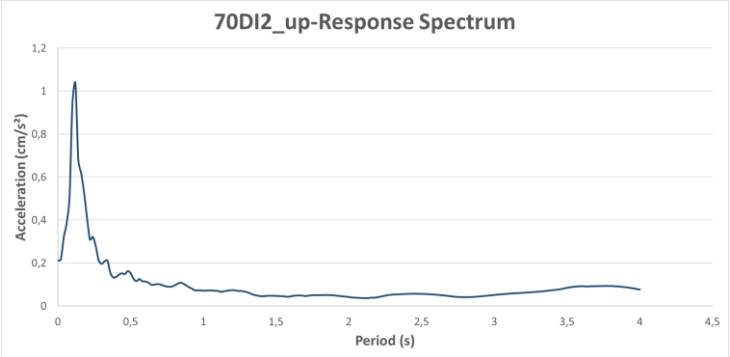

Figure C.111. Response Spectrum Graph of Ground Motion named 70DI2_up

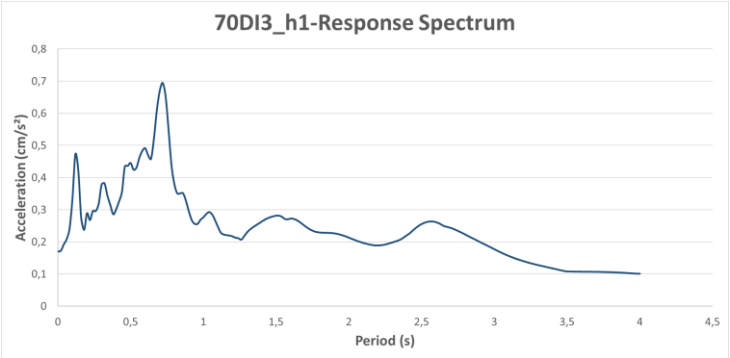

Figure C.112. Response Spectrum Graph of Ground Motion named 70DI3_h1

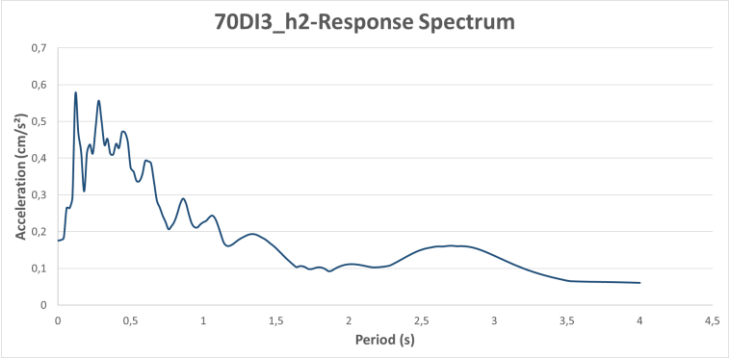

Figure C.113. Response Spectrum Graph of Ground Motion named 70DI3_h2

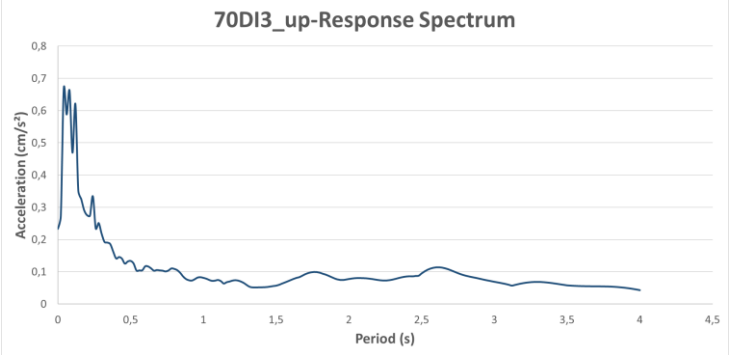

Figure C.114. Response Spectrum Graph of Ground Motion named 70DI3_up

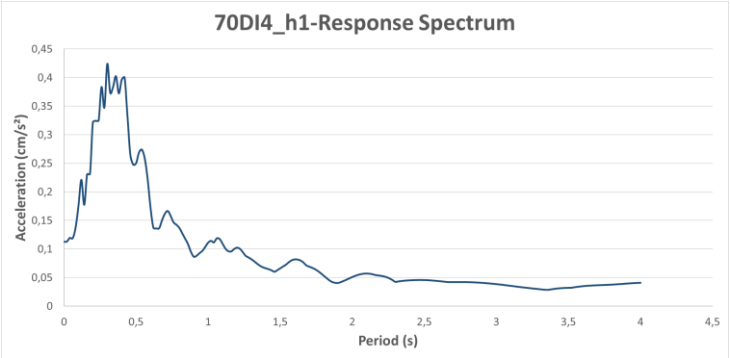

Figure C.115. Response Spectrum Graph of Ground Motion named 70DI4_h1

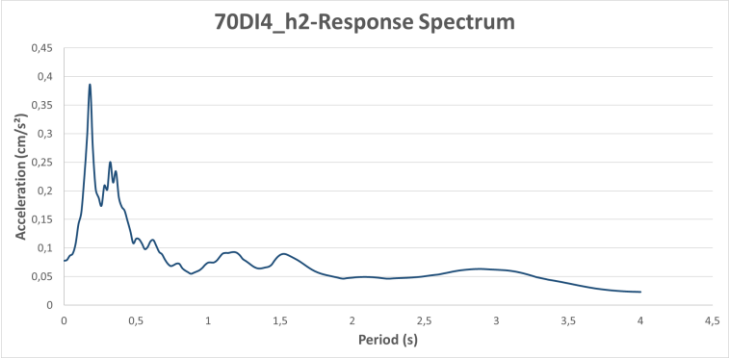

Figure C.116. Response Spectrum Graph of Ground Motion named 70DI4_h2

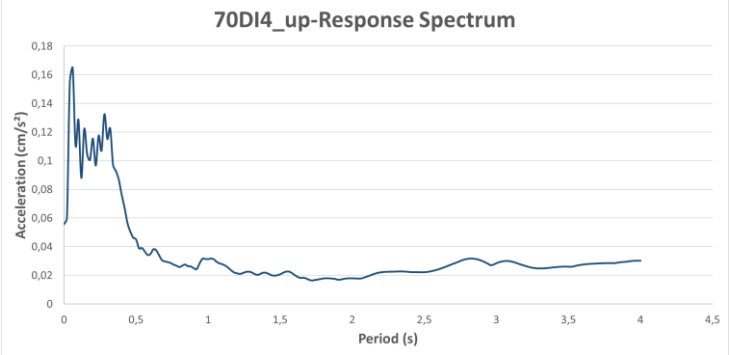

Figure C.117. Response Spectrum Graph of Ground Motion named 70DI4_up

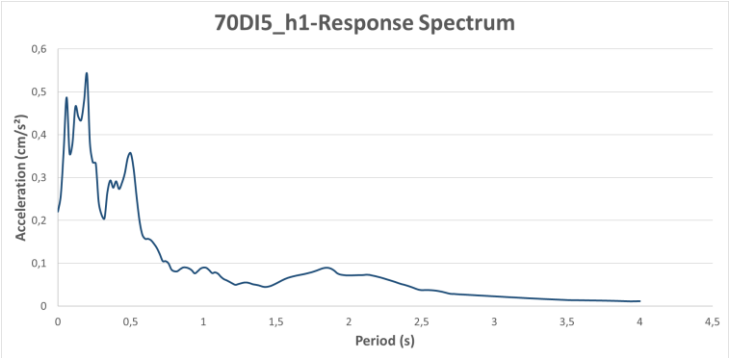

Figure C.118. Response Spectrum Graph of Ground Motion named 70DI5_h1

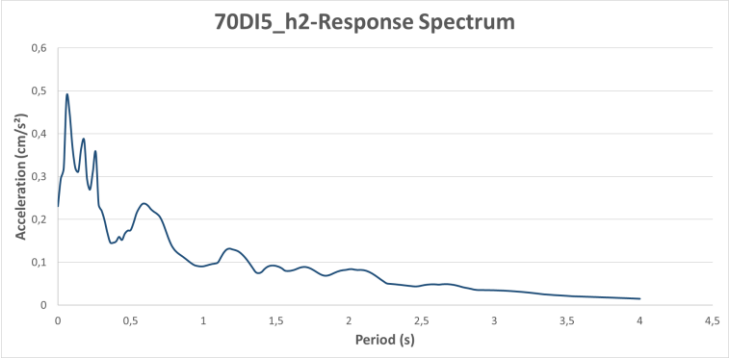

Figure C.119. Response Spectrum Graph of Ground Motion named 70DI5_h2

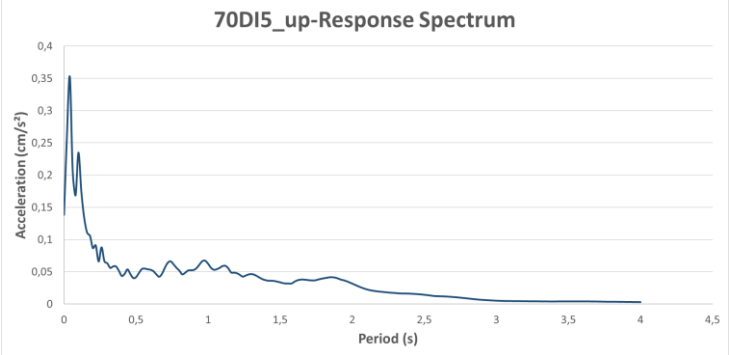

Figure C.120. Response Spectrum Graph of Ground Motion named 70DI5_up

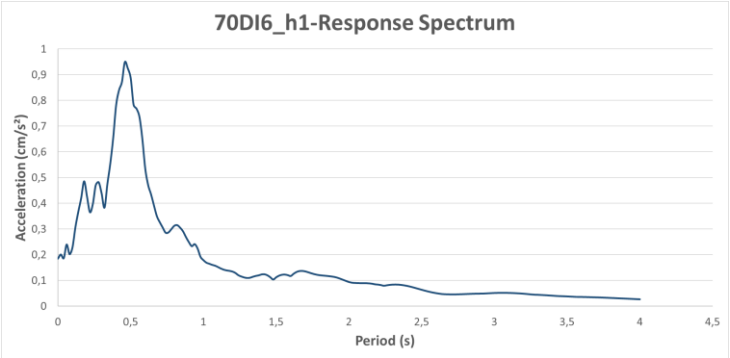

Figure C.121. Response Spectrum Graph of Ground Motion named 70DI6_h1

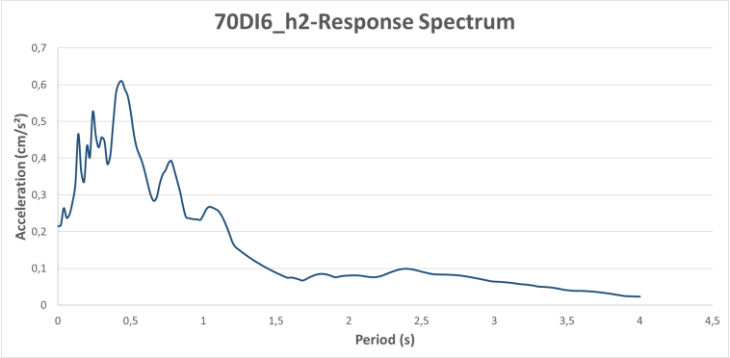

Figure C.122. Response Spectrum Graph of Ground Motion named 70DI6_h2

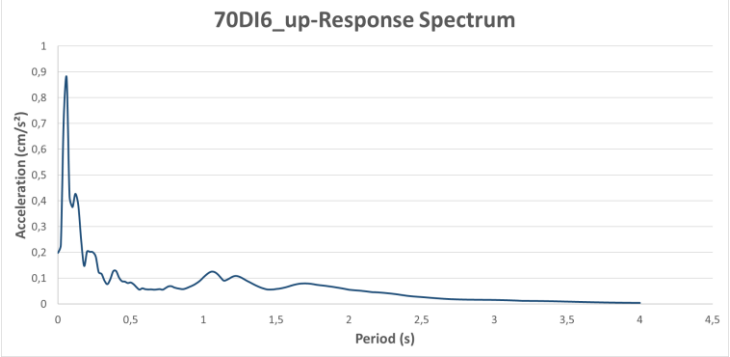

Figure C.123. Response Spectrum Graph of Ground Motion named 70DI6_up

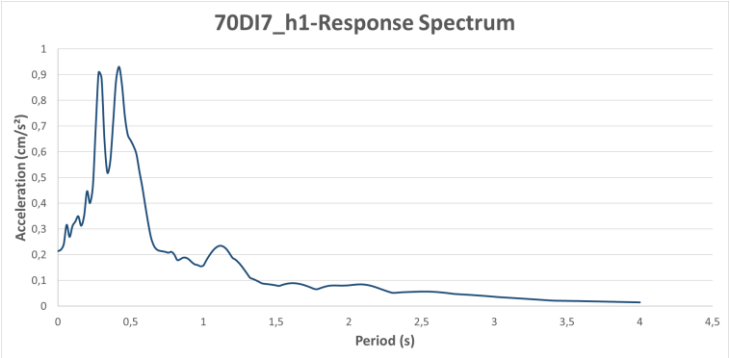

Figure C.124. Response Spectrum Graph of Ground Motion named 70DI7_h1

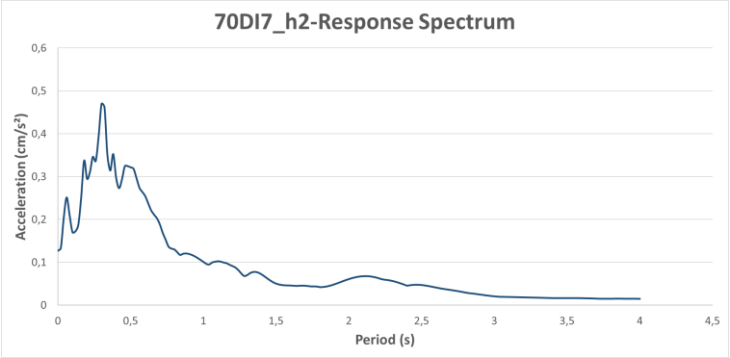

Figure C.125. Response Spectrum Graph of Ground Motion named 70DI7_h2

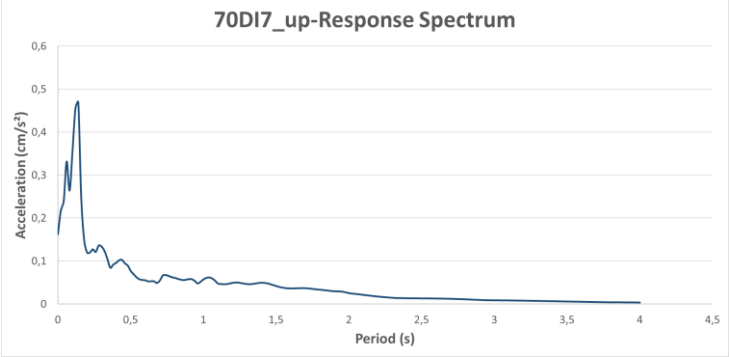

Figure C.126. Response Spectrum Graph of Ground Motion named 70DI7_up